THE ESCOUMINS SUPRACRUSTAL BELT: A RECORD OF MESOPROTEROZOIC (PINWARIAN) EVOLUTION OF THE LAURENTIAN MARGIN AND GRENVILLIAN MAGMATISM, CENTRAL GRENVILLE PROVINCE, QUEBEC, CANADA

by

© Pierre-Arthur Groulier

A thesis submitted to the School of Graduate Studies

in partial fulfillment of the requirements for the degree of

Doctor of Philosophy

Department of Earth Sciences

Memorial University of Newfoundland

September 2019

St. John's, Newfoundland and Labrador

Abstract

The Mesoproterozoic, Pinwarian-age (1.52 – 1.46 Ga) Escoumins supracrustal belt (southern central Grenville Province, Quebec) consists of a volcano-sedimentary sequence (Saint-Siméon Group) and its structural basement (Tadoussac Intrusive Suite), both deformed and metamorphosed to the amphibolite-facies during the Grenvillian orogeny (1.09 – 0.98 Ga). It represents preserved parts of an island arc built on crustal slivers rifted away from the southeastern Laurentian margin during a major Geon 15 extensional event. Change in arc dynamics led to the closure of the previously opened seaway and back-arc basins and to the final accretion of the island arc at about 1.39 Ga, as marked by the emplacement of a major 1.43 – 1.37 Ga arc-related plutonic belt. The Saint-Siméon Group is an oceanic island arc, rifted-arc and back-arc volcano-sedimentary succession that despite deformation and metamorphism, preserves well original characteristics of the rocks. Its middle member (Moulin-à-Baude Formation) consists of highly evolved alkaline felsic to intermediate volcanic rocks and ferrobasalt together with island arc tholeiite, back-arc basalt and arc basaltic andesite interpreted to reflect the rifting of the arc. Some rocks were extensively altered by synvolcanic hydrothermal fluids and show mineral assemblages typical of metamorphosed VMS-type deposits. The supracrustal belt represents higher crustal levels of the orogenic infrastructure in the Grenville and was intruded by diverse types of syn-to late-orogenic plutons: (1) ca. 1.08 Ga crust-derived magnesian felsic magmatism at the onset of the continental collision, (2) ca. 1.06 – 1.04 Ga ferroan and Ba – Sr enriched intermediate to felsic plutons fractionated from a mafic magma derived from partial melting of a Geon 14 subduction-modified subcontinental lithospheric mantle coeval with amphibolite-facies metamorphism in the

supracrustal rocks, and (3) ca. 0.99 – 0.98 Ga crust-derived peraluminous two-mica leucogranite bodies and pegmatite coeval with titanite growth and deformation. Despite the deformation and the metamorphic overprint, primary features are still preserved providing key information about the evolution of the southeastern Laurentian margin before the final continental collision. This study represents one of the first complete investigations of a polydeformed and metamorphosed volcano-sedimentary sequence and of its hydrothermal alteration assemblages within the Grenville Province.

Acknowledgments

I would like to start this acknowledgements section with extending my sincere gratitude and thanks to my supervisor Aphrodite Indares for her support, mentorship, and her guidance during the completion of this project. Our first meeting in the wilderness of the Manicuagan area led to a fruitful scientific collaboration, it helped me grow as a scientist and a geologist. Thank you for trusting me and for allowing me to lead this project the way I wanted to. You always put me back on track when I was lost and without confidence, you helped me focus and organize my ideas in order to make them stronger, for that I will always be thankful! I am looking forward to continuing working with you in the future on some other exciting projects in this full of surprise Grenville Province. Thanks to your trust I was able to spend more than five years on this wonderful island that is Newfoundland. Its astonishing landscapes, cliffs and the comforting presence of the ocean remembered me of home (without the snow and icebergs) facilitating my adaptation. I can now say proudly that I'm in a way a Newfoundlander and that it will always be part of who I am.

I would like also to thank and acknowledge my second supervisor Greg Dunning. Greg thank you for your help, expertise and mentorship during all these years. Your implication and contribution to this project is major and it was a privilege to learn from you in the lab and in the field. You always taught me to be more precise and to reach for excellence. As for Aphrodite, I am looking forward to continuing working with you in the future on some other exciting projects.

This entire PhD wouldn't have a been possible without the initial impulsion and driving force of Abdelali Moukhsil that put this project in motion and the logistic and

financial support of the Ministère de l'Énergie et des Ressources naturelles du Québec. "Mille merci" Ali, for being such a great mentor, for teaching me the secrets of the Grenville and for believing in me and pushing me to do a PhD.

I would like also to thank Steve Piercey, the final member of my supervisory committee. Steve it was always a pleasure to discuss with you about the secrets of mineral deposits and geochemistry applied to VMS environment. This thesis also received important contributions from George Jenner (igneous petrology and geochemistry) and Markus Wälle (LA-ICP-MS), their expertise in their fields greatly helped me to simplify my thoughts and to bring the best out of the data. I would also like to thank Toby Rivers, John Hanchar, Lyal Harris, Roger Mason, Luke Beranek, Joseph Hodych, Charles Hurich and other faculty members of the department at MUN for the numerous constructive discussions.

Amanda Languille, Sherri Strong, Pam King, Wanda Aylward, Dave Grant, Dylan Goudie of CREAIT and of the department at MUN are thanked for their technical support during the use of the various analytical techniques. Patrice Roy, James Moorhead, Fabien Solgadi, Jonathan Aubin and other members of the Ministère de l'Énergie et des Ressources naturelles du Québec are thanked for their help with the organization of the logistic and organization of the field work.

I would also like to thank my friends, fellow students and officemates (Vincent, Alice, Dilanka, Mackenzie, Arnaud, Fred, Marcus,…) for all their support. If my stay in Newfoundland was this great despite the harsh weather, it is mostly because of them.

François, thank you so much for your patience and help during these long days in the field. You were always here when I needed it, in Nancy as well as on this side of the

"pond". I know it was not always easy to support my changing mood especially when facing the flying vampires (black flies and other wonderful creatures) or when carrying a rock-saw up-hill in a forest but you were always ready and never complained. I will also never forget that you saved me from a pretty bad allergic reaction. Thanks for your support and your friendship, I am really proud to call you my friend. I want to tell you that you are a brilliant man and a great researcher, I wish you the best for your career that will without doubt be brilliant!

Carlos and Maria, the three of us constituted what I like to call the European trio! Always ready to talk, support each other's (especially during the long winters) and giving advices on how to handle the up and downs of the PhD life. Carlos I'm already missing our movie and gaming nights. I'm looking forward to continuing seeing both of you wherever we will be on Earth. I wish you the best for your PhD projects, stay strong!

Finally, I would like to thank the persons the most important in my life, the ones without whom I wouldn't be here today to defend this project: Florence, my sister Anaïs my parents, my grand-parents, and my two purring fur-balls. I would like to dedicate this thesis to all of them. Thank you for your love and unlimited support, I know it was not easy every day, but you managed to always find the proper words to help me stay concentrate and not lost my way. I am so proud of you and I love you.

Table of contents

Abstract ii

Acknowledgments iv

Table of contents vii

List of Tables xvi

List of figures xvii

List of Abbreviations and Symbols xxii

List of Appendices (in separate files) xxvi

Co-authorship Statement xxvii

Chapter 1 Introduction to the thesis 1

1.1 Larger context and aim of this thesis 1

1.2 Geological background 2

1.2.1 The Grenville Province 2

1.2.2 Location of the study area and previous work 6

1.3 Approach 7

1.3.1 Fieldwork 7

1.3.2 Petrography 8

1.3.3 Mineral chemistry 8

1.3.4 Whole-rock lithogeochemistry 9

1.3.5 U–Pb geochronology 9

1.3.6 Sm–Nd isotopic geochemistry 10

1.4 Structure of the thesis 10

1.5 References 13

Chapter 2 Peri-Laurentian, Pinwarian-age oceanic arc crust preserved in the Grenville Province: Insights from the Escoumins supracrustal belt 18

2.1 Abstract 18

2.2 Introduction 19

2.3 Geology of the Escoumins supracrustal belt 21

2.3.1 Tadoussac Intrusive Suite 23

2.3.2 Saint-Siméon Group 24

2.3.2.1 Saint-Paul-du-Nord Formation 24

2.3.2.2 Moulin-à-Baude Formation 25

2.3.2.3 The Port-aux-Quilles Formation 28

2.4 Geochemistry 29

2.4.1 Tadoussac Intrusive Suite 29

2.4.2 Volcanic rocks from the Saint-Siméon Group 30

2.4.2.1 Major element geochemistry 31

2.4.2.2 Trace element geochemistry 32

2.4.3 Tectonic environment 33

2.5 Geochronology 34

2.5.1 Analytical techniques 35

2.5.2 Samples and results 37
2.5.2.1 Dacitic tuff from the Saint-Onge synform (13-PA-32; 468768, 5363165) 37
2.5.2.2 Rhyolitic tuff from the Raymond synform (14-PA-95-A; 459148, 5348547) 38
2.5.2.3 Granodiorite, Tadoussac intrusive Suite (15-PA-125-A; 449918, 5340601) 39
2.5.2.4 Quartzite, lower part of the Port-aux-Quilles Formation (13-PA-2; 467066, 5356031) 39
2.6 Isotopic data 44
2.6.1 Analytical technique 44
2.6.2 Results 45
2.7 Discussion 46
2.7.1 Insights from field data and geochronology 46
2.7.2 Insights from geochemistry and Nd-isotopic data 49
2.7.3 Overall evolution of the ESB 52
2.7.4 Late Geon 15 to Geon 14 arc systems in the central-eastern Grenville Province 54
2.7.4.1 Tectonic model for the ESB 58
2.7.4.2 Preservation of the ESB 59
2.8 Conclusion 60
2.9 Acknowledgements 61

2.10 References 61

Chapter 3 Arc dynamics in the Mesoproterozoic Laurentian margin, Quebec 115

3.1 Abstract.....115

3.2 Introduction 115

3.3 The Southeastern Laurentian margin at Geon 15 to 13 116

3.4 Volcano-sedimentary belts in the central Grenville 118

3.5 Late Geon 15 to mid Geon 14 sedimentary basins.....118

3.6 Late Geon 15 to Geon 13 plutonic suites 120

3.7 Discussion.....122

3.7.1 Continental intra-arc / back-arc basins and rifting of crustal slivers along southeast Laurentia in Geon 15 122

3.7.2 Closure of the seaway and accretion of pericratonic island arcs to Laurentia during late Geon 14 to early Geon 13..... 123

3.8 Acknowledgements 124

3.9 References 125

Chapter 4 Recognition and documentation of a Mesoproterozoic sub-seafloor hydrothermal system within an oceanic arc, arc-rift and back-arc sequence preserved through Grenvillian metamorphism 135

4.1 Abstract.....135

4.2 Introduction 136

4.3 Regional setting 139

4.3.1 Quebecia terrane 139

4.3.2 Geology of the Saint-Siméon Group 140

4.4 Stratigraphy of the Moulin-à-Baude Formation 142

4.4.1 Lower Moulin-à-Baude Formation 143

4.4.2 Upper Moulin-à-Baude Formation 145

4.5 Sampling and analytical techniques 148

4.5.1 Whole-rock geochemistry 148

4.5.2 Electron probe microanalysis (EPMA) 148

4.6 Lithogeochemistry of the volcanic rocks 149

4.6.1 General characteristics 150

4.6.2 Geochemistry of the mafic rocks 151

4.6.2.1 M1 unit, lower part of the MAB 151

4.6.2.2 M2 unit, upper part of the MAB 152

4.6.2.3 M3 unit, upper part of the MAB 153

4.6.2.4 M4 ferrobasalt, upper part of the MAB 153

4.6.2.5 Tectonic environment 154

4.6.3 Geochemistry of felsic and intermediate rocks 155

4.6.3.1 F1 unit 155

4.6.3.2 F2 unit 156

4.6.3.3 I1 intermediate unit 157

4.6.3.4 Tectonic environment 158

4.7 Metamorphosed hydrothermal alteration assemblage, mineral chemistry and sulfide occurrences 159

4.7.1 Mafic volcanic and volcaniclastic rocks 160

4.7.1.1 Epidote, quartz 160

4.7.1.2 Amphibole, garnet ± phlogopite 160

4.7.1.3 Biotite, quartz 162

4.7.2 Felsic volcanic and volcaniclastic rocks 162

4.7.2.1 Magnetite, biotite ± epidote 162

4.7.2.2 Mn–Ca–Fe garnet, calcic amphibole, quartz, calcic plagioclase, biotite (epidote) 162

4.7.2.3 Albite, gedrite/anthophyllite and/or phlogopite, quartz, magnetite 163

4.7.2.4 Epidote, K-feldspar, biotite, quartz, carbonate, magnetite, plagioclase, muscovite 163

4.7.2.5 Phlogopite, K-feldspar, quartz, clinozoisite/zoisite, tourmaline 164

4.7.2.6 Muscovite, quartz, Fe oxides, tourmaline ± garnet 164

4.7.2.7 Sillimanite, muscovite, phlogopite, K-feldspar, magnetite, gahnite, tourmaline 165

4.7.3 Mafic to felsic protoliths 166

4.7.3.1 Skarn assemblage 166

4.7.3.2 Silica alteration 167

4.7.4 Paragenetic sequence of alteration and zonation of the alteration 168

4.7.5 Sulfide occurrences 168
4.7.6 Effect of the metamorphism 170
4.7.6.1 Desulphidation 170
4.7.6.2 Dehydration reactions in aluminous rocks 171
4.7.6.3 Dehydration reactions in chlorite ± sericite ± quartz ± albite altered rocks 172
4.7.6.4 Decarbonatation in skarns 173
4.8 Alteration geochemistry 175
4.9 Discussion 178
4.9.1 New input on the geochemistry and stratigraphy of the Moulin-à-Baude Formation 178
4.9.2 Evidence of VMS-style alteration and mineralization 179
4.9.3 Comparison with other metamorphosed VMS-deposits 181
4.9.3.1 The Montauban auriferous VMS deposit (Grenville Province, Quebec) 182
4.9.3.2 The Lalor deposit (Flin Flon Belt, Manitoba) 185
4.9.3.3 The Stollberg deposits (Fennoscandian Shield, Sweden) 186
4.10 Conclusion 188
4.11 Acknowledgements 190
4.12 Appendices 190
4.13 References 191

Chapter 5 Syn-orogenic magmatism over 100 m.y. in high crustal levels of the central Grenville Province: Characteristics, age and tectonic significance 254

5.1 Abstract 254

5.2 Introduction 255

5.3 Geological setting 257

5.3.1 Structural configuration of the ESB 259

5.3.2 Metamorphism 260

5.4 Analytical methods 261

5.5 Grenvillian-age plutonic rocks 263

5.5.1 General characteristics and petrography 263

5.5.1.1 Bon-Désir granite 263

5.5.1.2 Michaud quartz-monzonite and related intrusions 264

5.5.1.3 Biotite-rich felsic sill 266

5.5.1.4 Two-mica leucogranite 266

5.5.2 Geochronology 268

5.5.2.1 Bon-Désir granite (PA-107-A) 268

5.5.2.2 Michaud quartz monzonite (PA-187-A) 269

5.5.2.3 Biotite-rich felsic sill (PA-88-A) 269

5.5.2.4 Felsic pegmatite (PA-88-B) 270

5.5.2.5 Two-mica leucogranite (PA-29-A) 271

5.5.3 Whole-rock geochemistry 272

5.5.3.1 Major element geochemistry 272
5.5.3.2 Trace element geochemistry 273
5.5.3.3 Tectonic environment and magmatic-type signature 274
5.5.4 Sm-Nd isotopic data 276
5.5.4.1 Results 276
5.6 Discussion and conclusion 277
5.6.1 Summary of the Grenvillian age plutonic rocks 277
5.6.2 Relationships to metamorphism and deformation in the ESB 279
5.6.3 Implications for the Grenvillian orogeny 282
5.6.3.1 Early-Ottawan magmatism 283
5.6.3.2 Mid-Ottawan mantle-derived magmatism 283
5.6.3.3 Rigolet crust-derived magmatism 286
5.6.3.4 Tectonic plate organization 287
5.6.3.5 Conclusion 288
5.7 Acknowledgements 289
5.8 References 290
Chapter 6 Conclusions and directions for future research 324
6.1 Conclusion and key findings 324
6.2 Recommendations for future work 329
6.3 References 332
Bibliography and References 333

List of Tables

Table 2.1. Whole rock geochemistry of the plutonic rocks from the Tadoussac Intrusive Suite 94.

Table 2.2. Whole rock geochemistry of volcanic rocks from the Moulin-à-Baude Formation 97

Table 2.3. U-Pb data for rocks of the Escoumins region 106

Table 2.4. Detrital zircon (LA-ICP-MS) data from the quartzite 107

Table 2.5. Sm-Nd isotopic data for the plutonic and volcanic rocks of the Escoumins Supracrustal Belt 112

Table A2.1. UTM location of the samples 113

Table 4.1. Whole-rock geochemistry of the volcanic rocks and feeder conduits of the Moulin-à-Baude Formation 237

Table 4.2. Summary of the mineralogy of the different metamorphosed mineral alteration assemblage in the Moulin-à-Baude Formation 252

Table A4.1. Analytical conditions used to analyze minerals using Electron Probe Micro-Analyser (EPMA) 253

Table 5.1. U-Pb data for zircon and monazite 319

Table 5.2. Whole rock geochemistry of the different plutonic rocks 321

Table 5.3. Sm-Nd isotopic data of the different Grenvillian intrusions 323

List of figures

Figure 2.1: (a) Map of Proterozoic Laurentia displaying the extension of the Grenville. (b) Nd-model age map showing major crustal terranes of the Grenville Province in Canada with distinct crustal formation ages 77

Figure 2.2: Geological map of the Escoumins supracrustal belt. 78

Figure 2.3: Schematic stratigraphic section of the ESB. 79

Figure 2.4: Representative photographs of igneous and sedimentary rocks 80

Figure 2.5: Geochemistry of plutonic rocks of the Tadoussac Intrusive Suite. 83

Figure 2.6: Geochemistry of volcanic rocks from the Moulin-à-Baude Formation. 84

Figure 2.7: REE plots normalized to chondrite (a, c, e and g) or extended trace element diagram normalized to primitive mantle (b, d, f and h) for volcanic rocks. 85

Figure 2.8: Tectonic discrimination diagram for volcanic rocks. 86

Figure 2.9: Photomicrographs of selected zircon grains under a binocular microscope. 87

Figure 2.10: Cathodoluminescence images of representative zircon grains. 88

Figure 2.11: Concordia diagrams of CA-TIMS U/Pb analyses of zircon and titanite grains. 89

Figure 2.12: Cathodoluminescence images of representative zircon grains dated using LA-ICP-MS. 90

Figure 2.13: Histogram of age probability and concordia diagrams of LA-ICP-MS U/Pb analyses. 91

Figure 2.14: εNd versus age diagram. 92

Figure 2.15: Proposed model for the tectonic evolution of the ESB. 93

Figure 3.1: A: Geologic map of Proterozoic Laurentia; B: Schematic map of the Grenville in Canada; C: Geological map of the central Grenville Province. 130

Figure 3.2: U–Pb age ranges, geochemical signatures and tectonic setting for 1.6 to 1.35 Ga magmatic rocks and sedimentary basins from the Grenville and Granite-Rhyolite Province. 131

Figure 3.3: $^{207}Pb/^{206}Pb$ ages versus relative abundance of detrital zircon. 132

Figure 3.4: Tectonic discrimination diagrams for igneous rocks. 133

Figure 3.5: Sketches of the proposed evolution of the southeastern Laurentian margin in central and eastern Grenville from Geon 15 to early Geon 13. 134

Figure 4.1: A) Simplified map of the Proterozoic Laurentia; B) Schematic map of the Grenville in Canada; C) Geological map of the central Grenville Province. 208

Figure 4.2: Geological map of the southern central Grenville Province along the St Lawrence River. 209

Figure 4.3: Geological map of the Escoumins syncline. 210

Figure 4.4: Geological map of the southern Grandes-Bergeronnes syncline. 211

Figure 4.5: Stratigraphic log of the Saint-Siméon Group and of its basement. 212

Figure 4.6: Representative field photographs of rocks from the Saint-Siméon Group. 213

Figure 4.7: Representative field photographs of rocks from the Saint-Siméon Group. 214

Figure 4.8: a) Detailed geological maps of the southern limb of the Grandes-Bergeronnes syncline. b) Detailed geological maps of the northern limb of the Grandes-Bergeronnes syncline. 215

Figure 4.9: Representative field photographs of rocks from the Saint-Siméon Group. 216

Figure 4.10: Major and trace element discrimination plot for volcanic rocks of the Moulin-à-Baude Formation. 217

Figure 4.11: REE plots and extended trace element diagram for mafic volcanic rocks of the Moulin-à-Baude Formation. 219

Figure 4.12: Tectonic discrimination diagrams for mafic volcanic rocks from the Moulin-à-Baude Formation. 220

Figure 4.13: Tectonic discrimination diagrams for mafic volcanic rocks of the Moulin-à-Baude Formation. 222

Figure 4.14: REE plots and extended trace element diagram for felsic to intermediate volcanic rocks of the Moulin-à-Baude Formation. 223

Figure 4.15: Petrochemical affinity and tectonic discrimination diagrams for intermediate and felsic volcanic rocks from the Moulin-à-Baude Formation. 224

Figure 4.16: Compositional diagrams for amphibole, epidote and mica from unaltered and altered rocks of the Moulin-à-Baude Formation. 226

Figure 4.17: Ternary diagram for garnet composition from altered rocks of the Moulin-à-Baude Formation. 228

Figure 4.18: Representative photographs of mineral assemblages from altered basaltic rocks of the Moulin-à-Baude Formation. 229

Figure 4.19: Representative photographs of mineral assemblages from altered volcanic rocks of the Moulin-à-Baude Formation. 230

Figure 4.20: Representative photographs of mineral assemblages from altered volcanic rocks of the Moulin-à-Baude Formation. 231

Figure 4.21: Representative photographs of mineral assemblages from altered volcanic rocks of the Moulin-à-Baude Formation. 232
Figure 4.22: Representative photographs of mineral assemblages from skarns of the Moulin-à-Baude Formation. 233
Figure 4.23: Photomicrographs of skarn assemblages. 234
Figure 4.24: Photomicrographs showing desulphidation, dehydration and decarbonatation reactions. 235
Figure 4.25: Alteration geochemical diagrams. 236
Figure 5.1: Tectono-metamorphic map of the Grenville Province in Canada. 300
Figure 5.2: Geological map of the Escoumins supracrustal belt. 301
Figure 5.3: a) Interpreted structural map of the ESB from aeromagnetic survey map; b-c-d) stereonets of the planar and linear structures. 302
Figure 5.4: Representative field photographs of the structure in the studied rocks. 303
Figure 5.5: Concordia diagram U–Pb on zircon grains and titanite grains. 304
Figure 5.6: Representative field photographs of the studied plutonic rocks. 305
Figure 5.7: SEM–MLA false colour mineral maps of thin section from the studied plutons. 306
Figure 5.8: Photomicrographs of characteristic textures of the studied plutons. 307
Figure 5.9: Photomicrographs of selected zircon and monazite grains under a binocular microscope. 310
Figure 5.10: Cathodoluminescence images of representative zircon grains. 311
Figure 5.11: Concordia diagrams of TIMS U–Pb analyses of zircon and monazite grains. 312

Figure 5.12: Major and trace element discrimination plot for plutonic rocks. 313

Figure 5.13: Major and trace element discrimination diagrams for plutonic rocks. 315

Figure 5.14: Initial εNd vs age diagram for intrusive rocks from the ESB. 316

Figure 5.15: Summary of the U–Pb magmatic and metamorphic ages. 317

Figure 5.16: Proposed model for the tectono-magmatic evolution of the central Grenville Province during the Grenvillian orogeny. 318

List of Abbreviations and Symbols

Ma = Mega annum (latin), million years

Ga = Giga annum (latin), billion years

M.y. = million years

P = pressure

°C = degree Celsius

kV = kilo volt

nA = nano amper

CL = cathodoluminescence

Z = zircon fraction (geochronology)

T = titanite fraction (geochronology)

a.p.f.u. = atom per formula unit

wt. % = weight percent

ppm = parts per million

Mg# = magnesium number

LOI = loss on ignition

REE = rare earth elements

LREE = light rare earth elements

HREE = heavy rare earth elements

LILE = large-ion lithophile elements

LFSE = low field strength elements

HFSE = high field strength elements

MORB = mid-ocean ridge basalt

OIB = ocean island basalt

VAB = volcanic arc basalt

BABB = back-arc basin basalt

WPG = within-plate granite

VAG = volcanic arc granite

AI = alteration index

AAAI = advanced argillic alteration index

CCPI = chlorite-carbonate-pyrite index

CN = chondrite normalized

PN = primitive mantle normalized

UTM = Universal Transverse Mercator

SEM = scanning electron microscope

EPMA = electron probe microanalyzer

MLA = mineral liberation analysis

LA-ICP-MS = laser ablation inductively coupled plasma mass spectrometry

CA-ID-TIMS = chemical abrasion isotope dilution thermal ionization mass spectrometry

ESB = Escoumins supracrustal belt

SSG = Saint-Siméon Group

TIS = Tadoussac Intrusive Suite

SPDN = Saint-Paul-du-Nord Formation

MAB = Moulin-à-Baude Formation

PAQ = Port-aux-Quilles Formation

Mineral abbreviations

Ab = albite

Act = actinolite

Aln = allanite

Amp = Amphibole

Ap = apatite

Ath = Anthophyllite

Bt = biotite

Cb = carbonate

Cc = calcite

Ccp = chalcopyrite

Cl = chlorite

Cpx = clinopyroxene

Czo = clinozoisite

Cum = cummingtonite

Di = diopside

Ep = epidote

Ged = gedrite

Ghn = gahnite

Grt = garnet

Hbl = hornblende

k-fsp/kspar = K-feldspar

Mag = magnetite

Mc = microcline

Mus = muscovite

Or = orthoclase

Phl = phlogopite

Pl = plagioclase

Po = pyrrhotite

Py = pyrite

Qz = quartz

Scp = scapolite

Ser = sericite

Sil = sillimanite

Sp = sphalerite

Sul = sulfide

Tr = tremolite

Ttn = titanite

Tur = tourmaline

Zo = zoisite

Zrn = zircon

List of Appendices (in separate files)

Appendix 1. SEM-MLA false colour maps and analytical procedure.

Appendix 2. EPMA analyses of amphibole, epidote, mica and garnet from altered and unaltered rocks from the Moulin-à-Baude Formation.

Appendix 3. Mobility of elements tested using Zr as reference.

Appendix 4. List of samples (geochemistry, U-Pb, Sm-Nd) and UTM location.

Co-authorship Statement

This research project was first initiated by Abdelali Moukhsil (Ministère de l'Énergie et des Ressources naturelles) and was then designed by Aphrodite Indares (MUN), Greg Dunning (MUN) and Pierre-Arthur Groulier. The identification of specific questions to be examined was refined by Pierre-Arthur Groulier during the course of the study with the guidance of Aphrodite Indares and Greg Dunning. Field work was predominantly planned and carried out by the thesis author, Aphrodite Indares and Greg Dunning. Early visits with Abdelali Moukhsil in the study area during the summer 2013 helped discover the area and bring out some questions to be solved. All the samples used were collected by Pierre-Arthur Groulier during the summers 2013, 2014, 2015 and 2017. The samples used in this thesis for the different analytical techniques were prepared by Pierre-Arthur Groulier. Greg Dunning was instrumental for the U-Pb dating of the rocks with CA-TIMS. Pam King (MUN), Amanda Languille (MUN), Dave Grant (CREAIT – MUN) and Dylan Goudie (CREAIT – MUN) provided assistance with the sample preparation for the U-Pb dating. Markus Wälle aided with the use of the LA-ICP-MS and helped process and interpret the data. Wanda Aylward (TERRA Facility – MUN) is thanked for her help during the use of the SEM and of the EPMA machines. Sherri Strong (TERRA Facility – MUN) provided assistance during the preparation of the sample and the acquisition of Sm-Nd data with the TIMS. Lyal Harris (INRS) helped with interpreting the structure. François Turlin and Evelyne Sunatori provided field assistance during the summers 2014 and 2015 respectively.

Chapter 2 was published in *Precambrian Research* and co-authored by Aphrodite Indares, Greg Dunning, Abdelali Moukhsil, and Markus Wälle. Aphrodite Indares and

Greg Dunning provided editorial guidance and helped with the organization of the paper. The paper was reviewed by Trond Slagstad and Bernard Bingen and journal editor Randall Parrish provided editorial handling.

Chapter 3 is expected to be submitted to *Terra Nova*. This paper is co-authored by Aphrodite Indares, Greg Dunning and Abdelali Moukhsil. Aphrodite Indares and Greg Dunning provided editorial guidance and helped in shaping ideas. Abdelali Moukhsil contributed in providing geochemical analyses of some plutonic rocks used in this paper.

Chapter 4 is expected to be submitted to *Ore Geology Review* and is co-authored by Aphrodite Indares, Greg Dunning, Steve Piercey (MUN) and Abdelali Moukhsil. Aphrodite Indares, Greg Dunning and Steve Piercey provided editorial guidance and helped with the organization of the paper.

Chapter 5 was published in *Lithos* and co-authored by Aphrodite Indares, Greg Dunning, Abdelali Moukhsil and George Jenner. Aphrodite Indares, Greg Dunning, George Jenner provided editorial assistance. George Jenner contributed with the handling of the geochemistry and the Nd isotopes and helped refined the geodynamic model based on that. The paper was reviewed by Charles F. Gower and an anonymous reviewer and journal editor Nelson Eby provided editorial handling.

Chapter 1 Introduction to the thesis

1.1 Larger context and aim of this thesis

This thesis documents new field, petrological, geochemical and geochronological data from the central Grenville Province and discusses their implications for the evolution of the Southeastern Laurentian margin in the Mesoproterozoic and for magmatism during the subsequent Grenvillian orogeny.

Due to the extensive area of rocks that experienced high-grade metamorphism and deformation, the Grenville Province has been, and still is considered, one of the most complex and challenging geological provinces in Canada (cf. the "Grenville Problem" during the mid-fifties) and it is only recently that significant progress has been made in understanding its nature and evolution (see Rivers 2015 for a historical review of the evolution of thoughts and concepts). The geological evolution of the Grenville can be separated into two major stages: that of a long-lived active margin built at the margin of southeastern Laurentia from the Paleoproterozoic to the Mesoproterozoic (Rivers and Corrigan, 2000; Karlstrom et al., 2001; Whitmeyer and Karlstrom, 2007) referred to as the pre-Grenvillian phase, and that of a major continental collision between Laurentia and Amazonia that led to the formation of the Grenville Orogen (1.09 – 0.98 Ga; Rivers 1997) during the assembly of the supercontinent Rodinia (Li et al., 2008; Cawood et al., 2016). The Grenville is considered to be one of the best examples of a Large Hot (Long Duration) Orogen (LHO's; Beaumont et al., 2006; Rivers 2008). However, protracted high-grade metamorphism obscured to a large extent the original features of rock units and added more complexity to the already composite puzzle. Despite this, there are areas

where primary characteristics of the rocks can be revealed by careful integrated work of mapping, petrography, geochemistry and geochronology. An example is the recently recognized Escoumins supracrustal belt at the southern margin of the central Grenville Province that consists of an amphibolite-facies volcano-sedimentary belt and its plutonic basement and that was subsequently intruded by diverse Grenvillian-age plutons.

The objectives of this thesis are to: 1) elucidate the tectonic setting of the ESB using improved assessment of field relations, and new age and geochemical data; 2) place the ESB in the context of evolution of the southeastern Laurentian margin during Geons 15 to 13; 3) assess its economic potential by documenting metamorphosed syn-volcanic subseafloor hydrothermal alteration; and 4) provide insights on the role of the Grenvillian orogeny in the actual organization of the ESB based on structural patterns, metamorphic ages and syn-orogenic plutons.

This study represents a unique opportunity to assess arc dynamics during the pre-Grenvillian period as a result of the exceptional preservation of the primary features of the rocks but also to explore the link between deformation-metamorphism and magmatism in high crustal levels during a major continental collision.

1.2 Geological background

1.2.1 The Grenville Province

Studies of the evolution of the Laurentian margin in the Grenville Province led to the recognition of major arc systems that correspond to distinct pre-Grenvillian events (or orogenies): the Labradorian (1.71 – 1.60 Ga; Gower and Krogh, 2002; Gower et al., 2008), the Pinwarian (1.52 – 1.46 Ga; Tucker and Gower, 1990), the Elsonian (1.40 –

1.20 Ga) and the Elzevirian (1.25 – 1.18 Ga; Carr et al., 2000). The Labradorian and Pinwarian events in Canada are coeval with the formation of the 1.7 – 1.6 Ga Mazatzal and the 1.5 – 1.3 Ga Granite-Rhyolite Provinces in the USA (Karlstrom et al., 2001), which are considered as their western extensions. An important proportion of crust in the Grenville Province formed at 1.5 – 1.35 Ga (Pinwarian and younger). Rocks formed in continental arc to back-arc settings during this time interval were identified along most of the SE Laurentian margin, from the Grenville Province in Labrador (Canada) to the Granite-Rhyolite Province in the USA (Whitmeyer and Karlstrom, 2007). However, in the central Grenville Province, this pattern is disrupted by a ~1.5 Ga partly juvenile terrane defined on the basis of Sm–Nd data (Quebecia terrane; Dickin et al., 2010). This terrane includes remnants of well-preserved Pinwarian volcano-sedimentary sequences (Montauban and Escoumins supracrustal belts). Despite advances made in understanding the evolution of the southeastern Laurentia margin before the Grenvillian orogeny, major questions remain: 1) what is the relation between the Quebecia terrane and Laurentia, 2) does it represent a juvenile outboard arc or a Laurentian-derived terrane separated from Laurentia during a major rifting event, and 3) do the supracrustal belts found within Quebecia hold the key to unveiling the past evolution of the southeastern Laurentian margin during the Proterozoic?

The Grenvillian orogeny (1.09–0.98 Ga; Rivers 1997) in Canada has extensively reworked the SE Laurentian margin. It has been divided in two phases, the Ottawan (1.09–1.02 Ga) and Rigolet phase (1.00–0.98 Ga), and two major belts with distinct evolutions are recognized. The Allochthonous Belt (or hinterland) of the orogen is composed of far-travelled terranes with rocks of Mesoproterozoic age. Large parts of this

belt are characterized by high-grade Ottawan-age metamorphism, and the hinterland is limited to the north by the Allochthon Boundary Thrust (Rivers et al., 1989), which corresponds to a major site of tectonic transport. The Parautochthonous Belt consists of Archean and Paleoproterozoic crust reworked during the Rigolet orogenic phase through the final propagation of the orogen toward its foreland (Rivers et al., 2012), and ends to the NW at the Grenville Front. The hinterland represents the core of the orogen and consists of belts with distinctive metamorphic signatures: the Allochthonous high-*P* (aHP) and mid-*P* (dominant, aMP) belts that were metamorphosed under granulite-facies conditions and experienced anatexis during the Ottawan-phase of the orogeny (see Rivers, 2012) and the low-*P* belt (aLP) with mostly amphibolite facies rocks (Rivers 2008). In addition, the Orogenic Lid consists of rocks from the orogenic suprastructure that lack or has very little evidence of Grenvillian-age penetrative deformation and metamorphism (Rivers 2008). The hinterland is also characterized by a wide range of Ottawan- to Rigolet-age magmatism including anorthosite-mangerite-charnockite-granite (AMCG) suites, potassic to ultrapotassic intrusions, diverse types of granitoids and pegmatites (magnesian, ferroan and peraluminous) and ultramafic to mafic intrusions (Groulier et al., 2018b; Rivers et al., 2012 and references therein). Their spatial distribution was used to define the Interior Magmatic Belt (Gower et al., 1991; Gower and Krogh, 2002; Owen and Erdmer, 1990; Rivers 1997), also referred to as the thermal core of the orogen (Rivers et al., 2012). It has been proposed that the Grenvillian orogeny followed an evolution with: (1) lithospheric shortening and crustal thickening concomitant with the formation of an orogenic plateau in the early Ottawan-phase (Jamieson et al., 2007 & 2010; Rivers 2008, 2012; Hynes and Rivers, 2010), (2) broadening of the plateau with lateral extrusion

of crust and orogenic collapse in the mid- to late-Ottawan, and (3) propagation of the orogen into its foreland and development of the Parautochthonous Belt during the Rigolet together with further thinning of the crust in the hinterland (Rivers, 2012; after Dewey, 1988).

Only parts of the Laurentian side of the Grenville Orogen are preserved, the rest drifted away during the breakup of the supercontinent Rodinia during the Neoproterozoic. In addition, the emplacement of Appalachian rocks over Grenvillian basement (proven by the presence of Appalachian Mesoproterozoic outliers) during the Ordovician hid other parts of the puzzle. Pb isotopes seem to indicate that the southern outliers within the USA have a probable Amazonian affinity and in addition a New York – Alabama lineament recognized by geophysics was interpreted to represent a possible suture zone between Laurentia and Amazonia (see Hibbard and Karabinos, 2015 and references therein).

Because of the extensive high-grade metamorphism and deformation linked to Grenvillian orogeny, primary textures and original relations are severely to completely overprinted. Among the exceptions are the supracrustal belts (Wakeham – La Romaine, Montauban and Escoumins) from the low-*P* belt but only few studies have focussed on them (Corrigan, 1995; Bonnet and Corriveau, 2005). The Montauban, Wakeham and Escoumins supracrustal belts are characterized by coherent and well-preserved volcano-sedimentary sequences than can be used as a window into volcanic and sedimentary processes that occurred along the long-lived active SE Laurentian margin, providing key information on crust-forming processes. Such information can be later adapted to higher-grade metamorphic rocks from the rest of the Grenville Province. These preserved supracrustal belts also host base and precious metals occurrences which are unusual at the

scale of the province (Gauthier and Chartrand, 2005). The high-grade metamorphic conditions and the deformation have led many to exclude the Grenville Province from consideration as an exploration target for these kinds of ore deposits. For example, despite its small size, the Montauban supracrustal belt hosts the Zn–Pb–Au–Ag Montauban mine interpreted to represent a metamorphosed auriferous volcanogenic massive sulfide (VMS) deposit (Bernier et al., 1987; Bernier and Maclean, 1993; Tomkins 2007).

1.2.2 Location of the study area and previous work

This PhD thesis focuses on a previously poorly known Mesoproterozoic volcano-sedimentary belt with exceptionally well-preserved volcanic and sedimentary features located in the southern central part of the Grenville Province in Quebec, that extends from the towns of La Malbaie (to the south) to Forestville (to the north). This belt forms a ca. 150 km long by 30 km wide (in its widest portion) domain along the shore of the St-Lawrence River. It includes a supracrustal sequence known as the Saint-Siméon Group (Rondot 1986) together with its basement (Tadoussac Intrusive Suite) and will be referred to as the Escoumins Supracrustal Belt (ESB). The ESB is part of the low-*P* belt of the Grenville Province defined by Rivers (2008), and was metamorphosed to the amphibolite-facies. The area is accessible by a major highway and several logging roads and has good outcrop exposures below numerous power lines. Despite this, no modern geological mapping was done there since the 1980's. Miller (1973) first described the supracrustal rocks of the ESB while working in the vicinity of Saint-Siméon. In the 1970's and 1980's, several mapping campaigns lead by Rondot (1979, 1986 and 1989) and Morin

(1987) led to a better documentation of the different units and the presence of metavolcanic rocks was first mentioned. The mapping by Rondot (1979, 1986 and 1989) was mainly at the reconnaissance scale and took advantage of the first aeromagnetic geophysical map available at that time. In contrast, Morin (1987) did detailed mapping of a limited area in order to describe some mineral occurrences in the vicinity of the Bergeronnes. Rondot (1986) assigned the name of Saint-Siméon Group to the supracrustal rocks of the ESB, and separated it in three formations: Saint-Paul-du-Nord (lowest, dominantly sedimentary), Moulin-à-Baude (middle, volcanic) and Port-aux-Quilles (upper, sedimentary). The Saint-Siméon Group and the Tadoussac Intrusive Suite are intruded by a wide spectrum of younger plutonic rocks.

1.3 Approach

1.3.1 Fieldwork

Mapping was carried out in key areas, and samples of intrusive and supracrustal rocks were collected for lithogeochemistry, geochronology and petrography, to better constrain the distribution of the different rock units and their characteristics. This study was financed and supported by the Ministère de l'Énergie et des Ressources naturelles du Québec (geological survey of Quebec, MERN), and samples were collected during the summers 2013, 2014, 2015 and 2017. A multiscale approach was used for this thesis, with investigations ranging from the scale of the entire supracrustal belt to more detailed work at the scale of portions of synclines and at the outcrop scale. Pre-existing geological maps (Morin, 1986; Rondot and Dion, 1987) and new aeromagnetic maps (Benahmed and Intissar, 2015) produced by the MERN were used as a framework during this study. Three

reports submitted to the MERN were produced during this study and are available online on the SIGEOM website.

1.3.2 Petrography

Mineral assemblages and textures of metavolcanic, metasedimentary and plutonic rocks were investigated using an optical microscope and some with a Scanning Electron Microscope with Mineral Liberation Analysis software (SEM–MLA) in order to identify primary inherited and metamorphic textures but also to document the metamorphosed hydrothermal alteration. Samples selected for thin sections were sent to IOS services Géoscientifiques Inc. for preparation in Quebec. The petrography work was done in the microscopy lab of the Earth Sciences department at Memorial University of Newfoundland. Microstructures at the thin section scale were documented by false color mineralogical maps using SEM–MLA. This technique produces maps of mineral distribution and precise mineral abundances of thin sections, and highlights textures that are difficult to see using classic optical microscopy. The maps were produced at Memorial University of Newfoundland. Further details are presented in chapters 3 and 5.

1.3.3 Mineral chemistry

The composition of amphibole, epidote, garnet, muscovite and biotite from hydrothermally altered volcanic rocks were obtained using the electron probe micro-analyzer in the Department of Earth Sciences of Memorial University of Newfoundland, to better assess the types of alteration. The data can also be used as tracers of high-

temperature upflow zones and ore mineralization. Further details on this method are given in Chapter 3.

1.3.4 Whole-rock lithogeochemistry

Major and trace element lithogeochemistry was used to discriminate the different types of intrusive and volcanic rocks by magmatic affinity, and to provide critical information on the tectonic settings of formation and evolution of the sequence. In addition, together with petrography it was important for the documentation of the hydrothermal alteration. Whole-rock geochemical analyses were done at Activation Laboratories located in Ancaster, Ontario. The powdered samples were prepared using Li-metaborate and Li-tetraborate fusions. Geochemical analyses include major elements and a suite of 54 trace elements. The major and trace elements were analyzed by inductively coupled plasma (ICP) mass spectrometry. Detection limits are available on the Activation Laboratories website, precision and accuracy are consistent with the estimates given in Jenner (1996).

1.3.5 U–Pb geochronology

Geochronology is an important component of this research. The aims of the U–Pb dating in the context of this project are: (a) to constrain the age of volcanism in the ESB, the provenance and age of deposition of sedimentary units, and the age of major plutonic events by dating zircon and monazite, and (b) to constrain the age of metamorphism, using zircon, monazite and titanite. All the sample preparation and U–Pb dating were

done at the Department of Earth Sciences of Memorial University of Newfoundland. Details on the methods are presented in chapters 2 and 5.

1.3.6 Sm–Nd isotopic geochemistry

This technique was used in order to better determine the sources (juvenile versus reworked material) involved during the genesis of volcanic and plutonic rocks. Sm–Nd isotopic analyses were performed on rocks from the Tadoussac Intrusive Suite, Moulin-à-Baude Formation and on crosscutting Grenvillian plutons. The analyses were done at the Department of Earth Sciences of Memorial University of Newfoundland using the same powders that were used for whole-rock geochemistry. Further details on the method are presented in chapters 2 and 5.

1.4 Structure of the thesis

The thesis is in manuscript format and is divided into six chapters. Four chapters (Chapters 2 to 5) are written as manuscripts for publication in peer-reviewed scientific journals and two are already published. The first chapter provides a short introduction on the geological background of the study area and outlines the main questions that have to be solved together with the methods used in order to answer them. The connection between the different chapters of the thesis is explained in the following paragraphs. Chapters 2, 3 and 4 discuss pre-Grenvillian aspects of the study area, and some overlap between them is unavoidable. However, efforts have been made to provide a unique version of some of the repetitive aspects presented, such as the geological context.

The second chapter, titled "Peri-Laurentian, Pinwarian-age oceanic arc crust preserved in the Grenville Province: Insights from the Escoumins supracrustal belt" by authors Pierre-Arthur Groulier, Aphrodite Indares, Gregory Dunning, Abdelali Moukhsil and Markus Wälle is published in *Precambrian Research*, vol. 311, p. 37-64, 2018. This paper documents the geology, geochemistry and the stratigraphy of the supracrustal rocks and of their basement. It also provides for the first-time precise ages for volcanic rocks of the Saint-Siméon Group and for plutonic rocks of the Tadoussac Intrusive Suite. Detrital zircon ages from a Saint-Siméon Group quartzite show a clear genetic link between the supracrustal rocks and their basement, and also provides some critical information on the connection between this sequence and Laurentia. This chapter sets the geological foundation for the study.

Chapter 3 is titled "Arc dynamics in the Mesoproterozoic Laurentian margin, Quebec", by authors Pierre-Arthur Groulier, Aphrodite Indares, Greg Dunning and Abdelali Moukhsil. This manuscript will be submitted to *Terra Nova*. It integrates the results of the first chapter with other data from Geon 15 to 13 supracrustal and plutonic rocks of the central Grenville Province, to provide a model for the evolution of the southeastern Laurentian margin linked to arc dynamics.

Chapter 4, titled "Recognition and documentation of a Mesoproterozoic subseafloor hydrothermal system within an oceanic arc, arc rift and back-arc sequence preserved through Grenvillian metamorphism" will be submitted to *Ore Geology Review* with Aphrodite Indares, Steve Piercey, Greg Dunning and Abdelali Moukhsil as co-authors. This manuscript provides an extensive description of a volcanic sequence (Moulin-à-Baude Formation from the Saint-Siméon Group) located within the Grenville

Province. It documents the stratigraphy, physical volcanology and primary volcanic textures together with new maps, stratigraphic log and a more in-depth lithogeochemistry review of the mafic and felsic volcanic rocks. It also documents thoroughly the metamorphosed hydrothermal alteration assemblages associated with the volcanic rocks. The results provide evidence of syn-volcanic sub-seafloor hydrothermal alteration typical of VMS deposits. This paper also compares the type of hydrothermal alteration observed in the Escoumins supracrustal belt with other metamorphosed VMS deposits from the Grenville Province, Flin-Flon Belt and Fennoscandian Shield.

Chapter 5, titled "Syn-orogenic magmatism over 100 m.y. in high crustal levels of the central Grenville Province: characteristics, age and tectonic significance" by authors Pierre-Arthur Groulier, Aphrodite Indares, Greg Dunning, Abdelali Moukhsil and George Jenner is published in *Lithos*, vol. 312, p. 128-152, 2018. This paper focuses on the Grenvillian-age events reported in this thesis. It discusses the effect of deformation and metamorphism on the rock units of the ESB and concentrates on an in-depth study of Grenvillian-age intrusions. It provides new U–Pb dating of zircon, titanite and monazite from supracrustal and intrusive rocks together with field description, petrography, geochemistry and Nd geochemistry. This information offers a new timeline for the deformation and metamorphism in a portion of the low-*P* belt of the Grenville Province, and also highlights the importance of mantle-crust interaction in a major continental collision.

Chapter 6 summarizes the findings of this thesis and suggests directions that can be taken for future research in order to solve the problems and questions that remain.

1.5 References

Beaumont, C., Nguyen, M.H., Jamieson, R.A., and Ellis, S., 2006. Crustal flow modes in large hot orogens. In Channel Flow, Ductile Extrusion and Exhumation in Continental Collision Zones. Edited by R.D. Law, M.P. Searle, and L. Godin. Geological Society, London, Special Publication 268, 91–145.

Benahmed, S., Intissar, R., 2015. Levé magnétique aéroporté dans le secteur des Escoumins, Côte-Nord, Province de Grenville. Ministère de l'Énergie et des Ressources naturelles, Québec, DP 2015-04.

Bernier, L.R., Pouliot, G., MacLean, W.H., 1987. Geology and metamorphism of the Montauban north gold zone: a metamorphosed polymetallic exhalative deposit, Grenville Province, Quebec. Economic Geology, volume 82, 2076–2090.

Bernier, L.R., MacLean, W.H., 1993. Lithogeochemistry of a metamorphosed VMS alteration zone at Montauban Grenville Province, Quebec. Exploration and Mining Geology, volume 2(4), 367–386.

Bonnet, A.-L., Corriveau, L., La Flèche, M.R., 2005. Chemical inprit of highly metamorphosed volcanic-hosted hydrothermal alterations in the La Romaine Supracrustal Belt, easttern Grenville Province, Quebec. Canadian Journal of Earth Sciences, volume 42, 1783–1814.

Carr, S.D., Easton, R.M., Jamieson, R.A., Culshaw, N.G., 2000. Geologic transect across the Grenville Orogen of Ontario and New York. Canadian Journal of Earth Sciences, volume 37, 193–216.

Cawood, P.A., Strachan, R.A., Pisarevsky, S.A., Gladkochub, D.P., Murphy, J.B., 2016. Linking collisional and accretionary orogens during Rodinia assembly and

breakup: Implications for models of supercontinent cycles. Earth and Planetary Science Letters, volume 449, 118–126. doi:10.1016/j.epsl.2016.05.049

Corrigan, D., 1995. Mesoproterozoic evolution of the south-central Grenville orogen: structural, metamorphic, and geochronologic constraints from the Mauricie transect. PhD thesis, Carleton University, 282 p.

Corriveau, L., Bonnet, A.-L., 2005. Pinwarian (1.50 Ga) volcanism and hydrothermal activity at the eastern margin of the Wakeham Group, Grenville Province, Quebec. Canadian Journal of Earth Sciences, volume 42, 1749–1782.

Dickin, A.P., McNutt, R.H., Martin, C., Guo, A., 2010. The extent of juvenile crust in the Grenville Province: Nd isotope evidence. Geological Society of America Bulletin, volume 122(5-6), 870–883.

Gauthier, M., Chartrand, F., 2005. Metallogeny of the Grenville Province revisited. Canadian Journal of Earth Sciences, volume 42, 1719–1734.

Gower, C.F., Heaman, L.M., Loveridge, W.D., Sch.rer, U., and Tucker, R.D., 1991. Grenvillian granitoid plutonism in the eastern Grenville Province. Precambrian Research, 51: 315–336.

Gower, C.F., Krogh, T.E., 2002. A U-Pb geochronological review of the Proterozoic history of the eastern Grenville Province. Canadian Journal of Earth Sciences, volume 39, 795–829.

Gower, C.F., Kamo, S.L., Kwok, K., Krogh, T.E., 2008. Proterozoic southward accretion and Grenvillian orogenesis in the interior Grenville Province in eastern Labrador: Evidence from U-Pb geochronological investigations. Precambrian Research, volume 165, 61–95.

Hibbard, J., Karabinos, P., 2013. Disparate paths in the geologic evolution of the Northern and Southern Appalachians: a case for inherited contrasting crustal/lithospheric substrates. Geoscience Canada, volume 40, 303–317.

Hynes, A., Rivers, T., 2010. Protracted continental collision – evidence from the Grenville Orogen. Canadian Journal of Earth Sciences, volume 47, 591–620.

Jamieson, R.A., Beaumont, C., Nguyen, M.H., Culshaw, N.G., 2007. Synconvergent ductile flow in variable strength continental crust: numerical models with application to the western Grenville Province. Tectonics, volume 26, TC5005. https://doi.org/10.1029/2006TC002036.

Jamieson, R.A., Beaumont, C., Warren, C.J., Nguyen, M.H., 2010. The Grenville Orogen explained? Applications and limitations of integrating numerical models with geological and geophysical data. Canadian Journal of Earth Sciences, volume 47, 517–539.

Karlstrom, K.E., Ahall, K.-I., Harlan, S.S.,Williams, M.L., McLelland, J., Geissman, J.W., 2001. Long-lived (1.8-1.0 Ga) convergent orogen in southern Laurentia, its extensions to Australia and Baltica, and implications for refining Rodinia. Precambrian Research, volume 111, 5–30.

Li, Z.X., Bogdanova, S. V, Collins, A.S., Davidson, A., De Waele, B., Ernst, R.E., Fitzsimons, I.C.W., Fuck, R.A., Gladkochub, D.P., Jacobs, J., Karlstrom, K.E., Lu, S., Natapov, L.M., Pease, V., Pisarevsky, S.A., Thrane, K., Vernikovsky, V., 2008. Assembly, configuration, and break-up history of Rodinia: A synthesis. Precambrian Research, volume 160, 179–210. doi:10.1016/j.precamres.2007.04.021

Miller, M.L., 1973. Région de Saint-Siméon Tadoussac, Ministère de l'Énergie et des Ressources naturelles, Québec ; GM 159, 94 pages.

Morin, G., 1987a. Gîtologie de la région de Montauban. Ministère des ressources naturelles du Québec, MM 86-02, 59 p.

Owen, J.V., Erdmer, P., 1990. Middle Proterozoic geology of the Long Range inlier, Newfoundland: regional significance and tectonic implications. In: Gower, C.F., Rivers, T., Ryan, A.B. (Eds.), Mid-Proterozoic Laurentia-Baltica, Geological Association of Canada, Special Paper 38, 215–231.

Rivers, T., Corrigan, D., 2000. Convergent margin on southeastern Laurentia during the Mesoproterozoic: tectonic implications. Canadian Journal of Earth Sciences, volume 37, 359–383.

Rivers, T., Martignole, J., Gower, C.F., Davidson, A., 1989. New tectonic divisions of the Grenville Province, southeast Canadian shield. Tectonics, volume 8(1), 63–84. doi:10.1029/TC008i001p00063.

Rivers, T., 1997. Lithotectonic elements of the Grenville Province: a review and tectonic implications. Precambrian Research, volume 86, 117–154.

Rivers, T., 2008. Assembly and preservation of lower, mid and upper orogenic crust in the Grenville Province – Implications for the evolution of Large hot long-duration orogens. Precambrian Research, volume 167, 237–259.

Rivers, T., 2012. Upper-crustal orogenic lid and mid-crustal core complexes: signature of a collapsed orogenic plateau in the hinterland of the Grenville Province. Canadian Journal of Earth Sciences, volume 49, 1–42.

Rivers, T., Culshaw, N., Hynes, A., Indares, A., Jamieson, R., Martignole, J., 2012. The Grenville Orogen – A post-LITHOPROBE perspective, Chapter 3, in: Percival, J.A., Cook, F.A., and Clowes, R.M. (Eds.), Tectonic Styles in Canada: the LITHOPROBE Perspective. Geological Association of Canada, Special Paper 49, pp. 97–236.

Rivers, T., 2015. Tectonic setting and evolution of the Grenville Orogen: an assessment of progress over the last 40 years. Geoscience Canada, volume 42, 77–124. http://dx.doi.org/10.12789/geocanj.2014.41.057

Rondot, J., 1979. Reconnaissances Géologiques dans Charlevoix-Saguenay, Ministère de l'Énergie et des Ressources naturelles, Québec ; DPV-682, 44 pages.

Rondot, J., 1986. Géologie de la région de Forestville-Les Escoumins, Ministère de l'Énergie et des Ressources naturelles, Québec ; ET 85-05, 47 pages.

Rondot, J., 1989. Géologie de Charlevoix, Ministère de l'Énergie et des Ressources naturelles, Québec; MB 89-21, 606 pages.

Tomkins, A.G., 2007. Three mechanisms of ore re-mobilisation during amphibolite facies metamorphism at the Montauban Zn-Pb-Au-Ag deposit. Mineralium Deposita, volume 42, 627–637.

Tucker, R.D., Gower, C.F., 1990. Salient features of the Pinware terrane, Grenville Province, eastern Labrador. Geological Association of Canada, Mineralogical Association of Canada, Program with abstracts, volume 15, A133.

Whitmeyer, S.J., Karlstrom, K.E., 2007. Tectonic model for the Proterozoic growth of North America. Geosphere, volume 3(4), 220–259.

Chapter 2 Peri-Laurentian, Pinwarian-age oceanic arc crust preserved in the Grenville Province: Insights from the Escoumins supracrustal belt

2.1 Abstract

The remnants of an island arc system of Pinwarian age, the Escoumins supracrustal belt (ESB), are exposed for over 100 km in the Low-pressure belt of the Central Grenville Province (Canada), and are part of the Quebecia terrane. The ESB mainly consists of amphibolite-facies supracrustal rocks with well preserved primary textures (Saint-Siméon Group; SSG), and their plutonic counterpart (Tadoussac Intrusive Suite; TIS) that provide a record of the evolution of a Mesoproterozoic arc system. Granodiorite (1502 ±6 Ma) and tonalite of the TIS have calc-alkalic oceanic arc signatures, positive εNd (+2.66) with old model age (1672 Ma) consistent with remelting of previously formed juvenile mafic crust and interaction with an older crustal component, and are crosscut by younger within-plate granitoids. Tectonically above the TIS, the lowest formation of the SSG (Saint-Paul-du-Nord) consists of sedimentary rocks, and minor basalt, intruded by syn-volcanic juvenile (εNd = +5.21) tholeiitic gabbro and is interpreted to represent the remnants of an oceanic basin adjacent to an arc. The middle formation (Moulin-à-Baude) records an evolution from: (a) subalkaline tholeiitic to transitional arc basaltic andesite, basalt, and minor calc-alkalic volcanic arc 1492± 3 Ma dacite with crustal-derived signature (εNd = -0.77, model age of 1936 Ma), to (b) transitional to tholeiitic dacite–rhyodacite and 1464 +38/-32 Ma rhyolite, and (c) subalkaline juvenile (εNd = +3.91 – +4.92) tholeiitic basalts and FeTi basalts of arc rift and back-arc affinities. This formation is interpreted to represent an oceanic arc

undergoing rifting. Finally, the upper formation (Port-aux-Quilles) is composed of epiclastic sedimentary rocks with detrital zircon of Laurentian affinities, indicating proximity of the arc to Laurentia, but dominated by 1.5–1.47 Ga ages, showing a maximum age of deposition of 1476 ±10 Ma. The εNd and Nd-model ages indicate an association of mixed crustal and mantle-derived signatures typical of Quebecia crust combined with younger depleted mantle-derived basaltic magma. The data provide new insights on the organisation of Quebecia, and show that crust formed in an oceanic arc setting during late Geon 15 to Geon 14 constitutes a significant component of the central Grenville Province.

2.2 Introduction

The Grenville Province is a large hot orogen (Beaumont et al., 2010) built on the south-eastern margin of Laurentia at ~1.0 Ga (Fig. 2.1a). Much of the Grenville Province exposed in Canada has experienced granulite-facies metamorphism, which, together with deformation, has obscured to a large degree the characteristics of the original rock associations. Among the exceptions is the Low-pressure belt, which is discontinuously exposed in the southern part of the Province (Fig. 2.1b), is characterized by lower grade metamorphism, and is interpreted to represent shallow crustal levels of the orogenic infrastructure (Rivers, 2008).

At the scale of the continent, the southeastern Laurentian margin consists mainly of crust formed in arc systems over a period of several hundreds of million years, from the late Paleoproterozoic through most of the Mesoproterozoic (Whitmeyer and Karlstrom, 2007; Rivers et al., 2012). The long duration of this margin, as well as it

length (several thousands of km) led several authors (Rivers and Corrigan, 2000; Karlstrom et al., 2001) to compare it with the Andean margin. Growth of the southeastern Laurentian margin traditionally was attributed to distinct events (or orogenies) such as the Labradorian (1.71–1.60 Ga; Gower and Krogh, 2002; Gower et al., 2008), the Pinwarian (1.52–1.46 Ga; Tucker and Gower, 1990), the Elsonian (1.40–1.20 Ga) and the Elzevirian (1.25–1.18 Ga; Carr et al., 2000) events.

During Geon 14 there were major magmatic events in North America, which formed an important proportion of the crust in the Grenville Province. Largely overlapping with this time interval, the 1.52–1.46 Ga Pinwarian event was first defined in the eastern Grenville in Labrador (Pinware terrane; Gower et al. 1988), mainly overprinting older, labradorian crust. Subsequently, late Geon 15 to Geon 14 rocks inferred to have formed in continental arc to back-arc settings were identified in the western and central parts of the Grenville Province in Canada and in the Granite-Rhyolite Province in the USA (Fig. 2.1a; ex: Ketchum et al., 1998; McLelland et al., 2013; Slagstad et al., 2009; Augland et al., 2015), suggesting that this time period is marked by continental arc-related crustal growth along most of the southwestern margin of Laurentia.

In addition, Sm–Nd isotopic data led to the recognition in the Central Grenville Province of a distinct ~1.5 Ga terrane called “Quebecia” (Fig. 2.1b; Dickin and Higgins, 1992; Dickin 2000; Dickin et al., 2010), and inferred by these authors to represent juvenile crust. Most of this crust was metamorphosed into gneisses during the Grenvillian orogeny leading to a loss of primary texture, structure and information.

This contribution documents evidence for Pinwarian-age oceanic arc crust recently identified in the Low-pressure belt of the central Grenville Province in Quebec, near the town of Escoumins. This crust is exposed in the form of a volcano-sedimentary belt (Escoumins supracrustal belt; ESB; Groulier et al., 2015 and 2016) with well-preserved stratigraphic relationships, and offers a rare opportunity, in the context of the Grenville Province, to investigate the characteristics and evolution of a peri-Laurentian Mesoproterozoic island arc system. The ESB includes a supracrustal sequence, the Saint-Siméon Group (SSG, Rondot, 1986), with well-preserved volcanic and sedimentary features, and its potential igneous basement known as Tadoussac Complex (Rondot, 1977). Previous to this study, there was limited information about this belt and the ESB had not been considered in the development of recent models for the evolution of the Grenville Province (e.g., Rivers, 2008; Rivers and Hynes, 2010). A recent field campaign sponsored by the Geological Survey of Quebec (Groulier et al*.,* 2016) in conjunction with the acquisition of new aeromagnetic data (Benahmed and Intissar, 2015) provides a basis for a better understanding of the ESB. The objective of this paper is to present field relations, U–Pb zircon ages and the geochemical signature of the volcanic rocks and sub-volcanic intrusions of the ESB, and discuss the tectonic significance of this belt in the context of the evolution of the Laurentian margin.

2.3 Geology of the Escoumins supracrustal belt

The Escoumins supracrustal belt (ESB) is located in the southernmost part of the central Grenville Province, between Forestville and Saint-Siméon (Fig. 2.1b). It is composed of metasedimentary and metavolcanic rocks with their plutonic counterparts,

which together with younger plutonic suites, are arranged in an overall dome and basin map pattern (Fig. 2.2). The supracrustal rocks are exposed as coherent units in synforms in the Bergeronnes, Escoumins and Longuerive areas (Fig. 2.2) and in the Petit-Saguenay area in the SW, near Saint-Siméon (Fig. 2.1b). Moreover, in the north and west, they occur as rafts interleaved with orthogneisses. Based on accessibility and quality of outcrop, three synforms were investigated: Lac Raymond, Lac Saint-Onge and Baie-des-Bacon (Fig. 2.2). Throughout the area, the dominant metamorphic grade is lower to mid-amphibolite facies, as indicated by the presence of hornblende ± epidote in metamafic rocks and muscovite in aluminous metasedimentary rocks.

Miller (1973) was the first to describe the supracrustal rocks in the area, in the vicinity of Saint-Siméon, and he interpreted the sequence as sedimentary. Later, Rondot (1979, 1986 and 1989) and Morin (1987) documented the geological units more systematically and suggested the presence of metavolcanic rocks. In addition, an assemblage of "pink and grey" gneisses and migmatites (Tadoussac complex) was described by Rondot (1977) in a dome near Tadoussac and inferred to represent a basement (Rondot, 1989). In the north, a major lineament well defined in aeromagnetic data (Benahmed and Intissar, 2015) separates the ESB from granulite-facies gneissic complexes. Among these, best documented is the Cap-à-l'Est Complex, defined by Hébert and Lacoste (1998) and dated at 1391 +8/-7 Ma (Hébert and van Breemen 2004), north of the Tadoussac area. It consists of a calc-alkalic igneous suite with dioritic, granodioritic, monzonitic, granitic and syenitic components, enclosing rafts of supracrustal rocks, and amphibolites, and is inferred to have formed in a continental arc setting.

The following section documents the key field characteristics of the different lithologic associations of the ESB, based upon our observations, unless stated otherwise. Figure 2.3 represents a lithostratigraphic column of the ESB with a summary of the U–Pb ages, geochemical signatures and tectonic settings of the different igneous rocks, discussed in this contribution. Although all the rocks are metamorphosed, the prefix meta- is omitted from the rock names because we focus on primary features. As well, Groulier et al. (2016) identified diverse younger plutonic units associated with the ESB. These will be described in a separate contribution.

2.3.1 Tadoussac Intrusive Suite

The Tadoussac Complex is referred to here as Tadoussac Intrusive Suite (TIS) because the new field data collected in a dome between the towns of Tadoussac and Bergeronnes in the SW portion of the investigated area (Fig. 2.2) outlined a coherent polyphase batholith with rocks commonly preserving igneous textures. The inner and larger part of the TIS is composed of granodiorite, tonalite and gabbro, locally injected by granite, whereas the outer part consists of granite. The granodiorite varies in texture from fine-grained porphyry to a coarser-grained rock with K-feldspar megacrysts (Fig. 2.4a). The tonalite is coarse-grained with biotite phenocrysts. The granite in the outer part of the TIS is megacrystic, hornblende-bearing and foliated, whereas the granite sills emplaced within the granodiorite and gabbro are medium-grained and magnetite-rich. Both types of granite are pink and younger than the granodiorite and tonalite, which they crosscut. The contact between the TIS and the SSG is marked by a major lineament on aeromagnetic maps and is inferred to be tectonic. Tonalite, granodiorite and felsic orthogneisses were

also identified structurally below the SSG in the central and northern parts of the area (Fig. 2.2), however their linkage to the TIS remains unclear.

2.3.2 Saint-Siméon Group

The SSG represents the supracrustal sequence and has been divided into the Saint-Paul-du-Nord (lower), Moulin-à-Baude (middle) and Port-aux-Quilles (upper) formations, by Rondot (1977, 1979 and 1986) and Rondot and Lavergne (1984). This sequence is complex and displays at the scale of each synform a wide variety of rock types with interfingering relationships, lenticular units, and abrupt facies variations (Fig. 2.3).

2.3.2.1 Saint-Paul-du-Nord Formation

The Saint-Paul-du-Nord Formation, was defined as a clastic continental sequence by Rondot and Lavergne (1984). This formation is best exposed in locations A and B (Fig. 2.2) where, based on the new data, it is composed of thick layers of pelite, greywacke, and quartzite with a lesser amount of volcaniclastic rocks (tuffs; Fig. 2.4b). In addition, the lower part of the formation is locally injected by porphyritic and rapakivi high-K intermediate to felsic intrusions (syenite, monzogranite, granite and pegmatite) and by mafic-ultramafic sills and layered bodies. The pelitic rocks are muscovite±garnet-bearing schists, and the presence of sulfides and graphite (observed in location A) implies a reducing environment. The tuff horizons indicate volcanic activity coeval with sedimentation. The dominance of pelitic layers with no abrupt change in sedimentary

structures, the presence of tuffs and mafic intrusive rocks is suggestive of a marine basin adjacent to an arc, in contrast to the earlier interpretation of Rondot and Lavergne (1984).

2.3.2.2 Moulin-à-Baude Formation

The Moulin-à-Baude Formation was first defined by Rondot (1979) as an association of volcanic, volcaniclastic and volcanic-derived sedimentary rocks. New fieldwork revealed that these rocks contain primary volcanic textures, best preserved in the larger synforms (Lac Raymond, Lac Saint-Onge and Baie-des-Bacon, Fig. 2.2). The presence of felsic pumice in mafic tuffs and mafic fiamme in felsic tuffs implies that these are the products of bimodal volcanism. In addition, mafic and felsic dykes and sills occur in contact with volcanic rocks in every synform and may be feeder conduits. The same may hold for the mafic and ultramafic rocks intruding the lower formation, described earlier.

The most complex rock associations were observed in the Lac Raymond and Lac Saint-Onge synforms, and to facilitate the description we divided the Moulin-à-Baude Formation in three parts. The lower part (MAB1) is best exposed in location C (Fig. 2.2) and mainly consists of mafic rocks, capped by dacitic tuff. The mafic rocks are generally massive basalt and basaltic andesite, commonly vesicular, amygdaloidal, plagioclase- and/or hornblende-phyric, and locally pillowed (Fig. 2.4c and 2.4d). They are therefore interpreted to represent lava flows. In addition, mafic tuff with ash, crystal, lapilli and bombs, as well as volcanic breccia (Fig. 2.4e) and hyaloclastite are present, and some laminated mafic rocks may represent reworked tuff. This whole mafic sequence is crosscut by an extensive stockwork of quartz-epidote veins (Fig. 2.4f).

The dacitic tuff (locations C and D) has abundant fiamme with minor crystals and is characterized by more lithic fragments at the top of the deposit (ignimbrite?). Above this, a polymictic conglomerate with a pelitic and ash matrix marks a stratigraphic horizon (Fig. 2.4g). The cobbles and boulders have rounded shapes (now flattened) and are millimetric to almost metric in size. They consist of tonalite, granodiorite, granite, felsic porphyry, basalt, basaltic andesite, felsic volcanic and quartzite, which are typical lithologies of the Tadoussac Intrusive Suite, the Saint-Paul-du-Nord formation, and MAB1. We interpret this rock to have formed in a tectonically active volcanic basin, with the reworked rock fragments having a proximal source. Similar rocks were described in the Canadian Cordillera as marine-reworked lahar (Gunning et al., 2006).

The middle part of the Moulin-à-Baude Formation (MAB2) is best exposed in locations D and E (Fig. 2.2), and mainly consists of mafic rocks overlain by a composite felsic unit, with a complex rock association including sedimentary units on top. The mafic rocks are represented by hornblende-phyric basaltic flows with minor vesicules and amygdules, and tuff. The felsic unit consists of massive dacite to rhyodacite that grades locally into a crystal and lapilli-tuff (Fig. 2.4h), and rhyolite with clusters of biotite-muscovite, inferred to represent relics of fiamme (Fig. 2.4i). In addition, a porphyritic rhyolite was observed in location B, at the base of the middle part, right above the conglomerate.

Above the felsic unit, an assemblage of altered vesicular, amygdaloidal, porphyric (plagioclase and/or hornblende) basalt, biotite-phyric dacite (present in location D) and finely laminated felsic rocks (reworked tuffs) is present. The top of MAB2 in location D (Fig. 2.2) is marked by a composite exhalative unit (iron formation, exhalite and chert)

interlayered with basalt, calc-silicate rocks, pelite, greywacke and quartzite. The iron formation occurs as magnetitite beds in quartzite (Fig. 2.4j), and the exhalite consists of ortho-amphibole, epidote, clinopyroxene, scapolite, carbonate, quartz, tourmaline and garnet with varying amounts of sulfides (pyrrhotite, chalcopyrite, sphalerite and galena). The association of exhalative, sedimentary and reworked volcanogenic rocks indicates a break in the volcanic activity.

Finally, the upper part of the Moulin-à-Baude Formation (MAB3) is best exposed in location E (Fig. 2.2) and it consists of massive vesicular to amygdaloidal, locally porphyritic, basalt. As in the lower part, basaltic rocks in MAB2 and MAB3 show extensive quartz-epidote alteration.

The presence of pillowed basalt in MAB1 provides evidence of marine deposition and the widespread regional scale quartz-epidote alteration is typical of a sub-seafloor alteration system. In addition, the presence of vesicles in the basaltic rocks is suggestive of a shallow water-depth emplacement of the lava (< 500 m).

MAB2 also exhibits localized evidence of hydrothermal alteration. This is manifested by the presence of white micas–biotite–K-feldspar–quartz–magnetite and locally sillimanite (pseudomorph after andalusite)–tourmaline–sulfides in the felsic volcanic and sedimentary rocks, and by the presence of anthophyllite, gedrite, tremolite, diopside, Ca–Mn garnet, biotite, white mica, chlorite, epidote, quartz, K-feldspar, magnetite, sulfide, titanite and carbonate in the mafic volcanic rocks. The assemblage white mica and aluminosilicates represents a marker of argillic alteration close to some felsic volcanic centers. We interpret these alteration assemblages as a metamorphic equivalent of a hybrid epithermal-VMS system (Caté et al., 2015; Bailes et al., 2016;

Dubé et al., 2007; Galley et al., 2007). Finally, boudinaged quartz-carbonate-silicate veins enriched in Cu–Au (metamorphosed lode-gold veins? Eilu et al., 1999) locally occur in the basalt and the conglomerate. The alteration and the mineral potential of the Moulin-à-Baude Formation will be discussed in another paper.

2.3.2.3 The Port-aux-Quilles Formation

The Port-aux-Quilles Formation is best exposed in the location F (Fig. 2.2). This formation is dominated by thick deposits of quartzite, subarkose and greywacke with pelitic layers, and also contains minor basalt. Its base and lower part are characterized by impure quartzite with cross-bedding stratification (Fig. 2.4k), suggestive of deposition in shallow water, but above the cross-bedded quartzite, the arrangement of these rock units in alternating layers is consistent with deposition distal from the source (possibly turbidite, Fig. 2.4l) in a deeper-water environment. The lower part of the formation is crosscut by a mafic dyke swarm.

Finally, the core of the Baie-des-Bacon synform, on top of the Port-aux-Quilles Formation, hosts a different sequence of polymictic conglomerate, quartzite, arkose and marls with possible volcanic rocks, all of which are strongly hydrothermally altered. The conglomerate contains fragments of volcanic and sedimentary rocks (altered and non-altered), and fragments of quartz veins. This continental sequence appears to be younger that the SSG and will not be considered here.

2.4 Geochemistry

A subset of the least altered rocks was analyzed at Activation Laboratories (Ancaster, Ontario) for major elements and a suite of 54 trace elements. The major elements were analyzed by inductively coupled plasma mass spectrometry (ICP-MS) or atomic emission spectroscopy (AES) with metaborate/lithium tetraborate digestion and trace elements by ICP-MS, ICP-AES and instrumental neutron activation analysis (INAA) methods. Sample locations are reported in Table A2.1.

2.4.1 Tadoussac Intrusive Suite

The main rock types of the TIS, granodiorite, tonalite and granite, define two distinctive geochemical groups (Table 2.1). Both groups fall dominantly in the volcanic arc field in the ternary diagram Rb/30 vs Ta vs Hf (Fig. 2.5a), with two samples at the boundary with the within-plate field. However, analysed samples of the granodiorite and tonalite from the core of the TIS (Group 1) have a calc-alkaline signature whereas samples of the younger granite from the margin of TIS (Group 2) have a high-K to shoshonitic signature (Fig. 2.5b). In addition, Group 1 rocks are classified as volcanic arc granite (VAG) of I-type on the diagrams of Whalen et al. (1987, Fig. 2.5c) and Pearce et al. (1984, Fig. 2.5d), whereas Group 2 rocks mostly fall in the fields of the ocean ridge (OR) and within-plate granitoid (WPG) and are of A-type (Fig. 2.5c and d). On a primitive mantle-normalized extended trace elements diagram (Sun and McDonough, 1989; Fig 2.5e), the Group 1 samples show fractionation between LREE (light rare earth element) and HREE (heavy rare earth element), negative HFSE (high field strength element) and positive Sr anomalies. In comparison, the Group 2 samples are more

enriched in REEs and other trace elements and they still display negative HFSE anomalies. In chondrite normalized REE plots (Fig. 2.5f) the two groups have patterns with a strong negative slope implying fractionation between LREEs and HREEs. The Group 2 rocks are more enriched relative to chondrite and most of them have strong negative Eu anomalies implying fractionation of feldspar. The Group 1 rocks are less enriched and do not exhibit significant Eu anomalies.

2.4.2 Volcanic rocks from the Saint-Siméon Group

The chemical composition of the volcanic rocks is dependent not only on magmatic processes, but also on possible interactions with crustal material. Major elements (for fresh rocks) and trace elements (for both fresh and metamorphosed rocks) (Table 2.2) are used to characterize the evolutionary trend(s) of the representative samples from primitive to evolved magma (e.g., crystal fractionation processes), elemental mobility due to synvolcanic alteration and/or regional metamorphism, their chemical affinities, and their possible tectonic setting. The ESB is affected by amphibolite-facies metamorphism and the volcanic rocks locally display signs of hydrothermal alteration in a syn-volcanic environment (Groulier et al., 2015). Most of the major elements are mobile under such conditions, hence are not appropriate for geochemical interpretations using discrimination diagrams commonly used for fresh rocks. However, elements such as Ti, Al, P, Ta, Nb, Hf, Zr, Y, Th and REEs are interpreted to be immobile under low water-to-rock ratios during hydrothermal alteration and metamorphism (Winchester and Floyd, 1977; Barret and MacLean, 1994, 1999; Jenner 1996; Gifkins et al., 2005).

The bimodal, mafic-dominant character of the volcanism in the Saint-Siméon Group is demonstrated in Figure 2.6a (Pearce et al., 1982 after Winchester and Floyd, 1977). In this diagram, the mafic volcanic rocks fall in the fields of basalt and basaltic andesite, and the felsic rocks fall in the field of rhyolite-dacite with some straddling to the field of andesite. The whole sequence has a sub-alkaline signature. The basalts are present in both the Moulin-à-Baude and Port-aux-Quilles formations in every synform, whereas the felsic volcanic rocks were only observed in MAB1 and MAB2, in the Lac Raymond and Lac-Saint-Onge synforms (Fig. 2.2).

2.4.2.1 Major element geochemistry

The basaltic rocks of the SSG fall in 3 types: (a) basalt with low Fe and Ti content (TiO_2: 0.76–1.89 wt%; $Fe_2O_{3(t)}$: 9.44–14.55 wt%; Table 2.2 and Fig. 2.6b) and high Mg# (42–66); (b) FeTi basalt with high Fe and Ti (TiO_2: 2.22–3.52 wt%; $Fe_2O_{3(t)}$: 14.78–17.89 wt%; Table 2.2 and Fig. 2.6b) and lower Mg# (36–49); and (c) basaltic andesite, with lower Mg# (26–56) and higher SiO_2 (49.53–59.62 wt.%) and K_2O (0.41–3.9 wt.%; Table 2.2). In comparison, the basaltic rocks with low-Fe–Ti are more primitive with higher Mg# and lower SiO_2 (46.31–53.58) wt.% and K_2O (0.14 – 1.8 wt.%; Table 2.2). As recognized in the field, basaltic andesite is predominant in the MAB1. The basalt and FeTi basalt are distinguished by their geochemistry only and are predominant in MAB2 and MAB3. The FeTi basalt first appears as sills and dykes in MAB2 crosscutting basaltic andesite and sedimentary rocks. In MAB3 evolved FeTi basalt flows, sills and dykes are commonly associated with more primitive, low Fe and Ti basaltic flows, sills and tuffs.

Felsic volcanic rocks from the SSG (dacite to rhyolite) are characterized by SiO_2 in the range of 59.6 – 76.28 wt.%, Al_2O_3 11.05 – 16.66 wt.%, $Fe_2O_{3(t)}$ 2.25–10.88 wt% and TiO_2 0.09–0.99 wt.% (Table 2.2). Some silica and K_2O values have been modified during syn-volcanic hydrothermal alteration explaining why the values might be out of the normal range for the different rock types.

2.4.2.2 Trace element geochemistry

On a Zr vs Y diagram (Fig. 2.6c; Barret and MacLean 1999) most mafic rocks display a tholeiitic signature, with the basaltic andesite straddling into the transitional field. The felsic volcanic rocks were classified based on their stratigraphic location (Fig. 2.3). Dacitic rocks from MAB1 fall on the boundary between the calc-alkaline and the transitional fields (Fig. 2.6c), and dacite to rhyolite from MAB2 (Fig. 2.3) show an evolution from calc-alkaline to tholeiitic signatures, with most data falling on the transitional field. This evolution does not follow the stratigraphy. Felsic rocks with different signatures are found in the same stratigraphic horizons of the MAB2 and cannot be distinguished in the field.

All the basaltic rocks are variably enriched in REE relative to chondrite with a slightly HREE-depleted chondrite-normalized pattern (Fig. 2.7a; $[La/Sm]_N$: 0.89–1.75; $[La/Yb]_N$: 0.89–3.55, Table 2.2). In the Primitive Mantle-normalized extended trace elements diagram (Sun and McDonough, 1989; Fig. 2.7b) they display negative Nb, Ti, Al, V and Sc anomalies with no apparent to slightly positive Th anomalies and flat REE patterns.

The basaltic andesite is variably enriched in LREE ($[La/Yb]_N$: 1.47–9.57, Table 2.2) with weak Eu anomalies, and flat HREE patterns (Fig. 2.7c) and negative Nb, Ti, Al, V and Sc anomalies (Fig. 2.7d). The FeTi basalt is moderately enriched in LREE and HREE ($[La/Yb]_N$: 1.44–2.8, Table 2.2), has slightly negative Eu anomalies (Fig. 2.7e), and negative Nb, Al, V and Sc anomalies (Fig. 2.7f).

The analysed felsic volcanic rocks of the Moulin-à-Baude Formation have a range of REE patterns (Fig. 2.7g). The dacite from MAB1 (Table 2.2 and Fig. 2.3) exhibits strong fractionation between REE ($[La/Yb]_N$ of 7.75–9.08) typical of calc-alkaline magma with negative Eu anomalies (Fig. 2.7g), a strong positive Th anomaly and negative Nb, Ti, Al, V and Sc anomalies (Fig. 2.7h). The MAB2 felsic volcanic rocks (Table 2.2 and Fig. 2.3) show moderate fractionation between REE ($[La/Yb]_N$ of 0.97–4.71), with some having a negative Eu anomaly and one with a positive Eu anomaly, indicative of plagioclase accumulation. These rocks also show no apparent to positive Th, Zr, Hf anomalies and negative Nb, Ti, Al, V and Sc anomalies (Fig. 2.7h). The positive Zr anomaly might explain why some analyses of the MAB2 felsic rocks fall in the calc-alkaline field in Figure 2.6c.

2.4.3 Tectonic environment

In order to better constrain the environment of formation for the volcanic rocks of the SSG, selected tectonic discrimination diagrams were used. On the ternary diagram Nb*2 vs Zr/4 vs Y (Meschede, 1986; Fig. 2.8a), the basaltic andesite falls in the volcanic arc field and the basalt and FeTi basalt in the N-MORB field. In addition, a trend from the calc-alkaline and transitional fields toward the primitive volcanic arc tholeiites and back-

arc basin basalts (BABB) is defined on the ternary diagram La/10 vs Y/15 vs Nb/8 (Cabanis and Lecolle, 1989; Fig. 2.8b) by the basaltic rocks. On the Y vs Nb diagram (Pearce et al., 1984; Fig. 2.8c), felsic volcanic rocks of the SSG cluster around the boundary between the fields of volcanic arc (VAG) and ocean-ridge (ORG) to within-plate (WPG) granite. The MAB 1 dacite is I-type and VAG whereas MAB 2 felsic volcanic rocks are I-type to A-type and mostly ORG to WPG (Fig. 2.8c and 2.8d).

On the Nb/Yb vs Th/Yb diagram (Pearce 2014; Fig. 2.8e), the sources of the basaltic rocks of the ESB vary from N-MORB to E-MORB type. The mafic volcanic rocks plot above the mantle array due to relative high Th contents, and this is interpreted to reflect either subduction input with fluids ejected from the slab or interaction with a thicker crust (Pearce 2008). The oblique trend resulting from decreasing values in both ratios is consistent with a change in source from a more evolved arc-type to a more primitive MORB-like, or a change in proportions of the contribution from each source. Basaltic andesite from MAB1 have clear evidence of subduction input and interaction with a more evolved crust marked by the enrichment in Th. Basaltic rocks from MAB2 and MAB3 have lower Th/Yb and Nb/Yb ratios indicating a lower proportion of subduction component and less crustal interaction. The trend may indicate a change in tectonic settings from a more mature oceanic arc toward a more primitive oceanic arc.

2.5 Geochronology

Three samples were selected for CA-TIMS U–Pb dating of zircon in order to constrain the age range of the ESB and their locations are shown in Figure 2.2. A dacitic tuff (13-PA-32-A) from MAB1 and a rhyolitic tuff (14-PA-95-A) from MAB2 in the

Saint-Onge and the Lac Raymond synforms, respectively, were chosen for the purpose of determining the age of the volcanic sequence. In addition, a granodiorite (15-PA-125-A) from the core of the TIS was selected to test the hypothesis that it represents the base of the arc. Titanite was also analysed from the dacitic tuff.

A quartzite from the Port-aux-Quilles Formation was also collected for CA-LA-ICP-MS (Chemical Abrasion Laser Ablation) U–Pb dating of detrital zircon in order to constrain the maximum age of deposition and the source(s) of sediments.

2.5.1 Analytical techniques

Zircon analysed in this study was chemically abraded (cf. Mattinson 2005), whether analysed by laser ICP-MS or by ID-TIMS. The zircon grains were annealed for 36 hours at 1000°C. This was followed by etching in concentrated HF in a TEFLON pressure-dissolution bomb in an oven at 200°C for 5 hours. This procedure eliminates radiation-damaged, altered or metamict zones in zircon that cannot be restored with annealing thus virtually eliminating secondary lead loss. This results, for simple grains of one age, in concordant or near-concordant analyses by either instrument technique. For zircon grains with cores and overgrowths of different ages, this technique will eliminate secondary lead loss that would cause data points to fall below the correct mixing line. Typical zircon grains for each sample were also mounted in epoxy and imaged by CL (Deben cathodoluminescence detector) using the JSM-7100F field emission SEM from the TERRA Facility – CREAIT (Memorial University Earth Sciences Department) in order to describe their internal morphologies and to interpret their growth history. The current used varied from 10 to 15 kV.

The protocol used for CA-TIMS dating is detailed by Sparkes and Dunning (2014). The isotopic ratios were measured by either simultaneous measurement on multiple Faraday cups or, for small samples, by peak-jumping on one secondary electron multiplier using a Finnigan multicollector MAT 262 V TI mass spectrometer at the Earth Sciences Department of Memorial University. Several fractions, generally composed of a single grain, were analysed for each sample. The data are listed in Table 2.3. Titanite was physically abraded, and then fractions of one or two grains were analysed by TIMS using the same protocols for chemical separation and measurement as for zircon.

In the case of the quartzite, 170 zircon grains representative of the different populations observed were selected under the microscope and were prepared following the same annealing and etching protocols as for the CA-TIMS analyses. The prepared grains were then mounted in epoxy in grain mounts and polished followed by imaging, then analysis by LA-ICP-MS. The U-Pb age measurement with LA-ICP-MS was done on a GeoLas ArF 193nm excimer laser ablation system (Coherent, Göttingen, Germany) coupled to an Element XR (Thermo Fisher Scientific, Bremen, Germany). An in-house made teardrop-shaped ablation chamber was used. The chamber had space for a 1-inch mount containing the samples and a 10 mm mount containing the standards. Zircon 91500 (Wiedenbeck et al., 1995) was used as primary standard and the zircons Plešovice (Slama et al., 2008) and 02123 (Ketchum et al., 2001) were used as secondary standards. The ICP-MS was tuned to high sensitivity and a low oxide ratio (ThO^+/Th^+<0.3%). Data evaluation was done with iolite applying an exponential-linear downhole U/Pb fractionation correction model. Although ^{235}U was measured it was recalculated from the ^{238}U signal during data evaluation using a $^{238}U/^{235}U$ ratio of 138.818. The laser ablation

settings were: crater size of 30 μm, repetition rate of 5 Hz, fluence of 4 J/cm^2, 200 pulses and 1L/min He for the carrier gas flow. The ICP-MS settings were: 0.93 L/min for the sample gas flow, 0.9 L/min for the auxiliary gas flow, 16 L/min for the plasma gas flow, the plasma power was 1550 W. The measured isotopes and dwell times were ^{202}Hg (10 ms), ^{204,206,207,208}Pb (10, 50, 50, 10 ms), ^{232}Th (10 ms) and ^{235,238}U (50, 10 ms). The determined weighted average ^{206}Pb/^{238}U ages for the secondary standards were 340.5 ± 1.7 Ma (MSWD=2.8, n=55) and 299.2 ± 2.0 Ma (MSWD=2.0, n=25) for Plešovice and 02123, respectively.

All U-Pb zircon data is reported with 2σ uncertainties and all calculated ages using ISOPLOT are reported at the 95% confidence interval.

2.5.2 Samples and results

2.5.2.1 Dacitic tuff from the Saint-Onge synform (13-PA-32; 468768, 5363165)

This unit lies on the top of MAB1 in the Lac Saint-Onge synform (location C, Fig. 2.2 and Fig. 2.3). It is characterized by the presence of fiamme (assemblage of amphibole–biotite–titanite), few phenocrysts of plagioclase, amphibole and biotite and minor lithic fragments. The sample chosen for geochronology was homogeneous, without lithic fragments.

The zircon grains are subhedral (Fig. 2.9a) and some of them have inclusions and a turbid aspect probably due to radiation damage or alteration. They are 100 to 200 μm long and CL images display magmatic oscillatory zonation, with some grains having a homogeneous overgrowth whereas some have a distinct core (Fig. 2.10a).

Of the three fractions analyzed (Table 2.3), Z1 is concordant with a $^{207}Pb/^{206}Pb$ age of 1493 Ma and Z2 is 0.13% discordant with a $^{207}Pb/^{206}Pb$ age of 1491 Ma. A weighted average of these data (MSWD=0.54) is 1492 ± 3 Ma (Fig. 2.11a), which is interpreted as the crystallization age. Fraction Z3 occurs on a shallower discordia line that intersects the Concordia curve at ca. 1 Ga, inferred to represent the metamorphic age. Large, clear medium to dark brown titanite grains were also selected under the microscope. All four fractions analyzed are concordant (Table 2.3). T1 has a $^{206}Pb/^{238}U$ age of 982 Ma and T4 has a $^{206}Pb/^{238}U$ age of 984 Ma and together these give a weighted average 983 ± 3 Ma (MSWD=0.61; Fig. 2.11b). T2 has a $^{206}Pb/^{238}U$ age of 1001 Ma and T3 has a $^{206}Pb/^{238}U$ age of 1001 Ma. These data taken together give an age of 1001 ± 3 Ma (MSWD=0.002; Fig. 2.11b). Both ages are inferred to be metamorphic ages and are late Grenvillian.

2.5.2.2 Rhyolitic tuff from the Raymond synform (14-PA-95-A; 459148, 5348547)

This unit belongs to MAB2 (location D on Fig. 2.2, Fig. 2.3). The sample comes from a 2 to 4 meters thick layer of tuff with pumice. The zircon grains are prismatic and elongate (between 100 and 150 μm long) and many of the grains are turbid in plane light but some of them appear clear (Fig. 2.9b). In CL the zircon grains are complex with resorbed igneous cores (Fig. 2.10b). A second generation of zircon around the core appears dark and has only irregular zonation.

A calculated line fixed through the 1037 ± 10 Ma age from metamorphic overgrowths measured by laser ICP-MS (see below) and the 8 TIMS analyses yields an

upper intercept age of 1464 +38/-32 Ma (probability of fit 69%; Fig. 2.11c). We interpret the upper intercept as the igneous crystallization age and the lower intercept as the age of the metamorphic rims. The uncertainty on the upper intercept age can be explained by the fact that the data points are distant from the upper intercept due to the complexity of the grains with both igneous cores and relatively thick metamorphic overgrowths.

2.5.2.3 Granodiorite, Tadoussac intrusive Suite (15-PA-125-A; 449918, 5340601)

The granodiorite was collected at the core of the TIS. It is medium-grained, biotite-bearing and is cross-cut by mafic dykes. The zircon grains are fairly euhedral, large (some are up to 200 μm long and 50 to 100 μm wide), clear, but some are fractured (Fig. 2.9c). In CL, the grains show magmatic zonation and some show distinct cores (Fig. 2.10c). Six fractions were analyzed (Table 2.3), and four of these are co-linear (probability of fit= 85%) and yield an upper intercept age of igneous crystallization of 1502 ± 6 Ma (Fig. 2.11d). The lower intercept age tends toward 1000 Ma, indicating either the presence of Grenvillian metamorphic overgrowth, or Pb-loss. Fraction Z6 must contain inherited older zircon, likely as a core.

2.5.2.4 Quartzite, lower part of the Port-aux-Quilles Formation (13-PA-2; 467066, 5356031)

This impure quartzite was sampled in the western limb of the Saint-Onge synform, stratigraphically below a sequence of turbidite and above FeTi basalt. It is characterized by cross-bedding stratification highlighted by heavy mineral laminations. Several

populations of zircon were observed using a binocular microscope (euhedral prismatic, sub-euhedral, sub-rounded, rounded and of different size and colour, Fig. 2.9d). CL images of the zircon grains are consistent with the observations made using the binocular microscope: some zircon crystals display a complex history with inherited cores and different phases of igneous and metamorphic growth while others are simple and probably crystallized during a single event (Fig. 2.12). Only the concordant points (n=110) were kept for Figure 2.13 in order to avoid any bias and misinterpretation of the data. The measured isotopic ratios and ages are listed in Table 2.4. Concordia diagrams and histograms of age distribution are shown in Figure 2.13. $^{207}Pb/^{206}Pb$ ages were used for analyses older than 1.2 Ga and $^{206}Pb/^{238}U$ ages were used for the younger ones.

In Figure 2.13a, the histogram of age distribution shows a wide range of ages with different clusters in the Archean, Paleoproterozoic and Mesoproterozoic with increasingly high peaks toward younger ages. The oldest population corresponds to distinct cores of rounded and sub-rounded grains. These cores display magmatic oscillatory zoning and complex resorption textures with at least two generations of overgrowth (Fig. 2.12a). For example, a core with magmatic oscillatory zoning surrounded by thick bright metamorphic overgrowth gave an age of 2722 ± 18 Ma (Fig. 2.12a) whereas the metamorphic overgrowth gave a discordant Grenvillian age (1063 ± 22 Ma). Another core dated at 2754 ± 21 Ma is surrounded by a thick bright metamorphic overgrowth, which gave a discordant age of 1195 ± 26 Ma (Fig. 2.12a). The age obtained from the zircon cores of this Archean group cluster at 2800 – 2700 Ma (Fig. 2.13b), similar to the age range of igneous rocks from the Superior Province (Fig. 2.1a).

A gap in ages from ca. 2700 to 2530 Ma is observed in Figure 2.13b and the next age cluster is between 2530 and 2479 Ma. Among these, two zircon grains with sub-rounded to sub-euhedral shapes and magmatic zoning were dated respectively at 2531 ± 19 Ma, 2533 ± 23 Ma and 2531 ± 22 Ma (Fig. 2.12b) and are late Archean. One sub-rounded grain with simple magmatic zoning gave an early Paleoproterozoic age of 2479 ± 24 Ma (Fig. 2.12b). Igneous rocks with similar ages (late Archean to early Paleoproterozoic) occur in the Meta-Incognita and in the Core Zone domains of the Canadian shield (Fig. 2.1a).

The next set of concordant ages was obtained from sub-euhedral to rounded grains with magmatic zoning such as oscillatory and sector with thin metamorphic overgrowths (Fig.12c). They form two clusters, one at 2000 – 1970 Ma and another one at 1950 – 1900 Ma (Fig. 2.13c). These ages are Paleoproterozoic, and correlative with igneous units from the Torngat Orogen (Fig. 2.1a).

An important population of zircon has ages from 1900 to 1780 Ma (Fig. 2.13d). The grains are euhedral to subhedral, prismatic to sub-rounded, they all have the characteristics of magmatic zircon (e.g. oscillatory zoning) and some of them have metamorphic overgrowths with discordant ages (ex: 1177 ± 26 Ma; Fig. 2.12c) and concordant Grenvillian ages (ex:1066 ± 35 Ma; Fig. 2.12c). The older rim ages may result from the laser beam penetrating part of the older core in the interior of the grain. The age range of the magmatic zircon is similar to that of intrusive rocks in the Makkovik Province of southeastern Labrador (Fig. 2.1a).

A younger set of concordant ages comes from prismatic to sub-rounded grains with oscillatory zoning and thick bright magmatic overgrowths surrounding magmatic

cores while some grains have metamorphic overgrowths (Fig. 2.12d). The cores and the homogenous grains gave ages in the range of ca. 1.71 – 1.6 Ga (Fig. 2.13e), with the magmatic overgrowths dated at 1.57 – 1.48 Ga (broadly Pinwarian; Fig. 2.13f). Some metamorphic overgrowths gave discordant Grenvillian ages (ex:1077 ± 30 Ma; Fig. 2.12d). One cluster of five tightly overlapping concordant data gave a weighted average $^{207}Pb/^{206}Pb$ magmatic age of 1634 ± 10 Ma (MSDW=0.34), which is within the age range of the mid-Labradorian Mealy Mountains Intrusive Suite in Labrador (1650 – 1630 Ma; Gower et al., 2008). The Labradorian event in southeastern Labrador (Fig. 2.1a) and in the northern part of the Grenville Province in Quebec is characterized by igneous rocks of this 1710 – 1600 Ma age range and they have undergone Pinwarian or Grenvillian metamorphism.

Finally, the youngest ages provide a record of a continuous series of magmatic events and they represent the biggest peak (Fig. 2.13a, f and g). The dated grains include many sub-euhedral prisms with some sub-rounded examples and display oscillatory and/or sector zoning typical of igneous zircon (Fig. 2.12e). Some ages were obtained from overgrowths formed around older grains and interpreted to be magmatic in origin as they display oscillatory zoning, indicating the reworking and recycling of older crust and/or sediments. The ages vary from 1.58 to 1.47 Ga, and the youngest ages are from perfectly euhedral and prismatic magmatic grains. Sixteen tightly-clustered analyses yield a weighted average $^{207}Pb/^{206}Pb$ age of 1506 ± 3.5 Ma (MSWD=0.18; Fig. 2.12g), similar (within error) to the age of the TIS (1502 ± 6 Ma), and this suggests a proximity between the TIS and the supracrustal rocks. Some grains display thin darker metamorphic overgrowths with two yielding a Grenvillian age (1037 ± 10 Ma, weighted average

$^{206}Pb/^{238}U$, MSDW=0.48 and probability of concordance of 0.062; Fig. 2.13h). The youngest cluster of concordant ages is 1476 ± 10 Ma (weight average of $^{207}Pb/^{206}Pb$ age from seven overlapping grain analyses; MSDW=0.13; Fig. 2.13g). This age range corresponds to the Pinwarian event in Canada and these ages were obtained from both magmatic cores and rims (Fig. 2.12e and Table 2.4). The Geon 14 rims are surrounding magmatic cores of Geon 15 and Labradorian ages indicating a reworking of older crust. These youngest zircon prisms may be syn-volcanic, deposited in the basin during volcanic eruption.

In summary, based on the internal and external morphology of the grains analyzed, most Archean, Paleoproterozoic, Labradorian and Pinwarian ages are magmatic and were obtained from both igneous zircon and igneous overgrowths. Pinwarian ages were obtained for euhedral to sub-euhedral grains displaying magmatic oscillatory zoning or magmatic overgrowths. Most of the magmatic overgrowths are Geon 15 (1.60 to 1.52 Ga) to Pinwarian (1.52 to 1.46 Ga) in age whereas metamorphic overgrowths are Grenvillian (ca. 1.08 – 1.03 Ga). Two concordant Grenvillian-age overgrowths gave a crystallization age of 1037 ± 10 Ma (Fig. 13h). Apparently older rims with ages of ca. 1100 Ma may reflect the laser beam analysing part of both core and rim on some grains. Based on these observations, the maximum age of deposition for the quartzite was inferred using the youngest concordant magmatic grains of the annealed set, at 1476 ± 10 Ma (Fig. 2.13g and Table 2.4). This is consistent with the intercept age of the nearby volcanic rocks at 1464 +38/-32 Ma which may have provided a volcanic component to the basin.

2.6 Isotopic data

Sm–Nd isotopic data were acquired from two basaltic rocks of the Moulin-à-Baude Formation (one basalt from MAB2, Lac Raymond synform, and one FeTi basalt from MAB2, Lac Saint-Onge synform), and one sub-volcanic gabbronorite, intrusive in the sedimentary rocks of the Saint-Paul-du-Nord Formation (Baie-des-Bacon synform) to test the genetic link with the basalts from the Moulin-à-Baude Formation. Two rocks dated by U–Pb (dacitic tuff from the top of MAB1: 1492 ± 3 Ma; and granodiorite from the TIS: 1502 ± 6 Ma; Fig. 2.11) were also analysed in order to provide an insight on the source. The sample locations are shown in Figure 2.2. The Depleted Mantle line was obtained following the model of DePaolo (1981).

2.6.1 Analytical technique

Details of the sample preparation technique can be found in Valverde et al. (2012). Sm and Nd concentrations and the Nd isotopic composition were determined using a multi-collector Finnigan Mat 262 mass spectrometer (TERRA Facility – Memorial University Earth Sciences Department) in static mode for concentration determination, and dynamic mode for isotopic composition determination. Instrumental mass fractionation of Sm and Nd isotopes were corrected using a Raleigh law relative to $^{146}Nd/^{144}Nd = 0.7219$, $^{152}Sm/^{147}Sm = 1.783$. The reported $^{143}Nd/^{144}Nd$ ratios were corrected for the deviation from repeated analyses of the JNdi-1 ($^{143}Nd/^{144}Nd = 0.512115$, Tanaka et al., 2000) standard. This standard gave a 6-month mean value of $^{143}Nd/^{144}Nd = 0.512102 \pm 14$ (2SD, n=18), USGS whole rock reference material BCR-2 was also periodically analyzed with each analysis comprising a separate dissolution and thus

provided the best estimate of the reproducibility of an individual whole rock analysis. The results of our BCR-2 analyses over time are in agreement with the results reported by Raczek et al. (2003).

2.6.2 Results

Based on their stratigraphic position relative to the dated rocks, we assume that the crystallization ages of the basalts and the gabbronorite are bracketed between 1.5 and 1.49 Ga. The measured Nd isotope ratios were calculated back to the time of formation at 1.49 and 1.5 Ga (Table 2.5). These are expressed as the deviation from a chondritic uniform reservoir at each time. The basalt from MAB2 in the Lac Raymond synform (154-B) has an $\varepsilon Nd_{1.49}$ of 4.92, similar to the $\varepsilon Nd_{1.49}$ of 5.21 from the gabbronorite (291-A) from the Saint Paul du Nord formation in the Baie-des-Bacon synform. The FeTi basalt from MAB2 in the Lac Saint-Onge synform (91-B) has an $\varepsilon Nd_{1.49}$ of 3.91. The dacitic tuff (32-A) from MAB1 from location C has an $\varepsilon Nd_{1.49}$ of -0.8 and the granodiorite (125-A) of the TIS has an $\varepsilon Nd_{1.5}$ of 2.66.

The positive $\varepsilon Nd_{1.49}$ values of the mafic rocks are close to the values of the depleted mantle at that age. Figure 2.14 highlights the wide range of evolution lines for the samples, and also shows the field of the Quebecia crust (from Owens and Tomascak, 2002; Dickin and Higgins, 1992; Dickin 2000). These lines are consistent with varied degrees of interaction between a juvenile magma and older crustal material.

The evolution lines of the granodiorite from the TIS (125-A) and the dacitic tuff from MAB1 (32-A) fall within the Quebecia field. The negative $\varepsilon Nd_{1.49}$ value for the dacitic tuff indicates a greater assimilation of older crust. The gabbronorite (291-A) and

the basalt (154-B) were collected from different synforms and formations (Fig. 2.2), but they have similar back-arc tholeiitic signature, and isotopic signatures (Table 2.5 and Fig. 2.14), that are consistent with a source slightly more depleted than the depleted mantle at 1490 Ma and therefore permitting a cogenetic origin. This also suggests a direct access to the asthenospheric mantle with only minor crustal contamination and/or assimilation of subducted sediments. The FeTi basalt (91-B) has also a juvenile signature but slightly more enriched. These three mafic samples have similar evolution lines, above the Quebecia field (Fig. 2.14), implying the formation of a juvenile crust with a different signature than the Quebecia crust (Fig. 2.14).

2.7 Discussion

2.7.1 Insights from field data and geochronology

The new field data and U–Pb ages show that the Escoumins supracrustal belt (ESB) in the central Grenville Province in Quebec is a well-preserved Pinwarian-age volcano-sedimentary and plutonic rock association. The main lithologic divisions investigated are the Tadoussac Intrusive Suite (TIS), a polyphase batholith, dominated by granodiorite, tonalite, gabbro and granite at the base of the supracrustal sequence, and three formations that make up the Saint-Siméon Group and consist of metasedimentary and metavolcanic rocks. The Saint-Siméon Group is exposed in synformal structures, and the boundary between the western synform investigated and the TIS is a major shear zone (Fig. 2.2). All the investigated rock units display evidence of amphibolite-facies metamorphism.

The oldest protolith age of 1502 ± 6 Ma (Fig. 2.2) is provided by a granodiorite from the core of TIS. Volcanic rocks from the lower (MAB1) and middle part (MAB2) of the Moulin-à-Baude (middle formation of the Saint-Siméon Group) gave ages of 1492 ± 3 Ma (dacitic tuff; Lac Saint-Onge synform; Fig. 2.2), and 1464 +38/-32 Ma (rhyolitic tuff; Lac Raymond synform) and they fall in the Pinwarian age-range (1.52–1.46 Ga) as defined by Gower and Erdmer (1988).

The stratigraphy of the Saint-Siméon Group in each of the three synforms and its interpreted setting of formation can be summarised as follows (see also Fig. 2.3): (a) Deposition of a sedimentary sequence of mudstone, greywacke and sandstone (Saint-Paul-du-Nord Formation), in a marine basin adjacent to an arc, as suggested by the fine-grained laminations, the presence of tuff, mafic intrusions and the lack of evidence for shallow-water deposition; (b) Bimodal volcanism (Moulin-à-Baude Formation). This was mafic dominated (basalt and basaltic andesite) at the lower part of the formation (MAB1) and was followed by felsic-dominated volcanism (dacite, rhyodacite and rhyolite; top of MAB1 and MAB2) and then by mafic volcanism (basalt and FeTi basalt; MAB3) all in a marine environment, as attested by the presence of pillow basalts. Volcanism produced flows and tuffs interbedded with reworked tuffs and clastic sediments and was accompanied by sub-seafloor alteration leading to formation of regional scale quartz–epidote amoeboid patches and a stockwork of quartz–epidote veins. Locally the presence of andalusite-sillimanite-muscovite in felsic volcanic rocks is suggestive of an hybrid epithermal-VMS system (in MAB2). In addition, there is a record of sub-volcanic feeder conduits, which may be equivalent to the mafic sills and dykes that intrude the lower Saint-Paul-du-Nord formation. Finally, the polymictic conglomerate with syn-volcanic

granitoid fragments on the top of MAB1 is indicative of a tectonically active volcanic basin with quick uplift and erosion and is consistent with a decrease in water-depth from the lower to the upper part of the formation. This is supported by the presence of abundant vesicles in basaltic rocks higher in the stratigraphy (MAB2 and MAB3), which attest to a shallow extrusion of the lava; (c) Deposition of a thick sequence of sandstone–greywacke–mudstone interbedded with mafic sills and minor basalt (Port-aux-Quilles Formation). The presence of cross-bedding stratifications and stream ripples in the clastic rocks, which are most abundant in the lower part of the formation, is consistent with a dynamic shallow-marine environment. In contrast, the overlying turbiditic sequence likely formed in a quieter and deeper environment suggesting a rapid subsidence of the basin.

The 1476 ± 10 Ma maximum age of deposition obtained from a quartzite with cross-bedding stratification collected in the core of the Lac Saint-Onge synform (Fig. 2.2) is close to the age of the dated volcanic rocks, and therefore consistent with volcanism in a tectonically active and shallow water environment. The distribution of ages of detrital zircon reveals sources with Laurentian affinities: Superior (2.8 – 2.7 Ga), Meta-Incognita and Core Zone (2.5 – 2.4 Ga), New-Quebec and Torngat Orogens (2 – 1.9 Ga), Makkovikian (1.9 – 1.7 Ga), Labradorian (1.7 – 1.6 Ga), Geon 15 (1.6 – 1.5 Ga) and Pinwarian (1.52 – 1.46 Ga). The increasing abundance of detrital zircon from oldest to younger ages (Fig. 2.13a), reflects the spectra expected for sediment deposited in an extensional back-arc basin, where older detritus from a nearby older craton is less well preserved (Cawood et al., 2012). The main 1500 – 1476 Ma peak indicates that the main

source of sedimentary material is the arc and that some zircon may be derived from coeval ash deposits.

The 1001±3 and 983±3 ages obtained on titanite from the dacitic tuff and the 1037±10 Ma overgrowths on detrital zircon from the quartzite, indicate the presence of a Grenvillian overprint, consistent with the amphibolite-facies metamorphic assemblages in the ESB. The timing and significance of this metamorphism will be discussed in another paper (Groulier et al., 2018).

2.7.2 Insights from geochemistry and Nd-isotopic data

The majority of the TIS rocks have a volcanic arc granitoid signature and are of I-type (Fig. 2.5). Their negative HFSE anomalies are typical of a subduction zone and their trace elements patterns are consistent with a transitional to calc-alkalic signature. The widespread presence of biotite and hornblende in this suite is indicative of hydrous magmas enriched in volatiles, typical of supra-subduction magmatic arc zone. In contrast, the granite at the rim of the batholith has a within-plate, alkaline, A-type signature, enriched in incompatible elements (REE, Nb, Th, Zr and alkalis) and likely formed in an extensional environment. Most of the granite displays strong negative Eu anomalies consistent with a source where plagioclase is present (juvenile mafic crust or plagioclase-bearing asthenospheric mantle?). The 1502 ± 6 Ma granodiorite from the TIS has a positive εNd value of 2.66, implying remelting of mafic rock shortly after extraction from the mantle. The fact that it does not match the εNd value of the depleted mantle at the time of formation (εNd ~ 4–5) may be attributed to interaction of the magma with an older, Paleoproterozoic crust (T_{DM} of 1.67 Ga), and this is supported by the presence of

older inherited cores in some zircon grains of the granodiorite (Fig. 2.10). It is worth noting that the line connecting the εNd_0 and $\varepsilon Nd_{1.5}$ matches the domain of Quebecia crust (Fig. 2.13; Owens and Tomascak, 2002; Dickin and Higgins, 1992; Dickin, 2000). Dickin and Higgins (1992) obtained two depleted-mantle model ages of respectively 1.55 and 1.54 Ga from tonalites from the TIS (not shown in Fig. 2.2), consistent with a juvenile origin for the batholith. Collectively, these ages and our data, suggest that the batholith is polyphase with juvenile components showing no to little crustal contamination while others display a noticeable amount of contamination by older crustal material.

Based on trace element concentrations and REE patterns, the basaltic rocks of the SSG are inferred to have formed in an island arc setting from a slightly enriched source compared to the MOR. Most samples have Zr/Y ratios characteristic of tholeiitic magma with a few falling in the transitional field (Fig. 2.6c) indicating a primitive environment. The basaltic andesite, most common in MAB1, displays negative HFSE anomalies in some cases associated with positive Th anomalies and has high $[La/Yb]_N$ ratios (Fig. 2.7c and d). These signatures are typical of subduction zone magmas where HFSE elements are retained in the source, and the enrichment in Th marks the presence of a fluid exsolved from the dehydrating slab, or interaction with a thicker crust.

The basalt, and FeTi basalt present in MAB2 and MAB3 have REE and extended trace element patterns (Fig. 2.7a-b-e-f) that are consistent with a shallow mantle source where garnet is not present to hold HREEs during partial melting. The juvenile εNd values of these rocks (Table 2.5) indicate little or no interaction with older continental crust, and the data are consistent with direct melting of asthenospheric mantle, as for instance in a rifted arc environment. These basaltic rocks have a Nd isotopic signature

that is distinct from that of Quebecia (Fig. 2.14) and they also have younger model-ages, suggesting a younger episode of melt extraction from the mantle with no interaction with the previously formed oceanic arc crust. The basaltic rocks of the ESB show an overall pattern defined by volcanic arc signatures in the basaltic andesite, to arc-rift and back-arc basin signatures in the basalt and the FeTi basalt (Fig. 2.8b). Based on this information, the most coherent way to define the environment of formation for the basaltic rocks of the ESB is an oceanic island arc and back-arc or arc-rift environment.

The chemistry of the FeTi basalt in the SSG, its close spatial and temporal relationship with the island arc rocks (basaltic andesite) and its highly evolved signature, are consistent with a formation close to the volcanic arc front, from extensive fractionation in a shallow-level magma chamber. Such a process can explain the extreme enrichment in Fe–Ti–P and other trace elements. The FeTi basalt could therefore represent the rifting of the oceanic arc. This interpretation is consistent with observations made on modern oceanic arc and back-arc basins, which show that the magmas produced in rifted arcs and narrow back-arcs will still have the influence of the subduction zone expressed by negative anomalies in HFSE and positive anomalies in the fluid-mobile elements such as Th–Ba–Sr (Pearce et al., 1994; Pearce and Stern, 2006). It is only when the back-arc is more mature with a spreading centre spatially isolated from the subduction zone, that the chemistry of the magma will be more like classic MORB. In the ESB, all the analyzed basaltic rocks display an arc-like signature with the typical negative Nb anomalies, and there is no evidence of MOR-like magmatism. The more primitive signature of the high Mg# and low Fe–Ti basalt, suggests eruption from magma chambers

connected to the main magmatic feeder zone, allowing the magma chamber to be recharged more often and therefore avoiding any extreme magmatic fractionation.

The geochemical signatures of the dacitic to rhyolitic rocks from the Moulin-à-Baude Formation vary from calc-alkalic (MAB1) to transitional (dominant in MAB2) and tholeiitic (MAB2, Fig. 2.6c). Dacite in MAB1 is I-type and VAG whereas in MAB2 it is mostly A-type with an oceanic ridge and within-plate signature (Fig. 2.8c and d). This overall pattern is consistent with an arc environment undergoing an episode of rifting, as was suggested by the geochemistry of the mafic rocks. The dacitic tuff dated at 1.49 Ga (32-A) has an $\varepsilon Nd_{1.49}$ of -0.8 (Table 2.5). Its position below the CHUR line indicates the melting of an older crust or the interaction between a juvenile magma and older crust as suggested by its older model age (T_{DM} of 1936 Ma). Both cases are also supported by the presence of inherited cores in the zircon grains of the dated dacite. Its signature of I-type and VAG supports formation in a supra-subduction zone environment, adding more evidence of the co-existence of at least two distinct sources of magma for the volcanic rocks of the ESB.

2.7.3 Overall evolution of the ESB

It is proposed that the tonalite and granodiorite of the TIS represent the base of a Pinwarian-age oceanic arc with typical "Quebecia" Nd signature, which underwent a rifting event as suggested by the presence of younger A-type and within-plate intrusive rocks.

In the SSG, the lowest Saint-Paul-du-Nord Formation records a typical oceanic basin assemblage, intruded by syn-volcanic tholeiitic mafic bodies with primitive arc to

back-arc signatures similar to those from basalts of the intermediate, Moulin-à-Baude Formation. The latter formation is characterized in its lower part (MAB1) by a bimodal volcanic sequence of tholeiitic to transitional sub-alkaline basalt and basaltic andesite with oceanic arc affinities, and calc-alkaline dacite of I-type and VAG signatures. The middle part of the formation (MAB2) is dominated by a bimodal volcanic sequence of tholeiitic subalkaline basalt and A-type dacite to rhyolite with ORG to WPG signatures, and, towards the top, by sedimentary and volcanogenic rocks, exhalites, dykes and sills of FeTi basalt crosscutting the basaltic rocks. MAB3 is characterized by a mafic volcanic sequence of flows, tuffs and intrusive back-arc basalt and FeTi basalt, the association of interlayered island-arc tholeiite, back-arc basin basalt and FeTi basalt with WPG and VAG felsic volcanic rocks indicates a close spatial relation between the two sources. This type of environment has been observed in modern intra-oceanic arc system where rifting occurs directly at the location of the arc (Saunders and Tarney, 1984). The FeTi basalt represents highly differentiated rocks that are uncommon in modern mid-oceanic ridge environments, but are found in complex tectonic zones such as the Eastern Galapagos spreading center and in ancient intra-oceanic arc undergoing rifting (Barrie and Pattinson, 1999; DeWolfe et al., 2009a; DeWolfe et al., 2009b; Pearce et al., 1995). The absence of MORB-like basalt indicates that the rifting did not lead, in the ESB area, to the opening of a mature spreading centre.

Higher in the stratigraphy, the Port-aux-Quilles Formation is interpreted as the remnant of an intra-arc/back-arc basin filled by epiclastic sediments. The local presence of polymictic conglomerate combined with the observed variation in sedimentary structures (cross-bedding, turbidite) indicates a rapid subsidence of the basin in a

tectonically active environment. The presence of Archean and Paleoproterozoic zircon grains in the quartzite indicates that the oceanic arc/back-arc was proximal to Laurentia.

2.7.4 Late Geon 15 to Geon 14 arc systems in the central-eastern Grenville Province

Late Geon 15 to Geon 14 rocks formed in arc settings were first reported from the eastern Grenville in Labrador leading to the definition of the Pinwarian event (Pinware terrane; Gower et al. 1988). In this area 1.52–1.46 Ga old calc-alkalic granitoids (Gower and Krogh, 2002) are intrusive into Labradorian crust (1.71–1.60 Ga) and indicative of a continental arc system developed at the margin of Laurentia. Moreover, Tucker and Gower (1994) documented a high-grade metamorphic event, suggesting the development of a Pinwarian orogen between 1.47 and 1.45 Ga (see also review in Gower et al., 2008).

In addition, Pinwarian to mid-Geon 14 volcano-sedimentary belts have been identified in the Low-pressure belt along the southernmost parts of the central and eastern Grenville in Quebec. The Portneuf-Mauricie Domain, located at the western margin of Quebecia, consists of the volcano-sedimentary Montauban Group (Fig. 2.1b) dated at 1.45 Ga, and intruded by 1.40 to 1.37 Ga calc-alkalic dioritic to granodioritic plutons of La Bostonnais Complex (Nadeau and van Breemen, 1994; Corrigan, 1995; Sappin et al., 2011; Fig. 2.1b). The Montauban Group is known for its well-preserved tholeiitic pillow basalts metamorphosed to the amphibolite facies (Nadeau et al., 1992) and hosts the Montauban deposit interpreted to represent a metamorphosed gold-rich VMS deposit (Tomkins, 2007) or a metamorphosed exhalative system (Bernier et al., 1987). The Montauban Group is inferred to have formed in an island arc or back-arc tectonic setting (Corrigan and van Breemen, 1997; Sappin et al., 2011) with a northwest-dipping (current

coordinates) intra-oceanic subduction zone offshore from Laurentia (Sappin et al., 2009; Sappin et al., 2012). The range of geochemical signatures in La Bostonnais Complex (oldest plutons: mature oceanic arc; youngest plutons: transition to a continental arc) are interpreted to reflect the accretion of the Montauban oceanic arc to Laurentia at about 1.39 Ga (Corrigan et al., 1994).

Farther east, and outside Quebecia, La Romaine supracrustal belt is a 1.50 Ga volcanic belt (van Breemen and Corriveau, 2005; Fig. 2.1b) with locally preserved primary textures (ex: flow banding; Corriveau and Bonnet, 2005), metamorphosed under upper amphibolite to granulite-facies conditions. While the volcanic rocks are mainly felsic, the presence of coeval mafic dykes, sills, and scoria fragments in felsic tuffs suggest bimodal volcanism. This sequence is associated with calc-alkalic granodioritic to granitic intrusions of the Aguanish Complex (Fig. 2.1b) broadly coeval with the volcanism. To the north-west of this belt, the eastern Wakeham Group (Fig. 2.1b), is composed mainly of continental, arenaceous sedimentary rocks intruded by continental arc 1510 – 1495 Ma high-level plutons (Madore et al. 1997a, 1997b), and metamorphosed to the greenschist facies. Detrital zircon grains from an arenite range from 2.8 to 1.6 Ga (Madore et al., 1997a) meaning that the sedimentary sequence was deposited between 1.6 Ga and 1.51 Ga. La Romaine supracrustal belt is interpreted to be a subaerial to shallow submarine intra-arc volcanic sequence (Corriveau and Bonnet, 2005), whereas the eastern Wakeham Group is inferred to represent a continental back-arc basin (Rivers and Corrigan, 2000; Rivers et al., 2012), the closure of which is marked by the emplacement of the 1510 – 1495 Ma continental arc plutons.

The ESB is exposed between these two supracrustal belts (Montauban and Wakeham/La Romaine) and is part of the "Quebecia" terrane, which makes up an important part of the central Grenville Province (Fig. 2.1b; Dickin and Higgins, 1992; Dickin, 2000; Dickin et al., 2010; Vautour, 2015. Farther east, Pinwarian rocks have older model ages, and are intrusive into Labradorian crust in a continental arc setting (Labradoria; Fig. 2.1b). In contrast, the Quebecia terrane contains rocks derived from reworked crust with Labradorian to Makkovikian depleted mantle model ages, but also rocks with juvenile signatures (ex. Dickin et al., 2010 and this study) suggesting a complex organization. Island arc crust in Quebecia is represented by the ESB, the Montauban group (Fig. 2.1b) and the Cap-à-la-Mer mafic Complex. The latter is located north of the ESB, has Pinwarian model ages (Dickin et al., 2010) and was dated at 1506 ±13 Ma (Hébert and van Breemen 2004). However, within the ESB there is also evidence of Paleoproterozoic crustal components (ex. low εNd values, older depleted mantle model ages and presence of inherited zircons in some tonalitic rocks of the TIS and in the dated dacite of MAB 2). Older Paleoproterozoic model ages were also reported north of the ESB, in the Baie Comeau area (Dickin and Higgins 1992; Dickin et al. 2010), leading Vautour (2015) and Hynes (2010) to suggest the presence of a belt of older Paleoproterozoic crustal panels within Quebecia.

As also proposed by Hynes (2010), we suggest that these crustal panels might have been rifted away from Laurentia during a Geon 15 opening of a continental back-arc that evolved into an oceanic domain. This interpretation is also supported by the presence of two major metasedimentary sequences on opposite sides of Quebecia (Fig. 2.1b): (a) the Geon 15 Plus-Value Complex (PLV; Moukhsil et al., 2012; Lasalle et al., 2013), to

the north, intruded by ~1497 Ma granite with calc-alkaline signature (Bardoux plutonic suite), and interpreted to have formed in an intra-arc or continental back-arc environment (Augland et al., 2015); and (b) the Bourdon Complex, to the south (near the town of Baie-Comeau), which has a maximum deposition age of 1.49 Ga and detrital zircon age spectra (David et al., 2010) typical of a passive margin or rift basin (cf. Cawood et al., 2013).

This organisation indicates that the southeastern Laurentian margin in the central Grenville province experienced during Geon 15 a major extensional event that led to the opening of an oceanic basin. The emplacement of continental arc plutons (ex. Bardoux plutonic suite) within the northern sedimentary sequence (PLV) during early Geon 14, indicates a change in the tectonic setting, and the beginning of closure of the previously opened basins. The broadly coeval development of island arc sequences to the south built on oceanic crust with rifted fragments of Laurentia suggests the presence of two northwest dipping (current coordinates) subduction zones, one along Laurentia and one along the oceanic arc. The presence of a Geon 15 continental sedimentary basin (Eastern Wakeham) associated with a Pinwarian-age continental volcanic belt (La Romaine) and both intruded by late Geon 15 continental plutons (Aguanish Complex; Fig.2.1b) indicates that this extensional event affected also the eastern Grenville but didn't lead to the opening of an oceanic domain there.

An important question is when the ESB was accreted to Laurentia. Stitching plutons were not identified, but a potential candidate could be the ~1391 Ma Cap-à-l'Est gneissic Complex (Fig. 2.1b and 2.2), which was identified immediately north of the ESB, contains enclaves of the juvenile, ~1506 Ma Cap-à-la-Mer mafic Complex, and is inferred to have formed in a continental arc setting (Hébert and van Breemen 2004). This

would be comparable to the 1.4 to 1.37 Ga La Bostonnais Complex in the Portneuf-Mauricie area (Fig. 2.1b), farther west, which is inferred to have marked the accretion of the Montauban supracrustal belt (Sappin et al., 2009, 2011, 2012). The age, rock associations and tectonic environment of the latter, have similarities with the ESB. The two belts are located in the southeastern Grenville Province and are separated by the younger Parc des Laurentides gneissic dome (Fig. 2.1b). Therefore, they might represent remnants of one oceanic arc belt ("Quebecia"), that was accreted to Laurentia at 1.4– 1.37 Ga, and was disrupted during later events.

2.7.4.1 Tectonic model for the ESB

The late Geon 15 to Geon 14 period was the time of a major magmatic event at the scale of the Laurentian margin, and there is evidence of continental arc and back-arc magmatism (Granite-Rhyolite Province in the US, Wakeham and other continental calc-alkaline to alkaline intrusions in many parts of the Grenville Province in Canada) concomitant with oceanic island arc magmatism (Montauban and Escoumins supracrustal belts in the Central Grenville Province in Canada as part of the terrane "Quebecia").

We propose as a geodynamic model of evolution of the ESB that around 1.5 Ga, the TIS was an intra-oceanic arc (Fig. 2.15a). Within a few tens of million years (from 1.50 to 1.47 Ga), the arc matured and started rifting, with the opening of a nascent back-arc basin in the location of the volcanic arc front (Fig. 2.15b). This rifting of the arc may be attributed to slab-rollback, and accounts for the presence of arc-type rocks (basaltic andesite and I-type dacite and rhyodacite) interbedded with or crosscut by back-arc-type rocks (dykes and sills of back-arc basalt, FeTi basalt and A-type dacite to rhyolite). The

rifting led to the opening of a more mature back-arc basin with formation of magmatic chambers at shallow-levels in the crust and extrusion of back-arc basalt and FeTi basalt with juvenile εNd (Fig. 2.15c). They represent the formation of new juvenile crust directly from the melting of the asthenospheric mantle. The back-arc basin was later filled with epiclastic sediments derived from both the arc and Laurentia implying a peri-Laurentian location. The absence of MORB-like igneous rocks in the ESB indicates that rifting did not lead to the complete rupture of the arc and formation of new oceanic crust. The accretion of the arc to Laurentia may have happened by 1.39 Ga, with the intrusion of the continental calc-alkalic Cap-à-l'Est gneissic Complex (Fig. 2.15d).

2.7.4.2 Preservation of the ESB

The presence of volcanic belts in the southernmost part of the Grenville Province, along the north shore of the Saint-Lawrence River (Fig. 2.1b), is of particular interest because this implies the preservation of relativelly shallow crustal levels of the orogen (less metamorphosed rocks of arc and back-arc affinities) in this area. The preferred location of the supracrustal belts between igneous and highly deformed and metamorphosed terranes might be related to the structure of the orogen. For example, the Appalachian orogen in North-America is organized in promontories and embayments. The embayments are preferred places of preservation for the supracrustal sequences, they are closely linked to the nature of the colliding plates, to major inherited tectonic zones (such as syn-rift transform faults) and to the angle of collision between the two colliding plates. The organization of the Grenville orogen in its southern part might be explained

using the promontory-embayment organization with the Composite Arc Belt, Portneuf-Mauricie, Escoumins and Wakeham areas representing relicts of embayments.

2.8 Conclusion

- This study shows that shallow crustal levels of the Grenville orogen preserve primary features that provide a record of the evolution of pre-Grenvillian arc systems.
- The ESB represents a Pinwarian oceanic island arc and arc-rift sequence formed outboard from Laurentia and accreted to it during the Mesoproterozoic.
- Island arc rocks of the ESB have a Quebecia Nd-isotopic signature with some displaying older Paleoproterozoic model ages plausibly linked to the presence of older crustal panels rifted away from Laurentia. These variations in isotopic signature indicate that the Quebecia terrane has a complex organization and that only parts of it display true juvenile character. Hence, Quebecia is less coherent as an entity than previously thought and should be treated as a composite arc belt as proposed by Vautour (2015).
- Basalt formed during the rifting of the arc has a juvenile depleted mantle signature, highlighting a new episode of asthenosphere mantle melting and crust formation.
- Detrital zircon from a quartzite of the ESB, record an age spectrum typical of an oceanic back-arc or intra-arc basin with the oceanic arc as a dominant source of detritus, and a lesser contribution from their adjacent continent. This is one of the

first cases of detrital zircon being treated with chemical abrasion prior to laser-ICP-MS analysis. The Concordia plots demonstrate the very tight clustering of these high-quality reproducible data points, which we suggest allow us to calculate true ages of detritus due to removal of secondary lead-loss. Crust formed in an oceanic arc setting during late Geon 15 to Geon 14, constitutes a significant component of the central Grenville Province.

2.9 Acknowledgements

This contribution is part of the PhD of the first author and was funded by the Ministère de l'Énergie et des Ressources naturelles of Quebec (contribution number 8449-2017-2018-01) and by Natural Sciences Engineering Research Council of Canada (NSERC) discovery grant (200386) to the second author. The samples were collected by the first author during three field seasons (2013, 2014 and 2015). The authors would like to thank Dr. Jean-Luc Pilote for constructive discussion, Sherri Strong for Sm-Nd analyses, Amanda Langille and Pamela King for the preparation of the samples for the TIMS and LA-ICP-MS, Dr. François Turlin and Evelyne Sunatori for their assistance in the field. The authors are also grateful to Dr. Trond Slagstad and Dr. Bernard Bingen for their detailed reviews that led to a significant improvement of the paper, and to Dr. Randall Parrish for editorial handling.

2.10 References

Augland, L.E., Moukhsil, A., Solgadi, F., Indares, A., 2015. Pinwarian to Grenvillian magmatic evolution in the central Grenville Province: new constraints from ID-

TIMS U-Pb ages and coupled Lu-Hf S-MC-ICP-MS data. Canadian Journal of Earth Sciences, volume 52, 701–721.

Bailes, A.H., Galley, A.G., Paradis, S., Taylor, B.E., Pehrsson, S.J., Gibson, H.L., Gilmore, K., 2016. Variations in large synvolcanic alteration zones at Snow Lake, Manitoba, Canada, with proximity to associated volcanogenic massive sulfide deposits. Economic Geology, volume 111 (4), 933–962.

Barret, T.J., MacLean, W.H., 1994. Mass changes in hydrothermal alteration zones associated with VMS deposits of the Noranda Area. Exploration and Mining Geology, volume 3 (2), 131–160.

Barret, T.J, MacLean, W.H., 1999. Volcanic sequences, lithogeochemistry, and hydrothermal alteration in some bimodal volcanic-associated massive sulfide systems, in: C.T. Barrie and M.D. Hannington (Eds.), Volcanic-Associated Massive Sulfide Deposits: Processes and Examples in Modern and Ancient Environments. Society of Economic Geologists, Reviews in Economic Geology, volume 8, 101–131.

Barrie, T.C., and Pattinson, J., 1999. Fe-Ti basalts, High silica rhyolites and the role of magmatic heat in the genesis of the Kam-Kotia volcanic-associated massive sulfide deposit, Western Abitibi Subprovince, Canada. Economic Geology, Monograph 10, 577–592.

Beaumont, C., Jamieson, R., Nguyen, M., 2010. Models of large, hot orogens containing a collage of reworked and accreted terranes. Canadian Journal of Earth Sciences, volume 47, 485–515.

Benahmed, S., Intissar, R., 2015. Levé magnétique aéroporté dans le secteur des Escoumins, Côte-Nord, Province de Grenville. Ministère de l'Énergie et des Ressources naturelles, Québec ; DP 2015-04.

Bernier, L.R., Pouliot, G., MacLean, W.H., 1987. Geology and metamorphism of the Montauban north gold zone: a metamorphosed polymetallic exhalative deposit, Grenville Province, Quebec. Economic Geology, volume 82, 2076–2090.

Brown, G.C., Thorpe, R.S., Webb, P.C., 1984. The geochemical characteristics of granitoids in contrasting arcs and comments on magma sources. Journal of the Geological Society of London, volume 141, 413–426.

Cabanis, B., Lecolle, M., 1989. Le diagramme La/10-Y/15-Nb/8 ; un outil pour la discrimination des séries volcaniques et la mise en évidence des processus de mélange et/ou de contamination crustale. Comptes Rendus de l'Académie des Sciences, Série 2, Mécanique, Physique, Chimie, Sciences de l'Univers, Sciences de la Terre, volume 309 (20), 2023–2029.

Carr, S.D., Easton, R.M., Jamieson, R.A., Culshaw, N.G., 2000. Geologic transect across the Grenville Orogen of Ontario and New York. Canadian Journal of Earth Sciences, volume 37, 193–216.

Caté, A., Ross, P.-S., Gagne, S., 2015. Hydrothermal history and gold mineralization at the Lalor volcanogenic massive sulphide deposit, Snow Lake camp, Manitoba, Canada. 13th SGA biennal meeting, Nancy, France.

Cawood, P.A., Hawkesworth, C.J., Dhuime, B., 2012. Detrital zircon record and tectonic setting. Geology, volume 40, 875–878.

Colman-Sadd, S.P., Dunning, G.R., Dec, T., 1992. Dunnage-Gander relationships and Ordovician orogeny in central Newfoundland: a sediment provenance and U/Pb age study. American Journal of Science, volume 292, 317–355.

Corrigan, D., van Breemen, O., Hanmer, S., Nadeau, L., 1994. Arc accretion, crustal thickening, and post-collisional extension in the Grenville Province: constraints from the St. Maurice lithotectonic belt. Lithoprobe Meeting, Abitibi-Grenville Transect, Université de Montreal, Montreal, Quebec, Nov/Dec. 1994. Program with abstracts.

Corrigan, D., 1995. Mesoproterozoic evolution of the south-central Grenville orogen: structural, metamorphic, and geochronologic constraints from the Mauricie transect. PhD thesis, Carleton University, 282 p.

Corrigan, D., van Breemen, O., 1997. U-Pb age constraints for the lithotectonic evolution of the Grenville Province along the Mauricie transect, Quebec. Canadian Journal of Earth Sciences, volume 34, 299–316.

Corriveau, L., Bonnet, A.-L., 2005. Pinwarian (1.5 Ga) volcanism and hydrothermal activity at the eastern margin of the Wahekam Group, Grenville Province, Quebec. Canadian Journal of Earth Sciences, volume 42, 1749–1782.

David, J., Moukhsil, A., Dion, C., 2010. Datations U-Pb effectuées dans la Province de Grenville en 2008-2009. Ministère de l'Énergie et des Ressources naturelles du Québec, RP2010-10.

Defant, M.J., Drummond, M.S., 1990. Derivation of some modern arc magmas by melting of young subducted lithosphere. Nature, volume 347, 662–665.

Defant, M.J., Drummond, M.S., 1993. Mount St. Helens: potential example of the partial melting of the subducted lithosphere in a volcanic arc. Geology, volume 21, 541–550.

DePaolo, D.J., 1981. Neodynium isotopes in the Colorado Front Range and crust-mantle evolution in the Proterozoic. Nature, volume 291, 193–196.

DeWolfe, Y.M., Gibson, H.L., Lafrance, B., Bailes, A.H., 2009a. Volcanic reconstruction of Paleoproterozoic arc volcanoes: the Hidden and Louis formations, Flin-Flon, Manitoba, Canada. Canadian Journal of Earth Sciences, volume 46 (7), 481–508.

DeWolfe, Y.M., Gibson, H.L., Piercey, S.J, 2009b. Petrogenesis of the 1.9 Ga mafic hanging-wall sequence to the Flin-Flon, Callinan and Triple 7 massive sulphide deposits, Flin-Flon, Manitoba, Canada. Canadian Journal of Earth Sciences, volume 46 (7), 509–527.

Dickin, A.P., Higgins, M.D., 1992. Sm /Nd evidence for a major 1.5 Ga crust-forming event in the central Grenville Province. Geology, volume 20, 137–140.

Dickin, A.P., 2000. Crustal formation in the Grenville Province: Nd-isotope evidence. Canadian Journal of Earth Sciences, volume 37, 165–181.

Dickin, A.P., McNutt, R.H., Martin, C., Guo, A., 2010. The extent of juvenile crust in the Grenville Province: Nd isotope evidence. Geological Society of America Bulletin, volume 122 (5-6), 870–883.

Dubé, B., Gosselin, P., Mercier-Langevin, P., Hannington, M., Galley, A., 2007. Gold-rich volcanogenic massive sulphide deposits, in: W.D. Goodfellow (Ed.), Mineral Deposits of Canada; A synthesis of Major Deposit Types, District Metallogeny, the Evolution of Geological Provinces, and Exploration Methods. Geological

Association of Canada, Mineral Deposits Division, Special Publication No. 5, 75–94.

Eilu, P.K., Mathison, C.I., Groves, D.I., Allardyce, W.J., 1999. Atlas of alteration assemblages, styles and zoning in orogenic lode-gold deposits in a variety of host rocks and metamorphic settings. Geology and Geophysics Department (Centre for Strategic Mineral Deposits) & UWA Extension, The University of Western Australia, Publication 30, 50 p.

Embley, R.W., Jonasson, I.R., Perfit, M.R., Franklin, J.M., Tivey, M.A., Malahoff, A., Smith, M.F., Francis, T.J.G, 1988. Submersible investigation of an extinct hydrothermal system on the Galapagos ridge: sulfide mounds, stockwork zone, and differentiated lavas. Canadian Mineralogist, volume 26, 517–539.

Galley, A.G., Hannington, M.D., Jonasson, I., 2007. Volcanogenic massive sulphide deposits, in: W.D. Goodfellow (Ed.), Mineral Deposits of Canada; A synthesis of Major Deposit Types, District Metallogeny, the Evolution of Geological Provinces, and Exploration Methods. Geological Association of Canada, Mineral Deposits Division, Special Publication No. 5, 141–161.

Gehrels, G., Rusmore, M., Woodsworth, G., Crawford, M., Andronicos, C., Hollister, L., Patchett, J., Ducea, M., Butler, R., Klepeis, K., Davidson, C., Friedman, R., Haggart, J., Mahoney, B., Crawford, W., Pearson, D., Girardi, J., 2009. U-Th-Pb geochronology of the Coast Mountains batholith in north-coastal British Columbia: constraints on age and tectonic evolution. Geological Society of America Bulletin 121, 1341–1361.

Gifkins, C., Herrmann, W., Large, R.R., 2005. Altered volcanic rocks: a guide to description and interpretation; Centre for Ore Deposits Research; University of Tasmania, Hobart, Tasmania, Australia, 275 p.

Gower, C.F., Erdmer, P., 1988. Proterozoic metamorphism in the Grenville Province: a study in the Double Mer – Lake Melville area, eastern Labrador. Canadian Journal of Earth Sciences, volume 25, 1895–1905.

Gower, C.F., Krogh, T.E., 2002. A U-Pb geochronological review of the Proterozoic history of the eastern Grenville Province. Canadian Journal of Earth Sciences, volume 39, 795–829.

Gower, C.F., Kamo, S.L., Kwok, K., Krogh, T.E., 2008. Proterozoic southward accretion and Grenvillian orogenesis in the interior Grenville Province in eastern Labrador: Evidence from U-Pb geochronological investigations. Precambrian Research, volume 165, 61–95.

Groulier, P.-A., Indares, A., Dunning, G., Moukhsil, A., 2015. Géologie de la ceinture volcano-sédimentaire des Escoumins, Côte-Nord, Québec (rapport préliminaire), MB 2015-09, Énergie et Ressources naturelles, 57 p.

Groulier, P.-A., Indares, A.D., Dunning, G., Mouhksil, A., 2016. Géologie de la ceinture volcano-sédimentaire des Escoumins, Côte-Nord, Québec. MB 2016-07, Ministère de l'Énergie et des Ressources naturelles, 87 p.

Groulier, P.-A., Indares, A.D., Dunning, G., Mouhksil, A., Jenner, G., 2018. Syn-orogenic magmatism over 100 m.y. in high crustal levels of the central Grenville Province: characteristics, age and tectonic significance. Lithos, volume 312-313, 128–152.

Gunning, M.H., Hodder, R.W.H., Nelson, J.L., 2006. Contrasting volcanic styles within the Paleozoic Stikine assemblage, western Stikine terrane, northwestern British Columbia, in: M. Colpron and J.L. Nelson (Eds.), Paleozoic evolution and metallogeny of pericratonic terranes at the Ancient Pacific Margin of North America, Canadian and Alaskan Cordillera. Geological Association of Canada, Special Paper 45, 201–227.

Harris, N.B.W., Pearce, J.A., Tindle, A.G., 1986. Geochemical characteristics of collision-zone magmatism. In: Coward, M.P., Reis, A.C. (Eds.), Collision Tectonics, Geological Society, London, Special Publications no. 19, 67–81.

Hastie, A.R., Kerr, A.C., Pearce, J.A., Mitchell, S.F., 2007. Classification of altered island arc rocks using immobile trace elements: development of the Th – Co discrimination diagram. Journal of Petrology, volume 48, 2341–2357.

Hébert, C., Lacoste, P., 1998. Géologie de la region de Bagotville (22D/07). Ministère des Ressources naturelles, Québec, RG 97-06, 17 p.

Hébert, C., van Breemen, O., 2004. Mesoproterozoic basement, the Lac-Saint-Jean anorthosite suite and younger Grenvillian intrusions in the Saguenay region (Quebec): structural relationships and U-Pb geochronology, in: R.P. Tollo, L. Corriveau, J. McLelland, and M. Bartholomew (Eds.). Geological Society of America, Memoir 197, 65–79.

Hoffman, P.F., 1989. Precambrian geology and tectonic history of North America. In The Geology of North America: an Overview. Geological Society of America, Boulder, Colo., The Geology of North America, Vol. A., 447–512.

Hynes, E., 2010. Nd isotope delineation of crustal terranes in the Bancroft area of Ontario and the Saguenay and Baie Comeau regions of Central Quebec: ensialic rifting and arc formation. Msc thesis, McMaster University.

Jenner, G.A., 1996. Trace element geochemistry of igneous rocks: geochemical nomenclature and analytical geochemistry, in: D.A. Wyman (Ed.), Trace Element Geochemistry of Volcanic Rocks: Applications for Massive Sulfide Exploration. Geological Association of Canada, Short Course Notes, volume 12, 51–77.

Karlstrom, K.E., Ahall, K.-I., Harlan, S.S.,Williams, M.L., McLelland, J., Geissman, J.W., 2001. Long-lived (1.8-1.0 Ga) convergent orogen in southern Laurentia, its extensions to Australia and Baltica, and implications for refining Rodinia. Precambrian Research, volume 111, 5–30.

Ketchum, J.W.F., Heaman, L.M., Krogh., T.E., Culshaw, N.G., Jamieson, R.A., 1998. Timing and thermal influence of late orogenic extension in the lower crust: a U-Pb geochronological study from the southwest Grenville orogen, Canada. Precambrian Research, volume 89, 25–45.

Ketchum, J.W.F., Jackson, S.E., Culshaw, N.G., Barr, S.M., 2001. Depositional and tectonic setting of the Paleoproterozoic lower Aillik Group, Makkovik Province, Canada: evolution of a passive margin-foredeep sequence based on petrochemistry and U-Pb (TIMS and LAM-ICP-MS) geochronology. Precambrian Research, volume 105, 331–356.

Krogh, T.E., 1982. Improved accuracy of U-Pb zircon ages by the creation of more concordant systems using an air abrasion technique. Geochemica et Cosmochimica Acta, volume 46 (4), 637–649.

Lasalle, S., S., Fisher, C.M., Indares, A., and Dunning, G. 2013. Contrasting types of Grenvillian granulite facies aluminous gneisses: insights on protoliths and metamorphic events from zircon morphologies and ages. Precambrian Research, volume 228: 117–130.

Madore, L., Verpaelst, P., Choinière, J., Dion, D.-J., David, J., Lefebre, D., Marquis, R., Hocq, M. 1997*a*. Géologie de la région du Lac Briend. Ministère des ressources naturelles du Québec, RG96-05.

Madore, L., Verpaelst, P., Brisebois, D., Choinière, J., Dion, D.-J., David, J. 1997*b*. Géologie de la région du Lac Cormier. Ministère des ressources naturelles du Québec, RG97-08.

Mattinson, J.M., 2005. Zircon U-Pb chemical abrasion (‘‘CA-TIMS’’) method: combined annealing and multi-step partial dissolution analysis for improved precision and accuracy of zircon ages. Chemical Geology, volume 220, 47–66.

McLelland, J.M., Selleck, B.W., Bickford, M.E., 2013. Tectonic evolution of the Adirondack Mountains and Grenville Orogen inliers within the USA. Geoscience Canada, volume 40, 318–352.

Meschede, M., 1986. A method of discriminating between different types of mid-ocean ridge basalts and continental tholeiites with the Nb-Zr-Y diagram. Chemical Geology, volume 56, 207–218.

Miller, M.L., 1973. Région de Saint-Siméon Tadoussac, Ministère de l’Énergie et des Ressources naturelles, Québec ; GM 159, 94 p.

Miyashiro, A. 1974. Volcanic rock series in island arc and arctive continental margins. American Journal of Science, volume 274 (4), 321–355.

Morin, G., 1987. Gîtologie des régions de Sacré-Coeur et de Grandes-Bergeronnes, Ministère de l'Énergie et des Ressources naturelles, Québec ; ET 85-11, 25 p.

Morrison, G.W., 1980. Characteristics and tectonic setting of the shoshonite rock association. Lithos, volume 13, 97–108.

Moukhsil, A., Solgadi, F., Lacoste, P., Gagnon, M., David, J., 2012. Géologie de la region du lac du Milieu (SNRC 22O03, 22O04, 22O06, 22J13 et 22J14). Ministère des Ressources naturelles et de la Faune, RG 2012-01, 31 p.

Nadeau, L., van Breemen, O., Hebert, C., 1992. Géologie, âge et extension géographique du groupe de Montauban et du complexe de La Bostonnais. Ministère de l'Énergie et des Ressources, Québec, DV 92-03, 35–39.

Nadeau, L., van Breemen, O., 1994. Do the 1.45-1.39 Ga Montauban Group and the La Bostonnais complex constitute a Grenvillian accreted terrane? In Program with abstracts. Geological Association of Canada, volume 19, p. A81.

Owens., B.E., Tomascak, P.B., 2002. Mesoproterozoic lamprophyres in the Labrieville Massif, Quebec: clues to the origin of alkali anorthosites? Canadian Journal of Earth Sciences, volume 39, 983–997.

Pearce, J.A., 1982. Trace element characteristics of lavas from destructive plate boundaries. In: Thorpe, R.S. (Ed.), Orogenic Andesites. Wiley, Chichester, U.K., 528–548.

Pearce, J.A., Harris, B.W., Tindle, A.G., 1984. Trace element discrimination diagrams for the tectonic interpretation of granitic rocks. Journal of Petrology, volume 25 (4), 956–983.

Pearce, J.A., Ernewein, M., Bloomer, S.H., Parson, L.M., Murton, B.J., Johnson, L.E., 1994. Geochemistry of Lau Basin volcanic rocks: influence of ridge segmentation and arc proximity. In: Smellie, J.L. (Ed.), Volcanism Associated with Extension at Consuming Plate Margins, Geological Society of London, Special Publication No. 81, 53–75.

Pearce, J.A., Peate, D.W., 1995. Tectonic implications of the composition of volcanic arc magmas. Annual Review of Earth and Planetary Sciences, volume 23, 251–285.

Pearce, J.A., Stern, R.J, 2006. Origin of Back-Arc Basin Magmas: Trace Element and Isotope Perspectives, in: D.M. Christie et al., (Eds), Back-Arc Spreading Systems: Geological, Biological, Chemical and Physical Interactions. AGU Washington D.C., Geophysical Monograph Series 166, 63–86.

Pearce, J.A., 2008. Geochemical fingerprinting of oceanic basalts with applications to ophiolite classification and the search for Archean oceanic crust. Lithos, volume 100, 14–48.

Pearce, J.A., 2014. Immobile element fingerprinting of ophiolites. Elements, volume 10, 101–108.

Raczek, I., Jochum, K.P., Hofmann, A.W., 2003. Neodynium and Strontium Isotope Data for USGS Reference Materials BCR-1, BCR-2, BHVO-1, BHVO-2, AGV-1, AGV-2, GSP-1, GSP-2 and Eight MPI-DING Reference. Geostandards and Geoanalytical Research, volume 27 (2), 173–179.

Rivers, T., 1997. Lithotectonic elements of the Grenville Province: a review and tectonic implications. Precambrian Research, volume 86, 117–154.

Rivers, T., 2008. Assembly and preservation of lower, mid and upper orogenic crust in the Grenville Province – Implications for the evolution of Large hot long-duration orogens. Precambrian Research, volume 167, 237–259.

Rivers, T., Corrigan, D., 2000. Convergent margin on southeastern Laurentia during the Mesoproterozoic: tectonic implications. Canadian Journal of Earth Sciences, volume 37, 359–383.

Rivers, T., Culshaw, N., Hynes, A., Indares, A., Jamieson, R., Martignole, J., 2012. The Grenville Orogen – A post-LITHOPROBE perspective, Chapter 3, in: Percival, J.A., Cook, F.A., and Clowes, R.M. (Eds.), Tectonic Styles in Canada: the LITHOPROBE Perspective. Geological Association of Canada, Special Paper 49, 97–236.

Rondot, J., Marleau, J.R., 1977. La silice de Charlevoix, CIM Bull. 70, 105–115.

Rondot, J., 1979. Reconnaissances Géologiques dans Charlevoix-Saguenay, Ministère de l'Énergie et des Ressources naturelles, Québec ; DPV-682, 44 p.

Rondot, J., 1986. Géologie de la région de Forestville-Les Escoumins, Ministère de l'Énergie et des Ressources naturelles, Québec ; ET 85-05, 47 p.

Rondot, J., 1989. Géologie de Charlevoix, Ministère de l'Énergie et des Ressources naturelles, Québec ; MB 89-21, 606 p.

Rondot, J., Lavergne, G., 1984. Carte géologique de la région de Forestville-Les Escoumins, 2 cartes annotées, Ministère de l'Énergie et des Ressources naturelles, Québec ; DP 84-54.

Sappin, A.-A., Constantin, M., Clark, T., van Breemen, O., 2009. Geochemistry, geochronology, and geodynamic setting of Ni-Cu±PGE mineral prospects hosted

by mafic and ultramafic intrusions in the Portneuf-Mauricie Domain, Grenville Province, Quebec. Canadian Journal of Earth Sciences, volume 46, 331–353.

Sappin, A.-A., Constantin, M., Clark, T., 2011. Origin of magmatic sulfides in a Proterozoic island arc – an example from the Portneuf-Mauricie Domain, Grenville Province, Canada. Mineralium Deposita, volume 46 (3), 211–237.

Sappin, A.-A., Constantin, M., Clark, T., 2012. Petrology of mafic and ultramafic intrusions from the Portneuf-Mauricie Domain, Grenville Province, Canada: Implications for plutonic complexes in a Proterozoic island arc. Lithos, volume 154, 277–295.

Saunders, A.D., Tarney, J., 1984. Geochemical characteristics of basaltic volcanism within back-arc basins. In Marginal Basin Geology. Kokelaar, B.P. and Howells, M.F. (Eds.). Special Publication number 16 of the Geological Society, London, 59–76.

Slagstad., T., Culshaw, N.G., Daly, J.S., Jamieson, R.A., 2009. Westerm Grenville Province holds key to midcontinental Granite-Rhyolite Province enigma. Terra Nova, volume 21, 191–187.

Sláma, J., Košler, J., Condon, D.J., Crowley, J.L., Gerdes, A., Hanchar, J.M., Horstwood, M.S.A., Morris, G.A., Nasdala, L., Norberg., N., Schlategger, U., Schoene, B., Tubrett, M.N., Whitehouse, M.J., 2008. Plešovice zircon – A new natural reference material for U-Pb and Hf isotopic microanalysis. Chemical Geology, volume 249, 1–35.

Sparkes, G.W., Dunning, G.R, 2014. Late Neoproterozoic epithermal alteration and mineralization in the western Avalon zone: a summary of mineralogical

investigations and new U/Pb geochronological results. Current Research, Newfoundland and Labrador Department of Natural Resources, Geological Survey, Report 14-1, 99–128.

Stacey, J.S., Kramers, J.D., 1975. Approximation of terrestrial lead isotope evolution by a 2-stage model. Earth and Planetary Science Letters, volume 26 (2), 207–221.

Sun, S.S., McDonough, W.F., 1989. Chemical and isotopic systematics of oceanic basalts: Implications for mantle composition and processes, in Magmatism in the Ocean Basins, in: A.D. Saunders and M.J. Norry (Eds.). Geological Society of London, Special Publication No. 42, 313–345.

Tomkins, A.G., 2007. Three mechanisms of ore re-mobilisation during amphibolite facies metamorphism at the Montauban Zn-Pb-Au-Ag deposit. Mineralium Deposita, volume 42, 627–637.

Tucker, R.D., Gower, C.F., 1990. Salient features of the Pinware terrane, Grenville Province, eastern Labrador. Geological Association of Canada, Mineralogical Association of Canada, Program with abstracts, volume 15, A133.

Tucker, R.D, Gower, C.F., 1994. A U-Pb geochronological framework for the Pinware terrane, Grenville Province, southeast Labrador. Journal of Geology, volume 102, 67–78.

Valverde Cardenas, C., Indares, A., Jenner, G., 2012. Mafic and ultrapotassic rocks from the Canyon domain (central Grenville Province): geochemistry and tectonic implications. Canadian Journal of Earth Sciences, volume 49, 412–433.

van Breemen, O., Corriveau, L., 2005. U-Pb age constraints on arenaceous and volcanic rocks of the Wahekam Group, eastern Grenville Province. Canadian Journal of Earth Sciences, volume 42, 1677–1697.

Vautour, S., 2015. A new model for the Quebecia terrane in the Grenville Province as a composite arc belt: Sm-Nd evidence. MSc thesis, McMaster University, 66 p.

Veizer, J., Ala, D., Azmy, K., Bruckschen, P., Buhl, D., Bruhn, F., Carden, G.A.F., Diener, A., Ebneth, S., Godderis, Y., Jasper, T., Korte, C., Pawellek, F., Podlaha, O.G., Strauss, H., 1999. $^{87}Sr/^{86}Sr$, $\delta^{13}C$ and $\delta^{18}O$ evolution of Phanerozoic seawater. Chemical Geology, volume 161, 59–88.

Whalen, J.B., Currie, K.L., Chappell, B.W., 1987. A-type granites: geochemical characteristics, discrimination and petrogenesis. Contributions to Mineralogy and Petrology, volume 95, 407–419.

Whitmeyer, S.J., Karlstrom, K.E., 2007. Tectonic model for the Proterozoic growth of North America. Geosphere, volume 3, 220–259.

Wiedenbeck, M., Allé, P., Corfu, F., Griffin, W.L., Roddick, J.C., Spiegel, W., 1995. Three natural zircon standards for U-Th-Pb, Lu-Hf, trace element and REE analyses. Geostandards and Geoanalytical Research, volume 19, 1–23.

Winchester, J.A., Floyd, P.A., 1977. Geochemical discrimination of different magma series and their differentiation products using immobile elements. Chemical Geology, volume 20, 325–343.

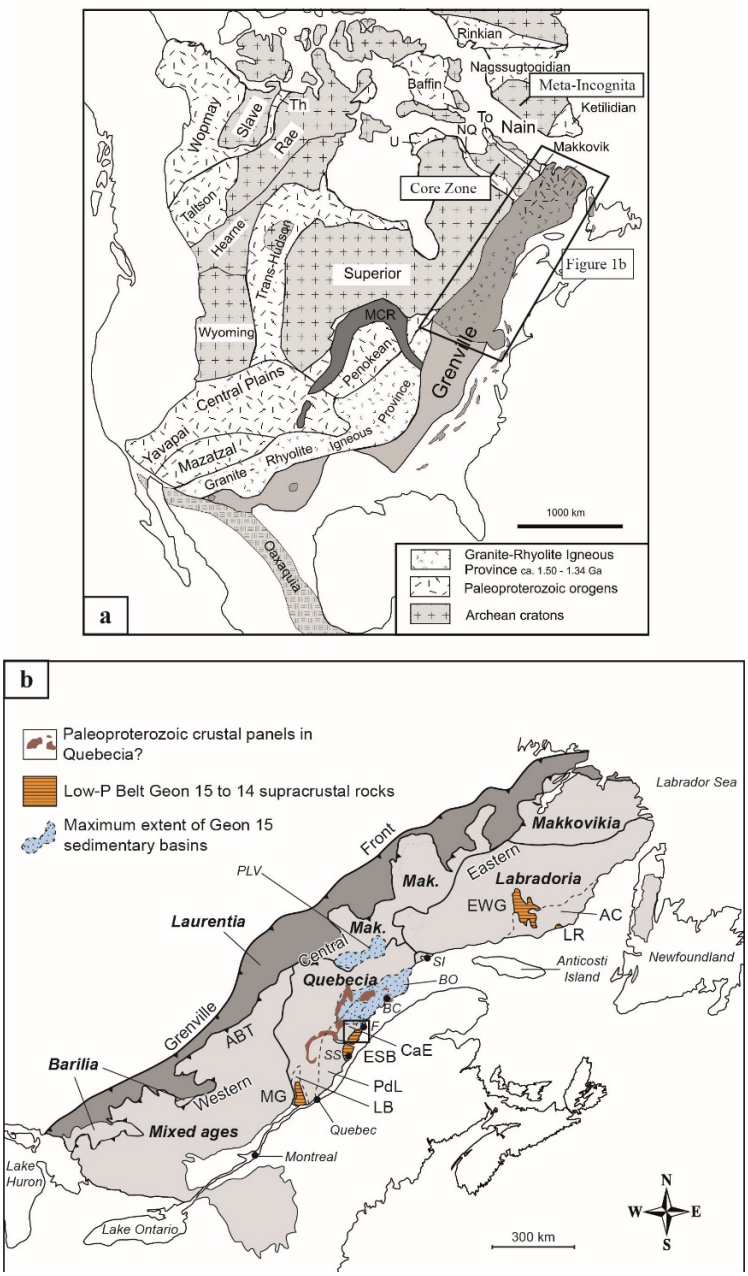

Figure 0.1: (a) Map of Proterozoic Laurentia displaying the extension of the Grenville with younger sequences omitted (modified from Rivers et al., 2012 and Hoffman 1989). Abbreviations: MCR – Mid-continent Rift, NQ – New Québec orogen, Th – Thelon orogen, To – Torngat orogen, U – Ungava orogen. **(b)** Nd-model age map showing major crustal terranes of the Grenville Province in Canada with distinct crustal formation ages: Laurentia (2.7 Ga), Barilia and Makkovikia (1.9 Ga), Labradoria (1.7 Ga), Quebecia (1.5 Ga) (modified from Dickin et al., 2010). The proposed extent of Paleoproterozoic crustal panels within Quebecia are from Hynes (2010) and Vautour (2015). Abbreviations: ABT – Allochthonous Boundary Thrust, AC – Aguanish Complex (1.5 Ga), BC – Baie Comeau, BO = Bourdon Complex, CaE = Cap-à-l'Est Complex (1.39 Ga), ESB = Escoumins Supracrustal Belt, EWG = Eastern Wakeham Group, F – Forestville, LB = La Bostonnais Complex (1.37 – 1.4 Ga), LR – La Romaine, Mak. – Makkovikian age crust, MG = Montauban Group, PdL = Parc des Laurentides Complex (1.34 – 1.39 Ga), PLV = Plus-Value Complex, SI – Sept Iles, SS – Saint-Siméon.

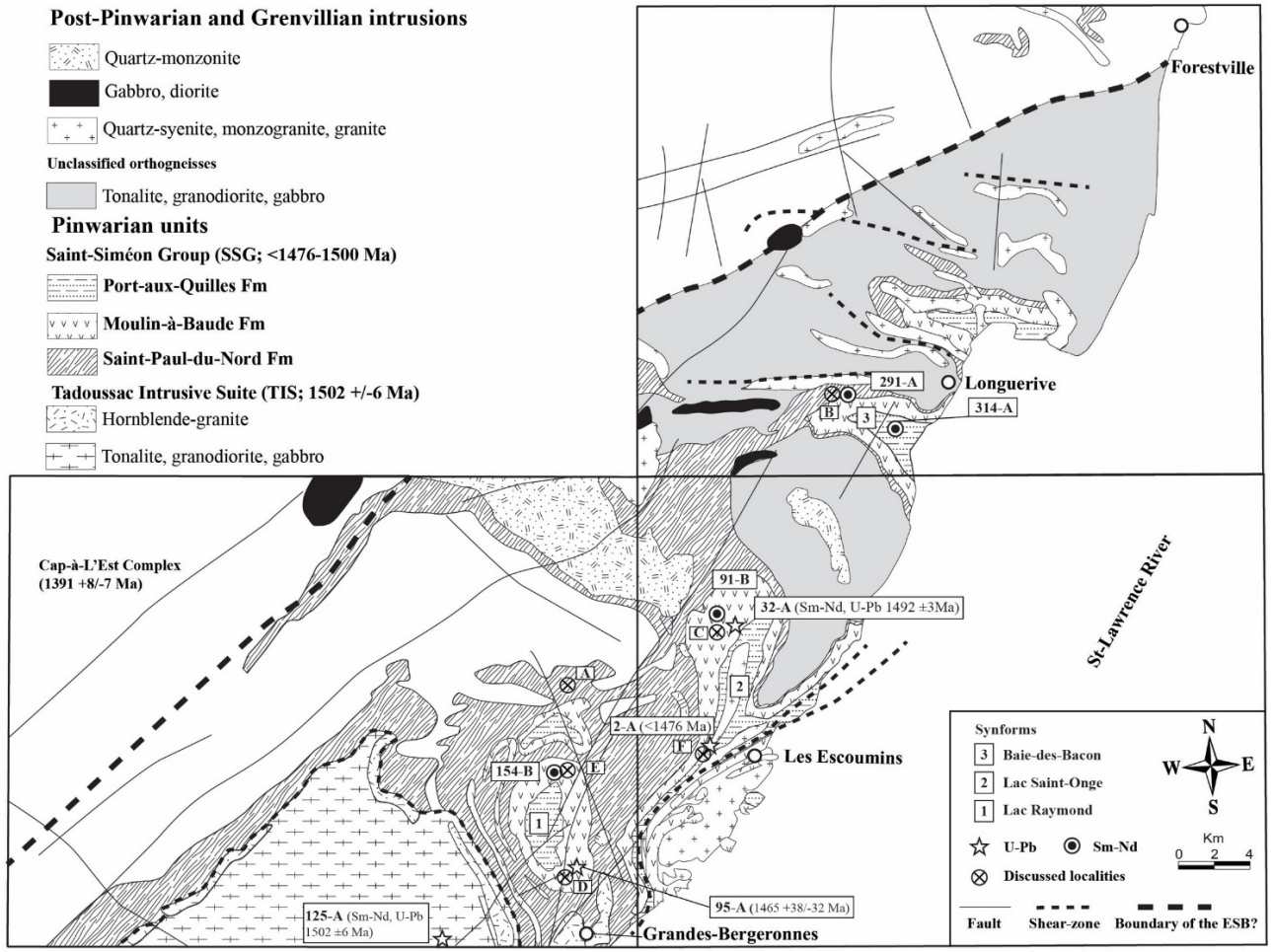

Figure 0.2: Geological map of the Escoumins supracrustal belt (ESB) (modified from Morin (1986), Rondot and Dion (1987) and updated from Groulier et al. (2016)). Age and localisation of the Cap-à-l'Est Complex are from Hébert and van Breemen (2004) and Hébert and Lacoste (1998).

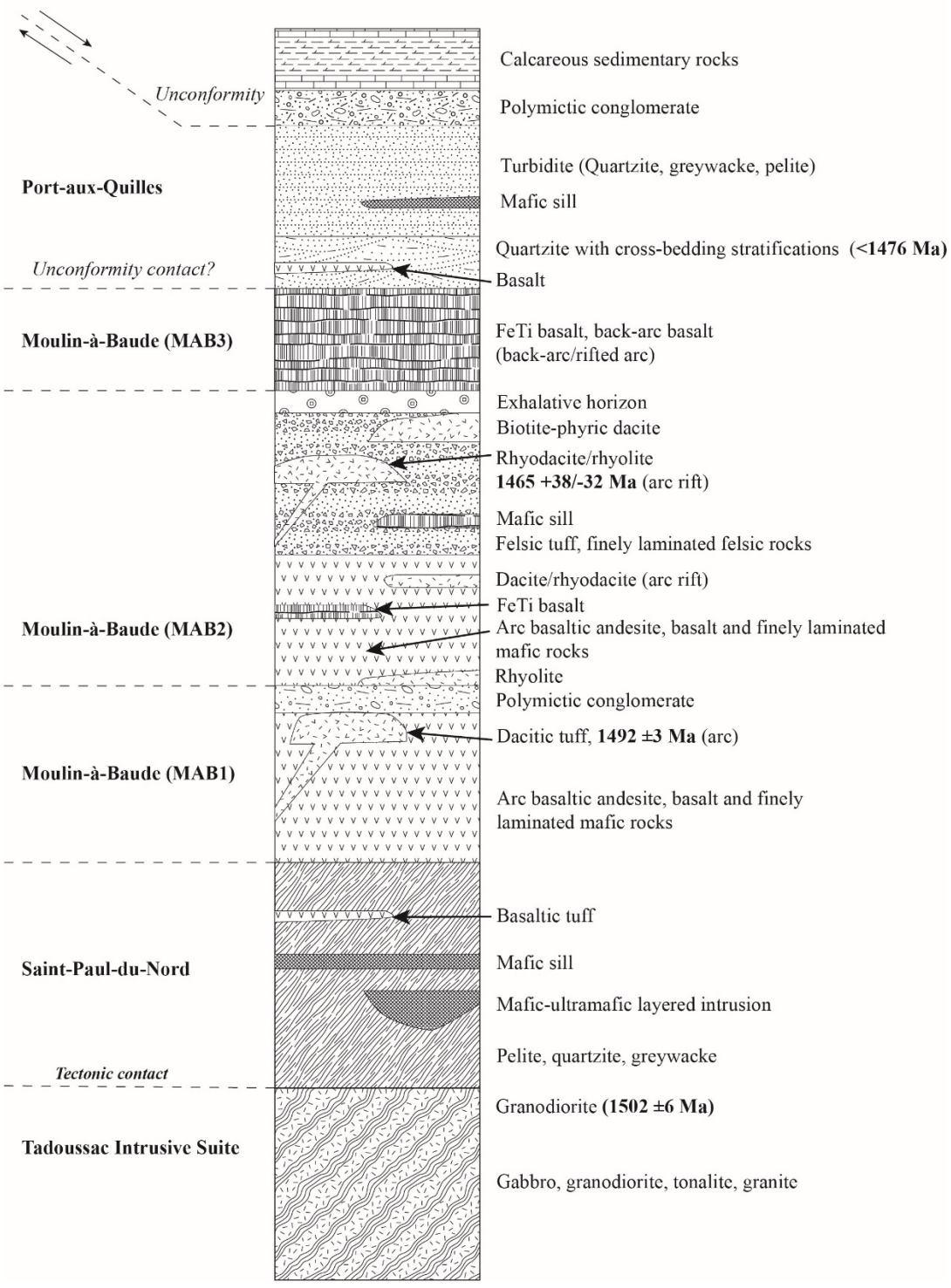

Figure 0.3: Schematic stratigraphic section of the ESB.

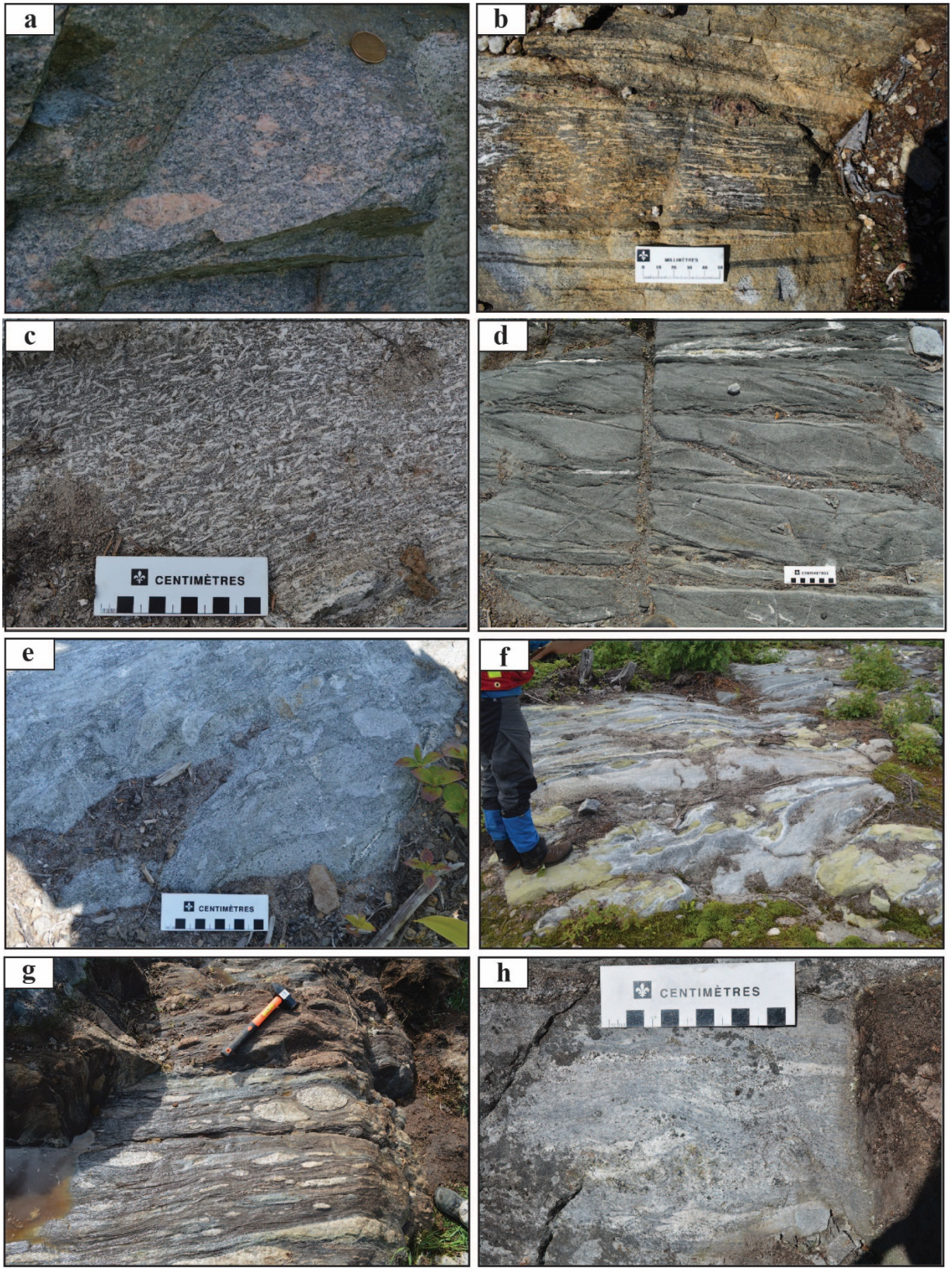
a
b
c
CENTIMÈTRES
d
e
CENTIMÈTRES
f
g
h
CENTIMÈTRES

(Previous page) **Figure 0.4: (a)** Granodiorite from the TIS with K-feldspar megacrysts. **(b)** Greywacke, quartzite and pelite assemblage with a bed of mafic lapilli tuff from the Saint-Paul-du-Nord Formation. **(c)** Plagioclase-phyric basalt from the Moulin-à-Baude Formation (MAB1). **(d)** Stretched pillowed basalt from the Moulin-à-Baude Formation (MAB1). **(e)** Autoclastic basaltic breccia from the Moulin-à-Baude Formation (MAB1). **(f)** Stockwork of quartz-epidote veins cross-cutting basaltic rocks of the Moulin-à-Baude Formation (MAB1). **(g)** Polymictic conglomerate marking the limit between MAB1 and MAB2 of the Moulin-à-Baude Formation in the Lac Saint-Onge synform. **(h)** Dacitic tuff with lapilli from MAB2 of the Moulin-à-Baude Formation.

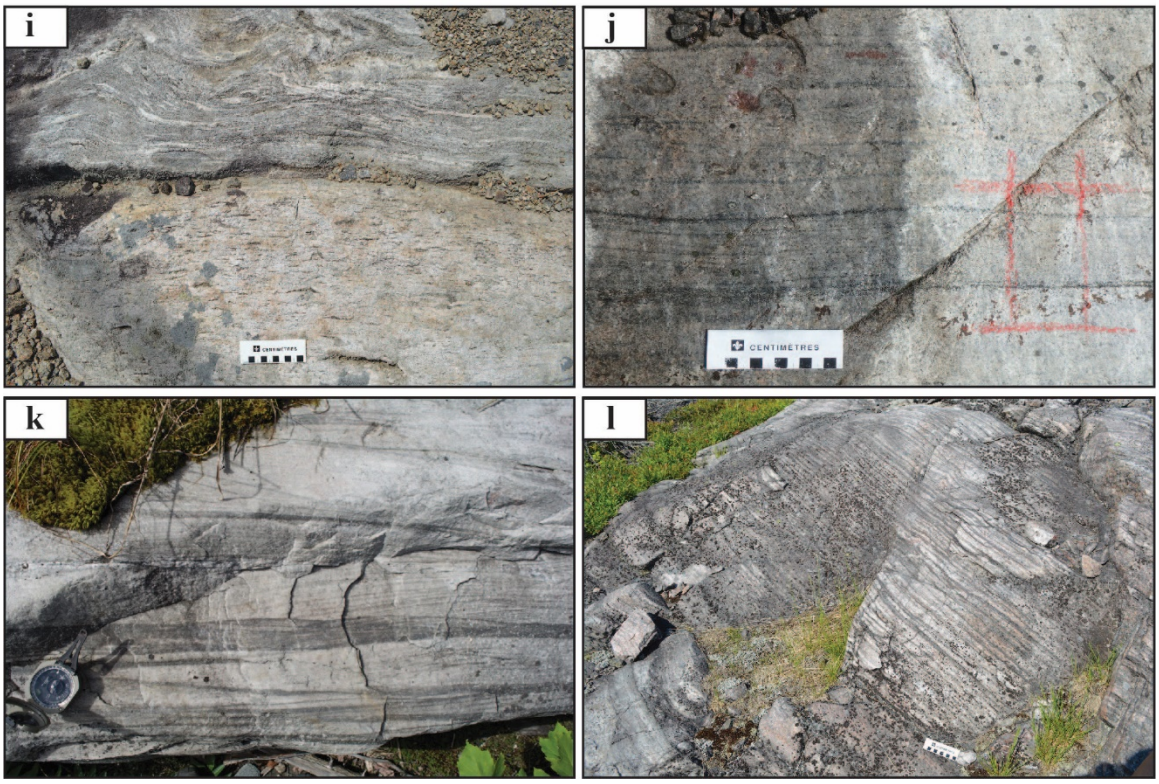

Figure 0.4 (continued): (i) Contact between a rhyolite with clasts of biotite-muscovite (bottom part of the picture) and a dacitic tuff with lapilli (upper part of the picture) from MAB2. **(j)** Impure quartzite (sub-litharenite) with cross-bedding stratification marked by the presence of heavy mineral enriched laminations from the contact between the Moulin-à-Baude and Port-aux-Quilles formations in the Baie-des-Bacon synform. **(k)** Quartzite and thin iron formation from the Moulin-à-Baude Formation. **(l)** Greywacke-quartzite-metapelite assemblage with thin laminae (rhythmites), Port-aux-Quilles Formation.

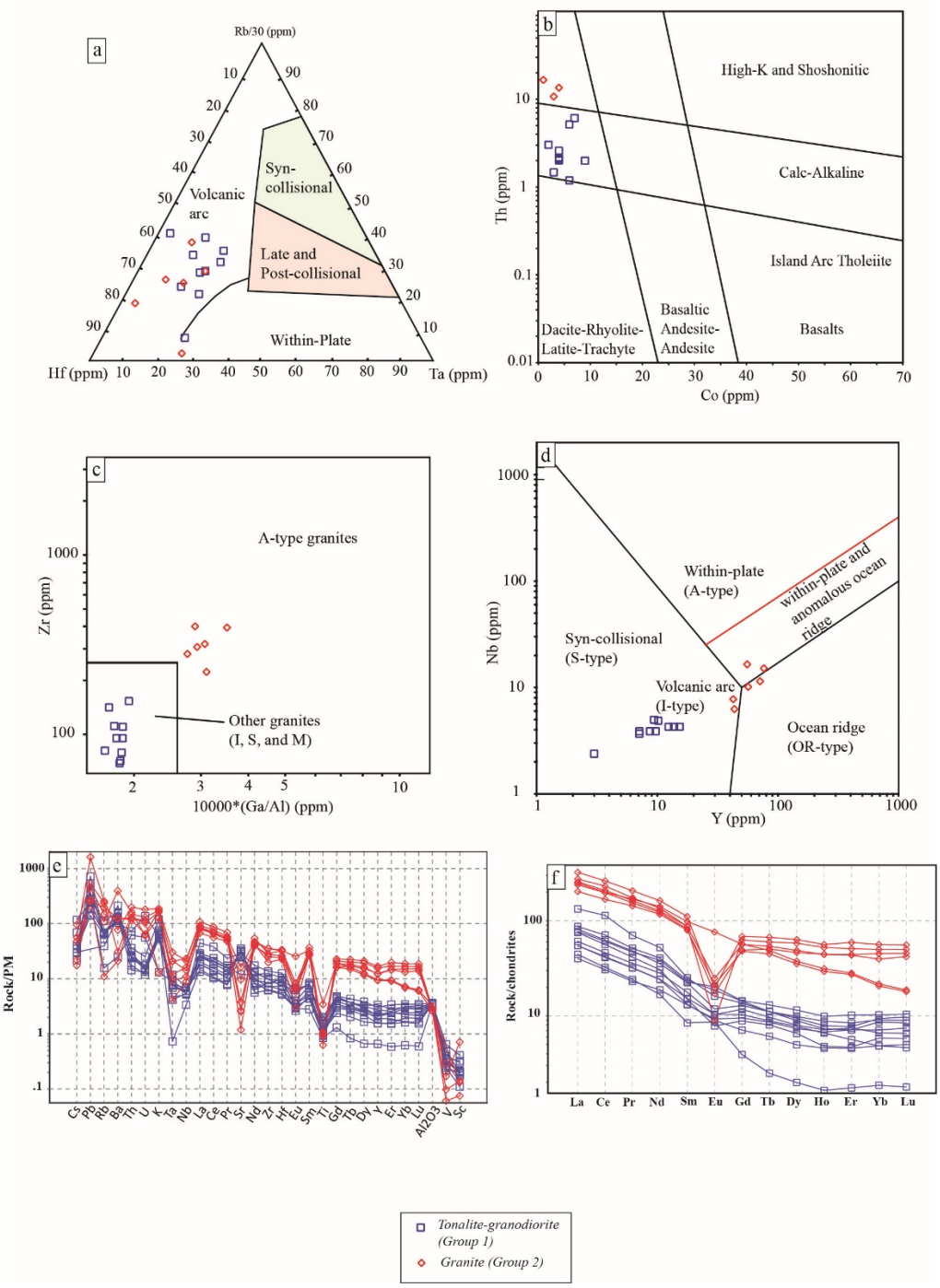

Figure 0.5: Geochemistry of plutonic rocks of the Tadoussac Intrusive Suite. **(a)** Rb/30 vs Ta vs Hf diagram for felsic igneous rocks (Harris et al., 1986). **(b)** Th vs Co for igneous rock classification (Hastie et al., 2007). **(c)** Diagram 10^4 Ga/Al vs Zr (Whalen et al., 1987). I-type = igneous source, S-type = crustal source, A-type = alkaline. **(d)** Y vs Nb from Pearce et al. (1984) for felsic volcanic and intrusive rocks. **(e)** Primitive mantle-normalized extended trace element diagram (Sun and McDonough, 1989). **(f)** REE normalized to chondrite (Sun and McDonough, 1989).

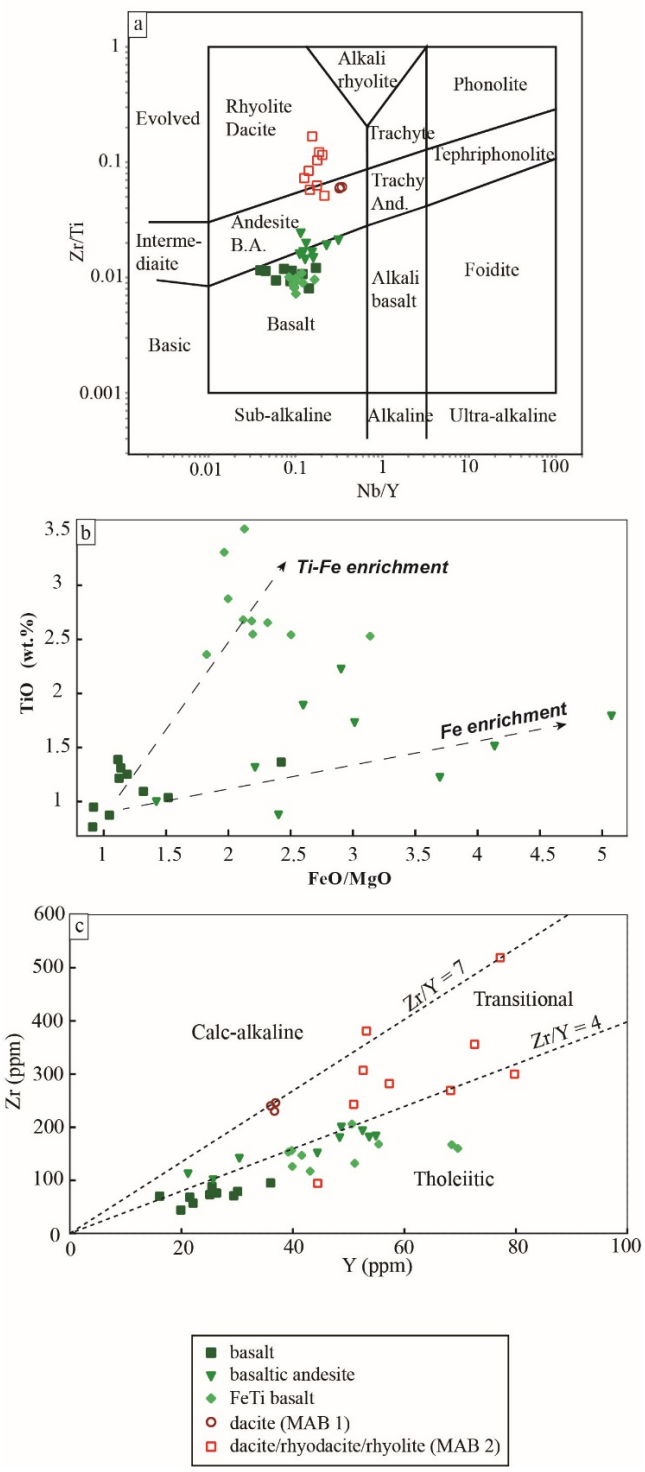

Figure 0.6: Geochemistry of volcanic rocks from the Moulin-à-Baude Formation. **(a)** Nb/Y vs Zr/Ti diagram for volcanic rock classification (Pearce et al., 1982 after Winchester and Floyd, 1977). **(b)** FeO/MgO vs TiO_2 diagram (Miyashiro 1974) for mafic rocks. **(c)** Y vs Zr plot for volcanic rocks (Barret and MacLean, 1999) showing general tholeiitic character of mafic rocks and wide scatter of felsic volcanic rocks.

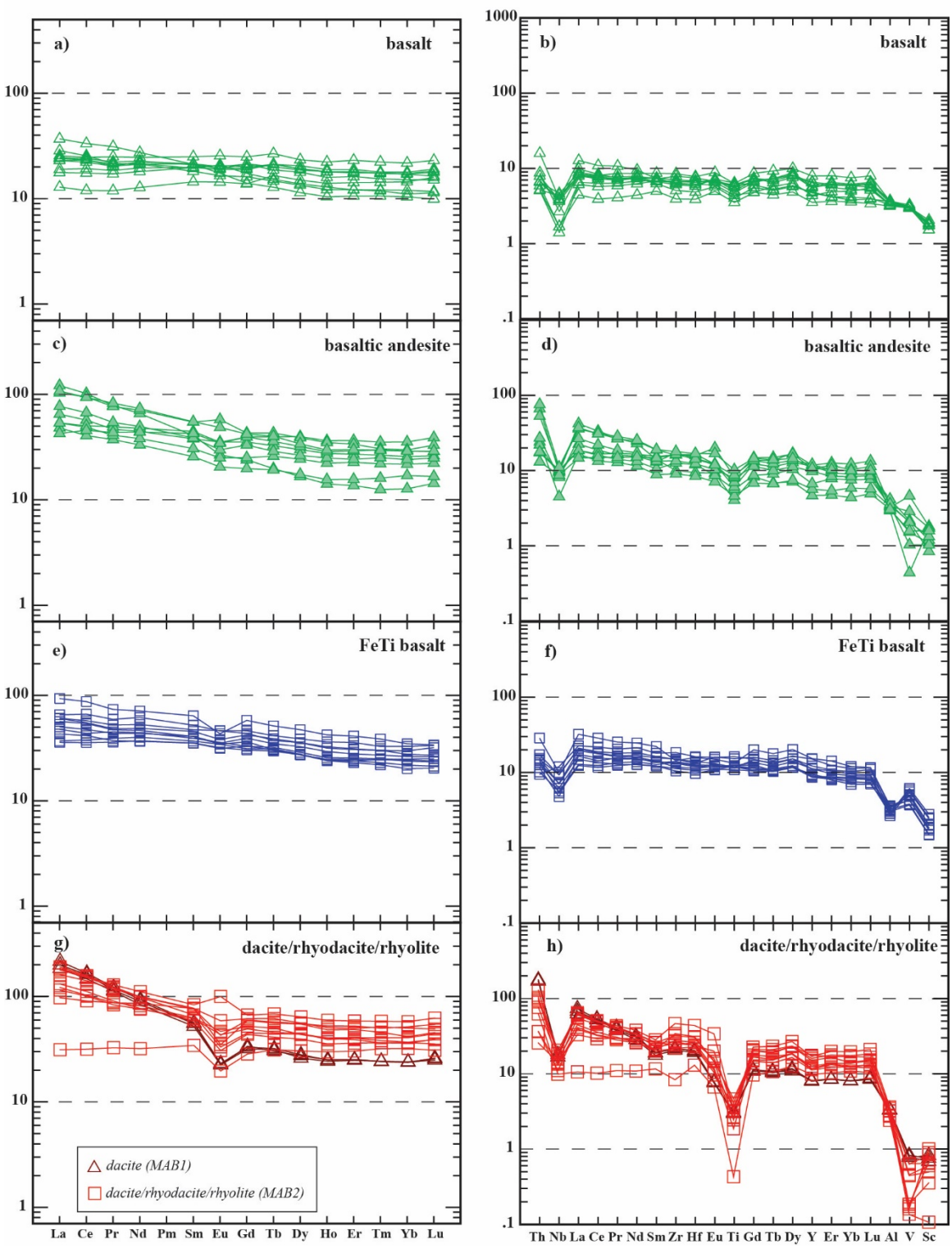

Figure 0.7: REE plots normalized to chondrite **(a, c, e and g)** or extended trace element diagram normalized to primitive mantle **(b, d, f and h)** showing groups of volcanic rocks. Values after Sun and McDonough (1989).

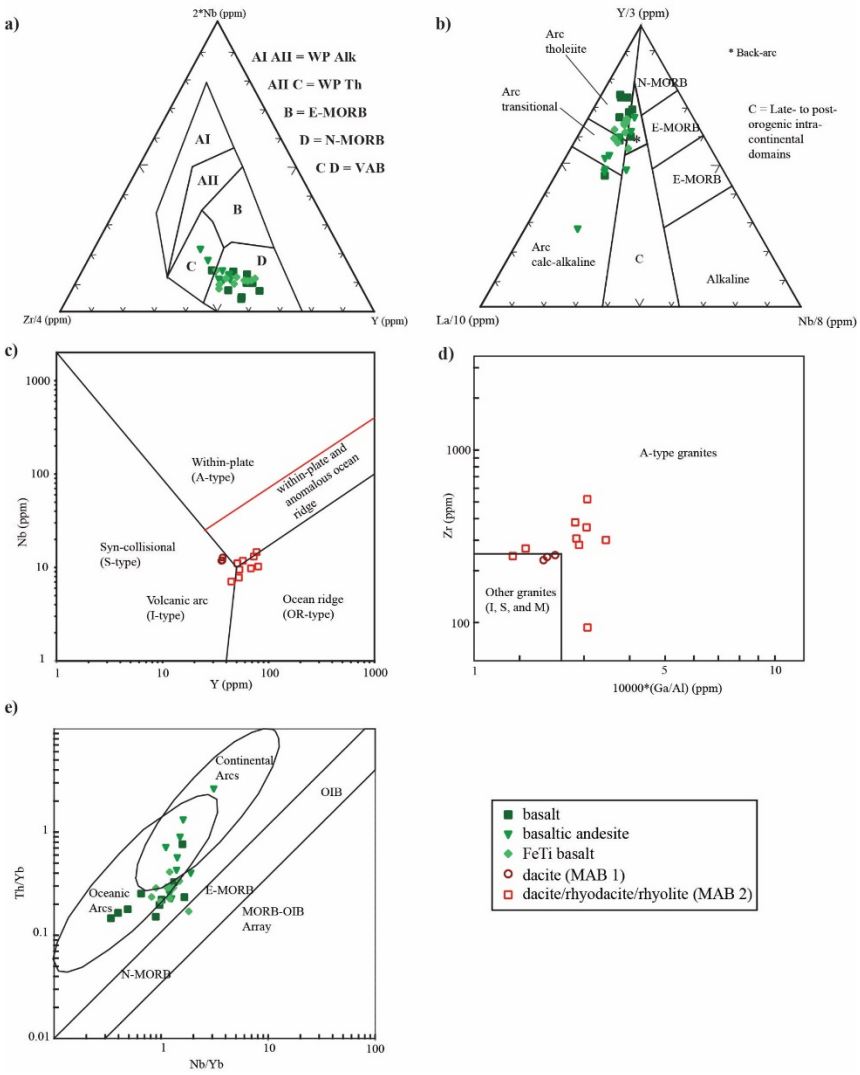

Figure 0.8: (a) Nb*2 vs Zr/4 vs Y diagram for volcanic rock tectonic discrimination (Meschede, 1986). AI-AII = within-plate alkali, AII-C= within-plate tholeiitic, B= E-MORB, D= N-MORB and CD= volcanic arc basalt. **(b)** Ternary diagram Y/15 vs La/10 vs Nb/8 for volcanic rock tectonic discrimination (Cabanis and Lecolle, 1989). **(c)** Y vs Nb diagram from Pearce et al. (1984) for felsic volcanic and intrusive rocks. **(d)** Plot of 10^4 Ga/Al vs Zr (Whalen et al., 1987). I-type = igneous source, S-type = crustal source, M-type = mantle-derived, A-type = alkaline. **(e)** Nb/Yb vs Th/Yb diagram from Pearce (2014).

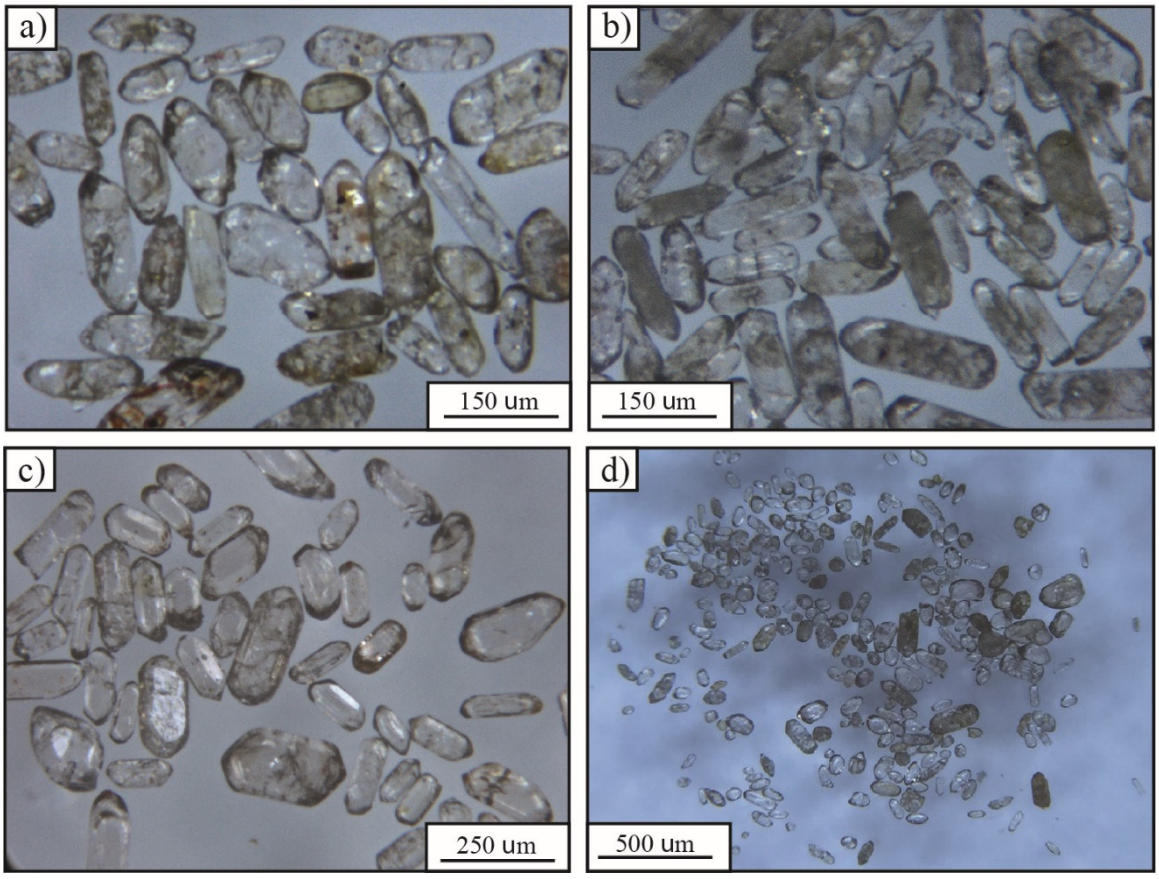

Figure 0.9: Photomicrographs of selected zircon grains under a binocular microscope. **(a)** dacitic tuff (13-PA-32-A); **(b)** rhyolitic tuff (15-PA-95-A); **(c)** granodiorite (15-PA-125-A); and **(d)** impure quartzite (13-PA-2).

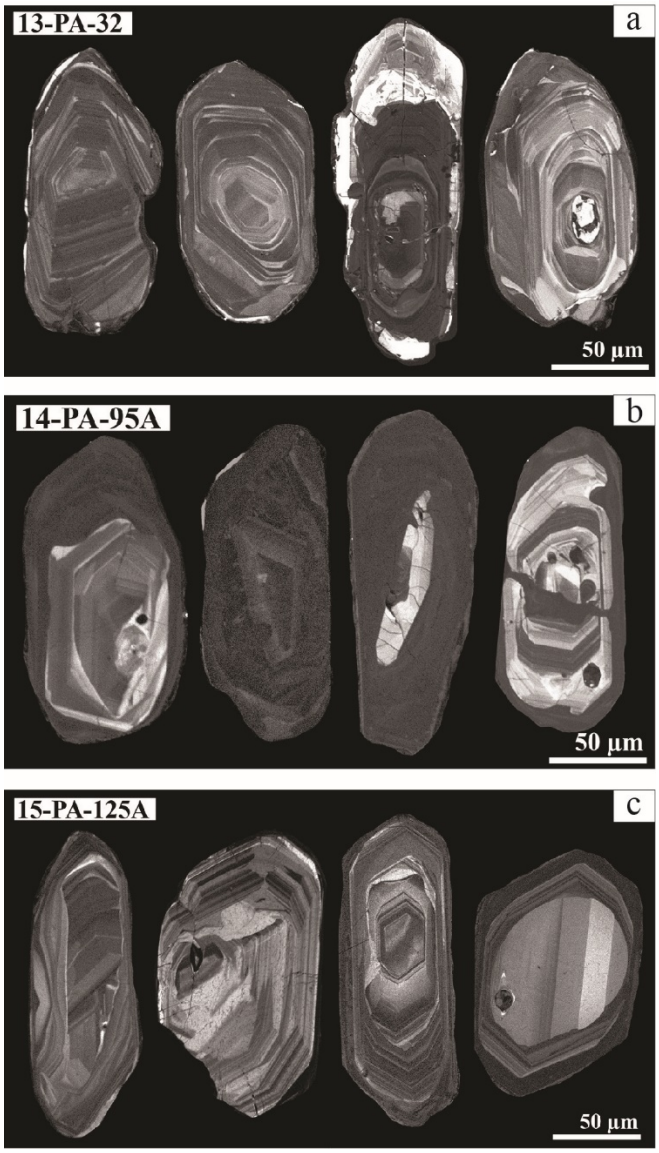

Figure 0.10: Cathodoluminescence images of representative zircon grains with igneous growth zoning and internal complexity, some with non-luminescent outer zones from: **(a)** dacitic tuff (13-PA-32-A); **(b)** rhyolitic tuff (15-PA-95-A); **(c)** granodiorite (15-PA-125-A).

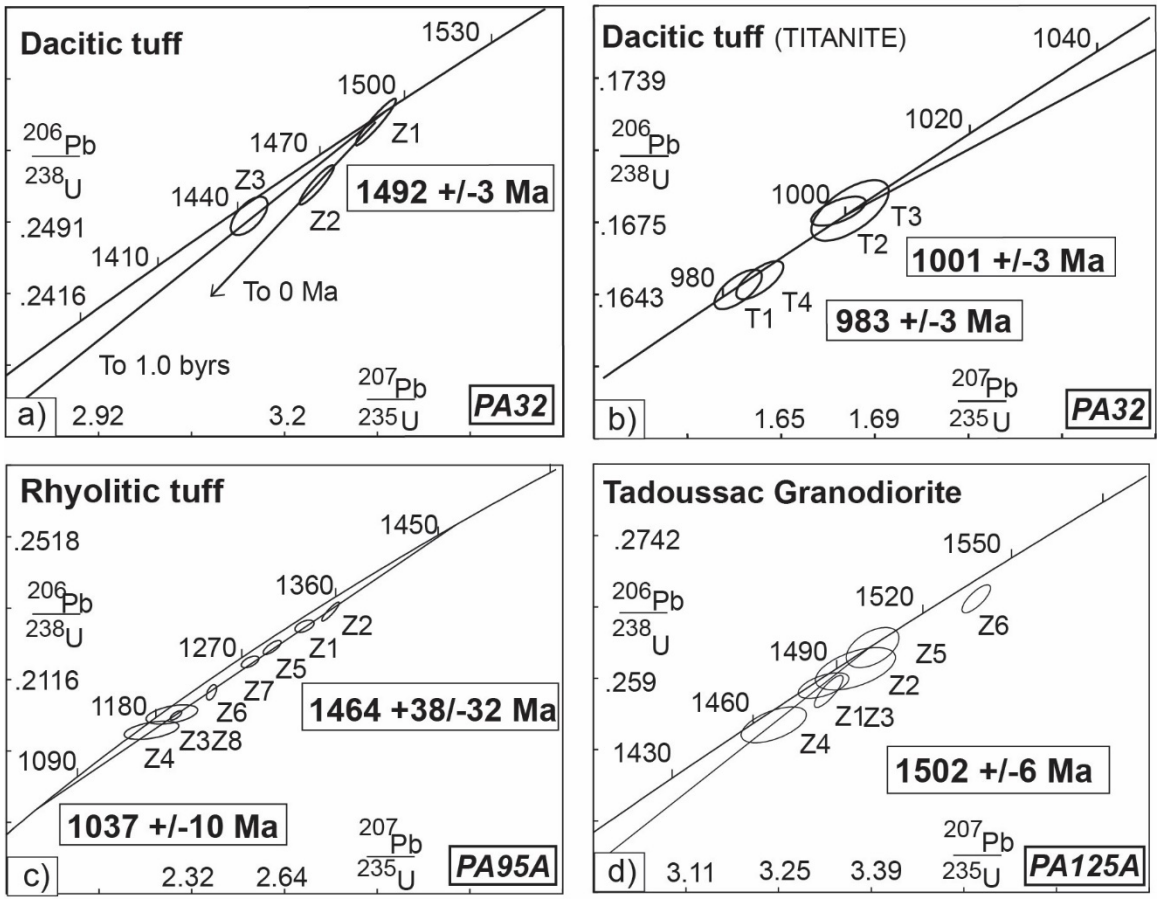

Figure 0.11: Concordia diagrams of CA-TIMS U/Pb analyses of zircon grains from: **(a)** dacitic tuff collected in the Moulin-à-Baude Formation (MAB1) in the Lac Saint-Onge synform; **(c)** rhyolitic tuff from the Moulin-à-Baude Formation (MAB2) sampled in the Lac Raymond synform; **(d)** granodiorite from the Tadoussac Intrusive Suite; and **(b)** concordia diagram of CA-TIMS U/Pb analyses of titanite grains dacitic tuff (PA-32-A).

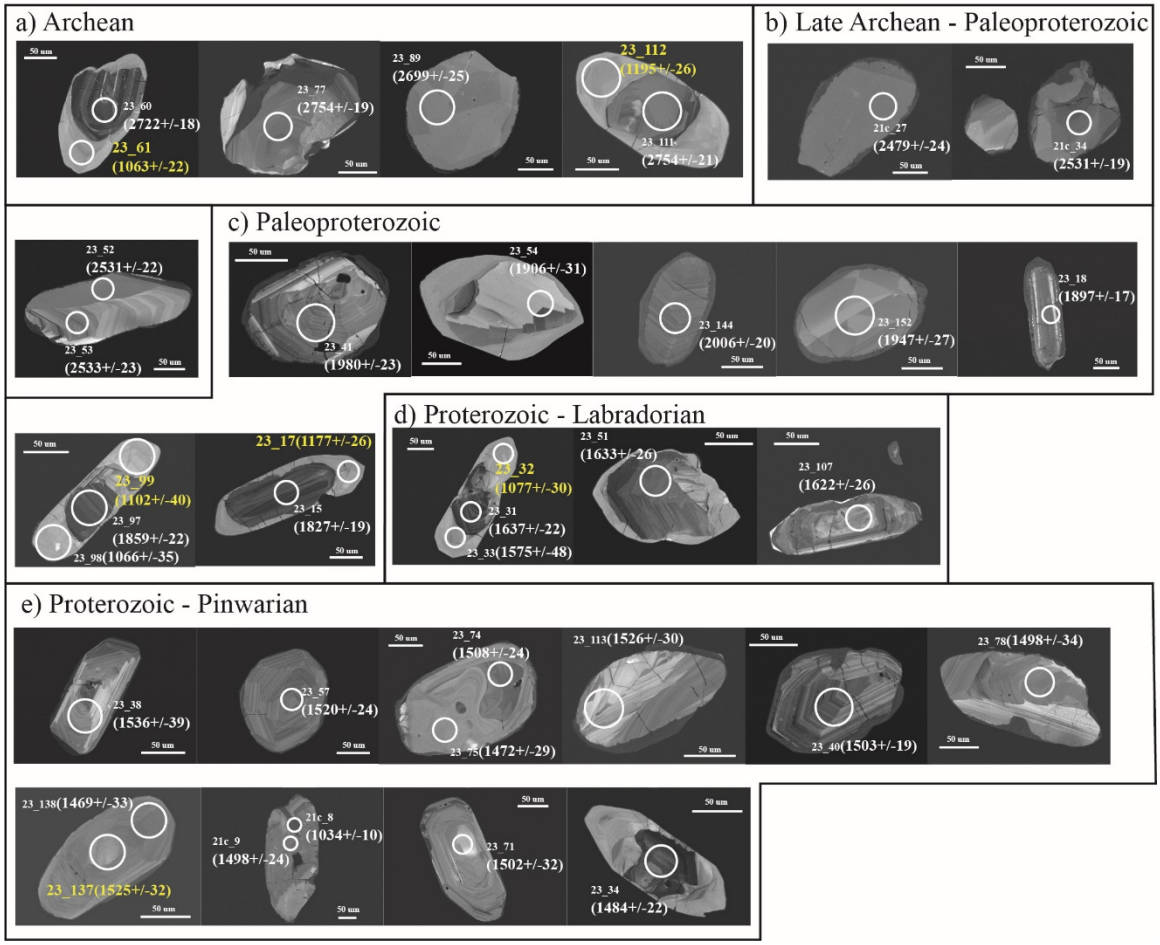

Figure 0.12: Cathodoluminescence images of representative zircon grains with igneous growth zoning and internal complexity, some with non-luminescent outer zones from an impure quartzite (13-PA-2). The white circles represent the area ablated and dated using LA-ICP-MS, the first numbers correspond to the number of the analysis and the ones in parenthesis correspond to the age. Yellow ages represent discordant data.

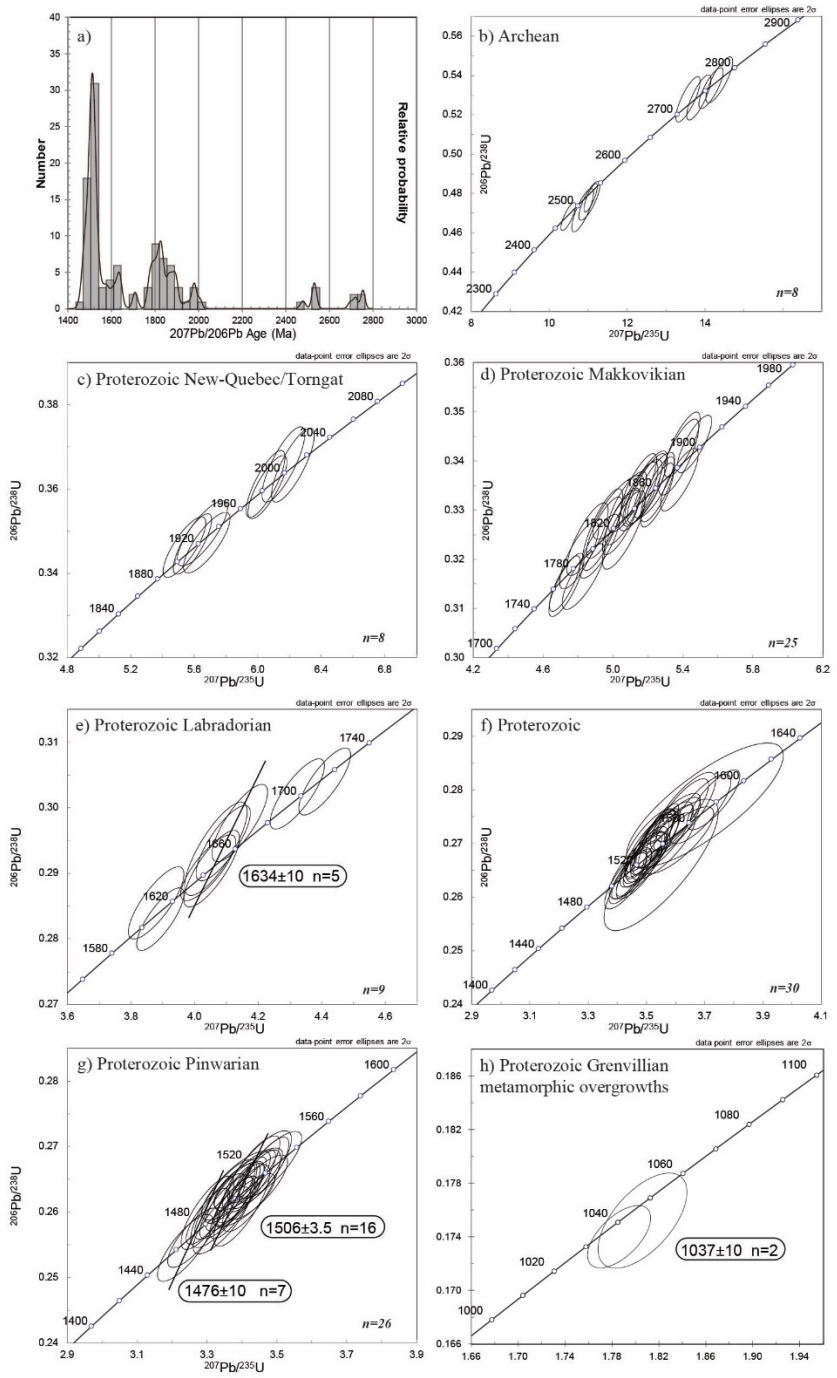

Figure 0.13: Results of CA-laser ICP-MS analysis of 130 detrital zircon from impure quartzite (13-PA-2) of the Port-aux-Quilles Formation. All zircon was chemically abraded (cf. Mattinson, 2005), annealed at 1000°C for 36 hours then HF etched at 200°C for 5 hours. **(a)** Histogram displaying relative abundance of detrital zircon versus $^{207}Pb/^{206}Pb$ ages. **(b to h)** Concordia diagrams of LA-ICP-MS U/Pb analyses. Ages have been calculated for selected sets of closely overlapping analyses.

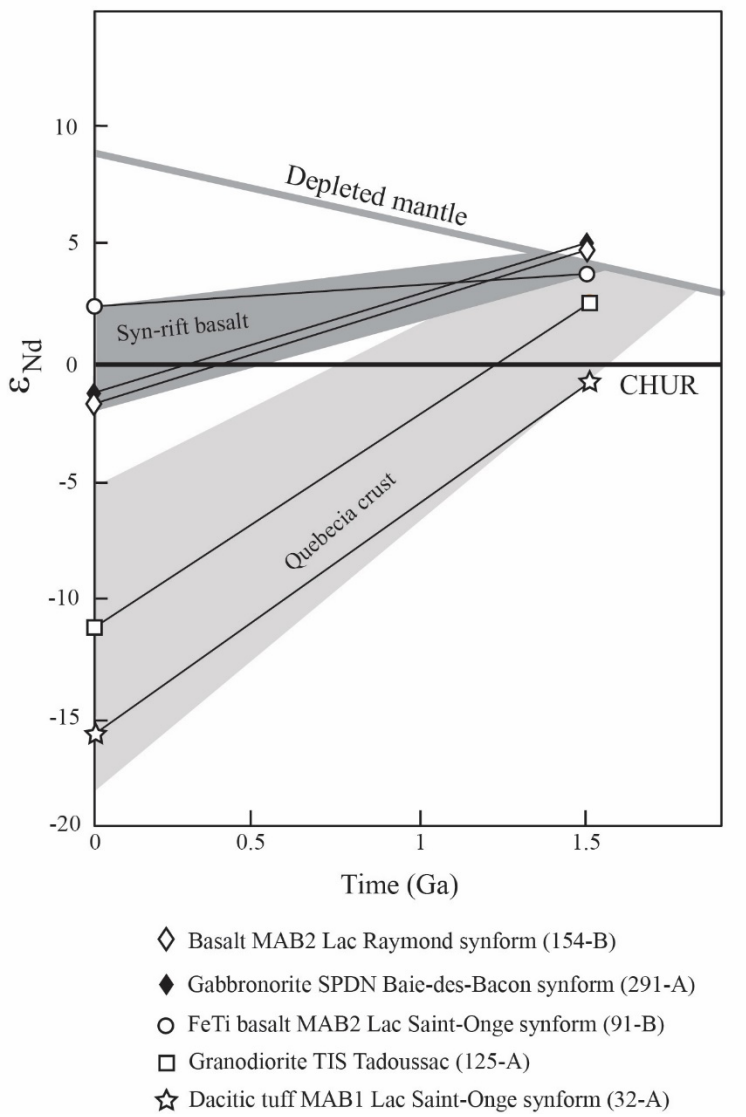

Figure 0.14: Initial εNd versus age diagram for volcanic and intrusive rocks from the ESB. Data for Quebecia crust are after Owens and Tomascak (2002) based on data by Dickin and Higgins (1992) and Dickin (2000). MAB: Moulin-à-Baude Formation; PAQ: Port-aux-Quilles Formation; TIS: Tadoussac Intrusive Suite.

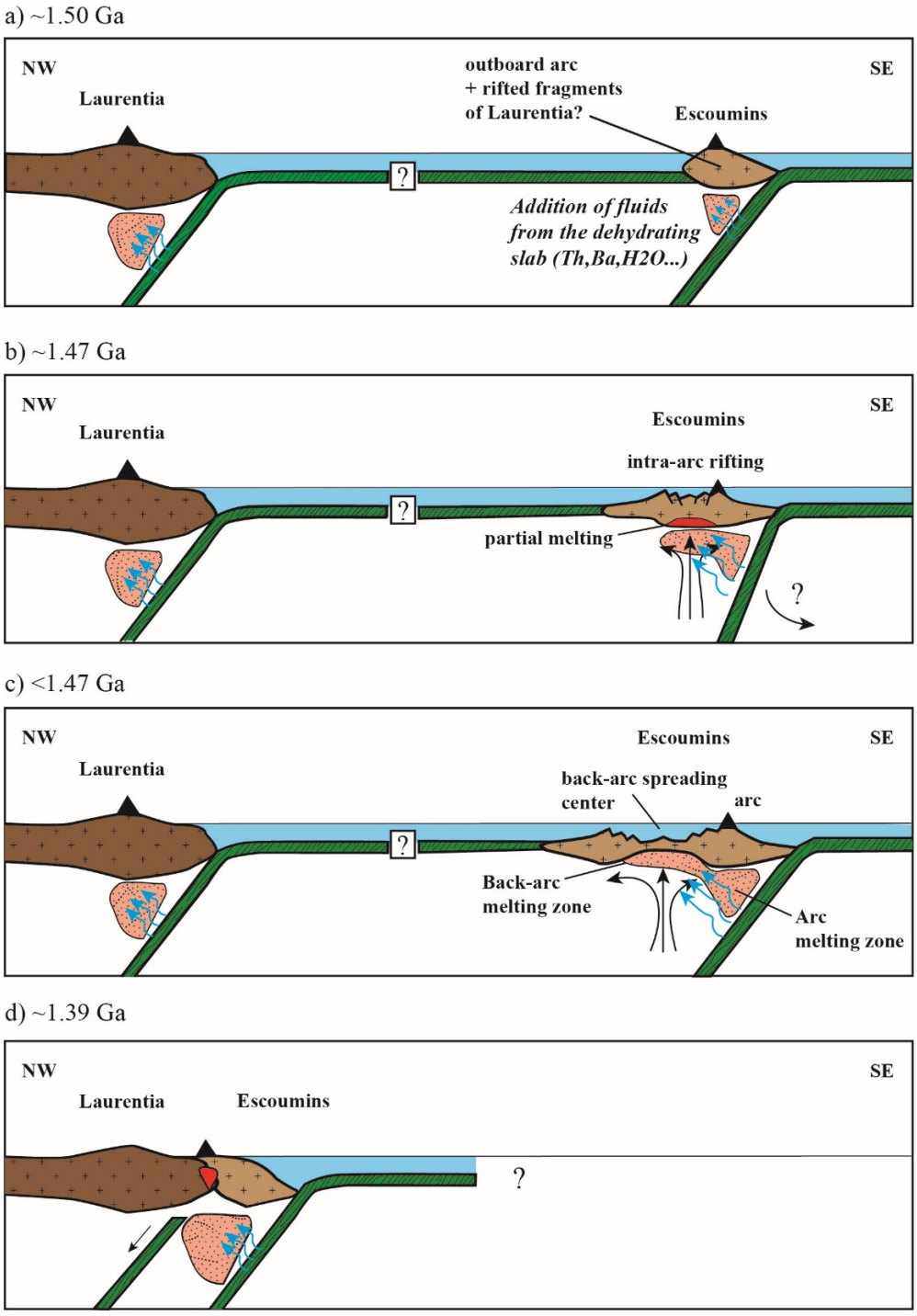

Figure 0.15: Proposed model for the tectonic evolution of the ESB. **(a)** At ~1.5 Ga, the ESB is an oceanic arc separated from Laurentian by an ocean. **(b)** At ~1.47 Ga the island arc experienced an intra-arc rifting event. **(c)** After 1.47 Ga the rifting led to the opening of a back-arc basin filled with basaltic rocks and then epiclastic sediments. **(d)** At ~1.39 Ga the island arc and back-arc is accreted to Laurentia.

Table 0.1: Whole rock geochemistry of the plutonic rocks from the Tadoussac Intrusive Suite, ordered by geochemical signature (calc-alkalic for the group 1 and alkalic for the group 2). Abbreviations: Ton.=tonalite; Grd.=granodiorite; Gra.=granite ; LOI=loss on ignition.

sample	54701	54708	54709	54719	54721	54727	53067	53068	54748	54718	54702	53077	54710	53078	54720	54349
Rock type	Ton.	Grd.	Grd.	Grd.	Grd.	Grd.	Ton.	Ton.	Grd.	Gra.	Ton.	Grd.	Gra.	Gra.	Gra.	Gra.
Group	1	1	1	1	1	1	1	1	1	1	2	2	2	2	2	2
SiO2(wt.%)	72.49	71.59	71.30	69.25	71.64	66.76	68.56	70.71	68.04	72.79	76.59	65.56	75.40	76.30	77.52	75.41
Al2O3	14.31	15.78	15.80	15.61	15.30	16.00	15.41	15.48	16.20	15.21	11.62	14.36	12.92	11.60	11.57	11.83
Fe2O3(T)	2.81	2.28	2.02	3.05	2.02	4.21	2.35	2.11	3.57	1.64	2.19	7.34	2.30	2.29	1.78	2.54
FeO	2.16	1.72	1.50	2.33	1.52	3.30	1.78	1.62	2.77	1.18	1.66	5.87	1.78	1.75	1.36	1.96
Fe2O3	0.44	0.39	0.37	0.49	0.35	0.58	0.39	0.33	0.52	0.35	0.36	0.89	0.35	0.37	0.28	0.38
MgO	0.41	0.73	0.70	1.11	0.61	1.55	0.76	0.54	1.04	0.44	0.23	0.52	0.15	0.12	0.08	0.27
MnO	0.028	0.049	0.046	0.060	0.050	0.079	0.045	0.037	0.085	0.030	0.018	0.101	0.022	0.018	0.022	0.035
CaO	2.63	2.80	2.59	3.58	2.46	4.03	2.91	2.91	3.52	1.79	1.86	2.67	0.67	0.79	0.53	0.49
Na2O	6.07	4.97	5.19	4.46	4.72	4.24	4.75	4.59	4.69	4.69	4.95	3.68	3.40	3.04	3.24	3.16
K2O	0.38	1.83	2.00	1.76	2.02	1.65	1.88	2.17	1.53	3.45	0.37	3.70	5.44	4.69	5.01	5.02
TiO2	0.289	0.241	0.220	0.342	0.203	0.428	0.238	0.181	0.368	0.196	0.210	0.735	0.197	0.217	0.134	0.230
P2O5	0.06	0.08	0.06	0.12	0.06	0.17	0.07	0.07	0.18	0.06	0.02	0.14	0.02	< 0.01	0.02	0.04
Cr2O3	0.01	0.01	0.01	0.01	0.01	0.01	< 0.01	< 0.01	0.01	0.01	0.01	< 0.01	0.01	< 0.01	0.01	< 0.01
LOI	0.81	0.50	0.53	0.63	0.50	0.46	0.77	1.24	0.56	0.50	0.39	0.42	0.30	0.35	0.25	0.45
Total	100.30	100.80	100.50	99.97	99.58	99.59	97.94	100.20	99.79	100.80	98.45	100.10	100.80	99.72	100.20	99.48
Sr (ppm)	253	686	692	603	650	514	683	748	519	544	204	346	54	80	25	56
Ba	177	791	941	733	1072	863	824	1483	901	1120	147	2760	540	851	216	881
Nb	4.3	4.9	3.9	3.9	3.7	4.3	3.9	2.4	4.3	5	10.2	6.3	15.2	7.8	11.5	16.6
V	29	29	26	40	22	53	28	20	33	18	24	14	8	< 5	5	< 5
Co	6	4	4	7	4	9	4	3	6	2	3	4	1	< 1	< 1	< 1
Ga	13	15	14	16	15	15	15	15	16	15	17	22	21	18	19	22
Ge	1.4	1.5	1.4	1.7	1.3	1.7	1.4	1.3	1.3	1.4	1.3	2.1	2.1	1.9	2.1	1.8
In	0.1	< 0.1	< 0.1	< 0.1	< 0.1	< 0.1	< 0.1	< 0.1	< 0.1	< 0.1	0.1	< 0.1	0.2	< 0.1	0.1	< 0.1

Sn	2	2	2	2	2	3	< 1	< 1	< 1	2	3	2	4	2	4	3
Cs	1.6	0.9	0.8	0.8	0.7	2.7	0.8	0.5	0.7	0.7	1.1	1.1	1.3	0.4	2.2	0.5
Pb	18	18	10	26	13	17	51	38	< 3	20	19	19	115	32	38	18
Be	2	2	2	1	1	2	1	1	1	2	1	2	3	2	3	3
Hf	3.2	2.6	2.0	3.9	2.3	2.8	1.7	1.6	2.3	3.0	7.4	9.9	10.1	8.1	7.0	10.4
Ta	0.37	0.32	0.32	0.31	0.19	0.31	0.17	0.03	0.28	0.49	0.87	0.17	1.24	0.38	0.49	0.85
W	0.8	< 0.5	0.6	1.5	1.2	1.1	< 0.5	< 0.5	< 0.5	< 0.5	1	0.8	0.7	< 0.5	0.8	0.6
Tl	0.05	0.25	0.23	0.35	0.28	0.29	0.25	0.21	0.14	0.46	0.08	0.42	1.18	0.55	0.96	0.66
Bi	0.3	< 0.1	< 0.1	0.2	< 0.1	0.2	< 0.1	< 0.1	< 0.1	< 0.1	< 0.1	< 0.1	< 0.1	< 0.1	< 0.1	< 0.1
Th	5.20	2.18	2.02	6.14	2.61	2.01	2.10	1.48	1.20	3.05	10.80	13.60	16.70	10.70	12.40	9.94
U	1.18	0.37	0.37	2.86	0.30	0.32	0.31	0.25	0.28	0.53	2.35	1.28	3.82	2.18	2.76	1.36
Rb	10	42	40	44	43	43	42	34	25	71	7	69	163	95	151	126
Y	12.4	10.2	8.7	9.7	7.1	13.8	7.1	3.0	15.3	9.4	56.7	43.6	76.4	42.6	71.1	55.6
Zr	141	95	81	153	79	111	71	69	110	95	281	400	319	307	223	394
La	19.3	14.4	13.0	31.6	17.8	18.3	13.0	10.5	20.6	9.5	56.6	59.3	76.6	48.1	60.8	65.1
Ce	38.5	28.3	25.7	69.8	34.5	37.3	25.2	19.8	43.4	18.8	121.0	122.0	161.0	103.0	128.0	142.0
Pr	4.47	3.32	2.98	6.52	3.84	4.34	2.96	2.24	4.77	2.14	14.30	15.70	19.20	13.30	15.10	16.20
Nd	16.20	12.90	11.10	23.90	14.00	17.60	11.00	7.66	18.50	8.59	55.90	64.40	74.30	53.50	57.90	62.00
Sm	3.31	2.62	2.26	3.72	2.21	3.35	1.96	1.25	3.51	1.93	12.10	14.50	16.40	11.80	12.90	12.90
Eu	0.665	0.582	0.585	0.907	0.441	1.140	0.506	0.486	1.050	0.524	0.967	4.290	1.110	1.190	0.500	1.400
Gd	2.56	2.33	2.05	2.71	1.76	2.87	1.41	0.78	2.84	1.89	9.77	11.30	13.60	9.54	12.50	11.20
Tb	0.40	0.35	0.32	0.40	0.29	0.47	0.22	0.09	0.40	0.31	1.82	1.76	2.42	1.62	2.16	1.95
Dy	2.32	1.96	1.90	2.19	1.61	2.83	1.22	0.49	2.42	1.81	11.40	9.25	15.60	8.67	14.30	12.00
Ho	0.43	0.39	0.36	0.40	0.26	0.54	0.25	0.09	0.48	0.37	2.43	1.71	3.07	1.60	2.86	2.41
Er	1.23	1.19	0.90	1.14	0.75	1.63	0.73	0.28	1.35	1.14	7.07	4.51	9.48	4.36	8.14	6.95
Tm	0.217	0.177	0.123	0.169	0.129	0.265	0.116	0.042	0.214	0.212	1.040	0.608	1.400	0.615	1.240	0.995
Yb	1.51	1.07	0.78	1.14	0.94	1.65	0.78	0.30	1.46	1.39	7.26	3.49	9.06	3.32	8.04	6.38
Lu	0.239	0.161	0.123	0.183	0.142	0.256	0.114	0.044	0.220	0.207	1.120	0.461	1.370	0.443	1.230	1.030

Cd	< 0.5	< 0.5	< 0.5	< 0.5	< 0.5	< 0.5	< 0.5	< 0.5	< 0.5	< 0.5	< 0.5	< 0.5	< 0.5	< 0.5	< 0.5	< 0.5
Cu	60	< 1	2	6	3	9	10	8	1	11	105	24	6	6	5	8
Ag	0.3	< 0.3	< 0.3	< 0.3	< 0.3	< 0.3	< 0.3	< 0.3	< 0.3	< 0.3	0.6	< 0.3	0.5	0.5	0.5	2.8
Ni	9	6	7	6	5	12	9	6	6	4	7	2	1	3	2	2
Mo	1	< 1	< 1	< 1	2	< 1	< 1	< 1	< 1	2	1	< 1	2	< 1	1	3
Zn	16	42	43	44	44	62	69	61	54	26	9	125	47	45	46	69
S	400	< 100	< 100	< 100	< 100	< 100	300	200	< 100	< 100	300	600	< 100	< 100	< 100	< 100
Au	< 2	< 2	< 2	< 2	< 2	< 2	< 2	< 2	< 2	< 2	< 2	< 2	< 2	< 2	< 2	< 2
As	5.5	< 0.5	< 0.5	< 0.5	< 0.5	< 0.5	4.9	4.2	< 0.5	< 0.5	5.2	< 0.5	< 0.5	2.6	< 0.5	< 0.5
Br	< 0.5	< 0.5	< 0.5	< 0.5	< 0.5	< 0.5	< 0.5	< 0.5	< 0.5	< 0.5	< 0.5	< 0.5	< 0.5	< 0.5	< 0.5	< 0.5
Cr	32	31	43	24	31	30	39	29	16	28	44	25	32	38	17	28
Sc	5.6	3.2	3.4	3.5	3.0	7.1	3.6	1.9	5.2	3.7	2.4	12.3	2.4	2.3	1.3	2.3
Sb	1.3	< 0.1	< 0.1	< 0.1	< 0.1	< 0.1	0.7	0.6	0.2	< 0.1	0.6	0.1	< 0.1	< 0.1	< 0.1	< 0.1
La/Yb	12.78	13.46	16.67	27.72	18.94	11.09	16.67	35.00	14.11	6.86	7.80	16.99	8.45	14.49	7.56	10.20
Th/Yb	3.44	2.04	2.59	5.39	2.78	1.22	2.69	4.93	0.82	2.19	1.49	3.90	1.84	3.22	1.54	1.56

Table 0.2: Whole rock geochemistry of volcanic rocks from the Moulin-à-Baude Formation. The felsic volcanic rocks are separated in three groups based on their signature and their stratigraphic position (dac.1 corresponds to calc-alkaline dacite from MAB1 (Group 1, loc.C), dac.2 and rhyod.2 correspond to transitional to calc-alkaline dacite and rhyodacite from MAB2 (Group 2, loc.E), and rhyo.3-dac.3 corresponds to tholeiitic rhyolite/dacite from MAB2 (Group 3, loc.D);Figures 4, 5 and 6). Abbreviations: bas.=basalt; B.A=basaltic andesite; FT-bas.=FeTi basalt; dac.=dacite; rhyod.=rhyodacite; rhyo.=rhyolite; LOI=loss on ignition.

sample	**54689**	**54758**	**53090**	**54367**	**54366**	**54369**	**54759**	**54760**	**54687**	**54783**	**54357**	**53082**	**54356**	**54764**	**54688**
Rock type	bas.	bas.	bas.	bas.	bas.	bas.	bas.	bas.	bas.	bas.	B.A	B.A	B.A	B.A	B.A
SiO2(wt.%)	46.32	49.23	53.58	46.83	47.63	49.26	47.99	48.89	46.31	50.12	59.62	53.91	60.57	51.34	56.96
Al2O3	14.86	15.24	14.57	16.94	17.20	16.20	15.26	15.24	16.88	16.81	14.24	15.52	15.83	19.27	15.94
Fe2O3tot	11.72	10.36	9.44	12.70	12.19	11.36	12.60	12.06	14.55	10.52	9.06	10.13	9.14	10.33	12.49
FeO	9.82	8.49	7.58	10.47	9.95	9.09	10.18	9.64	11.85	8.16	7.30	8.17	7.06	8.06	9.84
Fe2O3	0.92	1.02	1.10	1.19	1.24	1.37	1.40	1.46	1.52	1.54	1.03	1.15	1.37	1.47	1.66
MgO	10.79	8.12	8.26	6.90	7.55	8.09	8.57	8.47	4.89	7.33	3.04	5.74	1.91	3.64	2.38
MnO	0.202	0.183	0.160	0.213	0.195	0.204	0.208	0.199	0.249	0.186	0.156	0.171	0.138	0.217	0.254
CaO	9.12	10.23	7.37	9.01	9.61	8.68	10.26	9.15	10.12	9.82	4.34	7.42	5.55	8.60	6.02
Na2O	2.37	3.16	4.39	3.34	2.71	3.26	2.43	3.30	1.51	1.64	3.02	3.38	4.48	3.67	3.65
K2O	0.15	0.64	0.14	0.23	0.14	0.30	0.61	0.37	1.65	1.80	3.90	1.27	0.70	0.88	0.87
TiO2	0.765	0.874	0.949	1.037	1.094	1.216	1.252	1.310	1.365	1.389	0.876	0.998	1.222	1.315	1.511
P2O5	0.07	0.14	0.13	0.11	0.12	0.16	0.14	0.14	0.15	0.12	0.44	0.14	0.23	0.20	0.43
Cr2O3	0.08	0.05	0.04	< 0.01	< 0.01	0.04	0.06	0.07	< 0.01	0.03	< 0.01	< 0.01	< 0.01	0.01	< 0.01
LOI	1.57	1.78	0.92	0.77	0.68	0.87	1.17	0.77	1.23	1.26	0.80	1.29	0.40	0.77	0.46
Total	97.95	99.97	100.20	98.08	99.12	99.61	100.50	99.89	98.90	101.00	99.49	100.40	100.20	100.20	101.00
Sr(ppm)	192	296	368	188	222	306	351	391	168	251	402	205	311	317	280
Ba	23	85	31	28	31	60	197	265	202	495	761	271	200	192	285
Nb	1.2	2.7	2.8	1.0	1.2	1.9	2.6	2.8	3.3	3.1	6.7	3.2	7.0	6.1	7.2
V	250	248	245	242	255	245	252	258	268	253	124	234	172	178	85
Co	51	41	36	51	52	45	47	47	59	42	17	35	18	36	24
Ga	16	16	18	18	19	18	19	18	20	17	16	18	20	21	22

Ge	1.9	1.6	2.3	1.8	1.8	2.0	1.8	1.4	1.7	1.7	1.2	2.0	1.5	1.5	1.5
In	< 0.1	< 0.1	< 0.1	< 0.1	< 0.1	< 0.1	< 0.1	< 0.1	< 0.1	< 0.1	< 0.1	< 0.1	< 0.1	< 0.1	< 0.1
Sn	< 1	< 1	< 1	< 1	< 1	< 1	< 1	< 1	< 1	< 1	1	< 1	1	2	2
Cs	0.3	1.0	< 0.1	< 0.1	0.1	0.2	1.5	0.3	1.4	1.8	3.2	1.0	1.1	1.1	3.7
Pb	< 3	< 3	10	< 3	4	5	< 3	< 3	4	13	9	8	4	12	7
Be	< 1	< 1	< 1	< 1	< 1	< 1	1	< 1	< 1	< 1	2	< 1	2	2	< 1
Hf	1.2	1.5	1.9	2.1	2.0	2.3	1.9	2.1	2.4	1.8	2.9	2.6	3.7	4.5	5.1
Ta	0.06	0.15	0.14	0.05	0.05	0.08	0.13	0.16	0.14	0.20	0.33	0.17	0.46	0.36	0.47
W	< 0.5	< 0.5	< 0.5	< 0.5	< 0.5	< 0.5	< 0.5	1.7	< 0.5	< 0.5	0.9	0.9	0.9	0.6	0.6
Tl	< 0.05	0.12	0.06	< 0.05	0.07	< 0.05	0.11	< 0.05	0.25	0.25	0.93	0.24	0.20	0.11	0.12
Bi	0.1	< 0.1	< 0.1	< 0.1	< 0.1	< 0.1	< 0.1	< 0.1	0.2	< 0.1	< 0.1	< 0.1	< 0.1	0.2	0.1
Th	0.44	0.67	1.35	0.43	0.50	0.74	0.57	0.57	0.56	0.44	5.63	2.04	1.47	1.86	1.50
U	0.18	0.36	0.71	0.23	0.24	0.33	0.28	0.32	0.37	0.17	1.41	0.50	0.89	0.83	0.65
Rb	4	24	2	4	2	8	23	9	56	49	141	39	13	16	18
Y	19.9	22.1	16.1	25.1	26.3	25.5	29.4	30.1	36.0	21.5	21.2	25.7	30.4	52.5	53.7
Zr	44	57	70	73	76	88	71	79	95	68	112	101	141	193	181
La	3.05	6.76	8.75	4.19	4.50	5.82	5.45	5.70	6.06	5.46	28.80	11.40	12.70	15.40	12.70
Ce	7.31	15.60	20.40	10.70	11.80	14.70	13.60	14.30	15.10	14.20	62.40	24.90	29.90	34.90	30.90
Pr	1.13	2.05	2.96	1.63	1.76	2.12	1.93	1.94	2.37	2.02	7.45	3.54	3.89	4.44	4.68
Nd	5.96	9.93	12.80	8.44	9.13	10.60	9.94	10.40	11.50	10.10	30.80	15.50	17.80	20.80	22.30
Sm	2.21	2.78	3.24	3.02	3.04	3.21	3.27	3.28	3.82	2.96	6.23	3.93	4.69	5.80	6.82
Eu	0.834	0.959	1.010	1.100	1.200	1.130	1.170	1.110	1.480	1.210	1.550	1.190	1.450	2.050	2.040
Gd	2.84	3.31	2.88	3.89	4.12	3.98	4.36	4.40	5.12	3.57	4.93	4.06	5.16	7.27	8.10
Tb	0.62	0.55	0.48	0.79	0.79	0.79	0.70	0.75	1.00	0.57	0.74	0.72	0.97	1.22	1.48
Dy	3.81	3.41	2.90	4.88	5.21	4.89	4.53	4.75	5.94	3.51	4.22	4.43	6.17	7.60	10.10
Ho	0.79	0.69	0.59	1.01	1.07	1.02	0.90	1.02	1.26	0.73	0.80	0.88	1.26	1.56	2.06
Er	2.35	2.01	1.75	2.99	3.13	2.97	2.68	2.90	3.83	2.00	2.26	2.59	3.75	4.48	6.05
Tm	0.364	0.308	0.270	0.441	0.456	0.444	0.393	0.448	0.568	0.302	0.319	0.409	0.561	0.676	0.900

Yb	2.46	2.04	1.77	2.94	3.03	2.92	2.57	2.90	3.70	1.88	2.16	2.89	3.70	4.38	6.02
Lu	0.404	0.297	0.252	0.464	0.484	0.451	0.383	0.416	0.586	0.289	0.364	0.423	0.565	0.664	0.989
Cd	< 0.5	< 0.5	< 0.5	< 0.5	< 0.5	< 0.5	< 0.5	< 0.5	< 0.5	0.5	< 0.5	< 0.5	< 0.5	0.6	< 0.5
Cu	97	11	91	5	22	38	125	64	2	145	2	15	7	87	39
Ag	< 0.5	< 0.3	0.3	< 0.5	< 0.5	< 0.5	< 0.3	< 0.3	< 0.5	< 0.3	0.6	< 0.3	0.7	< 0.3	1.2
Ni	198	102	101	75	70	110	145	161	33	113	7	24	3	56	4
Mo	< 1	1	< 1	< 1	< 1	< 1	< 1	1	< 1	< 1	< 1	< 1	< 1	< 1	< 1
Zn	68	88	81	93	101	125	98	112	111	76	109	78	107	115	121
S	300	< 100	100	400	500	400	< 100	< 100	400	400	300	< 100	400	200	200
Au	< 2	< 2	< 2	< 2	< 2	< 2	< 2	< 2	< 2	< 2	< 2	< 2	< 2	< 2	< 2
As	< 0.5	< 0.5	< 0.5	< 0.5	< 0.5	< 0.5	< 0.5	< 0.5	1.1	< 0.5	< 0.5	2.5	1.5	< 0.5	< 0.5
Br	< 0.5	< 0.5	< 0.5	< 0.5	< 0.5	< 0.5	< 0.5	< 0.5	< 0.5	< 0.5	< 0.5	< 0.5	< 0.5	< 0.5	< 0.5
Cr	614	278	262	14	29	312	360	404	31	216	23	37	14	31	32
Fe	8.04	6.74	6.32	8.75	7.97	7.99	8.11	8.16	9.05	7.33	6.28	6.48	6.09	7.01	8.24
Ir	< 5	< 5	< 5	< 5	< 5	< 5	< 5	< 5	< 5	< 5	< 5	< 5	< 5	< 5	< 5
Na	1.58	2.18	3.03	2.28	1.83	2.22	1.62	2.16	0.89	1.34	2.08	2.23	3.02	2.62	2.27
Sc	34.9	32.4	26.1	29.6	30.1	32.1	29.6	31.3	26.0	32.3	18.7	29.6	14.4	20.4	17.6
Sb	0.4	1.2	0.6	< 0.1	< 0.1	0.4	0.5	< 0.1	0.4	< 0.1	< 0.1	0.3	< 0.1	0.5	0.3
(La/Sm)n	0.89	1.57	1.75	0.90	0.96	1.17	1.08	1.12	1.03	1.19	2.99	1.87	1.75	1.72	1.20
(La/Yb)n	0.89	2.38	3.55	1.02	1.07	1.43	1.52	1.41	1.18	2.08	9.57	2.83	2.46	2.52	1.51
(Th/La)n	1.17	0.80	1.25	0.83	0.90	1.03	0.85	0.81	0.75	0.65	1.58	1.45	0.94	0.98	0.95
(Nb/La)n	0.38	0.38	0.31	0.23	0.26	0.31	0.46	0.47	0.52	0.55	0.22	0.27	0.53	0.38	0.55
Mg#	66	63	66	54	57	61	60	61	42	62	43	56	33	45	30

Table 2.2: (cont.)

sample	54765	54362	54761	53081	53091	54766	53086	53087	54779	54780	54782	54767	54770	54763
Rock type	B.A	B.A	B.A	B.A	FT-bas.	FT-bas.	FT-bas.	FT-bas.	FT-bas.	FT-bas.	FT-bas.	FT-bas.	FT-bas.	FT-bas.
SiO2(wt.%)	53.43	58.15	49.53	52.61	49.13	52.55	46.18	45.82	47.71	48.98	47.89	47.17	44.29	44.34
Al2O3	14.92	13.60	16.65	14.08	12.30	14.03	15.46	14.44	13.16	13.25	14.87	16.71	16.17	15.98
Fe2O3tot	13.58	13.16	14.77	12.95	14.88	15.83	17.89	16.20	17.32	16.80	15.63	14.78	16.89	17.63
FeO	10.64	10.20	11.57	9.61	11.25	11.95	13.82	12.27	13.20	12.71	11.63	10.69	12.21	12.69
Fe2O3	1.88	1.94	2.04	2.37	2.51	2.68	2.69	2.70	2.81	2.82	2.83	3.03	3.46	3.67
MgO	3.53	2.01	4.45	3.31	6.16	3.81	5.52	5.59	5.70	5.81	5.49	5.35	6.21	5.96
MnO	0.221	0.291	0.245	0.269	0.235	0.229	0.262	0.205	0.261	0.262	0.202	0.116	0.248	0.246
CaO	7.35	5.01	7.34	7.35	8.76	6.84	8.84	8.51	9.40	9.19	8.26	6.81	8.64	8.68
Na2O	3.81	3.71	3.65	3.07	2.75	2.88	2.70	3.16	1.19	1.16	2.26	1.09	2.04	2.89
K2O	1.02	1.56	0.41	1.51	0.21	1.25	0.12	0.10	0.70	0.97	2.57	3.33	0.62	0.17
TiO2	1.730	1.791	1.890	2.224	2.360	2.530	2.542	2.548	2.655	2.670	2.682	2.876	3.306	3.522
P2O5	0.28	0.81	0.28	0.52	0.28	0.42	0.32	0.32	0.32	0.29	0.28	0.48	0.50	0.51
Cr2O3	0.01	< 0.01	0.01	< 0.01	0.02	0.01	0.01	0.01	0.03	0.03	0.02	0.01	0.01	0.02
LOI	0.52	0.29	1.03	0.67	0.54	0.30	0.41	0.52	0.75	0.88	0.73	1.42	0.34	0.33
Total	100.40	100.40	100.30	99.41	98.42	100.70	100.20	98.07	99.18	100.30	100.90	100.10	99.25	100.30
Sr(ppm)	379	402	272	512	316	489	278	264	312	296	246	195	270	389
Ba	336	806	172	309	31	525	42	46	144	174	266	270	225	20
Nb	5.8	7.6	6.2	7.9	3.8	6.6	3.4	4.0	4.4	5.0	5.1	7.1	6.7	8.5
V	377	36	168	129	453	302	407	417	478	503	313	349	392	354
Co	33	15	41	27	45	42	59	56	38	46	44	71	53	52
Ga	20	21	24	20	22	22	24	24	18	22	22	25	26	22
Ge	1.6	1.9	1.8	2.4	3.0	1.7	2.0	2.6	1.5	1.7	1.7	1.3	1.3	1.7
In	< 0.1	< 0.1	< 0.1	< 0.1	< 0.1	0.1	< 0.1	< 0.1	0.1	0.1	0.1	0.1	0.1	0.1

Sn	1	2	2	3	1	2	1	1	1	1	1	2	2	2
Cs	0.6	10.5	0.5	1.8	< 0.1	20.4	< 0.1	< 0.1	0.5	0.5	11.2	2.8	0.9	0.2
Pb	< 3	14	< 3	27	10	< 3	12	7	< 3	< 3	10	11	< 3	10
Be	1	2	2	2	2	2	1	1	1	1	2	2	2	2
Hf	3.8	4.9	4.4	5.2	3.3	4.3	3.9	3.8	3.0	3.5	3.7	4.9	4.1	5.0
Ta	0.35	0.45	0.36	0.55	0.20	0.38	0.34	0.20	0.25	0.32	0.36	0.44	0.38	0.57
W	< 0.5	0.7	0.6	1.0	0.5	1.1	0.8	0.8	0.6	< 0.5	2.7	2.3	0.5	0.6
Tl	0.10	0.37	< 0.05	0.24	< 0.05	2.12	< 0.05	< 0.05	0.1	0.16	0.51	0.64	0.11	< 0.05
Bi	< 0.1	0.2	< 0.1	< 0.1	< 0.1	0.5	< 0.1	< 0.1	< 0.1	< 0.1	0.1	0.2	< 0.1	< 0.1
Th	2.30	4.49	1.11	6.41	1.22	1.46	0.98	0.86	1.08	1.31	1.15	2.43	1.26	0.80
U	0.82	1.61	0.51	2.63	0.44	0.64	0.35	0.37	0.41	0.53	0.49	3.18	0.74	0.31
Rb	21	69	10	38	2	356	2	1	15	25	85	67	28	4
Y	44.4	48.4	54.9	48.7	39.9	55.4	39.8	39.2	43.1	51.1	41.6	69.6	68.5	50.6
Zr	151	180	183	200	126	168	156	153	117	132	147	160	167	206
La	18.30	24.50	10.10	25.50	8.48	14.30	11.30	8.76	10.20	11.90	13.40	22.10	14.40	15.50
Ce	41.00	57.90	27.90	57.40	21.80	33.70	26.70	23.10	25.40	29.10	33.10	53.40	35.20	40.60
Pr	5.15	7.30	4.13	7.85	3.42	4.58	4.28	3.71	3.53	4.14	4.48	6.99	4.98	5.63
Nd	23.20	33.00	20.50	34.30	17.30	22.70	20.70	18.70	17.10	20.40	21.70	33.20	24.70	28.80
Sm	5.91	8.35	6.52	8.42	5.40	6.97	6.00	5.64	5.39	6.23	6.23	9.80	7.22	7.98
Eu	1.730	3.350	2.000	2.820	1.850	2.210	2.080	1.990	1.820	2.040	1.990	2.510	2.690	2.670
Gd	6.80	8.84	8.12	8.64	6.23	8.67	6.74	6.41	6.78	8.07	7.46	11.90	9.48	8.94
Tb	1.08	1.61	1.34	1.50	1.11	1.45	1.20	1.16	1.13	1.30	1.14	1.92	1.55	1.40
Dy	6.71	9.85	8.14	8.62	6.92	9.04	7.32	7.04	6.94	8.29	6.95	12.00	9.82	9.03
Ho	1.41	1.98	1.62	1.68	1.40	1.84	1.45	1.36	1.39	1.66	1.36	2.39	2.05	1.79
Er	4.01	5.58	4.81	4.95	4.08	5.16	4.21	3.94	3.96	4.60	3.81	6.80	5.91	5.06
Tm	0.640	0.778	0.761	0.751	0.621	0.765	0.639	0.634	0.587	0.691	0.559	0.983	0.836	0.769
Yb	4.10	5.06	4.94	4.91	4.24	5.06	4.17	4.04	3.70	4.47	3.43	5.91	5.57	4.69
Lu	0.633	0.838	0.729	0.736	0.636	0.811	0.605	0.595	0.540	0.665	0.518	0.859	0.849	0.687

Cd	0.6	< 0.5	< 0.5	< 0.5	0.6	< 0.5	< 0.5	< 0.5	0.6	0.7	< 0.5	1.0	< 0.5	0.7
Cu	61	2	42	73	79	38	176	120	145	102	14	44	47	77
Ag	0.3	0.9	< 0.3	< 0.3	< 0.3	< 0.3	< 0.3	< 0.3	< 0.3	< 0.3	< 0.3	< 0.3	< 0.3	< 0.3
Ni	12	2	37	5	54	33	83	76	49	49	37	40	47	92
Mo	< 1	< 1	< 1	< 1	< 1	< 1	< 1	< 1	< 1	< 1	< 1	1	< 1	< 1
Zn	103	151	142	139	110	137	122	110	127	124	192	166	146	131
S	100	300	100	100	< 100	< 100	< 100	< 100	100	< 100	300	3900	700	800
Au	< 2	< 2	< 2	< 2	< 2	< 2	< 2	< 2	< 2	< 2	< 2	< 2	< 2	< 2
As	6.3	< 0.5	< 0.5	2.5	< 0.5	< 0.5	2.0	2.1	< 0.5	< 0.5	< 0.5	462.0	< 0.5	< 0.5
Br	< 0.5	< 0.5	< 0.5	< 0.5	< 0.5	< 0.5	< 0.5	< 0.5	< 0.5	< 0.5	< 0.5	< 0.5	< 0.5	< 0.5
Cr	30	< 5	46	17	130	28	78	80	146	170	88	36	61	109
Fe	8.86	8.81	9.68	8.29	9.39	9.67	11.30	9.91	10.10	10.80	9.26	8.69	10.80	11.50
Ir	< 5	< 5	< 5	< 5	< 5	< 5	< 5	< 5	< 5	< 5	< 5	< 5	< 5	< 5
Na	2.75	2.53	2.48	2.08	1.77	2.02	1.76	2.13	0.80	0.81	1.53	0.76	1.45	2.02
Sc	31.0	29.2	22.7	27.2	41.5	25.2	34.1	34.7	43.1	47.6	25.7	29.3	31.3	30.7
Sb	0.7	< 0.1	0.4	1.0	0.2	0.8	0.3	0.6	0.4	0.7	1.1	1.0	0.3	0.5
(La/Sm)n	2.00	1.90	1.00	1.96	1.01	1.33	1.22	1.00	1.22	1.23	1.39	1.46	1.29	1.26
(La/Yb)n	3.20	3.47	1.47	3.73	1.44	2.03	1.94	1.56	1.98	1.91	2.80	2.68	1.86	2.37
(Th/La)n	1.02	1.48	0.89	2.03	1.16	0.83	0.70	0.79	0.86	0.89	0.69	0.89	0.71	0.42
(Nb/La)n	0.31	0.30	0.59	0.30	0.43	0.44	0.29	0.44	0.42	0.40	0.37	0.31	0.45	0.53
Mg#	37	26	41	38	49	36	42	45	43	45	46	47	48	46

Table 2.2: (cont.)

sample	54682	54343	54354	54738	54741	54740	54716	54715	54739	54737	53076	54697
Rock type	dac.1	dac.1	dac.1	dac.2	dac.2	dac.2	dac.2	rhyod.2	rhyod.2	rhyod.2	rhyo.3	dac.3
SiO2(wt.%)	65.77	65.57	64.79	66.82	62.75	65.57	64.54	72.38	65.76	76.28	72.39	59.60
Al2O3	15.45	15.11	15.10	14.80	14.65	12.56	16.66	12.74	14.88	11.05	12.93	15.93
Fe2O3tot	5.52	5.98	5.65	7.34	9.61	10.88	6.88	6.05	6.68	2.98	2.25	10.61
FeO	4.30	4.70	4.41	5.83	7.69	8.96	5.48	4.89	5.42	2.21	1.83	8.89
Fe2O3	0.79	0.81	0.80	0.93	1.15	1.02	0.85	0.68	0.71	0.55	0.24	0.83
MgO	1.60	1.55	1.76	0.75	0.54	0.76	1.08	0.28	1.25	0.61	0.69	0.78
MnO	0.079	0.068	0.088	0.074	0.118	0.140	0.090	0.054	0.112	0.101	0.038	0.167
CaO	3.29	3.09	2.67	2.80	2.19	3.72	2.57	2.41	2.43	2.26	1.99	5.10
Na2O	3.02	3.17	3.30	5.57	1.78	2.92	2.05	4.20	2.44	2.36	1.77	3.24
K2O	4.34	3.63	3.89	0.33	6.80	1.38	4.06	1.04	4.62	1.81	5.41	1.31
TiO2	0.638	0.663	0.651	0.778	0.998	0.874	0.699	0.525	0.563	0.401	0.092	0.678
P2O5	0.17	0.17	0.16	0.22	0.46	0.43	0.12	0.18	0.17	0.10	< 0.01	0.40
Cr2O3	< 0.01	< 0.01	< 0.01	0.01	< 0.01	0.01	0.01	0.01	0.01	0.01	< 0.01	< 0.01
LOI	0.79	1.14	0.97	0.37	0.40	0.51	1.82	0.40	0.76	0.74	0.54	0.66
Total	100.70	100.10	99.01	99.87	100.30	99.74	100.60	100.30	99.65	98.67	98.48	98.87
Sr(ppm)	243	301	232	213	262	144	141	200	113	144	164	190
Ba	794	819	674	148	1256	337	1078	60	1219	889	743	281
Nb	11.9	12.8	11.8	11.1	9.5	7.8	14.6	9.8	13.1	11.8	7.0	10.1
V	67	64	63	51	13	14	52	36	37	15	11	15
Co	11	11	10	11	7	9	6	10	10	2	3	8
Ga	19	20	19	15	22	19	27	14	24	17	21	29
Ge	1.7	1.9	1.9	2.3	1.8	2.1	2.2	1.6	2.3	2.2	2.6	3.8
In	< 0.1	< 0.1	< 0.1	0.1	0.1	0.2	0.2	0.2	0.2	0.2	< 0.1	< 0.1
Sn	2	3	2	4	3	4	4	4	5	4	3	2

Cs	3.3	11.1	3.8	0.7	3.7	2.0	3.0	2.2	2.5	3.6	3.3	2.0
Pb	27	26	23	12	16	17	26	98	14	38	20	7
Be	3	3	3	2	2	2	3	4	2	3	2	2
Hf	5.9	6.1	6.3	7.0	9.6	8.1	13.5	8.0	9.4	7.4	4.0	7.3
Ta	0.97	0.90	0.88	0.80	0.60	0.59	1.11	0.93	1.02	1.08	0.61	0.59
W	1.0	3.1	2.5	0.9	1.1	0.6	1.1	1.3	1.1	1.2	< 0.5	1.4
Tl	0.58	0.86	0.89	0.11	0.94	0.34	0.58	0.25	0.67	0.48	0.59	0.22
Bi	< 0.1	< 0.1	< 0.1	< 0.1	0.1	0.1	< 0.1	0.2	0.1	0.1	0.1	< 0.1
Th	14.40	14.50	15.00	6.45	3.07	3.09	8.37	8.76	7.94	10.90	5.29	2.17
U	4.51	4.34	3.50	1.85	1.31	0.97	2.58	2.70	2.92	2.55	1.32	1.08
Rb	162	144	171	11	160	36	93	37	92	70	100	45
Y	36.7	36.9	36.0	50.9	53.2	52.6	77.2	68.3	72.6	57.3	44.5	79.7
Zr	230	246	240	243	381	307	519	269	356	282	93	298
La	42.90	46.20	50.10	30.60	26.70	28.30	42.90	37.40	41.60	44.40	7.23	22.60
Ce	88.40	97.00	100.00	66.80	60.40	61.40	92.60	84.70	90.80	94.60	18.90	54.40
Pr	10.40	10.70	11.40	8.41	7.76	8.14	12.00	10.90	11.50	11.20	3.03	8.12
Nd	38.20	41.00	42.80	35.20	34.70	37.40	50.90	45.70	45.40	45.00	14.60	39.40
Sm	7.79	8.27	8.44	8.83	9.22	9.36	12.50	11.60	11.40	10.00	5.13	11.50
Eu	1.270	1.270	1.310	1.740	2.460	2.650	5.680	1.980	2.430	1.880	1.110	3.340
Gd	6.42	6.77	6.66	8.80	9.88	10.50	13.40	11.90	12.00	9.05	5.71	12.40
Tb	1.14	1.11	1.17	1.50	1.67	1.83	2.50	2.05	2.10	1.63	1.14	2.26
Dy	6.46	6.79	6.95	9.80	11.10	10.80	15.90	13.60	13.70	10.90	7.54	13.90
Ho	1.34	1.39	1.38	1.96	2.16	2.22	3.29	2.67	2.91	2.24	1.65	2.80
Er	4.00	4.07	4.07	5.83	6.52	6.30	9.48	7.86	8.50	6.56	4.91	8.09
Tm	0.605	0.600	0.603	0.908	0.950	0.906	1.450	1.140	1.250	1.010	0.796	1.280
Yb	3.97	3.93	3.96	6.07	6.14	6.00	9.60	6.92	8.58	6.76	5.33	8.34
Lu	0.638	0.645	0.618	0.880	0.965	0.980	1.550	1.130	1.350	1.100	0.766	1.220
Cd	< 0.5	< 0.5	< 0.5	< 0.5	< 0.5	< 0.5	< 0.5	< 0.5	< 0.5	< 0.5	< 0.5	< 0.5

Cu	8	15	< 1	13	< 1	2	< 1	5	2	6	3	159
Ag	1.1	1.9	1.7	0.4	0.4	< 0.3	0.6	0.7	0.6	< 0.3	< 0.3	< 0.3
Ni	8	9	8	8	3	3	6	8	7	< 1	5	10
Mo	< 1	< 1	< 1	< 1	2	< 1	< 1	< 1	1	4	< 1	< 1
Zn	83	92	90	76	90	112	88	51	118	82	100	144
S	200	1800	200	< 100	< 100	< 100	< 100	< 100	< 100	< 100	100	200
Au	< 2	< 2	< 2	< 2	< 2	< 2	11	< 2	< 2	< 2	2	< 2
As	2.5	3.9	< 0.5	4.8	< 0.5	< 0.5	< 0.5	5.1	< 0.5	0.9	3.0	2.9
Br	< 0.5	< 0.5	< 0.5	< 0.5	< 0.5	< 0.5	< 0.5	< 0.5	< 0.5	< 0.5	< 0.5	< 0.5
Cr	52	52	54	36	15	22	31	66	21	35	27	45
Fe	4.07	3.95	4.11	4.86	6.55	7.14	4.61	4.37	4.37	2.01	1.56	7.49
Ir	< 5	< 5	< 5	< 5	< 5	< 5	< 5	< 5	< 5	< 5	< 5	< 5
Na	1.94	1.70	2.41	3.83	1.32	2.05	1.42	2.99	1.73	1.74	1.32	2.10
Sc	12.8	11.6	13.9	14.2	17.1	15.2	10.9	8.4	10.2	6.0	1.8	11.2
Sb	0.8	1.7	1.3	0.4	< 0.1	0.4	< 0.1	0.3	0.3	0.4	0.8	1.1
(La/Sm)n	3.56	3.61	3.84	2.24	1.87	1.95	2.22	2.08	2.36	2.87	0.91	1.27
(La/Yb)n	7.75	8.44	9.08	3.62	3.12	3.38	3.21	3.88	3.48	4.71	0.97	1.94
(Th/La)n	2.71	2.54	2.42	1.70	0.93	0.88	1.58	1.89	1.54	1.98	5.91	0.78
(Nb/La)n	0.27	0.27	0.23	0.35	0.34	0.27	0.33	0.25	0.30	0.26	0.93	0.43
Mg#	40	37	42	19	11	13	26	9	29	33	40	14

TABLE 2.3: U-Pb DATA FOR ROCKS OF THE ESCOUMINS REGION

Fraction	Weight [mg]	Concentration U	Concentration Pb rad [ppm]	Measured total common Pb [pg]	Measured 206Pb/204Pb	Corrected Atomic Ratios * 208Pb/206Pb	206Pb/238U	+/-	207Pb/235U	+/-	207Pb/206Pb	+/-	Age [Ma] 206Pb/238U	Age [Ma] 207Pb/235U	Age [Ma] 207Pb/206Pb
Dacitic tuff (13-PA-32; UTM 468768,5363165)															
Z1 1 euh prm	0.002	810	215.7	5.5	3631	0.0997	0.25957	200	3.3378	250	0.09326	22	1488	1490	1493
Z2 2 euh prm	0.003	182	47.3	2.2	3961	0.1018	0.25299	168	3.2489	212	0.09314	24	1454	1469	1491
Z3 1 euh prm	0.002	329	85.8	6.1	1286	0.1225	0.24973	164	3.1470	228	0.09140	56	1437	1444	1455
T1 1 lrg clr med brn	0.002	1297	202.3	19	1447	0.0310	0.16452	72	1.6317	82	0.07193	28	982	982	984
T2 2 lrg clr brn	0.004	606	97.1	29	901	0.0375	0.16802	110	1.6795	136	0.07250	46	1001	1001	1000
T3 1 lrg clr med brn	0.002	579	91.9	10	1201	0.0265	0.16799	52	1.6745	94	0.07229	32	1001	999	994
T4 2 lrg clr brn	0.004	606	94.7	16	1537	0.0309	0.16493	68	1.6409	82	0.07216	26	984	986	990
Rhyolitic Tuff (14-PA-95A; UTM 459148,5348547)															
Z1 5 best euh prm	0.005	63	14.5	15	307	0.0909	0.22661	140	2.7093	268	0.08671	76	1317	1331	1354
Z2 2 euh prm	0.002	466	108.4	21	668	0.0842	0.23071	216	2.7990	246	0.08799	34	1338	1355	1382
Z3 2 best euh prm	0.002	26	5.2	9	92	0.0644	0.20176	222	2.2518	728	0.08095	234	1185	1197	1220
Z4 2 best euh prm	0.002	32	6.1	10	97	0.0489	0.19732	210	2.1814	774	0.08018	254	1161	1175	1201
Z5 1 prm abr	0.002	202	44.3	7	656	0.0714	0.22063	160	2.5977	252	0.08539	56	1285	1300	1324
Z6 3 sml prm abr	0.002	789	160.5	5	2915	0.0540	0.20801	174	2.3884	142	0.08328	62	1218	1239	1276
Z7 1 sml prm abr	0.002	330	70.3	17	409	0.0616	0.21656	132	2.5214	248	0.08444	70	1264	1278	1303
Z8 1 sml prm abr	0.002	437	86.4	14	592	0.0606	0.20152	104	2.2659	164	0.08155	42	1183	1202	1235
Tadoussac Granodiorite (15-PA-125A; UTM 449918,5340601)															
Z1 2 prms	0.002	574	155.9	28	687	0.1320	0.25760	140	3.3258	176	0.09364	30	1478	1487	1501
Z2 1 clr prm	0.001	243	64.4	42	112	0.0932	0.26001	184	3.3662	494	0.09390	116	1490	1497	1506
Z3 1 clr prm	0.001	190	53.9	16	216	0.1854	0.25822	112	3.3179	314	0.09319	74	1481	1485	1492
Z4 1 clr prm	0.001	325	83.8	34	170	0.0885	0.25404	156	3.2428	404	0.09258	96	1459	1467	1479
Z5 2 clr prm	0.002	90	25.4	12	261	0.1552	0.26227	174	3.3922	326	0.09381	80	1501	1503	1504
Z6 2 clr prm	0.002	376	106.8	20	634	0.1372	0.26746	122	3.5489	176	0.09623	30	1528	1538	1552

Notes: Z=zircon, T= titanite, 1,2 =number of grains, lrg=large, clr=clear, med=medium, prm =prism, euh=euhedral, med= medium, brn =brown, abr = physically abraded (Krogh, 1982).
All zircon was chemically abraded (Mattinson, 2005). Weights were estimated so U and Pb concentrations are approximate.
* Atomic ratios corrected for fractionation, spike, laboratory blank of 1-2 picograms of common lead, and initial common lead at the age of the sample calculated from the model of Stacey and Kramers (1975), and 0.3 picogram U blank. Two sigma uncertainties are reported after the ratios and refer to the final digits.

Table 2.4: Zircon (LA-ICP-MS) data from the quartzite (13-PA-2) collected in the lower part of the Port-aux-Quilles Formation. The U and Th contents corresponds to approximate concentrations.

				RATIO						AGE						
	U	Th	U/Th	207Pb/		206Pb/		207Pb/		207Pb/		206Pb/		207Pb/		
points	(ppm)	(ppm)		235U	2SE	238U	2SE	206Pb	2SE	235U	2SE	238U	2SE	206Pb	2SE	Conc.
23_77	227	282	0.79	14.370	0.280	0.5379	0.0096	0.1914	0.0022	2769	18	2774	41	2754	19	100%
23_111	213	159	1.32	14.150	0.250	0.5336	0.0086	0.1914	0.0024	2756	17	2756	35	2754	21	100%
23_60	403	174	2.31	13.840	0.260	0.5290	0.0094	0.1877	0.0021	2731	18	2736	40	2722	18	100%
23_89	89	266	0.33	13.560	0.250	0.5278	0.0094	0.1851	0.0028	2718	17	2727	40	2699	25	100%
23_52	197	126	1.56	11.030	0.220	0.4763	0.0081	0.1673	0.0022	2520	19	2510	36	2531	22	100%
21c_34	262	256	1.05	11.070	0.140	0.4778	0.0059	0.1673	0.0019	2526	12	2518	26	2531	19	100%
23_53	192	194	0.99	10.860	0.230	0.4716	0.0090	0.1675	0.0023	2502	20	2485	39	2533	23	99%
21c_27	184	388	0.47	10.490	0.150	0.4683	0.0058	0.1622	0.0023	2475	14	2474	26	2479	24	100%
23_144	808	505	1.58	6.220	0.110	0.3657	0.0072	0.1234	0.0014	2005	16	2010	33	2006	20	100%
23_41	316	365	0.86	6.060	0.100	0.3605	0.0061	0.1216	0.0016	1981	14	1985	28	1980	23	100%
23_122	708	250	2.78	6.160	0.110	0.3658	0.0073	0.1217	0.0016	1994	15	2006	35	1981	23	101%
23_168	1153	1748	0.65	6.050	0.100	0.3612	0.0065	0.1215	0.0013	1982	14	1987	31	1978	19	100%
23_152	241	145	1.66	5.680	0.120	0.3473	0.0059	0.1194	0.0018	1925	18	1922	27	1947	27	100%
23_54	163	283	0.57	5.650	0.130	0.3495	0.0063	0.1167	0.0020	1918	20	1932	31	1906	31	101%
23_108	534	528	0.99	5.588	0.098	0.3470	0.0059	0.1162	0.0013	1909	15	1917	28	1899	20	100%
23_94	305	133	2.28	5.540	0.110	0.3462	0.0059	0.1149	0.0015	1901	16	1914	28	1878	24	101%
23_175	2440	858	2.83	5.465	0.080	0.3435	0.0048	0.1154	0.0011	1892	12	1902	23	1886	17	101%
23_18	674	374	1.81	5.380	0.088	0.3362	0.0052	0.1161	0.0011	1879	14	1866	25	1897	17	99%
23_179	566	301	1.88	5.255	0.080	0.3342	0.0054	0.1146	0.0014	1858	13	1856	26	1874	22	100%
23_174	537	370	1.45	5.395	0.083	0.3433	0.0054	0.1145	0.0014	1882	13	1900	26	1872	22	101%
23_119	932	795	1.18	5.254	0.078	0.3331	0.0053	0.1136	0.0013	1859	13	1851	25	1858	21	100%
23_97	648	242	2.65	5.375	0.095	0.3408	0.0063	0.1137	0.0014	1877	15	1887	30	1859	22	101%
23_140	333	195	1.70	5.234	0.096	0.3351	0.0055	0.1131	0.0017	1855	16	1861	27	1850	27	100%

23_37	420	250	1.68	5.060	0.100	0.3260	0.0065	0.1121	0.0013	1824	17	1816	31	1834	21	100%
23_154	380	252	1.50	5.046	0.088	0.3277	0.0055	0.1118	0.0016	1823	14	1828	27	1829	26	100%
23_165	793	267	3.01	5.190	0.100	0.3346	0.0061	0.1120	0.0015	1846	17	1858	29	1832	24	101%
23_118	763	200	3.82	5.168	0.092	0.3335	0.0056	0.1118	0.0013	1843	15	1856	27	1829	21	101%
23_15	315	219	1.45	5.148	0.083	0.3350	0.0053	0.1117	0.0012	1844	14	1863	26	1827	19	101%
23_95	288	498	0.63	5.147	0.091	0.3328	0.0057	0.1112	0.0015	1840	15	1852	28	1819	24	101%
23_100	796	217	3.66	5.195	0.092	0.3344	0.0058	0.1117	0.0014	1847	15	1857	28	1827	23	101%
21_36	488	177	2.79	5.055	0.082	0.3285	0.0046	0.1109	0.0013	1825	14	1830	22	1814	21	100%
23_131	302	198	1.52	5.081	0.089	0.3317	0.0050	0.1105	0.0016	1828	15	1845	24	1808	26	101%
23_160	855	370	2.29	4.940	0.095	0.3261	0.0068	0.1104	0.0016	1805	16	1816	33	1806	26	101%
23_150	105	99	1.05	5.030	0.120	0.3306	0.0053	0.1104	0.0023	1818	20	1839	25	1806	38	101%
23_92	241	121	1.95	4.921	0.093	0.3227	0.0053	0.1100	0.0016	1802	16	1800	26	1799	26	100%
23_30	279	232	1.21	4.949	0.084	0.3264	0.0051	0.1092	0.0014	1808	14	1819	25	1786	23	101%
23_139	349	349	0.99	4.830	0.100	0.3165	0.0055	0.1098	0.0016	1783	17	1773	28	1796	27	99%
23_157	469	322	1.47	4.855	0.097	0.3241	0.0060	0.1094	0.0016	1792	17	1807	29	1789	27	101%
21c_28	381	552	0.67	4.724	0.072	0.3151	0.0046	0.1087	0.0014	1768	13	1767	22	1778	23	100%
23_115	357	249	1.41	4.732	0.082	0.3148	0.0053	0.1088	0.0014	1770	14	1762	26	1779	23	100%
23_93	484	490	0.97	4.806	0.090	0.3208	0.0056	0.1082	0.0012	1781	16	1791	27	1769	20	101%
23_130	531	545	0.96	4.409	0.066	0.3040	0.0042	0.1050	0.0012	1712	12	1709	21	1714	21	100%
23_177	1224	198	6.38	4.323	0.070	0.3021	0.0044	0.1044	0.0011	1695	14	1700	22	1704	19	100%
23_48	706	540	1.31	4.054	0.071	0.2907	0.0048	0.1009	0.0012	1640	14	1643	24	1641	22	100%
23_31	456	373	1.24	4.142	0.072	0.2977	0.0048	0.1007	0.0012	1659	14	1678	24	1637	22	101%
21c_30	310	193	1.60	4.043	0.070	0.2909	0.0041	0.1005	0.0013	1641	14	1645	20	1633	24	100%
23_51	245	114	2.16	4.090	0.070	0.2946	0.0047	0.1005	0.0014	1650	14	1662	23	1633	26	101%
23_107	483	348	1.36	4.067	0.080	0.2937	0.0058	0.0999	0.0014	1643	16	1657	29	1622	26	101%
23_50	665	886	0.75	3.892	0.060	0.2830	0.0039	0.0992	0.0011	1609	12	1605	19	1609	21	100%
21c_38	191	162	1.19	3.879	0.072	0.2855	0.0045	0.0983	0.0017	1604	15	1617	22	1592	32	101%
23_33	81	24	3.44	3.700	0.220	0.2772	0.0095	0.0997	0.0063	1568	47	1575	48	1618	118	100%

23_180	334	303	1.10	3.730	0.075	0.2782	0.0046	0.0975	0.0015	1572	16	1583	23	1577	29	101%
23_109	519	274	1.91	3.550	0.160	0.2660	0.0100	0.0968	0.0024	1532	35	1520	52	1563	46	99%
23_159	222	162	1.36	3.685	0.086	0.2764	0.0053	0.0970	0.0018	1564	19	1571	27	1567	35	100%
23_181	100	80	1.27	3.610	0.100	0.2706	0.0051	0.0975	0.0026	1542	24	1541	26	1577	50	100%
21c_14	498	427	1.11	3.593	0.055	0.2730	0.0035	0.0951	0.0011	1547	12	1555	18	1530	22	101%
23_27	627	291	2.12	3.437	0.065	0.2635	0.0047	0.0952	0.0013	1513	15	1505	24	1532	26	99%
23_163	308	176	1.73	3.566	0.076	0.2715	0.0052	0.0957	0.0017	1538	17	1546	26	1542	33	101%
23_167	660	422	1.56	3.626	0.091	0.2760	0.0060	0.0947	0.0016	1552	20	1569	30	1522	32	101%
23_11	1435	654	2.20	3.441	0.049	0.2641	0.0037	0.0945	0.0008	1511	11	1510	19	1519	16	100%
23_8	1583	953	1.65	3.457	0.050	0.2646	0.0036	0.0945	0.0009	1515	12	1512	19	1518	18	100%
23_56	172	106	1.62	3.557	0.091	0.2695	0.0051	0.0950	0.0018	1531	20	1536	26	1528	36	100%
23_121	551	247	2.20	3.533	0.065	0.2701	0.0049	0.0945	0.0012	1532	14	1539	25	1518	24	100%
23_182	623	336	1.86	3.502	0.062	0.2693	0.0045	0.0949	0.0014	1524	14	1536	23	1526	28	101%
23_113	218	342	0.64	3.592	0.076	0.2730	0.0046	0.0949	0.0015	1542	17	1554	23	1526	30	101%
23_38	101	59	1.74	3.473	0.082	0.2660	0.0051	0.0954	0.0020	1516	19	1518	26	1536	39	100%
23_136	1111	531	2.07	3.531	0.054	0.2709	0.0045	0.0944	0.0011	1533	12	1544	23	1516	22	101%
23_57	465	301	1.53	3.475	0.065	0.2652	0.0045	0.0946	0.0012	1517	15	1514	23	1520	24	100%
23_68	835	514	1.61	3.437	0.053	0.2635	0.0039	0.0945	0.0011	1510	12	1506	20	1518	22	100%
23_13	290	152	1.96	3.511	0.073	0.2706	0.0048	0.0946	0.0015	1527	17	1542	24	1520	30	101%
23_42	724	443	1.63	3.492	0.067	0.2675	0.0046	0.0945	0.0013	1521	15	1526	24	1518	26	100%
23_74	570	363	1.57	3.495	0.061	0.2670	0.0042	0.0940	0.0012	1522	14	1524	21	1508	24	100%
23_143	1320	665	1.99	3.517	0.060	0.2700	0.0047	0.0942	0.0011	1527	14	1539	24	1512	22	101%
23_123	473	248	1.88	3.624	0.073	0.2762	0.0048	0.0942	0.0015	1554	16	1573	24	1512	30	101%
21c_13	660	266	2.42	3.490	0.052	0.2675	0.0033	0.0943	0.0012	1523	11	1529	17	1514	24	100%
21c_11	1008	554	1.90	3.555	0.045	0.2737	0.0031	0.0941	0.0011	1539	10	1559	16	1510	22	101%
23_106	883	432	2.03	3.492	0.057	0.2675	0.0040	0.0941	0.0011	1525	13	1527	20	1510	22	100%
23_117	961	617	1.55	3.539	0.064	0.2710	0.0045	0.0940	0.0012	1533	14	1547	22	1508	24	101%
23_86	207	129	1.59	3.586	0.082	0.2739	0.0045	0.0946	0.0020	1542	17	1559	23	1520	40	101%

23_79	616	390	1.58	3.521	0.074	0.2694	0.0054	0.0941	0.0013	1526	17	1535	27	1510	26	101%
23_40	1217	603	2.03	3.463	0.058	0.2664	0.0041	0.09375	0.00092	1515	13	1521	21	1503	19	100%
23_78	220	135	1.61	3.443	0.081	0.2662	0.0051	0.09350	0.00170	1511	20	1519	26	1498	34	101%
23_10	630	583	1.08	3.432	0.052	0.2650	0.0037	0.09397	0.00096	1509	12	1514	19	1508	19	100%
23_155	570	299	1.90	3.434	0.061	0.2665	0.0042	0.09410	0.00130	1509	13	1521	21	1510	26	101%
23_36	605	332	1.84	3.428	0.068	0.2632	0.0051	0.09490	0.00120	1505	15	1503	26	1526	24	100%
23_166	856	651	1.31	3.399	0.066	0.2610	0.0051	0.09470	0.00120	1500	15	1493	26	1522	24	100%
23_9	518	439	1.26	3.372	0.052	0.2606	0.0038	0.09399	0.00099	1495	12	1492	20	1508	20	100%
23_14	436	243	1.83	3.397	0.056	0.2629	0.0037	0.09380	0.00120	1502	13	1504	19	1504	24	100%
23_12	202	183	1.11	3.342	0.067	0.2587	0.0042	0.09390	0.00150	1486	16	1482	22	1506	30	100%
23_19	1428	641	2.26	3.393	0.058	0.2627	0.0041	0.09370	0.00093	1499	13	1502	21	1502	19	100%
23_72	302	165	1.84	3.444	0.071	0.2638	0.0040	0.09370	0.00150	1509	16	1508	21	1502	30	100%
21c_15	238	185	1.28	3.411	0.068	0.2618	0.0033	0.09390	0.00160	1502	16	1498	17	1506	32	100%
21c_9	311	217	1.62	3.382	0.052	0.2617	0.0031	0.09350	0.00120	1497	12	1498	16	1498	24	100%
23_176	335	233	1.43	3.365	0.059	0.2628	0.0037	0.09340	0.00130	1494	14	1503	19	1496	26	101%
23_71	216	161	1.35	3.481	0.074	0.2672	0.0042	0.09370	0.00160	1517	17	1525	22	1502	32	101%
21c_19	258	150	1.68	3.394	0.062	0.2645	0.0032	0.09300	0.00150	1499	14	1512	16	1488	31	101%
23_34	640	382	1.68	3.374	0.064	0.2624	0.0043	0.09280	0.00110	1493	15	1500	22	1484	22	100%
23_133	345	269	1.29	3.354	0.062	0.2608	0.0040	0.09310	0.00130	1489	15	1493	20	1490	26	100%
23_162	230	97	2.28	3.348	0.078	0.2613	0.0055	0.09330	0.00180	1485	18	1494	28	1494	37	101%
21c_39	533	224	2.39	3.302	0.051	0.2593	0.0035	0.09270	0.00120	1481	12	1485	18	1482	25	100%
21c_35	1040	541	2.01	3.337	0.060	0.2609	0.0041	0.09220	0.00100	1487	14	1493	21	1472	21	100%
21c_31	310	216	1.42	3.261	0.060	0.2561	0.0037	0.09240	0.00130	1469	14	1469	19	1476	27	100%
23_129	183	142	1.28	3.383	0.080	0.2640	0.0043	0.09260	0.00180	1493	18	1509	22	1480	37	101%
23_75	406	203	1.98	3.301	0.062	0.2599	0.0046	0.09220	0.00140	1476	15	1488	24	1472	29	101%
23_132	188	177	1.06	3.418	0.080	0.2650	0.0039	0.09270	0.00170	1501	18	1514	20	1482	35	101%
23_138	353	256	1.36	3.238	0.065	0.2545	0.0042	0.09210	0.00160	1461	16	1460	22	1469	33	100%
23_26	507	31	22.00	2.152	0.070	0.1950	0.0044	0.07910	0.00180	1161	23	1147	24	1175	45	99%

21c_8	1605	7	275.00	1.786	0.022	0.1740	0.0019	0.07435	0.00069	1039.8	7.9	1034	10	1051	19	99%
23_28	1484	5	325.00	1.806	0.031	0.1752	0.0029	0.07421	0.00078	1045	11	1040	16	1047	21	100%

Table 2.5: Sm-Nd isotopic data for the plutonic and volcanic rocks of the Escoumins Supracrustal Belt.

Sample	Outcrop	Lithology	Synform	Formation	Age (Ga)	Zone	Nd (ppm)	Sm (ppm)	147Sm/144Nd	143Nd/144Nd	2s	$\varepsilon_{Nd}(0)$	$\varepsilon_{Nd}(1.5)$	T De Paolo	TDM2
54776	291-A	gabbronorite	Baie-des-Bacon	MAB	1.49	19	15.20	4.11	0.1633	0.512575	8	-1.2	5.21	1406	1738
53091	91-B	FeTi basalt	Saint-Onge	MAB	1.49	19	17.82	5.58	0.1893	0.512763	7	2.4	3.91	1727	2416
54758	154-B	basalt	Lac Raymond	MAB	1.49	19	10.07	2.71	0.1625	0.512552	7	-1.7	4.92	1451	1779
54708	125-A1	granodiorite	-	TIS	1.502	19	11.77	2.42	0.1243	0.512059	6	-11.3	2.66	1672	1857
54343	32-A	dacitic tuff	Saint-Onge	MAB	1.49	19	37.88	7.40	0.1180	0.511826	7	-15.8	-0.77	1936	2103

Table A2.1: UTM location of the samples used in this chapter. Abbreviations: Ton. = Tonalite, Grd. = Granodiorite, Gra. = Granite, bas. = basalt, B.A = basaltic andesite, FT-bas = FeTi basalt, dac. = dacite, rhyod. = rhyodacite.

Sample	rock type	UTM zone	East	North
54701	Ton.	19	469379	5363958
54708	Grd.	19	449918	5340601
54709	Grd.	19	449918	5340601
54719	Grd.	19	444534	5340159
54721	Grd.	19	447133	5334358
54727	Grd.	19	476632	5384908
53067	Ton.	19	449955	5340643
53068	Ton.	19	430706	5329086
54748	Grd.	19	476886	5384499
54718	Gra.	19	453291	5345042
54702	Ton.	19	469379	5363958
53077	Grd.	19	450877	5341963
54710	Gra.	19	450246	5340762
53078	Gra.	19	450877	5341963
54720	Gra.	19	434498	5345801
54349	Gra.	19	458299	5343483
54689	bas.	19	5347899	458723
54758	bas.	19	5354274	458771
53090	bas.	19	5365784	469017
54367	bas.	19	5349114	459025
54366	bas.	19	5349114	459025
54369	bas.	19	5349114	459025
54759	bas.	19	5354274	458771
54760	bas.	19	5354202	458781
54687	bas.	19	5347943	458693
54783	bas.	19	5374597	477625
54357	B.A	19	5349838	460415
53082	B.A	19	5325269	435354
54356	B.A	19	5349114	459025
54764	B.A	19	5354245	458666
54688	B.A	19	5348126	458769
54765	B.A	19	5354200	458569
54362	B.A	19	5347854	458722
54761	B.A	19	5354207	458756
53081	B.A	19	5325317	433878
53091	FT-bas.	19	5365784	469017
54766	FT-bas.	19	5354185	458489

53086	FT-bas.	19	5364050	468230
53087	FT-bas.	19	5364050	468230
54779	FT-bas.	19	5375346	473160
54780	FT-bas.	19	5375346	473160
54782	FT-bas.	19	5374917	477876
54767	FT-bas.	19	5354200	458420
54770	FT-bas.	19	5354163	458460
54763	FT-bas.	19	5354245	458666
54682	dac.1	19	5363685	468740
54343	dac.1	19	5363165	468768
54354	dac.1	19	5363263	468818
54738	dac.2	19	5354274	458771
54741	dac.2	19	5354195	458687
54740	dac.2	19	5354245	458685
54716	dac.2	19	5354184	458657
54715	rhyod.2	19	5354207	458756
54739	rhyod.2	19	5354202	458717
54737	rhyod.2	19	5353932	457596
53076	rhyo.3	19	5348547	459148
54697	dac.3	19	5348406	459203

Chapter 3 Arc dynamics in the Mesoproterozoic Laurentian margin, Quebec

3.1 Abstract

Quebecia is a unique Geon 15 to 13 composite arc belt in the central Grenville Province, separating crustal segments that were parts of continental arc systems at that time. It consists of ca. 1.5 Ga metasedimentary sequences indicative of earlier rifting of the Laurentian margin, remnants of 1.50 to 1.45 Ga peri-Laurentian oceanic arcs to the south built on rifted crustal slivers, a major 1.4 to 1.3 Ga felsic plutonic belt potentially marking the time of accretion to Laurentia, and the only 1.3 Ga anorthosites in the Grenville, the latter implying mafic underplating at the base of the crust predating by a few million years their emplacement. Differences between Quebecia and continental arcs elsewhere in the Grenville attest to lateral variations in subduction dynamics under Laurentia comparable to the modern-day Andean system.

3.2 Introduction

The Grenville Province (Fig. 3.1a) is largely composed of remnant arc systems active at the SE margin of Laurentia from late Paleoproterozoic through Mesoproterozoic (Rivers and Corrigan, 2000), and later (at ~1.0 Ga) involved in continental collision during the assembly of the supercontinent Rodinia (Li et al., 2008). Major crust forming events in the Grenville at 1.71 – 1.60 Ga (Labradorian), and 1.52 – 1.46 Ga (Pinwarian; see Gower and Krogh, 2002) extending to 1.3 Ga (Nadeau and van Breemen, 1994; Corrigan and van Breemen, 1997; Ratcliffe et al., 1991; Sappin et al., 2009), are broadly coeval with the formation of the 1.7 – 1.6 Ga Mazatzal and the 1.5 – 1.3 Ga Granite-

Rhyolite Provinces farther west (Whitmeyer and Karlstrom, 2007). Most widespread crust formation seems to characterize the Pinwarian extending to early Geon 13, with development of continental arcs to the east and west and a composite, partly juvenile terrane (Quebecia terrane; see Dickin et al., 2010) with a recently recognized peri-Laurentian arc system exposed in the central Grenville Province (Fig. 3.1b) (Groulier et al., 2018).

New insights into the configuration and evolution of the SE Laurentian margin from Geon 15 to 13 are offered by integrating recent data from the peri-Laurentian arc in the framework of Quebecia and vicinity, and lateral variations along the SE Laurentian margin are linked to subduction dynamics.

3.3 The Southeastern Laurentian margin at Geon 15 to 13

Tectonic environments, ages and chemistry of key units formed at 1.5 to 1.3 Ga are summarized in Figure 3.2. In the central and SW part of the United States, the 1.50 – 1.34 Ga Granite-Rhyolite Province is characterized by calc-alkalic and ferroan igneous rocks and is divided into a 1.50 – 1.44 Ga eastern part and a 1.40 – 1.34 Ga southern part. A “Nd-line” separates internal and external domains with model ages older and younger than 1.55 Ga, inferred to represent reworked crust in a continental arc and back-arc setting, and juvenile arc terranes accreted to Laurentia, respectively (Van Schmus et al., 2007). Reworked equivalents can be traced northeastwards in the Grenville Province as far as the Central Gneiss Belt in Ontario (Slagstad et al., 2009).

In the eastern Grenville in Labrador, 1.5 to 1.4 Ga calc-alkalic granitoids with Paleoproterozoic Nd T_{DM} model ages (Dickin et al., 2010) are intrusive into Labradorian

age crust (Gower and Krogh, 2002), consistent with a continental arc built on older crust (Labradoria terrane, Fig. 3.1b). These are crosscut by the 1.46 Ga Shabogamo and the 1.43 Ga Michael tholeiitic gabbro dyke swarms (Gower and Krogh, 2002) (Fig. 3.1b). In the southern part of the study area, the late Geon 15 La Romaine supracrustal belt (van Breemen and Corriveau, 2005) (Fig. 3.1b) represents the remnants of a continental back-arc system including a subaerial to shallow marine intra-arc volcanic sequence (Corriveau and Bonnet, 2005) and continental, shallow to deeper submarine siliciclastic sedimentary rocks (eastern Wakeham Group; Fig. 3.1b), (see van Breemen and Corriveau, 2005). The whole sequence is intruded by 1.51 to 1.49 Ga shallow-level calc-alkalic plutons (Kataht Plutonic Suite; see Brisebois and Clark, 2003) interpreted to signal the closure of the back-arc.

In the central Grenville Province, the ~1.5 Ga Quebecia terrane (Fig. 3.1b) is defined on the basis of Sm–Nd data (see Dickin et al., 2010). Recently, Groulier et al. (2018) proposed that Quebecia represents a composite arc belt with continental and oceanic arc and back-arc rocks built on older crustal panels rifted from Laurentia during Geon 15. Main crustal elements recognized in Quebecia are: (a) early and mid-Geon 14 volcano-sedimentary belts to the south (Escoumins supracrustal belt, ESB) and SW (Montauban group); (b) late Geon 15 metasedimentary sequences in the north (Plus Value complex, PLV) and SE (Bourdon Complex); (c) Geon 15 to early Geon 13 felsic to intermediate plutonic suites; and (d) Geon 13 Rivière Pentecôte and De La Blâche anorthosites (Fig. 3.1c).

3.4 Volcano-sedimentary belts in the central Grenville

The ESB (Fig. 3.1b) is composed of the Saint-Siméon Group (Fig. 3.1c), a 1.49 to 1.46 Ga bimodal sub-aerial to marine volcanic sequence and its 1.5 Ga structural basement of calc-alkalic and high-K to shoshonitic granitoids (Tadoussac Intrusive Suite; Fig. 3.1c). The ESB is inferred to have formed in a peri-Laurentian oceanic arc and rifted-arc environment. This is recorded by 1.49 Ga calc-alkalic to transitional mafic and felsic volcanic rocks with evidence of crustal contamination, covered by younger transitional to tholeiitic juvenile basalt and ferrobasalt and A-type dacite to rhyolite (Groulier et al., 2018).

On the southwestern margin of Quebecia, the Porneuf-Mauricie Domain consists of the ca. 1.45 Ga marine island arc and back-arc Montauban Group (Fig. 3.1b and c) inferred to have formed along a NW-dipping (current coordinates) intra-oceanic subduction zone offshore from Laurentia. This group is intruded by calc-alkalic plutons of the 1.40 – 1.37 Ga La Bostonnais Complex (Fig. 3.1c) emplaced in a mature island arc (oldest rocks) and continental arc (youngest) settings, suggesting the accretion of the Montauban oceanic arc to Laurentia at about 1.39 Ga (Corrigan and van Breemen, 1997; Sappin et al., 2009).

3.5 Late Geon 15 to mid Geon 14 sedimentary basins

The most regionally significant sedimentary sequences are the late Geon 15 PLV, and Bourdon complexes, to the north and south, respectively (Fig. 3.1b, 3.1c). In addition, the Port-aux-Quilles Formation is a sedimentary sequence in the Saint-Siméon Group (Fig. 3.1c) and for comparison, we also discuss the eastern Wakeham group, associated

with La Romaine continental arc to the east. Histograms with age distribution of detrital zircon compiled from the literature are included in Figure 3.3.

The PLV consists of metapsammite, metapelite, quartzite, scarce calc-silicate rocks and marble with minor mafic sills and is intruded by the ~1497 Ma Bardoux plutonic Suite (Fig. 3.1c; Augland et al., 2015). Detrital zircon ranges from early Geon 14 to the Archean (ca. 2.7 – 2.8 Ga) with a dominant Paleoproterozoic peak at ca. 1.7 – 1.8 Ga (Fig. 3.3a). The PLV zircon age spectrum is typical of foreland to passive margin basins (see Cawood et al., 2012), which is an indication of a more evolved extensional basin.

The Bourdon Complex (Fig. 3.1b, 3.1c) is composed of metapelite, metapsammite, marble, quartzite and iron formation (Moukhsil et al., 2009). Detrital zircon show a wide range of ages with clusters in the Archean, Paleo- and Mesoproterozoic, and a maximum around 1.8 – 1.9 Ga with younger ages around 1.5 Ga (Fig. 3.3b). When compared to the PLV (Fig. 3.3a), the Bourdon Complex histogram has fewer zircon close to the depositional age, and this is typical of rift basins.

The late Geon 15 eastern Wakeham Group (Fig. 3.1a) consists of continental shallow submarine to submarine arenaceous sedimentary rocks with minor conglomerate, marble, mudrock and volcanic rocks (Brisebois and Clark, 2003). Detrital zircon show a similar pattern to that of the Bourdon Complex, with a spread of ages from the Archean to ca. 1.5 Ga and a significant peak at ca. 1.8 – 1.9 Ga (Fig. 3.3c). However, the youngest peak appears bigger than the one from the Bourdon Complex suggesting a more proximal magmatic source, which could be linked to the presence of the La Romaine volcanic belt

to the SE, and is consistent with formation in a continental back-arc or intra-arc environment.

The Port-aux-Quilles Formation (upper member of the Saint-Simeon Group, ESB Fig. 3.1b, 3.1c) consists of quartzite, subarkose, metapsammite, greywacke, metapelite with minor basalt, mafic dykes and sills and has a younger age limit of deposition at 1.476 Ga (Groulier et al., 2018). Detrital zircon cluster in the Archean, Paleoproterozoic and Mesoproterozoic with increasingly high peaks toward younger ages, typical of back-arc basins (Fig. 3.3d). The younger ages match 1.46 Ga felsic volcanic rocks in the supracrustal belt, the 1.5 Ga peak is interpreted to reflect proximity to the ca. 1.5 Ga Tadoussac Intrusive Suite.

3.6 Late Geon 15 to Geon 13 plutonic suites

Plutonic suites in Quebecia are mostly distributed along a SW – NE trending belt (Fig. 3.1c). The PLV is intruded by the 1497 Ma Bardoux, the ca. 1434 – 1413 Ma Hulot Complex and the ca. 1390 Ma Castoreum Plutonic Suite (Fig. 3.1c) (Augland et al. 2015). To the south, the ca. 1390 Ma Cap-a-l'Est, Parc des Laurentides and Charlevoix granitoids (Hébert and van Breemen, 2004), (Fig. 3.1c), contain metasedimentary rafts of the Bourdon Complex. Finally, the ca. 1360 Ma Rivière Pentecôte and ca. 1327 Ma De La Blâche anorthosites (Martignole et al., 1993; Gobeil et al., 2002) are exposed in the NW and central parts of Quebecia, respectively. Geochemically characterised suites are discussed from the oldest to the youngest, with trends based on selected trace elements (compiled and shown in Fig. 3.4).

The 1.5 Ga Tadoussac Intrusive Suite (Fig. 3.1c) has juvenile components and is composed of arc-related granodiorite, trondhjemite to tonalite and arc-rift megacrystic granite (Groulier et al., 2018). There is a clear separation between calc-alkalic arc components and the alkaline arc-rift rocks. Nd model ages from arc-related rocks vary from 1.54 to 1.67 Ga (Dickin et al., 2010; Groulier et al., 2018) demonstrating that part of this suite interacted with older crust and suggesting a polyphase origin with juvenile components showing no to little crustal contamination.

The 1.49 Ga Bardoux Plutonic Suite (Fig. 3.1c). ranges from continental arc to within-plate, typical of an evolution towards a more mature arc that experienced some extension (ex. intra-arc rifting). Zircon εHf values (2.3 – 4.7) and depleted mantle model ages of 1.9 to 2.05 Ga (Augland et al., 2015) suggest interaction with an older Paleoproterozoic component and formation in an active continental margin.

Collectively, data from the ca. 1.43 – 1.39 Ga Hulot Complex and Castoreum Plutonic Suite and Cap-a-l'Est Complex follow a trend from a juvenile arc toward a more mature arc and a high temperature extensional environment (arc-rift). The εHf values for 1434 Ma rocks of the Hulot Complex range from 8.4 to 10.7 with depleted mantle ages of 1.6 Ga, and indicate a strong juvenile input with some interactions with a 1.6 Ga crust (Augland et al. 2015). Younger components of the Hulot Complex (1413 Ma) have lower εHf values of 6.3 – 8.0 and older depleted mantle ages (> 1.73 Ga). These data suggest that the arc was more primitive and thinner around 1.43 Ga and more mature ca. 1.41 Ga with more interaction with older continental crust. The geochemistry of the 1.39 Ga Castoreum and Cap-a-l'Est complexes appears to be more evolved with higher high-field strength elements contents.

3.7 Discussion

3.7.1 Continental intra-arc / back-arc basins and rifting of crustal slivers along southeast Laurentia in Geon 15

The data from the central/eastern Grenville Province point to major extension along the SE Laurentian margin during Geon 15 (Fig. 3.5a), as a result of upper-plate extension in an active continent-ocean convergent setting (Fig. 3.5b). This was well registered in the eastern and central Grenville Province where the rifting of the continental margin arc led in the eastern Grenville to the opening of a continental intra-arc (La Romaine) and a shallow marine continental back-arc (Wakeham Group), and to the separation of crustal slivers in the central Grenville Province and opening of a seaway (Fig. 3.5a, b). This led to the formation of an oceanic island arc (the Escoumins and Montauban supracrustal belts) partly built on previously rifted fragments of Laurentian margin (Groulier et al., 2018). In the eastern Grenville Province, the continental to shallow marine continental back-arc rock succession indicates a less advance stage of rifting. This difference between the central and eastern Grenville Province may indicate that the extension was greater in the former, implying a possible northward "unzipping" rift, possibly similar to the opening mechanism of the Mesozoic Rocas Verdes Basin in southern Andes (Stern and de Wit, 1997; Parada et al., 2007). On the Laurentian side after rifting, the PLV and Bourdon sedimentary basins respectively exposed on the northern and southern side of Quebecia (Fig. 3.1b and c), indicate the presence of a passive margin. In Figure 3.5a the Bourdon Complex is placed on the Laurentian side rather than

on the rifted crustal sliver based on the lack of ca. 1.5 Ga detrital zircon that would be expected close to an active arc (see Cawood et al., 2012).

In the eastern Grenville Province, the emplacement of the ca. 1.51 – 1.49 Ga arc-related plutons of the Kataht Plutonic Suite within the continental back-arc sequence support a basin inversion. These plutons show evidence of interaction between a juvenile magma and Paleoproterozoic crust (εNd 0.11 – 2.9, T_{DM} 1.79 – 2.0 Ga; Brisebois and Clark, 2003) indicating that the rifting didn't lead to complete rupture of the crust. In the central Grenville Province, the emplacement of the 1.49 Ga Bardoux Plutonic Suite within the PLV Complex also indicates the transformation of the passive margin into an active one via the formation of a new subduction zone (Fig. 3.5a, b). The Escoumins island arc preserves evidence of a rifting event at ca. 1.49 – 1.46 Ga with formation of arc-rift and back-arc related felsic and juvenile mafic volcanic rocks. These imply direct asthenospheric melting with little to no crustal contamination in thinned crust in a supra-subduction environment (Fig. 3.5a, b). Groulier et al. (2018) proposed that this rifting was linked to slab-rollback and led to the opening of an intra-arc/back-arc basin later filled with epiclastic sediments (the Port-aux-Quilles Formation). Such evolution was also proposed by Sappin et al. (2009).

3.7.2 Closure of the seaway and accretion of pericratonic island arcs to Laurentia during late Geon 14 to early Geon 13

The emplacement of the margin-parallel 1450 Ma and 1425 Ma Michael and Shabogamo gabbro dyke swarms is attributed to the formation of an asthenospheric

window or back-arc extension (see Rogers et al., 2019), probably formed by the subduction of the spreading centre (Fig.5a, b). For comparison, in the Andes, such a process is linked to the emplacement of voluminous continental flood basalt (Parada et al., 2007; Stern et al., 2007). In the Grenville Province, basalt formed in this environment was not observed, however this could be due to the lack of preservation of pre-Grenvillian upper crust.

The emplacement of voluminous 1.43 – 1.37 Ga continental arc plutonic complexes along the entire central Grenville Province marks the final closure of the seaway and the accretion of the pericratonic island arcs to Laurentia (Fig. 3.5a, b). The 1.39 – 1.37 Ga La Bostonais and the 1.39 Ga Cap-a-l'Est complexes may represent stitching plutons emplaced within or in proximity to the oceanic arc sequences (e.g. Corrigan and van Breemen, 1997). The Hulot and Castoreum complexes farther north were more likely emplaced in the already existing active continental margin. In addition, two ca. 1.36 – 1.33 anorthositic complexes emplaced in the northern part of Quebecia, represent the only Geon 13 anorthosites reported in the Grenville Province. This suggests that an important quantity of mafic magma may have been present at the Moho earlier.

3.8 Acknowledgements

The authors acknowledge support from the Ministère de l'Énergie et des Ressources naturelles du Québec (contribution n°8450-2018-2019-05) and from the Natural Sciences and Engineering Research Council of Canada Discovery Grant program.

3.9 References

Augland, L.E., Moukhsil, A., Solgadi, F., Indares, A., 2015. Pinwarian to Grenvillian magmatic evolution in the central Grenville Province: new constraints from ID-TIMS U-Pb ages and coupled Lu-Hf S-MC-ICP-MS data. Canadian Journal of Earth Sciences, vol. 52, p. 701–721.

Bickford, M.E., Van Schmus, W.R., Karlstrom, K.E., Mueller, P.A., Kamenov, G.D., 2015. Mesoproterozoic-trans-Laurentian magmatism: a synthesis of continent-wide age distributions, new SIMS U-Pb ages, zircon saturation temperatures, and Hf and Nd isotopic compositions. Precambrian Research, vol. 265, p. 286–312.

Brisebois, D., Clark, T., 2003. Géologie et ressources minérales de la partie est de la Province de Grenville. Ministère des Ressources naturelles de la Faune et des Parcs, Québec, DV 2002-03, 419 p.

Cawood, P.A., Hawkesworth, C.J., Dhuime, B., 2012. Detrital zircon record and tectonic setting. Geology, vol. 40, p. 875–878.

Corrigan, D., van Breemen, O., 1997. U-Pb age constraints for the lithotectonic evolution of the Grenville Province along the Mauricie transect, Quebec. Canadian Journal of Earth Sciences, vol. 34, p. 299–316.

Corriveau, L., Bonnet, A.-L., 2005. Pinwarian (1.5 Ga) volcanism and hydrothermal activity at the eastern margin of the Wahekam Group, Grenville Province, Quebec. Canadian Journal of Earth Sciences, vol. 42, p. 1749–1782.

David, J., Moukhsil, A., Clark, T., Hébert, C., Nantel, S., Dion, C., Sappin, A.-A., 2009. Datations U-Pb effectuées dans les provinces de Grenville et de Churchill en 2006-2007. Ministère des Ressources naturelles et de la Faune, RP 2009-03, 32 p.

David, J., Moukhsil, A., Dion, C., 2010. Datation U-Pb effectuées dans la Province de Grenville en 2008-2009. Ministère des Ressources naturelles et de la Faune, RP 2010-10, 18 p.

Dickin, A.P., McNutt, R.H., Martin, C., Guo, A., 2010. The extent of juvenile crust in the Grenville Province: Nd isotope evidence. Geological Society of America. Bulletin, vol. 122 (5–6), p. 870–883.

Gobeil, A., Hébert, C., Clark, T., Beaumier, M., Perreault, S., 2002. Géologie de la région du lac De La Blache (22K/03 et 22K/04). Ministère des Ressources naturelles et de la Faune, RG 2002-01, 49 p.

Gorton, M.P., Schandl, E.S., 2000. From continents to island arcs: a geochemical index of tectonic setting for arc-related and within-plate felsic to intermediate volcanic rocks. Canadian Mineralogist, vol. 38, p. 1065–1073.

Gower, C.F., Krogh, T.E., 2002. A U-Pb geochronological review of the Proterozoic history of the eastern Grenville Province. Canadian Journal of Earth Sciences, vol. 39, p. 795–829.

Groulier, P.-A., Indares, A.D., Dunning, G., Mouhksil, A., Wälle, M., 2018. Peri-Laurentian, Pinwarian-age oceanic arc crust preserved in the Grenville Province: insights from the Escoumins Supracrustal Belt. Precambrian Research, vol. 311, p. 37–64.

Hébert, C., van Breemen, O., 2004. Mesoproterozoic basement, the Lac-Saint-Jean anorthosite suite and younger Grenvillian intrusions in the Saguenay region (Quebec): structural relationships and U-Pb geochronology. Geological Society of America, Memoir 197, p. 65–79.

Hoffman, P.F., 1989. Precambrian geology and tectonic history of North America. In: The Geology of North America: an Overview. Geological Society of America, Boulder, Colo, pp. 447–512 The Geology of North America, Vol. A.

Lasalle, S.S., Fisher, C.M., Indares, A., Dunning, G., 2013. Contrasting types of Grenvillian granulite facies aluminous gneisses: insights on protoliths and metamorphic events from zircon morphologies and ages. Precambrian Research, vol. 228, p. 117–130.

Li, Z.X., Bogdanova, S.V., Collins, A.S., Davidson, A., De Waele, B., Ernst, R.E., Fitzsimons, I.C.W., Fuck, R.A., Gladkochub, D.P., Jacobs, J., Karlstrom, K.E., Lu, S., Natapov, L.M., Pease, V., Pisarevsky, S.A., Thrane, K., Vernikovsky, V., 2008. Assembly, configuration, and break-up history of Rodinia: a synthesis. Precambrian Research, vol. 160, p. 179–210.

Martignole, J., Machado, N., Nantel, S., 1993. Timing of Intrusion and Deformation of the Rivière-Pentecôte Anorthosite (Grenville Province). The Journal of Geology, vol. 01, p. 652–658.

Moukhsil, A., Lacoste, P., Gobeil, A., David, J., 2009. Synthèse géologique de la région de Baie-Comeau (SNRC 22F). Ministère des Ressources naturelles et de la Faune, RG 2009-03, 28 p.

Parada, M.A., Lopez-Escobar, L., Oliveros, V., Fuentes, F., Morata, D., Calderon, M., Aguirre, L., Feraud, G., Espinoza, F., Moreno, H., Figueroa, O., Munoz Bravo, J., Troncoso Vasquez, R., Stern, C.R., 2007. In: Moreno, T., Gibbons, W. (Eds.), The Geology of Chile. The Geological Society, London., p. 147–178.

Pearce, J.A., Harris, B.W., Tindle, A.G., 1984. Trace element discrimination diagrams for the tectonic interpretation of granitic rocks. Journal of Petrology, vol. 25 (4), p. 956–983.

Rivers, T., Corrigan, D., 2000. Convergent margin on southeastern Laurentia during the Mesoproterozoic: tectonic implications. Canadian Journal of Earth Sciences, vol. 37, p. 359–383.

Roger, C., Cousens, B., Ernst, R.E., Söderlund, U., Phosphorus and potassium metasomatic enrichment in the mantle source of the c. 1450–1425 Ma Michael – Shabogamo gabbro of eastern Laurentia. Journal of Petrology, vol. 60, No. 1, p.57–84.

Sappin, A.-A., Constantin, M., Clark, T, van Breemen, O., 2009. Geochemistry, geochronology, and geodynamic setting of Ni-Cu±PGE mineral prospects hosted by mafic and ultramafic intrusions in the Portneuf-Mauricie Domain, Grenville Province, Quebec. Canadian Journal of Earth Sciences, vol. 46, p. 331–353.

Slagstad, T., Culshaw, N.G., Daly, J.S., Jamieson, R.A., 2009. Westerm Grenville Province holds key to midcontinental Granite-Rhyolite Province enigma. Terra Nova, vol. 21, p. 191–187.

Stern, C.R., de Wit, M.J., 1997. The Rocas Verdes “Greenstone Belt”, Southernmost South America. In: de Wit, M.J., Ashwal, L.D. (Eds.), Greenstone Belts. Oxford monographs on geology and geophysics, vol. 35, p. 791–801.

Stern, C.R., Moreno, H., Lopez-Escobar, L., Clavero, J.E., Lara, L.E., Naranjo, J.A., Parada, M.A., Skewes, M.A., 2007. Chilean volcanoes. In: Moreno, T., Gibbons, W. (Eds.), The Geology of Chile. The Geological Society, London., p. 147–178.

van Breemen, O., Corriveau, L., 2005. U-Pb age constraints on arenaceous and volcanic rocks of the Wahekam Group, eastern Grenville Province. Canadian Journal of Earth Sciences, vol. 42, p. 1677–1697.

Van Schmus, W.R., Schneider, D.A., Holm, D.K., Dodson, S., Nelson, B.K., 2007. New insights into the north-central United States based on U-Pb, Sm-Nd, and Ar-Ar geochronology. Precambrian Research, vol. 157, p. 80–105.

Whitmeyer, S.J., Karlstrom, K.E., 2007. Tectonic model for the Proterozoic growth of North America. Geosphere, vol. 3, p. 220–259.

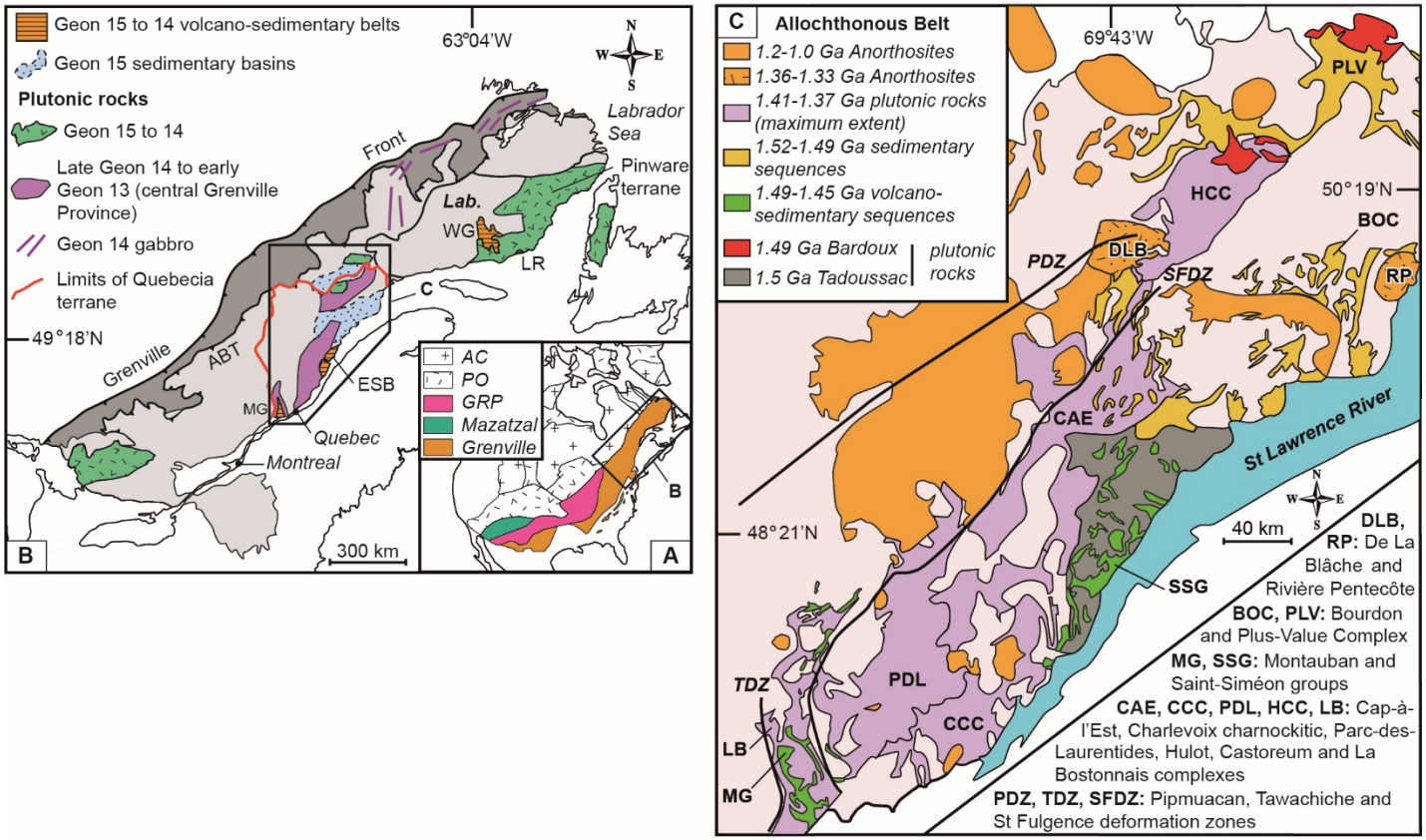

Figure 0.1: A: The Mazatzal, Grenville and Granite-Rhyolite Provinces (GRP) in the framework of the Proterozoic Laurentia (modified from Hoffman 1989). AC: Archean cratons; PO: Paleoproterozoic orogens; **B:** Schematic map of the Grenville in Canada (modified from Groulier et al., 2018) ABT – Allochthonous Boundary Thrust; ESB – Escoumins Supracrustal Belt, Lab. – Labradoria; LR – La Romaine supracrustal belt; MG – Montauban Group; WG – Wakeham Group; **C:** Geological map of the central Grenville Province.

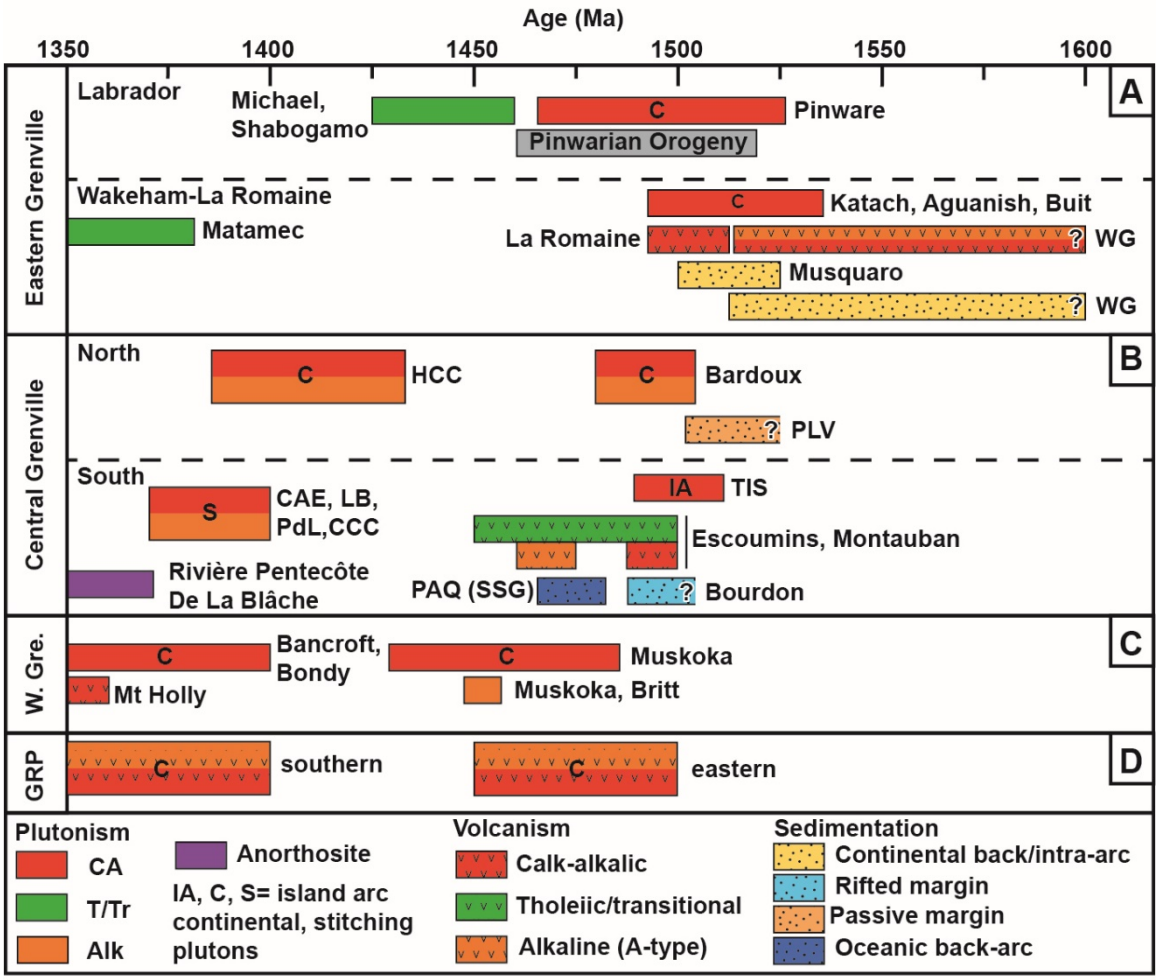

Plutonism: CA–calc-alkaline; **T/Tr**–tholeiitic/transitional; **Alk**–alkaline. **Rock units: CAE**–Cap-a-l'Est Complex; **CCC**–Charlevoix charnockitic Complex; **GRP**–Granite-Rhyolite Province; **HCC**–Hulot Castoreum complexes; **LB**–La Bostonnais Complex; **PAQ**–Port-aux-Quilles; **PLV**–Plus-Value Complex; **PdL**–Parc des Laurentides Complex; **SSG**–Saint-Simeon Group; **TIS**–Tadoussac Intrusive Suite; **WG**–Wakeham Group

Figure 0.2: U–Pb age ranges, geochemical signatures and tectonic setting for 1.6 to 1.35 Ga magmatic rocks and sedimentary basins from the **A:** Eastern Grenville (Gower and Krogh, 2002; van Breemen and Corriveau, 2005); **B:** Central Grenville (see Martignole et al., 1993; Gobeil et al., 2002; Augland et al., 2015; Groulier et al., 2018); **C:** Western Grenville (Slagstad et al., 2009; Rivers and Corrigan, 2000); and **D:** Granite-Rhyolite Province (see Bickford et al., 2015).

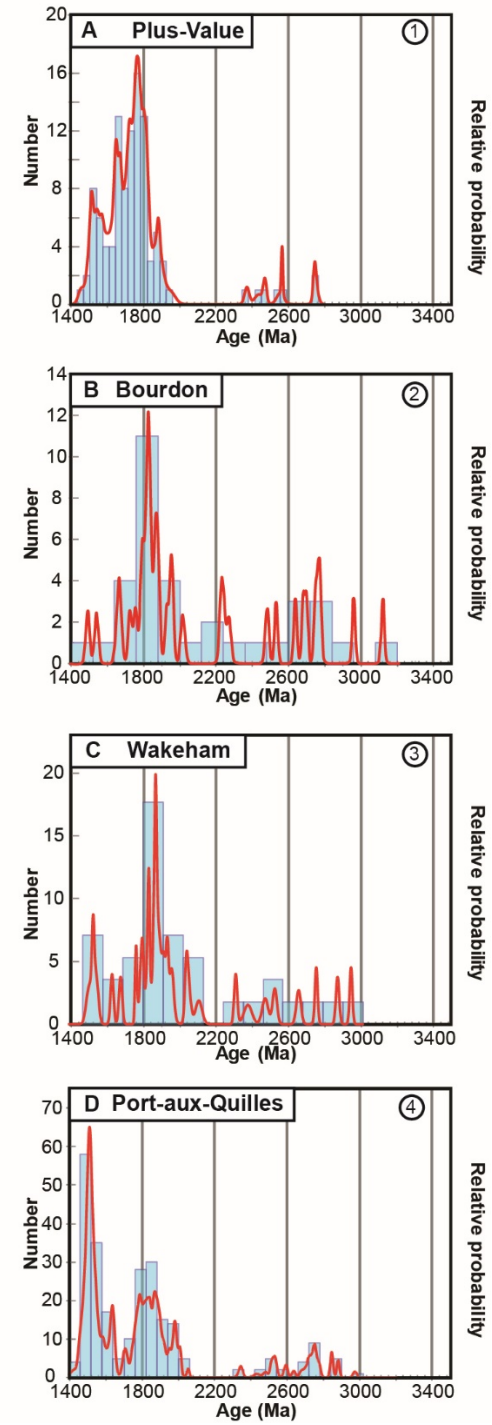

Figure 0.3: $^{207}Pb/^{206}Pb$ ages versus relative abundance of detrital zircon for **A:** PLV Complex (data from Lasalle et al., 2013), **B:** Bourdon Complex (data from David et al., 2010), **C:** La Romaine belt (data from van Breemen and Corriveau, 2005), and **D:** Port-aux-Quilles Formation (Saint-Siméon Group; data from Groulier et al., 2018). To avoid lead-loss bias only values with less than 5% discordance were used.

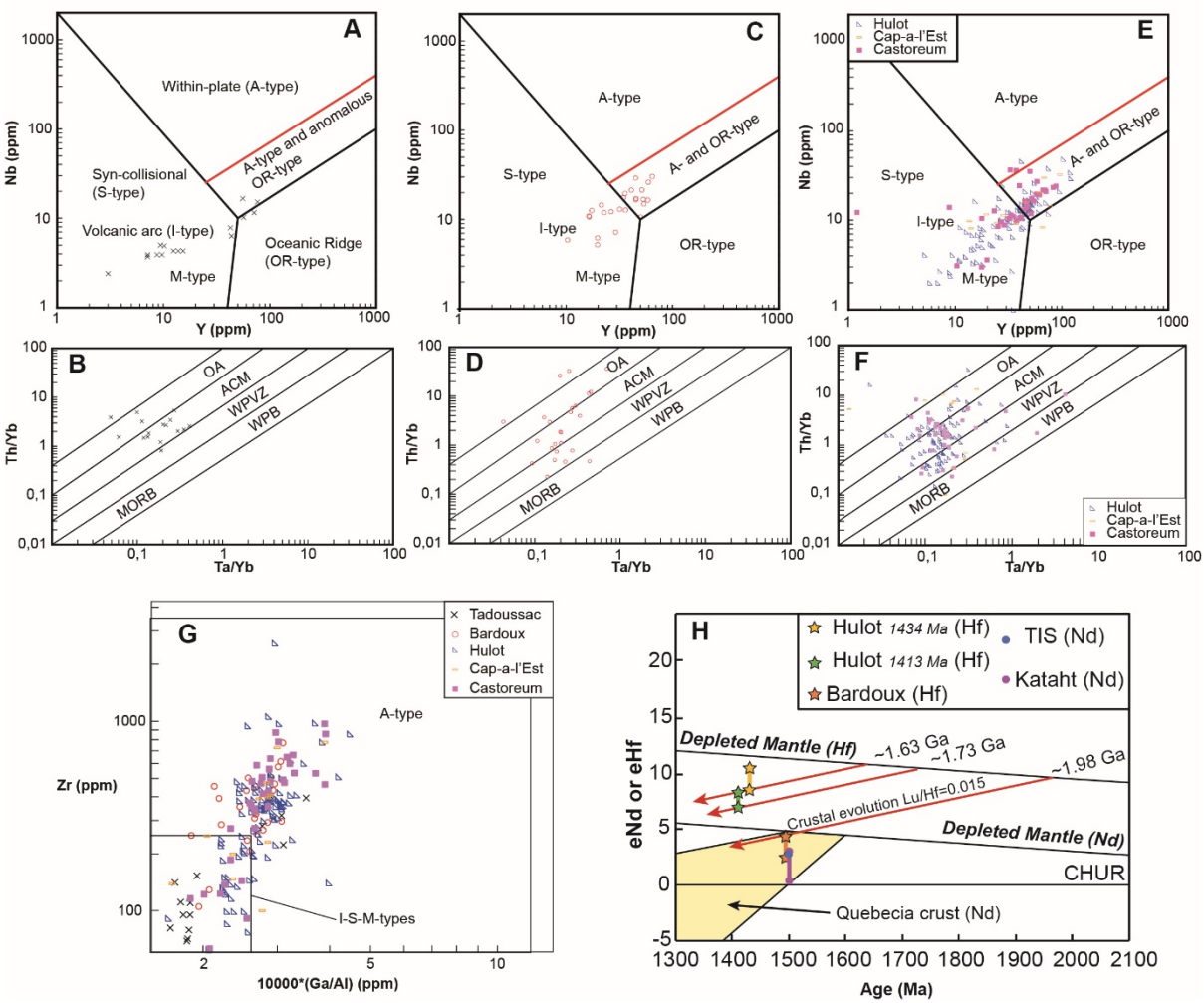

Figure 0.4: Whole rock lithogeochemistry were obtained from the Quebec Geological Survey Sigéom website. **A**, **C** and **E**: Y versus Nb plots (values in ppm) from Pearce et al. (1984) for the Tadoussac Intrusive Suite (**A**), Bardoux Plutonic Suite (**B**), and the Hulot, Cap-à-l'Est and Castoreum complexes (**C**). **B**, **D** and **F**: Diagrams Ta/Yb versus Th/Yb from Gorton and Schandl (2000) for the Tadoussac Intrusive Suite (**B**), Bardoux Plutonic Suite (**D**), and the Hulot, Cap-à-l'Est and Castoreum complexes (**F**). Abbreviations: ACM – Active Continental Margin, OA – Oceanic Arc, MORB – Mid-Oceanic Ridge Basalt, WPB – Within-Plate Basalt, WPVZ – Within-Plate Volcanic Zone. G: Diagram 10^4*(Ga/Al) vs Zr (Whalen et al., 1987). I-type = igneous source, S-type = crustal source, M-type = mantle-derived, A-type = alkaline. H: age (in Ma) versus εNd or εHf for intrusive rocks from the central (Tadoussac Intrusive Suite, Bardoux Plutonic Suite, Hulot Complex) and eastern (Kataht Plutonic Suite) Grenville Province. εNd values are from Brisebois and Clark (2003) and Groulier et al. (2018). εHf values are from Augland et al. (2015). Abbreviations: CHUR – Chondritic Uniform Reservoir.

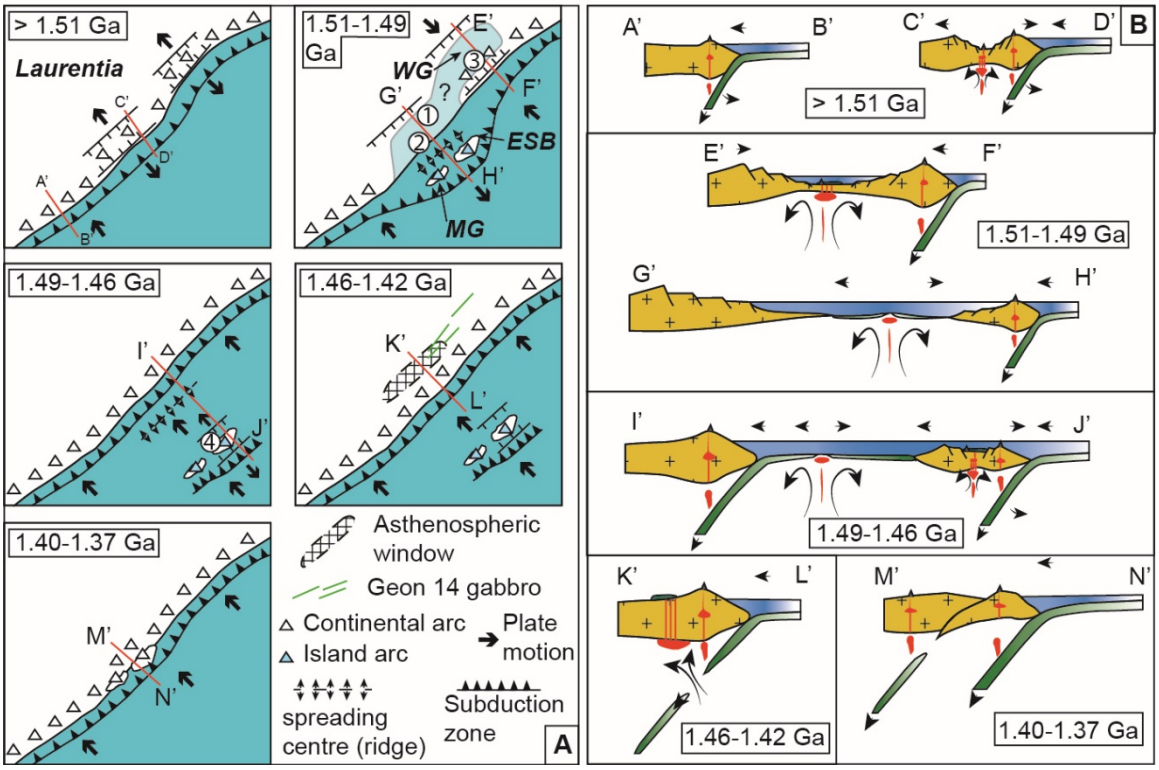

Figure 0.5: Sketches of the proposed evolution of the southeastern Laurentian margin in central and eastern Grenville from Geon 15 to early Geon 13. **A.** Map view. Circles with numbers refer to the sedimentary basins (1 – PLV; 2 – Bourdon; 3 – La Romaine; 4 – Port-aux-Quilles); labelled red lines correspond to the cross-sections in Figure 3b. Abbreviations: ESB – Escoumins Supracrustal Belt, MG – Montauban Group, WG – Wakeham Group; **B:** cross section view. The arrows show the direction of the plate and mantle motions.

Chapter 4 Recognition and documentation of a Mesoproterozoic sub-seafloor hydrothermal system within an oceanic arc, arc-rift and back-arc sequence preserved through Grenvillian metamorphism

4.1 Abstract

The Saint-Siméon Group, located in the south-central Grenville Province (Quebec), represents remnants of a Pinwarian (1.52 – 1.46 Ga) volcano-sedimentary sequence metamorphosed to the amphibolite facies during the Grenvillian orogeny (1.09 – 0.98 Ga). Its middle member (Moulin-à-Baude Formation) is a preserved part of a marine oceanic arc, arc-rift and back-arc sequence built on rifted Laurentian slivers. From the stratigraphic base to the top it consists of: calc-alkaline basalt, basaltic andesite and FII-type dacite; and island arc tholeiite and back-arc basalt, transitional basaltic andesite, ferrobasalt and alkaline FIII- to FIV-type dacite – rhyodacite – andesite together with sedimentary and exhalative rocks. Parts of the formation are extensively altered by synvolcanic hydrothermal fluids.

Based on field and petrographic observations the alteration assemblages are summarised as: (1) quartz – epidote in the lower part of the volcanic sequence, (2) magnetite – biotite, (3) albite – orthoamphibole – biotite – quartz – magnetite, (4) phlogopite – K-feldspar – quartz – clinozoisite/zoisite – tourmaline, (5) aluminous (sillimanite – muscovite) and potassic assemblages within felsic to intermediate volcanic rocks potentially synchronous with (6) amphibole – garnet and biotite – quartz alteration in mafic rocks and (7) silicification in the upper part of the volcanic sequence. In

addition, a skarn alteration (8) is late in the sequence and is locally crosscut by quartz – sericite (Mn) alteration.

The thickness of the alteration zones varies from less than a meter to tens of meters, and they can be semi-conformable or discordant. The assemblage (3) corresponds to Na-altered rocks (spillites) while the others experienced Na-loss together with various gains in Si, Mg, Fe, K, Ca and Mn. These alteration zones are interpreted to represent metamorphic equivalents of albite, chlorite, sericite, quartz, carbonate, clinozoisite/zoisite and argillic altered rocks typically found within VMS-deposits.

4.2 Introduction

The Grenville Province extends from the southeastern United States to the coast of Labrador in Canada (Fig. 4.1a) and was formed during the assembly of the supercontinent Rodinia (Li et al., 2008; Cawood et al., 2016), by continental collision with Amazonia. An important portion of the Grenville Province in Canada represents the remnants of continental and oceanic arcs and back-arcs formed at the SE Laurentian margin from the late Paleoproterozoic (~1.7 Ga) through most of the Mesoproterozoic (Whitmeyer and Karlstrom, 2007). These arc sequences were deformed and metamorphosed during the 1.09 – 0.98 Ga Grenvillian orogeny (Rivers and Corrigan, 2000; Rivers et al.; 2012). The Mesoproterozoic SE Laurentian margin is often compared to the Andean margin as it shares similar length (several thousands of km) and long duration of magmatic activity (Rivers and Corrigan, 2000; Karlstrom et al., 2001; Whitmeyer and Karlstrom, 2007).

One of the main crust-forming events at the scale of the SE Laurentian margin is the Pinwarian Orogeny (1.52 – 1.46 Ga; Tucker and Gower, 1990). Rocks of this age

formed in arc and back-arc settings have been identified along the entire southeastern Laurentian margin (Gower and Erdmer, 1988; Ketchum et al., 1998; McLelland et al., 2013; Slagstad et al., 2009; Karlstrom et al., 2001; Whitmeyer and Karlstrom, 2007). Most of these rocks have continental arc affinities (Gower and Krogh, 2002) but this is not the case for the central Grenville Province where remnants of island arc rocks are preserved in the Quebecia terrane (MacLean et al., 1982; Bernier and MacLean 1993; Groulier et al., 2018a).

In terms of economic potential, the Grenville Province hosts the largest hard rock ilmenite deposit in the world (lac Tio mine) and is actively explored for Fe–Ti±V±P and Ni–Cu deposits associated with the numerous anorthosite massifs and other mafic-ultramafic intrusions. In addition, the Grenville Province has a significant potential for pegmatite-skarn-veins hosted U- or Mo-occurrences (Sangster et al., 1992), industrial minerals (graphite, silicium metal, sillimanite, garnet) and rare metals (i.e. Nb–Ta–Zr–Y–REE) with the Crevier (Groulier et al., in review), Niobec, Kipawa deposits and numerous LREE-rich pegmatitic granite showings (Turlin et al., 2017). However, it remains little explored for shallow-level base and precious metals such as volcanogenic massive sulphides (VMS), iron-oxide-copper-gold (IOCG), epithermal or porphyry-type deposits, for which there is strong potential due to the presence of supracrustal belts and intrusions formed in prospective tectonic environments (Gauthier and Chartrand, 2005). This is because high-grade metamorphism (Rivers et al., 2012 and references therein) and deformation, during the Grenvillian orogeny, obscured to a large part the primary characteristics of the rocks. There are however several exceptions such as: (a) two metamorphosed auriferous VMS deposits have been mined in Pinwarian and Elzevirian

(1.3 – 1.2 Ga) volcanic sequences, the Zn–Pb–Au–Ag Montauban (Stamatelopoulou-Seymour and MacLean, 1984; Bernier et al., 1987; Sangster et al., 1992; Bernier and MacLean, 1993; Tomkins 2007) and the Calumet Zn–Pb–Cu–Au–Ag deposits (Williams 1990; Sangster et al., 1992) ; (b) the world-class "SEDEX" marble-hosted Zn–Pb deposits of the Balmat-Edwards-Pierrepont district (New York State, USA; Whelan et al., 1984) and smaller occurrences on the Canadian-side of the province (Gauthier and Brown, 1986; Gauthier and Chartrand, 2005); (c) iron-oxide ± copper-gold (IOCG) deposits such as the Cu-REE-U-Au-Mo-F Kwyjibo prospect (Gauthier et al., 2004) and the historical mines of the low-Ti magnetite Lyon Mountains deposits within the Adirondack Mountains (Gauthier and Chartrand, 2005). The western extension of the Grenville Province in the United States, the Granite-Rhyolite Province is also known for its IOCG and iron-oxide-apatite (IOA) deposits (see Nold et al., 2013; Day et al., 2016). These instances highlight the underexploited potential of the Grenville Province for base and precious metals mineralization and it has become crucial to better recognize, understand and define the different types of hydrothermal alteration zones associated with these types of deposits where they are overprinted by high-grade metamorphism (amphibolite to granulite-facies).

Some of the amphibolite-facies areas of the Grenville Province have preserved the original characteristics of the rocks (Martignole et al., 1994; Corriveau and Bonnet, 2005). The recently documented Escoumins supracrustal belt (ESB) in the southern central Grenville Province (Fig. 4.1b), is characterized by supracrustal rocks (Saint-Siméon Group) with well-preserved stratigraphic relationships, primary textures and evidence of complex hydrothermal alteration patterns (Groulier et al., 2018a). The ESB

consists of remnants of a peri-Laurentian Pinwarian (1.52 – 1.46 Ga) submarine to subaerial oceanic island arc and arc-rift/back-arc sequence built on crustal slivers rifted away from Laurentia during Geon 15 (Groulier et al., 2018a and chapter 3 of this thesis). This contribution focuses on hydrothermal alteration in the Saint-Siméon Group and provides new key information on the lithostratigraphy (primary volcanic textures, metamorphic mineral assemblage and petrogenesis of the volcanic rocks), metamorphosed hydrothermal mineral assemblage and alteration geochemistry. These reveal new prospective zones for VMS-type mineralization, and highlight the importance of a multiscale and multi-technique approach and have implications for similar belts in highly deformed and metamorphosed terranes.

4.3 Regional setting

4.3.1 Quebecia terrane

The ESB is part of Quebecia that represents a distinct ~1.5 Ga terrane defined by Sm–Nd isotope geochemistry (Dickin and Higgins, 1992; Dickin 2000; Dickin et al., 2010; Fig. 4.1b). It consists of a composite belt of oceanic arc and back-arc rocks built on older crustal panels rifted away from Laurentia during Geon 15 and accreted to Laurentia around ~1.4 Ga, as suggested by the presence of voluminous 1.41 – 1.37 Ga continental arc stitching plutons (Corrigan and van Breemen, 1997; Groulier et al., 2018a and chapter 3 of this thesis; Fig. 4.1b and c). Two 1.49 – 1.45 Ga submarine to potentially subaerial island arc and back-arc volcano-sedimentary sequences, the Montauban Group and the Saint-Siméon Group (SSG), are located in the southern part of Quebecia (Fig. 1c). They are intruded by calc-alkalic plutons of the 1.40 – 1.37 Ga La Bostonnais and Cap-à-l'Est

complexes reflecting the accretion of the oceanic arcs to Laurentia (Corrigan et al., 1994; Corrigan and van Breemen, 1997; Sappin et al., 2009; Groulier et al., 2018 and chapter 3 of this thesis). The SSG represents the remnants of a 1.49 – 1.46 Ga volcano-sedimentary sequence metamorphosed to the amphibolite facies during the Grenvillian Orogeny (Groulier et al., 2018a; Groulier et al., 2018b), and extends over 140 km from the town of La Malbaie in the SW to Forestville in the NE (Fig. 4.1b). The supracrustal rocks of the SSG are arranged in an overall dome and basin map pattern and they lie tectonically above the 1.5 Ga Tadoussac Intrusive Suite which represents their basement (Fig. 4.2; Groulier et al. 2018a), and younger plutonic rocks. Other supracrustal sequences exposed in the SW, close to the town of La Malbaie (La Malbaie Group) consist of metasedimentary and metavolcanic rocks that represent potential lateral equivalents of the SSG (Fig. 4.2). Further south and west, the Saint-Tite-des-Caps and Martres groups have less amphibolite and more marble implying a different environment of deposition but their ages remain unknown.

4.3.2 Geology of the Saint-Siméon Group

The SSG was divided into the Saint-Paul-du-Nord (lower), Moulin-à-Baude (middle – MAB) and Port-aux-Quilles (upper) formations by Rondot (1977, 1979 and 1986) and Rondot and Lavergne (1984), and was dated and documented by Groulier et al. (2018a). In this contribution we focus on two synclinal structures, the Grandes-Bergeronnes and Escoumins synclines (Fig. 4.2, 4.3 and 4.4), that were further investigated to refine the volcanic stratigraphy of the SSG, and study the hydrothermal alteration. The supracrustal sequence is complex and displays at the scale of each syncline

a wide variety of rock types with interfingering relationships, lenticular units, and abrupt facies variations.

The lower Saint-Paul-du-Nord Formation consists of planar-stratified centimetric to metric layers of metapelite, quartzite and greywacke with a lesser amount of volcaniclastic rocks, amphibolite and iron formation intruded by syn-volcanic mafic and ultramafic bodies. Metapelite is dominant and consists of garnet – muscovite ± sillimanite (locally pyrite and graphite-bearing) schist. These rocks are also crosscut by foliated, porphyroclastic high-K granitoids and by late Grenvillian (0.98 – 0.90 Ga) muscovite – biotite ± tourmaline ± garnet ± beryl pegmatites and leucogranite (Groulier et al., 2018b). The rock assemblage is typical of a marine sedimentary system where interlayered mudstone and sandstone can be deposited below wave base by suspension settling.

The MAB (Fig. 4.5) consists of a bimodal volcanic sequence with horizons of sedimentary rocks (volcanic-derived, detrital and chemical), and conglomerate together with volcanic feeder conduits. This formation hosts the hydrothermal alteration zones that are described in this study, and will be discussed in more detail in the next section.

The upper Port-aux-Quilles Formation is composed of a thick assemblage of dominant quartzite and subarkose (locally ferruginous) with minor wacke and metapelite. Amphibolite horizons parallel to the bedding may represent mafic sills (usually coarse-grained and hornblende-phyric) and scarce basaltic flows (fine-grained and massive). In the lower part of the formation the quartzite shows cross-bedding stratification (Fig. 6a) and stream ripples suggestive of deposition in a dynamic shallow water environment. Above it, centimeter to decimeter-thick planar-stratified layers are more consistent with

rhythmites deposited in deeper water environment (Fig. 4.6b). Detrital zircon from a cross-bedded quartzite gave a maximum deposition age of 1476 ±10 Ma with detrital zircon age spectrum typical of back-arc basins with peri-Laurentian sedimentary sources (Groulier et al., 2018a and chapter 3 of this thesis). The younger ages are coeval with the 1464 +38/-32 Ma age from the upper part of the MAB and the 1.5 Ga peak is interpreted to reflect the proximity to the Tadoussac Intrusive Suite (Groulier et al., 2018a). The evolution from a shallow water dynamic environment towards a deeper marine turbiditic sequence is consistent with a marine basin that experienced rapid subsidence. The lower volume of igneous rocks in the upper formation of the SSG suggests decreasing magmatic activity potentially linked to a migration of the magmatic zone or to the ending of back-arc magmatism.

4.4 Stratigraphy of the Moulin-à-Baude Formation

This section presents refined field description of the volcanic rocks of the MAB from the Escoumins and Grandes-Bergeronnes synclines, based on new detailed geological maps. The Escoumins syncline (Fig. 4.2) is an elongated northeast-southwest structure with a more developed western limb (Fig. 4.3). The MAB represents a band up to 3 km wide in the western limb and narrows to 200–300 m in the eastern limb. The Grandes-Bergeronnes syncline (Fig. 4.2) has a north-south pancake shape and the MAB forms a continuous belt of <1 km (western limb) to ~2 km thick (southeastern limb) around the upper Port-aux-Quilles Formation. Most of the eastern limb of the syncline is however concealed under quaternary deposits (Fig. 4.4). New geological mapping

together with detailed geochemistry (introduced in section 5) permitted separation of the MAB into a lower and upper parts. Volcanic rocks are named following the classification of McPhie et al. (1993). Figure 4.5 shows a schematic stratigraphic log of the Tadoussac Intrusive Suite and the SSG. Although all the rocks are metamorphosed, the prefix meta- is omitted from the rock names.

4.4.1 Lower Moulin-à-Baude Formation

The lower part of the MAB mainly consists of basalt and basaltic andesite crosscut by a regional stockwork of quartz-epidote (and other calc-silicate minerals) veins. The basaltic rocks are composed of plagioclase, hornblende with minor quartz, titanite and Fe-Ti oxides. They are generally fine-grained, locally amygdaloidal and some horizons display a preserved porphyritic texture defined by hornblende (Fig. 4.6c) or plagioclase phenocrysts (Fig. 4.6d). This sequence also includes tuffs, and flows. Some tuff horizons have juvenile mafic clasts together with felsic lapilli in a mafic groundmass indicating a bimodal volcanic activity. Rare volcanic breccias and hyaloclastites have fragments of mafic to intermediate intrusive and volcanic rocks in a basaltic groundmass (Fig. 4.6e). The lava flows are usually decimeter- to meter- thick, interlayered with tuffs. They are hornblende- or plagioclase-phyric, fine-grained massive and homogeneous or pillowed (Fig. 4.6f). The pillows are generally deformed, flattened and polarity indicators such as peduncles or quartz cavities are not conclusive. Hornblende and plagioclase-phyric mafic dykes crosscut the volcanic rocks and based on their chemistry they are interpreted to be feeder conduits for the overlying basalts (Groulier et al. 2018a). The types of volcanic rocks together with the lack of sedimentary rocks in this part of the lower MAB and the

widespread quartz-epidote veins indicates a submarine mafic-dominated effusive to explosive-type of volcanism with few breaks in the volcanic activity.

The top of this mafic volcanic sequence is marked by a horizon of sedimentary rocks. In the Escoumins syncline it corresponds to a thin interval of quartzite (locally pyrite- or hematite-bearing) whereas in the Grandes-Bergeronnes syncline the horizon consists of metapelite injected by felsic intrusions, coarse-grained and undeformed younger granite and by boudinated pegmatite. This sedimentary interval separates the basaltic rocks from a thick deposit of dacitic tuff dated at 1492 ±3 Ma (Groulier et al., 2018). In the Escoumins syncline the dacitic tuff is characterized by flattened amphibole – biotite – titanite fiamme (Fig. 4.6g) and it grades into a crystal (plagioclase with minor quartz) and lithic tuff towards the top. In the southwestern limb of the Grandes-Bergeronnes syncline, this felsic horizon has minor quartz eyes (Fig. 4.6h), lacks amphibole and fiamme or crystal-lithic textures but is instead characterized by laminar beddings that represents flow-banding or volcaniclastic lamina. In this location, the widespread presence of microcline and muscovite is suggestive of a potassic alteration. The dacitic tuff with the fiamme and crystal-lithic textures is consistent with explosive felsic volcanism and is associated with a polymictic conglomerate with pelitic and ash matrix. This is a stratigraphic marker horizon that can be followed in both synclines (Fig. 4.3, 4.5 and 4.8). The cobbles and boulders are matrix-supported, have rounded shapes (now flattened) and are of diverse origins (sedimentary, volcanic and plutonic) and sizes (millimetric to metric) (Fig. 4.7a). The biggest ones consist of felsic intrusive rocks (tonalite, trondhjemite, granodiorite and granite) typical of the Tadoussac Intrusive Suite.

Cobbles of plagioclase-phyric basalt from the underlying rock unit are also observed. This conglomerate is interpreted to have formed in a tectonically active volcanic basin, with a proximal source for the rock fragments (Groulier et al., 2018a). It implies a rapid exhumation and erosion of the ~1.5 Ga arc (Tadoussac Intrusive Suite) and of the underlying supracrustal rocks sequence indicating that parts of the arc were possibly shallow submarine to sub-aerial.

4.4.2 Upper Moulin-à-Baude Formation

Field observations of the upper MAB were based on the southern and northern limb of the Grandes-Bergeronnes syncline where powerline corridors provide exceptional exposures of the bedrock (Fig. 4.8). Parts of the upper MAB are extensively altered and host unusual mineral assemblages (discussed in section 6). The upper MAB (Fig. 4.5 and 4.8) starts with a thin horizon of massive and homogeneous felsic volcanic rocks that cover the conglomerate. A thick horizon (up to 280 meters thick) of basalt and basaltic andesite together with their gabbroic feeder conduits is found stratigraphically above. The basalt is fine-grained, locally highly amygdaloidal (Fig. 4.7b) and forms dominant massive flows. Locally, the basalt exhibits primary textures such as lobes or isolated pillows (Fig. 4.7c), tuff and breccia or hyaloclastite (Fig. 4.7d). Hyaloclastite and pillows are indicative of submarine volcanic eruption. Feeder gabbroic rocks are coarser-grained (Fig. 4.7e) and locally hornblende-phyric. The grain-size is a good differentiation factor between intrusive and extrusive mafic rocks, however due to the thickness of some basaltic horizons, it is still possible that some of the hornblende-phyric rocks represent lava flows. The dominant massive flow morphology makes polarity observation difficult,

though, hyaloclastite, amygdales and silica-filled pipes (more abundant toward the base of the flow) can be potentially used in order to determine the top of the sequence. Massive basaltic flows are interpreted to form during short, voluminous eruptions with high effusion rate potentially linked to fissure-like eruption (Gibson et al., 1999). Modern subaqueous massive flows are usually characterized by dominant massive facies overlain by hyaloclastite and very rare pillows. This mafic unit is characterized by the presence of patches and veins of quartz-epidote alteration, locally carbonates, sericitized plagioclase, anthophyllite and garnet.

In the Grandes-Bergeronnes syncline, a composite felsic unit composed of andesitic to dacitic-rhyodacitic volcanic, sub-volcanic, and volcaniclastic rocks with minor mafic horizons (lava flows and sills) is found stratigraphically above the basaltic rocks (Fig. 4.5 and 4.8). This felsic unit consists of massive to laminar felsic volcanic rocks interpreted to represent coherent felsic bodies (lava flows, lobes and domes) that laterally grade toward hyaloclastites, volcaniclastics rocks and possibly debris-flows together with their sub-volcanic sills and dykes (Fig. 4.7f and 4.7g). A high-silica leucocratic felsic volcanic rock, dated at 1468 +38/-32 Ma (Groulier et al., 2018), with clasts of biotite-muscovite and their breccia/hyaloclastite (Fig. 4.7h and 4.9a) may be a metamorphosed equivalent of lava-like ignimbrite with pumice but also lava lobes or lava flows as in some place relicts of flow-banding texture seem to be preserved. The biotite-muscovite clasts are commonly surrounded by a halo of K-feldspar (Fig. 4.9b). Tourmaline and garnet are present locally, and may represent products of the alteration of the rock during the passage of fluids creating a false pyroclastic texture. The proportion of amphibolite (volcanic or intrusive), tuff (Fig. 4.9c), planar-bedded ash-tuff – volcanic

siltstone and sandstone (Fig. 4.9d) with minor volcanic mudstone, chemical sediments (chert, calcareous rocks) and other volcanic-derived sedimentary rocks (Fig. 4.9e and 4.9f) increases toward the top of this unit.

Felsic tuff and volcaniclastic rocks were also observed together with exhalative Ba-rich chert horizons (Fig. 4.9e) in the northern limb of the Grandes-Bergeronnes syncline (Fig. 4.8b). In addition, this horizon contains calc-silicate rocks with skarn mineral assemblage (diopside, carbonate, tremolite/ actinolite, clinozoisite/zoisite, phlogopite, quartz, anorthite, microcline, titanite, scapolite, garnet and sometimes a Mn-rich muscovite variety called wilsonite; see section 6 for more details). In the northern part of the Grandes-Bergeronnes syncline, altered basaltic and felsic volcanic rocks are together with a horizon of intermediate to felsic amphibole and sulfide-bearing laminated tuffite (Fig. 4.9g) with anomalous Zn–Pb contents (1620 ppm Zn and 622 ppm Pb). This tuffite likely formed by a mixture of volcanic ash and sulfide-rich chemical sediments. These rock units are consistent with the presence of a potentially metal-rich hydrothermal-exhalative horizon within the sequence. The tuffite can be used as a metallotect in order to find massive sulfide lens (as for the Matagami VMS district with the Key tuffite; see Genna et al., 2014). Finally, on top of the felsic composite unit, massive and locally highly amygdaloidal basaltic flows (Fig. 4.9h) marks the end of the MAB. The high proportion of vesicles is indicative of volatile-rich magma and together with lapilli tuff is suggestive of a shallow water-depth emplacement of the lava.

4.5 Sampling and analytical techniques

The rock samples used for this study were collected by the first author during the summers 2013, 2014, 2015 and 2017. Mineral assemblages from non-altered and altered mafic to felsic volcanic rocks were documented using field observations, detail petrographic studies and lithogeochemistry. In addition to optical microscopy, microstructures at the thin section scale were documented by SEM–MLA false color mineralogical maps that are not discussed here, but are shown in Appendix 1.

4.5.1 Whole-rock geochemistry

Whole-rock major and trace element analyses were performed by Actlabs (Ancaster, Ontario). The powdered samples were prepared using Li-metaborate and Li-tetraborate fusions. Major elements were analyzed by inductively coupled plasma (ICP) and trace elements were analyzed by ICP-mass spectrometry (MS). The data are reported in Table 4.1. Some of the non-altered rocks geochemistry data were used in Groulier et al. (2018a), this study represents a more refined investigation that also incorporates altered rocks. Detection limits are available on the Actlabs website. Precision and accuracy are consistent with the estimates given in Jenner (1996).

4.5.2 Electron probe microanalysis (EPMA)

Major and trace element composition of selected minerals were measured using a JEOL JXA 8230 electron microprobe at MUN. Detailed analytical methods of major and trace element analyses and results are provided in Table A4.1 and Appendix 2.

4.6 Lithogeochemistry of the volcanic rocks

Trace elements are commonly used to determine chemical affinities and possible tectonic setting of formation for ancient volcanic rocks based on recent analogues (Pearce et al., 1984; Pearce 2008; Ross and Bédard, 2009). Lithogeochemistry is also instrumental for assessing prospective areas for VMS deposits (Lesher et al., 1986; Hart et al., 2004; Piercey, 2010, 2011) and their different types of alteration (see Barrett and McLean, 1994a, b; Piercey, 2008). In localities where the SSG is extensively altered, finding least altered rocks for some units is challenging. Criteria for the selection of the least altered samples were (1) Na_2O content ranging between 2 and 5 weight percent, (2) no anomalous contents in Ca, Mg, Mn, Fe or Si, (3) low loss on ignition (LOI), metals (Cu, Zn, Pb) and S contents (4), no anomalous metamorphic mineral assemblage in thin section and preserved primary volcanic textures in hand specimen. Most of the major elements are mobile in VMS-related hydrothermal system, elements such as Ti, Al, P, some high field strength elements –HFSE– (Nb, Ta, Zr, Hf, Th and rare earth elements – REE) are usually interpreted to be immobile under low water-to-rock ratios alteration (Winchester and Floyd, 1977; Barrett and MacLean, 1994, 1999; Jenner, 1996; Gifkins et al., 2005). Exceptions are presented in section 7.

For this reason, in order to determine primary characteristics of the bimodal volcanic sequence (chemical affinity and tectonic settings), the mobility of "immobile" elements has been tested using Zr as a reference (see Appendix 3). For mafic volcanic rocks, most tested elements seem to be immobile and Rb appears to be mobile under certain conditions. It is more complex for felsic volcanic rocks, as some anomalous samples can be potentially linked to heterogeneity in the sample (cf. volcaniclastic rocks)

or to the remobilization of certain elements during the passage of hydrothermal fluids. In some altered felsic volcanic rocks Zr, most REEs and Y appeared to be mobile. However, in this study both least altered and altered samples will be use in the different diagrams presented.

4.6.1 General characteristics

Volcanic rocks from the MAB were separated based on their stratigraphic position and immobile elements composition. This formation consists of a sub-alkaline bimodal volcanic sequence (Fig. 4.10a) composed by basalt and basaltic andesite together with intermediate to felsic volcanic rocks of andesitic to rhyolitic composition. Four different types of mafic volcanic rocks (M1 to M4) and three types of intermediate to felsic volcanic rocks (I1, F1 and F2) have been recognized: M1 and F1 in the lower MAB, M2 in the lower portion of upper part MAB; and, M3-M4 and I1-F2 in the upper portion of upper MAB (see Fig. 4.5). Based on the Th/Yb versus Zr/Y diagram (Ross and Bédard, 2009; Fig. 4.10b) M1 is transitional to calc-alkalic, F1 is calc-alkalic, M2 is tholeiitic, M3 and M4 are tholeiitic to transitional (dominant). F2 follows a clear fractionation trend between the calc-alkalic to transitional fields (consistent with fractionation of plagioclase – hornblende – biotite – ilmenite and traces minerals such as apatite – titanite – zircon – allanite; see Ross and Bédard, 2009) and I1 follows a trend in the transitional to the calc-alkalic fields. For comparison, La versus Yb (Fig. 4.10c) and Zr versus Y (Fig. 4.10d) diagrams from MacLean and Barrett (1993) and Barrett and MacLean (1994) are provided. Mafic rocks usually display the same magmatic affinities as on the Ross and Bédard (2009) diagram, however felsic volcanic rocks show a more complex and

scattered distribution together with different magmatic affinities more likely due to the remobilization of some of these elements due to hydrothermal alteration. TiO_2 versus Zr (Fig. 10e) and Al_2O_3 versus Zr (Fig. 4.10f) are useful to highlight superposed effect of fractionation (following different fractionation trends depending on the magmatic affinity) and alteration (lines that passes through the origin and that connect altered and least altered samples). For instance, on the TiO_2 versus Zr diagram volcanic rocks from the upper MAB (M2, M3, I1 and F2 at the exception of the M4 ferrobasalts) follow a typical tholeiitic trend. Several alteration lines are discernible and are consistent with mass gain or loss from multiple precursors. Similar tholeiitic trends with decreasing aluminum content with fractionation and alteration lines are visible on the Al_2O_3 versus Zr diagram. The red arrow, with strongly decreasing Zr compared to Al_2O_3 values, represents a trend of altered felsic to intermediate rocks. This unusual alteration trend is possibly linked to Zr remobilization.

4.6.2 Geochemistry of the mafic rocks

4.6.2.1 M1 unit, lower part of the MAB

This unit is a complex succession of coherent flows and volcaniclastic rocks of mafic to intermediate or (minor) felsic composition crosscut by syn- to potentially post-volcanic dykes. This complexity also appears in geochemistry with different trace element compositions and further work would be necessary in order to better discriminate the different types of volcanic rocks. On chrondrite-normalized REE plot (Fig. 4.11a), M1 rocks display strong fractionation between light and heavy REE (La/Yb_{cn} = 1.47 – 8.2; cn = chondrite normalized) and Th/Yb ratio (0.21 – 2.21) typical of transitional to calc-

alkaline rocks (Ross and Bédard, 2009). At least two distinct patterns are discernible suggesting that M1 is likely composed by different types of basaltic rocks, consistently with the field observations. Furthermore, hydrothermally altered rocks exhibit variations in REE patterns with increase or decrease in values linked to mass gain or loss. On a primitive mantle-normalized extended trace element diagram, M1 rocks display negative anomalies in HFSE (Nb and sometimes Ti), a positive anomaly in Th and an enrichment in LREE compared to HREE (Fig. 4.11b).

4.6.2.2 M2 unit, upper part of the MAB

M2 basalts in the upper part of MAB are a coherent unit of massive to amygdaloidal lava flows together with hornblende-phyric syn-volcanic intrusive and extrusive rocks. They are characterized by flat REE patterns (La/Yb_{cn} = 0.79 – 3.36) and Th/Yb ratio (0.15 – 0.76) typical of tholeiitic rocks (Fig. 4.11c; Ross and Bédard, 2009), flat patterns on a primitive mantle-normalized extended trace elements diagram with unnoticeable to weak fractionation between LREE and HREE, weak negative anomaly in Ti, negative anomaly in Nb and positive anomaly in Th (Fig. 4.11d). This unit is relatively primitive. The least altered samples have low Nb (1 – 2.8 ppm), Zr (71 – 88 ppm) and P (0.11 – 0.16 wt.% P_2O_5) content and high Co (45 – 52 ppm), V (242 – 258 ppm), Ni (70 – 161 ppm), Mg (6.9 – 8.57 wt.% MgO) content. They are juvenile (εNd_t of 4.92 – 5.21; Groulier et al., 2018a) and have a signature typical of island arc tholeiite or Th-enriched back-arc basin basalt.

4.6.2.3 *M3 unit, upper part of the MAB*

Basaltic rocks from this unit are closely associated to the I1 and F2 intermediate and felsic volcanic rocks. They are evolved basaltic andesite enriched in Zr (106 – 199 ppm), Nb (4.1 – 17.7 ppm) and P (0.19 – 0.81 wt.% P_2O_5). On a chondrite-normalized REE plot (Fig. 4.11e), they display a strong overall enrichment in REE with a fractionation between LREE and HREE (La/Yb_{cn} = 1.39 – 4.42) and Th/Yb ratio (0.22 – 1.19) typical of transitional to calc-alkaline rocks (Ross and Bédard, 2009). On a primitive mantle-normalized extended trace elements diagram they display a positive Th anomaly, negative Nb, Ti, Al and V anomalies (Fig. 4.11f).

4.6.2.4 M4 ferrobasalt, upper part of the MAB

M4 ferrobasalts are found in the upper MAB within and stratigraphically above the felsic composite, and the M3 units. Altered and less altered samples are characterized by high $Fe_2O_{3\ tot}$ (13.65 – 18.42 wt.%), P_2O_5 (0.24 – 0.51 wt.%), TiO_2 (~2.1 – 3.5 wt.%), Nb (3.1 – 10.1 ppm), Zr (144 – 213 ppm), Co (42 – 71 ppm) and V (279 – 392 ppm) content. These rocks are highly evolved as suggested by the overall enrichment in REE and HFSE. On a chrondite-normalized REE plot (Fig. 11g), they show an enrichment in LREE (La/Yb_{cn} = 1.36 – 2.54) and have Th/Yb ratio (0.18 – 0.41) typical of transitional rocks (Ross and Bédard, 2009). On a primitive mantle-normalized extended trace elements diagram they display a weak negative anomaly in Nb, positive Th and V anomalies, and lack a negative Ti anomaly (Fig. 4.11h). Their REE and extended trace elements patterns share similarities with OIB- or E-MORB rocks, the enrichment in Th and the negative Nb anomaly are however not consistent with such rocks. They more

likely represent back-arc basalt formed from the melting of an enriched source. Their Nd isotopes indicates that they are juvenile (εNd_t of 3.91; Groulier et al., 2018a) and they more likely form from a more enriched mantle source than the M2 unit or that it interacted with crustal material.

4.6.2.5 Tectonic environment

On the Agrawal et al (2008) and Condie (2003) diagrams the basaltic rocks of the SSG fall in the arc (dominant) to E-MORB fields (Fig. 4.12a and 4.12b). Basalts from the upper part of the formation (M3 and M4) straddle the enriched-MORB and oceanic plateau basalts fields while the others fall dominantly in the arc field. On the Y–La–Nb (Fig. 4.12c) and Hf–Th–Ta (Fig. 4.12d) ternary discrimination diagrams of Cabanis and Lecolle (1989) and Wood (1980) the basaltic rocks display a similar arc environment trend. In these two diagrams M1 and M3 basalts fall in the calc-alkaline to transitional arc field while the others fall in the tholeiitic field. On the Pearce (2014) diagram (Fig. 4.12e), they fall dominantly in the volcanic arc array above the MORB-OIB array. The data mostly plot in the oceanic arcs field, and the oblique trend suggests interaction of the magma with more evolved crust. On the TiO_2/Yb-Nb/Yb plot (Fig. 4.12f) from Pearce (2008) most of the mafic volcanic rocks fall in the N- and E-MORB fields (shallow melting of the mantle), with some of the M4 rocks in the OIB tholeiitic field, following a trend of plume-ridge interaction. In the Ti–V diagram (from Shervais, 1982), M1 rocks straddle in the arc tholeiite to MORB/back-arc fields (Fig. 4.13a), and the others fall in the MORB/back-arc basin basalt (M2) and ocean island-alkali basalt fields (M3, M4). The high Ti and V contents of the M4 rocks are consistent with continental-crust

associated extensional volcanic environment (Piercey, 2010). M4 rocks are characterized as ferrobasalt or FeTi basalt based on their extreme enrichment in Ti and Fe (Fig. 4.13b).

4.6.3 Geochemistry of felsic and intermediate rocks

Felsic and intermediate volcanic rocks from the MAB are describe using the classification from Lesher et al. (1986) and Hart et al. (2006). FI rocks have high Zr/Y and La/Yb ratios, low HFSE contents and are enriched in LREE consistent with calc-alkaline signatures while FIII and FIV rocks have lower Zr/Y and La/Yb ratios and are enriched in HFSE. FII-types are intermediate between the two groups. FIII and FIV rocks are interpreted to have formed from melting of hydrated mafic crust at shallow levels (<10 km) and high temperature (>900°C) in rifting environment, FII rocks formed at mid-crustal levels (10–15 km) and lower temperature (<900°C) and finally FI rocks are interpreted to have formed from low temperature (<750°C) melting at greater depth (>30 km) (Hart et al., 2006).

4.6.3.1 F1 unit

This unit is located above the M1 unit of lower MAB. It is a thick deposit of tuff with fiamme texture grading toward a crystal, lapilli and lithic fragments variety toward the top, and is hornblende, biotite and titanite-rich. The least altered samples have SiO_2 (65 wt. %) content typical of dacite, and more K_2O (3.63 – 4.34 wt.%) than Na_2O (3.02 – 3.30 wt.%). F1 rocks have calc-alkalic affinities (Ross and Bédard, 2009), Yb_{CN} values and $[La/Yb]_{CN}$ ratios like FII-type felsic volcanic rocks (Fig. 4.15a), and Y values and

Zr/Y ratio similar to FII- and FIII-type rocks (Fig. 4.15b) (Lesher et al., 1986; Hart et al., 2004). Least altered samples are characterized by relatively high Nb (12 ppm), Th (14 – 15 ppm), Y (36 – 37 ppm) and Zr (230 – 246 ppm) content. On a chondrite-normalized REE diagram (Fig. 4.14a) they display a strong enrichment in LREE compared to HREE (La/Yb_{CN} = 7.34-8.59) with a negative Eu anomaly (Eu* = 0.52-0.55). On a primitive mantle-normalized plot this unit shows a strong positive Th anomaly, negative Nb, Eu, Ti and V anomalies (Fig. 4.14b). The zircon saturation temperature (T_{Zr} = 854 – 858°C) calculated from the formula of Watson and Harrison (1983) and adapted by Hanchar and Watson (2003) is within the temperature range for FII-type felsic volcanic rocks. This unit was dated by Groulier et al. (2018a) at 1492 ±3 Ma, inherited cores within zircon grains were observed using cathodoluminescence imaging. It gave slightly negative εNd_t (-0.8) together with a Paleoproterozoic calculated Nd depleted mantle age (T_{DM} = 1.94 Ga) consistent with mixing between a juvenile magma and older crust or remelting of an older crust.

4.6.3.2 F2 unit

This unit is part of the upper composite felsic unit of MAB. Least altered samples have relatively high silica content (66.82 – 76.82 wt.% SiO_2), are sodic with more Na_2O (2.36 – 5.57 wt.%) than K_2O (0.33 – 1.81 wt.%) typical of dacitic to rhyodacitic rocks. This unit has calc-alkalic to transitional affinities (Ross and Bédard, 2009), Yb_{CN} values and $[La/Yb]_{CN}$ ratios like FIIIa- and FIV-type felsic volcanic rocks (Fig. 4.15a), and Y values and Zr/Y ratio similar to FII-, FIIIa- and FIIIb-type rocks (Fig. 4.15b) (Lesher et

al., 1986; Hart et al., 2004). They have intermediate Nb (9.8 – 11.8 ppm) and Th (6.45 – 10.9 ppm) contents, high Y (50.9 – 68.3 ppm) and Zr (243 – 282 ppm) content. On a chondrite-normalized REE plot (Fig. 4.14c), they display a strong fractionation of REE with a significant enrichment in LREE compared to HREE (La/Yb_{CN} = 0.78-4.46, average of 2.82) with a strong Eu negative anomaly (Eu*=0.52–0.60 for the least altered rocks). On a primitive mantle-normalized plot this unit is characterized by a positive Th anomaly, and negative Nb, Eu, Ti, Al and V anomalies (Fig. 4.14d). The calculated zircon saturation temperature (T_{Zr}= 857 – 866°C). One rock from this unit was dated at 1464 +38/-32 Ma by Groulier et al. (2018a).

4.6.3.3 I1 intermediate unit

This unit is part of the upper composite felsic unit of MAB. Least altered samples are intermediate (59.6 – 61.61 wt.% SiO_2) andesitic rocks, with more Na_2O (3.24 – 4.92 wt.%) than K_2O (1.31 – 2.03 wt.%). This andesitic unit has transitional to calc-alkalic affinities (Ross and Bédard, 2009), Yb_{CN} values and $[La/Yb]_{CN}$ ratios like FIIIa- and FIV-type felsic volcanic rocks (Fig. 4.15a), and Y values and Zr/Y ratio similar to FII-, FIIIa- and FIIIb-type rocks (Fig. 4.15b) (Lesher et al., 1986; Hart et al., 2004). They also have low Th (2.17 – 2.52 ppm) content but are enriched in other HFSE such as Nb (10.1 – 19.8 ppm), Y (32.5 – 93.1 ppm) and Zr (298 – 324 ppm). On a chondrite-normalized diagram (Fig. 4.14e), the andesitic rocks are characterized by less fractionation between LREE and HREE (La/Yb_{CN} = 0.31-4.13, average of 2.32) and a smaller negative Eu anomaly (Eu*=0.79-0.85) compared to the other two units. Some altered samples show an extreme

depletion of REE consistent with a gain of mass during the passage of a hydrothermal fluid while a strongly muscovite-carbonate-microcline altered one is characterized by a positive Eu anomaly (Eu*=1.34). On a primitive mantle-normalized plot, I1 rocks are characterized by weak to absent Th positive anomaly, weak Nb negative anomaly, positive Zr and Hf anomalies and negative Ti, Al and V anomalies (Fig. 4.14f). They have the highest calculated zircon saturation temperature (T_{Zr}= 879 – 892°C) which is consistent with the elevated concentration of HFSE.

4.6.3.4 Tectonic environment

On a Nb–Y plot (Fig. 4.15c) from Pearce et al. (1984), the felsic volcanic rocks of MAB fall in the volcanic arc (VAG), oceanic ridge (ORG) and within-plate granites (WPG) fields. F1 rock data plot within the VAG field whereas F2 and I1 rock data straddle the VAG toward the ORG and WPG fields. On the Zr versus Ga/Al diagram (Fig. 4.15d), F1 data points plot in the I-, S- and M-type field, and most of the F2 and I1 data points plot in the A-type field. Overall, the F1 unit is calc-alkaline, FII-type and arc-related. Such rocks with high $[La/Yb]_{CN}$ and Zr/Y ratios and with negative Y anomaly are interpreted to form by deep to intermediate (30–10 km) low-degree partial melting at low temperature (~650 to ~1000°C) where garnet (HREE retention) and amphibole (Y retention) are stable in the residue (Lesher et al., 1986; Hart et al., 2004). F2 and I1 units have a calc-alkaline to transitional affinity and are mostly alkaline (A-type). They have lower $[La/Yb]_{CN}$ and Zr/Y ratios with higher contents in HFSE typical of FIIIa to FIV-types rhyolite. These rocks are interpreted to have formed at low-pressure (<10 km) and

high temperature (~900 to ~1100°C) low to moderate partial melting of tholeiitic basaltic crust in an extensional environment (Hart et al., 2004). These three units can be well separated using the Hf–Th–Ta (Fig. 4.15e) ternary discrimination diagrams of Wood (1980) and the Th/Yb–Nb/Yb diagram (Fig. 4.15f) of Pearce (2008). These two diagrams show a decrease in the Th content of the felsic volcanic rocks and an increase in HFSE (Hf, Ta, Nb, Yb). It can be interpreted as a decreasing interaction of the juvenile magma with older material during the thinning of the crust or a decreasing subduction input of Th.

4.7 Metamorphosed hydrothermal alteration assemblage, mineral chemistry and sulfide occurrences

The supracrustal rocks of the SSG were metamorphosed to the amphibolite facies during the Grenvillian orogeny (Groulier et al., 2018b). Least altered intermediate to felsic volcanic rocks have quartz, plagioclase dominant over K-feldspar, amphibole and/or biotite with trace of Fe-Ti oxides, zircon and apatite. Least altered basaltic rocks are garnet-free and contain plagioclase, hornblende (magnesio- and tschermakitic hornblende composition, Fig. 4.16b), ilmenite with minor quartz, epidote and titanite. Therefore, the presence of minerals such as aluminum-rich epidote (clinozoisite/zoisite which represent polymorphs [$Ca_2Al_3Si_2O_{12}(OH)$]), REE-bearing epidote (allanite), garnet, diopside, Fe–Mg amphibole (anthophyllite-gedrite or cummingtonite), aluminosilicate (sillimanite) or excessive proportion of albite, potassium feldspar, quartz, biotite or muscovite within metamorphosed volcanic and sedimentary rocks of the MAB is indicative of change of the chemistry of the rock by pre-metamorphic hydrothermal

alteration. For the purpose of this study we will refer to the calc-silicate alteration assemblage as “skarn” following the denomination of Jansson et al. (2013) for similar types of rocks, even though they are not related to an intrusion. Table 4.2 summarizes the different types of alteration. Figures 4.16 and 4.17 display compositional diagrams for the analyzed alteration minerals.

4.7.1 Mafic volcanic and volcaniclastic rocks

4.7.1.1 Epidote, quartz

Epidote – quartz alteration is common in the basaltic rocks from the lower MAB (M1 unit), and is also observed in the upper mafic to felsic units. It is manifested by concordant and discordant veins, veinlets, sub-circular patches and sometimes as pervasive replacement of entire horizons. In basaltic rocks, the original amphibole – plagioclase assemblage is entirely replaced by a core of quartz surrounded by epidote, magnetite porphyroblasts and sericitized plagioclase (Fig. 4.18a). Other calcic minerals present are titanite, grossular, calcite and diopside (Fig. 4.18b). This alteration is usually barren, but in the presence of sulfides it is linked to some Cu, Au and Ag anomalies.

4.7.1.2 Amphibole, garnet ± phlogopite

This alteration is usually observed in the M3 and M4 units of the upper MAB, where it forms veins, concordant horizons and discordant pipes of amphibole or amphibole – garnet ± biotite rich rocks with variable proportions of quartz, plagioclase, oxides and sulfides. The amphiboles are either calcic (tschermakitic hornblende) or

ferromagnesian in composition (orthoamphibole anthophyllite – gedrite or monoclinic cummingtonite – grunerite series) (Fig. 4.16b and 4.16c). Three main assemblages were recognized: (1) garnet – cummingtonite – calcic amphibole ± biotite (Fig. 4.19c, 4.19d and 4.19e); (2) garnet – gedrite (with minor anthophyllite) – biotite (Fig. 4.19f, 4.19g); and (3) calcic amphibole – garnet – biotite. Garnet is the almandine end-member and it has varying contents of Ca, Mg and Mn (mean calculated composition is $Almandine_{61–70}$ $Pyrope_{9–21}$ $Grossular_{6–23}$ $Spessartine_{2–5}$) (Fig. 4.17a, 4.17b, 4.17c). Amphibole can form up to 90% of the volume of the rocks, garnet (> 20% and up to 50 vol.%) can appear as centimeter-size porphyroblasts, facilitating the field recognition of this type of alteration. When biotite is a minor constituent of the rock (< 5 vol.%), it has anomalous values in Ba (up to 0.6 wt.% BaO) and is Mg-rich (with X_{Fe} of ~0.4; Fig. 4.16d). Biotite is more Fe-rich (X_{Fe} of ~0.54; Fig. 4.16d) and it has lower Ba content (BaO <0.1 wt.%) in samples with higher proportion of biotite (>5 vol.%) and no Fe–Mg amphiboles. Biotite together with gedrite and garnet is Mg-rich (X_{Fe} = 0.34-0.37; Fig. 4.16d), low Ba (0.11 and 0.28 wt.% BaO) and Mn (<0.3 wt.% MnO) contents. Disseminated sulfides (chalcopyrite, pyrrhotite, pyrite) and magnetite are in some case part of the mineral assemblage. This alteration is principally hosted within a fragmental and silica-rich mafic rock unit which may be a hydrothermal breccia, a hyaloclastite, or a pyroclastic breccia. Amphibole – garnet ± biotite altered rocks are in close relation with biotite – quartz altered basaltic rocks, quartz-rich alteration zones, skarns, albite – FeMg amphibole/biotite – quartz altered felsic rocks and phlogopite – quartz – microcline – clinozoisite/zoisite – tourmaline altered felsic rocks.

4.7.1.3 Biotite, quartz

The biotite – quartz alteration was observed in the western limb of the Escoumins syncline in the M1 unit and within the M4 unit in the Grandes-Bergeronnes syncline. The altered rocks appear dark and rusted on weathered surfaces and they are usually in the proximity of amphibole – garnet ± biotite altered mafic rocks. The proportion of biotite versus amphibole increases toward the maximum zone of biotitization (Fig. 19a, 19b) that forms veins and discordant corridor of alteration. Biotite has X_{Fe} of 0.5 (Fig. 4.16d), and has low Ba content (<0.1 wt.% BaO) with trace values in Mn (0.15-0.20 wt.% MnO). Biotitization is commonly associated with silicification and disseminated sulfides (pyrrhotite, chalcopyrite, pyrite and As–Ni–Co sulfides from the gersdorffite – cobaltite solid solution).

4.7.2 Felsic volcanic and volcaniclastic rocks

4.7.2.1 *Magnetite, biotite ± epidote*

The magnetite – biotite ± epidote alteration is subtle, pervasive but can also appear as veins. It consists of millimeter-sized magnetite porphyroblasts and biotite disseminated within the altered rock.

4.7.2.2 *Mn–Ca–Fe garnet, calcic amphibole, quartz, calcic plagioclase, biotite (epidote)*

This alteration affects andesitic rocks of the I1 unit. It consists of veins of orange Mn-Ca-rich almandine garnet ($Almandine_{34-37}$ $Grossular_{29-32}$ $Spessartine_{23-26}$ with up to 11

wt.% MnO and 13 wt.% CaO; Fig. 4.17a, 4.17b, 4.17c) together with quartz, calcic plagioclase, calcic amphibole (ferro-tschermakite; Fig. 4.16b), magnetite, biotite (X_{Fe} = 0.54 – 0.59 with up to 0.52 wt.% MnO; Fig. 4.16d), calcite, epidote, titanite and apatite (Fig. 4.19c, 4.19d). Garnet forms up to 5 vol.% of the rock.

4.7.2.3 Albite, gedrite/anthophyllite and/or phlogopite, quartz, magnetite

This alteration assemblage affects I1 and F2 rocks of the Grandes-Bergeronnes syncline at proximity to M3 and M4 mafic volcanic rocks. The altered rocks have a bleached (white to beige) color due to the high proportion of albite. They are also characterized by the presence of millimeter- to centimeter-sized acicular to radiating needles of orthoamphibole (Fig. 4.19e and 4.19f) or by high proportion of biotite (Fig. 4.19g and 4.19h), and magnetite as disseminated grains or crosscutting veins. This alteration is crosscut by centimeter-sized quartz veins. The orthoamphiboles are anthophyllite and gedrite (Fig. 4.16c) and biotite is Mg-rich (X_{Fe} of 0.3–0.4; Fig. 4.16d). The orthoamphiboles are locally retrogressed to quartz–chlorite–biotite.

4.7.2.4 Epidote, K-feldspar, biotite, quartz, carbonate, magnetite, plagioclase, muscovite

This alteration assemblage is well-developed in the composite felsic unit in the northern limb of the Grandes-Bergeronnes syncline. The alteration is pervasive, or forms a stockwork of veins (Fig. 4.20a). It is locally overprinted by a pervasive muscovite alteration that can totally obliterate the previous alteration assemblage and is crosscut by boudinaged skarn veins of calcic amphibole, epidote, quartz and minor diopside (Fig. 4.20b). The alteration mineral assemblage consists of allanite, epidote, K-feldspar, biotite,

quartz together with carbonate, magnetite, muscovite, plagioclase and tourmaline (Fig. 4.20c and 4.20d). Some of the analyzed epidote grains straddle to the Fe-rich epidote pole (Fig. 4.16a) and biotite is Fe-rich (X_{Fe} of ~0.65; Fig. 4.16d).

4.7.2.5 Phlogopite, K-feldspar, quartz, clinozoisite/zoisite, tourmaline

This alteration assemblage is observed within the composite felsic unit in the Grandes-Bergeronnes syncline (northern and southern limb) within the F2 and I1 intermediate to felsic rocks. Its mineralogy is complex and consists of phlogopite (Mg-rich biotite based on EDX measurement), K-feldspar, quartz, clinozoisite/zoisite (based on thin section observation) with minor calcite, muscovite, plagioclase, calcic amphibole, tourmaline, epidote, titanite, sulfides and Fe oxides (Fig. 4.20e and 4.20f). The alteration is pervasive and replaces the original mineral assemblage of the host rock but can also form veins. It is characterized by high proportion of potassic, calcic and magnesian minerals together with clinozoisite-zoisite, and tourmaline is the dravite (Fe–Mg) variety (EDX measurement). This alteration grades laterally toward aluminous rocks (muscovite and sillimanite altered rocks).

4.7.2.6 Muscovite, quartz, Fe oxides, tourmaline ± garnet

This alteration assemblage is observed in the composite felsic unit (I1 and F2 rocks). Some of the muscovite altered rocks are characterized by a greyish to pinkish-reddish colour due to hematite-staining (Fig. 4.20g), others take a spotted look due to porphyroblasts of muscovite (together with quartz ± sillimanite; Fig. 4.20h, 4.21a, 4.21b).

The altered rock has a schistose aspect due to high proportions of muscovite (up to 50 vol.%), biotite is generally Mg-rich (X_{Fe} <0.5; Fig. 4.16d) and the white mica has a phengitic muscovite to phengite composition (Fig. 4.16e, 4.16f). The whole-rock Ba anomalies (sometimes >1000 ppm) are consistent with high-Ba contents of muscovite (up to 0.62 wt.% BaO; Fig. 4.16g). This alteration seems to overprint the phlogopite – K-feldspar – quartz – clinozoisite/zoisite, and the albite-altered rocks.

4.7.2.7 Sillimanite, muscovite, phlogopite, K-feldspar, magnetite, gahnite, tourmaline

These altered rocks have important proportions of aluminous minerals (sillimanite and muscovite). Sillimanite can represent more than 50% of the volume of the rock, and forms aggregates of fine needles (fibrolite) and/or euhedral elongated crystals. The overal mineral assemblage is quartz, K-feldspar, muscovite, biotite, magnetite and tourmaline, and sometimes gahnite rims magnetite crystals. Aluminosilicate altered rocks are intimately associated with the composite felsic unit (I1 and F2 rocks) and in the southern limb of the Grandes-Bergeronnes syncline the proportion of sillimanite increases toward the zone of maximum alteration that forms a spectacular discordant pipe of metasomatic rocks. Sillimanite is disseminated or forms veins (Fig. 4.21c), pseudomorphs after andalusite (Fig. 4.21d) and nodules (Fig. 4.21e and 4.21f). The metasomatic rocks, that have lost all their primary characteristics, are in sharp concordant to discordant contact with less altered rocks and they are characterized by an important proportion of magnetite with grains of gahnite at the edge (with trace of Mn and Mg) (Fig. 4.21g). Biotite has X_{Fe} <0.5 (Fig. 4.16d) and can have anomalous contents of Mn (up to 0.87 wt.% MnO), low Ba (<0.07 wt.% BaO), quantifiable F (up to 0.5 wt.%) and high Zn (up to 0.24 wt.%

ZnO). Muscovite has variable X_{Fe} (0.34–0.64), lower Mn content (<0.07 wt.% MnO; Fig. 4.16g) but higher X_{Fe} (0.64) and Ba content (<0.21 wt.%) than biotite. Tourmaline is commonly found within the discordant pipe zone (Fig. 4.21h). In the southern limb of the synform, the nodular variety is observed alongside the discordant aluminosilicate-rich metasomatic rock following a dacitic – rhyodacitic rock. Trace minerals such as zircon and REE-bearing minerals (xenotime, monazite, apatite and allanite) were observed using the SEM, potentially indicating that the hydrothermal fluid had the ability to carry and remobilize chemical elements interpreted to be immobile.

4.7.3 Mafic to felsic protoliths

4.7.3.1 Skarn assemblage

The skarn alteration is one of the last that affected the volcanic sequence, in the upper MAB. This alteration is usually intense, obliterates the primary textures of the rocks and forms veins and discordant pipes that crosscut already altered rocks (quartz – phlogopite – K-feldspar – clinozoisite/zoisite or amphibole – garnet – biotite alteration type). The typical mineral assemblage is diopside, calcic amphibole (tremolite-actinolite dominant with minor actinolitic hornblende, magnesio-hornblende, tschermakitic hornblende and pargasite with up to 1.1 wt.% MnO; Fig. 4.16b), K-feldspar, epidote (up to 0.5 wt.% MnO), clinozoisite/zoisite, quartz, calcite, biotite (generally Mg-rich, Fig. 4.16d) with up to 0.87 atomic % of Cu, andradite garnet ($Andradite_{76}$ $Grossular_{15}$ $Almandine_4$ with low Al and Mn; Fig. 4.17), grossular garnet, magnetite, F-bearing titanite (up to 1.88 atomic % F) with minor FeMg amphiboles (anthophyllite-gedrite and cummingtonite), sulfides, scapolite and tourmaline (see Fig. 4.22a-g and 4.23a-f for field

photographs, hand specimen and some microphotographs of skarn mineral assemblages). Furthermore, some arsenopyrite grains with trace of Ga (up to 1.68 atomic %) have also been identified using the SEM imagery and EDX measurement. The altered rocks have a typical pale green colour due high proportion of diopside (up to 90% of the volume of the rock), or take a rusty patina in the presence of disseminated sulfides (Fig. 4.22c). The skarn rocks are sometimes crosscut by veins of quartz and pink- to lilac-coloured white mica (Mn-rich with up to 2 wt.% MnO and up to 0,6 wt.% BaO; Fig. 4.22d, 4.22e, 4.22f). The skarn veins are usually boudinaged (see Fig. 4.20b, 4.22c, 4.22e and 4.22g). Whole-rock analyses have high contents of CaO (ranging from 10.7 to 15.7 wt.%), MgO (up to 8.6 wt.%) and trace elements such as Mo (up to 65 ppm), Be (up to 24 ppm), Zn (up to 286 ppm) and Pb (up to 156 ppm).

4.7.3.2 Silica alteration

Silica alteration is common in the upper MAB, where it forms discordant quartz-rich veins and more or less pervasive silica-alteration of the basaltic and felsic to intermediate volcanic rocks. It is locally associated with the muscovite – microcline – biotite ± albite or with the skarn alterations. Two important silica-rich zones are found next to garnet – amphibole – biotite altered basaltic rocks. It can form a breccia with more or less altered fragments of mafic volcanic rocks enclosed in a silica-rich matrix.

4.7.4 Paragenetic sequence of alteration and zonation of the alteration

Based on field and petrographic observations the sequence of alteration is the following: (1) quartz – epidote in the lower part of the volcanic sequence, (2) magnetite – biotite, (3) albite – orthoamphibole – biotite – quartz – magnetite, (4) phlogopite – K-feldspar – quartz – clinozoisite/zoisite – tourmaline, (5) aluminous (sillimanite – muscovite) and potassic assemblages within felsic to intermediate volcanic rocks potentially synchronous with (6) amphibole – garnet and biotite – quartz alterations in mafic rocks and (7) silicification in the upper part of the volcanic sequence. The (8) skarn alteration is late in the sequence but is sometimes crosscut by a quartz – sericite (Mn) alteration type.

4.7.5 Sulfide occurrences

Sulfides form disseminated grains, stringers or as thin sulfide-rich horizons transposed subparallel to the main S2 foliation. Sulfides are mostly observed in the upper MAB, linked to the skarns (Zn–Pb–Fe–Cu sulfides), biotite – quartz (Fe–As–Ni–Co–Cu sulfides) and amphibole – garnet ± biotite alterations (Fe–Cu sulfides). Cu-rich sulfides such as bornite, covellite and chalcocite are hosted in some quartz – epidote veins and within the potassic and ferromagnesian alteration zones (biotite, phlogopite, Fe–Mg amphibole). Sulfides are rare or absent in the lower part of the composite felsic unit where magnetite is dominant. In the aluminosilicate alteration zone, the widespread presence of magnetite together with gahnite and Zn-bearing biotite may indicate the former presence of Fe–Zn sulfides later transformed to oxides and silicate minerals. In

some other samples, the high proportion of magnetite with relict sulfides is consistent with this observation (see section 4.7.6.1 for more details).

The Escoumins and Grandes-Bergeronnes synclines have several small base and precious metal showings (see Fig. 4.3, 4.4, 4.8). In the Grandes-Bergeronnes syncline, the Cu–Ag "ligne hydro" showing consists of disseminated chalcocite, bornite, digenite, chalcopyrite (up to 25% of the rock volume) divided in two mineralized tabular lumps of metric size within hydrothermally altered volcanic rocks, with up to 10.6% Cu and 185 g/t Ag on selected samples and 0.25% Cu over 7 meters. The mineralization is associated to biotite-schists and albite – gedrite and/or biotite – magnetite – quartz altered rocks within the composite felsic unit and mafic, M3 to M4 units of upper MAB. Further north and along the same stratigraphic horizon, altered felsic rocks with muscovite, biotite, chlorite, microcline, hematite, quartz and albite have anomalous values in Cu (up to 1320 ppm Cu) indicating the presence of a prospective horizon for Cu mineralization. The "Pylone 300" showing is hosted within a centimeter to decimeter wide quartz – carbonate – titanite – apatite vein that crosscuts basaltic rocks. The vein also contains bornite, covellite, chalcocite, pyrrhotite and malachite, and has anomalous values in copper, silver and gold (1.75 % Cu, 7.5 g/t Ag and 470 ppb Au). Stratigraphically above, in the upper part of the composite felsic unit and within a banded sequence of skarn, exhalative, metavolcanic and metasedimentary rocks, two base metal occurrences in the northern and southern limbs of the Grandes-Bergeronnes syncline potentially mark a base metal-rich exhalative horizon. The "Bas-de-Soie" Zn–Pb occurrence (0.29% Zn and 0.16% Pb) in the southern limb is hosted in alternating quartz – phlogopite – K-felspar – clinozoisite/zoisite – tourmaline, quartz and skarn altered rocks together with garnet –

amphibole – biotite altered mafic volcanic rocks. The mineralization is hosted in sub-horizontal sulfide-rich skarn layers (pyrrhotite, pyrite with minor sphalerite, chalcopyrite and galena). In the same stratigraphic horizon but in the northern limb, a meter-wide hornblende-bearing felsic tuffite has disseminated sulfides (clusters of pyrrhotite – pyrite – chalcopyrite – sphalerite – galena) coupled to Zn and Pb anomalous values (1620 ppm Zn and 622 ppm Pb). This tuffite is closely associated with an aluminous and potassic altered rock with nodules of sillimanite – quartz and tourmaline.

4.7.6 Effect of the metamorphism

The rocks of this study experienced low-pressure amphibolite-grade metamorphism, and the least altered basaltic rocks are garnet-free and contain plagioclase – hornblende – ilmenite ± titanite ± quartz ± epidote. Least altered felsic to intermediate volcanic rocks have quartz – plagioclase dominant over potassium feldspar – amphibole and/or biotite with trace of Fe-Ti oxides, zircon and apatite. Altered rocks are characterized by metamorphic mineral assemblages that recorded different types of metamorphic reactions. Metamorphic-induced desulphidation, dehydration and decarbonatation reactions are presented in the following sections.

4.7.6.1 Desulphidation

Evidence of desulphidation is found in some thin sections where pyrite (FeS_2) is rimmed by pyrrhotite (FeS) and magnetite (Fe_3O_4) consistent with reactions (1) and (2), liberating sulfur (see Fig. 4.24a for the first reaction). Reaction (3) happens when water is

added to the system and pyrite reacts with water to form pyrrhotite releasing H_2S and SO_2 (Tomkins, 2007).

(1) Pyrite ($2FeS_2$) = Pyrrhotite ($2FeS$) + S_2

(2) Pyrrhotite ($6FeS$) + $4O_2$ = Magnetite ($2Fe_3O_4$) + $3S_2$

(3) Pyrite ($3FeS_2$) + $2H_2O$ = Pyrrhotite ($3FeS$) + $2H_2S$ + SO_2

The addition of water in reaction (3) is more likely to happen during the dehydration of hydrous phases with increasing metamorphic temperatures across the greenschist to amphibolite facies transition, as proposed for the Lalor deposit by Caté (2016). H_2S released during this reaction can later react with silicate minerals to form new sulfides following the reaction (4).

(4) H_2S + Fe-Mg minerals + ½ O_2 = FeS + Mg-richer mineral + H_2O

This kind of reaction was described in the Montauban deposit where sulfur-rich fluid reacted with the surrounding amphibolite to form magnesian minerals such as tremolite, anthophyllite-gedrite or phlogopite (Tomkins, 2007). In garnet-altered rocks, sulfides are mostly observed as inclusions within garnet while magnetite is disseminated within the groundmass (Fig. 4.24b). This texture suggests that it was shielded by the growth of garnet and protected from the desulphidation event during the syn- to post peak metamorphism.

4.7.6.2 Dehydration reactions in aluminous rocks

Dehydration reactions imply consumption of a hydrous mineral in order to form less hydrous to anhydrous minerals. Different evidence of dehydration reactions is

observed in thin sections while others can be inferred based on the actual metamorphic assemblage. In some muscovite altered rocks, muscovite is rimmed by quartz, sillimanite and sometimes K-feldspar consistent with reaction (5) (Fig. 4.24c).

(5) Muscovite + Quartz = Sillimanite + K-feldspar + H_2O

The discordant pipe in the southern limb of the Grandes-Bergeronnes syncline is characterized by sillimanite-rich metasomatic rocks. It implies that the hydrothermal fluid was acidic enough to form hydrous aluminum-rich minerals such as clay (kaolinite) or pyrophyllite minerals. Dehydration of such minerals during the formation of aluminosilicate minerals would release water and form quartz following reaction (6).

(6) Pyrophyllite = Andalusite/Sillimanite + Quartz + H_2O

In the highly altered samples excess of sillimanite – quartz together seems to indicate that this reaction more likely happened (see Fig. 4.21c, 4.21d and 4.24d).

4.7.6.3 Dehydration reactions in chlorite ± sericite ± quartz ± albite altered rocks

In amphibole – garnet ± biotite (interpreted to represent gains in Mg–Fe±K based on the mineral assemblage) and biotite – quartz (gains in K–Mg–Fe–Si) altered basaltic rocks are usually interpreted to represent metamorphosed chlorite, quartz and sericite alteration assemblage (Caté 2016; Bonnet and Corriveau, 2006; Bailes et al., 2016). Such assemblages are not stable at higher pressure and temperature conditions. Chlorite – sericite – quartz would react to form a new set of metamorphic minerals for example: (i) garnet – hornblende – biotite, (ii) garnet – cummingtonite – hornblende – biotite, (iii) garnet – gedrite/anthophyllite – biotite or (iv) biotite – quartz.

In the felsic to intermediate volcanic rocks, the mineral assemblages albite – gedrite/anthophyllite and/or biotite – quartz (gains in Na–Fe–Mg–Si±K) and phlogopite – K-feldspar – quartz – clinozoisite/zoisite ± carbonate (gains in K–Fe–Mg–Si–Ca) represent metamorphic equivalents of the albite – chlorite – quartz ± sericite and sericite – chlorite – quartz – carbonate – clinozoisite/zoisite alteration assemblages.

The proportion between quartz (Si), albite (Na), sericite (K), chlorite (Mg-Fe) and carbonate (Ca-Mg) together with the ratio Al–alkalis of the rock will determine the final metamorphic assemblage. Some of the possible reactions involved are the following:

(7) Chlorite + Quartz = Fe-rich Garnet (almandine) + Mg-richer Chlorite + H_2O

(8) Muscovite + Chlorite + Quartz = Mg-richer Chlorite + Biotite + Garnet + H_2O

(9) Talc = Anthophyllite + Qtz + H_2O

(10) Chlorite + Garnet + Hornblende = Fe-Mg amphibole (cummingtonite–grunerite) + Anorthite

4.7.6.4 Decarbonatation in skarns

In the skarns, the pre-metamorphic alteration mineral assemblage probably consisted of carbonate (dolomite – calcite), quartz with varying amount of potassic minerals (k-feldspar and sericite), chlorite and talc. During metamorphism these minerals would react to form the observed mineral assemblages following reactions (11), (12), (13), (14) and releasing CO_2 (see Spear 1993).

(11) Dol + Qz + H_2O = Tlc + Cc + CO_2

(12) Dol + Qz + Tlc = Tr + CO_2

(13) $Dol + Qz + H_2O = Cc + Tr + CO_2$

(14) $Dol + Qz = Di + CO_2$

(15) $Tr + Qz + Cc = Di + H_2O + CO_2$

(16) $Dol + Kfs + H_2O = Phl + Cc + CO_2$

The samples with dominant diopside ($CaMgSi_2O_6$) are usually characterized by an assemblage of diopside – quartz – carbonate with minor tremolite [$Ca_2(Mg_{5-4.5}Fe^{2+}_{0-0.5})Si_8O_{22}(OH)_2$] or actinolite [$Ca2(Mg_{4.5-2.5}Fe^{2+}_{0.5-2.5})Si_8O_{22}(OH)_2$]. In anhydrous rocks, diopside would form preferentially, while hydrous rocks would favor the formation of amphibole. In high XMg hydrous rocks, tremolite would form preferentially while actinolite would form in rocks with more Fe available. The presence of alumina in the bulk composition of the rock would favor the formation of Ca, Mg or Fe-rich aluminous minerals. For example, phlogopite (if the rocks are also potassic and hydrous), calcic aluminous amphibole (for example pargasite or hornblende), gedrite and potentially epidote-group minerals or garnet. Diopsidite (fig. 4.24e) would therefore more likely form from reaction (14) with reaction of dolomite and quartz to form diopside. However, in some other assemblage, the presence of tremolite – actinolite together with diopside and sometimes calcite would indicate that reaction (12), (13) or potentially (15) happened (see Fig. 4.24f, 4.24g). The assemblage diopside – microcline – phlogopite commonly observed in some of the skarns (Fig. 4.24h), is more likely reached via reaction (15) and (16). Finally, calcic – aluminous and silica-rich hydrous assemblage will form preferably clinozoisite-zoisite ($Ca_2Al_3(Si_2O_7)(SiO_4)O(OH)$ while anhydrous ones will form anorthite ($CaAl_2Si_2O_8$) and potentially calcic garnet and scapolite.

4.8 Alteration geochemistry

Amphibolite-facies metamorphism is interpreted to be isochemical, therefore metamorphosed alteration zones are expected to preserve the imprint of the chemical changes of the protolith induced by fluid-rock interaction during syn-volcanic alteration (e.g. Bonnet et al., 2005 and references therein). Most major elements are mobile during alteration, hence are inappropriate for most geochemical interpretations (ex. discrimination diagrams), but they can be used to quantify alteration. In some seafloor massive sulfide deposits, the mixing of modified seawater with magmatic fluids decreases the pH and adds B, P and volatiles such as HF, HCl, CO_2, SO_2 to the hydrothermal system (Douville et al., 1999). Such fluid chemistry can have a significant impact on the behaviour of "immobile" elements by enhancing their mobility (Jiang et al., 2004; Salvi and William-Jones, 1996; Gammons et al., 2002; Migdisov et al., 2009). The mobility of "immobile" elements in alteration pipes below volcanogenic massive sulfide deposits have been questioned as early as 1984 for REEs (Campbell et al., 1984) and was demonstrated in both modern and ancient volcanogenic massive sulfide environments in more recent studies (Craddock et al., 2010; Genna et al., 2014). Hydrothermal tourmaline, fluorapatite, xenotime, monazite, allanite, zircon, F-bearing titanite and biotite were recognized in some alteration assemblages from MAB implying that the mobility of some elements (Zr, Hf, Th, Nb, Ce, Y and REEs) might have been increased. For this reason, and due to the lack of "least altered" samples for some of the volcanic rock units, mass balance calculation was not attempted. However, different indexes and diagrams provide viable alternatives to these calculations in order to better constrain alteration types.

The Hughes (1973) diagram and the Spitz-Darling index (Spitz and Darling, 1978) versus Na_2O diagram are commonly used to discriminate between weakly altered igneous rocks, semi-conformable Na metasomatism (spillitization) and discordant pipe-like zones of Na loss and K gain (Piercey, 2008). In the Hughes diagram (Fig. 4.25a), some of the mafic (M1 to M4 groups), skarn, intermediate (I1) and felsic (F2) rocks display evidence of potassic metasomatism while some of the I1 and F2 rocks show a strong Na metasomatism. In the Figure 4.25b, the K-altered rocks experienced Na-loss together with an increasing Spitz-Darling index typical of VMS-altered rocks (Piercey, 2008). Na-altered rocks have values higher than 5 wt.%.

The Hashimoto alteration index (Ishikawa et al., 1976) versus the chlorite–carbonate–pyrite index (Large et al., 2001) box plot can be used to identify alteration trends within a volcanic sequence (Fig. 4.25c). The types of alteration described in section 6 are consistent with a complex hydrothermal history reflected in the AI versus CCPI diagram. Trends observed for the felsic to intermediate rocks include: (1) a decrease in the AI and CCPI indexes that corresponds to albite – orthoamphibole – biotite – magnetite altered rocks, (2) a strong increase in the AI and decrease of the CCPI indexes in direction of the sericite – muscovite – K-feldspar fields for potassic and aluminous altered rocks (3) an increase in the AI with a more or less constant CCPI in direction of the biotite – phlogopite field, (4) a strong increase in the CCPI index with a slightly increasing AI index toward the fields of calc-silicate and ferromagnesian minerals typical of the skarns (one trend is more calcic and the other one more potassic) and (5) increasing values in the AI and CCPI indexes for the phlogopite – k-feldspar – quartz – clinozoisite/zoisite altered rocks. Concerning the mafic rocks, the trend (6) in direction of

the biotite – phlogopite field (increasing AI and slightly decreasing CCPI indexes) correspond to biotite – quartz altered basalts. The trend (7) in direction of the ferromagnesian minerals fields corresponds to FeMg amphibole (anthophyllite-gedrite/cummingtonite) and garnet ± biotite/phlogopite altered basalts and the trend (8) corresponds to epidosites (quartz – epidote ± Ca garnet altered rocks).

On the advance argillic alteration index (AAAI) versus alteration index (AI) four trends are discernable: (1) toward the muscovite – kaolinite – pyrophyllite fields; (2) toward the chlorite – muscovite fields; (3) toward the calcite – epidote and (4) toward the calcite and chlorite fields (Fig. 4.25d). Altered intermediate and felsic rocks following the trend (1) are characterized by aluminous and potassic alteration assemblage. The trend (2) corresponds to Fe–Mg amphibole – garnet ± biotite altered rocks while the trend (4) corresponds to skarns.

Alkali – Al_2O_3 molar ratio plots (Fig. 4.25e) were first used to quantify alteration in metasedimentary rocks (Davies and Whitehead, 1994) and then for felsic volcanic rocks (Davies and Whitehead, 2006). The trend (1) in the intermediate to felsic volcanic rocks corresponds to a gain in Na (spillite) in direction of the albite field, the trend (2) corresponds to a loss of Na and a gain in K that correspond to a shift of the chemical composition of the rocks toward the K-feldspar – biotite fields. The trend (3) is linked to major depletion of Na together with a gain in K toward the muscovite field and then a loss of K toward the clay minerals and chlorite fields. The mafic rocks are characterized by either a major loss in Na followed by a gain in K (trend 4) or by a gain in Na (spillite, trend 5).

4.9 Discussion

4.9.1 New input on the geochemistry and stratigraphy of the Moulin-à-Baude Formation

This study, building upon Groulier et al. (2018a) shows that it is possible to recognize, map and study, at a high level of detail the different supracrustal rocks and alteration zones in polydeformed and metamorphosed terranes and it represents one of the first of this kind for an hydrothermally altered volcano-sedimentary sequence in the Grenville Province. The ESB is a Pinwarian-age volcano-sedimentary sequence (Saint-Siméon Group) together with its basement (Tadoussac Intrusive Suite), exposed in the central Grenville Province. The SSG consists of remnants of a submarine bimodal oceanic arc to arc-rift and back-arc volcanic sequence (Moulin-à-Baude Formation) emplaced on rifted fragments of the Laurentian margin. Such a setting led to the formation of highly evolved felsic (A-type) and mafic volcanic rocks (ferrobasalt). The lower part of the volcanic succession has all the characteristics of an oceanic arc sequence (calc-alkaline dominant signature) with evidence of submarine effusive to explosive volcanism. The felsic volcanic rocks are calc-alkaline, FII-type, have inherited zircon cores together with slightly negative εNd_t and older Nd model ages indicative of interaction with an older crust (unit F1). The upper part is characterized by arc-rift and back-arc related high-temperature volcanic rocks. Their signatures vary from calc-alkaline to tholeiitic. Juvenile tholeiitic island arc to back-arc basalt (M2 unit) are covered by transitional to tholeiitic arc-related basaltic andesite (M3) and juvenile arc-rift related ferrobasalt (M4). The felsic and intermediate volcanic rocks show a similar evolution with arc and arc-rift signatures. The dacite-rhyodacite rocks (F2 unit) have a high-silica

content, are alkaline (A-type) with calc-alkaline to transitional affinity and fall within the FIIIa- to FIV-type fields. The andesitic rocks (I1 unit) are also alkaline, transitional to calc-alkaline and FIIIa- to FIV-type. However, they have higher Zr saturation temperature, higher HFSE with lower Th content and they show less fractionation between LREEs and HREEs together with lower Eu anomalies. Rocks from the F2 unit have a stronger arc-signature while I1 rocks display more characteristics of rift magma.

4.9.2 Evidence of VMS-style alteration and mineralization

Different types of metamorphosed alteration mineral assemblage were documented in the field and using petrography, mineral chemistry and lithogeochemistry. The lowermost quartz – epidote alteration is widespread (regional) and semi-conformable and it has all the characteristics of modern subseafloor epidosite formed during the interaction of modified seawater with rocks.

Stratigraphically above, the basaltic andesites are characterized by the appearance of porphyroblasts of garnet (<5 vol.%) together with quartz and biotite. They are affected by a subtle but pervasive biotite – magnetite alteration and by veins of (Mn-Ca-Fe) garnet – quartz – calcite – amphibole – Ca-plagioclase – biotite. Mn- and Ca-rich garnet are commonly described in metamorphosed VMS and exhalative hydrothermal deposits and can be used as a vector toward mineralization (Dubé et al., 2007; Jansson et al., 2013; Dubé et al., 2014).

Above it, the andesitic rocks are albite – gedrite/anthophyllite ± biotite ± quartz altered and laterally the alteration within the felsic and intermediate volcanic rocks becomes more potassic (phlogopite – K-feldspar – quartz – clinozoisite/zoisite –

tourmaline) and then aluminous (muscovite – quartz – tourmaline ± garnet) with a core of sillimanite – muscovite – phlogopite – K-feldspar – quartz – tourmaline – magnetite – gahnite alteration. Stratigraphically above, the skarn mineral assemblage (diopside – tremolite – actinolite – phlogopite – carbonate – K-feldspar – FeMg amphibole – titanite – anorthite ± garnet ± sulfides) and garnet – amphibole – biotite ± quartz altered mafic rocks are in close spatial relation with the previous alterations and are associated with a silicification. The epidote (Fe-rich, allanite) – biotite – magnetite – quartz – K-feldspar – plagioclase – carbonate alteration within felsic to intermediate volcanic rocks seems to be limited to the northern limb of the syncline.

The whole-rock geochemistry indicates four major types of alteration trends: (1) Na metasomatism (semi-conformable spillitization) associated with enrichment in K – Fe – Mg – Si; (2) K metasomatism (keratophyre) with enrichment in Fe – Mg –Si – Ca; (3) skarn alteration (Ca – Mg) with enrichment in Fe – K – Si – Mn; (4) Ferromagnesian alteration (Fe – Mg) with enrichment in K – Si. The last three assemblages are generally pervasive to discordant and linked to Na losses.

The metamorphosed mineral assemblages and alteration geochemistry are consistent with different metamorphosed types of classic VMS alteration: (i) quartz – epidote, (ii) albite – chlorite ± quartz ± sericite, (iii) chlorite – sericite – quartz – clinozoisite/zoisite – tourmaline ± carbonate, (iv) quartz – sericite, (v) argillic alteration, (vi) chlorite ± quartz ± sericite, (vii) dolomite – quartz ± chlorite ± sericite ± clinozoisite/zoisite and (viii) silicification. The aluminous discordant zone (sillimanite and muscovite-rich) is consistent with an argillic alteration that formed during the passage of an acidic hydrothermal fluid (Mercier-Langevin et al., 2015 and references therein),

leading to the formation of kaolinite-pyrophyllite prior to metamorphism. This type of alteration in submarine volcanogenic environment is unusual and appears related to shallow-submarine hybrid VMS-epithermal deposits generally enriched in gold (Dubé et al., 2007; Dubé et al., 2014; Mercier-Langevin et al., 2015). The sulfide occurrences are consistent with a lower Cu (± Au – Ag) and an upper Zn – Pb zones. Such metal distribution is often described in VMS deposits with a lower core of high-temperature Cu-rich ore and an upper Zn – Pb massive sulfide zone formed at lower temperature (see Galley et al., 2007). The Cu-zone is spatially associated with metamorphic equivalent of quartz – sericite, chlorite ± sericite ± quartz ± clinozoisite/ zoisite and argillic alteration zones while the Zn – Pb zone is dominantly hosted by skarns and silica-rich rocks. Volcanic sandstone – siltstone, exhalative sediments and the metal-rich tuffite are markers of a break in the volcanic activity and of active exhalative systems prospective for VMS-deposits.

4.9.3 Comparison with other metamorphosed VMS-deposits

The metamorphosed alteration assemblages from the SSG have a lot in common with the ones from some amphibolite-grade VMS deposits. In this section they will be compared with a similar age auriferous VMS deposit from the Grenville Province (Montauban) that was most likely part of the same island arc sequence (Figures 1b and 1c). Other good comparatives are the Paleoproterozoic Lalor (Flin Flon Belt) and Stollberg (Fennoscandian Shield) deposits as they are well-documented and share similarities (metamorphic conditions and mineral assemblages) with the ones presented in this study.

4.9.3.1 The Montauban auriferous VMS deposit (Grenville Province, Quebec)

The Montauban deposit was metamorphosed at the upper amphibolite facies (T = 650°C, P = 6 kb; Bernier et al., 1987) during the Grenvillian Orogeny. The Montauban shares a similar geological evolution with the Escoumins supracrustal belt as it represents a stratiform deposit hosted by the ~1.44 Ga Montauban Group, an island arc and back-arc volcanic and sedimentary sequence (Corrigan and van Breemen, 1997; Sappin et al., 2011) accreted to Laurentia at about 1.39 Ga (Corrigan et al., 1994; Sappin et al., 2011). A total of 2.7 Mt at 6.8% Zn, 2.3% Pb, 1.3 g/t Au and 131 g/t Ag and 0.9 Mt of precious metal ore grading at 3.6 g/t Au and 17.7 g/t Ag have been exploited leading to the extraction of 2571 kg of gold and 8068 kg of silver (Nadeau et al., 2008).

The Montauban deposit is divided in a central Zn-Pb-Ag-Au massive sulfide zone hosted mainly in a tremolite – diopside rock and is flanked along strike by north and south gold zones within a narrow (100 m) mine sequence of variably altered intermediate to felsic volcanic or volcaniclastic rocks (Bernier et al., 1987; Bernier and MacLean, 1993). The north gold zone (grading at 4.27 g/t Au) is hosted within quartz-rich gahnite – garnet – tourmaline, cordierite – biotite and cordierite – anthophyllite gneisses while the south gold zone (grading at 3.70 g/t Au) is hosted within a muscovite schist (Sangster et al., 1992).

Cordierite – anthophyllite rocks are interpreted to represent metamorphosed equivalent of chlorite – talc altered felsic volcanic rocks and the cordierite-biotite rocks represent a K-enriched variety of this type of alteration (chlorite – talc – sericite; Bernier and MacLean, 1993). Such assemblages were not observed within altered felsic to

intermediate volcanic rocks of the SSG, this is possibly linked to the absence of highly altered samples with alteration and AI and CCPI indexes > 80.

The tremolite – diopside (phlogopite, anorthite, calcite, dolomite, scapolite, titanite, apatite, dravite, zircon) calc-silicate rocks are interpreted to either represent metamorphosed exhalative carbonate-massive sulfide zone (Stamatelopoulou-Seymour and MacLean, 1977), silica-rich calcareous and dolomitic rocks formed by mixing between marine carbonate and detrital volcanic rocks (Prahbu and Webber, 1984) or Ca-Mg altered volcanic rocks (see Bernier and MacLean, 1993). The latter hypothesis is also favored for the skarns of this study as they have trace elements signatures of felsic to intermediate volcanic rocks together with negative Eu anomaly. The skarns share similar mineral assemblages to the ones from the Montauban together with anomalies in Zn–Pb. They are also characterized by the presence of wilsonite a rare pink to lilac-coloured Mn-rich white mica.

In the Montauban sequence, the nodular sillimanite gneiss (sillimanite – quartz – biotite) is well-developed next to the cordierite – anthophyllite rocks and locally envelops the calc-silicate rocks. It is interpreted to represent a quartz – sericite (clay?) alteration zone with potentially a minor chloritic component. In the ESB, the nodular sillimanite rocks also represent meter-wide horizons that can be followed along strike. They consist of nodules of sillimanite fibrolite, quartz and muscovite together with Mg-rich biotite, K-feldspar and tourmaline. They are associated with aluminous and potassic altered rocks and phlogopite – K-feldspar – quartz – zoisite/clinozoisite – tourmaline altered rocks from felsic to intermediate protoliths and also garnet – amphibole ± biotite or biotite – quartz altered basaltic rocks. The main difference with Montauban is the presence of a

discordant pipe of sillimanite-rich altered rocks that represents the core of the hydrothermal system in the southern limb of the Grandes-Bergeronnes syncline.

Bernier and MacLean (1993) interpreted the auriferous quartz-rich gahnite – tourmaline – garnet zone as a metamorphosed silica-rich alteration pipe that represent the core of the hydrothermal system. Within the auriferous zone, garnet is manganiferous (up to 25 wt.% MnO), biotite is enriched in Ba and the tourmaline is the dravite (magnesian) type. In the SSG, two zones of quartz-rich breccia with altered (garnet – amphibole – quartz) mafic clasts can represent equivalent of a silica-rich alteration pipe, the host rock is however basaltic. Mn- and Ca-rich almandine garnet (up to 11.3 wt.% MnO and up to 13 wt.% CaO) have been analyzed within an altered andesite and some other altered rocks are characterized by Ca-rich garnet (andradite variety) while analyzed garnets from altered basaltic rocks are generally almandine with lower contents of Mn and Ca.

The hydrothermal alteration at the Montauban deposit is organized with a silica-rich core surrounded by quartz – sericite ± chlorite (nodular sillimanite gneiss), chlorite – talc (anthophyllite – cordierite rocks), chlorite – sericite ± quartz (cordierite – biotite) and chlorite – carbonate (diopside – tremolite) alteration zones. This is consistent with the alteration observed in a Kuroko-type VMS deposits (Bernier and MacLean, 1993). The gold-rich zone is characterized by electrum, sulphosalts and Au–Ag–Sb–As-bearing "epithermal-suite" ore minerals typical of gold-rich VMS deposits (Bernier et al., 1987; Tomkins 2007; Brueckner et al., 2014). Although the origin of the Montauban deposit remained a source of debate for an extended period of time, it is now accepted to

represent a metamorphosed auriferous VMS exhalative type of deposit (Bernier et al., 1987; Morin, 1987a; Bernier and MacLean, 1993; Tomkins, 2007).

4.9.3.2 The Lalor deposit (Flin Flon Belt, Manitoba)

The Zn–Cu–Au Lalor deposit is found within the Snow Lake arc assemblage of the Paleoproterozoic Flin Flon belt, and was metamorphosed at the amphibolite-facies during the Trans-Hudson orogeny (T = 550 – 600°C and P = 5-6 kbar; see Caté 2016 and references therein). The hydrothermal alteration spectrum at the Lalor deposit is complex and can be described based on the location within the stratigraphy and the impact on the chemistry of the rocks: (i) distal semi-conformable, (ii) pervasive and intense proximal (Mg–Fe, K–Mg–Fe, Mg–Ca and K) within the footwall of the deposit and (iii) hangingwall alterations (Caté 2016).

The proximal (i) Mg–Fe, (ii) K–Fe–Mg, (iii) Mg–Ca and (iv) K alterations affects both mafic and felsic volcanic rocks. The spatial distribution of the alteration zones indicates a symmetrical organization with a core of Mg–Fe alteration (chloritic) surrounded by K–Mg–Fe (chlorite – sericite), and K (sericite) alterations. Close to the lower massive sulfide lens and in the upper part of the footwall alteration zone is found the Mg–Ca alteration (chlorite – carbonate) (Caté, 2016). The Mg–Fe alteration hosts the Cu–Au mineralization while the Mg–Ca alteration is in direct contact with the lower massive sulfide lens. The Mg–Fe alteration consists of an assemblage of chlorite – FeMg amphibole – cordierite ± biotite ± garnet ± quartz ± gahnite ± staurolite ± feldspar

(Mercier-Langevin et al., 2014; Caté, 2016). This alteration is very similar to the amphibole – garnet ± biotite alteration assemblage in the basaltic rocks of the Escoumins.

The K–Fe–Mg alteration alternates with the Fe–Mg alteration and is characterized by the assemblage biotite – Ca-amphibole – FeMg amphibole – chlorite – cordierite together with aluminous minerals (garnet, staurolite, aluminosilicate, muscovite). This alteration can represent an analogue to the biotite – garnet – amphibole (basaltic rocks), biotite – quartz (basaltic rocks), phlogopite – k-feldspar – quartz – clinozoisite/zoisite – tourmaline alteration assemblage of the Escoumins. This assemblage appears to be overprinted by aluminous assemblage (muscovite – sillimanite).

The Mg–Ca alteration consists of chlorite – carbonate ± Ca-amphibole and chlorite – actinolite together with diopside, quartz, titanite, anorthite, biotite and talc (Caté, 2016). The mineral assemblage and chemical signature of this alteration is very similar to the skarns of the Escoumins, it is however characterized by a lower grade metamorphic mineral assemblage.

The K alteration is associated with the upper Zn-rich lens and it corresponds to muscovite-altered rocks together with quartz, biotite, aluminosilicate and pyrite consistent with sericitic pre-metamorphic alteration (Caté, 2016). The K alteration is similar to the muscovite and sillimanite-altered rocks of the SSG.

4.9.3.3 The Stollberg deposits (Fennoscandian Shield, Sweden)

The Stollberg mining field (which is part of the broader Bergslagen district) consists of massive sulfide (Zn–Pb–Ag) and massive Mn-rich magnetite mineralization

metamorphosed to the amphibolite-facies. The stratigraphy of the deposits consists of a thick sequence of 1.91-1.89 Ga calc-alkaline felsic volcanic and volcaniclastic rocks with minor mafic and sedimentary intervals emplaced during the waning stage of the rhyolitic volcanism (Jansson et al., 2013) in a subaerial to shallow subaqueous continental back-arc (Allen et al., 1996; Allen et al., 2003). The main ore zone is hosted within a sequence of skarns and calcic to dolomitic marble (locally stromatolitic), Jansson et al. (2013) interpreted the skarns to be a metamorphosed combination of altered rhyolite, limestone and hydrothermal sediments. The Stollberg geodynamic environment and rocks succession are very different from the Escoumins, however they share some similarities concerning the alteration assemblages.

In the footwall of the Stollberg deposit, altered rocks consist from the base to the top of: (1) gedrite – quartz – albite ± garnet interpreted to represent a metamorphosed chlorite – albite alteration assemblage with gains in Na–Fe–Mg; (2) biotite – quartz ± garnet (K–Fe–Mg altered rocks after a sericite – chlorite assemblage); (3) garnet – amphibole – biotite ± gahnite ± cordierite rocks (chlorite – sericite); (5) silicification; (6) skarn assemblage (hedenbergite, diopside, garnet, Ca-amphibole) (Jansson et al., 2013). The contact between gedrite – albite versus biotite-rich assemblage is interpreted to represent an alteration front between sodic and potassic-rich alteration (Jansson et al., 2013). These alteration patterns are very similar to the ones from the SSG.

4.10 Conclusion

- Building upon Groulier et al. (2018a), this study represents one of the first complete investigations of a polydeformed and metamorphosed volcano-sedimentary sequence and of its hydrothermal alteration assemblages within the Grenville Province. Despite the deformation and the metamorphic overprint, primary textures and information are still preserved.
- The geochemistry of the volcanic rocks from the middle Moulin-à-Baude Formation records an evolution from a calc-alkaline mafic – felsic volcanic island arc sequence (lower part) toward a rifted-arc and back-arc succession with calc-alkaline to tholeiitic mafic, intermediate and felsic volcanic rocks (upper part).
- The magmatism from the upper part of the formation is characteristic of a high-temperature geothermal gradient with primitive tholeiitic island arc to back-arc basalt covered by alkaline andesitic to rhyodacitic rocks, transitional basaltic andesite, highly evolved ferrobasalt and syn-volcanic mafic to felsic intrusive rocks. In the upper part of the formation, an increasing volume of volcaniclastic, volcanic-derived sedimentary and exhalative rocks seem to indicate breaks in the volcanic activity.
- In the Grandes-Bergeronnes syncline, the entire formation exhibits evidence of hydrothermal alteration. Field observations, petrography and geochemistry of the altered volcanic rocks are consistent with different types of metamorphosed subseafloor and syn-volcanic hydrothermal alterations with from the bottom to the top of the stratigraphy can be summarized as: (1) regional quartz – epidote; (2) albite – quartz – gedrite/anthophyllite – biotite – magnetite interpreted to represent a

metamorphosed albite – chlorite ± sericite assemblage (K–Fe–Mg); (3) phlogopite – K-feldspar – quartz – clinozoisite/zoisite – tourmaline ± calcite after chlorite – sericite – quartz – clinozoisite/zoisite ± carbonate (K– Fe–Mg–Ca); (4) aluminous muscovite-altered rocks (K metasomatism, quartz – sericite), (5) sillimanite and muscovite-rich rocks (argillic alteration), (6) amphibole – garnet ± biotite altered rocks (Fe–Mg±K, after chlorite ± sericite ± quartz); (7) skarns (after carbonate – quartz ± chlorite ± sericite) and (8) quartz. The alteration assemblages in the upper part of the stratigraphy are generally intense, pervasive to discordant and linked to Na losses (except for the spillite).

- The alteration shows a zonation between Na-altered and K-altered felsic to intermediate volcanic rocks. Within the K-altered rocks the proportion between phlogopite/biotite – microcline – clinozoisite/zoisite and muscovite ± sillimanite is interpreted to mark a zonation between K–Mg–Fe–Ca and more aluminous K±Fe±Mg altered rocks.
- The sillimanite-rich discordant pipe represents a metamorphosed equivalent of an argillic alteration zone.
- Based on field observations and geochemical signatures, the skarns are interpreted to represent metamorphosed carbonate – quartz ± sericite ± chlorite altered volcanic rocks. Their Zr/Ti and Th/Yb ratios are consistent with felsic to intermediate protoliths (units F2 and I1).

- In addition to the promising geodynamic environment, this study shows that the alteration assemblages and their chemical signatures are similar to the ones observed in some metamorphosed VMS-deposits.
- This approach can be reproduced in polydeformed and metamorphosed terranes in order to determine favourable zones for VMS-type deposits.

4.11 Acknowledgements

This contribution is part of the PhD of the first author and was funded by the Ministère de l'Énergie et des Ressources naturelles of Quebec and by Natural Sciences Engineering Research Council of Canada (NSERC) discovery grant (200386) to the second author. The authors would like to thank Dr. François Turlin and Evelyne Sunatori for their assistance in the field, Dr. Wanda Aylward for her assistance with the EPMA analyses.

4.12 Appendices

Table A4.1: EPMA analytical conditions

Appendix 1 SEM-MLA maps

Appendix 2 Table of microprobe analyses for the different alteration minerals.

Appendix 3 Mobility of elements tested versus Zr.

4.13 References

Agrawal, S., Guevara, M., Verma, S.P., 2008. Tectonic discrimination of basic and ultrabasic volcanic rocks through log-transformed ratios of immobile trace elements, International Geology Review, volume 50(12), 1057–1079.

Allen, R.L, Lundström, I., Ripa, M., Simeonov, A., and Christofferson, H., 1996. Facies analysis of a 1.9 Ga, continental margin, back-arc, felsic caldera province with diverse Zn-Pb-Ag-(Cu-Au) sulfide and Fe oxide deposits, Bergslagen region, Sweden. Economic Geology, volume 91, 979–1008.

Ames, D.E., Galley, A.G., Kjarsgaard, I.M.K., Tardif, N., Taylor, B.E., 2016. Hanging-wall vectoring for buried volcanogenic massive sulfide deposits, Paleoproterozoic Flin Flon Mining Camp, Manitoba, Canada. Economic Geology, volume 111, 963–1000.

Bailes, A.H., Galley, A.G., Paradis, S., Taylor, B.E., 2016. Variations in large synvolcanic alteration zones at Snow Lake, Manitoba, Canada, with proximity to associated volcanogenic massive sulfide deposits. Economic Geology, volume 111, 933–962.

Barret, T.J., MacLean, W.H., 1994a. Mass changes in hydrothermal alteration zones associated with VMS deposits of the Noranda Area. Exploration and Mining Geology, volume 3(2), 131–160.

Barret, T.J., MacLean, W.H., 1994b. Chemostratigraphy and hydrothermal alteration in exploration for VHMS deposits in greenstones and younger volcanic rocks, in Lentz, D.R., ed., Alteration and Alteration Processes associated with Ore-forming

Systems: Geological Association of Canada, Short Course Notes, volume 11, 433–467.

Barret, T.J, MacLean, W.H., 1999. Volcanic sequences, lithogeochemistry, and hydrothermal alteration in some bimodal volcanic-associated massive sulfide systems, in: C.T. Barrie and M.D. Hannington (Eds.), Volcanic-Associated Massive Sulfide Deposits: Processes and Examples in Modern and Ancient Environments. Society of Economic Geologists, Reviews in Economic Geology, volume 8, 101–131.

Bernier, L.R., Pouliot, G., MacLean, W.H., 1987. Geology and metamorphism of the Montauban north gold zone: a metamorphosed polymetallic exhalative deposit, Grenville Province, Quebec. Economic Geology, volume 82, 2076–2090.

Bernier, L.R., MacLean, W.H., 1993. Lithogeochemistry of a metamorphosed VMS alteration zone at Montauban Grenville Province, Quebec. Exploration and Mining Geology, volume 2(4), 367–386.

Bonnet, A.-L., Corriveau, L., 2006. Atlas et outils de reconnaissance de systèmes hydrothermaux métamorphisés dans les terrains gneissiques. DIVEX, 94 pages.

Brisebois, D., Clark, T., 2003. Géologie et ressources minérales de la partie est de la Province de Grenville. Ministère des Ressources naturelles de la Faune et des Parcs, Québec, DV 2002-03, 419 p.

Brueckner, S.M., Piercey, S.J., Sylvester, P.J., Maloney, S., Pilgrim, L., 2014. Evidence for syngenetic precious metal enrichment in an Appalachian volcanogenic massive sulfide system: the 1806 Zone, Ming Mine, Newfoundland, Canada. Economic Geology, volume 109, 1611–1642.

Cabanis, B., Lecolle, M., 1989. Le diagramme La/10-Y/15-Nb/8 ; un outil pour la discrimination des séries volcaniques et la mise en évidence des processus de mélange et/ou de contamination crustale. Comptes Rendus de l'Académie des Sciences, Série 2, Mécanique, Physique, Chimie, Sciences de l'Univers, Sciences de la Terre, volume 309(20), 2023–2029.

Campbell, I.H., Lesher, C.M., Coad, P., Franklin, J.M., Gorton, M.P., Thurston, P.C., 1984. Rare-Earth element mobility in alteration pipes below massive Cu-Zn sulfide deposits. Chemical Geology, volume 45, 181–202.

Carr, S.D., Easton, R.M., Jamieson, R.A., Culshaw, N.G., 2000. Geologic transect across the Grenville Orogen of Ontario and New York. Canadian Journal of Earth Sciences, volume 37, 193–216.

Caté, A., 2016. Geology of the Paleoproterozoic Zn-Cu-Au Lalor volcanogenic massive sulphide deposit and its gold-rich lenses, Snow Lake, Manitoba. PhD thesis, Université du Québec, Institut National de la Recherche Scientifique, 384 p.

Cawood, P.A., Strachan, R.A., Pisarevsky, S.A., Gladkochub, D.P., Murphy, J.B., 2016. Linking collisional and accretionary orogens during Rodinia assembly and breakup: Implications for models of supercontinent cycles. Earth and Planetary Science Letters, volume 449, 118–126. doi:10.1016/j.epsl.2016.05.049

Condie, K.C., 2003. Incompatible element ratios in oceanic basalts and komatiites: tracking deep mantle sources and continental growth rates with time. Geochemistry Geophysics Geosystems, volume 4 (1), 1005. doi:10.1029/2002GC000333.

Corrigan, D., van Breemen, O., Hanmer, S., Nadeau, L., 1994. Arc accretion, crustal thickening, and post-collisional extension in the Grenville Province: constraints from the St. Maurice lithotectonic belt. Lithoprobe Meeting, Abitibi-Grenville Transect, Université de Montreal, Montreal, Quebec, Nov/Dec. 1994. Program with abstracts.

Corrigan, D., 1995. Mesoproterozoic evolution of the south-central Grenville orogen: structural, metamorphic, and geochronologic constraints from the Mauricie transect. PhD thesis, Carleton University, 282 p.

Corrigan, D., van Breemen, O., 1997. U-Pb age constraints for the lithotectonic evolution of the Grenville Province along the Mauricie transect, Quebec. Canadian Journal of Earth Sciences, volume 34, 299–316.

Corriveau, L., Bonnet, A.-L., 2005. Pinwarian (1.5 Ga) volcanism and hydrothermal activity at the eastern margin of the Wahekam Group, Grenville Province, Quebec. Canadian Journal of Earth Sciences, volume 42, 1749–1782.

Craddock, P.R., Bach, W., Seewald, J.S., Rouxel, O.J., Reeves, E., Tivey, M.K., 2010. Rare earth element abundances in hydrothermal fluids from the Manus Basin, Papua New Guinea: Indicators of sub-seafloor hydrothermal processes in back-arc basins. Geochemica et Cosmochimica Acta, volume 74, 5494–5513.

Davies, J.F., Whitehead, R.E., 1994. Molar ratios in the study of unaltered and hydrothermally altered greywackes and shales. Chemical Geology, volume 111, 85–100.

Davies, J.F., Whitehead, R.E., 2006. Alkali-Alumina and MgO-Alumina molar ratios of altered and unaltered rhyolites. Exploration and Mining Geology, volume 15(1-2), 75–88.

Day, W.C., Slack, J.F., Ayuso, R.A., Seeger, C.M., 2016. Regional geologic and petrologic framework for iron oxide ± apatite ± rare earth element and iron oxide copper-gold deposits of the Mesoproterozoic St. Francois Mountains Terrane, Southeast Missouri, USA. Economic Geology, volume 111, 1825–1858.

Dickin, A.P., Higgins, M.D., 1992. Sm /Nd evidence for a major 1.5 Ga crust-forming event in the central Grenville Province. Geology, volume 20, 137–140.

Dickin, A.P., 2000. Crustal formation in the Grenville Province: Nd-isotope evidence. Canadian Journal of Earth Sciences, volume 37, 165–181.

Dickin, A.P., McNutt, R.H., Martin, C., Guo, A., 2010. The extent of juvenile crust in the Grenville Province: Nd isotope evidence. Geological Society of America Bulletin, volume 122(5-6), 870–883.

Douville, E., Bienvenu, P., Charlou, J.L., Donval, J.P., Fouquet, Y., Appriou, P., Gamo, T., 1999. Yttrium and rare earth elements in fluids from various deep-sea hydrothermal systems. Goechimica et Cosmochimica Acta, volume 63(5), 627–643.

Dubé, B., Mercier-Langevin, P., Hannington, M., Lafrance, B., Gosselin, G., Gosselin, P., 2007. The LaRonde Penna World-Class Au-Rich Volcanogenic Massive Sulfide Deposit, Abitibi, Québec: Mineralogy and Geochemistry of Alteration and Implications for Genesis and Exploration. Society of Economic Geologist, volume 102, 633–666.

Dubé, B., Mercier-Langevin, P., Kjarsgaard, I., Hannington, M., Bécu, V., Côté, J., Moorhead, J., Legault, M., Bédard, N., 2014. The Bousquet 2-Dumagami World-Class Archean Au-Rich Volcanogenic Massive Sulfide Deposit, Abitibi, Quebec: Metamorphosed Submarine Advanced Argillic Alteration Footprint and Genesis. Society of Economic Geologist, volume 109, 121–166.

Galley, A.G., Hannington, M.D., Jonasson, I.R., 2007. Volcanogenic massive sulphide deposits, in Goodfellow, W.D., ed., Mineral Deposits of Canada: a synthesis of major deposit-types, District Metallogeny, the evolution of Geological Provinces, and Exploration Methods: Geological Association of Canada, Mineral Deposits Division, Special Publication No. 5, 141–161.

Gammons, C.H., Wood, S.A., Li, Y., 2002. Complexation of the rare earth elements with aqueous chloride at 200 °C and 300 °C and saturated water vapor pressure, in Hellmann, R. and Wood, S.A., eds., Water-Rock interactions, Ore Deposits, and Environmental Geochemistry: A tribute to David A. Crerar. The Geological Society, Special Publication No. 7, 191–207.

Gauthier, M., Brown, A.C., 1986. Zinc and iron metallogeny in the Maniwaki-Gracefield District southwestern Quebec. Economic Geology, volume 81, 89–112.

Gauthier, M., Chartrand, F., Cayer, A., David, J., 2004. The Kwyjibo Cu-REE-U-Au-Mo-F property, Quebec : a Mesoproterozoic polymetallic iron oxide deposit in the northeastern Grenville Province. Economic Geology, volume 99, 1177–1196.

Gauthier, M., Chartrand, F., 2005. Metallogeny of the Grenville Province revisited. Canadian Journal of Earth Sciences, volume 42, 1719–1734.

Genna, D., Gaboury, D., Roy, G., 2014. The Key Tuffite, Matagami Camp, Abitibi Greenstone Belt, Canada: petrogenesis and implications for VMS formation and exploration. Mineralium Deposita, volume 49, 489–512.

Gifkins, C., Herrmann, W., Large, R.R., 2005. Altered volcanic rocks: a guide to description and interpretation; Centre for Ore Deposits Research; University of Tasmania, Hobart, Tasmania, Australia, 275 p.

Gower, C.F., Erdmer, P., 1988. Proterozoic metamorphism in the Grenville Province: a study in the Double Mer – Lake Melville area, eastern Labrador. Canadian Journal of Earth Sciences, volume 25, 1895–1905.

Gower, C.F., Krogh, T.E., 2002. A U-Pb geochronological review of the Proterozoic history of the eastern Grenville Province. Canadian Journal of Earth Sciences, volume 39, 795–829.

Gower, C.F., Kamo, S.L., Kwok, K., Krogh, T.E., 2008. Proterozoic southward accretion and Grenvillian orogenesis in the interior Grenville Province in eastern Labrador: Evidence from U-Pb geochronological investigations. Precambrian Research, volume 165, 61–95.

Groulier, P.-A., Indares, A., Dunning, G., Mouhksil, A., Wälle, M., 2018. Peri-Laurentian, Pinwarian-age oceanic arc crust preserved in the Grenville Province: insights from the Escoumins Supracrustal Belt. Precambrian Research, volume 311, 37–64. https://doi.org/10.1016/j.precamres.2018.04.001.

Groulier, P.-A., Indares, A., Dunning, G., Mouhksil, A., Jenner, G., 2018b. Syn-orogenic magmatism over 100 m.y. in high crustal levels of the central Grenville Province: characteristics, age and tectonic significance. Lithos, volume 312-313, 128–152.

Groulier, P.-A., Turlin, F., André-Mayer, A.S., Ohbebstetter, D., Crépon, A., Boulvais, P., Poujol, M., Rollion-Bard, C., Zeh, A., Moukhsil, A., Solgadi, F., El Basbas, A., in review for Journal of Petrology. Silicate-carbonate liquid immiscibility: insights from the Crevier alkaline intrusion (Quebec).

Hanchar, J.M., Watson, E.B., 2003. Zircon saturation thermometry. Reviews in Mineralogy and Geochemistry, volume 53(1), 89–112.

Hart, T.R., Gibson, H.L., Lesher, C.M., 2004. Trace element geochemistry and petrogenesis of felsic volcanic rocks associated with volcanogenic massive Cu-Zn-Pb sulfide deposits. Economic Geology, volume 99, 1003–1013.

Hawthorne, F. C., Kato, A., Kisch, H. J., Krivovichev, V. G., Linthout, K., Laird, J., Maresch, W. V., Schumacher, J. C., Stephenson, N. C. N., Whittaker, E. J. W. (1997). Nomenclature of amphiboles: report of the subcommittee on amphiboles of the International Mineralogical Association, Commission on New Minerals and Mineral Names. The Canadian Mineralogist, volume 35, 219–246.

Hughes, C.J., 1973. Spilites, keratophyres, and the igneous spectrum. Geological Magazine, volume 109, 513–527.

Ishikawa, Y., Sawaguchi, T., Ywaya, S., Horiuchi, M., 1976. Delineation of prospecting targets for Kuroko deposits based on modes of volcanism of underlying dacite and alteration haloes. Mining Geology, volume 26, 105–117.

Jansson, N.F., Erismann, F., Lundstam, E., Allen, R.L., 2013. Evolution of the Paleoproterozoic volcanic-limestone-hydrothermal sediment succession and Zn-Pb-Ag and Iron Oxide deposits at Stollberg, Bergslagen Region, Sweden. Economic Geology, volume 108, 309–335.

Jenner, G.A., 1996. Trace element geochemistry of igneous rocks: geochemical nomenclature and analytical geochemistry, in: D.A. Wyman (Ed.), Trace Element Geochemistry of Volcanic Rocks: Applications for Massive Sulfide Exploration. Geological Association of Canada, Short Course Notes, volume 12, 51–77.

Jiang, S.-Y., Wang, R.-C., Xu, X.-S., Zhao, K.-D., 2004. Mobility of high field strength elements (HFSE) in magmatic-, metamorphic-, and submarine-hydrothermal systems. Physics and Chemistry of the Earth, volume 30, 1020–1029.

Karlstrom, K.E., Ahall, K.-I., Harlan, S.S.,Williams, M.L., McLelland, J., Geissman, J.W., 2001. Long-lived (1.8-1.0 Ga) convergent orogen in southern Laurentia, its extensions to Australia and Baltica, and implications for refining Rodinia. Precambrian Research, volume 111, 5–30.

Ketchum, J.W.F., Heaman, L.M., Krogh., T.E., Culshaw, N.G., Jamieson, R.A., 1998. Timing and thermal influence of late orogenic extension in the lower crust: a U-Pb geochronological study from the southwest Grenville orogen, Canada. Precambrian Research, volume 89, 25–45.

Large, R.R., Gemmell, J.B., Paulick, H., 2001. The alteration box plot: a simple approach to understanding the relationship between alteration mineralogy and lithogeochemistry associated with volcanic-hosted massive sulfide deposits. Economic Geology, volume 96, 957–971.

Lesher, C.M., Goodwin, A.M., Campbell, I.H., Gorton, M.P., 1986. Trace-element geochemistry of ore-associated and barren, felsic metavolcanics rocks in the Superior Province, Canada. Canadian Journal of Earth Sciences, volume 23, 222–237.

Li, Z.X., Bogdanova, S. V, Collins, A.S., Davidson, A., De Waele, B., Ernst, R.E., Fitzsimons, I.C.W., Fuck, R.A., Gladkochub, D.P., Jacobs, J., Karlstrom, K.E., Lu, S., Natapov, L.M., Pease, V., Pisarevsky, S.A., Thrane, K., Vernikovsky, V., 2008. Assembly, configuration, and break-up history of Rodinia: A synthesis. Precambrian Research, volume 160, 179–210. doi:10.1016/j.precamres.2007.04.021

McDonough, W.F., Sun, S.S., 1995. The composition of the Earth. Chemical Geology, volume 120, 228 p.

MacLean, W.H., Seymour, K.S., Prabhu, M.K., 1982. Sr, Y, Zr, Nb, Ti, and REE in Grenville amphibolites at Montauban-les-Mines, Quebec. Canadian Journal of Earth Sciences, volume 19, 633–644.

MacLean, W.H., Barrett, T.J., 1993. Lithogeochemical techniques using immobile elements. Journal of Geochemical Exploration, volume 48, 109–133.

Madore, L., Verpaelst, P., Choinière, J., Dion, D.-J., David, J., Lefebre, D., Marquis, R., Hocq, M. 1997*a*. Géologie de la région du Lac Briend. Ministère des ressources naturelles du Québec, RG 96-05.

Madore, L., Verpaelst, P., Brisebois, D., Choinière, J., Dion, D.-J., David, J. 1997*b*. Géologie de la région du Lac Cormier. Ministère des ressources naturelles du Québec, RG 97-08.

McDonough, W.F., Sun, S.-S., 1995. The composition of the Earth. Chemical Geology, volume 120, 228p.

McLelland, J.M., Selleck, B.W., Bickford, M.E., 2013. Tectonic evolution of the Adirondack Mountains and Grenville Orogen inliers within the USA. Geoscience Canada, volume 40, 318–352.

Mercier-Langevin, P., Caté, A., and Ross, P.-S. (2014a) Whole-rock oxygen isotope mapping, Lalor auriferous VMS deposit footwall alteration zones, Snow Lake, west-central Manitoba (NTS 63K16). Report of activities 2014, Manitoba Mineral Resources, Manitoba Geological Survey, 94–103.

Mercier-Langevin, P., Hannington, M.D., Dubé, B., Piercey, S.J., Peter, J.M., and Pehrsson, S.J., 2015. Precious metal enrichment processes in volcanogenic massive sulphide deposits — A summary of key features, with an emphasis on TIGI-4 research contributions, In: Targeted Geoscience Initiative 4: Contributions to the Understanding of Volcanogenic Massive Sulphide Deposit Genesis and Exploration Methods Development, (ed.) J.M. Peter and P. Mercier-Langevin; Geological Survey of Canada, Open File 7853, 117–130.

Migdisov, A.A., Williams-Jones, A.E., Wagner, T., 2009. An experimental study of the solubility and speciation of the Rare Earth Elements (III) in fluoride- and chloride-bearing aqueous solutions at temperatures up to 300 °C. Geochemica et Cosmochimica Acta, volume 73, 7087–7109.

Morin, G., 1987a. Gîtologie de la région de Montauban. Ministère des ressources naturelles du Québec, MM 86-02, 59 p.

Morin, G., 1987b. Gîtologie des régions de Sacré-Cœur et de Grandes-Bergeronnes. Ministère des ressources naturelles du Québec, ET 85-11, 25 p.

Nadeau, L., Brouillette, P., Hébert, C., 2008. Arc magmatism, continental collision and exhumation : the Mesoproterozoic evolution of the south-central Grenville Province, Portneuf-Mauricie region, Quebec. Field trip B3, GAC-MAC-SEG-GSA Joint Annual Meeting, Québec, Canada.

Nold, J.L., Dudley, M.A., Davidson, P., 2013. The Southeast Missouri (USA) Proterozoic iron metallogenic province - Types of deposits and genetic relationships to magnetite-apatite and iron oxide-copper-gold deposits. Ore Geology Reviews, volume 57, 154–171.

Pearce, J.A., Harris, B.W., Tindle, A.G., 1984. Trace element discrimination diagrams for the tectonic interpretation of granitic rocks. Journal of Petrology, volume 25(4), 956–983.

Pearce, J.A., 2008. Geochemical fingerprinting of oceanic basalts with applications to ophiolite classification and the search for Archean oceanic crust. Lithos, volume 100, 14–48.

Pearce, J.A., 2014. Immobile element fingerprinting of ophiolites. Elements, volume 10, 101–108.

Piercey, S.J., 2008. Lithogeochemistry of volcanic rocks associated with volcanogenic massive sulphide deposits and applications to exploration, in Submarine Volcanism and Mineralization: Modern Through Ancient, (eds.) B. Cousens and S. Piercey; Geological Association of Canada, Short Course 29-30 May 2008, Quebec City, Canada, 25 p.

Piercey, S.J., 2010. An overview of petrochemistry in the regional exploration for volcanogenic massive sulphide (VMS) deposits. Geochemistry: Exploration, Environment, Analysis, volume 10, 1–18, doi 10.1144/1467-7873/09-221.

Piercey, S.J., 2011. The setting, style, and role of magmatism in the formation of volcanogenic massive sulfide deposits. Mineralium Deposita, volume 46(5), 449–471.

Prahbu, M.K., Webber, G.R., 1984. Origin of quartzofeldspathic gneisses at Montauban-les-mines, Quebec, Canadian Journal of Earth Sciences, volume 21, 336–345.

Rivers, T., Corrigan, D., 2000. Convergent margin on southeastern Laurentia during the Mesoproterozoic: tectonic implications. Canadian Journal of Earth Sciences, volume 37, 359–383.

Rivers, T., Culshaw, N., Hynes, A., Indares, A., Jamieson, R., Martignole, J., 2012. The Grenville Orogen – A post-LITHOPROBE perspective, Chapter 3, in: Percival, J.A., Cook, F.A., and Clowes, R.M. (Eds.), Tectonic Styles in Canada: the LITHOPROBE Perspective. Geological Association of Canada, Special Paper 49, 97–236.

Rondot, J., Marleau, J.R., 1977. La silice de Charlevoix, CIM Bull. 70, 105–115.

Rondot, J., 1979. Reconnaissances Géologiques dans Charlevoix-Saguenay, Ministère de l'Énergie et des Ressources naturelles, Québec ; DPV-682, 44 p.

Rondot, J., 1986. Géologie de la région de Forestville-Les Escoumins, Ministère de l'Énergie et des Ressources naturelles, Québec ; ET 85-05, 47 p.

Rondot, J., 1989. Géologie de Charlevoix, Ministère de l'Énergie et des Ressources naturelles, Québec; MB 89-21, 606 p.

Rondot, J., Lavergne, G., 1984. Carte géologique de la région de Forestville-Les Escoumins, 2 cartes annotées, Ministère de l'Énergie et des Ressources naturelles, Québec ; DP 84-54.

Ross, P.-S., Bédard, J.H., 2009. Magmatic affinity of modern and ancient subalkaline volcanic rocks determined from trace-element discriminant diagrams. Canadian Journal of Earth Sciences, volume 46, 823–839.

Rucks, T.W., Piercey, S.J., Ryan, J.J., Villeneuve, M.E., Creaser, R.A., 2006. Mid- to Late Paleozoic K-feldspar Augen granitoids in the Yukon-Tanana Terrane, Yukon, Canda: Implications for crustal growth and tectonic evolution of the Northern Cordillera. Geological Society of America Bulletin, volume 118, 1212–1231.

Salvi, S., William-Jones, A.E., 1996. The role of hydrothermal processes in concentrating high-field strength elements in the Strange Lake peralkaline complex, northeastern Canada. Geochimica et Cosmochimica Acta, volume 60 (11), 1917–1932.

Sangster, A.L., Gauthier, M., Gower, C.F., 1992. Metallogeny of structural zones, Grenville Province, northeastern North America. Precambrian Research, volume 58, 401–426.

Sappin., A.-A., Constantin, M., Clark, T., van Breemen, O., 2009. Geochemistry, geochronology, and geodynamic setting of Ni-Cu±PGE mineral prospects hosted by mafic and ultramafic intrusions in the Portneuf-Mauricie Domain, Grenville Province, Quebec. Canadian Journal of Earth Sciences, volume 46, 331–353.

Sappin., A.-A., Constantin, M., Clark, T., 2011. Origin of magmatic sulfides in a Proterozoic island arc – an example from the Portneuf-Mauricie Domain, Grenville Province, Canada. Mineralium Deposita, volume 46(3), 211–237.

Shervais, J.W., 1982. Ti-V plots and the petrogenesis of modern and ophiolitic lavas. Earth and Planetary Science Letters, volume 59, 101–118.

Slagstad., T., Culshaw, N.G., Daly, J.S., Jamieson, R.A., 2009. Westerm Grenville Province holds key to midcontinental Granite-Rhyolite Province enigma. Terra Nova, volume 21, 191–187.

Spear, F.S., 1993. Metamorphic phase equilibria and pressure-temperature-time paths. Mineralogical Society of America, Washington, D.C., short-course notes, Monograph volume 1, 799 p.

Spitz, G., Darling, R., 1978. Major and minor element lithogeochemical anomalies surrounding the Louvem copper deposit, Val D'Or, Quebec. Canadian Journal of Earth Sciences, volume 15, 1161–1169.

Stamatelopoulou-Seymour, K., MacLean, W.H., 1984. Metamorphosed volcanogenic ores at Montauban, Grenville Province, Quebec. Canadian Mineralogist, volume 22, 595–604.

Sun, S.-S., McDonough, W. F. 1989. Chemical and isotopic systematics of oceanic basalts: implications for mantle composition and processes. Geological Society, London, Special Publications 42, 313–345.

Tomkins, A.G., 2007. Three mechanisms of ore re-mobilisation during amphibolite facies metamorphism at the Montauban Zn-Pb-Au-Ag deposit. Mineralium Deposita, volume 42, 627–637.

Tucker, R.D., Gower, C.F., 1990. Salient features of the Pinware terrane, Grenville Province, eastern Labrador. Geological Association of Canada, Mineralogical Association of Canada, Program with abstracts, volume 15, A133.

Turlin, F., André-Mayer, A.-S., Moukhsil, A., Vanderhaeghe, O., Gervais, F., Solgadi, F., Groulier, P.-A., Poujol, M., 2017. Unusual LREE-rich, peraluminous, monazite- or allanite-bearing pegmatitic granite in the central Grenville Province, Québec. Ore Geology Reviews, volume 89, 627–667.

van Breemen, O., Corriveau, L., 2005. U-Pb age constraints on arenaceous and volcanic rocks of the Wahekam Group, eastern Grenville Province. Canadian Journal of Earth Sciences, volume 42, 1677–1697.

Watson, E.B., Harrison, T.M., 1983. Zircon saturation revisited: temperature and composition effects in a variety of crustal magma types. Earth and Planetary Science Letters, volume 64, 295–304.

Whalen, J.B., Currie, K.L., Chappell, B.W., 1987. A-type granites: geochemical characteristics, discrimination and petrogenesis. Contribution to Mineralogy and Petrology, volume 95, 407–419. doi:10.1007/BF00402202

Whelan, J.F., Rye, R.O., DeLorraine, W., 1984. The Balmat-Edwards Zinc-Lead Deposits – Synsedimentary ore from Mississippi Valley-Type fluids. Economic Geology, volume 79, 239–265.

Whitmeyer, S.J., Karlstrom, K.E., 2007. Tectonic model for the Proterozoic growth of North America. Geosphere, volume 3(4), 220–259.

Winchester, J.A., Floyd, P.A., 1977. Geochemical discrimination of different magma series and their differentiation products using immobile elements. Chemical Geology, volume 20, 325–343.

Williams, P.J., 1990. Evidence for a late metamorphic origin of disseminated gold mineralization in Grenville gneisses at Calumet, Quebec. Economic Geology, volume 85, 164–171.

Williams, N.C., Davidson, G.J., 2004. Possible submarine advanced argillic alteration at the Basin Lake prospect, Western Tasmania, Australia. Economic Geology, volume 99, 987–1002.

Wood, D. A. (1980) The application of a Th Hf Ta diagram to problems of tectonomagmatic classification and to establishing the nature of crustal contamination of basaltic lavas of the British Tertiary Volcanic Province. Earth and Planetary Science Letters, volume 50 (1), 11–30.

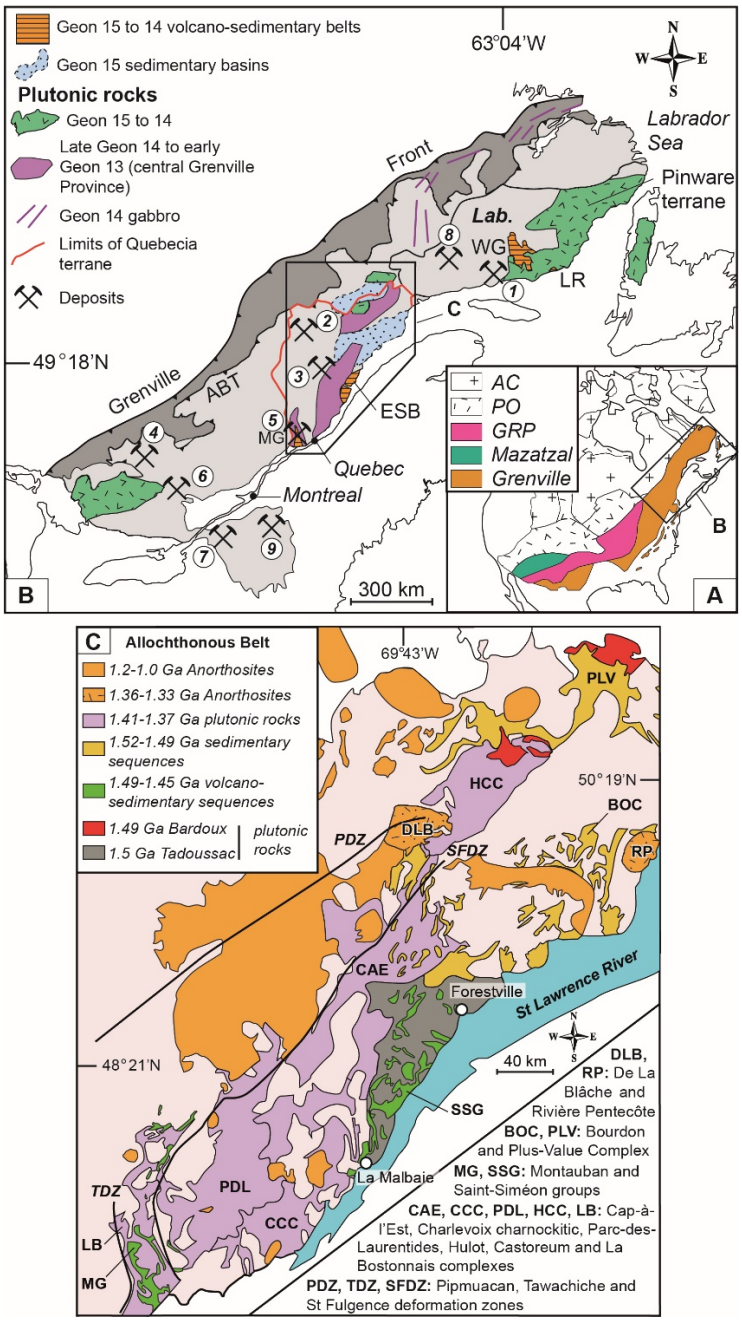

Figure 0.1: A) Simplified map of the Proterozoic Laurentia (modified from Hoffman 1989) with the location of the Mazatzal, Granite-Rhyolite Province (GRP) and Grenville Provinces. AC – Archean cratons; PO – Paleoproterozoic orogens; **B)** Schematic map of the Grenville in Canada (modified from Groulier et al., 2018) ABT – Allochthonous Boundary Thrust; ESB – Escoumins Supracrustal Belt, Lab. – Labradoria; LR – La Romaine supracrustal belt; MG – Montauban Group; WG – Wakeham Group. List of ore deposits and occurrences: 1) Lac Tio (Fe – Ti), 2) Crevier (Nb – Ta), 3) Niobec (Nb – REE), 4) Kipawa (REE – Zr), 5) Montauban (Zn – Pb – Au – Ag), 6) Calumet (Zn – Pb – Cu – Au – Ag), 7) Balmat – Edwards – Pierrepont (Zn – Pb), 8) Kwyjibo (Fe – REE – Cu – Au – Mo – U – F) and 9) Lyon Mountains (Fe – REE – P); **C**) Geological map of the central Grenville Province (this thesis chapter 3).

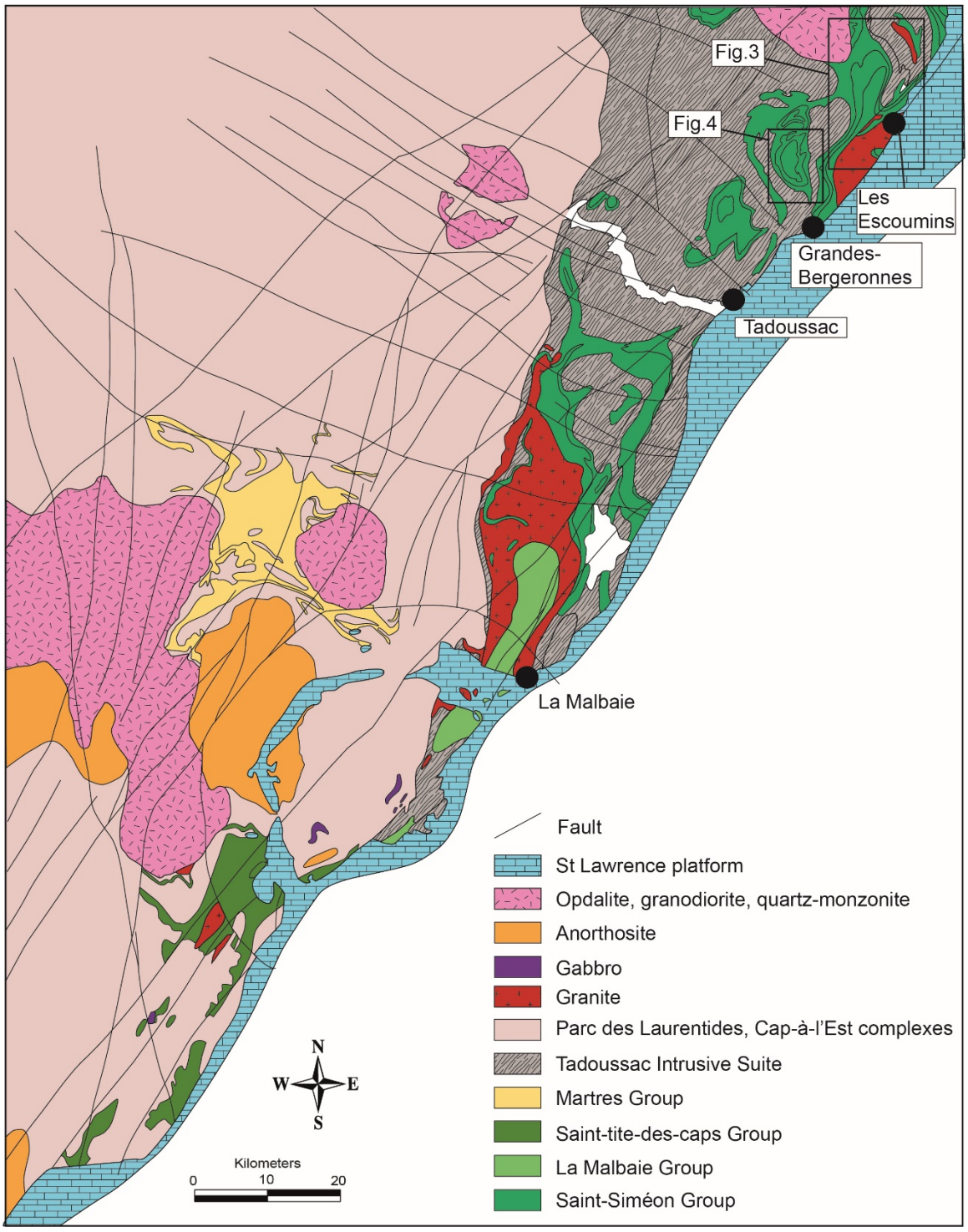

Figure 0.2: Geological map of the southern central Grenville Province along the St Lawrence River (modified after Rondot 1989).

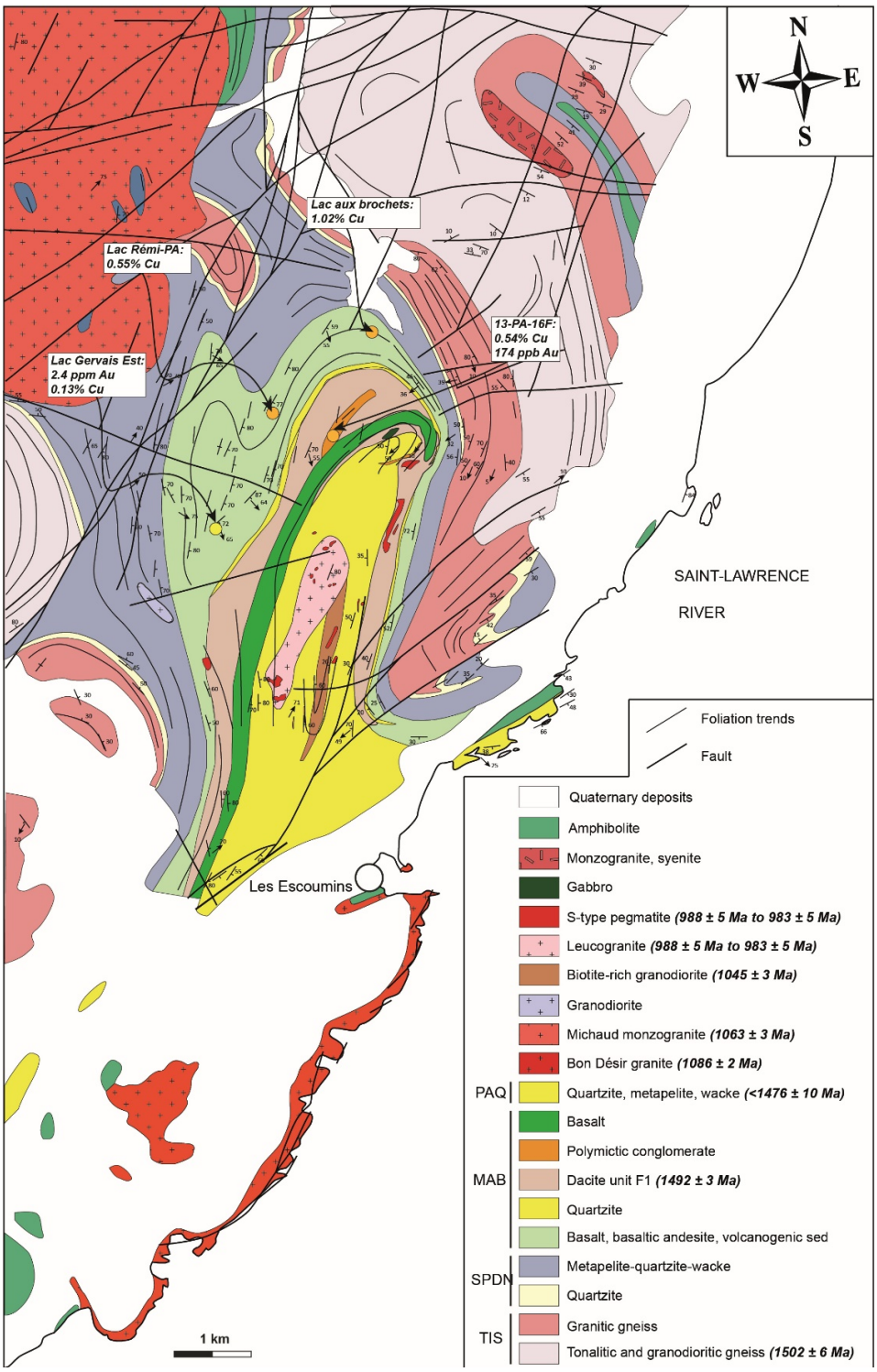

Figure 0.3: Geological map of the Escoumins syncline (modified after Rondot 1986). TIS – Tadoussac Intrusive Suite; SPDN – Saint-Paul-du-Nord Formation; MAB – Moulin-à-Baude Formation; PAQ – Port-aux-Quilles Formation. The colored circles represent mineral occurrences (orange for Cu and yellow for Au).

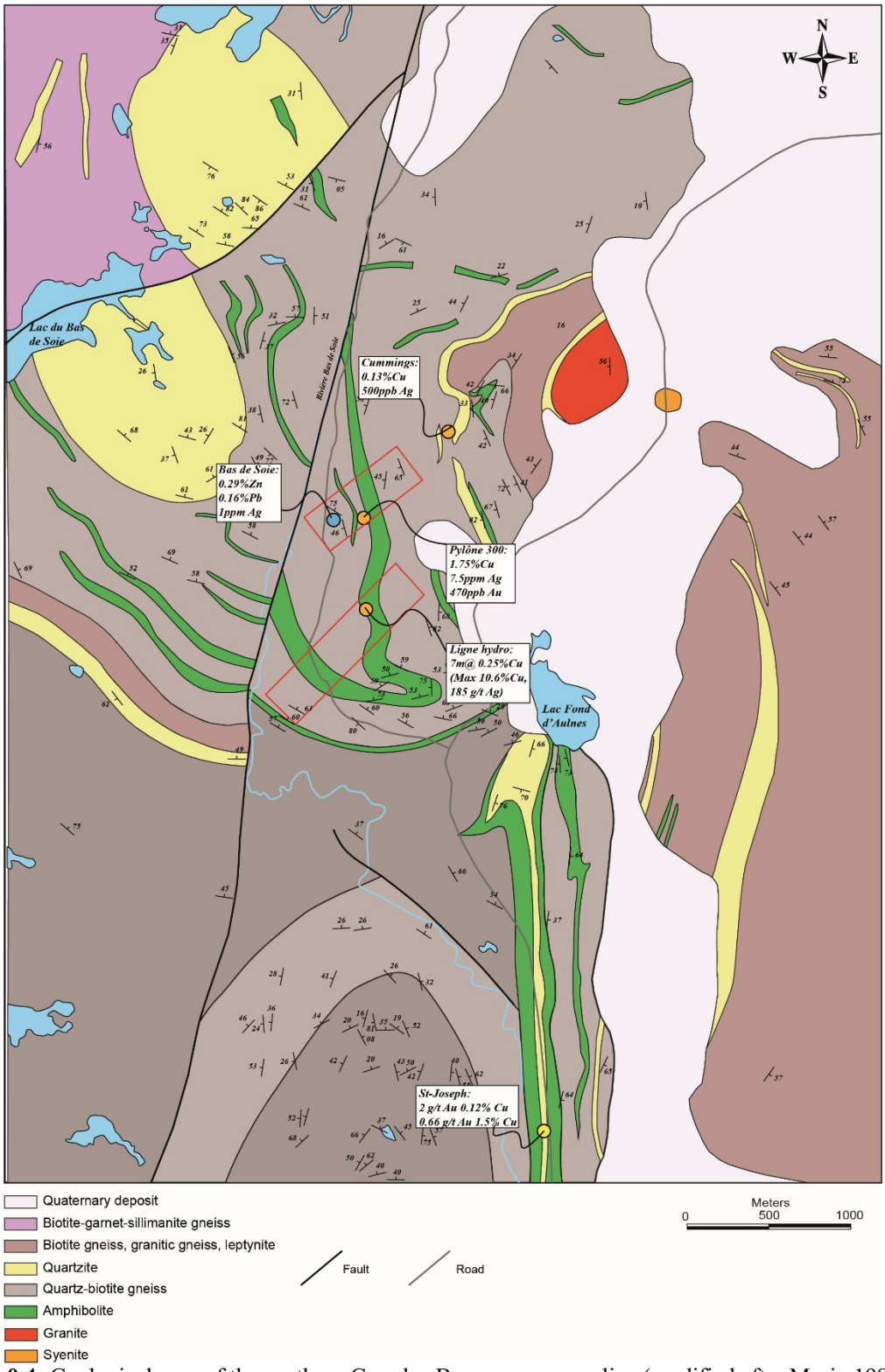

Figure 0.4: Geological map of the southern Grandes-Bergeronnes syncline (modified after Morin 1987b). The colored circles represent mineral occurrences (orange for Cu, blue for Zn – Pb and yellow for Au). The red rectangles correspond to the area mapped in Figure 4.8a.

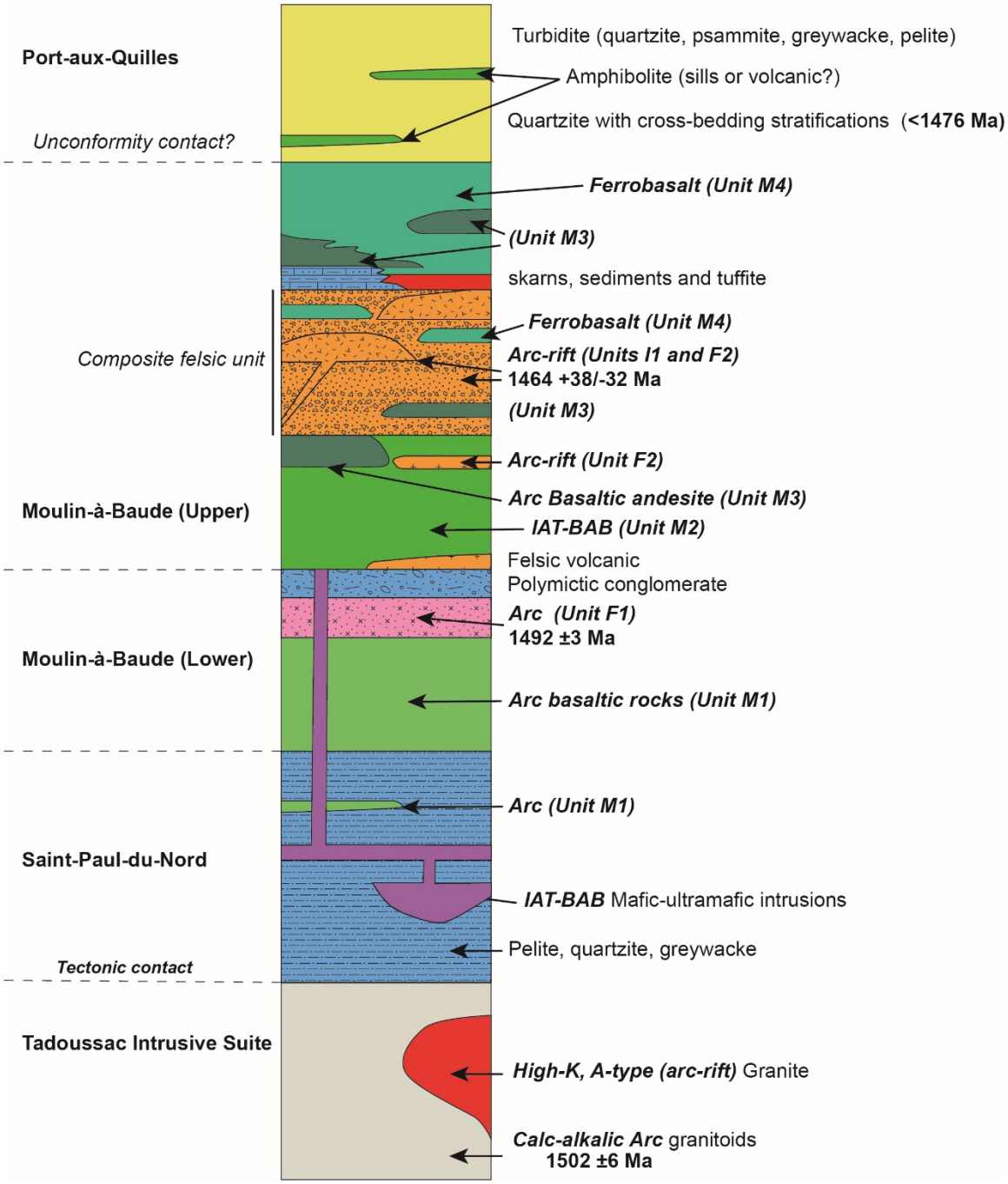

Figure 0.5: Stratigraphic log of the Saint-Siméon Group and of its basement (Tadoussac Intrusive Suite). U-Pb ages are from Groulier et al. (2018a).

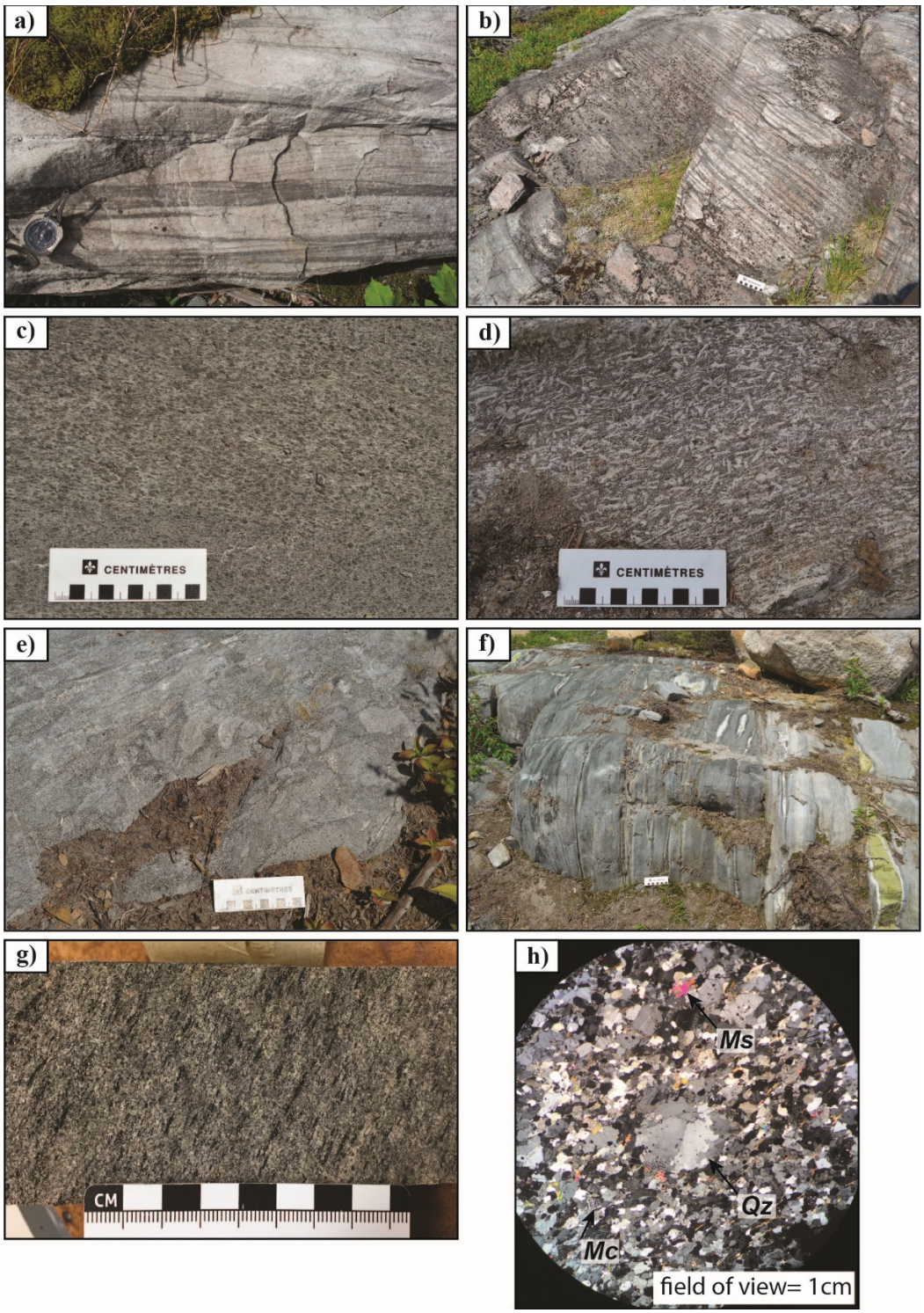

Figure 0.6: Field photographs of: **a)** Cross-bedding stratifications in a quartzite; **b)** Turbiditic sequence with alternating quartzitic and pelitic layers; **c)** Hornblende-phyric gabbro; **d)** Plagioclase-phyric basalt; **e)** Mafic tuff with mafic fragments; **f)** contact between deformed pillow basalt and intermediate volcanic rocks; **g)** dacitic tuff with fiamme texture; **h)** photomicrographs of a quartz eye in a slightly altered felsic volcanic rock (cross-polarized light, CPL).

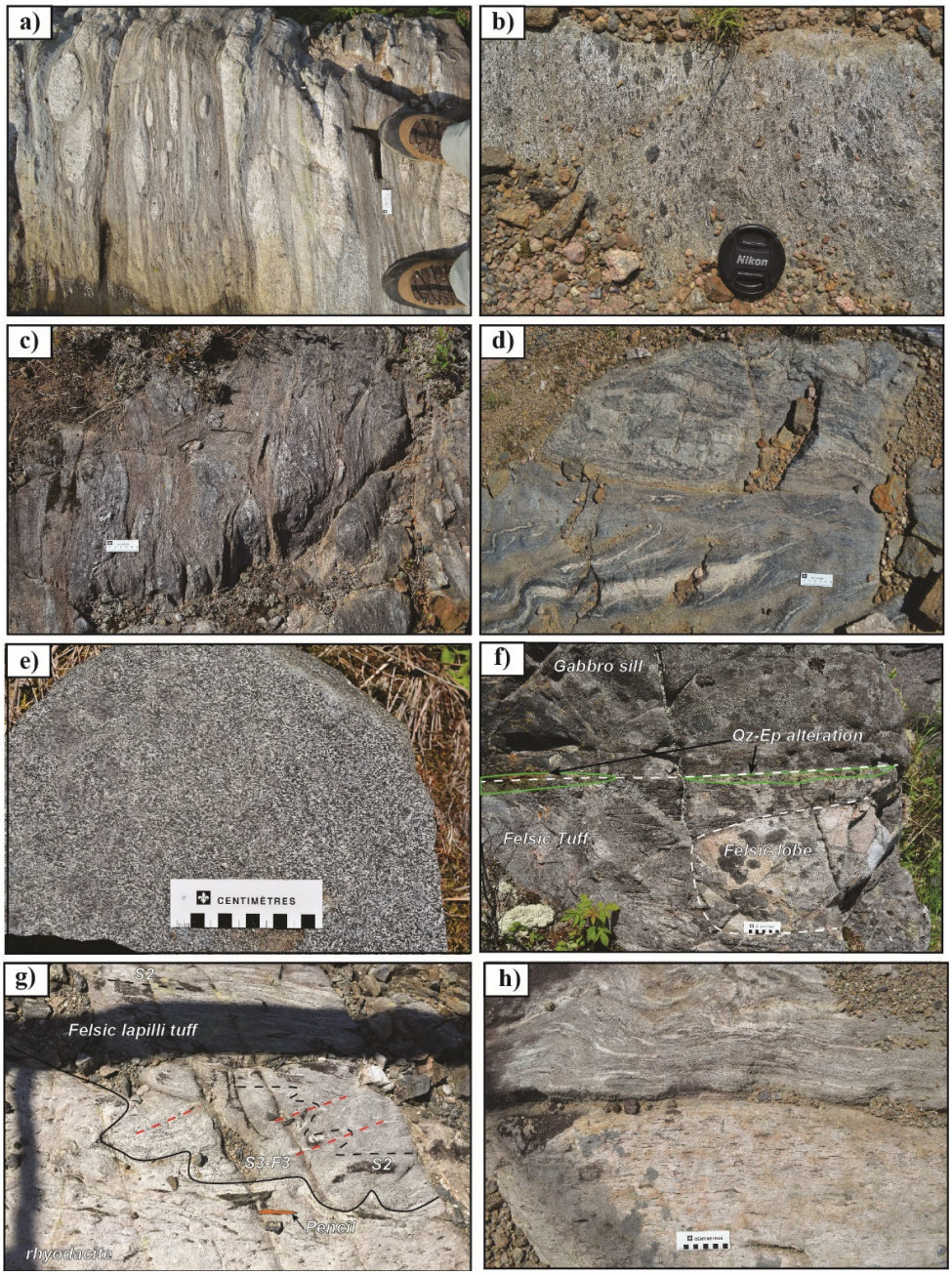

Figure 0.7: Field photographs of: **a)** Polymictic conglomerate with rounded pebbles of intrusive, extrusive and sedimentary rocks (the scale on the right represents 5 cm); **b)** Amygdaloidal basalt; **c)** Isolated pillow basalt (the scale represents 5 cm); **d)** Contact between a massive basaltic flow and its hyaloclastite (upper part) crosscut by hydrothermal veins of quartz-sericite (lower part), the scale represents 5 cm; **e)** Gabbro sill; **f)** Felsic lobe and gabbro sill intrusive within an intermediate to felsic tuff, the contact between the tuff and the gabbro is altered; **g)** Contact (solid black line) between a high-silica rhyodacite and a felsic lapilli tuff (the dashed black line represents S2 and the red dashed line represents S3 and F3 fold axis). The pencil, highlighted in orange, is 13.5 cm long; **h)** Contact between a high-silica rhyodacite (lower part) and a tuff breccia that contains juvenile clasts of the adjacent rhyodacite (upper part), the scale represents 10 cm.

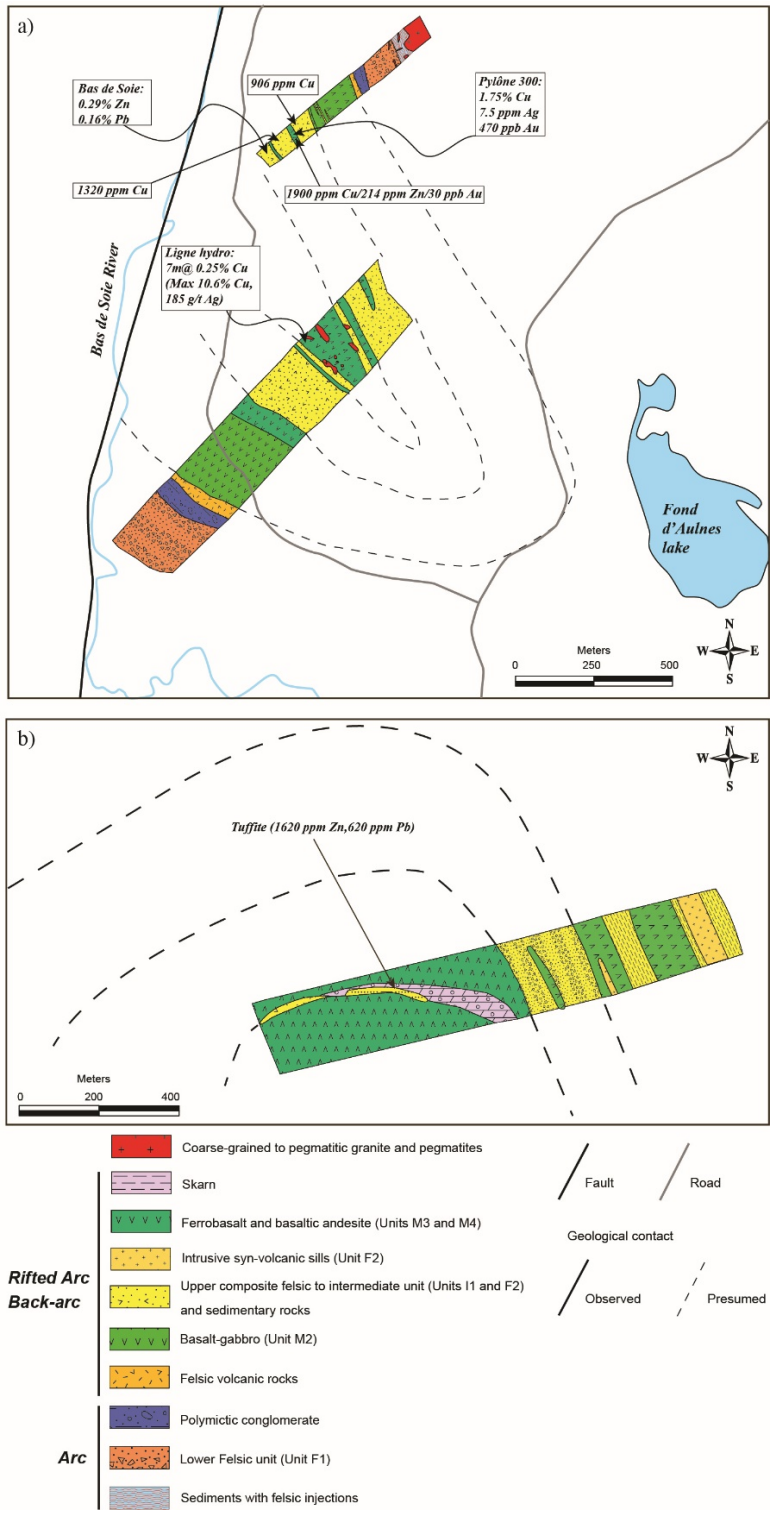

Figure 0.8: a) Detailed geological maps of the southern limb of the Grandes-Bergeronnes syncline. The arrows mark the location of the mineral occurrences and anomalous base and precious metals analyses. **b)** Detailed geological maps of the northern limb of the Grandes-Bergeronnes syncline, the arrow marks the location of the tuffite with anomalous Zn-Pb contents.

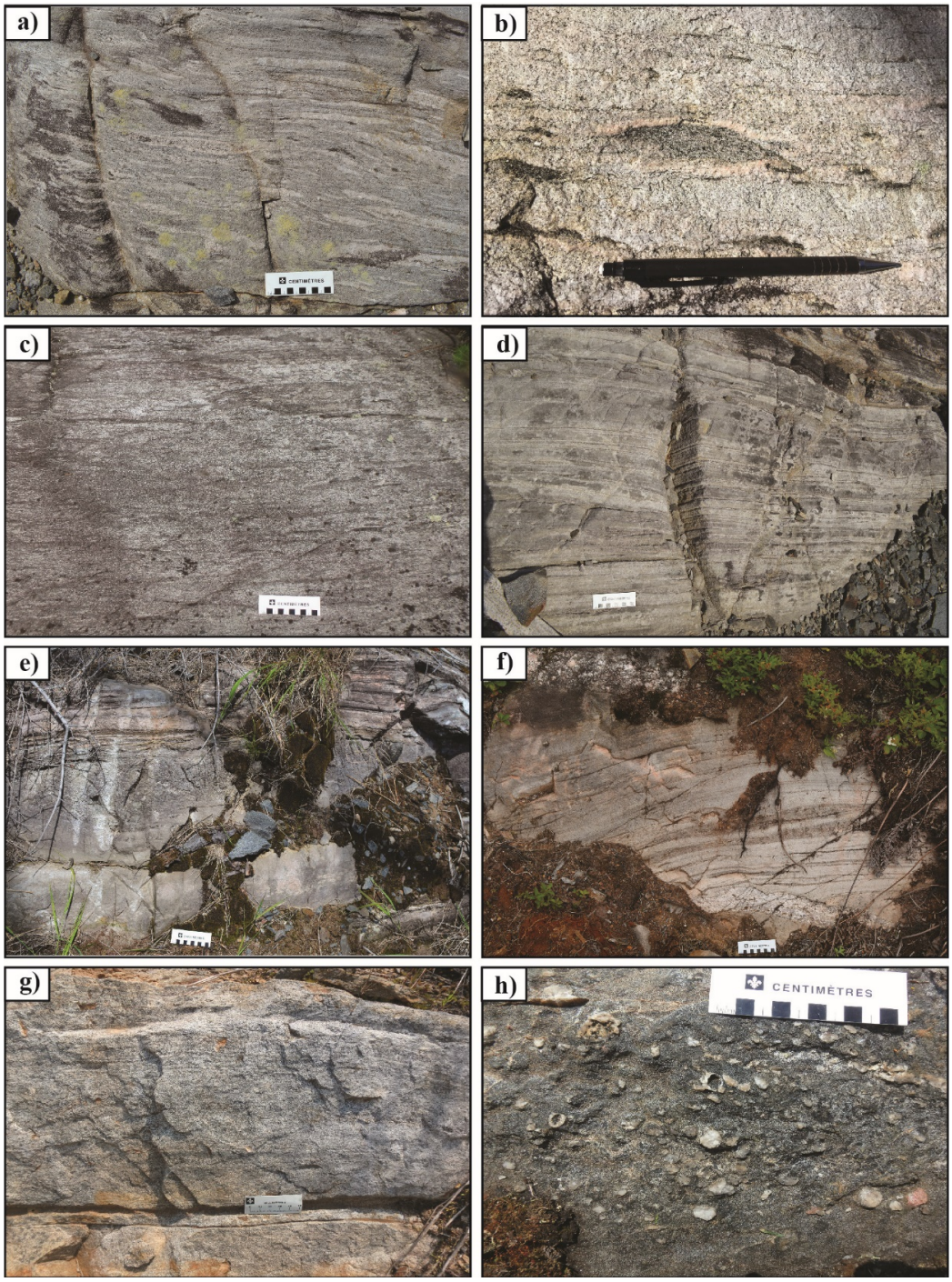

Figure 0.9: Field photographs of: **a)** Felsic lapilli tuff with juvenile fragments; **b)** Possible false pyroclastic texture in an altered felsic volcanic rock or recrystallized pumice in a felsic tuff (the pencil is 13.5 cm long; **c)** Felsic lapilli tuff; **d)** Planar-bedded felsic volcaniclastic rocks; **e)** Sequence of chert (lower and middle) together with felsic tuff and volcaniclastic mudstone; **f)** Volcanic-derived sedimentary rocks crosscut by pegmatites; **g)** Layered tuffite with anomalous content in Zn-Pb; **h)** Amygdaloidal basalt.

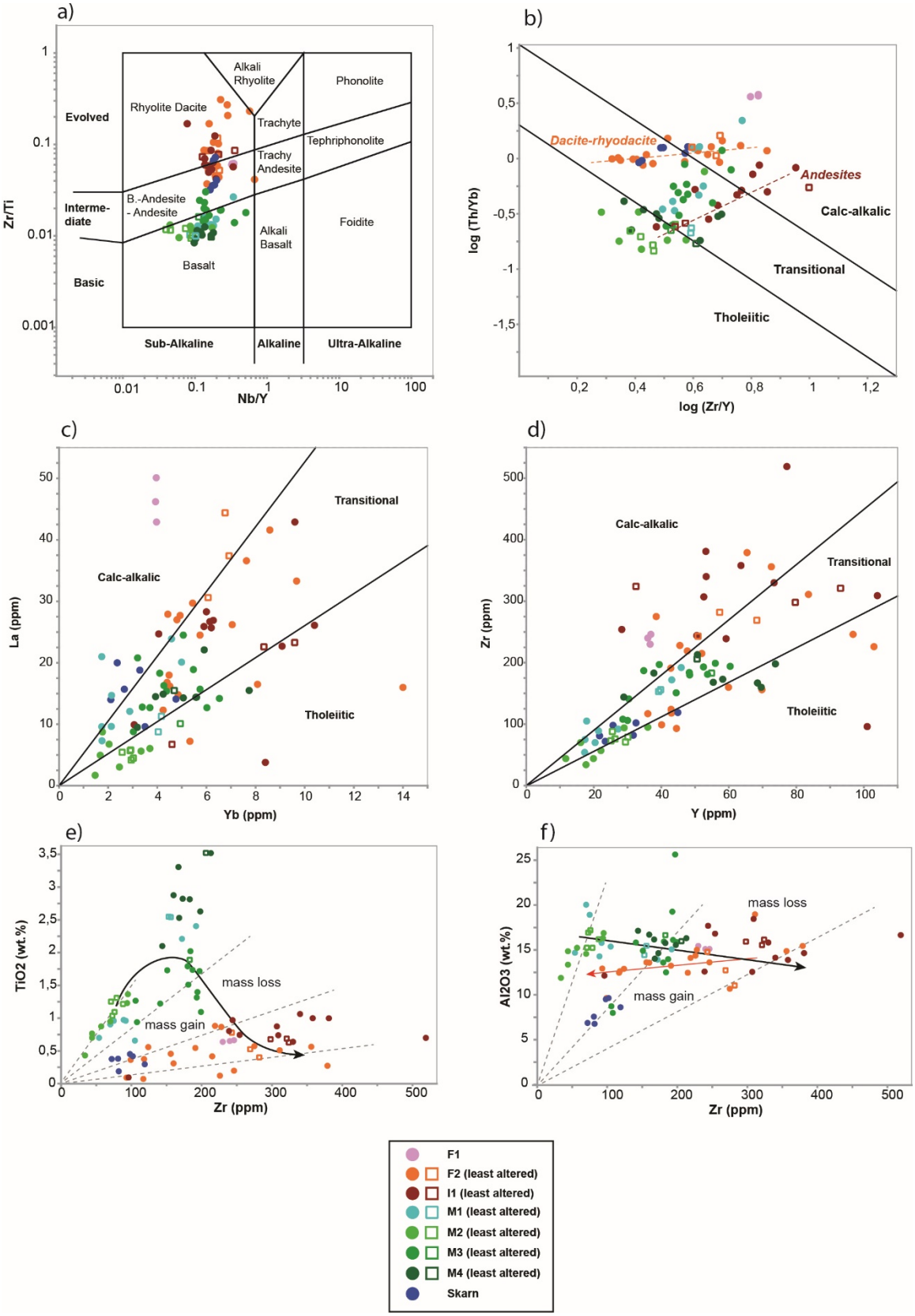
a)
Zr/Ti
Nb/Y
Alkali Rhyolite
Phonolite
Rhyolite Dacite
Evolved
Trachyte
Tephriphonolite
Trachy Andesite
B.-Andesite - Andesite
Interme-diate
Alkali Basalt
Foidite
Basalt
Basic
Sub-Alkaline
Alkaline
Ultra-Alkaline
b)
log (Th/Yb)
log (Zr/Y)
Dacite-rhyodacite
Andesites
Calc-alkalic
Transitional
Tholeiitic
c)
La (ppm)
Yb (ppm)
Transitional
Calc-alkalic
Tholeiitic
d)
Zr (ppm)
Y (ppm)
Calc-alkalic
Transitional
Tholeiitic
e)
TiO2 (wt.%)
Zr (ppm)
mass loss
mass gain
f)
Al2O3 (wt.%)
Zr (ppm)
mass loss
mass gain
F1
F2 (least altered)
I1 (least altered)
M1 (least altered)
M2 (least altered)
M3 (least altered)
M4 (least altered)
Skarn

(previous page) **Figure 0.10:** Geochemistry of volcanic rocks from the Moulin-à-Baude Formation. **a)** Nb/Y vs Zr/Ti diagram for volcanic rock classification (Pearce 1982); **b)** Log (Zr/Ti) vs log (Th/Yb) diagram from Ross and Bédard (2009) to determine the magmatic affinity of the volcanic rocks; **c)** Yb vs La and **d)** Zr vs Y discrimination diagrams of magmatic affinity using element ratios from MacLean and Barrett (1993) and Barrett and MacLean (1994); **e)** Diagram TiO_2 vs Zr with a fractionation trend (solid arrow) that link the least altered samples (except for the M4 unit). The dashed lines that pass through the origin represent alteration lines; **f)** Al_2O_3 vs Zr plot with a fractionation trend (solid black arrow) and alteration lines (dashed lines). The red solid arrow represents an alteration trend with remobilization of Zr.

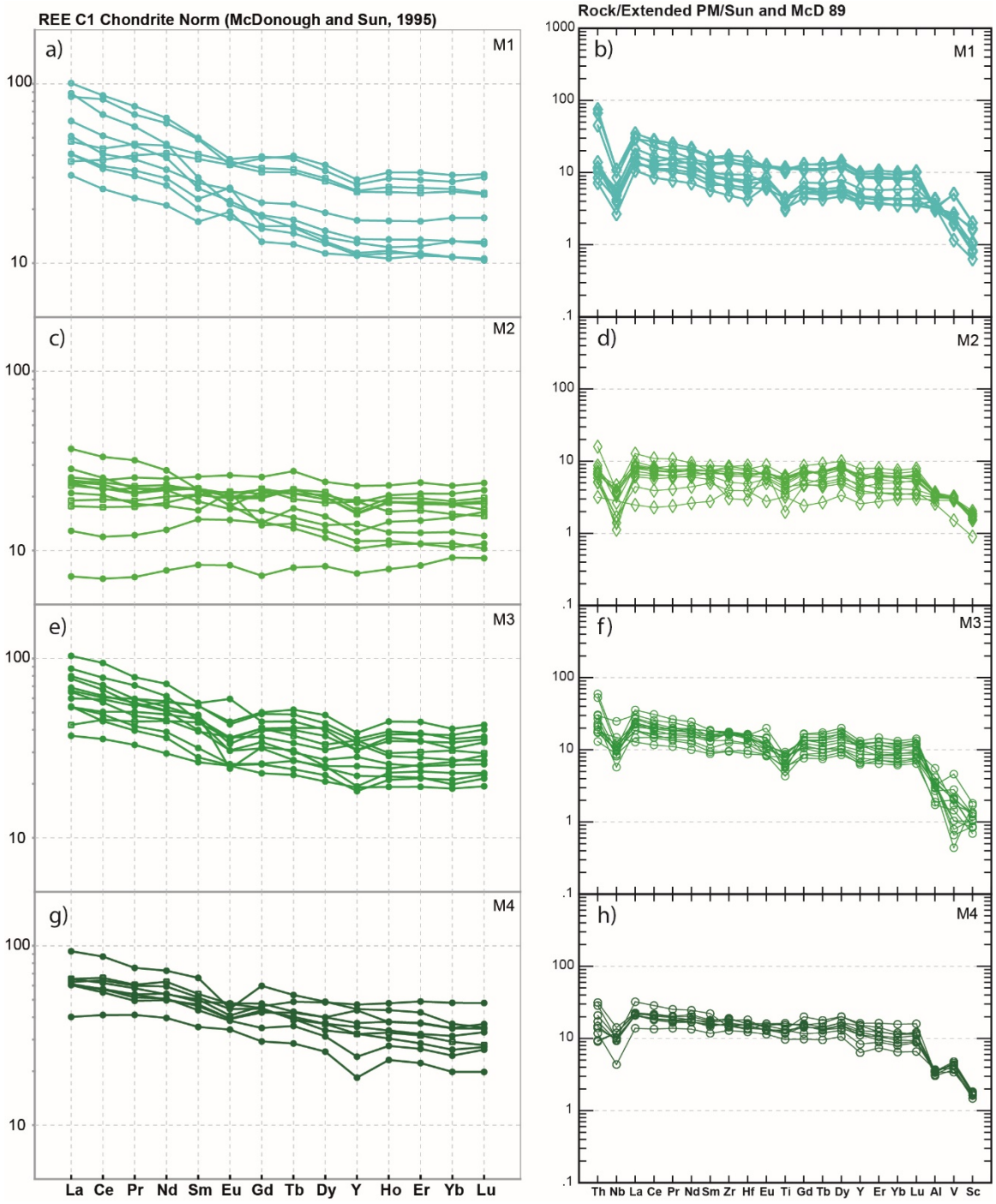

Figure 0.11: REE plots normalized to chondrite **(a, c, e, g)** or extended trace element diagram normalized to primitive mantle **(b, d, f, h)** showing the different groups of mafic volcanic rocks from the Moulin-à-Baude Formation. Values after Sun and McDonough (1989) for the normalization to the primitive mantle and McDonough and Sun (1995) for the chondritic values.

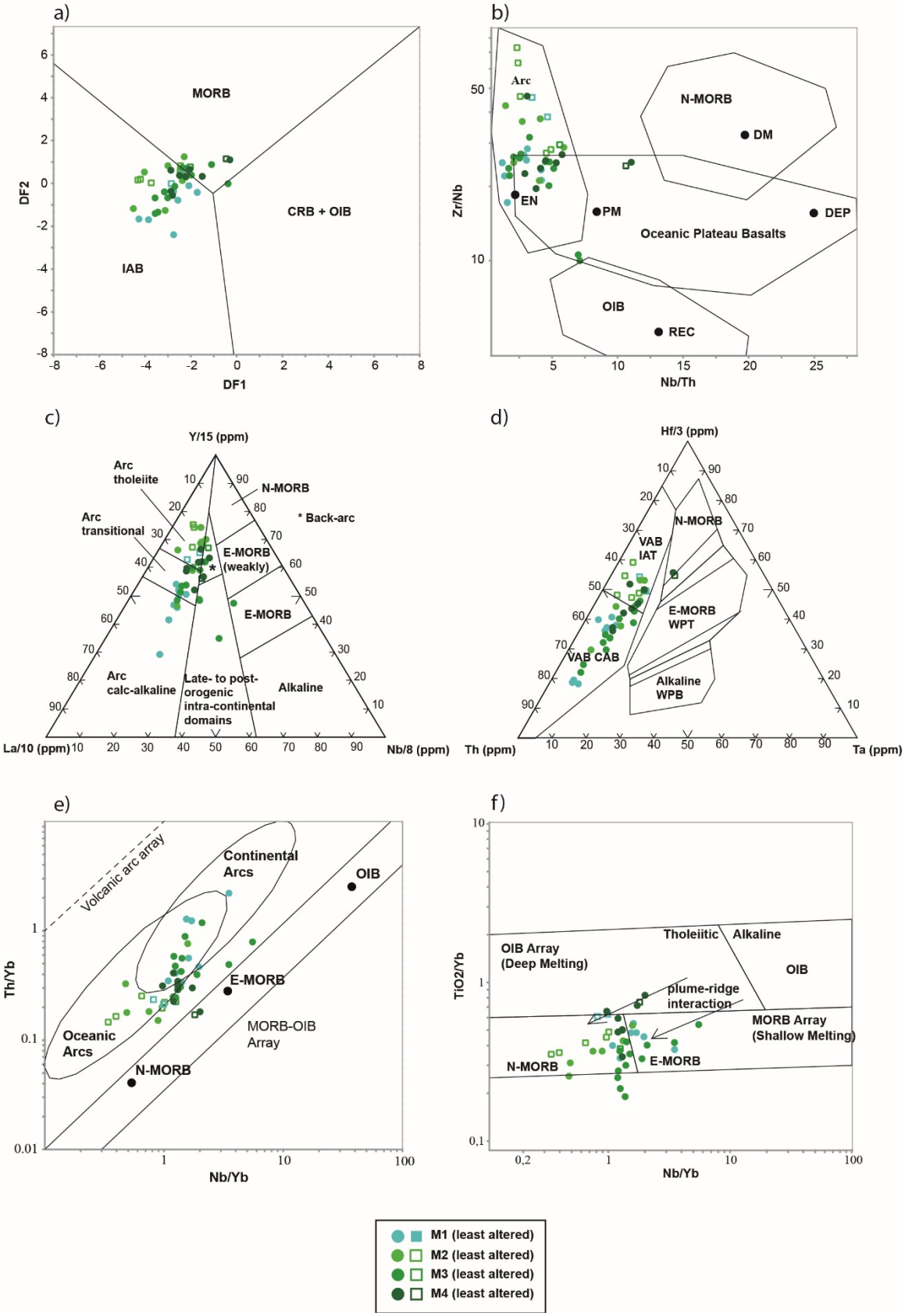
a)
MORB
CRB + OIB
IAB
DF2
DF1
b)
Arc
N-MORB
DM
EN
PM
DEP
Oceanic Plateau Basalts
OIB
REC
Zr/Nb
Nb/Th
c)
Y/15 (ppm)
Arc tholeiite
N-MORB
* Back-arc
Arc transitional
E-MORB (weakly)
E-MORB
Arc calc-alkaline
Late- to post-orogenic intra-continental domains
Alkaline
La/10 (ppm)
Nb/8 (ppm)
d)
Hf/3 (ppm)
N-MORB
VAB IAT
E-MORB WPT
VAB CAB
Alkaline WPB
Th (ppm)
Ta (ppm)
e)
Volcanic arc array
Continental Arcs
OIB
E-MORB
MORB-OIB Array
Oceanic Arcs
N-MORB
Th/Yb
Nb/Yb
f)
Tholeiitic
Alkaline
OIB Array (Deep Melting)
OIB
plume-ridge interaction
MORB Array (Shallow Melting)
N-MORB
E-MORB
TiO2/Yb
Nb/Yb
M1 (least altered)
M2 (least altered)
M3 (least altered)
M4 (least altered)

(previous page) **Figure 0.12:** Tectonic discrimination diagrams for mafic volcanic rocks from the Moulin-à-Baude Formation: **a)** DF2 vs DF1 diagram (Agrawal et al., 2008). DF1 = 0.3518 $\log_e$ {La/Th) + 0.6013 $\log_e$ (Sm/Th) – 1.3450 $\log_e$ (Yb/Th) + 2.1056 $\log_e$ (Nb/Th) – 5.4763. DF2 = –0.3050 $\log_e$ (La/Th) – 1.1801 $\log_e$ (Sm/Th) + 1.6189 $\log_e$ (Yb/Th) + 1.2260 $\log_e$ (Nb/Th) – 0.9944. IAB – Island arc basalt, MORB – Mid-ocean ridge basalt, CRB – Continental rift basalt, OIB – Ocean island basalt; **b)** Zr/Nb – Nb/Th plot from Condie (2003). EN – enriched mantle source, PM – primitive mantle, DM – depleted mantle, DEP – depleted mantle source, REC – recycled components; **c)** Ternary diagram Y/15 – Nb/8 – La/10 (Cabanis and Lecolle, 1989); **d)** ternary diagram Hf/3 – Ta – Th (Wood 1980); **e)** Nb/Yb – Th/Yb plot from Pearce (2014); **f)** TiO_2/Yb – Nb/Yb diagram from Pearce (2008). Symbols are as in Figure 10.

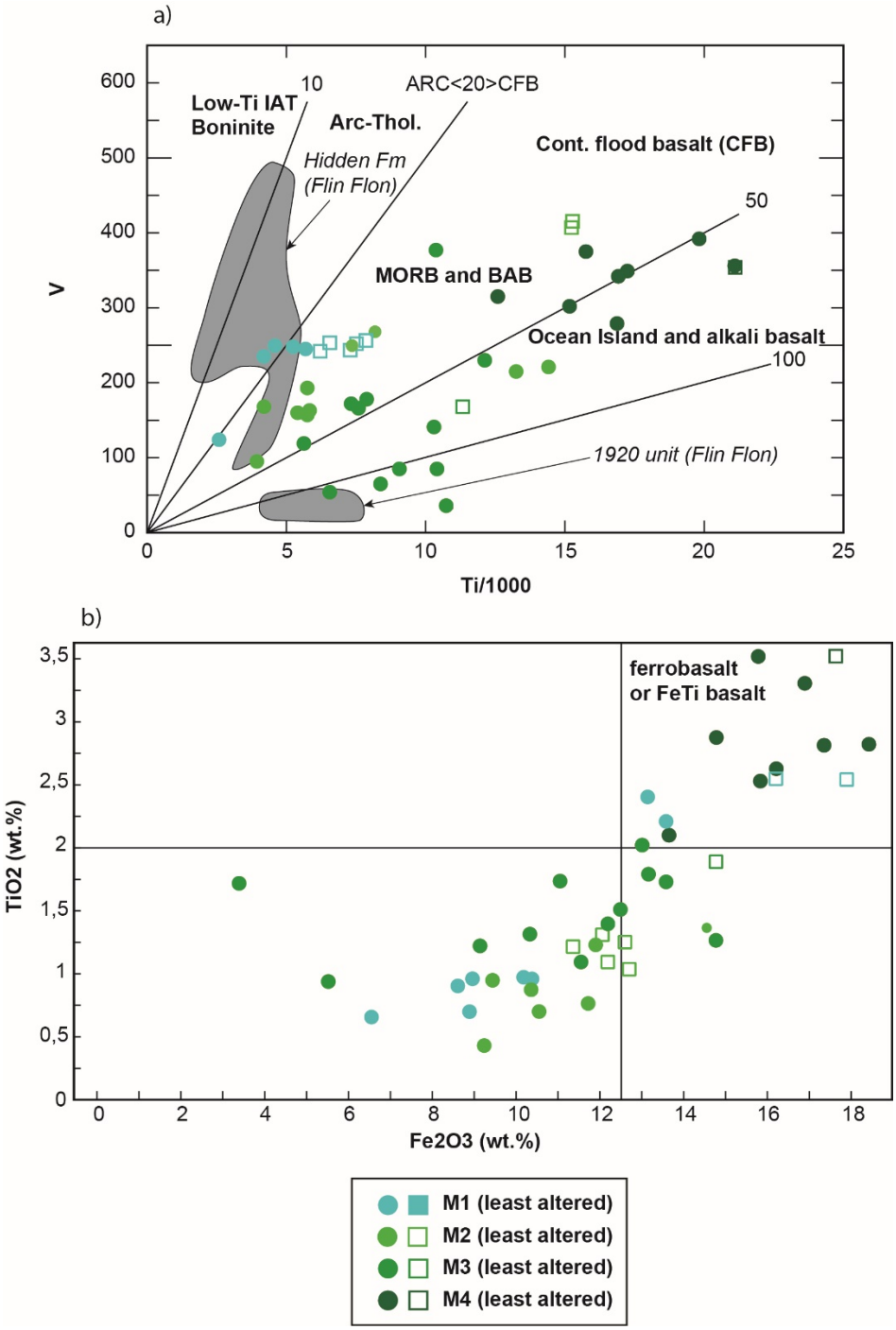

Figure 0.13: a) Ti – V discrimination diagram from Shervais (1982) for mafic volcanic rocks from the Moulin-à-Baude Formation, for comparison basaltic rocks from the Hidden Formation and 1920 unit (Flin Flon belt) are plotted (Ames et al., 2016). IAT – island arc tholeiite, BAB – back-arc basin basalt; **b)** TiO_2 – Fe_2O_3 plot to separate ferrobasalt or FeTi basalt from classic basalt. Symbols are as in Figure 10.

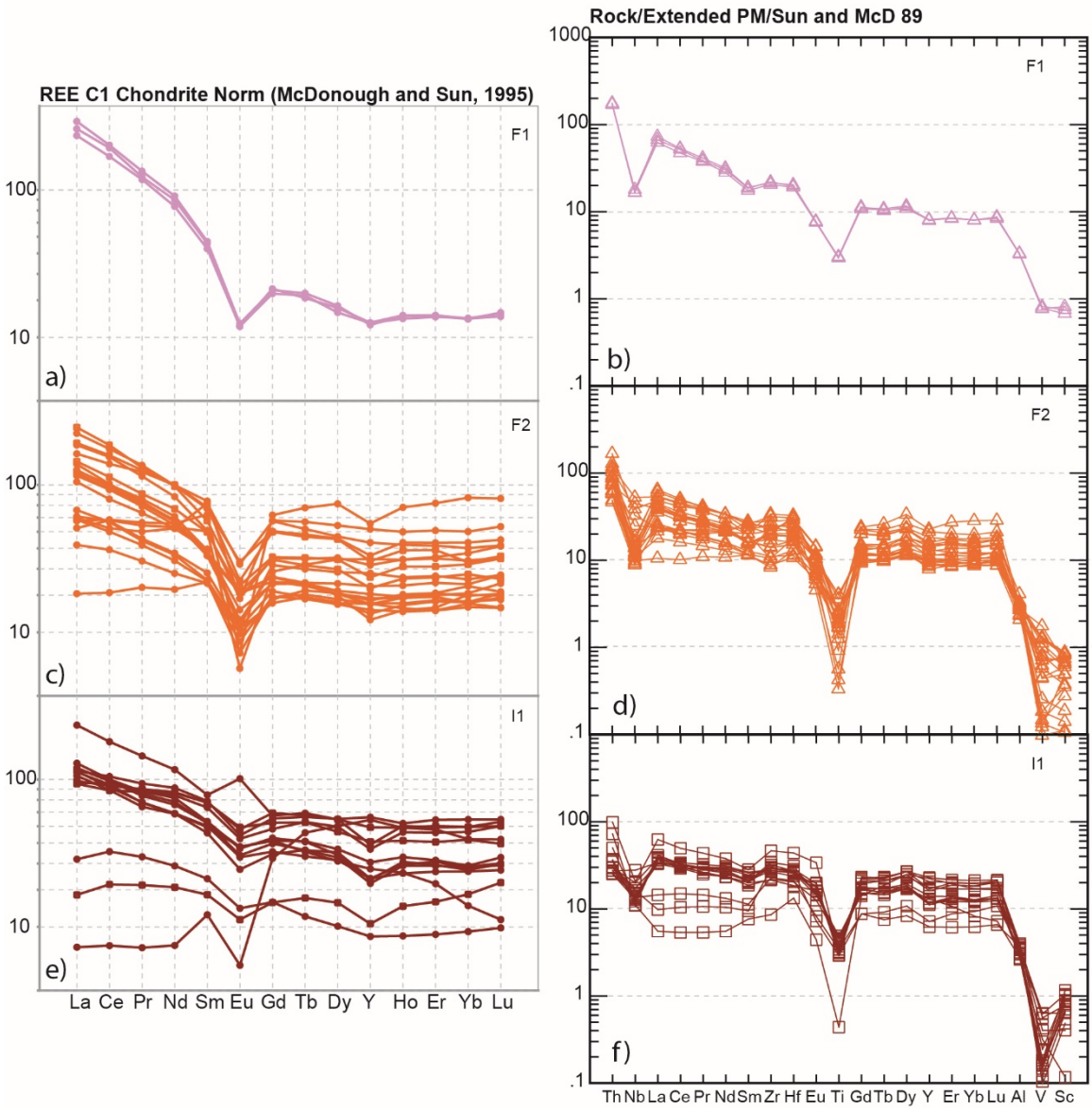

Figure 0.14: REE plots normalized to chondrite **(a, c, e)** or extended trace element diagram normalized to primitive mantle **(b, d, f)** showing the different groups of intermediate and felsic volcanic rocks from the Moulin-à-Baude Formation. Values after McDonough and Sun (1995).

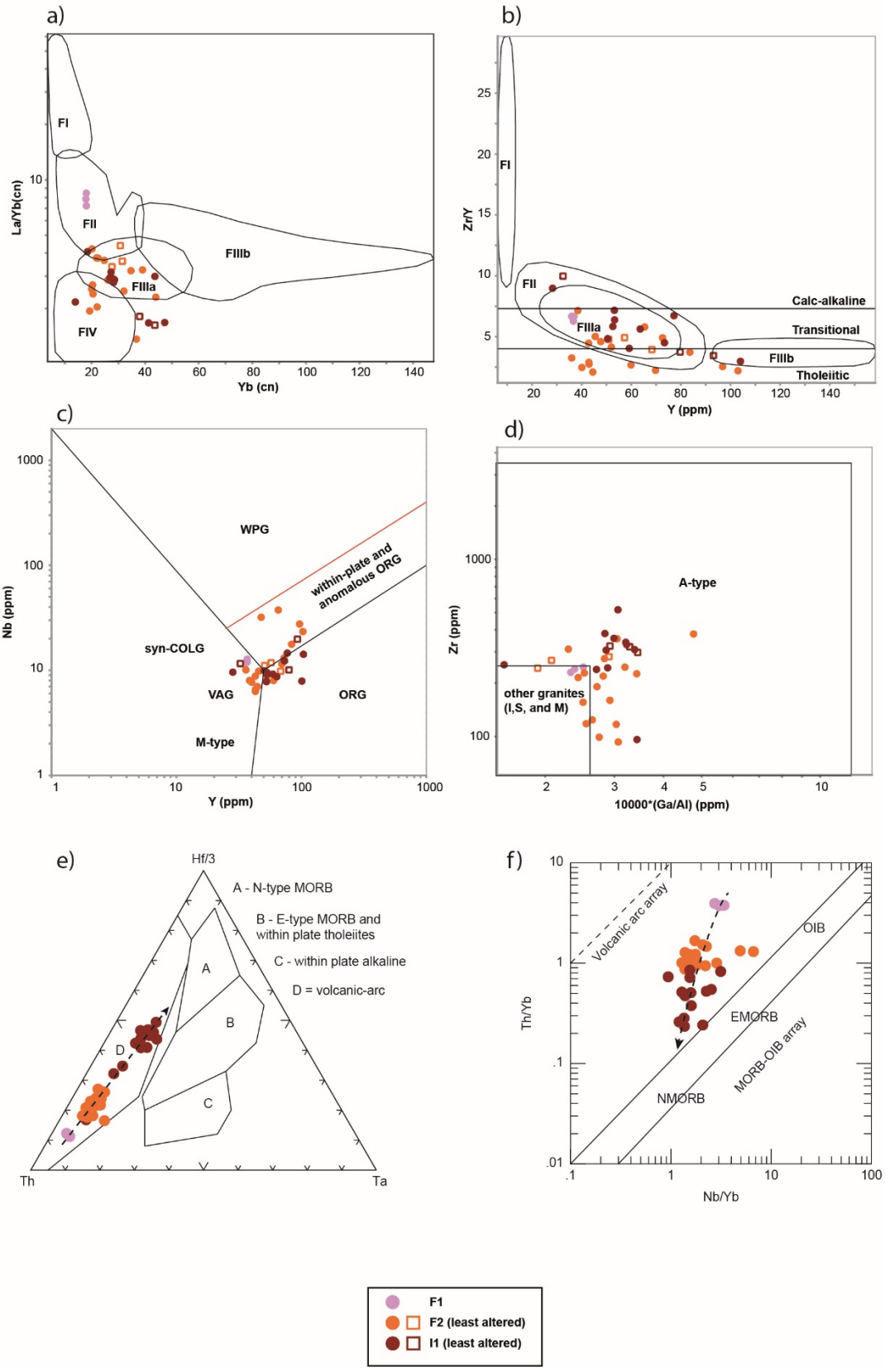
a)
FI
FII
FIIIb
FIIIa
FIV
La/Yb(cn)
Yb (cn)
b)
FI
FII
FIIIa
FIIIb
Calc-alkaline
Transitional
Tholeiitic
Zr/Y
Y (ppm)
c)
WPG
within-plate and anomalous ORG
syn-COLG
VAG
ORG
M-type
Nb (ppm)
Y (ppm)
d)
A-type
other granites (I,S, and M)
Zr (ppm)
10000*(Ga/Al) (ppm)
e)
Hf/3
A - N-type MORB
B - E-type MORB and within plate tholeiites
C - within plate alkaline
D = volcanic-arc
A
B
C
D
Th
Ta
f)
Volcanic arc array
OIB
EMORB
MORB-OIB array
NMORB
Th/Yb
Nb/Yb
F1
F2 (least altered)
I1 (least altered)

(previous page) **Figure 0.15:** Petrochemical affinity and tectonic discrimination diagrams for intermediate and felsic volcanic rocks from the Moulin-à-Baude Formation. **a)** $[La/Yb]_{CN} - Yb_{CN}$ diagram from Hart et al. (2004). CN – chondrite normalized, values after McDonough and Sun (1995); **b)** Zr/Y – Y plot from Lesher et al. (1986); **c)** Nb – Y diagram from Pearce et al. (1984); **d)** Zr – 10^4*(Ga/Al) plot from Whalen et al. (1987). I-type = igneous source, S-type = crustal source, A-type = alkaline; **e)** ternary diagram Hf/3 – Ta – Th (Wood 1980), the dashed line shows the evolution trend from arc to arc-rift rocks; **f)** Nb/Yb – Th/Yb plot from Pearce (2008), the dashed line shows the evolution trend from arc to arc-rift rocks. Symbols are as in Figure 10.

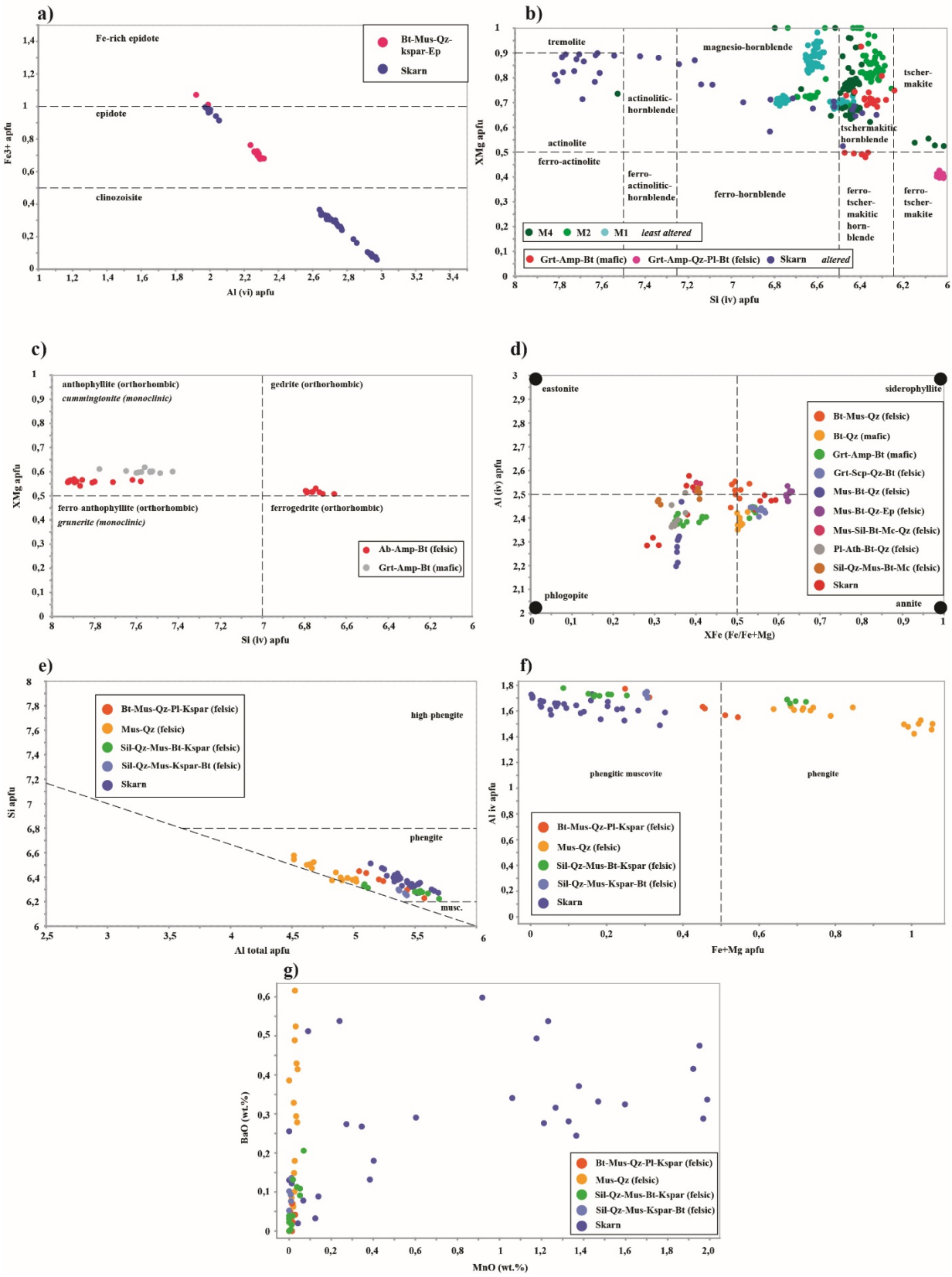
a)
Fe-rich epidote
epidote
clinozoisite
Bt-Mus-Qz-kspar-Ep
Skarn
Fe3+ apfu
Al (vi) apfu
b)
tremolite
magnesio-hornblende
tscher-makite
actinolitic-hornblende
tschermakitic hornblende
actinolite
ferro-actinolite
ferro-actinolitic-hornblende
ferro-hornblende
ferro-tscher-makitic horn-blende
ferro-tscher-makite
M4 M2 M1 least altered
Grt-Amp-Bt (mafic) Grt-Amp-Qz-Pl-Bt (felsic) Skarn altered
XMg apfu
Si (iv) apfu
c)
anthophyllite (orthorhombic)
cummingtonite (monoclinic)
gedrite (orthorhombic)
ferro anthophyllite (orthorhombic)
grunerite (monoclinic)
ferrogedrite (orthorhombic)
Ab-Amp-Bt (felsic)
Grt-Amp-Bt (mafic)
XMg apfu
Si (iv) apfu
d)
eastonite
siderophyllite
phlogopite
annite
Bt-Mus-Qz (felsic)
Bt-Qz (mafic)
Grt-Amp-Bt (mafic)
Grt-Scp-Qz-Bt (felsic)
Mus-Bt-Qz (felsic)
Mus-Bt-Qz-Ep (felsic)
Mus-Sil-Bt-Mc-Qz (felsic)
Pl-Ath-Bt-Qz (felsic)
Sil-Qz-Mus-Bt-Mc (felsic)
Skarn
Al (iv) apfu
XFe (Fe/Fe+Mg)
e)
high phengite
phengite
musc.
Bt-Mus-Qz-Pl-Kspar (felsic)
Mus-Qz (felsic)
Sil-Qz-Mus-Bt-Kspar (felsic)
Sil-Qz-Mus-Kspar-Bt (felsic)
Skarn
Si apfu
Al total apfu
f)
phengitic muscovite
phengite
Bt-Mus-Qz-Pl-Kspar (felsic)
Mus-Qz (felsic)
Sil-Qz-Mus-Bt-Kspar (felsic)
Sil-Qz-Mus-Kspar-Bt (felsic)
Skarn
Al iv apfu
Fe+Mg apfu
g)
Bt-Mus-Qz-Pl-Kspar (felsic)
Mus-Qz (felsic)
Sil-Qz-Mus-Bt-Kspar (felsic)
Sil-Qz-Mus-Kspar-Bt (felsic)
Skarn
BaO (wt.%)
MnO (wt.%)

(previous page) **Figure 0.16: a)** Bimodal plot of Fe^{3+} vs Al(vi) (atom per formula unit – apfu) with epidote mineral compositions fields from altered rocks of the Moulin-à-Baude Formation. **b)** XMg vs Si(iv) (apfu) diagram with calcic amphibole composition fields from Hawthorne et al. (1997) for least-altered mafic rocks from the M1, M2 and M4 units and altered rocks. **c)** FeMg amphibole classification diagram XMg vs Si (apfu) (Hawthorne et al., 1997). **d)** Al(iv) vs XFe (apfu) bimodal plot for biotite, the black dots represent the end-member compositions. **e)** Si vs Al_{tot} (apfu) bimodal plot for white mica with the fields of muscovite, phengite and high-silica phengite. **f)** Bimodal plot of Al(iv) vs Fe+Mg (apfu) for white mica with the fields of phengitic muscovite and phengite. **g)** BaO (wt.%) vs MnO (wt.%) bimodal plot with white mica analyses from altered rocks, the high-Mn ones from the skarns are the pink to lilac wilsonite.

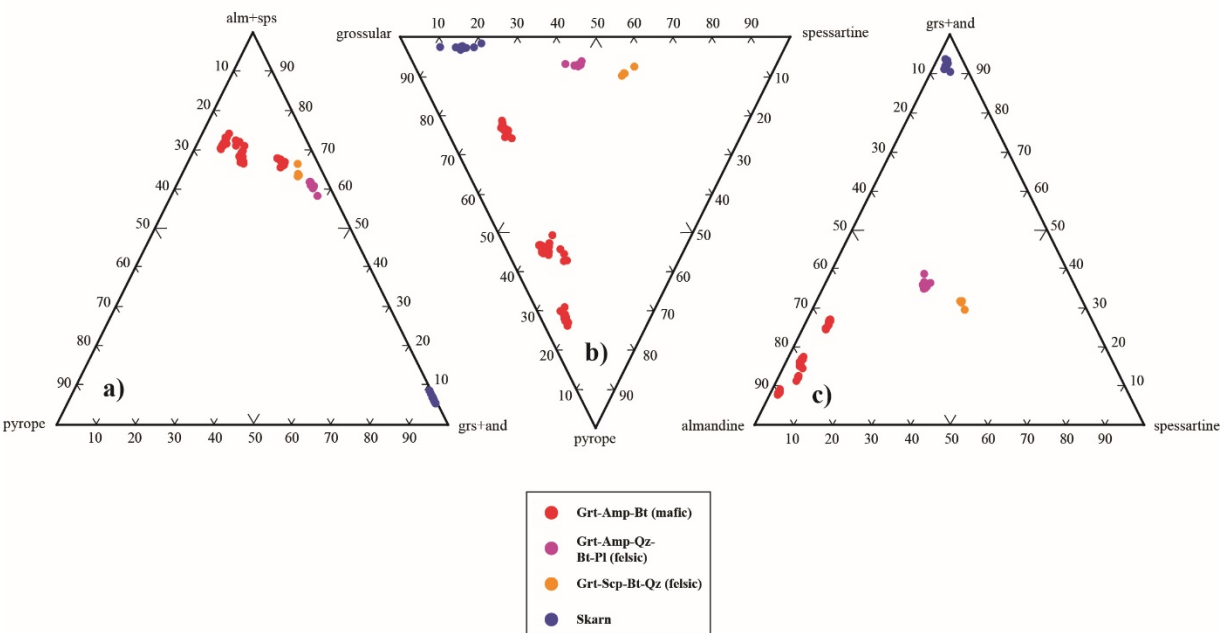

Figure 0.17: Ternary diagram illustrating the composition of garnet from altered rocks, each corner represents an end-member type (alm – almandine; sps – spessartine; grs – grossular; and – andradite). **a)** almandine+spessartine – grossular+andradite – pyrope. **b)** pyrope – grossular – spessartine. **c)** grossular+andradite – spessartine – almandine.

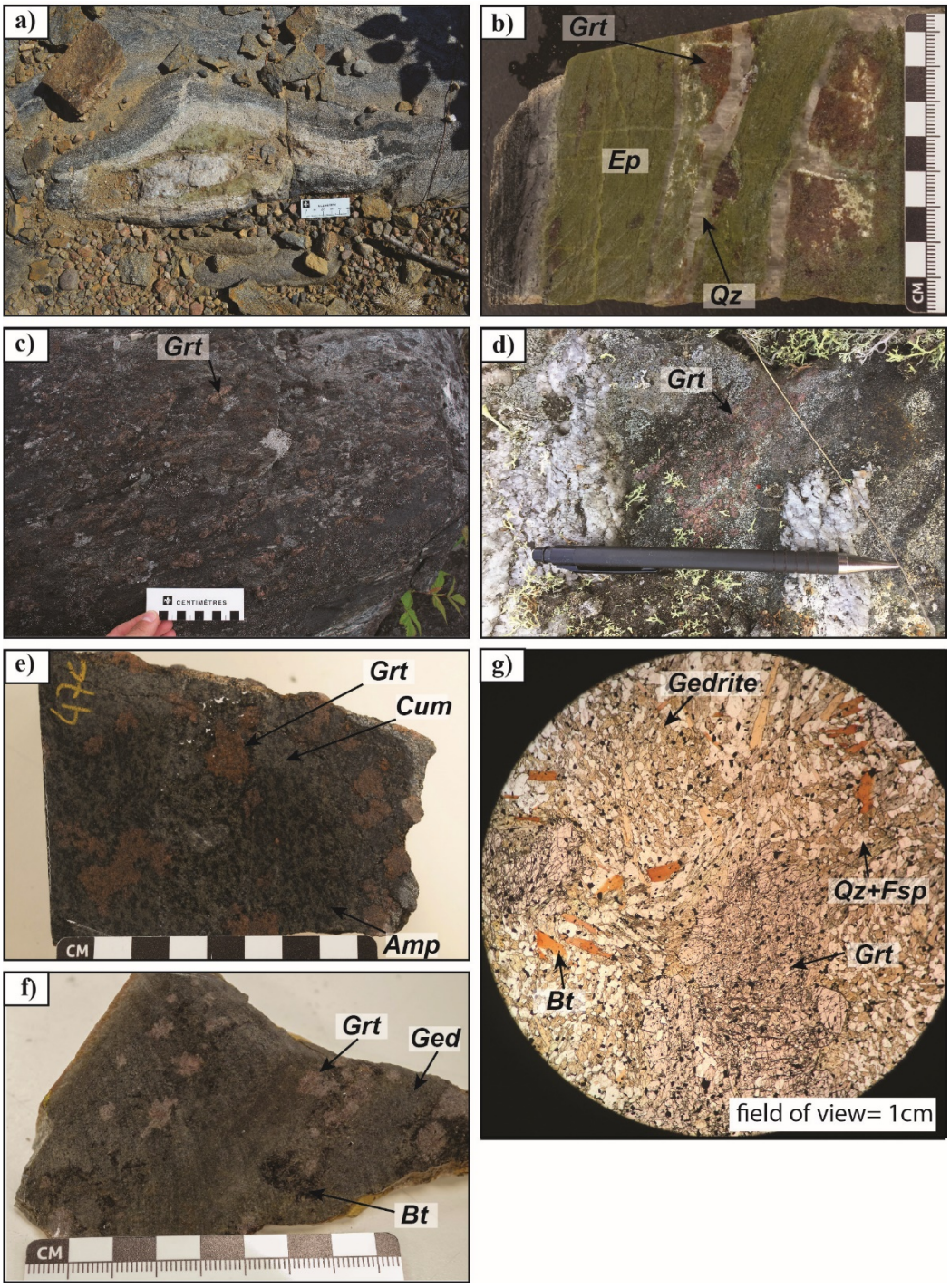

Figure 0.18: Photographs of mineral assemblages from altered basaltic rocks of the Moulin-à-Baude Formation: **a)** Quartz – epidote alteration amass; **b)** Quartz – epidote – grossular – titanite – calcic amphibole – diopside alteration vein; **c)** Porphyroblasts of garnet together with FeMg and calcic amphibole, biotite and quartz assemblage; **d)** Garnet – cummingtonite ± biotite ± sericite ± quartz assemblage and crosscuting quartz veins; **e)** Garnet – cummingtonite – calcic amphibole ± biotite ± sericite ± quartz; **f)** Gedrite ± anthophyllite – garnet – biotite ± quartz altered basalt; **g)** Gedrite – garnet – biotite altered basalt (plane polarized light – PPL).

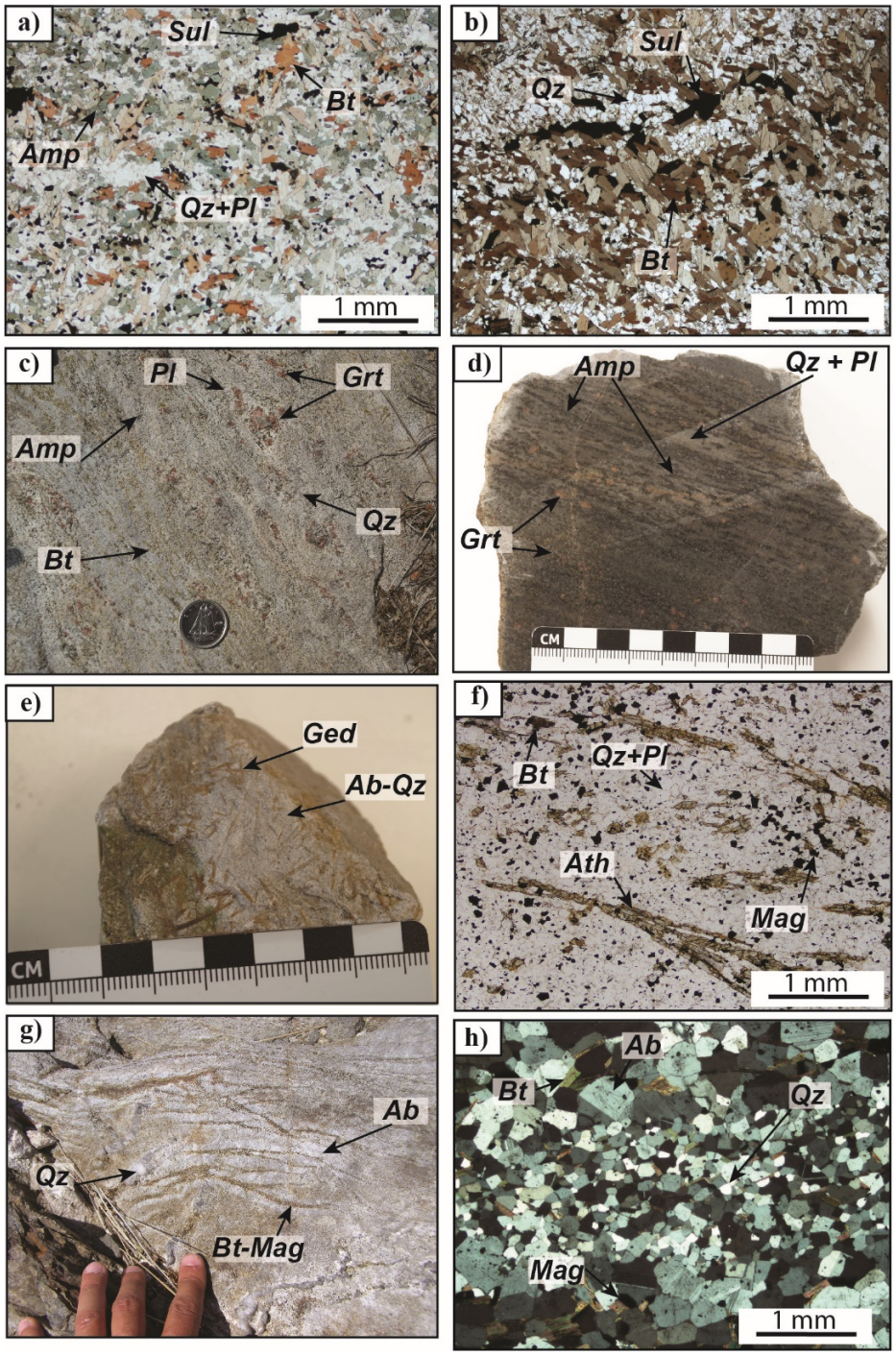

Figure 0.19: Photographs of mineral assemblages from altered volcanic rocks of the Moulin-à-Baude Formation: **a)** Biotite – sulfides ± quartz altered basalt (PPL); **b)** biotite – sulfides – quartz altered basalt (PPL); **c)** Mn-Ca-Fe garnet – quartz – amphibole – biotite altered andesite; **d)** Mn-Ca-Fe garnet – quartz – amphibole altered andesite; **e)** Albite – gedrite – quartz altered andesite; **f)** Anthophyllite – biotite – magnetite – quartz – albite assemblage in an altered andesite; **g)** Veins of quartz and biotite – magnetite – albite crosscutting an altered andesite (PPL); h) biotite – albite – quartz – magnetite assemblage in an altered andesite (cross-polarized light – CPL).

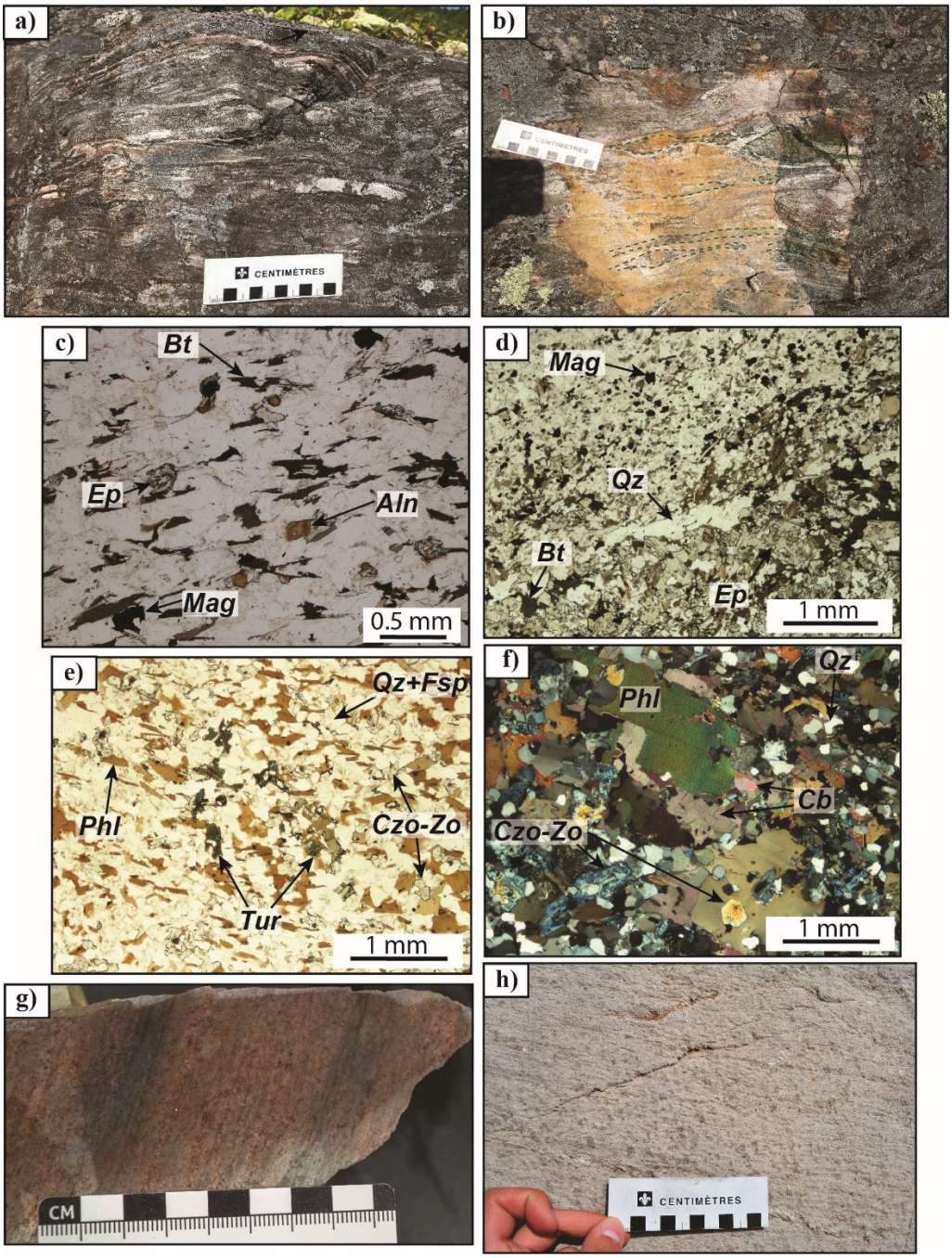

Figure 0.20: Photographs of mineral assemblages from altered felsic to intermediate volcanic rocks of the Moulin-à-Baude Formation: **a)** Stockwork of veins (microcline – plagioclase – biotite – carbonate – epidote – calcic amphibole – magnetite/hematite – quartz ± muscovite) crosscutting an andesitic tuff; **b)** boudinated skarn veins (delineate by green dashed lines) crosscutting an altered andesitic tuff; **c)** biotite – allanite – epidote and magnetite altered andesitic tuff (PPL); **d)** vein of biotite – epidote – quartz – magnetite crosscutting an altered andesitic tuff (PPL); **e)** phlogopite – quartz – k-feldspar – clinozoisite/zoisite – tourmaline altered dacite (PPL); **f)** Phlogopite – carbonate – clinozoisite/zoisite – quartz altered dacite (CPL); **g)** muscovite – hematite – microcline – quartz – biotite ± chlorite altered felsic volcanic rock; **h)** quartz – muscovite (porphyroblast) ± garnet altered felsic volcanic rocks.

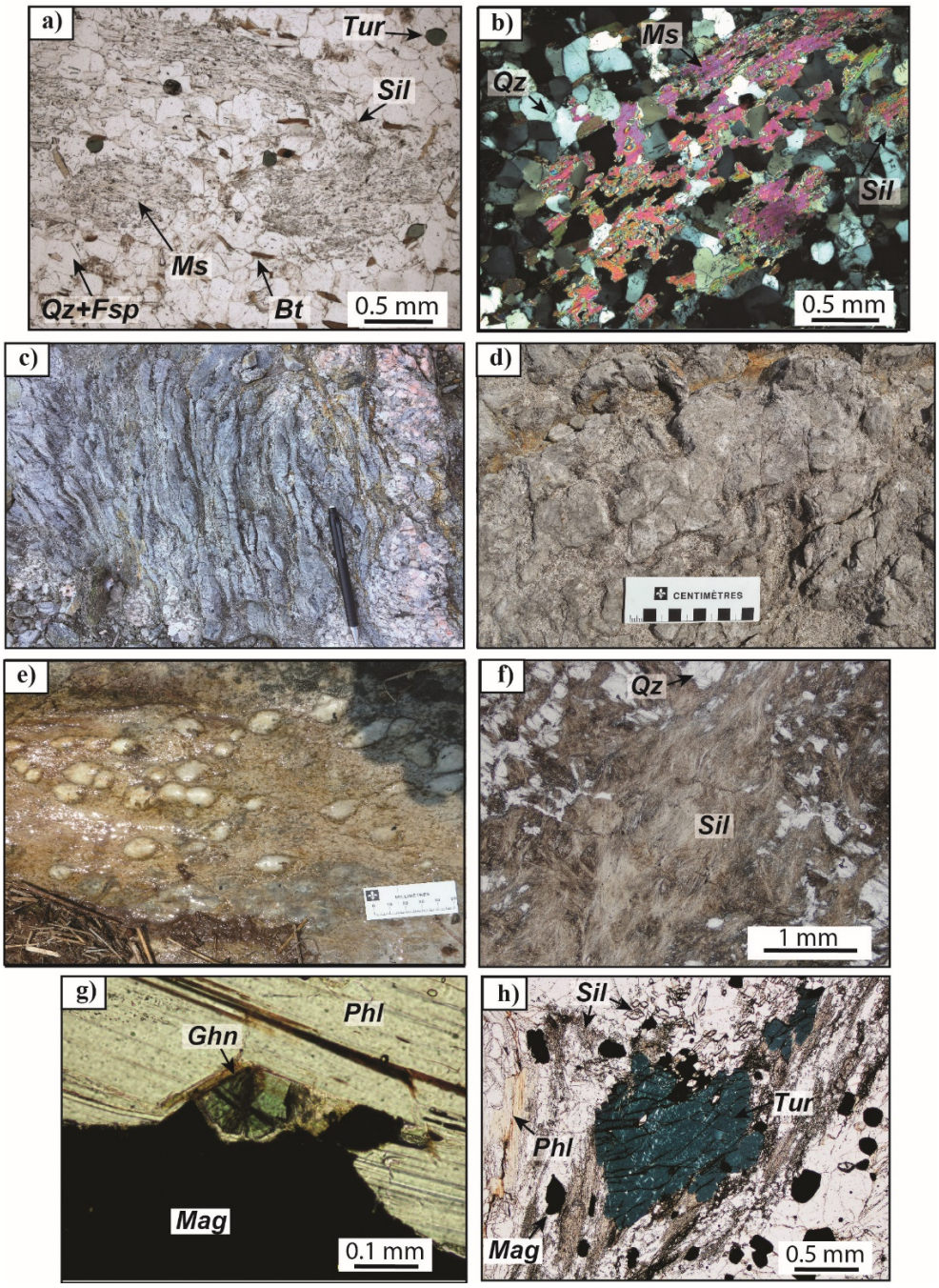

Figure 0.21: Photographs of mineral assemblages from altered felsic to intermediate volcanic rocks of the Moulin-à-Baude Formation: **a)** muscovite (porphyroblast) – sillimanite – microcline – biotite-tourmaline altered felsic volcanic rock (PPL); **b)** Muscovite porphyroblast reacting into a quartz – sillimanite assemblage within an altered felsic volcanic rock (CPL); **c)** Veins of sillimanite and granitic injections (right and lower part) crosscutting a muscovite – microcline – phlogopite – magnetite altered felsic volcanic rock (the pencil is 13.5 cm long); **d)** Sillimanite (fibrolite) pseudomorph after andalusite in an altered felsic volcanic rock; **e)** Nodules of sillimanite (fibrolite) – quartz in a quartz – microcline – muscovite – phlogopite – tourmaline altered felsic volcanic rock; **f)** Nodule of sillimanite (fibrolite) – quartz (PPL); **g)** Grain of gahnite at the contact between magnetite and phlogopite (PPL); **h)** Sillimanite (fibrolite and euhedral grains) – phlogopite – magnetite – tourmaline altered felsic volcanic rock (PPL)

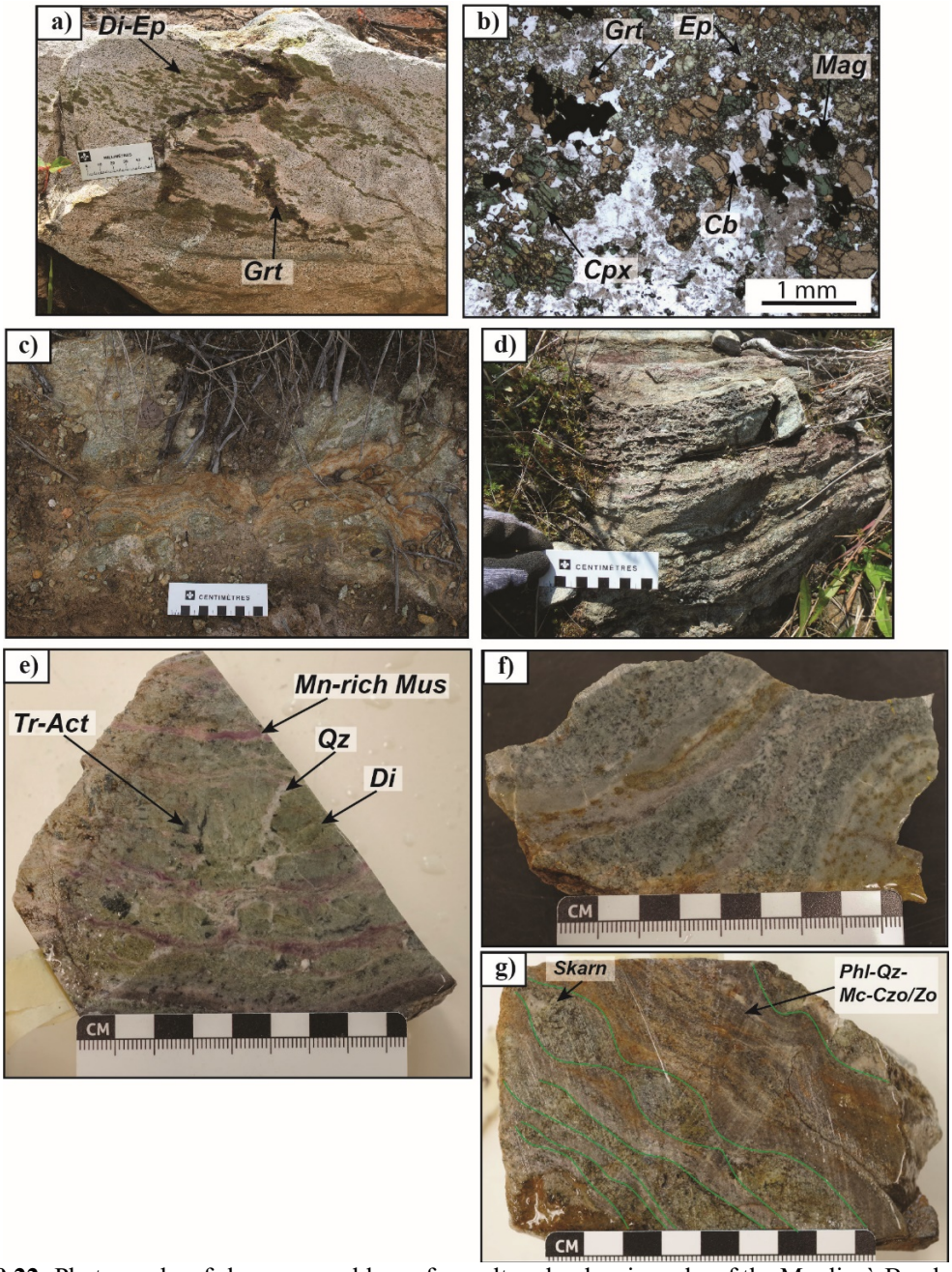

Figure 0.22: Photographs of skarns assemblages from altered volcanic rocks of the Moulin-à-Baude Formation:**a)** folded vein of garnet (andradite) – magnetite crosscutting a clinopyroxene – epidote – garnet (andradite) – calcic amphibole – carbonate – magnetite – quartz altered volcanic rock; **b)** garnet (andradite) – epidote – clinopyroxene – carbonate – magnetite ± quartz assemblage (PPL); **c)** diopside – tremolite/actinolite – clinozoisite/zoisite – carbonate – quartz ± muscovite ± phlogopite ± microcline skarn displaying some evidence of boudinage together with sulfides-rich veins; **d)** banded skarns and veins of quartz and Mn-rich pink to lilac white mica (wilsonite variety); **e)** diopside – tremolite/actinolite – clinozoisite/zoisite skarn crosscuts by veins of quartz and pink to lilac colored Mn-rich white mica; **f)** banded sample with skarn assemblage (greenish) and quartz alteration (white); **g)** boudinated veins of skarn assemblage (diopside-tremolite-actinolite delineated by green solid lines) crosscutting a phlogopite – microcline – clinozoisite/zoisite – quartz altered felsic volcanic rock.

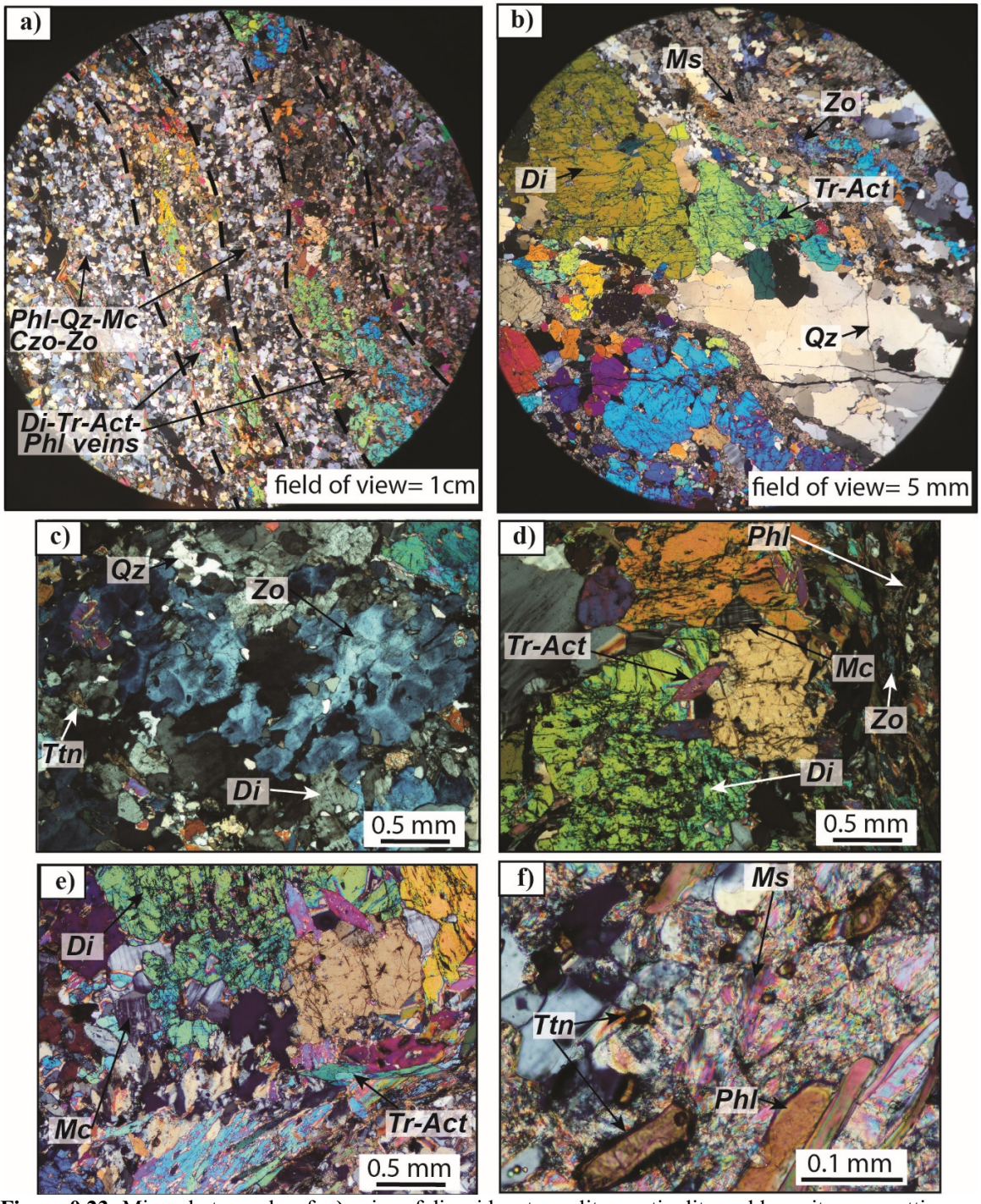

Figure 0.23: Microphotographs of: **a)** veins of diopside – tremolite – actinolite – phlogopite crosscutting a phlogopite – microcline ± clinozoisite/zoisite ± quartz altered felsic volcanic rock (CPL); **b)** a vein of diopside – quartz and sericitised plagioclage crosscutting a clinozoisite/zoisite – quartz – sericite altered rock (CPL); **c)** zoned zoisite together with diopside – quartz – titanite in a skarn assemblage (CPL); **d)** diopside – tremolite – actinolite – phlogopite – k-feldspar – zoisite assemblage in a boudinated skarn vein (CPL); **e)** diopside – microcline – tremolite – actinolite assemblage in a skarn vein (CPL); **f)** titanite – muscovite – phlogopite assemblage in an altered felsic volcanic rock crosscut by skarn veins (CPL).

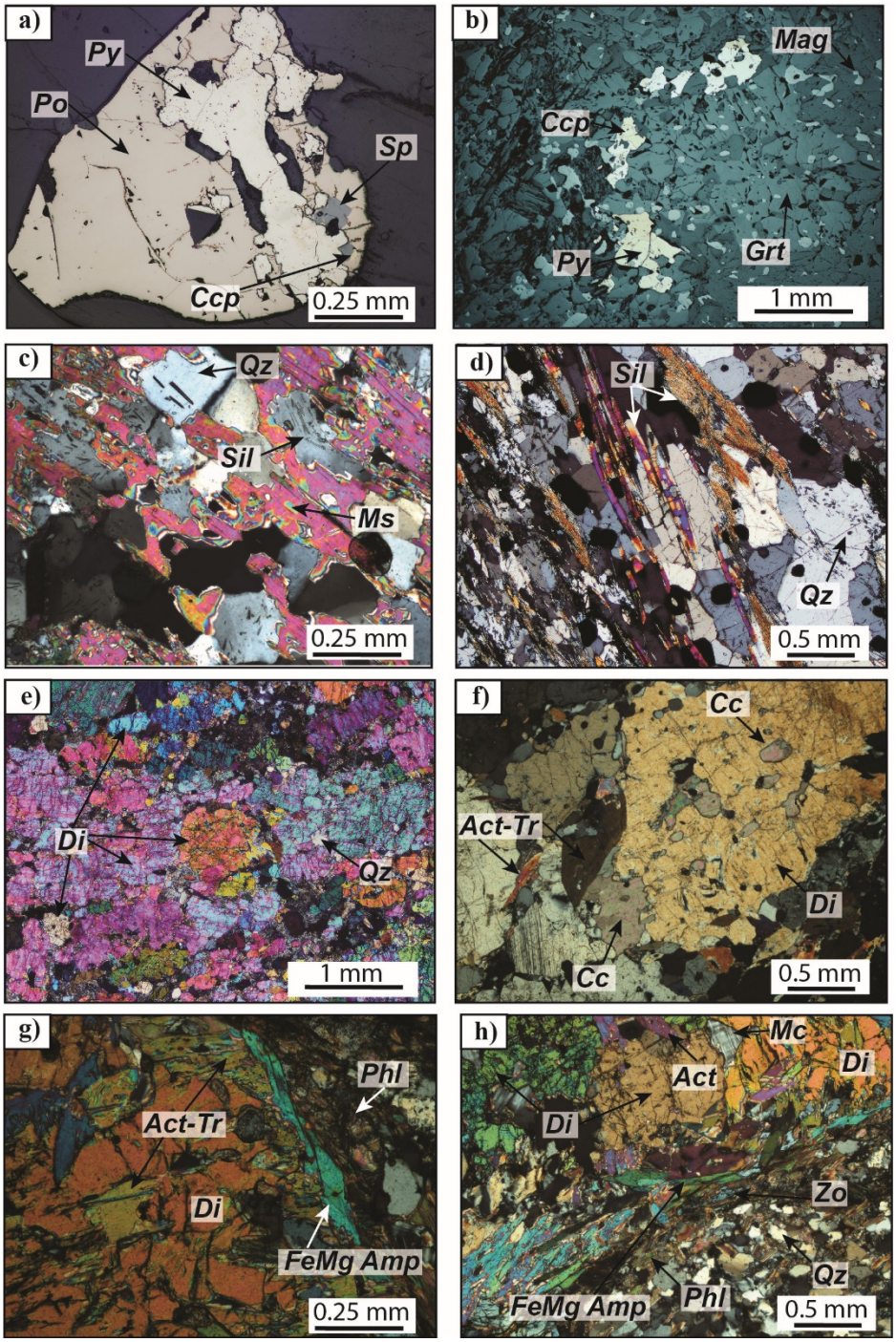

Figure 0.24: Microphotographs of: **a)** pyrite that transformed into pyrrhotite together with sphalerite and chalcopyrite (reflected light); **b)** sulfides (pyrite, chalcopyrite) inclusions within a garnet (reflected light); **c)** muscovite porphyroblast that transforms into quartz – sillimanite (CPL); **d)** euhedral sillimanite and sillimanite fibrolite together with quartz and magnetite (CPL); **e)** diopside-rich altered rock with minor quartz (CPL); **f)** calcite and tremolite – actinolite within diopside grains (CPL); **g)** close intergrowth between diopside and tremolite – actinolite rimmed by FeMg amphibole and phlogopite (CPL); **h)** boudin of diopside – tremolite – actinolite – microcline rimmed by FeMg amphibole – phlogopite – clinozoisite/zoisite (CPL).

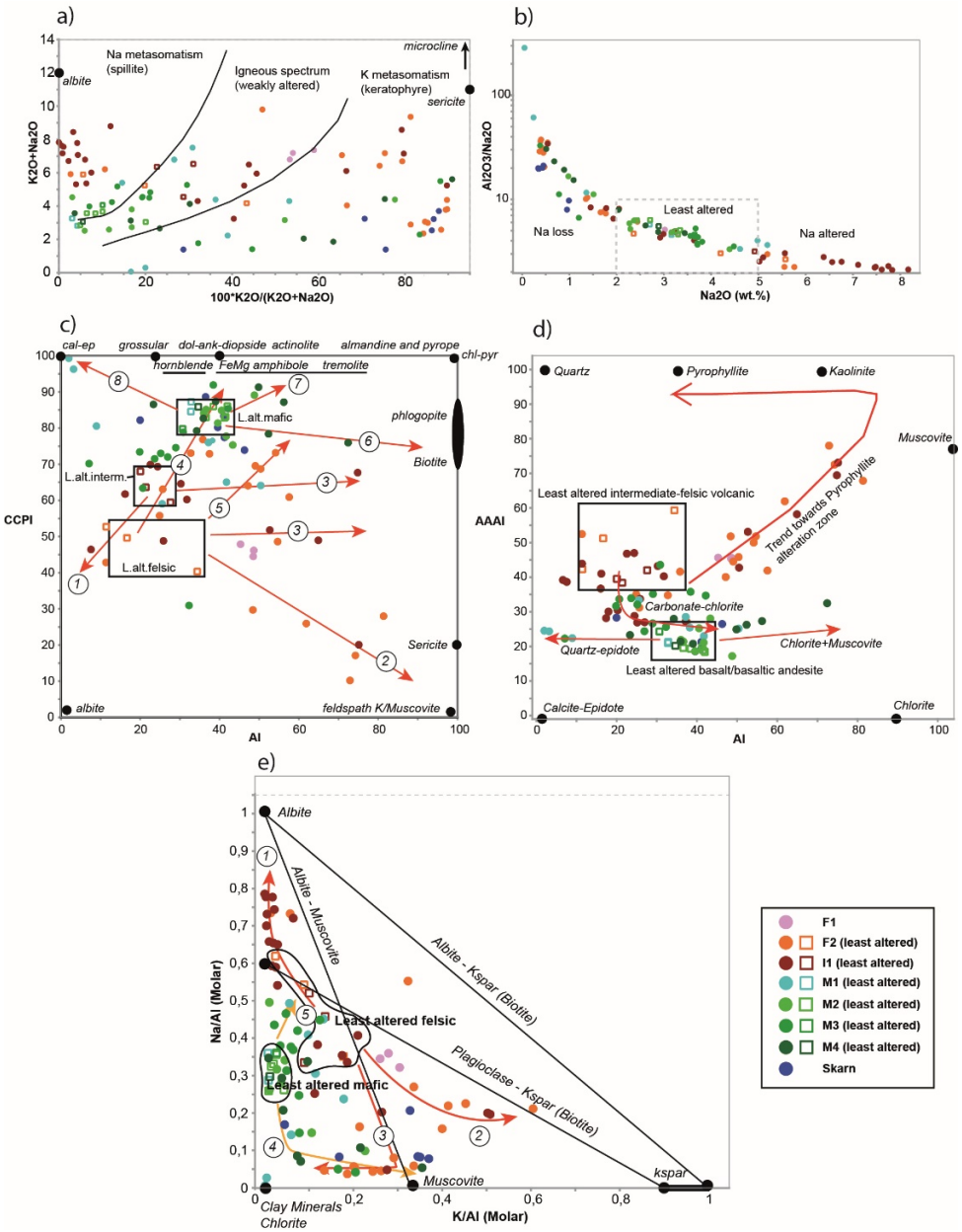

Figure 0.25: a) The Hughes (1973) diagram ($K_2O + Na_2O$) versus the index $100*K_2O/(K_2O+Na_2O)$ diagram outline fresh to weakly altered, Na-altered and K-altered igneous rocks; **b)** Spitz-Darlin index (Al_2O_3/Na_2O; Spitz and Darling, 1978) versus Na_2O to outline fresh to weakly altered rocks from those that experienced Na-gain and Na-losses (diagram from Ruks et al., 2006); **c)** CCPI (chlorite-carbonate-pyrite index = $100*(Fe_2O_{3T}+MgO)/(Fe_2O_{3T} + MgO + K_2O + Na_2O)$; Large et al., 2001) – AI (alteration index= $100*(K_2O+MgO)/(K_2O+MgO+CaO+Na_2O)$; Ishikawa et al., 1976) alteration box plot. It contains the fields of the least altered rocks (mafic, intermediate and felsic) and the nodes for different alteration minerals. Arrays and numbers represent the different types of alteration; **d)** AAAI (advanced argillic alteration index = $100*SiO_2/(SiO_2+10MgO+10CaO+Na_2O)$; Williams and Davidson, 2004) – AI (alteration index) alteration box plot. It contains the fields of the least altered volcanic rocks together with alteration mineral nodes, the arrows represent different alteration trends; **e)** molar ratio (Na/Al – K/Al) plot showing the fields of least altered mafic, intermediate and felsic volcanic rocks together with different mineral nodes. The arrows represent alteration trends. Symbols are as in Figure 10.

Table 0.1 Whole-rock geochemistry of the volcanic rocks and feeder conduits of the Moulin-à-Baude Formation ordered by units. Felsic (F1 and F2), intermediate (I1) and mafic (M1, M2, M3, M4).

Analyse	54682	54343	54354	54371	54737	68407	54738	54715	54739	68405	68401	68402	68408
Sample	15	32A	33C	10D	149A	15PA57A	154F	157B	158A	17PA12B	17PA16A1	17PA16A2	17PA17A
Group	F1	F1	F1	F2	F2	F2	F2	F2	F2	F2	F2	F2	F2
least altered					*		*	*					
SiO2 (wt.%)	65,77	65,57	64,79	67,09	76,28	68,35	66,82	72,38	65,76	70,33	63,42	62,75	72,38
Al2O3	15,45	15,11	15,10	10,68	11,05	15,45	14,80	12,74	14,88	13,62	14,12	15,02	12,46
Fe2O3(T)	5,52	5,98	5,65	6,99	2,98	4,21	7,34	6,05	6,68	2,93	7,95	8,19	5,51
FeO	4,30	4,70	4,41	5,70	2,21	3,44	5,83	4,89	5,42	2,35	6,29	6,52	4,49
Fe2O3	0,79	0,81	0,80	0,72	0,55	0,42	0,93	0,68	0,71	0,35	1,03	1,02	0,57
MgO	1,60	1,55	1,76	2,10	0,61	0,70	0,75	0,28	1,25	1,29	2,08	2,11	0,16
MnO	0,08	0,07	0,09	0,11	0,10	0,02	0,07	0,05	0,11	0,02	0,14	0,14	0,02
CaO	3,29	3,09	2,67	6,95	2,26	0,47	2,80	2,41	2,43	0,29	5,03	5,31	0,85
Na2O	3,02	3,17	3,30	0,37	2,36	5,19	5,57	4,20	2,44	1,75	0,39	0,40	5,55
K2O	4,34	3,63	3,89	1,98	1,81	4,61	0,33	1,04	4,62	7,61	3,42	3,38	0,66
TiO2	0,638	0,663	0,651	0,573	0,401	0,273	0,778	0,525	0,563	0,198	0,882	0,866	0,417
P2O5	0,17	0,17	0,16	0,10	0,10	0,02	0,22	0,18	0,17	0,05	0,18	0,16	0,11
Cr2O3	< 0.01	< 0.01	< 0.01	< 0.01	0,01	< 0.01	0,01	0,01	0,01	< 0.01	0,01	0,01	< 0.01
LOI	0,79	1,14	0,97	2,16	0,74	0,66	0,37	0,40	0,76	0,96	2,05	1,99	0,55
Total	100,70	100,10	99,01	99,11	98,67	99,96	99,87	100,30	99,65	99,04	99,65	100,30	98,67
Ti[1](ppm)	3825	3975	3903	3435	2404	1637	4664	3147	3375	1187	5288	5192	2500
Sr	243	301	232	164	144	67	213	200	113	74	120	128	107
Ba	794	819	674	235	889	1248	148	60	1219	480	772	755	129
Nb	11,9	12,8	11,8	8,0	11,8	37,5	11,1	9,8	13,1	27,6	32,0	9,8	8,4
V	67	64	63	80	15	12	51	36	37	21	107	104	10
Co	11	11	10	12	2	3	11	10	10	3	17	17	2
Ga	19	20	19	16	17	39	15	14	24	23	21	20	16
Ge	1,7	1,9	1,9	1,4	2,2	1,3	2,3	1,6	2,3	1,6	1,9	1,8	1,0
In	< 0.1	< 0.1	< 0.1	< 0.1	0,2	0,3	0,1	0,2	0,2	0,1	< 0.1	< 0.1	< 0.1
Sn	2,0	3,0	2,0	1,0	4,0	5,0	4,0	4,0	5,0	5,0	2,0	2,0	2,0
Cs	3,3	11,1	3,8	2,8	3,6	3,1	0,7	2,2	2,5	4,7	4,2	3,7	0,5
Pb	27	26	23	7	38	6	12	98	14	31	7	7	6
Be	3	3	3	2	3	3	2	4	2	2	2	2	1
Hf	5,9	6,1	6,3	6,4	7,4	10,1	7,0	8,0	9,4	9,0	5,9	6,2	5,8
Ta	0,97	0,90	0,88	0,47	1,08	1,04	0,80	0,93	1,02	1,21	0,67	0,57	0,64
W	1,0	3,1	2,5	0,6	1,2	0,5	0,9	1,3	1,1	0,8	0,9	0,8	0,8
Tl	0,58	0,86	0,89	0,34	0,48	0,72	0,11	0,25	0,67	0,91	0,57	0,63	< 0.05
Bi	< 0.1	< 0.1	< 0.1	< 0.1	0,1	< 0.1	< 0.1	0,2	0,1	< 0.1	0,3	0,3	< 0.1
Th	14,40	14,50	15,00	5,27	10,90	10,00	6,45	8,76	7,94	9,50	6,13	6,42	6,42
U	4,51	4,34	3,50	2,89	2,55	2,87	1,85	2,70	2,92	4,23	1,92	1,83	2,10
Rb	162	144	171	77	70	147	11	37	92	160	147	139	12
Y	36,7	36,9	36,0	38,5	57,3	65,4	50,9	68,3	72,6	96,8	47,7	45,5	52,0
Zr	230	246	240	275	282	379	243	269	356	246	219	228	215
La	42,9	46,2	50,1	18,0	44,4	36,6	30,6	37,4	41,6	33,3	27,0	27,9	29,7
Ce	88,4	97,0	100,0	40,9	94,6	83,1	66,8	84,7	90,8	77,1	58,5	60,1	61,9
Pr	10,40	10,70	11,40	5,04	11,20	10,20	8,41	10,90	11,50	10,70	7,57	7,67	7,75
Nd	38,2	41,0	42,8	21,3	45,0	40,2	35,2	45,7	45,4	45,6	30,6	31,1	30,6
Sm	7,79	8,27	8,44	5,23	10,00	8,99	8,83	11,60	11,40	12,40	7,13	6,95	6,83
Eu	1,27	1,27	1,31	1,17	1,88	1,63	1,74	1,98	2,43	1,63	1,75	1,73	1,29
Gd	6,42	6,77	6,66	5,48	9,05	8,95	8,80	11,90	12,00	13,50	7,24	6,92	6,88
Tb	1,14	1,11	1,17	1,06	1,63	1,61	1,50	2,05	2,10	2,41	1,23	1,20	1,24
Dy	6,46	6,79	6,95	6,85	10,90	11,10	9,80	13,60	13,70	15,80	7,74	7,50	8,38
Ho	1,34	1,39	1,38	1,47	2,24	2,42	1,96	2,67	2,91	3,27	1,61	1,59	1,82

Er	4,00	4,07	4,07	4,48	6,56	7,28	5,83	7,86	8,50	9,72	4,89	4,71	5,50
Tm	0,605	0,600	0,603	0,669	1,010	1,130	0,908	1,140	1,250	1,480	0,728	0,713	0,799
Yb	3,97	3,93	3,96	4,48	6,76	7,63	6,07	6,92	8,58	9,67	4,80	4,43	5,44
Lu	0,638	0,645	0,618	0,752	1,100	1,260	0,880	1,130	1,350	1,560	0,748	0,720	0,918
Cd	< 0.5	< 0.5	< 0.5	< 0.5	< 0.5	< 0.5	< 0.5	< 0.5	< 0.5	< 0.5	< 0.5	< 0.5	< 0.5
Cu	8	15	< 1	57	6	906	13	5	2	6	< 1	< 1	5
Ag	1,1	1,9	1,7	2,1	< 0.3	1,3	0,4	0,7	0,6	0,6	< 0.3	< 0.3	0,6
Ni	8	9	8	13	< 1	2	8	8	7	5	28	27	3
Mo	< 1	< 1	< 1	2	4	3	< 1	< 1	1	< 2	< 2	< 2	< 2
Zn	83	92	90	99	82	93	76	51	118	238	89	87	39
S	200	1800	200	5700	< 100	200	< 100	< 100	< 100	< 100	< 100	< 100	< 100
Au	< 2	< 2	< 2	< 2	< 2	< 2	< 2	< 2	< 2	3	< 2	< 2	< 2
As	2,5	3,9	< 0.5	13,0	0,9	3,1	4,8	5,1	< 0.5	3,6	3,1	3,4	4,4
Sc	12,8	11,6	13,9	10,2	6,0	4,7	14,2	8,4	10,2	3,2	15,0	14,6	8,5
Sb	0,8	1,7	1,3	0,5	0,4	0,7	0,4	0,3	0,3	0,4	1,9	2,0	1,0
Eu/Eu*[2]	0,55	0,52	0,53	0,67	0,60	0,56	0,60	0,52	0,63	0,38	0,74	0,76	0,58
log(Th/Yb)	0,56	0,57	0,58	0,07	0,21	0,12	0,03	0,10	-0,03	-0,01	0,11	0,16	0,07
log(Zr/Y)	0,80	0,82	0,82	0,85	0,69	0,76	0,68	0,60	0,69	0,41	0,66	0,70	0,62
La/Ybcn[3]	7,34	7,99	8,59	2,73	4,46	3,26	3,42	3,67	3,29	2,34	3,82	4,28	3,71
Zr/TiO2	360,50	371,04	368,66	479,93	703,24	1388,28	312,34	512,38	632,33	1242,42	248,30	263,28	515,59
Al2O3/TiO2	24,22	22,79	23,20	18,64	27,56	56,59	19,02	24,27	26,43	68,79	16,01	17,34	29,88
Tzr (cels)[4]	854	858	854		864	897	857	866	888	845	844	846	839
AI[5]	48	45	49	36	34	48	11	17	55	81	50	49	11
CCPI[6]	49	53	51	79	46	33	58	55	53	31	72	73	48
AAAI[7]	45	46	46	42	59	52	42	51	52	68	46	45	52

Table 4.1 (cont.)

Analyse	68417	68409	68416	54798	54799	54749	53076	67641	68415	54677	54740	54741	54742
Sample	17PA22B	17PA7A	17PA8B	216A1	216A2	217A(tuffite)	95A1	17PA23A	17PA8A	13PA10A1	159BC	160A	160B
Group	F2	F2	F2	F2	F2	F2	F2	F2	F2	F2	I1	I1	I1
least altered													
SiO2 (wt.%)	67,78	66,73	66,24	74,19	79,83	67,45	72,39	58,12	64,41	63,25	65,57	62,75	60,98
Al2O3	13,58	13,62	12,63	14,37	12,46	12,90	12,93	18,97	9,64	13,25	12,56	14,65	13,89
Fe2O3(T)	6,68	4,91	4,03	1,00	0,64	5,63	2,25	4,40	4,20	5,81	10,88	9,61	10,70
FeO	5,66	3,91	3,19	0,66	0,38	4,47	1,83	3,40	3,35	4,65	8,96	7,69	8,68
Fe2O3	0,46	0,61	0,53	0,27	0,22	0,71	0,24	0,66	0,51	0,70	1,02	1,15	1,15
MgO	2,50	3,29	3,62	0,72	0,35	2,99	0,69	1,54	4,87	2,35	0,76	0,54	0,86
MnO	0,08	0,09	0,11	0,02	0,01	0,07	0,04	0,11	0,14	0,16	0,14	0,12	0,19
CaO	3,84	5,35	5,11	0,71	0,24	3,75	1,99	10,73	11,98	9,21	3,72	2,19	4,16
Na2O	0,44	1,35	0,45	1,38	1,66	5,76	1,77	0,54	0,47	0,30	2,92	1,78	2,99
K2O	2,55	2,69	3,92	5,31	4,76	0,16	5,41	2,35	2,59	2,28	1,38	6,80	2,24
TiO2	0,309	0,456	0,375	0,122	0,072	0,558	0,092	0,510	0,363	0,545	0,874	0,998	0,999
P2O5	0,05	0,14	0,08	0,02	0,01	0,14	0,01	0,09	0,09	0,11	0,43	0,46	0,51
Cr2O3	0,01	0,01	0,01	< 0.01	0,01	0,01	< 0.01	< 0.01	0,01	0,01	0,01	< 0.01	< 0.01
LOI	2,21	1,34	2,08	1,10	0,68	0,54	0,54	2,94	1,71	2,22	0,51	0,40	1,14
Total	100,00	99,96	98,64	98,94	100,70	99,95	98,48	100,30	100,50	99,48	99,74	100,30	98,64
Ti[1] (ppm)	1852	2734	2248	731	432	3345	552	3058	2176	3267	5240	5983	5989
Sr	115	236	248	44	33	176	164	347	397	151	144	262	211
Ba	230	385	770	501	503	74	743	304	452	230	337	1256	607
Nb	8,0	11,5	6,6	23,4	10,1	6,3	7,0	17,7	7,7	8,8	7,8	9,5	8,7
V	47	91	64	15	8	144	11	58	67	101	14	13	15
Co	8	9	7	2	1	13	3	5	8	12	9	7	12
Ga	21	18	17	26	20	18	21	23	14	19	19	22	22
Ge	1,7	2,3	1,9	1,2	1,2	0,8	2,6	1,8	1,5	1,4	2,1	1,8	2,2
In	0,1	< 0.1	< 0.1	0,5	0,2	< 0.1	< 0.1	0,1	< 0.1	< 0.1	0,2	0,1	0,2
Sn	3,0	3,0	2,0	10,0	6,0	4,0	3,0	4,0	2,0	2,0	4,0	3,0	4,0
Cs	6,9	6,9	9,3	5,7	3,5	0,1	3,3	2,4	5,1	3,3	2,0	3,7	1,6
Pb	< 3	8	8	7	6	622	20	12	15	11	17	16	73
Be	2	3	2	2	1	1	2	4	1	2	2	2	2
Hf	5,2	4,7	4,0	9,8	5,5	3,5	4,0	9,0	3,3	5,0	8,1	9,6	8,4
Ta	0,61	0,55	0,42	2,66	0,86	0,45	0,61	0,81	0,41	0,57	0,59	0,60	0,62
W	< 0.5	< 0.5	< 0.5	< 0.5	< 0.5	< 0.5	< 0.5	< 0.5	0,8	1,4	0,6	1,1	1,1
Tl	0,72	0,48	0,84	0,56	0,42	0,07	0,59	0,35	0,41	0,25	0,34	0,94	0,33
Bi	0,5	0,2	0,2	< 0.1	< 0.1	0,1	0,1	0,3	0,1	0,2	0,1	0,1	0,2
Th	5,01	6,80	4,89	14,20	7,38	3,96	5,29	7,58	4,18	5,36	3,09	3,07	2,95
U	1,92	2,23	2,54	6,06	2,11	2,65	1,32	4,97	3,09	2,19	0,97	1,31	1,05
Rb	118	110	155	105	79	2	100	78	86	70	36	160	57
Y	59,9	69,8	43,0	103,0	36,0	42,9	44,5	83,6	40,1	42,8	52,6	53,2	63,6
Zr	160	156	118	226	117	124	93	311	99	191	307	381	358
La	24,5	26,2	16,2	16,0	14,8	16,8	7,2	16,5	12,3	27,7	28,3	26,7	26,9
Ce	52,5	58,2	36,8	41,9	41,6	41,3	18,9	38,2	30,2	61,3	61,4	60,4	60,2
Pr	6,83	7,35	4,81	6,15	5,96	5,16	3,03	5,57	4,04	7,97	8,14	7,76	7,96
Nd	28,4	29,5	20,0	30,0	28,8	21,7	14,6	28,4	17,4	32,4	37,4	34,7	35,8
Sm	7,31	7,33	5,18	10,70	8,91	5,66	5,13	12,10	5,06	7,25	9,36	9,22	9,18
Eu	1,20	1,28	0,90	0,90	0,76	1,19	1,11	2,37	1,02	1,44	2,65	2,46	2,70
Gd	8,29	7,72	5,84	14,30	7,29	6,23	5,71	13,40	5,87	6,74	10,50	9,88	10,20
Tb	1,44	1,51	1,09	2,81	1,24	1,06	1,14	2,23	1,04	1,23	1,83	1,67	1,84
Dy	9,49	10,90	7,06	20,00	7,36	6,76	7,54	14,00	6,68	7,48	10,80	11,10	11,50
Ho	1,99	2,41	1,50	4,27	1,39	1,42	1,65	2,84	1,37	1,59	2,22	2,16	2,34

Er	5,92	7,16	4,54	13,10	4,19	4,06	4,91	8,24	4,06	4,79	6,30	6,52	6,63
Tm	0,864	1,060	0,683	2,080	0,683	0,672	0,796	1,210	0,632	0,731	0,906	0,950	1,020
Yb	5,74	7,05	4,51	14,00	4,85	4,40	5,33	8,08	4,24	4,93	6,00	6,14	6,28
Lu	0,920	1,110	0,703	2,120	0,734	0,646	0,766	1,270	0,643	0,839	0,980	0,965	1,050
Cd	< 0.5	< 0.5	< 0.5	< 0.5	< 0.5	4,2	< 0.5	< 0.5	< 0.5	< 0.5	< 0.5	< 0.5	< 0.5
Cu	1320	14	31	4	2	38	3	23	15	39	2	< 1	2
Ag	0,4	< 0.3	< 0.3	0,5	0,3	1,1	< 0.3	< 0.3	< 0.3	1,1	< 0.3	0,4	< 0.3
Ni	8	13	11	4	3	15	5	8	12	16	3	3	3
Mo	2	< 2	< 2	1	3	< 1	< 1	4	3	9	< 1	2	< 1
Zn	105	101	77	46	15	1620	100	48	80	79	112	90	135
S	8600	< 100	1600	< 100	100	5800	100	1700	1300	6000	< 100	< 100	< 100
Au	< 2	< 2	3	< 2	< 2	< 2	2	< 2	< 2	< 2	< 2	< 2	< 2
As	1,5	1,1	4,4	5,8	3,8	< 0.5	3,0	33,0	41,5	24,9	< 0.5	< 0.5	2,4
Sc	6,4	10,9	11,6	2,4	1,9	11,4	1,8	12,6	8,3	13,9	15,2	17,1	19,8
Sb	0,7	0,2	0,4	0,3	0,5	< 0.1	0,8	0,7	0,7	0,8	0,4	< 0.1	< 0.1
Eu/Eu*[2]	0,47	0,52	0,50	0,22	0,29	0,61	0,63	0,57	0,57	0,63	0,82	0,79	0,85
log(Th/Yb)	-0,06	-0,02	0,04	0,01	0,18	-0,05	0,00	-0,03	-0,01	0,04	-0,29	-0,30	-0,33
log(Zr/Y)	0,43	0,35	0,44	0,34	0,51	0,46	0,32	0,57	0,39	0,65	0,77	0,86	0,75
La/Ybcn[3]	2,90	2,52	2,44	0,78	2,07	2,59	0,92	1,39	1,97	3,82	3,20	2,95	2,91
Zr/TiO2	517,80	342,11	314,67	1852,46	1625,00	222,22	1010,87	609,80	272,73	350,46	351,26	381,76	358,36
Al2O3/TiO2	43,95	29,87	33,68	117,79	173,06	23,12	140,54	37,20	26,56	24,31	14,37	14,68	13,90
Tzr (cels)[4]	796	823	800	808	755		768	899	823		885	902	904
AI[5]	54	47	58	74	73	25	62	26	37	33	24	65	30
CCPI[6]	75	67	64	20	13	59	29	67	75	76	73	54	69
AAAI[7]	50	40	42	73	78	35	62	31	27	35	47	58	43

Table 4.1 (cont.)

Analyse	54716	54743	54791	68410	68406	68404	54347	54348	54790	54697	54346
Sample	161B	162B	163F	17PA13	17PA15	17PA9	45A	46A	97A	97B	13PA44
Group	I1	I1	I1	I1	I1	I1	I1	I1	I1	I1	I1
least altered					*					*	*
SiO2 (wt.%)	64,54	64,73	65,68	63,53	60,05	76,58	59,97	59,86	58,45	59,60	61,63
Al2O3	16,66	14,14	12,59	16,82	15,55	12,14	15,83	17,69	18,46	15,93	16,16
Fe2O3(T)	6,88	9,18	8,49	7,34	12,06	1,45	9,64	7,86	12,14	10,61	10,36
FeO	5,48	7,24	6,85	5,86	10,20	1,10	8,05	6,13	10,23	8,89	8,71
Fe2O3	0,85	1,21	0,95	0,89	0,84	0,25	0,79	1,12	0,89	0,83	0,78
MgO	1,08	1,33	0,67	0,69	0,93	0,70	0,97	2,26	0,74	0,78	0,88
MnO	0,09	0,14	0,07	0,05	0,21	0,02	0,25	0,09	0,07	0,17	0,10
CaO	2,57	2,88	4,87	1,92	3,79	0,67	4,70	1,75	1,29	5,10	3,13
Na2O	2,05	5,10	1,93	7,48	4,92	1,45	3,23	7,75	0,54	3,24	4,50
K2O	4,06	0,21	1,31	0,08	1,44	5,70	2,72	1,05	4,70	1,31	2,03
TiO2	0,699	1,063	0,803	0,744	0,688	0,095	0,639	0,969	0,739	0,678	0,629
P2O5	0,12	0,38	0,26	0,27	0,39	0,04	0,39	0,45	0,30	0,40	0,38
Cr2O3	0,01	0,01	0,01	< 0.01	< 0.01	< 0.01	< 0.01	< 0.01	< 0.01	< 0.01	< 0.01
LOI	1,82	0,43	3,30	0,61	0,60	0,88	0,91	0,91	2,94	0,66	0,90
Total	100,60	99,60	99,97	99,54	100,60	99,72	99,24	100,60	100,40	98,87	100,70
Ti[1] (ppm)	4191	6373	4814	4460	4125	570	3831	5809	4430	4065	3771
Sr	141	177	242	361	301	66	198	211	119	190	260
Ba	1078	52	369	58	377	726	524	456	650	281	747
Nb	14,6	9,1	9,2	9,6	19,8	7,9	12,3	9,9	14,2	10,1	11,6
V	52	51	12	33	13	26	10	46	20	15	8
Co	6	13	9	8	12	1	11	17	8	8	10
Ga	27	24	18	14	27	22	27	27	33	29	25
Ge	2,2	2,3	0,9	1,5	1,6	1,4	1,8	1,8	2,7	3,8	1,6
In	0,2	0,2	< 0.1	< 0.1	0,1	< 0.1	< 0.1	< 0.1	0,3	< 0.1	< 0.1
Sn	4,0	3,0	1,0	2,0	2,0	3,0	3,0	2,0	4,0	2,0	3,0
Cs	3,0	0,5	1,6	0,3	2,1	3,6	2,8	3,0	6,3	2,0	1,8
Pb	26	43	17	5	6	20	7	6	5	7	5
Be	3	2	2	< 1	2	2	2	2	2	2	2
Hf	13,5	7,9	5,7	6,5	8,8	4,1	8,5	6,3	7,9	7,3	8,3
Ta	1,11	0,70	0,61	0,62	0,69	0,62	0,65	0,58	0,88	0,59	0,74
W	1,1	0,6	0,7	< 0.5	1,8	< 0.5	1,5	3,1	15,3	1,4	1,2
Tl	0,58	0,08	0,29	< 0.05	0,22	0,52	0,33	0,21	0,47	0,22	0,32
Bi	< 0.1	< 0.1	< 0.1	< 0.1	0,2	< 0.1	< 0.1	< 0.1	< 0.1	< 0.1	< 0.1
Th	8,37	4,25	2,13	2,53	2,32	6,14	2,57	2,34	2,51	2,17	2,52
U	2,58	1,86	0,63	0,87	1,06	3,29	1,63	1,22	1,12	1,08	1,08
Rb	93	5	43	2	38	124	66	34	133	45	59
Y	77,2	53,3	59,2	28,3	93,1	101,0	73,4	50,5	104,0	79,7	32,5
Zr	519	340	239	254	321	96	330	244	309	298	324
La	42,9	25,9	24,7	9,9	23,3	3,8	22,7	25,7	26,1	22,6	6,7
Ce	92,6	56,4	54,6	27,9	57,2	10,0	59,3	58,0	63,3	54,4	19,5
Pr	12,00	7,24	6,89	3,99	8,36	1,48	8,11	7,20	8,88	8,12	2,93
Nd	50,9	31,6	31,4	17,8	39,8	7,5	38,4	31,5	41,7	39,4	14,1
Sm	12,50	8,90	8,80	5,01	11,50	3,38	10,90	8,26	11,70	11,50	4,21
Eu	5,68	2,41	2,70	1,38	3,27	0,74	2,95	2,11	3,06	3,34	1,22
Gd	13,40	9,05	10,20	5,22	13,80	8,41	11,60	8,82	13,00	12,40	5,20
Tb	2,50	1,56	1,64	0,81	2,44	2,02	2,27	1,67	2,40	2,26	0,99
Dy	15,90	10,20	10,10	4,96	15,90	14,80	14,70	10,50	16,00	13,90	6,41
Ho	3,29	1,96	1,97	0,99	3,23	3,22	3,07	2,13	3,38	2,80	1,37

Er	9,48	5,85	5,13	2,95	9,64	9,27	8,95	6,23	10,30	8,09	4,21
Tm	1,450	0,910	0,712	0,447	1,410	1,340	1,350	0,936	1,570	1,280	0,662
Yb	9,60	5,90	4,06	3,06	9,59	8,40	9,08	6,20	10,40	8,34	4,60
Lu	1,550	0,915	0,533	0,487	1,480	1,280	1,480	0,987	1,590	1,220	0,798
Cd	< 0.5	< 0.5	0,8	< 0.5	< 0.5	< 0.5	< 0.5	< 0.5	< 0.5	< 0.5	< 0.5
Cu	< 1	2	54	3	7	6	6	1	87	159	7
Ag	0,6	0,5	1,4	0,5	0,6	< 0.3	2,7	1,9	< 0.3	< 0.3	2,7
Ni	6	9	5	6	2	3	4	5	4	10	3
Mo	< 1	< 1	5	< 2	< 2	< 2	4	< 1	1	< 1	2
Zn	88	83	82	48	156	87	182	197	94	144	103
S	< 100	< 100	43000	< 100	< 100	< 100	400	200	300	200	500
Au	11	< 2	270	< 2	< 2	< 2	< 2	< 2	< 2	< 2	< 2
As	< 0.5	< 0.5	376,0	1,5	7,0	2,5	< 0.5	< 0.5	1,6	2,9	< 0.5
Sc	10,9	17,9	13,9	6,9	12,0	2,0	11,0	13,4	17,7	11,2	8,3
Sb	< 0.1	< 0.1	1,4	0,6	0,2	0,2	0,9	1,0	1,2	1,1	< 0.1
Eu/Eu*[2]	1,34	0,82	0,87	0,82	0,79	0,42	0,80	0,76	0,76	0,85	0,80
log(Th/Yb)	-0,06	-0,14	-0,28	-0,08	-0,62	-0,14	-0,55	-0,42	-0,62	-0,58	-0,26
log(Zr/Y)	0,83	0,80	0,61	0,95	0,54	-0,02	0,65	0,68	0,47	0,57	1,00
La/Ybcn[3]	3,04	2,98	4,13	2,20	1,65	0,31	1,70	2,82	1,70	1,84	0,99
Zr/TiO2	742,49	319,85	297,63	341,40	466,57	1010,53	516,43	251,81	418,13	439,53	515,10
Al2O3/TiO2	23,83	13,30	15,68	22,61	22,60	127,79	24,77	18,26	24,98	23,50	25,69
Tzr (cels)[4]	907	891		858	892	756	895		785	879	
AI[5]	53	16	23	8	21	75	32	26	75	20	28
CCPI[6]	57	66	74	52	67	23	64	53	71	71	63
AAAI[7]	53	41	47	39	38	73	40	34	69	40	42

Table 4.1 (cont.)

Analyse	23	24	21	22	14	15	16	17	18	19	20
Sample	bt gneiss	bt schist	bt-sill	bt-sill	pl-qtz(hbl	pl-qtz(hbl)	pl-qtz(hbl)	pl-qtz(hbl)	pl-qtz(hbl)	pl-qtz(hbl)	pl-qtz(hbl)
Group	I1	I1	I1	I1	I1	I1	I1	I1	I1	I1	I1
least altered											
SiO2 (wt.%)	63,50	51,30	62,40	65,10	65,40	53,30	53,80	53,10	56,30	56,30	58,70
Al2O3	14,70	17,80	17,30	16,40	12,70	16,90	16,70	17,00	16,40	16,50	16,10
Fe2O3(T)	6,67	11,10	6,64	7,29	10,90	10,70	13,60	10,40	9,85	10,30	10,80
MgO	2,88	4,84	1,49	0,67	0,65	3,30	2,20	3,65	2,37	3,15	2,68
MnO	0,11	0,12	0,05	0,03	0,07	0,18	0,14	0,17	0,11	1,12	0,13
CaO	1,98	2,49	1,10	1,60	2,69	5,61	3,21	3,96	5,42	3,30	3,11
Na2O	3,64	6,38	8,17	7,83	5,02	5,56	7,11	6,76	6,56	7,46	7,61
K2O	2,85	0,41	0,28	0,00	0,34	0,45	0,06	0,31	0,15	0,33	0,04
TiO2	0,800	1,620	0,740	0,560	1,070	1,210	1,090	1,270	1,250	1,290	1,280
P2O5	0,10	0,37	0,25	0,29	0,21	0,17	0,28	0,26	0,22	0,26	0,28
LOI	0,96	2,60	1,12	0,57	0,89	1,21	0,64	0,81	0,64	0,59	0,71
Ti[1] (ppm)	4796	9712	4436	3357	6415	7254	6535	7614	7494	7734	7674
Sr	136	142	102	86	171	223	299	300	658	217	151
Ba	922	73	63	25	140	262	495	290	702	88	55
V	66	154	33	45	115	164	137	141	137	109	99
Co	20	39	8	5	12	36	28	35	32	29	24
Pb	< 3	< 3	17	21	< 3	< 3	< 3	< 3	< 3	< 3	< 3
Be	3	3	2	4	2	2	2	2	2	2	3
Y	23,0	28,0	17,0	20,0	53,0	28,0	48,0	40,0	24,0	40,0	35,0
Cd	30,0	26,0	25,0	24,0	28,0	27,0	28,0	29,0	29,0	29,0	30,0
Cu	23	17	14	26	12	11	12300	5100	24	24	16
Ag	< 0.3	< 0.3	< 0.3	< 0.3	< 0.3	< 0.3	29,0	11,0	< 0.3	< 0.3	< 0.3
Ni	35	121	39	58	38	84	81	96	100	76	78
Mo	< 1	< 1	< 1	15	< 1	< 1	< 1	< 1	< 1	< 1	< 1
Zn	121	153	98	56	65	143	100	131	129	118	111
S	< 100	< 100	< 100	< 100	< 100	< 100	0,19	0,05	< 100	< 100	< 100
Sc	15,0	23,0	8,0	8,0	26,0	34,0	26,0	25,0	21,0	21,0	19,0
Al2O3/TiO2	18,38	10,99	23,38	29,29	11,87	13,97	15,32	13,39	13,12	12,79	12,58
AI[5]	50	37	16	7	11	25	18	27	17	24	20
CCPI[6]	60	70	49	50	68	70	69	67	65	63	64
AAAI[7]	43	27	37	39	44	27	30	27	28	29	30

Table 4.1 (cont.)

Analyse	54792	54793	54794	54795	54796	54797	54694	54695	53080	53086	53087	53088	54696
Sample	168A	169C1	169C2	169C3	197B1	197B2	14PA81-12	14PA81-13	14PA81-2	14PA81-4	14PA81-6	14PA81-7/1	14PA81-7/2
Group	skarn	skarn	skarn	skarn	skarn	skarn	M1	M1	M1	M1	M1	M1	M1
least altered										*	*		
SiO2 (wt.%)	66,49	62,74	57,62	61,06	57,76	63,53	54,53	55,81	61,81	46,18	45,82	49,54	48,85
Al2O3	9,64	9,51	7,57	6,87	8,62	6,77	14,69	14,29	15,38	15,46	14,44	18,92	20,04
Fe2O3(T)	4,28	5,18	5,49	5,70	3,65	3,55	8,89	10,18	6,55	17,89	16,20	8,96	8,61
FeO	3,37	4,16	4,51	4,70	2,91	2,92	7,31	8,23	5,22	13,82	12,27	7,14	6,87
Fe2O3	0,57	0,60	0,53	0,53	0,45	0,34	0,85	1,12	0,81	2,69	2,70	1,11	1,05
MgO	3,04	6,32	8,60	7,98	8,12	7,92	0,48	0,33	2,56	5,52	5,59	6,28	5,77
MnO	0,17	0,17	0,22	0,20	0,22	0,22	0,13	0,14	0,11	0,26	0,21	0,11	0,16
CaO	12,80	10,66	15,70	14,23	15,13	15,28	16,20	16,79	5,16	8,84	8,51	3,28	5,60
Na2O	0,99	0,45	0,95	0,35	0,43	0,34	0,24	0,05	4,61	2,70	3,16	5,19	4,98
K2O	0,40	3,25	2,29	2,19	2,79	1,05	0,06	0,01	0,79	0,12	0,10	2,32	1,81
TiO2	0,418	0,452	0,381	0,376	0,296	0,189	0,700	0,973	0,657	2,542	2,548	0,960	0,904
P2O5	0,10	0,10	0,12	0,10	0,06	0,05	0,18	0,31	0,20	0,32	0,32	0,19	0,23
Cr2O3	0,01	0,01	0,01	0,01	0,01	0,01	0,02	0,01	0,01	0,01	0,01	0,02	0,02
LOI	1,71	1,32	1,02	0,89	1,77	1,90	1,90	1,48	0,86	0,41	0,52	1,81	2,19
Total	100,00	100,10	99,94	99,94	98,84	100,80	98,16	100,70	99,31	100,20	98,07	98,08	100,50
Ti[1] (ppm)	2506	2710	2284	2254	1775	1133	4197	5833	3939	15240	15276	5755	5420
Sr	264	261	240	218	299	223	678	1000	574	278	264	215	252
Ba	162	667	608	508	829	321	13	14	305	42	46	261	230
Nb	6,5	4,8	3,8	3,8	8,1	6,1	1,9	4,2	6,1	3,4	4,0	2,8	3,0
V	344	320	271	290	119	160	168	163	95	407	417	157	160
Co	11	12	9	12	6	4	3	2	16	59	56	35	33
Ga	14	11	9	9	13	11	22	29	19	24	24	19	22
Ge	3,1	1,1	1,2	1,2	1,4	1,2	3,4	5,9	2,6	2,0	2,6	2,0	2,6
In	0,1	< 0.1	< 0.1	< 0.1	< 0.1	< 0.1	< 0.1	< 0.1	< 0.1	< 0.1	< 0.1	< 0.1	< 0.1
Sn	6,0	2,0	2,0	1,0	2,0	2,0	< 1	< 1	2,0	1,0	1,0	< 1	< 1
Cs	5,9	12,0	5,5	5,2	4,1	1,6	< 0.1	< 0.1	0,8	< 0.1	< 0.1	3,0	2,2
Pb	18	156	113	21	23	11	10	14	28	12	7	4	4
Be	24	2	5	2	2	2	< 1	< 1	2	1	1	1	1
Hf	2,9	2,5	2,3	1,9	3,9	2,9	1,3	2,2	2,9	3,9	3,8	1,9	1,7
Ta	0,44	0,36	0,33	0,31	0,64	0,53	0,04	0,19	0,45	0,34	0,20	0,13	0,10
W	11,1	7,6	< 0.5	< 0.5	2,8	< 0.5	0,6	0,6	0,9	0,8	0,8	< 0.5	< 0.5
Tl	0,16	0,95	0,86	0,55	0,57	0,15	< 0.05	< 0.05	0,12	< 0.05	< 0.05	0,27	0,26
Bi	1,4	0,2	0,3	0,2	0,2	< 0.1	< 0.1	< 0.1	0,1	< 0.1	< 0.1	< 0.1	< 0.1
Th	4,13	3,40	2,65	2,64	4,57	3,22	0,61	1,00	3,84	0,98	0,86	0,98	0,72
U	7,86	7,62	4,62	5,66	6,57	4,94	0,56	1,01	1,23	0,35	0,37	0,43	0,43
Rb	19	129	107	75	105	42	2	< 1	17	2	1	51	40
Y	32,5	25,7	21,7	23,4	44,9	31,7	17,3	21,4	17,9	39,8	39,2	17,4	20,4
Zr	102	98	81	72	119	82	54	89	105	156	153	75	70
La	18,8	15,7	20,0	14,0	14,1	9,6	7,3	14,7	21,0	11,3	8,8	9,6	9,7
Ce	40,7	35,9	37,2	31,3	33,4	21,8	15,9	31,5	41,3	26,7	23,1	20,6	21,3
Pr	4,91	4,36	4,38	4,11	4,43	2,86	2,14	4,20	5,36	4,28	3,71	2,84	3,05
Nd	20,8	18,5	19,1	17,5	19,5	13,2	9,6	17,7	21,1	20,7	18,7	12,4	13,6
Sm	5,19	4,54	4,19	4,20	5,89	4,19	2,52	3,87	4,44	6,00	5,64	2,98	3,38
Eu	1,02	1,01	0,99	1,01	0,90	0,67	1,09	1,25	1,20	2,08	1,99	1,01	1,48
Gd	5,49	4,67	4,54	4,40	6,91	5,15	2,62	3,69	3,62	6,74	6,41	3,10	3,20
Tb	0,94	0,76	0,68	0,69	1,19	0,91	0,46	0,63	0,57	1,20	1,16	0,53	0,58
Dy	5,89	4,75	4,36	4,18	7,68	5,81	2,79	3,73	3,25	7,32	7,04	3,17	3,43
Ho	1,11	0,95	0,81	0,80	1,55	1,16	0,58	0,74	0,64	1,45	1,36	0,62	0,67

Er	3,24	2,62	2,38	2,26	4,55	3,46	1,76	2,16	1,79	4,21	3,94	1,82	1,99
Tm	0,512	0,399	0,358	0,330	0,712	0,541	0,269	0,330	0,265	0,639	0,634	0,269	0,318
Yb	3,29	2,66	2,37	2,11	4,76	3,50	1,75	2,14	1,74	4,17	4,04	1,74	2,13
Lu	0,489	0,401	0,371	0,325	0,697	0,517	0,255	0,315	0,258	0,605	0,595	0,261	0,325
Cd	0,7	0,9	1,3	1,2	0,7	0,7	< 0.5	< 0.5	< 0.5	< 0.5	< 0.5	< 0.5	< 0.5
Cu	34	40	8	15	16	2	2230	356	7	176	120	10	5540
Ag	< 0.3	0,4	< 0.3	< 0.3	< 0.3	< 0.3	1,1	< 0.3	< 0.3	< 0.3	< 0.3	< 0.3	0,9
Ni	17	17	13	16	9	7	17	16	27	83	76	99	99
Mo	50	65	13	20	4	4	< 1	< 1	< 1	< 1	< 1	< 1	< 1
Zn	86	286	249	85	118	108	11	14	87	122	110	115	107
S	1700	600	200	300	100	< 100	1900	300	100	< 100	< 100	< 100	1800
Au	< 2	< 2	< 2	< 2	< 2	< 2	43	8	< 2	< 2	< 2	< 2	< 2
As	24,0	34,2	20,4	55,2	8,4	8,6	3,8	19,4	8,3	2,0	2,1	1,3	< 0.5
Sc	10,4	10,8	9,4	8,9	7,5	4,4	14,3	13,6	10,8	34,1	34,7	18,5	17,5
Sb	1,3	0,7	0,5	0,6	0,6	0,4	1,7	5,0	2,3	0,3	0,6	< 0.1	0,9
Eu/Eu*[2]	0,58	0,67	0,69	0,72	0,43	0,44	1,30	1,01	0,91	1,00	1,01	1,02	1,38
log(Th/Yb)	0,10	0,11	0,05	0,10	-0,02	-0,04	-0,46	-0,33	0,34	-0,63	-0,67	-0,25	-0,47
log(Zr/Y)	0,50	0,58	0,57	0,49	0,42	0,41	0,49	0,62	0,77	0,59	0,59	0,63	0,54
La/Ybcn[3]	3,88	4,01	5,73	4,51	2,01	1,87	2,84	4,67	8,20	1,84	1,47	3,75	3,08
Zr/TiO2	244,02	216,81	212,60	191,49	402,03	433,86	77,14	91,47	159,82	61,37	60,05	78,13	77,43
Al2O3/TiO2	23,06	21,04	19,87	18,27	29,12	35,82	20,99	14,69	23,41	6,08	5,67	19,71	22,17
AI[5]	20	46	40	41	41	36	3	2	26	33	33	50	42
CCPI[6]	84	76	81	84	79	89	97	99	63	89	87	67	68
AAAI[7]	28	26	19	21	20	21	24	25	33	21	21	25	23

Table 4.1 (cont.)

Analyse	53071	54692	54376	53083	54758	54759	54760	54681	54369	54366	54367	54370	54687
Sample	14PA81-8	13PA22A1	13PA22	78	154B	154C	156A	20A1	55B	55C	55D	58B	7A
Group	M1	M1	M1	M2	M2	M2	M2	M2	M2	M2	M2	M2	M2
least altered						*	*		*	*	*		
SiO2 (wt.%)	51,66	52,14	50,78	52,94	49,23	47,99	48,89	51,87	49,26	47,63	46,83	57,16	46,31
Al2O3	15,79	13,92	15,07	13,36	15,24	15,26	15,24	16,32	16,20	17,20	16,94	11,89	16,88
Fe2O3(T)	10,38	13,58	13,14	10,55	10,36	12,60	12,06	11,90	11,36	12,19	12,70	9,24	14,55
FeO	8,43	10,20	9,62	8,82	8,49	10,18	9,64	9,56	9,09	9,95	10,47	7,87	11,85
Fe2O3	1,11	2,36	2,55	0,85	1,02	1,40	1,46	1,38	1,37	1,24	1,19	0,58	1,52
MgO	0,81	3,42	4,70	6,83	8,12	8,57	8,47	3,83	8,09	7,55	6,90	6,68	4,89
MnO	0,22	0,17	0,22	0,18	0,18	0,21	0,20	0,27	0,20	0,20	0,21	0,22	0,25
CaO	15,73	7,63	7,37	10,35	10,23	10,26	9,15	8,49	8,68	9,61	9,01	7,96	10,12
Na2O	1,36	2,01	2,80	2,27	3,16	2,43	3,30	0,98	3,26	2,71	3,34	2,29	1,51
K2O	0,87	2,29	1,59	0,46	0,64	0,61	0,37	3,41	0,30	0,14	0,23	0,30	1,65
TiO2	0,960	2,210	2,404	0,701	0,874	1,252	1,310	1,230	1,216	1,094	1,037	0,431	1,365
P2O5	0,23	0,46	0,54	0,04	0,14	0,14	0,14	0,14	0,16	0,12	0,11	0,20	0,15
Cr2O3	0,02	< 0.01	< 0.01	0,08	0,05	0,06	0,07	< 0.01	0,04	< 0.01	< 0.01	< 0.01	< 0.01
LOI	1,80	1,44	0,69	1,12	1,78	1,17	0,77	1,97	0,87	0,68	0,77	1,73	1,23
Total	100,60	99,27	99,29	99,35	99,97	100,50	99,89	100,40	99,61	99,12	98,08	98,11	98,90
Ti[1] (ppm)	5755	13249	14412	4203	5240	7506	7854	7374	7290	6559	6217	2584	8183
Sr	1165	110	115	122	296	351	391	211	306	222	188	121	168
Ba	216	432	235	103	85	197	265	1110	60	31	28	107	202
Nb	3,6	7,8	7,7	< 0.2	2,7	2,6	2,8	2,5	1,9	1,2	1,0	0,8	3,3
V	193	215	221	234	248	252	258	249	245	255	242	124	268
Co	6	30	32	39	41	47	47	46	45	52	51	46	59
Ga	25	21	23	14	16	19	18	18	18	19	18	21	20
Ge	5,6	1,9	2,0	1,4	1,6	1,8	1,4	1,3	2,0	1,8	1,8	1,9	1,7
In	< 0.1	< 0.1	< 0.1	< 0.1	< 0.1	< 0.1	< 0.1	< 0.1	< 0.1	< 0.1	< 0.1	< 0.1	< 0.1
Sn	1,0	2,0	2,0	< 1	< 1	< 1	< 1	< 1	< 1	< 1	< 1	< 1	< 1
Cs	< 0.1	1,3	0,9	1,4	1,0	1,5	0,3	0,8	0,2	0,1	< 0.1	0,4	1,4
Pb	24	8	6	8	< 3	< 3	< 3	5	5	4	< 3	< 3	4
Be	< 1	2	1	< 1	< 1	1	< 1	< 1	< 1	< 1	< 1	1	< 1
Hf	2,4	4,3	5,1	1,2	1,5	1,9	2,1	2,7	2,3	2,0	2,1	0,9	2,4
Ta	0,16	0,50	0,57	< 0.01	0,15	0,13	0,16	0,18	0,08	0,05	0,05	< 0.01	0,14
W	0,5	1,5	0,8	1,2	< 0.5	< 0.5	1,7	0,6	< 0.5	< 0.5	< 0.5	< 0.5	< 0.5
Tl	0,13	0,37	0,25	0,10	0,12	0,11	< 0.05	0,39	< 0.05	0,07	< 0.05	< 0.05	0,25
Bi	< 0.1	0,2	0,3	0,4	< 0.1	< 0.1	< 0.1	< 0.1	< 0.1	< 0.1	< 0.1	0,5	0,2
Th	1,18	5,66	6,38	0,27	0,67	0,57	0,57	0,61	0,74	0,50	0,43	0,55	0,56
U	0,78	2,33	2,57	0,18	0,36	0,28	0,32	0,41	0,33	0,24	0,23	0,31	0,37
Rb	14	77	47	12	24	23	9	117	8	2	4	8	56
Y	27,2	43,1	45,9	11,7	22,1	29,4	30,1	29,0	25,5	26,3	25,1	17,7	36,0
Zr	92	172	192	44	57	71	79	94	88	76	73	34	95
La	12,1	23,9	20,1	1,7	6,8	5,5	5,7	5,6	5,8	4,5	4,2	5,0	6,1
Ce	24,9	52,8	50,3	4,3	15,6	13,6	14,3	13,4	14,7	11,8	10,7	12,5	15,1
Pr	3,52	6,96	6,26	0,66	2,05	1,93	1,94	2,06	2,12	1,76	1,63	1,69	2,37
Nd	15,2	29,5	27,6	3,5	9,9	9,9	10,4	10,1	10,6	9,1	8,4	8,1	11,5
Sm	4,15	7,39	7,26	1,23	2,78	3,27	3,28	3,27	3,21	3,04	3,02	2,48	3,82
Eu	1,45	2,14	1,99	0,47	0,96	1,17	1,11	1,00	1,13	1,20	1,10	1,19	1,48
Gd	4,33	7,83	7,64	1,44	3,31	4,36	4,40	4,20	3,98	4,12	3,89	2,75	5,12
Tb	0,77	1,38	1,43	0,29	0,55	0,70	0,75	0,75	0,79	0,79	0,79	0,51	1,00
Dy	4,70	8,06	8,68	2,01	3,41	4,53	4,75	5,03	4,89	5,21	4,88	3,16	5,94
Ho	0,94	1,62	1,75	0,43	0,69	0,90	1,02	1,11	1,02	1,07	1,01	0,62	1,26

Er	2,74	4,66	5,13	1,32	2,01	2,68	2,90	3,32	2,97	3,13	2,99	1,74	3,83
Tm	0,420	0,689	0,784	0,211	0,308	0,393	0,448	0,499	0,444	0,456	0,441	0,257	0,568
Yb	2,88	4,58	4,99	1,47	2,04	2,57	2,90	3,34	2,92	3,03	2,94	1,68	3,70
Lu	0,440	0,742	0,770	0,223	0,297	0,383	0,416	0,534	0,451	0,484	0,464	0,269	0,586
Cd	< 0.5	< 0.5	< 0.5	< 0.5	< 0.5	< 0.5	< 0.5	< 0.5	< 0.5	< 0.5	< 0.5	< 0.5	< 0.5
Cu	394	11	396	11	11	125	64	2	38	22	5	1900	2
Ag	< 0.3	0,5	1,5	< 0.3	< 0.3	< 0.3	< 0.3	< 0.5	< 0.5	< 0.5	< 0.5	< 0.5	< 0.5
Ni	10	6	10	197	102	145	161	35	110	70	75	71	33
Mo	< 1	< 1	< 1	< 1	1	< 1	1	< 1	< 1	< 1	< 1	< 1	< 1
Zn	52	138	155	68	88	98	112	86	125	101	93	214	111
S	100	300	500	< 100	< 100	< 100	< 100	300	400	500	400	700	400
Au	60	14	16	< 2	< 2	< 2	< 2	< 2	< 2	< 2	< 2	32	< 2
As	7,1	3,7	< 0.5	< 0.5	< 0.5	< 0.5	< 0.5	< 0.5	< 0.5	< 0.5	< 0.5	4,6	1,1
Sc	17,5	28,8	27,5	27,9	32,4	29,6	31,3	26,2	32,1	30,1	29,6	15,4	26,0
Sb	3,8	0,9	0,5	1,3	1,2	0,5	< 0.1	1,5	0,4	< 0.1	< 0.1	1,4	0,4
Eu/Eu*[2]	1,05	0,86	0,82	1,07	0,97	0,95	0,89	0,82	0,97	1,04	0,98	1,39	1,02
log(Th/Yb)	-0,39	0,09	0,11	-0,74	-0,48	-0,65	-0,71	-0,74	-0,60	-0,78	-0,83	-0,48	-0,82
log(Zr/Y)	0,53	0,60	0,62	0,58	0,41	0,38	0,42	0,51	0,54	0,46	0,46	0,28	0,42
La/Ybcn[3]	2,85	3,54	2,74	0,79	2,25	1,44	1,34	1,15	1,35	1,01	0,97	2,01	1,11
Zr/TiO2	95,83	77,83	79,87	62,77	65,22	56,71	60,31	76,42	72,37	69,47	70,40	78,89	69,60
Al2O3/TiO2	16,45	6,30	6,27	19,06	17,44	12,19	11,63	13,27	13,32	15,72	16,34	27,59	12,37
AI[5]	9	37	38	37	40	42	42	43	41	38	37	41	36
CCPI[6]	83	80	80	86	83	87	85	78	85	87	85	86	86
AAAI[7]	22	29	25	21	19	18	19	28	20	19	20	25	22

Table 4.1 (cont.)

Analyse	53090	54689	54362	54363	54359	54761	54764	54765	68411	68403	54744	54356	54683
Sample	91A	9A	40	43	10F	157A	162C	165A	17PA2B	17PA5	171C	55E	8A
Group	M2	M2	M3	M3	M3	M3	M3	M3	M3	M3	M3	M3	M3
least altered						*							
SiO2 (wt.%)	53,58	46,32	58,15	57,06	58,12	49,53	51,34	53,43	61,88	52,57	74,21	60,57	57,56
Al2O3	14,57	14,86	13,60	16,12	12,51	16,65	19,27	14,92	8,73	13,98	7,99	15,83	15,88
Fe2O3(T)	9,44	11,72	13,16	12,19	13,01	14,77	10,33	13,58	14,77	11,05	5,52	9,14	11,55
FeO	7,58	9,82	10,20	9,67	9,85	11,57	8,06	10,64	12,14	8,33	4,03	7,06	9,37
Fe2O3	1,10	0,92	1,94	1,55	2,17	2,04	1,47	1,88	1,42	1,89	1,09	1,37	1,24
MgO	8,26	10,79	2,01	2,03	3,51	4,45	3,64	3,53	3,88	1,04	2,57	1,91	1,93
MnO	0,16	0,20	0,29	0,24	0,16	0,25	0,22	0,22	0,18	0,26	0,10	0,14	0,23
CaO	7,37	9,12	5,01	6,57	7,05	7,34	8,60	7,35	6,45	13,60	5,84	5,55	5,72
Na2O	4,39	2,37	3,71	3,72	0,38	3,65	3,67	3,81	0,78	3,70	1,20	4,48	3,56
K2O	0,14	0,15	1,56	0,52	1,91	0,41	0,88	1,02	0,63	0,28	0,57	0,70	0,94
TiO2	0,949	0,765	1,791	1,398	2,022	1,890	1,315	1,730	1,266	1,736	0,939	1,222	1,094
P2O5	0,13	0,07	0,81	0,44	0,36	0,28	0,20	0,28	0,20	0,44	0,19	0,23	0,44
Cr2O3	0,04	0,08	< 0.01	< 0.01	< 0.01	0,01	0,01	0,01	0,01	< 0.01	0,01	< 0.01	< 0.01
LOI	0,92	1,57	0,29	0,35	1,14	1,03	0,77	0,52	0,76	1,64	1,38	0,40	0,62
Total	100,20	97,95	100,40	100,60	100,20	100,30	100,20	100,40	99,53	100,30	100,50	100,20	99,52
Ti[1] (ppm)	5689	4586	10737	8381	12122	11331	7884	10372	7590	10407	5629	7326	6559
Sr	368	192	402	284	114	272	317	379	79	474	140	311	244
Ba	31	23	806	207	171	172	192	336	66	311	124	200	467
Nb	2,8	1,2	7,6	8,2	6,8	6,2	6,1	5,8	10,6	17,7	4,1	7,0	7,9
V	245	250	36	65	230	168	178	377	166	85	119	172	54
Co	36	51	15	20	32	41	36	33	26	28	15	18	18
Ga	18	16	21	23	21	24	21	20	14	14	10	20	23
Ge	2,3	1,9	1,9	2,1	2,1	1,8	1,5	1,6	1,3	1,1	1,6	1,5	1,7
In	< 0.1	< 0.1	< 0.1	< 0.1	< 0.1	< 0.1	< 0.1	< 0.1	< 0.1	< 0.1	0,1	< 0.1	< 0.1
Sn	< 1	< 1	2,0	2,0	2,0	2,0	2,0	1,0	1,0	1,0	3,0	1,0	2,0
Cs	< 0.1	0,3	10,5	0,6	3,0	0,5	1,1	0,6	0,3	0,2	0,6	1,1	1,6
Pb	10	< 3	14	5	7	< 3	12	< 3	< 3	6	38	4	5
Be	< 1	< 1	2	1	2	2	2	1	< 1	< 1	1	2	1
Hf	1,9	1,2	4,9	5,0	4,8	4,4	4,5	3,8	2,7	4,6	3,0	3,7	5,1
Ta	0,14	0,06	0,45	0,46	0,38	0,36	0,36	0,35	0,27	0,46	0,37	0,46	0,51
W	< 0.5	< 0.5	0,7	0,6	1,4	0,6	0,6	< 0.5	1,5	1,5	1,8	0,9	1,0
Tl	0,06	< 0.05	0,37	0,08	0,41	< 0.05	0,11	0,10	< 0.05	< 0.05	0,15	0,20	< 0.05
Bi	< 0.1	0,1	0,2	< 0.1	< 0.1	< 0.1	0,2	< 0.1	< 0.1	0,5	0,2	< 0.1	< 0.1
Th	1,35	0,44	4,49	1,60	2,60	1,11	1,86	2,30	1,49	2,53	1,98	1,47	1,76
U	0,71	0,18	1,61	0,73	1,15	0,51	0,83	0,82	0,96	0,69	2,89	0,89	0,81
Rb	2	4	69	8	60	10	16	21	10	6	15	13	20
Y	16,1	19,9	48,4	60,4	48,3	54,9	52,5	44,4	30,0	34,8	28,6	30,4	56,0
Zr	70	44	180	194	184	183	193	151	106	187	108	141	199
La	8,8	3,1	24,5	14,2	18,9	10,1	15,4	18,3	8,8	20,8	12,8	12,7	15,7
Ce	20,4	7,3	57,9	36,3	43,5	27,9	34,9	41,0	21,8	47,9	27,4	29,9	37,1
Pr	2,96	1,13	7,30	5,05	5,52	4,13	4,44	5,15	3,06	6,57	3,68	3,89	5,53
Nd	12,8	6,0	33,0	26,1	24,6	20,5	20,8	23,2	13,5	28,2	16,5	17,8	26,4
Sm	3,24	2,21	8,35	8,05	7,05	6,52	5,80	5,91	3,91	6,66	4,16	4,69	8,08
Eu	1,01	0,83	3,35	2,50	1,88	2,00	2,05	1,73	1,42	1,72	1,43	1,45	2,42
Gd	2,88	2,84	8,84	9,97	7,90	8,12	7,27	6,80	4,56	6,28	5,11	5,16	9,77
Tb	0,48	0,62	1,61	1,87	1,44	1,34	1,22	1,08	0,81	0,98	0,87	0,97	1,76
Dy	2,90	3,81	9,85	11,90	9,10	8,14	7,60	6,71	5,07	6,03	5,50	6,17	10,70
Ho	0,59	0,79	1,98	2,43	1,89	1,62	1,56	1,41	1,05	1,20	1,15	1,26	2,14

Er	1,75	2,35	5,58	7,09	5,51	4,81	4,48	4,01	3,08	3,47	3,43	3,75	6,15
Tm	0,270	0,364	0,778	1,030	0,822	0,761	0,676	0,640	0,452	0,488	0,512	0,561	0,900
Yb	1,77	2,46	5,06	6,53	5,47	4,94	4,38	4,10	3,03	3,20	3,39	3,70	5,74
Lu	0,252	0,404	0,838	1,050	0,871	0,729	0,664	0,633	0,477	0,527	0,554	0,565	0,903
Cd	< 0.5	< 0.5	< 0.5	< 0.5	< 0.5	< 0.5	0,6	0,6	< 0.5	< 0.5	< 0.5	< 0.5	< 0.5
Cu	91	97	2	27	34	42	87	61	48	< 1	8	7	17
Ag	0,3	< 0.5	0,9	1,0	1,2	< 0.3	< 0.3	0,3	< 0.3	< 0.3	< 0.3	0,7	1,0
Ni	101	198	2	4	23	37	56	12	22	49	13	3	4
Mo	< 1	< 1	< 1	1	< 1	< 1	< 1	< 1	2	< 2	< 1	< 1	< 1
Zn	81	68	151	130	154	142	115	103	129	34	59	107	112
S	100	300	300	300	1700	100	200	100	1500	< 100	500	400	200
Au	< 2	< 2	< 2	< 2	< 2	< 2	< 2	< 2	< 2	< 2	< 2	< 2	< 2
As	< 0.5	< 0.5	< 0.5	< 0.5	19,7	< 0.5	< 0.5	6,3	15,0	15,3	59,9	1,5	< 0.5
Sc	26,1	34,9	29,2	18,4	21,8	22,7	20,4	31,0	14,3	14,4	11,8	14,4	14,8
Sb	0,6	0,4	< 0.1	< 0.1	1,3	0,4	0,5	0,7	0,7	11,1	0,7	< 0.1	0,3
Eu/Eu*[2]	1,01	1,02	1,19	0,85	0,77	0,84	0,96	0,83	1,03	0,81	0,95	0,90	0,83
log(Th/Yb)	-0,12	-0,75	-0,05	-0,61	-0,32	-0,65	-0,37	-0,25	-0,31	-0,10	-0,23	-0,40	-0,51
log(Zr/Y)	0,64	0,34	0,57	0,51	0,58	0,52	0,57	0,53	0,55	0,73	0,58	0,67	0,55
La/Ybcn[3]	3,36	0,84	3,29	1,48	2,35	1,39	2,39	3,03	1,97	4,42	2,57	2,33	1,86
Zr/TiO2	73,76	57,52	100,50	138,77	91,00	96,83	146,77	87,28	83,73	107,72	115,02	115,38	181,90
Al2O3/TiO2	15,35	19,42	7,59	11,53	6,19	8,81	14,65	8,62	6,90	8,05	8,51	12,95	14,52
AI[5]	42	49	29	20	42	31	27	29	38	7	31	21	24
CCPI[6]	80	90	74	77	88	83	75	78	93	75	82	68	75
AAAI[7]	21	17	35	32	35	24	24	27	36	22	44	34	34

Table 4.1 (cont.)

Analyse	54688	54684	54374	54762	54763	54766	68412	68414	54767	54770	54364
Sample	8B	13PA10B1	19	161A	162A	169B	17PA2C	17PA2D	171B	197A	47C
Group	M3	M3	M4	M4	M4	M4	M4	M4	M4	M4	M4
least altered					*						
SiO2 (wt.%)	56,96	46,64	48,43	46,40	44,34	52,55	49,91	45,94	47,17	44,29	47,08
Al2O3	15,94	25,64	17,14	16,31	15,98	14,03	14,64	15,56	16,71	16,17	15,77
Fe2O3(T)	12,49	3,39	13,65	15,78	17,63	15,83	18,42	16,21	14,78	16,89	17,35
FeO	9,84	1,38	10,36	11,01	12,69	11,95	14,04	12,21	10,69	12,21	13,08
Fe2O3	1,66	1,87	2,25	3,67	3,67	2,68	2,97	2,78	3,03	3,46	2,96
MgO	2,38	1,08	2,83	6,03	5,96	3,81	7,23	5,51	5,35	6,21	6,48
MnO	0,25	0,12	0,17	0,25	0,25	0,23	0,14	0,12	0,12	0,25	0,29
CaO	6,02	11,78	12,23	7,55	8,68	6,84	3,43	3,53	6,81	8,64	7,03
Na2O	3,65	0,65	0,89	3,44	2,89	2,88	2,61	0,51	1,09	2,04	0,68
K2O	0,87	4,85	1,16	0,13	0,17	1,25	0,52	5,10	3,33	0,62	1,18
TiO2	1,511	1,718	2,100	3,519	3,522	2,530	2,822	2,628	2,876	3,306	2,814
P2O5	0,43	0,50	0,24	0,51	0,51	0,42	0,45	0,36	0,48	0,50	0,37
Cr2O3	< 0.01	< 0.01	0,01	0,02	0,02	0,01	0,01	0,01	0,01	0,01	0,01
LOI	0,46	3,94	0,88	0,41	0,33	0,30	0,11	3,50	1,42	0,34	0,17
Total	101,00	100,30	99,72	100,30	100,30	100,70	100,30	98,97	100,10	99,25	99,23
Ti[1] (ppm)	9059	10300	12590	21097	21115	15168	16918	15755	17242	19820	16870
Sr	280	303	344	405	389	489	258	148	195	270	260
Ba	285	513	126	20	20	525	125	421	270	225	290
Nb	7,2	8,9	3,1	8,5	8,5	6,6	7,3	10,1	7,1	6,7	6,8
V	85	141	315	356	354	302	342	375	349	392	279
Co	24	6	43	53	52	42	51	68	71	53	58
Ga	22	28	23	23	22	22	24	26	25	26	22
Ge	1,5	1,7	2,8	1,5	1,7	1,7	1,2	1,3	1,3	1,3	2,0
In	< 0.1	< 0.1	< 0.1	0,1	0,1	0,1	0,1	< 0.1	0,1	0,1	< 0.1
Sn	2,0	4,0	1,0	2,0	2,0	2,0	2,0	1,0	2,0	2,0	1,0
Cs	3,7	3,8	0,4	0,2	0,2	20,4	1,0	5,1	2,8	0,9	0,3
Pb	7	17	5	30	10	< 3	7	11	11	< 3	10
Be	< 1	4	1	2	2	2	1	1	2	2	1
Hf	5,1	4,8	3,8	4,9	5,0	4,3	4,7	5,6	4,9	4,1	4,7
Ta	0,47	0,53	0,17	0,52	0,57	0,38	0,37	0,46	0,44	0,38	0,38
W	0,6	1,7	0,6	1,8	0,6	1,1	1,7	0,9	2,3	0,5	1,2
Tl	0,12	0,81	0,22	0,07	< 0.05	2,12	< 0.05	0,79	0,64	0,11	0,14
Bi	0,1	0,8	< 0.1	< 0.1	< 0.1	0,5	< 0.1	0,4	0,2	< 0.1	0,2
Th	1,50	5,06	1,00	0,77	0,80	1,46	1,77	2,67	2,43	1,26	1,18
U	0,65	2,39	0,39	0,28	0,31	0,64	0,82	5,17	3,18	0,74	0,32
Rb	18	162	37	2	4	356	15	132	67	28	50
Y	53,7	39,4	28,9	50,7	50,6	55,4	58,2	73,8	69,6	68,5	37,8
Zr	181	197	144	213	206	168	173	198	160	167	183
La	12,7	16,3	9,5	14,9	15,5	14,3	14,4	15,5	22,1	14,4	14,5
Ce	30,9	38,0	25,2	39,3	40,6	33,7	34,9	38,0	53,4	35,2	35,1
Pr	4,68	5,26	3,82	5,56	5,63	4,58	4,95	5,38	6,99	4,98	4,78
Nd	22,3	23,5	18,1	27,1	28,8	22,7	23,0	24,5	33,2	24,7	23,2
Sm	6,82	7,17	5,22	7,63	7,98	6,97	6,83	7,44	9,80	7,22	6,47
Eu	2,04	1,37	1,92	2,50	2,67	2,21	2,20	2,30	2,51	2,69	2,15
Gd	8,10	6,37	5,83	8,87	8,94	8,67	8,45	9,16	11,90	9,48	6,93
Tb	1,48	1,11	1,03	1,41	1,40	1,45	1,53	1,76	1,92	1,55	1,29
Dy	10,10	6,18	6,32	8,30	9,03	9,04	9,82	11,90	12,00	9,82	7,69
Ho	2,06	1,33	1,26	1,66	1,79	1,84	2,06	2,61	2,39	2,05	1,51

Er	6,05	4,08	3,55	4,57	5,06	5,16	5,95	7,83	6,80	5,91	4,26
Tm	0,900	0,624	0,497	0,662	0,769	0,765	0,842	1,170	0,983	0,836	0,600
Yb	6,02	4,27	3,19	4,24	4,69	5,06	5,60	7,74	5,91	5,57	3,93
Lu	0,989	0,709	0,487	0,670	0,687	0,811	0,901	1,180	0,859	0,849	0,648
Cd	< 0.5	< 0.5	< 0.5	0,7	0,7	< 0.5	< 0.5	< 0.5	1	< 0.5	< 0.5
Cu	39	7	205	141	77	38	5	109	44	47	12
Ag	1,2	1,0	0,8	< 0.3	< 0.3	< 0.3	< 0.3	< 0.3	< 0.3	< 0.3	1,3
Ni	4	6	55	89	92	33	41	50	40	47	95
Mo	< 1	< 1	< 1	< 1	< 1	< 1	< 2	4	1	< 1	< 1
Zn	121	57	100	143	131	137	201	149	166	146	183
S	200	1300	700	2200	800	< 100	< 100	10300	3900	700	400
Au	< 2	< 2	< 2	< 2	< 2	< 2	8	< 2	< 2	< 2	< 2
As	< 0.5	21,9	4,2	< 0.5	< 0.5	< 0.5	1,4	627,0	462,0	< 0.5	< 0.5
Sc	17,6	23,1	27,9	31,1	30,7	25,2	30,3	29,1	29,3	31,3	27,6
Sb	0,3	0,5	2,1	0,6	0,5	0,8	< 0.1	1,0	1,0	0,3	< 0.1
Eu/Eu*[2]	0,84	0,62	1,06	0,93	0,97	0,87	0,88	0,85	0,71	0,99	0,98
log(Th/Yb)	-0,60	0,07	-0,50	-0,74	-0,77	-0,54	-0,50	-0,46	-0,39	-0,65	-0,52
log(Zr/Y)	0,53	0,70	0,70	0,62	0,61	0,48	0,47	0,43	0,36	0,39	0,68
La/Ybcn[3]	1,43	2,59	2,03	2,39	2,25	1,92	1,75	1,36	2,54	1,76	2,51
Zr/TiO2	119,79	114,67	68,57	60,53	58,49	66,40	61,30	75,34	55,63	50,51	65,03
Al2O3/TiO2	10,55	14,92	8,16	4,63	4,54	5,55	5,19	5,92	5,81	4,89	5,60
AI[5]	25	32	23	36	35	34	56	72	52	39	50
CCPI[6]	77	45	89	86	89	83	89	79	82	90	93
AAAI[7]	32	26	23	21	20	28	27	32	26	21	25

[1]Calculated from TiO_2; 10000 x (TiO_2/0.5993)
[2]Eu/Eu* = $Eu_n/(Gd_n + Sm_n)^{0.5}$ (Normalized to Primitive Mantle) (Sun and McDonough, 1989)
[3]Normalized to Chondrite (cn) value (Sun and McDonough, 1995)
[4]Temperature of zirconium saturation (Tzr) in Celsius, calculated from the formula of Watson and Harrison (1983) and adapted by Hanchar and Watson (2003).
[5]Alteration Index (AI = 100*(K_2O+MgO)/(K_2O+MgO+CaO+Na_2O)) (Ishikawa et al., 1976)
[6]Chlorite-carbonate-pyrite index (CCPI = 100*(Fe_2O_{3T}+MgO)/(Fe_2O_{3T}+MgO+K_2O+Na_2O)) (Large et al., 2001)
[7]Advanced argillic alteration index (AAAI = 100*SiO_2/(SiO_2+10MgO+10CaO+Na_2O)) (Williams and Davidson, 2004)

Table 0.2 Summary of the mineralogy of the different metamorphosed mineral alteration assemblage in the Moulin-à-Baude Formation

Main mineralogical assemblage	**Associated minerals**
Mafic	
Quartz – epidote	Diopside, sericite, amphibole, carbonate, magnetite, titanite, garnet (grossular), scapolite, apatite, sulfides
Amphibole – Garnet – Biotite	Ca-amphibole, cummingtonite, gedrite, anthophyllite, almandine, quartz, biotite, phlogopite, plagioclase, sulfides
Biotite – quartz	Biotite, quartz, phlogopite, sulfides, plagioclase
Felsic to intermediate	
Magnetite – biotite – epidote	
(Mn-Ca-Fe) garnet – quartz – Amphibole – anorthite – biotite	Calcic amphibole, titanite, epidote, magnetite, apatite
Albite – FeMg amphibole/biotite	Quartz, anthophyllite, gedrite, phlogopite, magnetite, sulfides
Epidote – biotite – k-feldspar – quartz – carbonate – magnetite	Muscovite, plagioclase, allanite, Fe-epidote
Phlogopite – k-feldspar – quartz – clinozoisite/zoisite	Tourmaline, sulfides, calcite, muscovite, epidote
Muscovite – quartz	K-feldspar, sericite, tourmaline, garnet, hematite, magnetite, biotite, sulfides, chlorite
Sillimanite – muscovite – phlogopite	Microcline, magnetite, gahnite, tourmaline, xenotime, zircon, allanite, sericite
Mafic to felsic	
Skarn	Diopside, tremolite, actinolite, phlogopite, garnet, microcline, clinozoisite/zoisite, Mn-muscovite (wilsonite), epidote, hornblende, pargasite, scapolite, calcite, muscovite, quartz, anthophyllite, cummingtonite, sulfides
Silicification	

Table A4.1 : Analytical conditions used to analyze minerals using Electron Probe Micro-Analyser (EPMA).

Mineral	Accelerating voltage	Beam current	10 sec	20 sec	30 sec	40 sec
Amphibole	15 kV	20 nA	*K(α)*: F	*K(α)*: K, Na, Al, Si, Mg	*K(α)*: Ni	*K(α)*: Ti, Mn, Ca, Fe
Epidote	15 kV	20 nA		*K(α)*: Al, Si, Mg		*K(α)*: Mn, Ti, Ca, Fe
Garnet	15 kV	20 nA	*K(α)*: Cr	*K(α)*: Al, Si, Mg		*K(α)*: Mn, Ti, Ca, Fe
Biotite & Muscovite	15 kV	20 nA	*K(α)*: F, Cl, Na, Zn. *L(α)*: Ba	*K(α)*: K, Si	*K(α)*: Ca, Al, Mg	*K(α)*: Ti, Mn, Fe

Chapter 5 Syn-orogenic magmatism over 100 m.y. in high crustal levels of the central Grenville Province: Characteristics, age and tectonic significance

5.1 Abstract

The Escoumins supracrustal belt (ESB) represents higher levels of the infrastructure of a large hot orogen, exposed in a broadly dome and basin pattern. It consists of remnants of a Pinwarian-age (1.52–1.46 Ga) oceanic arc and arc-rift sequence, preserved in the Low-*P* Belt of the central Grenville Province, and was intruded by diverse Grenvillian-age plutons. The plutonic rocks range from quartz monzodiorite to granite and have intrusion ages covering a time interval of ~100 My, that represents the entire range of the Grenvillian orogeny. Moreover, the ages, field relations and geochemical signatures of the different intrusions can be matched with different documented stages of the orogeny. The oldest pluton, the magnesian, biotite-bearing Bon-Désir granite (1086 ±2Ma), has positive εNd (+ 0.6), T_{DM}=1.52 Ga, and is attributed to melting of a juvenile Pinwarian crust as a result of slab break-off, at the onset of continental collision. The ferroan and Ba–Sr enriched, biotite-, amphibole- and clinopyroxene-bearing Michaud plutonic suite (1063 ±3 Ma) and biotite-rich felsic sill (1045 ±3 Ma) have εNd (-0.01 – +0.8) and T_{DM}= 1.45–1.48 Ga. Their geochemistry is consistent with fractionation of a mafic magma derived from melting of a Geon 14 subduction-modified subcontinental lithospheric mantle. This magmatism is consistent with convective thinning of subcontinental lithosphere, potentially linked to tectonic extrusion and orogenic collapse. This collapse ultimately led to the juxtaposition of the

low-*P* Belt with the high-*T* mid-*P* Belt in the hinterland of the Grenville Province and to amphibolite-facies metamorphism in the former, producing metamorphic zircon overgrowths at 1037 ±10 Ma. Finally, 988 ±5 Ma to 983 ±5 Ma syn-kinematic peraluminous two-mica garnetiferous leucogranite bodies and pegmatites with inherited 1055 ±2 Ma metamorphic monazite were derived from melting of previously metamorphosed deeper levels of the low-*P* Belt. This is consistent with a high geothermal gradient linked to thinning of the crust in a Basin and Range setting. The geochemical and age pattern of Grenvillian-age magmatism in the ESB, in conjunction with the overall architecture of the Province, suggests that Laurentia was the upper plate during the Grenvillian orogeny.

5.2 Introduction

The Grenville Province represents the remnants of a large hot orogen (Beaumont et al., 2010) built on the SE Laurentian margin during the Mesoproterozoic (Rivers et al., 2012) by a major collision between Laurentia and Amazonia (Cawood et al., 2016; Li et al., 2008). In Canada, it exposes a wide range of crustal levels that were metamorphosed at different depths, temperatures and times, during the Grenvillian orogeny (Fig. 5.1). For instance, the orogenic hinterland (or Allochthonous Belt of Rivers et al., 1989) is an assembly of high-*P* to mid-*P* (dominant) granulite facies rock units that were metamorphosed and experienced widespread anatexis during the Ottawan phase of the orogeny (1.09–1.02 Ma; see Rivers, 2012), capped to the south-east by low-*P*, mostly amphibolite-facies units (low-*P* belt of Rivers, 2008). Collectively these three belts represent the orogenic infrastructure (Culshaw et al., 2006). In addition, both in the NE

and the SW parts of the hinterland, the orogenic suprastructure is locally exposed (Orogenic Lid of Rivers, 2008). This includes the highest crustal levels of the orogen, which are characterized by no perceptible to low-grade Grenvillian age metamorphism. In contrast, the Parautochthonous Belt to the NE was metamorphosed from greenschist-facies conditions at the Grenville front, to high-*P* granulite and eclogite-facies conditions near the overlying hinterland to the SW, during the waning stage of the orogeny (Rigolet phase; 1.00–0.98 Ga) and was developed during the outward propagation of the orogen onto its foreland (Rivers et al., 2012).

The hinterland is also characterized by Ottawan- to Rigolet-age magmatism including anorthosite–mangerite–charnockite–granite (AMCG) suites, peraluminous granite, potassic to ultrapotassic intrusions and ultramafic to mafic intrusions of crustal and mantle source (Turlin et al., 2017; Rivers et al., 2012, and references herein). The distribution of Grenvillian-age plutons was the basis for the definition of the Interior Magmatic Belt (Owen and Erdmer, 1990; Gower et al., 1991; Rivers, 1997; Gower and Krogh, 2002) in the central and southern part of the mid-*P* hinterland, also referred to as the thermal core of the orogen (Rivers et al., 2012).

The Grenvillian-age AMCG rocks mainly occur as 1.1 Ga suites along two ~NS trending corridors that divide the hinterland in three parts, western, central and eastern (Fig. 5.1; Indares and Moukhsil, 2013). Grenvillian-age plutonic rocks are particularly abundant and diverse in the mid-*P* hinterland of the central Grenville (Owens and Tomascak, 2002; Hébert et al., 2009; Moukhsil et al. 2009; Dunning and Indares, 2010; Augland et al., 2015). The diverse and protracted character of Grenvillian-age magmatism

in the hinterland is clearly an important feature, but its significance in the context of the orogeny is still poorly explored.

The Escoumins Supracrustal Belt (ESB) is part of the Low-*P* Belt of the central Grenville Province in Quebec (Fig. 5.1; Groulier et al. 2018), and mainly consists of the Pinwarian-age (1.52 – 1.46 Ga) metasedimentary and metavolcanic rocks of the Saint-Siméon Group (SSG) with their plutonic counterpart (Tadoussac Intrusive Suite or TIS; Fig. 5.2). In addition, Grenvillian-age plutonic rocks intrusive into the ESB were also identified, implying that such rocks are present in all the crustal levels of the orogenic infrastructure. This contribution documents the distribution, U–Pb ages, geochemistry and Sm–Nd signatures of these Grenvillian-age plutonic rocks, and discusses their relation to metamorphism and deformation of the ESB. The results are used to propose a model for the origin of this magmatism in the context of the Grenvillian orogeny, and the implications for the evolution of a large, long duration, hot orogen are discussed.

5.3 Geological setting

The Escoumins Supracrustal Belt (ESB) is located in the southern part of the Central Grenville Province in Quebec (Canada) and is exposed discontinuously for over 100 km in the Saint-Siméon – Forestville area (Fig. 5.1). Part of it consists of the amphibolite-facies Saint-Siméon Group, a peri-Laurentian, Pinwarian age (1.52 – 1.46 Ga) supracrustal sequence inferred to have been accreted to Laurentia around ~1.4 Ga (Groulier et al., 2018). The supracrustal rocks are exposed in synforms (namely Lac Raymond, Lac Saint-Onge and Baie-des-Bacon; Fig. 5.2) separated by antiforms of orthogneisses and plutonic bodies in an overall dome and basin map pattern (Fig. 5.2).

The Saint Siméon Group is divided into three formations. The lowest, Saint-Paul-du-Nord Formation, is mainly composed of metasedimentary rocks intruded by syn-volcanic mafic sills and dykes with oceanic arc and back-arc signature and is interpreted to be the relict of an oceanic basin adjacent to an arc. The middle, Moulin-à-Baude Formation, is an assemblage of metavolcanic rocks with subordinate metasedimentary rocks, representing an evolution from an oceanic arc to an immature oceanic rifted-arc/back-arc. A rhyolite and a dacite from this formation were dated respectively at 1465 +38/-32 Ma and 1492 ±3 Ma (Groulier et al., 2018). Finally, the highest, Port-aux-Quilles Formation, is composed mainly of metasedimentary rocks (maximum age of deposition of 1476 ±10 Ma; Groulier et al., 2018) with scarce basaltic dykes and it is inferred to be the relict of an oceanic back-arc basin filled during rapid subsidence with clastic sediments.

A syn-volcanic Pinwarian batholith, the Tadoussac Intrusive Suite is exposed in the westernmost antiform (Fig. 5.2), in tectonic contact with the Saint-Siméon Group. This suite is dominated by granodiorite dated at 1502 ±6 Ma (Groulier et al., 2018), and is inferred to represent the base of the oceanic arc. Plutonic rocks and orthogneisses in the other antiforms are not dated and may represent equivalents of the Tadoussac Intrusive suite, and/or stitching plutons emplaced during and after the accretion of the ESB to Laurentia in a continental arc environment. These are correlated with the Cap-à-l'Est complex defined farther north by Hébert and Lacoste (1998) and dated at 1391 +8/-7 Ma by Hébert and van Breemen (2004).

In addition, there are several Grenvillian-age plutonic bodies that are the focus of this contribution: the several tens of km^2 Bon-Désir granite and Michaud quartz monzonite in the southern and northern part of the belt, respectively, and an assortment of

granodiorite and quartz monzodiorite stocks, felsic pegmatite dykes, and two-mica garnetiferous leucogranite stocks intrusive into the Port-aux-Quilles Formation in the core of the Lac Saint-Onge synform (Fig. 5.2).

5.3.1 Structural configuration of the ESB

The overall structural pattern of the ESB (Fig. 5.3a) is well constrained by recent aeromagnetic data, and a sequence of deformation events was inferred based on structural data from the supracrustal rocks. A schistosity S_1 marked by the orientation of mafic minerals is locally preserved and associated with hook-shape F_1 folds (Fig. 5.4a). S_1 and F_1 are folded by F_2 isoclinal folds with steeply dipping axial surfaces that follow the general orientation of the different synforms (Fig. 5.4a and b). The dominant schistosity at the scale of the belt is S_2, which is defined by axial planes of isoclinal F_2 folds and is sub-parallel to S_0 indicating a strong transposition. Moreover, a lineation L_2 marked by the preferred orientation of minerals such as amphibole or plagioclase laths in metabasalt, and fragments, clasts and pillows in metatuff and metabasalt is observed in the Raymond and Saint-Onge synforms. L2 is plunging WSW in the lac Raymond synform (Fig. 5.3b), dominantly SSW in the Lac Saint-Onge synform (Fig. 5.3c) and ENE in the Baie-des-Bacon synform (Fig. 5.3d). D2 folds and S_2 are dominantly trending N-S in the south and E-W in the north, as shown by the shape of synforms in Fig. 5.3, and axial planes are generally steeply dipping (Fig 5.3b-d). In addition, in the Escoumins and Grandes-Bergeronnes areas (Fig. 5.2), the F_2 folds and S_2 are folded by open F_3 folds with E-W steeply dipping axial planes (Fig. 5.4b) producing locally a crenulation schistosity S_3 and

an intersection lineation L_{2-3} (Fig. 5.3). The combination of D2 and D3 is responsible for the configuration of the belt (Fig. 5.2 and 5.3).

The ESB is limited to the NE by a major shear zone that separates it from granulite-facies complexes of the central Grenville. A second major deformation zone is identified on the northern edge of the Bon-Désir Granite. This zone is associated with a dextral movement and an anticlockwise rotation of the Lac Pelletier antiform (Fig. 5.3).

5.3.2 Metamorphism

The rocks are variably affected by metamorphic recrystallization. The presence of garnet – muscovite – biotite ± sillimanite in pelitic schists and hornblende – plagioclase – quartz – titanite – ilmenite ± epidote in basaltic rocks of the Saint-Siméon Group is indicative of amphibolite facies metamorphism. The widespread presence of hornblende in the Tadoussac Intrusive Suite, and the absence of metamorphic orthopyroxene are also consistent with amphibolite-facies metamorphism in the domes. Finally, immediately north of the major shear-zone that marks the northern limit of the ESB, a metagabbro contains leucosome with quartz – plagioclase – pyroxene (ortho and/or clino) – hornblende, attesting to partial melting at granulite-facies conditions.

Available metamorphic ages are published in Groulier et al. (2018), and summarized in figure 5.5. Overgrowths, interpreted as metamorphic, on annealed and etched detrital zircon grains from a quartzite of the Port-aux-Quilles Formation (Lac Raymond synform; Fig. 5.2) dated by LA–ICP–MS yielded a weighted average $^{206}Pb/^{238}U$ age of 1037 ±10 Ma, which is a late-Ottawan age. In addition, two distinct

generations of titanite from a dacitic tuff of the Moulin-à-Baude Formation (lac St Onge synform; Fig. 5.2) dated by TIMS yielded U–Pb ages of 1001 ±3 Ma and 983 ±3 Ma, which are Rigolet ages.

5.4 Analytical methods

In addition to optical microscopy, microstructures at the thin section scale were documented by false color mineralogical maps produced by a FEI Quanta 400 scanning electron microscope (SEM) at Memorial University with a Mineral Liberation Analysis (MLA) software (JKTech, University of Queensland, Australia), at operating conditions of 25 kV accelerating voltage and 10 nA beam current.

For U–Pb geochronology, samples were processed by standard techniques of crushing and mineral separation and zircon was prepared as previously described (Groulier et al., 2018). All zircon grains were annealed at 1000°C for 36 hours, and then etched in concentrated HF acid in a Teflon capsule at 200°C in an oven for 5 hours. Lead and U isotopic ratios were measured by thermal ionization mass spectrometry, and results calculated using ISOPLOT for weighted averages of $^{206}Pb/^{238}U$ or $^{207}Pb/^{206}Pb$ ages. Uncertainties on the ages are reported at the 95% confidence interval. For two samples, single monazite crystals were also analyzed, after cleaning in dilute distilled nitric acid and water, followed by dissolution and small- scale HCl ion exchange chemistry. In these cases, the $^{207}Pb/^{235}U$ ages are adopted as the best age estimate. The data are listed in Table 5.1.

Whole-rock major and trace element analyses were performed by Actlabs (Ancaster, Ontario). The samples were chosen based on their homogeneity, lack of

alteration and to be representative of the whole plutonic body. The powdered samples were prepared using Li-metaborate and Li-tetraborate fusions. Major elements were analyzed by inductively coupled plasma (ICP) and trace elements were analyzed by ICP-mass spectrometry (MS). The data are reported in Table 5.2. Detection limits are available on the Actlabs website. Precision and accuracy are consistent with the estimates given in Jenner (1996).

Details on the sample preparation technique for the Sm-Nd isotopic analyzes can be found in Valverde et al. (2012). Sm and Nd concentrations and isotopic compositions were determined using a multi-collector Finnigan Mat 262 mass spectrometer (TERRA Facility – Memorial University Earth Sciences Department) in static mode for concentration determination, and dynamic mode for isotopic composition determination. Instrumental mass fractionation of Sm and Nd isotopes were corrected using a Raleigh law relative to $^{146}Nd/^{144}Nd = 0.7219$, $^{152}Sm/^{147}Sm = 1.783$. The reported $^{143}Nd/^{144}Nd$ ratios are corrected for deviation from the JNdi-1 standard ($^{143}Nd/^{144}Nd = 0.512115$, Tanaka et al., 2000). Replicates of the standard gave a mean value of $^{143}Nd/^{144}Nd = 0.512102 \pm 14$ (2SD, n=18) for JNdi-1. We also periodically analyze USGS whole rock reference material BCR-2. The results of our BCR-2 analyses over time are in agreement with the results reported by Raczek et al. (2003). The Sm-Nd isotopic data are listed in Table 5.3.

5.5 Grenvillian-age plutonic rocks

5.5.1 General characteristics and petrography

This section documents the field characteristics of the investigated plutonic bodies complemented by the petrography of the sampled rocks. Note that the field names used in Figure 5.2, are used throughout the paper to distinguish the different samples. However, we note that geochemical classification of the samples, does produce somewhat different rock names, whether based on simple bulk chemistry plots or normative schemes. Regardless of the nomenclature, it is the field relations and ages of the granitoids that are most important aspect for this paper.

5.5.1.1 Bon-Désir granite

The Bon-Désir granite, named by Rondot (1986), is a ~10 km long polyphase pluton exposed along the northern shore of the Saint-Lawrence River, close to the town of Les Escoumins (Fig. 5.2). Its predominant facies is a coarse-grained pinkish to greyish biotite granite. In the central part of the pluton, it has a megacrystic texture and is crosscut by a medium-grained greyish granite. The absence of chilled margins is consistent with a cogenetic origin and coexistence of the two facies as different crystal mushes. At the edge of the intrusion, the granite displays development of a gneissic fabric that grades locally into centimetric-wide ultramylonite. The Bon-Désir granite contains minor amounts of cm-scale mafic-rich bodies (Fig. 5.6a), whose origin is not clear. Also present are minor amounts of xenoliths of quartzite from the Saint-Siméon Group.

In thin section, the granite consists of partly recrystallized coarse-grained quartz and alkali-feldspar in a finer-grained groundmass of quartz, alkali feldspar, plagioclase and minor biotite, with trace amounts of apatite Fe–Ti oxides and zircon (Fig. 5.7a). The coarse-grained quartz is elongated, has undulatory extinction and shows sub-grain migration (Fig. 5.8a), and the alkali feldspar are perthitic, show porphyroclastic texture and are locally rimmed by myrmekite (Fig 5.8b). Quartz in the groundmass is fine-grained, with polygonal and granoblastic texture. The biotite is closely associated with apatite and Fe–Ti oxides, and is locally chloritized. The textures both at the outcrop and at the thin section scale indicate that the Bon-Désir granite is deformed.

5.5.1.2 Michaud quartz-monzonite and related intrusions

The Michaud quartz monzonite has been described as the Bonhomme-Michaud charnockite or granodiorite (Rondot 1986), and is the largest pluton in terms of area (approximatively 8 km by 15 km, Fig. 5.2). It has a greenish to pinkish colour on fresh surfaces and consists of perthitic feldspar megacrysts (Fig. 5.6b), amphibole, biotite, quartz and Fe–Ti oxides. Some feldspar megacrysts have a thin mantle or rim of plagioclase around a K-feldspar core. The pluton contains abundant decametric rafts of metasedimentary rocks (Fig 5.2). The rafts are commonly observed in the field and in regional magnetic surveys, due to their low magnetic-signatures. The high proportion of these rafts in the central part of the intrusion suggests that the exposed surface of the pluton is close to the roof of the magmatic chamber.

In thin section the perthitic K-feldspar megacrysts (up to 2–3 cm long; Fig. 5.7b, 5.8c) are rimmed by myrmekite, in a medium- to coarse-grained groundmass of quartz

and euhedral perthite, with clusters of biotite, amphibole and resorbed clinopyroxene. These clusters also contain euhedral and zoned zircon, titanite, allanite, euhedral apatite and interstitial Fe–Ti oxides (Fig. 5.8d). The euhedral perthite grains are surrounded by rims of finer-grained plagioclase and quartz with minor K-feldspar. The euhedral plagioclase is zoned and partly sericitized. Some biotite grains have rutile inclusions.

Other smaller plutonic bodies are associated with the Michaud quartz monzonite. One of them is a granodiorite stock located a few kilometers south of the Michaud pluton in the western limb of the Saint-Onge synform. This stock cross-cuts metasedimentary rocks of the Saint-Paul-du-Nord Formation and is characterized by a circular positive magnetic anomaly on the aeromagnetic map. The stock has a beige to greenish color, is fine- to medium-grained with a porphyritic texture defined by plagioclase (Fig. 5.6c). In thin section, the rock consists of euhedral and zoned plagioclase phenocrysts (Fig. 5.7c, 5.8e) in a granoblastic groundmass of quartz, K-feldspar, plagioclase, biotite, and amphibole (sometimes twined) with quartz inclusions (Fig. 5.8f). Euhedral zircon, apatite and interstitial Fe-Ti oxides (ilmenite with hematite exsolution) surrounded by titanite (Fig. 5.8f), occur in trace amounts. The plagioclase phenocrysts have sericitized and corroded calcic cores surrounded by Na-rich rims (Fig. 5.7c).

In addition, a strongly magnetic fine grained and porphyritic quartz monzodiorite dyke is in sharp contact with the surrounding granitic orthogneisses, is located one to two kilometers west of the Michaud pluton, and is oriented N325 with a 38° dip toward the NE. This rock is dark in color, and displays a magmatic foliation defined by the preferred orientation of plagioclase phenocrysts. In thin section, the plagioclase phenocrysts are

euhedral and zoned with an inclusion-bearing core, in a very fine-grained groundmass of clinopyroxene, biotite, quartz, feldspar and Fe–Ti oxides (Fig. 5.7d, 5.8g-h).

5.5.1.3 Biotite-rich felsic sill

This is a SW-NE-trending sill, several hundred meters long and up to 100 meters wide, in sharp contact with the metasedimentary rocks of the Port-aux-Quilles Formation in the Saint-Onge synform (Fig. 5.2). It is medium grained and composed of an intermediate (dark grey color) and a felsic (light grey) facies. Both facies consist of quartz, biotite, plagioclase, K-feldspar and Fe–Ti oxides. The sill has numerous angular metasedimentary rock fragments and is crosscut by meter to decameter wide felsic pegmatite dykes (Fig. 5.6d), and quartz veins. It displays a foliation marked by the preferred orientation of biotite, the quartz veins are folded by D2 isoclinal folds, and the felsic pegmatite dykes are boudinaged, consistently with layer-parallel extension.

The biotite-rich felsic sill is medium-grained and mainly consists of quartz, biotite, plagioclase and K-feldspar and has a significant concentration of trace minerals (~5 %) as apatite, titanite, Fe–Ti oxides, zircon and allanite (Fig. 5.7e, 5.8i). It is also characterized by a common chlorite-carbonate replacement of the primary biotite (Fig. 5.8j). Other biotite grains are partially chloritized and locally replaced by white mica.

5.5.1.4 Two-mica leucogranite

The leucogranite was observed in the core of the Saint-Onge synform (Fig. 5.2), as small (less than a kilometer across) magmatic bodies intrusive in the metasedimentary rocks of the Port-aux-Quilles Formation. The contacts with the country rocks are diffuse.

The leucogranite bodies are quartz-rich (>30%) and biotite, muscovite, K-feldspar and garnet-bearing (Fig. 5.6e). They are mildly foliated and contain quartz veins with isoclinal folds (Fig. 5.4e). In thin section, the leucogranite is coarse-grained and characterized by the presence of muscovite, minor biotite and poikiloblastic garnet (Fig. 5.7f). The feldspars are sodic and potassic (microcline-dominant, albite, orthoclase; Fig. 5.8k) and the plagioclase is commonly zoned with a sericitized core surrounded by a rim of unaltered albite (Fig. 5.7f, 5.8l). Two generations of muscovite are observed; the first is euhedral, locally exhibiting simple twinning, and a late one grown along fractures. Quartz is generally interstitial, but there are also some inclusions of quartz within feldspar. Trace minerals such as uraninite, monazite and zircon were observed using SEM.

Despite the deformation features observed in the field, in thin section the leucogranite does not display any microstructural evidence of deformation or recrystallization, such as undulose extinction of quartz, subgrain rotation recrystallization, deformed twins in feldspar or rotated garnets (Fig. 5.7f, 5.8k and 5.8l). Some muscovite–garnet–tourmaline pegmatites spatially (see below) linked to the leucogranite stocks are characterized by syn-kinematic crystallization (Fig. 5.6e). Taken together, all these observations are consistent with crystallization coeval with some degree of deformation.

The leucogranite is crosscut by muscovite+garnet+tourmaline ± beryl-bearing-pegmatites that occur sporadically in the ESB. The mineralogy of these pegmatites is consistent with a peraluminous chemical signature and they would approach the Li-Cs-Ta (LCT) family of pegmatite defined by Černý and Ercit (2005). Some of these pegmatites are also characterized by miarolitic cavities consistent with an hypabyssal (i.e. shallow

level) emplacement (London, 2008; Ginsburg, 1984). Based on field relations, these are the youngest magmatic rocks observed in the ESB.

5.5.2 Geochronology

Five intrusions were sampled for CA-TIMS U–Pb dating of zircon (all) and monazite (leucogranite, pegmatite) in order to elucidate the age of post-Pinwarian magmatism in the Escoumins supracrustal belt, constrain their relation to metamorphism, and place age limits on the deformation. The sampled locations are shown in Figure 5.2 and their Universal Transverse Mercator (UTM) coordinates are given in Table 5.1. The core of the Bon-Désir granite (PA-107-A) was sampled along the shore of the St-Lawrence River. In the sampled location, the granite is homogeneous and is characterized by a foliation defined by megacrystic K-feldspar and biotite. The core of the Michaud quartz monzonite (PA-187-A) was sampled in a massive zone. The biotite-rich felsic sill (PA-88-A) and a boudinaged felsic pegmatite (PA-88-B) were sampled in their type location, in the core of the Saint-Onge synform (Fig. 5.2). Finally, a two-mica leucogranite (PA-29A) was sampled in the core of the Saint-Onge synform.

5.5.2.1 Bon-Désir granite (PA-107-A)

This coarse-grained to megacrystic granite yielded a large amount of high quality zircon (elongate prisms with some rounding of edges up to 250 μm long and 100 μm wide, Fig. 5.9a). Most grains are clear and pristine, but some are turbid. In cathodoluminescence (CL) images, the grains show oscillatory magmatic zonation and

some distinct cores (Fig. 5.10a). Seven analyses were carried out of 1, 2 or 3 grains per fraction (Table 5.1). One grain is very discordant and is not discussed further, not shown on Figure 5.11a. Six analyses are clustered with $^{206}Pb/^{238}U$ ages between 1084–1088 Ma, and the weighted average of these is 1086 ±2 Ma (MSWD =0.26).

5.5.2.2 Michaud quartz monzonite (PA-187-A)

The Michaud sample is characterized by abundant euhedral and pristine zircon (spectacular in thin section). The grains are commonly longer than 200 μm and up to 300 μm for 100 μm wide and have inclusions (Fig. 5.9b). In CL images, they display spectacular magmatic oscillatory and sector zoning and some exhibit distinct cores (Fig. 5.10b). Five analyses of zircon from this rock (4 of single grains) yielded 5 overlapping concordant points (Fig. 5.11b), with a range of $^{206}Pb/^{238}U$ ages from 1058–1065, and $^{207}Pb/^{206}Pb$ ages from 1062 to 1066 Ma. The weighted average $^{207}Pb/^{206}Pb$ age (MSWD = 0.13) of 1063 ±3 Ma is accepted as the age of crystallization of this intrusion.

5.5.2.3 Biotite-rich felsic sill (PA-88-A)

This sample yielded abundant large long prisms (Fig. 5.9c) with high – U contents (Table 5.1) and these were significantly corroded after chemical abrasion. In CL images, the grains are characterized by simple transverse magmatic zoning, and in some cases sector zoning, and lack inherited cores and inclusions (Fig. 5.10c). Three analyses were carried out of 2, 3 or 5 crystals, and while all are concordant and overlapping, these show still a hint of lead-loss with $^{206}Pb/^{238}U$ ages from 1037–1044, but with consistent

$^{207}Pb/^{206}Pb$ ages from 1044–1046 Ma. The weighted average $^{207}Pb/^{206}Pb$ age of 1045 ±3 Ma (MSWD = 0.13, Fig. 5.11c) is accepted as the age of crystallization of this rock.

5.5.2.4 Felsic pegmatite (PA-88-B)

The zircon grains from the pegmatite are euhedral, dark and turbid (Fig. 5.9d). Some grains are tiny and spherical, whereas others are elongated (up to 500 μm in length for 100 μm wide). In CL they appear altered with recrystallized domains, cross-cutting veins and disturbed magmatic oscillatory zoning (Fig. 5.10d) that we interpret to result from metamictization due to high-U content and possibly late hydrothermal alteration. After chemical abrasion, many of these zircon crystals were reduced to fluff. Four surviving single grains were analysed and these are discordant indicating that the crystal structure was too badly damaged to be restored by annealing. This likely led to further lead-loss in grains Z1 and Z2 during leaching in HF acid. However, 3 of 4 analyses have consistent $^{207}Pb/^{206}Pb$ ages of 986 ±6 to 990 ±8.5 Ma and yield a weighted average age of 988 ±5 Ma (MSWD= 0.46, 95% C.I., ISOPLOT). This is interpreted to be the age of igneous crystallization of this rock.

Euhedral monazite (Fig. 5.9e) is of high quality and three analyses of single monazite crystals yielded two points with overlapping $^{207}Pb/^{235}U$ ages of 1055–1056 Ma (Fig. 5.11d, weighted average = 1055 ±2 Ma) and one younger grain at 1039 ±3.5 Ma. We interpret this 1055 ±2 Ma age to represent inherited monazite grains from the metamorphic country rocks in the melt region formed during a high-T metamorphic event. The younger age (1039 ±3.5 Ma) is interpreted as a mixed age between an older

core (more likely 1055 ±2 Ma) and young overgrowth of the igneous age of the pegmatite.

5.5.2.5 Two-mica leucogranite (PA-29-A)

The leucogranite sample has euhedral zircon with well-defined edges and oscillatory zoning visible under a binocular microscope (Fig. 5.9f). Most of the grains are dark and turbid, and they vary in size from less than 100 μm to up to 300 μm in length for 50 to 100 μm in width. In CL images, they display magmatic oscillatory zoning and some have distinct cores (Fig. 5.10e). Four single zircon analyses are discordant, demonstrating the presence of older cores, likely inherited from the melt region. Three analyses are colinear (38% prob. of fit), with intercept ages of 2153 +207/-188 Ma and 995 +10/-12 Ma. The lower intercept age overlaps with the $^{207}Pb/^{235}U$ ages of both of the youngest single monazite crystals reported below.

This leucogranite also contains high quality monazite (Fig. 5.9g) with perfect crystal shape. Four single monazite crystals were analyzed (Fig. 5.11e) and these plot at 4 different positions on Concordia between 1037 and 983 Ma (Fig. 5.11e), indicating the likely presence of different age domains in these crystals. The youngest grain (M1) yields a $^{207}Pb/^{235}U$ age of 983 ±5 Ma, the oldest grain (M2) yields a $^{207}Pb/^{235}U$ age of 1037 ±3 Ma and M3 yields a $^{207}Pb/^{235}U$ age of 994 ±3 Ma (all at 2 sigma). As the youngest monazite age of 983 ±5 Ma is of high quality and concordant, and overlaps with the zircon lower intercept age, we interpret that it corresponds to the age of igneous crystallization of the leucogranite.

5.5.3 Whole-rock geochemistry

5.5.3.1 Major element geochemistry

Table 2 lists the names for the samples based on the Q-ANOR normative classification plot, which may be a better estimate of a modal mineral classification. Based on this classification, the rocks studied show a wide range of composition corresponding to quartz monzodiorite to granite (Fig. 5.12a). The data is also shown on the Peccerillo and Taylor (1976) K_2O versus SiO_2 plot (Fig. 5.12b) that indicates the potassic nature of the samples.

The discriminant plot of Debon and Le Fort (1988; Fig. 5.12c) was used to link the mineralogy of the plutonic rocks to their chemical signature. The A ordinate represents the peraluminosity of the magma, whereas the B abscissa is equivalent to a colouration index and a marker of fractionation (the lowest values are linked to the more fractionated rocks; (Cuney and Kyser, 2009). Values of A higher than 0 are indicative of peraluminous magmas and can be associated with Al-rich minerals such as muscovite, garnet, whereas negative A values are characteristic of metaluminous or peralkaline magmas that would crystallize amphibole, pyroxene, and titanite (Cuney and Kyser, 2009). The Bon-Désir granite plots at the edge between the Peraluminous (sector III) and Metaluminous (sector IV) fields and has low B values consistent with a mineral assemblage dominated by quartz and feldspar. The Michaud quartz monzonite also plots between sectors III and IV but has higher B values, and the quartz monzodiorite and granodiorite rocks associated with it fall between sectors IV and V at higher B values consistent with the abundances of mafic phases such as amphibole, clinopyroxene and Fe–Ti oxides in this suite. The biotite-rich felsic sill falls between sectors III and IV with

the most mafic sample close to the biotite field. Finally, the two-mica leucogranite falls between sectors I and II, near the quartz-feldspar pole, but the thin section and field observation indicates that muscovite is dominant over biotite.

On the molar proportion A/NK versus A/CNK diagram (Maniar and Piccoli, 1989; Fig. 5.12d) the samples range from metaluminous to slightly peraluminous (A/CNK values ≤ 1.1). The quartz monzodiorite and granodiorite are clearly separate from the other samples in terms of their silica contents and A/CNK ratios. Strickly, any sample with an A/CNK ratio greater than 1 is peraluminous, however, the dashed line at A/CNK of 1.1 indicates that metaluminous rocks may pass over this boundary to slightly peraluminous by differentiation.

The Michaud plutonic suite and the biotite-rich felsic sill are characterized by higher values of TiO_2 (ranging from 1.2 to 3.6 wt.%), P_2O_5 (ranging from 0.5 to 1.7 wt.%), MgO (ranging from 1.3 to 3.4 wt.%) and Fe_2O_{3T} (6.0 to 12.8 wt.%), whereas the Bon-Desir- and leuco-granites do not exhibit such enrichment in these elements (Table 5.2).

5.5.3.2 Trace element geochemistry

On the primitive mantle-normalized extended plot and chondrite plot (Sun and McDonough, 1989; Fig. 5.12e,f), the Bon-Désir granite and the leucogranite display strong negative Eu-anomalies and positive anomalies in low field strength elements (LFSE), such as Pb, U and Th. They also exhibit strong negative anomalies in HFSE (Nb–Ta and Ti), and in Sr and P. The Bon-Désir granite is enriched in light rare-earth elements (LREE) compared to heavy rare-earth elements (HREE) as shown by the ratio

$[La/Yb]_n$ of 6.85 – 6.92 (Table 5.2). The leucogranite is characterized by an enrichment in both LREE and HREE ($[La/Yb]_n$ of 1.82 – 2.04; Table 5.2) with a depletion in medium rare-earth elements (MREE) and a negative Eu anomaly.

The other intrusions share similar patterns with enrichment in LFSE (Ba, Sr, Pb), LREE, some HFSE (P, Zr), and with negative anomalies in Nb-Ta (Fig. 5.12e). Note that the lower silica quartz monzodiorite do not have as well developed a negative Nb-Ta anomaly. They are characterized by a strong enrichment in Ba (>1000 ppm and up to 2726 ppm, respectively) and Sr (>500 ppm and up to 941 ppm respectively) (Table 5.2). Their chondrite-normalized REE patterns are characterized by fractionation between LREE and HREE ($[La/Yb]_n$ of 9.62 – 27.14; Table 5.2 and Fig. 5.12f) with only minor negative-Eu anomalies or no Eu anomalies.

5.5.3.3 Tectonic environment and magmatic-type signature

On the Zr vs 10^4Ga/Al diagram (Whalen et al., 1987; Fig. 5.13a), most rocks (the Bon-Désir granite, the Michaud plutonic suite and the biotite-rich felsic sill) plot in the A-type field known also as alkaline or anorogenic/within-plate granitoid field (Bonin, 2007; Frost and Frost, 2011). On the diagram of Pearce et al (1984; Fig. 5.13b), all data plot in the within-plate granitoid (WPG) field near the boundary with the volcanic arc granitoid (VAG) field. The Bon-Désir granite falls at the boundary between the two fields, and, together with the leucogranite, close to the syn-collisional granitoid (syn-COLG) field.

The Fe-index versus silica diagram from Frost et al. (2001; Fig. 5.13c) is used to discriminate between ferroan (rocks that experienced an iron enrichment through fractionation) and magnesian rocks. Frost et al. (2001) and Frost and Frost (2011) have

demonstrated that A-type rocks mostly fall in the ferroan field, whereas Cordilleran granites formed in a continental arc are mostly magnesian, and peraluminous leucogranites plots in both fields but with high silica values (Fig. 5.13c). The Michaud plutonic suite and the biotite-rich fesic sill fall in the ferroan field. The Bon-Désir granite plots in the highly evolved Cordilleran magnesian granite field (high silica) and the two-mica leucogranite plots in the field of peraluminous leucogranite. They are both very close to the boundary between magnesian (Bon-Désir) and ferroan fields (two-mica leucogranite).

The modified alkali-lime index versus silica diagram was proposed by Frost et al. (2001) to better constrain the boundaries between the calcic, calc-alkalic, alkali-calcic and alkali granitoid series. All the analysed plutonic rocks fall in the alkali-calcic field or on the limit with the calc-alkalic field (Fig. 5.13d). Frost and Frost (2008) calculated that fractional crystallization would lead to trends parallel to the boundaries of the different series, and the Michaud plutonic suite exhibits such a trend, consistent with their increase in silica and alkali contents due to quartz and alkali feldspar crystallization. The two-mica leucogranite is highly evolved and its chemistry reflects the dominance of albite – K-feldspar – quartz. The chemistry of the other plutonic rocks reflects a more calcic composition of plagioclase and the presence of more mafic phases such as hornblende, biotite and pyroxene.

5.5.4 Sm-Nd isotopic data

Sm–Nd isotopic data were acquired for all the described plutonic rocks in order to provide insight on the sources involved and also to test the proposed genetic link between the different intrusions of the Michaud plutonic suite.

5.5.4.1 Results

The initial Nd isotopic composition of the samples ($\varepsilon Nd_{(t)}$) ranges from slightly negative (-0.4) to slightly positive (0.8). The Bon-Désir granite has a positive εNd of 0.6 with a T_{DM} of 1517 Ma, the Michaud quartz monzonite has a positive εNd of 0.7 and T_{DM} of 1478 Ma, very similar to that of the quartz monzodiorite (εNd =0.8 and T_{DM} of 1456 Ma) and of the granodiorite (εNd=0.8 and T_{DM} of 1450 Ma). The biotite-rich felsic sill has an εNd of -0.1 and T_{DM} of 1450 Ma and finally the two-mica leucogranite has an εNd of -0.4. Given the wide range in age and chemistry of the granitoids, this range of initial Nd isotopic composition is surprisingly small.

Figure 5.14 illustrates the variation in εNd versus time and provides a comparison to possible source materials at the time of formation. At 1Ga asthenospheric mantle would be characterized by a positive εNd of about +5. If this mantle was involved in the formation of the granitoids, then it would have had to mix with strongly negative Quebecia crust at 1Ga (Dickin and Higgins, 1992; Groulier et al., 2018), to arrive at the near chondritic values. That is there would be a vertical mixing line at 1Ga between crust and mantle. The alternative and more viable option at this point would appear to be melting at 1 Ga of 1.45-1.52 crust derived from the depleted mantle.

5.6 Discussion and conclusion

5.6.1 Summary of the Grenvillian age plutonic rocks

The Escoumins supracrustal belt (ESB) represents a remnant of a Pinwarian oceanic arc and back-arc accreted to Laurentia during the Mesoproterozoic (Groulier et al., 2018), preserved in the Low-*P* Belt of the central Grenville Province. It was intruded by diverse Grenvillian-age plutonic rocks, ranging from monzodiorite to granite, with intrusion and metamorphic ages covering a time interval of ~100 My. The following section summarizes their main characteristics.

1) The oldest pluton is the Bon-Désir granite (1086 ±2 Ma), exposed in the southern part of the belt. This is a polyphase, coarse-grained to megacrystic, foliated, biotite-bearing pluton, with scarce xenoliths of country rocks. Based on geochemistry the Bon-Désir granite can be classified as a magnesian, alkali-calcic to calc-alkalic pluton, which also is high-K and slightly peraluminous. On tectonic discrimination diagrams, the granite falls at the boundary between the volcanic arc and within-plate granitoids. Its has a pronounced negative Nb–Ta anomaly and negative Eu-anomaly. These features plus the enrichment in LFSE, which are typically found in continental crust, is consistent with a dominant crustal source. The positive initial εNd (+0.6) and its T_{DM} of 1517 Ma indicate that this source may be of Pinwarian-age. The Pinwarian depleted mantle age is similar to the age of the Escoumins island arc indicating that the Bon-Désir granite could have formed from the melting of crust formed in that earlier event.

2) The Michaud quartz monzonite (1063 ±3 Ma) is the largest pluton in the ESB. It is characterized by megacrystic K-feldspar, and, together with smaller bodies of quartz monzodiorite and granodiorite associated to it, contains notable amounts of amphibole, biotite, clinopyroxene Fe–Ti oxides, zircon, allanite, apatite and titanite. The Michaud plutonic suite is classified as within-plate, metaluminous, alkali-calcic and ferroan. Their Geon 14 T_{DM} and their slightly positive εNd appears to be similar to the Nd isotopic value of the crust-derived Bon-Désir granite, however, the Michaud plutonic suite has some critical differences. The suite is characterized by LREE enrichment and somewhat depleted HREE relative to the Bon-Désir granite. Furthermore it lacks a negative Eu-anomaly and the strong enrichment in LILE, Fe, Ti, P, may be more consistent with partial melting of a more mafic source.

3) The biotite-rich felsic sill (1045 ±3 Ma) is an hectometric sill with notable amounts of Fe–Ti oxides, titanite, apatite, allanite and zircon, abundant angular xenoliths of quartzite and is intruded by a swarm of felsic pegmatite (988 ±5 Ma). The biotite-rich felsic sill is classified as within-plate, metaluminous and alkali-calcic. It is also characterized by an enrichment in LREE, LILE, Zr, Nb, Fe, Ti, and P. The biotite-rich felsic sill has a slightly negative εNd (-0.01) and a calculated depleted mantle age of 1.45 Ga. The fractionation between LREE and HREE coupled to the absence of Eu negative anomaly is consistent with a more mafic source than that for the Bon-Desir granite. It bears geochemical similarities with the Ba–Sr rich Michaud plutonic suite.

4) The felsic pegmatite (988 ±5 Ma) and the two-mica garnetiferous leucogranite (983 ±5 Ma) form stocks intrusive into metasedimentary rocks of the upper formation of the Saint-Siméon Group and are crosscut by muscovite – garnet – tourmaline ± beryl-

bearing pegmatites with miarolitic cavities, consistent with emplacement of these pegmatites at high levels in the crust. The leucogranite is characterized by Na–K feldspar (microcline – orthoclase – albite) and muscovite over biotite. The leucogranite has a negative initial εNd (-0.4). It has a geochemical signature of crust-derived, S-type peraluminous granitoids, and is enriched in lithophile elements, such as U, Th, K, Cs, Rb and Pb, and in LREEs and HREEs with a strong negative anomaly in Eu. This can be explained by the presence of plagioclase in the source (Eu retention during melting) and by the presence of monazite and garnet in the leucogranite (LREEs and HREEs retention respectively).

5.6.2 Relationships to metamorphism and deformation in the ESB

Figure 5.15 represents a summary of the U–Pb crystallization and metamorphic ages obtained on the igneous rocks and on supracrustal rocks from the ESB presented in this study.

1) The 1086 ±2 Ma Bon-Désir granite is bounded to the north by a major deformation zone, and to the south by the St Lawrence River and the brittle faults of the St Lawrence graben. The relation between the northern deformation zone and the pluton is not observed due to lack of exposure. However aeromagnetic patterns (Fig. 5.3), as well as the presence of porphyroclastic textures, foliation parallel to the schistosity of the surrounding country rocks and a gneissic fabric in the northeastern rim of the pluton with localized ultramylonite, are consistent with emplacement of the Bon-Désir granite prior to this deformation. Therefore, this deformation zone is younger than 1086 Ma.

2) The 1063 ±3 Ma Michaud quartz monzonite has a reversed sigmoid shape (similar to σ-object in thin section, visible in aeromagnetic maps; see Fig. 5.3) and is located against the shear-zone representing the NW boundary of the ESB. Therefore, this shear zone was active at or after 1063 Ma.

3) Structural observations in the 1045 ±3 Ma biotite-rich felsic sill, such as a foliation parallel to the dominant S_2 schistosity in the surrounding supracrustal rocks, the presence of crosscutting quartz veins outlining isoclinal F2 folds, and the boudinage of 988 ±5 Ma felsic pegmatites which are oriented in the same direction, indicate that the sill pre-dates the main D2 deformation in the ESB.

Overgrowths on zircon from a quartzite sampled in the central part of the Lac Saint-Onge synform, a few kilometers south from the sill (Fig. 5.2), gave a U–Pb age of 1037 ±10 Ma. These rims are unzoned and have high U (1400–1600 ppm) and extremely low Th (near detection limit) contents typical of zircon crystallized from metamorphic fluids (Groulier et al., 2018). This typically happens at amphibolite facies metamorphic conditions or higher, therefore we propose that 1037 ±10 Ma corresponds to the age of the amphibolite facies metamorphism in the ESB.

4) The 988 ±5 Ma felsic pegmatites are boudinaged and the 983 ±5 Ma two-mica leucogranite stocks in the Lac Saint-Onge synform are foliated, and contain quartz-veins that outline F2 isoclinal folds. However, in thin section the leucogranite does not display any evidence of deformation or recrystallization, and we infer that crystallization was syn to late-D2. Therefore, they these rocks provide the tightest constraint on the age of the D2 deformation in the ESB.

Such rocks commonly form in continental crust experiencing deformation, metamorphism and partial melting. In the French Armorican Variscan belt, such leucogranites were linked to partial melting of the crust during extension associated with lithospheric thinning, and they are closely linked to major shear-zones (Ballouard et al., 2017). Inherited monazite grains from the felsic pegmatite and the leucogranite gave a metamorphic age of 1055 ±2 Ma and some mixed ages between the older metamorphic core and the newly formed younger igneous rims. We suggest that the older age (1055 ±2 Ma) represents the metamorphic age of the source and that this source experienced melting during the Rigolet (ca. 990 to 980 Ma) allowing the newly-formed peraluminous magma to sample the previously formed metamorphic monazite. Since the presently underlying Mid-*P* Belt had already experienced melting during the Ottawan (Rivers et al., 2012), leaving a non-fertile residuum behind, we suggest that the source of the peraluminous magmatism in the ESB was located at deep crustal levels of the Low-*P* Belt. The fact that it is not part of the Mid-*P* Belt is also supported by the presence of Parautochthonous-derived, Rigolet-age peraluminous felsic pegmatites found in the northern part of the Mid-*P* Belt of the central Grenville Province (Turlin 2017).

The igneous crystallization age from magmatic zircon and monazite grains fall in the range of the ages obtained on two generations of titanite from a dacitic tuff in the same synform (1001 ±3 Ma and 983 ±3 Ma U–Pb ages, dated by ID–TIMS; Groulier et al., 2018; Fig. 5.2 and 5.15). Therefore, these titanite ages are inferred to represent the age of a thermal event associated with the emplacement of the leucogranite and the pegmatites.

5.6.3 Implications for the Grenvillian orogeny

Plutonic rocks of Grenvillian age which intrude the ESB, as well as the age of metamorphism, provide constraints on the evolution of the Low-*P* Belt of the central Grenville during the Grenvillian orogeny as they cover almost the entire time interval of the orogeny (ca. 1086–983 Ma).

The Grenvillian orogeny has been described in the literature in terms of a continuous evolution, broadly inspired by the orogenic model evolution proposed by Dewey (1988), and including (1) lithospheric shortening and thickening concomitant with the creation of an orogenic plateau in the early Ottawan phase (ex: Jamieson et al., 2007, 2010, Rivers 2008, 2012, Hynes and Rivers, 2010) ; (2) broadening of the orogenic plateau and development of a network of conjugate strike-slip faults associated with lateral tectonic extrusion and orogenic collapse in the mid to late Ottawan and (3) NW propagation of the orogen and development of the Parautochthonous Belt during the Rigolet phase (1000 Ma – 980 Ma), with further thinning of the crust and a development of a horst and graben configuration in the orogenic hinterland (Rivers, 2012). The term ‘orogenic collapse’ is used here in a general sense (after Rivers 2012), as there is not consensus on the mechanism and timing of the ‘destructive’ phase of the Grenvillian orogeny. This mechanism would be some combination of decrease in strength of the middle crust below the plateau, with: end of convergence and gravitational spreading (ex. see Jamieson et al., 2010 and Vanderhaeghe 2012); and or removal of the thickened mantle lithosphere (Corrigan and Hanmer 1997) in an overall convergent setting. The Grenvillian-age plutonic rocks of the ESB can be attributed, and provide constraints, to specific stages in the orogenic evolution (Fig. 5.16).

5.6.3.1 Early-Ottawan magmatism

The 1086 ±2 Ma Bon-Désir granite bears similarities to the K-rich calc-alkalic granitoid-type (KCG) of Barbarin (1999). In the timeframe of the Grenvillian orogeny, the emplacement of this granite corresponds to the early Ottawan phase, associated with the development of an orogenic plateau in the core of the orogen. The positive εNd (+0.6) and Pinwarian-age T_{DM} (1517 Ma), and the magnesian signature of the Bon-Désir granite are consistent with melting of a Geon 15 juvenile (meta)igneous rock. Furthermore, the geochemistry of the Bon-Désir granite indicates that crust was probably formed in an arc environment (negative Nb–Ta anomalies). In this context of early continental collision (4 million years after the assumed beginning of the collision), the source of heat for this magmatic event could have been a mantle-derived magma associated with slab retreat or break-off (Fig. 5.16a). The Bon-Désir granite itself is highly evolved and shows no evidence of this mantle, but evidence of mafic underplating and SCLM melting is provided by the ca. 1080 Ma components of the CRUML (Château-Richer, St-Urbain, Mattawa and Labrieville) and Pipmuacan anorthositic massifs within the central Grenville Province, ca. 50 km west of the ESB (Hébert et al., 2009; Rivers et al., 2012).

5.6.3.2 Mid-Ottawan mantle-derived magmatism

The emplacement of the 1063 ±3 Ma Michaud plutonic suite is broadly coeval with motion along the sinistral strike-slip shear zone at the NW boundary of the ESB (Fig. 5.3). This boundary is subparallel to a major NE-striking transpressional shear-zone system in the central Grenville Province, known as the St-Fulgence deformation zone

which has been active at the same time during the Grenvillian orogeny (Fig. 5.1; Hébert et al., 2009 Hébert and Lacoste, 1998). Therefore, it is interpreted to be contemporaneous with the broadening of the plateau and the development of strike slip faults allowing lateral tectonic extrusion of crustal material (Rivers 2012). In addition, strong geochemical similarities between this suite and the younger 1045 ±3 Ma biotite-rich felsic sill suggest a broadly similar setting of formation for these two types of rocks, both of which are enriched in Ba and Sr.

It is now widely recognized that Ba–Sr enriched plutons are associated with subduction or subduction-modified source (arc-source or mantle-source; Corriveau and Morin, 2000; Liu et al., 2017), and attest to addition of fluids coming from the dehydrating slab and sediments into the mantle (Plank and Langmuir, 1998 and Fowler et al., 2008). The Grenville Province is built on southeastern Laurentia, which evolved from a long-lived active margin into a major continental collision zone, and this long history of subduction would have extensively impacted the mantle beneath it (Rivers and Corrigan, 2000; Rivers et al., 2012; Witmeyer and Karlstrom, 2007). From a more regional point of view, the ESB is inferred to represent remnants of a Pinwarian (1.46 – 1.52 Ga) oceanic island arc and back-arc accreted to Laurentia around 1.4 Ga (Groulier et al., 2018). The presence in the ESB of enriched potassic Grenvillian Ba–Sr mantle-derived igneous rocks such as the 1063 ±3 Ma Michaud plutonic suite and the 1045 ±3 Ma biotite-rich felsic sill is consistent with the presence of an enriched and metasomatized Geon 14 (T_{DM}=ca. 1.45-1.48 Ga) SCLM below the central Grenville Province. The within-plate geochemical signature of the Michaud plutonic suite and of the biotite-rich felsic sill is consistent with emplacement during an extensional event, such as orogenic collapse. In this context, the

melting of the enriched and metasomatized mantle can be attributed to thinning (ex. by convective removal or delamination) of the overthickened orogenic mantle lithosphere and rise of asthenospheric material, as proposed for the Grenville by Corrigan and Hanmer (1997). The induced upwelling of the asthenosphere would lead to the melting of the metasomatized SCLM and to the formation of Ba–Sr-enriched potassic magmas (Fig. 5.16b). We recognize that this model is highly speculative and relies heavily on the ferroan and A-type characteristics of the 1045 to 1063 Ma granitoids. It is possible that rather than a direct SCLM connection, melting of earlier underplated mafic crust formed at 1.48-1.52 is also possible. Nonetheless a new source of heat for melting is required 20-40 Ma after the formation of the Bon-Desir granite. This type of timing is consistent with delamination models for the formation of A-type magmas (Whalen et al., 1996).

Collectively, such rocks attest to protracted magmatism derived from enriched mantle, and emplaced in a within plate setting, at different parts of the Grenville, throughout the early to middle Ottawan. This type of magmatism may be compared to the potassic, ultrapotassic and shoshonitic magmatism and volcanism (latite and adakite) in the Tibetan plateau. This volcanism has occured sporadically since early stages of the collision (45 Ma), and is concentrated in orogen-perpendicular extension corridors contemporaneous with rapid uplift of the plateau (Liu et al., 2014). There is a possibility that the potassic to ultrapotassic alkaline event in the Grenville was associated with concomitant volcanism.

5.6.3.3 Rigolet crust-derived magmatism

The 983 ±5 Ma two-mica leucogranite stocks and their associated pegmatites (988 ±5 Ma) are peraluminous, consistent with crustal melting of deeper crustal levels during the Rigolet phase, and emplacement of the magmas in relatively shallow crustal levels. Peraluminous two-mica leucogranites are rare in the Grenville Province, perhaps due to limited preservation of the upper orogenic crust.

The leucogranites from the ESB (Saint-Onge synform) are synchronous with the growth of the 1001 ±3 Ma to 983 ±3 Ma titanite grains in a meta-dacitic tuff from the same synform indicating a connection between them. The later stages of the Grenvillian orogeny are inferred to represent advanced crustal thinning by extension, that ultimately led to an organization of the crust in a system of horst and graben (Basin and Range style; Rivers 2008). It is therefore conceivable that the juxtaposition of hot and weak middle-crust with colder and higher crustal levels via the reactivation of pre-existing and newly formed faults coupled to asthenosphere upwelling would lead to heat transmission and partial melting at the base of the low-*P* Belt. The peraluminous magma formed would rise in the crust and would contribute to heat the overlying crust (Fig. 5.16c).

The leucogranite and pegmatite bodies display evidence of deformation by D2, suggesting that the main structural configuration of the ESB was achieved during the Rigolet period. This configuration in domes and basins, with steep axial planes is characteristic of the suprastructure of the orogen, and contrasts with that of the middle orogenic crust which is characterized by older, sub-horizontal structures linked to ductile flow (Rivers 2008).

It is worth noting that the Rigolet-age magmatism and deformation in the low-*P* ESB is coeval with within-plate and alkaline-dominated late- to post-tectonic magmatism (Fig. 5.17c) in the mid-*P* Belt of the central-eastern Grenville, as for instance the 993 ±3 Ma La Galissonière felsic plutonic suite (Bourne, 1991) and the 988–985 Ma Grandes Pointes alkaline plutonic Suite (Hébert et al. 2009). This type of magmatism is mantle-derived and continued intermittently until ca. 957 Ma (ex the nepheline-syenite and carbonatite Crevier alkaline complex in the central Grenville Province; Groulier et al., 2018).

5.6.3.4 Tectonic plate organization

The model of slab break off invoked for the generation of the Bon-Désir granite, only makes sense if the final subduction was under Laurentia, *e,g,* if Laurentia was the upper plate during the Grenvillian collision with Amazonia. This is also consistent with the overall architecture of the Grenville Province, when compared to the modern Himalayas-Tibet orogen. However, it is the opposite of the current interpretation, which is mainly based on the deep burial during the orogeny of the crust currently exposed in the Grenville Province (see Hynes and Rivers 2010).

We would argue that the high-grade metamorphism does not represent a proof of Laurentia being subducted below Amazonia as it is still possible to have such conditions in the upper plate. For instance, numerous studies have demonstrated that the double-thickness crust in Tibet, which is part of the Upper Plate in the Eurasia-India collision, is experiencing partial melting and emplacement of syn-orogenic igneous rocks, including potassic to ultrapotassic volcanic and intrusive rocks (Pham et al., 1986; Hacker et al.,

2014; Liu et al. 2017). Therefore, deeper levels of the Tibetan crust may be equivalent of the high to Mid-*P* Belts of the Grenville Province.

The southeastern Laurentian margin was the site of a long-lived active subduction zone before the final continental collision (Whitmeyer and Karlstrom, 2007; Rivers et al., 2012; Rivers and Corrigan, 2000) that led to the outboard formation from the Superior craton nucleus (with thick and cold SCLM root) of Paleoproterozoic and Mesoproterozoic arc belts with thinner and subduction-modified and metasomatized SCLM. These belts experienced anomalous heat conditions resulting in the development of hot and weak lithosphere, prone to deformation and compression, as it became pinched between the two strong and cold cratons of Laurentia and Amazonia during the Grenvillian continental collision. This ultimately led to the propagation of the orogeny toward the interior of Laurentia and of the Superior Province. The model proposed in this paper best fits the observations made in the central Grenville Province.

5.6.3.5 Conclusion

The ESB in the central Grenville Province, represents higher levels of the infrastructure of a large hot orogen, exposed in a broadly dome and basin pattern, and intruded by diverse synorogenic plutonic bodies. These provide record of one hundred million years of tectono-magmatic evolution, covering the entire range of the Grenvillian orogeny, and include:

(1) early Ottawan-age, crust-derived plutons (Bon-Désir granite) potentially linked to slab breakoff (or retreat), at the onset of continental collision, to

(2) mid-Ottawan-age plutons, dykes and sills (Michaud suite and biotite-rich felsic sill) derived from enriched and metasomatized mantle sources in a context of lithospheric thinning and orogenic collapse predating by a few million years the regional amphibolite-facies metamorphism in the ESB, and to:

(3) Rigolet-age leucogranite stocks and pegmatites of crustal origin, with associated thermal overprint in the country rocks manifested by titanite growth, and deformation in the ESB.

The new data highlight the active role of the mantle throughout the Ottawan phase of the Grenvillian orogeny, and suggest a plate organization for the Grenvillian collision with Laurentia as the upper plate.

5.7 Acknowledgements

This contribution is part of the PhD of the first author and was funded by the Ministère de l'Énergie et des Ressources naturelles of Quebec (contribution number 8449-2017-2018-01) and by Natural Sciences Engineering Research Council of Canada (NSERC) Discovery grant (200386) to the second author. The samples were collected by the first author during three field seasons (2013, 2014 and 2015). The authors would like to thank Sherri Strong for Sm-Nd analyses, Amanda Langille for the CL images, Pamela King for sample preparation and technical work in the U-Pb lab, Dr. David Grant and Dylan Goudie for their assistance during the use of the SEM-MLA, Dr. Lyal Harris for his help interpreting the structure, Dr. François Turlin and Evelyne Sunatori for their assistance in the field. The authors are also grateful to Dr. Charles F. Gower and an

anonymous reviewer for their detailed reviews that led to a significant improvement of the paper, and to Dr. Nelson Eby for editorial handling.

5.8 References

Augland, L.E., Moukhsil, A., Solgadi, F., Indares, A., 2015. Pinwarian to Grenvillian magmatic evolution in the central Grenville Province: new constraints from ID-TIMS U-Pb ages and coupled Lu-Hf S-MC-ICP-MS data. Canadian Journal of Earth Sciences, volume 52, 1–21. doi:10.1139/cjes-2014-0232

Ballouard, C., Poujol, M., Boulvais, P., Zeh, A., 2017. Crustal recycling and juvenile addition during lithospheric wrenching : the Pontivy-Rostrenen magmatic complex, Armorican Massif (France), Variscan belt. Gondwana Research, volume 49, 222–247. doi:10.1016/j.gr.2017.06.002

Barbarin, B., 1999. A review of the relationships between granitoid types, their origins and their geodynamic environments. Lithos, volume 46, 605–626. doi:10.1016/S0024-4937(98)00085-1

Beaumont, C., Jamieson, R., Nguyen, M., 2010. Models of large, hot orogens containing a collage of reworked and accreted terranes. Canadian Journal of Earth Sciences, volume 47, 485–515. doi:10.1139/E10-002

Bonin, B., 2007. A-type granites and related rocks: Evolution of a concept, problems and prospects. Lithos, volume 97, 1–29. doi:10.1016/j.lithos.2006.12.007

Bourne, J., 1991. The geochemistry of the La Galissonniere Pluton: a Middle Proterozoic late-orogenic intrusion from the eastern Grenville Province, Quebec. Canadian Journal of Earth Sciences, volume 28, 37–43.

Cawood, P.A., Strachan, R.A., Pisarevsky, S.A., Gladkochub, D.P., Murphy, J.B., 2016. Linking collisional and accretionary orogens during Rodinia assembly and breakup: Implications for models of supercontinent cycles. Earth and Planetary Science Letters, volume 449, 118–126. doi:10.1016/j.epsl.2016.05.049

Černý, P., Ercit, T.S., 2005. The classification of granitic pegmatites revisited. Canadian Mineralogist, volume 43, 2005–2026. doi:10.2113/gscanmin.43.6.2005

Chen, B., Xiaoping, L., Wilde, S.A., Yuan, C., Wang, Q., Xia, X., Zhang, Z., 2017. Delamination of lithospheric mantle evidenced by Cenozoic potassic rocks in Yunnan, SW China: a contribution to uplift of the Eastern Tibetan Plateau. Lithos, volume 284-285, 709–729.

Corrigan, D., Hanmer, S., 1997. Anorthosites and related granitoids in the Grenville Orogen: a product of convective thinning of the lithosphere? Geology, volume 25, 61–64. doi:10.1130/0091-7613(1997)025<0061:AARGIT>2.3.CO;2

Corriveau, L., Heaman, L.M., Marcantonio, F., and van Breemen, O., 1990. 1.1 Ga K-rich alkaline plutonism in the SW Grenville Province. Contribution to Mineralogy and Petrology, volume 105, 473–485.

Corriveau, L., Morin, D., 2000. Modelling 3D architecture of western Grenville from surface geology, xenoliths, styles of magma emplacement, and Lithoprobe reflectors. Canadian Journal of Earth Sciences, volume 37, 235–251. doi:10.1139/e99-121

Culshaw, N.G., Beaumont, C., Jamieson, R.A., 2006. The orogenic superstructure-infrastructure concept: revisited, quantified, and revived. Geology, volume 34, 733–736.

Cuney, M., Kyser, K., 2009. Chapter 7: Hydrothermal Uranium Deposits Related to Igneous Rocks. Mineralogical Association of Canada.

Debon, F., and Le Fort, P. 1988. A cationic classification of common plutonic rocks and magmatic associations: principles, method, applications. Bulletin de Minéralogie, volume 111, 493–510.

De Paolo, D. J. 1988. Neodymium isotope geochemistry. Springer-Verlag. 187 p.

Dewey, J.F., 1988. Extensional collapse of orogens. Tectonics, volume 7 (6), 1123–1139.

Dickin, A.P., Higgins, M.D., 1992. Sm /Nd evidence for a major 1.5 Ga crust-forming event in the central Grenville Province. Geology, volume 20, 137–140.

Dickin, A.P., 2000. Crustal formation in the Grenville Province: Nd-isotope evidence. Canadian Journal of Earth Sciences, volume 37, 165–181.

Dunning, G., Indares, A., 2010. New insights on the 1.7–1.0Ga crustal evolution of the central Grenville Province from the Manicouagan – Baie Comeau transect. Precambrian Research, volume 180, 204–226. doi:10.1016/j.precamres.2010.04.005

Fowler, M.B., Kocks, H., Darbyshire, D.P.F., Greenwood, P.B., 2008. Petrogenesis of high Ba-Sr plutons from the Northern Highlands Terrane of the British Caledonian Province. Lithos, volume 105, 129–148. doi:10.1016/j.lithos.2008.03.003

Frost, B.R., Barnes, C.G., Collins, W.J., Arculus, R.J., Ellis, D.J., Frost, C.D., 2001. A Geochemical Classification for Granitic Rocks. Journal of Petrology, volume 42, 2033–2048. doi:10.1093/petrology/42.11.2033

Frost, B.R., Frost, C.D., 2008. A geochemical classification for feldspathic igneous rocks. Journal of Petrology, volume 49, 1955–1969. doi:10.1093/petrology/egn054

Frost, C.D., Frost, B.R., 2011. On ferroan (A-type) granitoids: Their compositional variability and modes of origin. Journal of Petrology, volume 52, 39–53. doi:10.1093/petrology/egq070

Ginsburg, A.I., 1984. The geological condition of the location and the formation of granitic pegmatites. International Geological Congress, 27th, Proceedings 15, 245–260.

Gower, C.F., Heaman, L.M., Loveridge, W.D., Schärer, U., and Tucker, R.D., 1991. Grenvillian granitoid plutonism in the eastern Grenville Province. Precambrian Research, volume 51, 315–336.

Gower, C.F., Krogh, T.E., 2002. A U–Pb geochronological review of the Proterozoic history of the eastern Grenville Province. Canadian Journal of Earth Sciences, volume 39, 795–829. doi:10.1139/e01-090

Groulier, P.-A., Indares, A.D., Dunning, G., Mouhksil, A., and Wälle, M., 2018. Peri-Laurentian, Pinwarian-age oceanic arc crust preserved in the Grenville Province: insights from the Escoumins Supracrustal Belt. Precambrian Research, volume 311, 37–64. https://doi.org/10.1016/j.precamres.2018.04.001

Hébert, C., and Lacoste, P., 1998. Géologie de la région de Bagotville (SNRC 22D/07). RG 97-06, Ministère des ressources naturelles et de la faune, Gouvernement du Québec.

Hébert, C. and van Breemen, O. 2004. Mesoproterozoic basement of the Lac St. Jean anorthosite suite and younger Grenvillian intrusions in the Saguenay region, Québec: Structural relationships and U-Pb geochronology. In Proterozoic Tectonic Evolution of the Grenville Orogen in North America. Edited by R.P. Tollo, L.,

Corriveau, J. McLelland, and M.J. Bartholomew. Geological Society of America, Memoir 197, 65–79.

Hébert, C., van Breemen, O., and Cadieux, A-M. 2009. Région du reservoir Pipmuacan (SNRC 22E): Synthèse géologique. RG 2009-01, Ministère des ressources naturelles et de la faune, Gouvernement du Québec.

Higgins, M.D., van Breemen, O., 1996. Three generations of AMCG magmatism, contact metamorphism and tectonism in the Saguenay – Lac-Saint-Jean region, Grenville Province, Canada. Precambrian Research, volume 79 (3-4), 327–346.

Hynes, A., and Rivers, T., 2010. Protracted continental collision – evidence from the Grenville Orogen. Canadian Journal of Earth Sciences, volume 47, 591–620.

Indares, A., Moukhsil, A., 2013. Geon 12 crustal extension in the central Grenville Province, implications for the orogenic architecture, and potential influence on the emplacement of anorthosites. Canadian Journal of Earth Sciences, volume 50, 955–966. doi:10.1139/cjes-2012-0161

Jamieson, R. A., Beaumont, C., Nguyen, M. H., and Culshaw, N. G. 2007. Synconvergent ductile flow in variable strength continental crust: numerical models with application to the western Grenville Province. Tectonics, 26: TC5005, doi: 10.1029/ 2006TC002036.

Jamieson, R.A., Beaumont, C., Warren, C.J., and Nguyen, M.H. 2010. The Grenville Orogen explained? Applications and limitations of integrating numerical models with geological and geophysical data. Canadian Journal of Earth Sciences, volume 47, 517–539.

Jenner, G.A. 1996. Trace element geochemistry of igneous rocks: geochemical

nomenclature and analytical geochemistry. In Trace Element Geochemistry of Volcanic Rocks. Edited by D.A. Wyman. Geological Association of Canada, Short Course Notes 12, 51–77.

Li, Z.X., Bogdanova, S. V, Collins, A.S., Davidson, A., De Waele, B., Ernst, R.E., Fitzsimons, I.C.W., Fuck, R.A., Gladkochub, D.P., Jacobs, J., Karlstrom, K.E., Lu, S., Natapov, L.M., Pease, V., Pisarevsky, S.A., Thrane, K., Vernikovsky, V., 2008. Assembly, configuration, and break-up history of Rodinia: A synthesis. Precambrian Research, volume 160, 179–210. doi:10.1016/j.precamres.2007.04.021

Liu, D., Zhao, Z., Zhu, D.C., Niu, Y., DePaolo, D.J., Harrison, T.M., Mo, X., Dong, G., Zhou, S., Sun, C., Zhang, Z., Liu, J., 2014. Postcollisional potassic and ultrapotassic rocks in southern Tibet: Mantle and crustal origins in response to India-Asia collision and convergence. Geochimica et Cosmochimica Acta, volume 143, 207–231. doi:10.1016/j.gca.2014.03.031

Liu, Z., Liao, S.-Y., Wang, J.-R., Ma, Z., Liu, Y.-X., Wang, D.-B., Tang, Y., Yang, J., 2017. Petrogenesis of late Eocene Ba-Sr potassic rocks from Western Yangtze Block, SE Tibet : a magmatic response to the Indo-Asian collision. Journal of Asian Earth Sciences, volume 135, 95–109.

London, D., 2008. Pegmatites. Canadian Mineralogist Special Publication 10, 368p.

Maniar, P.D., Piccoli, P.M., 1989. Tectonic discrimination of granitoids. Geological Society of America Bulletin doi:10.1130/0016-7606(1989)101<0635:TDOG>2.3.CO

Moukhsil, A., Clark, T., Hébert, C., and Labbé, J.-Y., 2009. Géologie de la région de

Baie-Comeau – Labrieville (feuillets SNRC 22F01, 22F02, 22F03, 22F04, 22F05 et 22F06). RP 2009-01, Ministère des ressources naturelles et de la faune, Gouvernement du Québec.

Owen, J.V. and Erdmer, P. 1990. Middle Proterozoic geology of the Long Range Inlier, Newfoundland: Regional significance and tectonic implications. In Mid-Proterozoic Laurentia-Baltica. Edited by C.F. Gower, T. Rivers, and A.B. Ryan. Geological Association of Canada, Special Paper 38, 215–231.

Owens, B.E., Tomascak, P.B., 2002. Mesoproterozoic lamprophyres in the Labrieville Massif, Quebec: clues to the origin of alkalic anorthosites? Canadian Journal of Earth Sciences, volume 39, 983–997. doi:https://doi-org.qe2a-proxy.mun.ca/10.1139/e02-010

Pearce, J.A., Harris, B.W., Tindle, A.G., 1984. Trace element discrimination diagrams for the tectonic interpretation of granitic rocks. Journal of Petrology, volume 25 (4), 956–983.

Peccerillo, A., Taylor, S.R., 1976. Rare earth elements in East Carpathian volcanic rocks. Earth and Planetary Science Letters, volume 32, 121–126. doi:10.1016/0012-821X(76)90050-9

Plank, T., Langmuir, C.H., 1998. The chemical composition of subducting sediment and its consequences for the crust and mantle. Chemical Geology, volume 145, 325–394. doi:10.1016/S0009-2541(97)00150-2

Raczek, I., Jochum, K.P., Hofmann, A.W., 2003. Neodynium and Strontium Isotope Data for USGS Reference Materials BCR-1, BCR-2, BHVO-1, BHVO-2, AGV-1, AGV-2, GSP-1, GSP-2 and Eight MPI-DING Reference. Geostandards and

Geoanalytical Research, volume 27 (2), 173–179.

Rivers, T., 2012. Upper-crustal orogenic lid and mid-crustal core complexes: signature of a collapsed orogenic plateau in the hinterland of the Grenville Province. Canadian Journal of Earth Sciences, volume 49, 1–42.

Rivers, T., 2008. Assembly and preservation of lower, mid, and upper orogenic crust in the Grenville Province-Implications for the evolution of large hot long-duration orogens. Precambrian Research, volume 167, 237–259. doi:10.1016/j.precamres.2008.08.005

Rivers, T., 1997. Lithotectonic elements of the Grenville Province: review and tectonic implications. Precambrian Research, volume 86, 117–154. doi:10.1016/S0301-9268(97)00038-7

Rivers, T., Martignole, J., Gower., C.F., and Davidson, A. 1989. New tectonic divisions of the Grenville Province, southeast Canadian Shield. Tectonics, 8: 63–84.

Rivers, T., Corrigan, D., 2000. Convergent margin on southeastern Laurentia during the Mesoproterozoic : tectonic implications. Canadian Journal of Earth Sciences, volume 37, 359–383.

Rivers, T., Culshaw, N., Hynes, A., Indares, A., Jamieson, R., Martignole, J., 2012. The Grenville. Orogen — A post-LITHOPROBE perspective. Chapter 3, Tectonic Styles in Canada: The LITHOPROBE Perspective. Edited by J.A. Percival, F.A. Cook, and R.M. Clowes. Geological Association of Canada, Special Paper 49.

Rondot, J., 1986. Géologie de la région de Forestville-Les Escoumins, Ministère de l'Énergie et des Ressources naturelles, Québec ; ET 85-05, 47 p.

Sun, S.S., McDonough, W.F., 1989. Chemical and isotopic systematics of oceanic

basalts: Implications for mantle composition and processes, in Magmatism in the Ocean Basins, in: A.D. Saunders and M.J. Norry (Eds.). Geological Society of London, Special Publication No. 42, 313–345.

Tanaka, T., Togashi, S., Kamioka, H., Amakawa, H., Kagami, H., Hamamoto, T., Yuhara, M., Orihashi, Y., Yoneda, S., Shimizu, H., Kunimaru, T., Takahashi, K., Yanagi, T., Nakano, T., Fujimaki, H., Shinjo, R., Asahara, Y., Tanimizu, M., Dragusanu, C., 2000. JNdi-1: A neodymium isotopic reference in consistency with LaJolla neodymium. Chemical Geology, volume 168, 279–281. doi:10.1016/S0009-2541(00)00198-4

Turlin, F., André-Mayer, A.-S., Moukhsil, A., Vanderhaeghe, O., Gervais, F., Solgadi, F., Groulier, P.-A., Poujol, M., 2017. Unusual LREE-rich, peraluminous, monazite- or allanite-bearing pegmatitic granite in the central Grenville Province, Québec. Ore Geology Reviews, volume 89, 627–667.

Turlin, F., 2017. Les granites pegmatitiques enrichis en éléments de terres rares légères marqueurs des processus de croissance et de différenciation crustale : Exemple de la Province Protérozoïque de Grenville, Québec. PhD thesis, Université de Lorraine, France, 448 p.

Valverde Cardenas, C., Indares, A., Jenner, G., 2012. Mafic and ultrapotassic rocks from the Canyon domain (central Grenville Province): geochemistry and tectonic implications. Canadian Journal of Earth Sciences, volume 49, 412–433. doi:10.1139/e11-065

Vanderhaeghe, O, 2012. The thermal–mechanical evolution of crustal orogenic belts at convergence plate boundaries: a reappraisal of the orogenic cycle. Journal of

Geodynamics, volume 56–57, 124–145.

Whalen, J.B., Currie, K.L., Chappell, B.W., 1987. A-type granites: geochemical characteristics, discrimination and petrogenesis. Contribution to Mineralogy and Petrology, volume 95, 407–419. doi:10.1007/BF00402202

Whalen, J., Jenner, G.A., Longstaffe, F.J., Robert, F. and Gariepy, C., 1996. Geochemical and isotopic (O, Nd, Pb, Sr) constraints on A-type granite petrogenesis based on the Topsails Igneous Suite, Newfoundland Appalachians. Journal of Petrology, volume 37, 1463–1489.

Whitmeyer, S.J., Karlstrom, K.E., 2007. Tectonic model for the Proterozoic growth of North America. Geosphere, volume 3(4), 220–259.

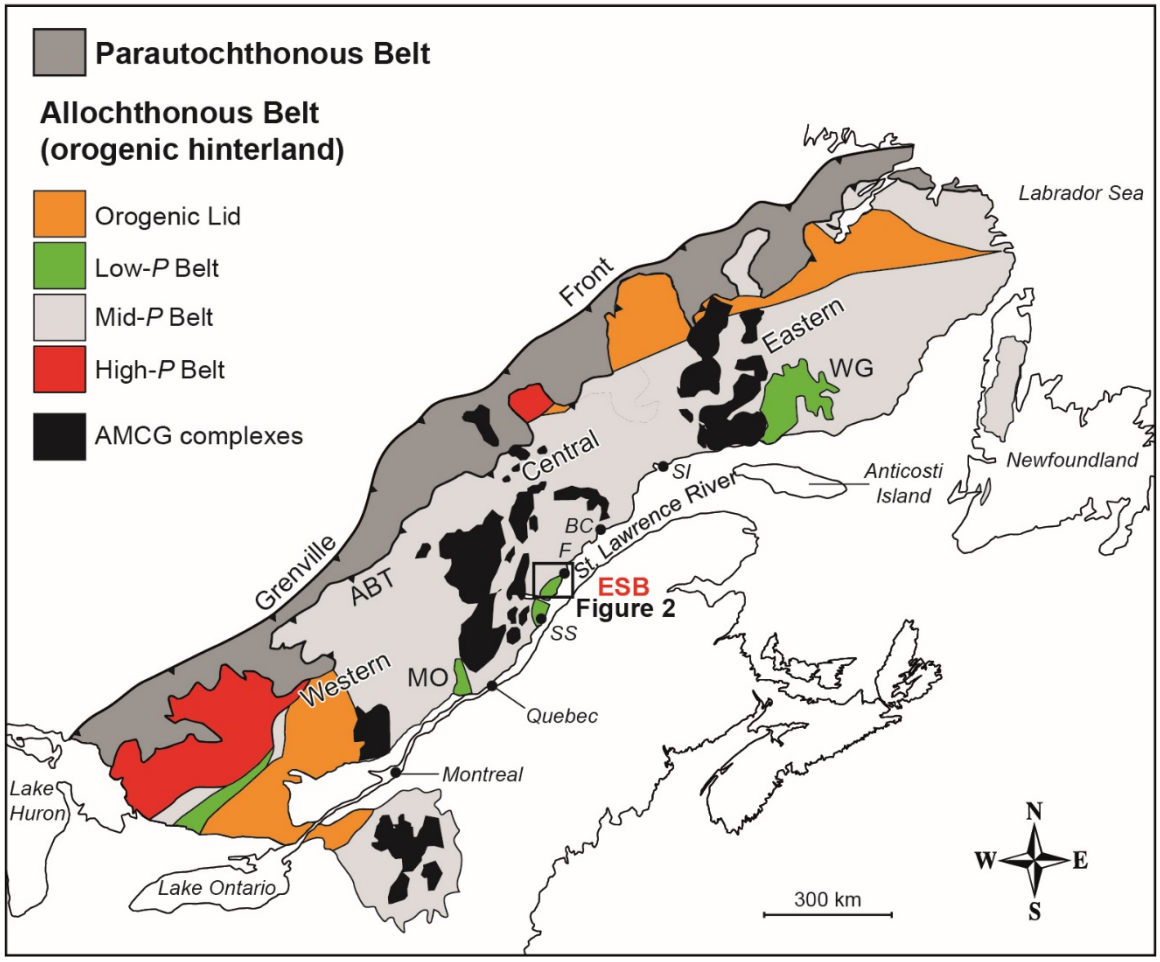

Figure 0.1: Tectono-metamorphic map of the Grenville Province in Canada (modified from Rivers et al., 2012) presenting the location of the different metamorphic belts and of the anorthositic massifs. Area of Escoumins supracrustal belt shown by box.

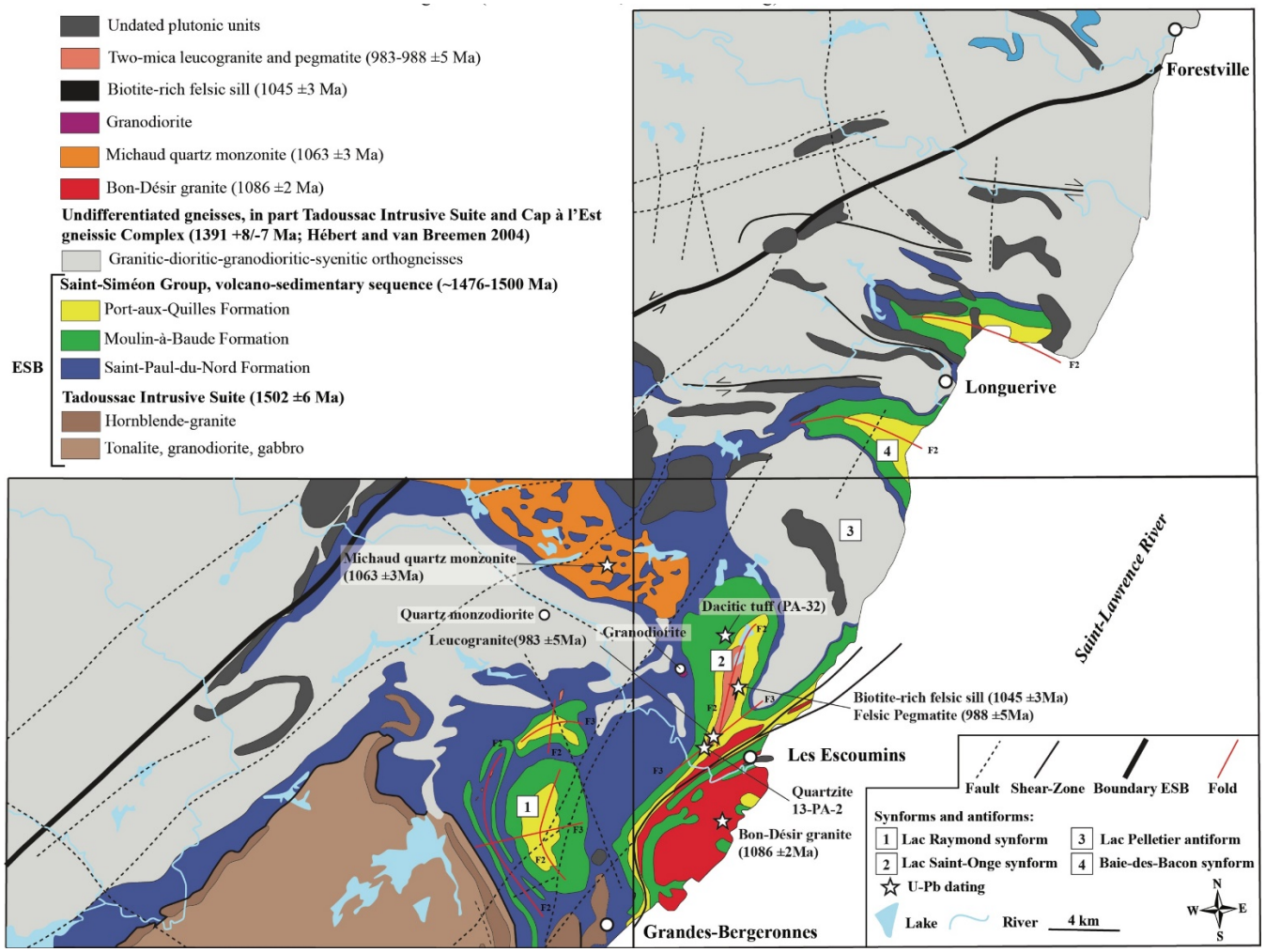

Figure 0.2: Geological map of the Escoumins supracrustal belt (ESB) updated from Groulier et al. (2016).

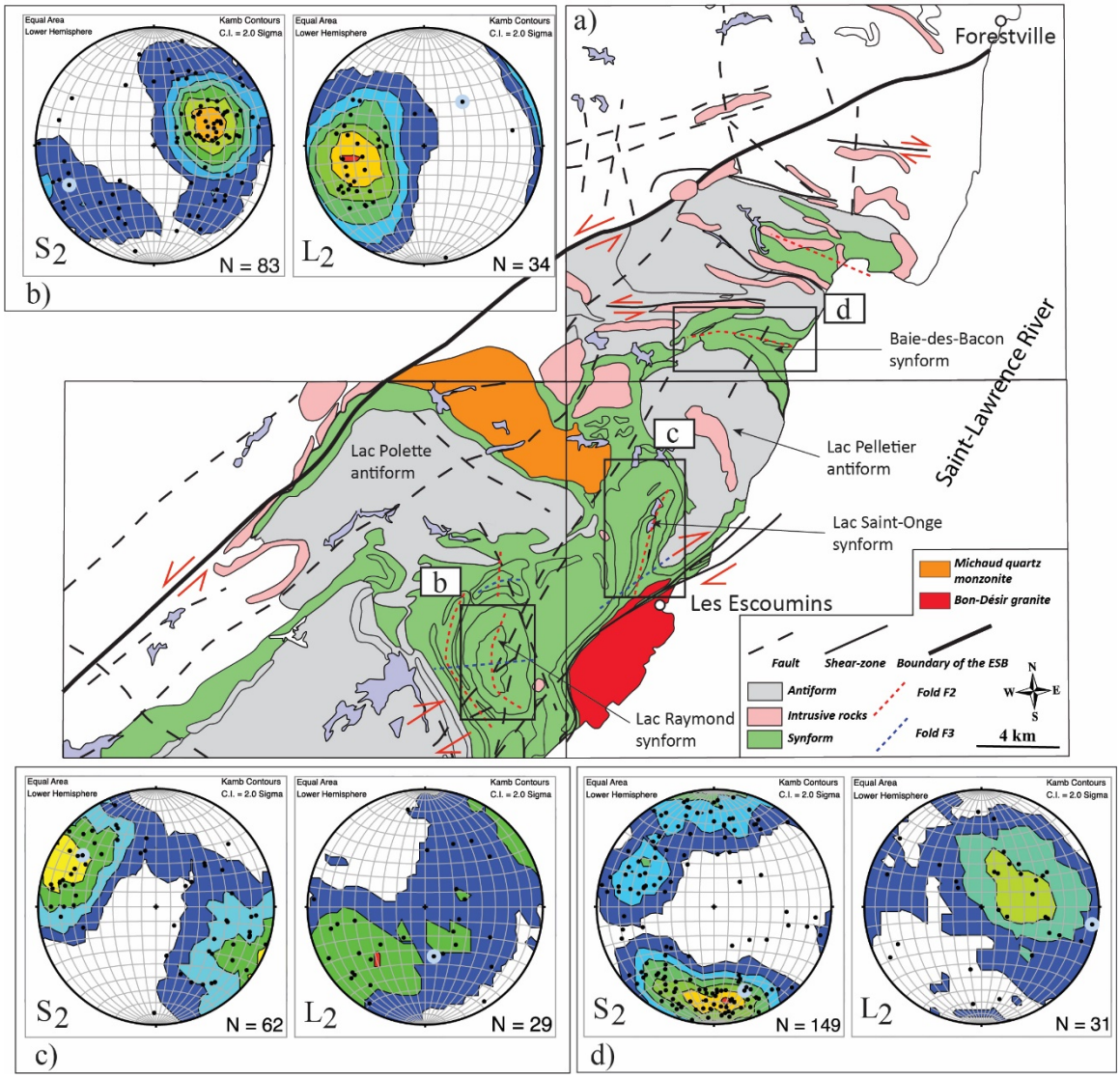

Figure 0.3: a) Interpreted structural map of the ESB from aeromagnetic survey map; **b-c-d)** stereonets of the planar (schistosity, on the left) and linear structures (right) for the three different synforms.

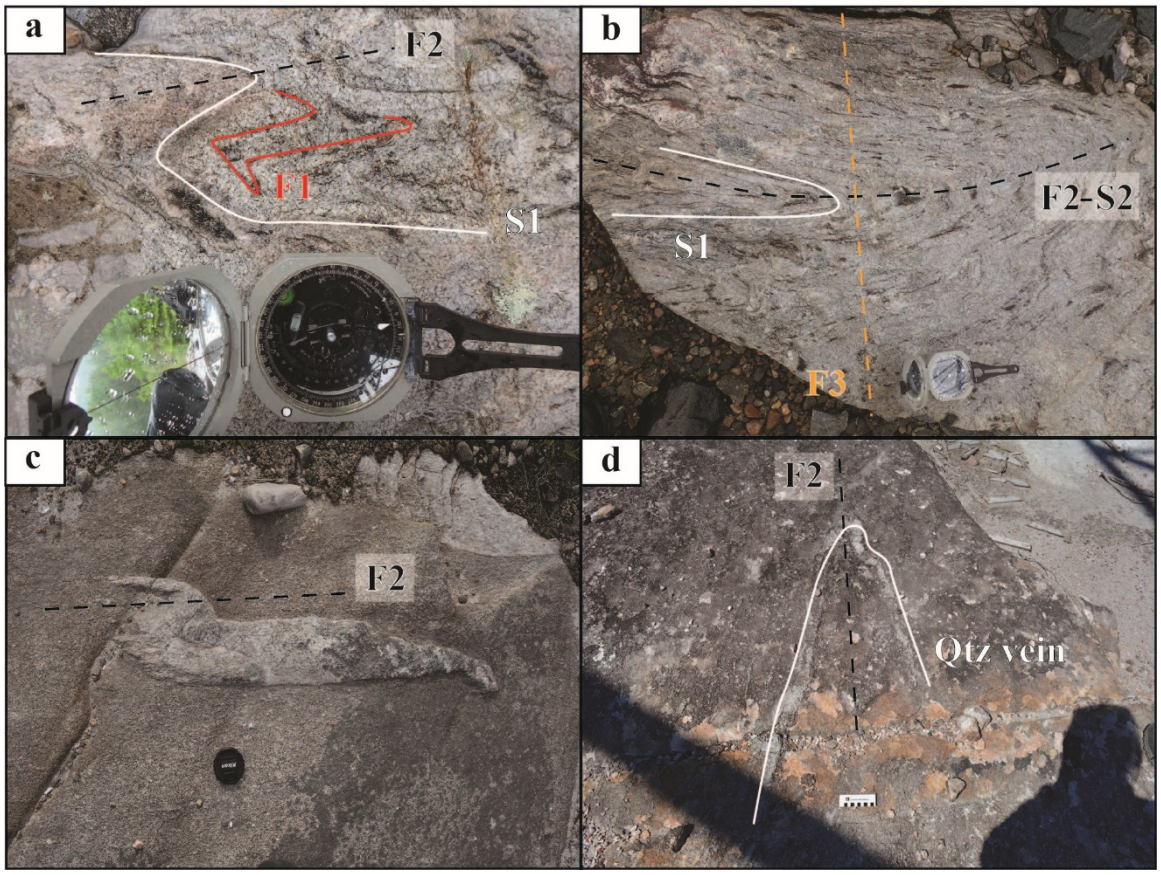

Figure 0.4: Field photographs of: **a)** F2 folds folding S1 schistosity and F1 fold in a rhyolite; **b)** three deformations events are represented in this photograph with an early schistosity S1 isoclinaly folded by a F2 fold which is associated with a S2 schistosity. S2 and F2 are folded by an open fold F3; **c)** quartz vein folded by F2 folds within the biotite-rich felsic sill (PA-88a), the main schistosity in the sill is parallel to the planar axis of these folds and **d)** Isoclinal F2 fold within the leucogranite marked by the presence of a quartz vein.

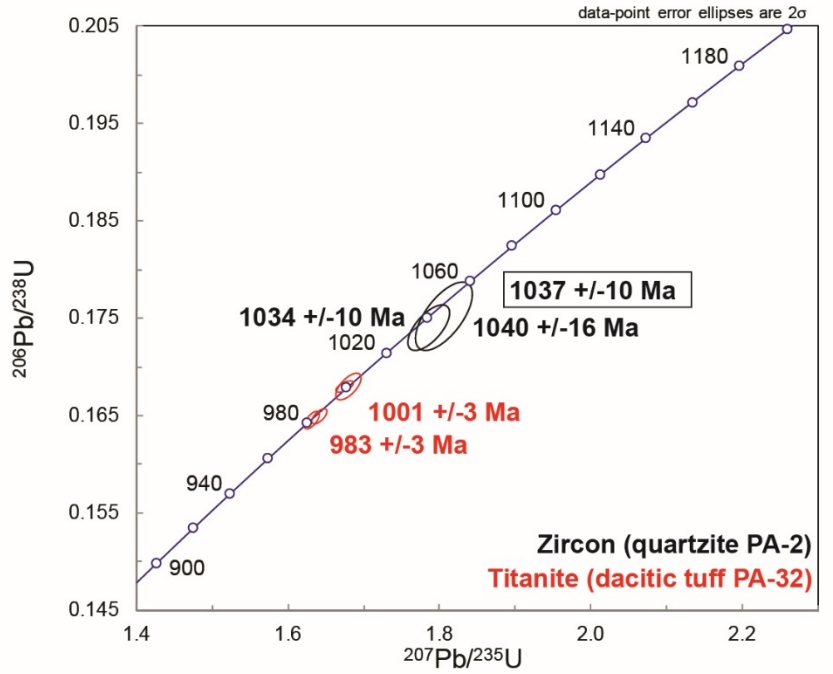

Figure 0.5: Concordia diagram U–Pb on zircon grains analysed by LA-ICP-MS (metamorphic overgrowths from detrital grains of a quartzite, PA-2) and titanite grains analysed by TIMS (from a dacitic ignimbrite, PA-32). Both rocks were sampled in the Saint-Onge synform.

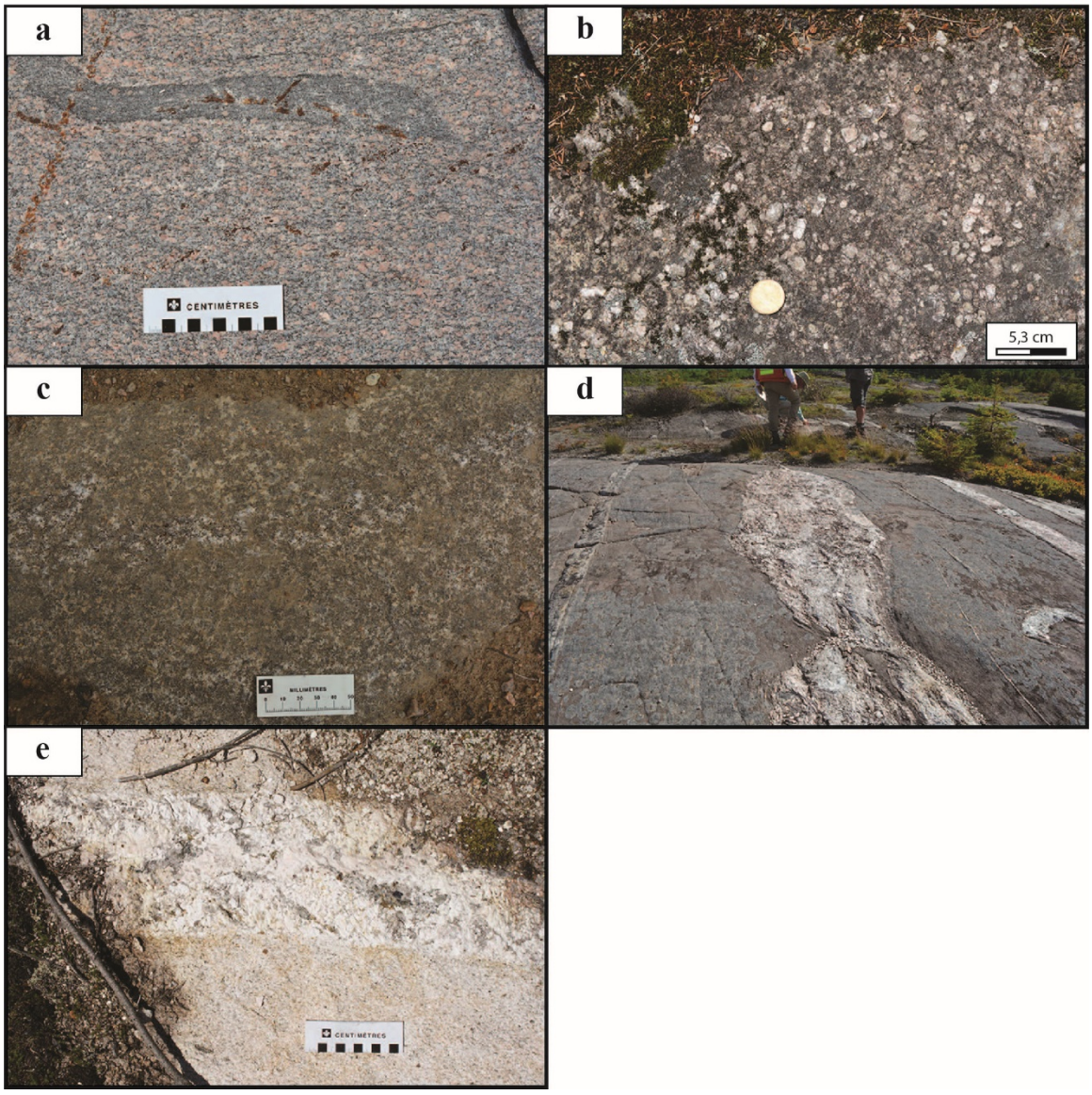

Figure 0.6: Outcrop photos of: **a)** Bon-Désir granite with mafic patch; **b)** Michaud quartz monzonite; **c)** granodiorite; **d)** biotite-rich fesic sill with felsic pegmatite and quartz veins; and **e)** two-mica leucogranite cross-cut by a muscovite –tourmaline and garnet-bearing pegmatite.

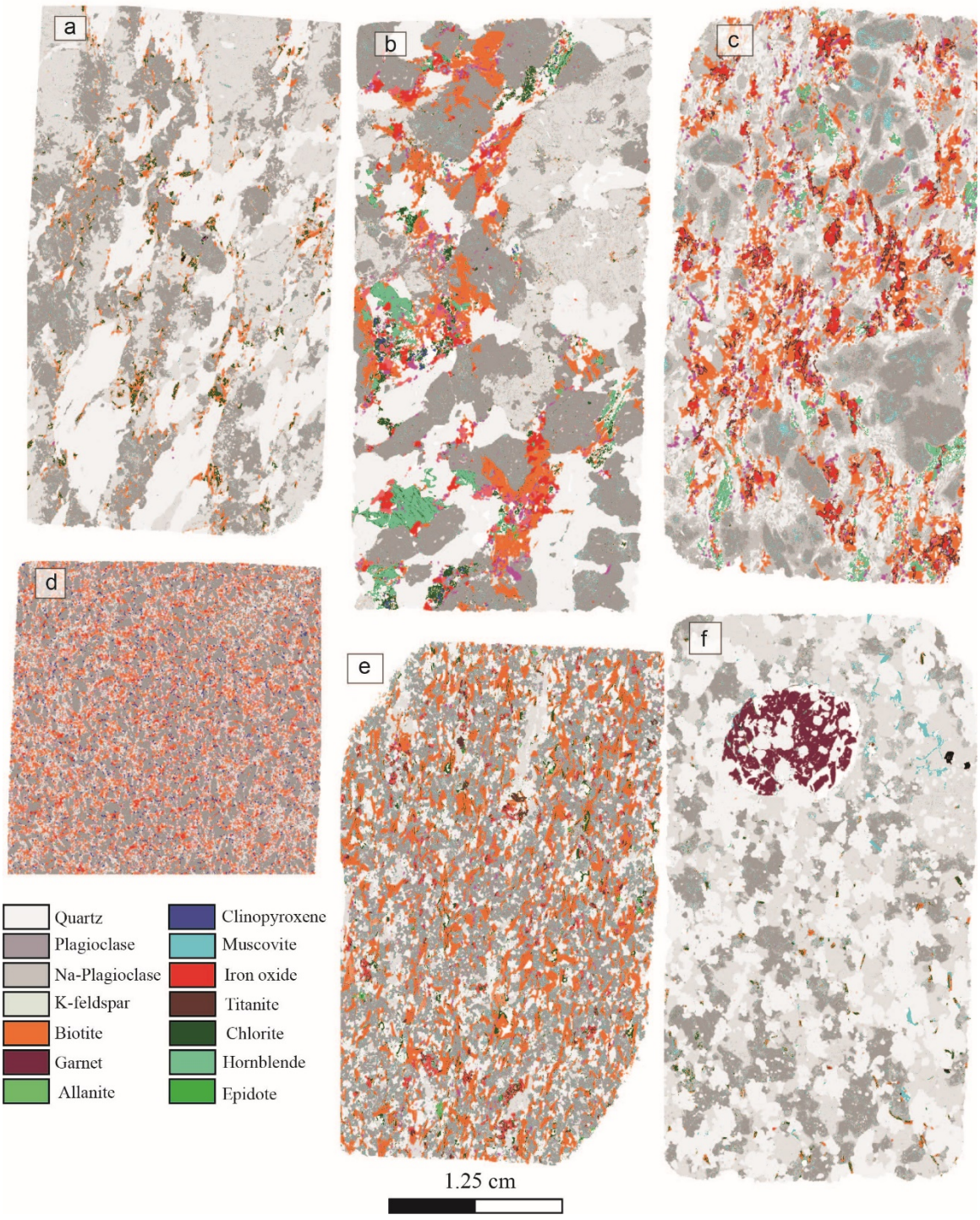

Figure 0.7: SEM–MLA false colour mineral maps of thin section showing the distribution of minerals for: **a)** Bon-Désir granite; **b)** Michaud quartz monzonite; **c)** granodiorite; **d)** quartz monzodiorite; **e)** biotite-rich felsic sill; and **f)** two-mica leucogranite.

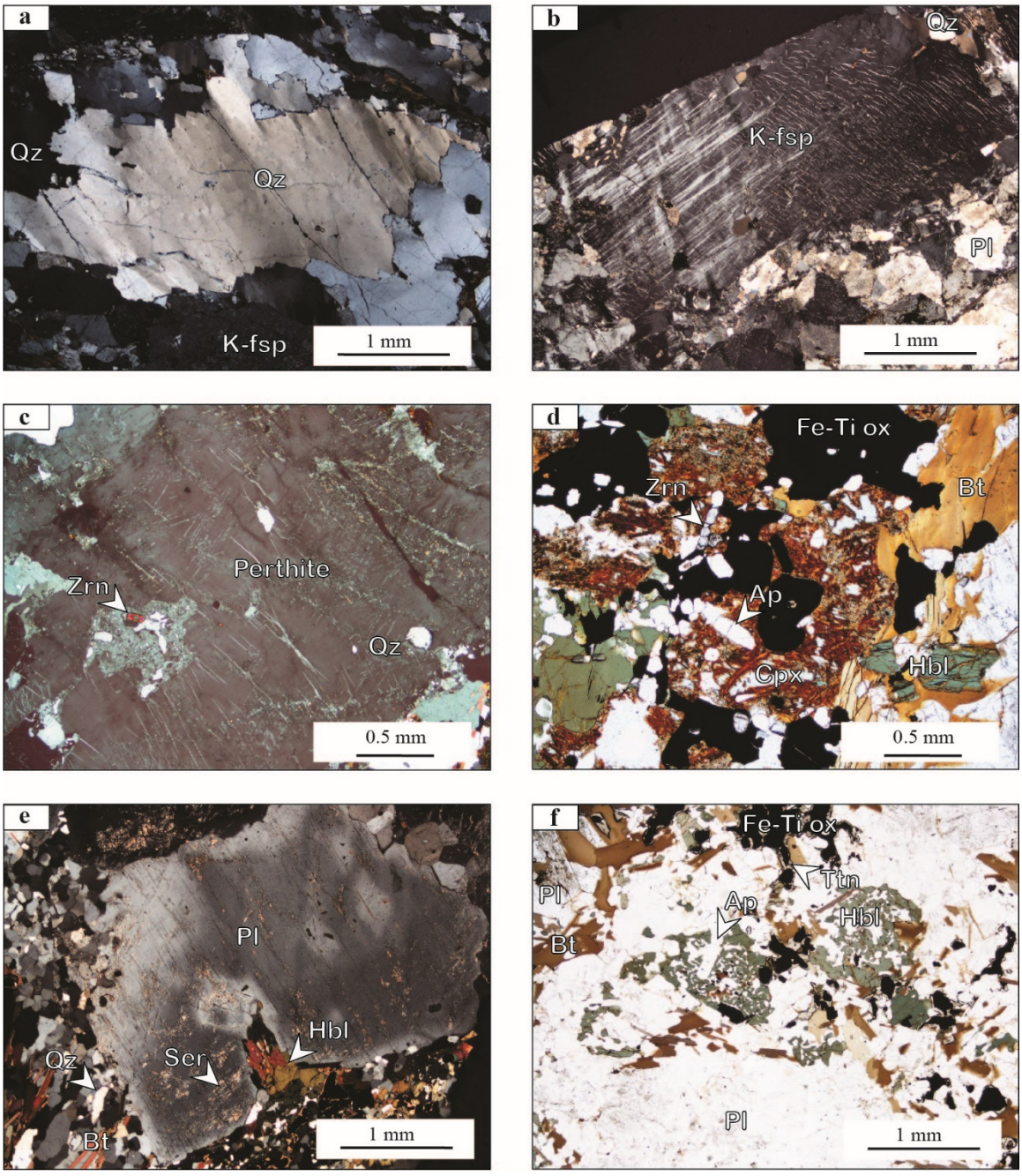

Figure 0.8: Photomicrographs of characteristic textures: **a)** deformed quartz (cross-polarized light, CPL), Bon-Désir granite; **b)** K-feldspar (perthite) megacryst in a recrystallized groundmass (CPL), Bon-Désir granite; **c)** K-feldspar megacrysts (perthite) with inclusion of quartz and zircon (CPL), Michaud quartz monzonite; **d)** a mass of trace minerals (apatite, zircon, Fe–Ti oxides) associated with relict clinopyroxene, hornblende and biotite (LPNA), Michaud quartz monzonite; **e)** zoned plagioclase (CPL) in the granodiorite stock; **f)** cluster of ferromagnesian minerals (hornblende, biotite, Fe-Ti oxides, titanite) associated with apatite (plane polarized light, PPL), granodiorite stock.

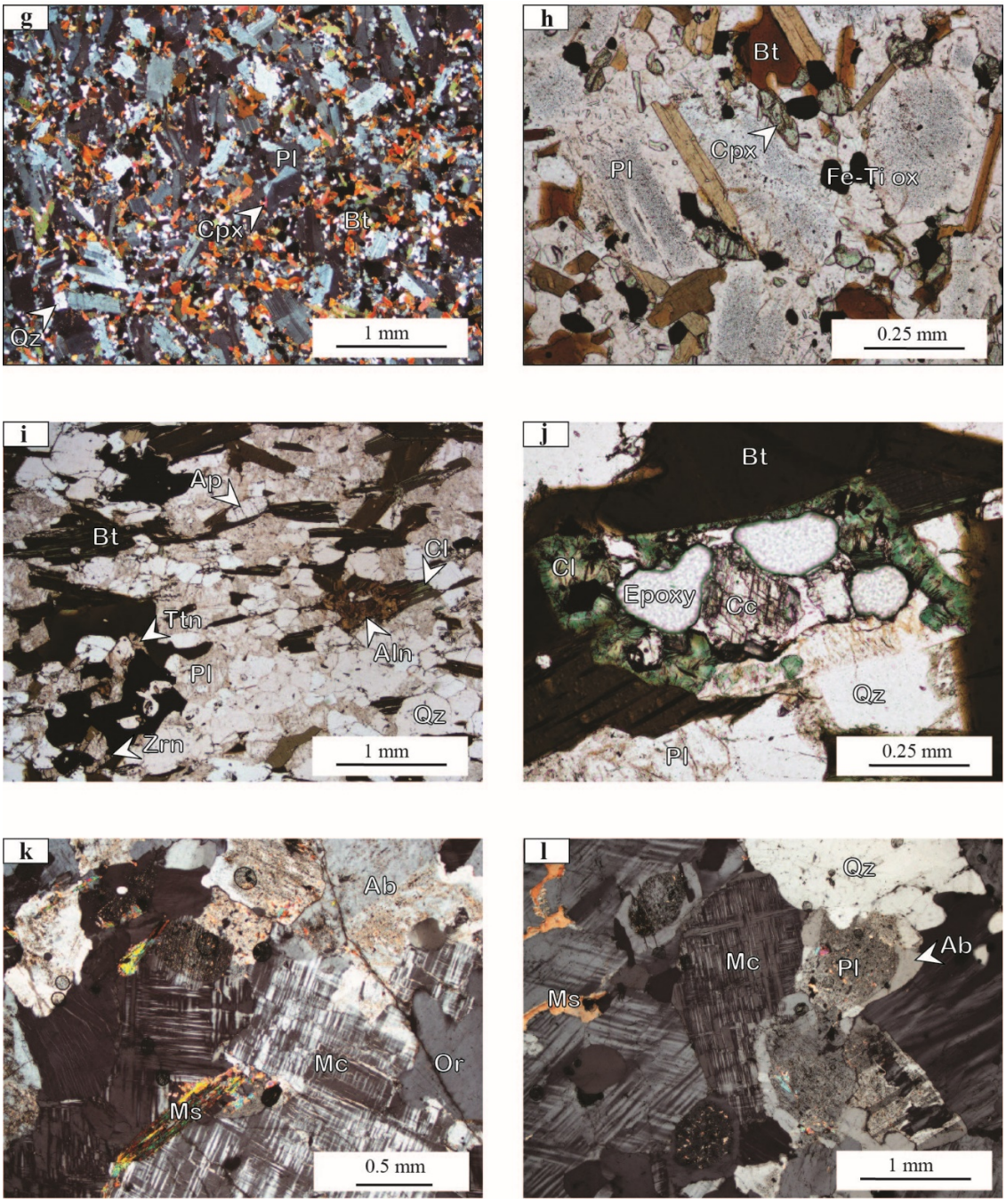

Figure 5.8 (cont.): **g)** porphyritic texture marked by the presence of plagioclase phenocryst in the quartz monzodiorite dyke (CPL); **h)** zoned plagioclase phenocryst with inclusions, important proportion of ferromagnesian minerals (CPL), quartz monzodiorite dyke; **i)** foliated texture in the biotite-rich felsic sill (PPL), important proportion of trace minerals (zircon, apatite, titanite, Fe–Ti oxides and allanite); **j)** example of an altered biotite replaced by chlorite and calcite within the biotite-rich felsic sill (PPL); **k)** groundmass enriched in K-feldspar and albite with muscovite (CPL), two-mica leucogranite; **l)** zoned plagioclase with albite rim, interstitial muscovite, quartz and K-feldspar (CPL), two-mica leucogranite.

Mineral abbreviations used for Figure 5.8: Qz = quartz; K-fsp = k-feldspar; Zrn = zircon; Ap = apatite; Fe-Ti ox = Fe-Ti oxides; Bt = biotite; Hbl = hornblende; Cpx = clinopyroxene; Pl = plagioclase; Ser = sericite; Ttn = titanite; Aln = allanite; Cl = chlorite; Cc = calcite; Mc = microcline; Ab = albite; Ms = muscovite; Or = orthoclase.:

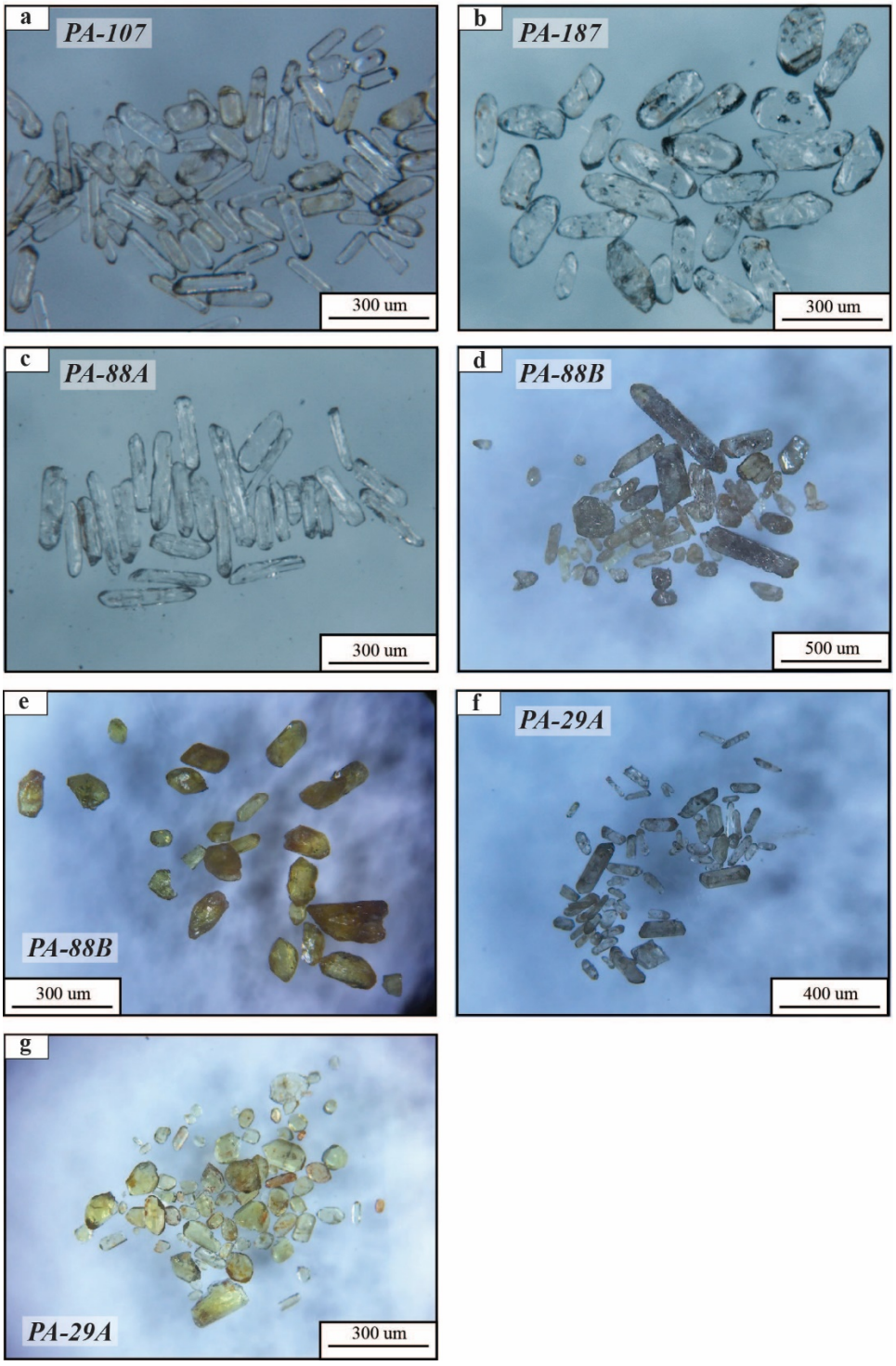

Figure 0.9: Photomicrographs of selected zircon and monazite grains under a binocular microscope: **a)** zircon, Bon-Désir granite (PA-107-A); **b)** zircon, Michaud quartz monzonite (PA-187-A); **c)** zircon, biotite-rich felsic sill (PA-88-A); **d)** zircon, felsic pegmatite (PA-88-B) **e)** monazite, felsic pegmatite (PA-88-B); **f)** zircon, two-mica leucogranite (PA-29-A); and **g)** monazite, two-mica leucogranite (PA-29-A).

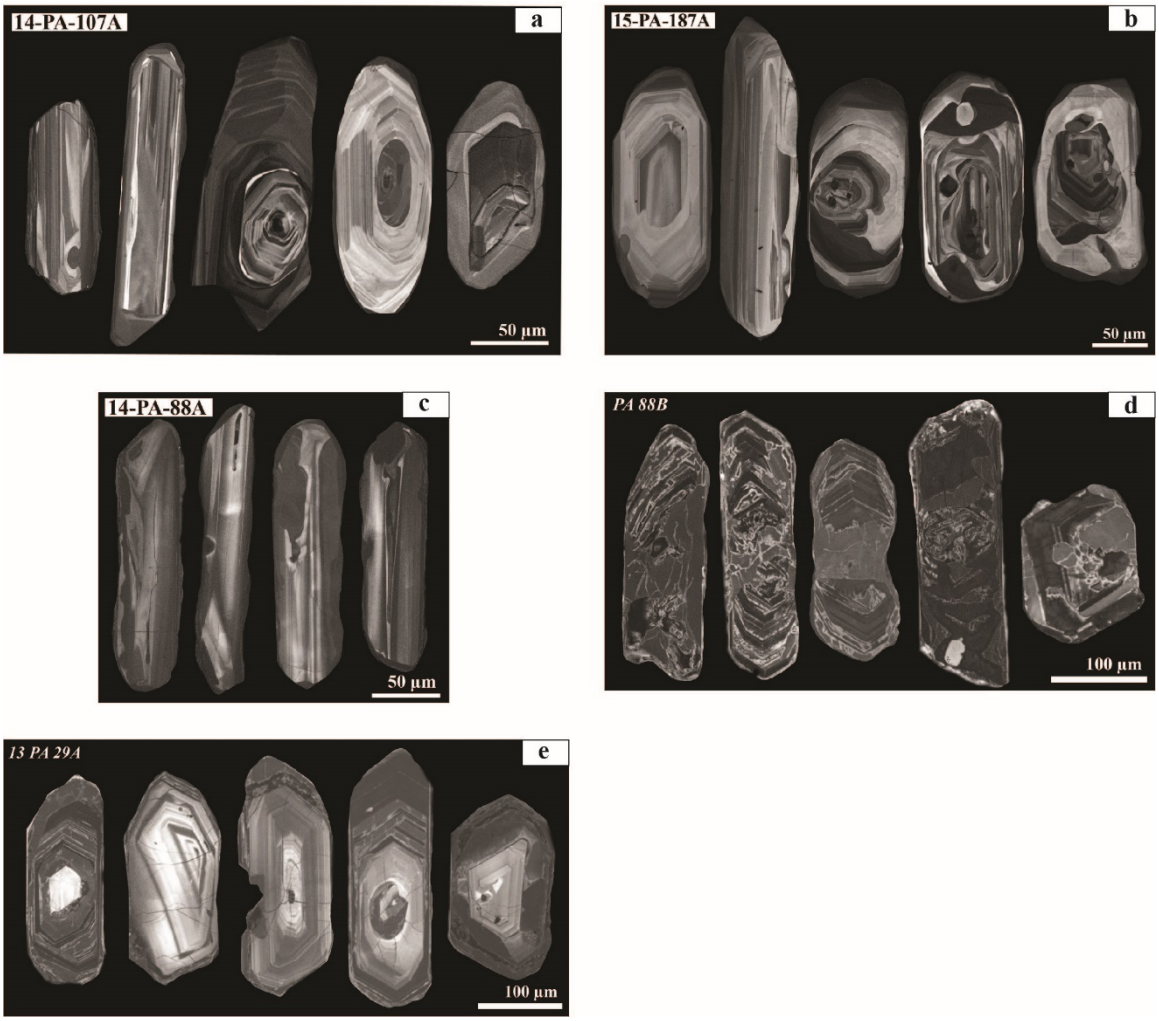

Figure 0.10: Cathodoluminescence images of representative zircon grains with igneous growth zoning from: **a)** Bon-Désir granite (PA-107-A); **b)** Michaud quartz monzonite (PA-187-A); **c)** biotite-rich felsic sill (PA-88-A); **d)** felsic pegmatite (PA-88B); and **e)** two-mica leucogranite (PA-29-A).

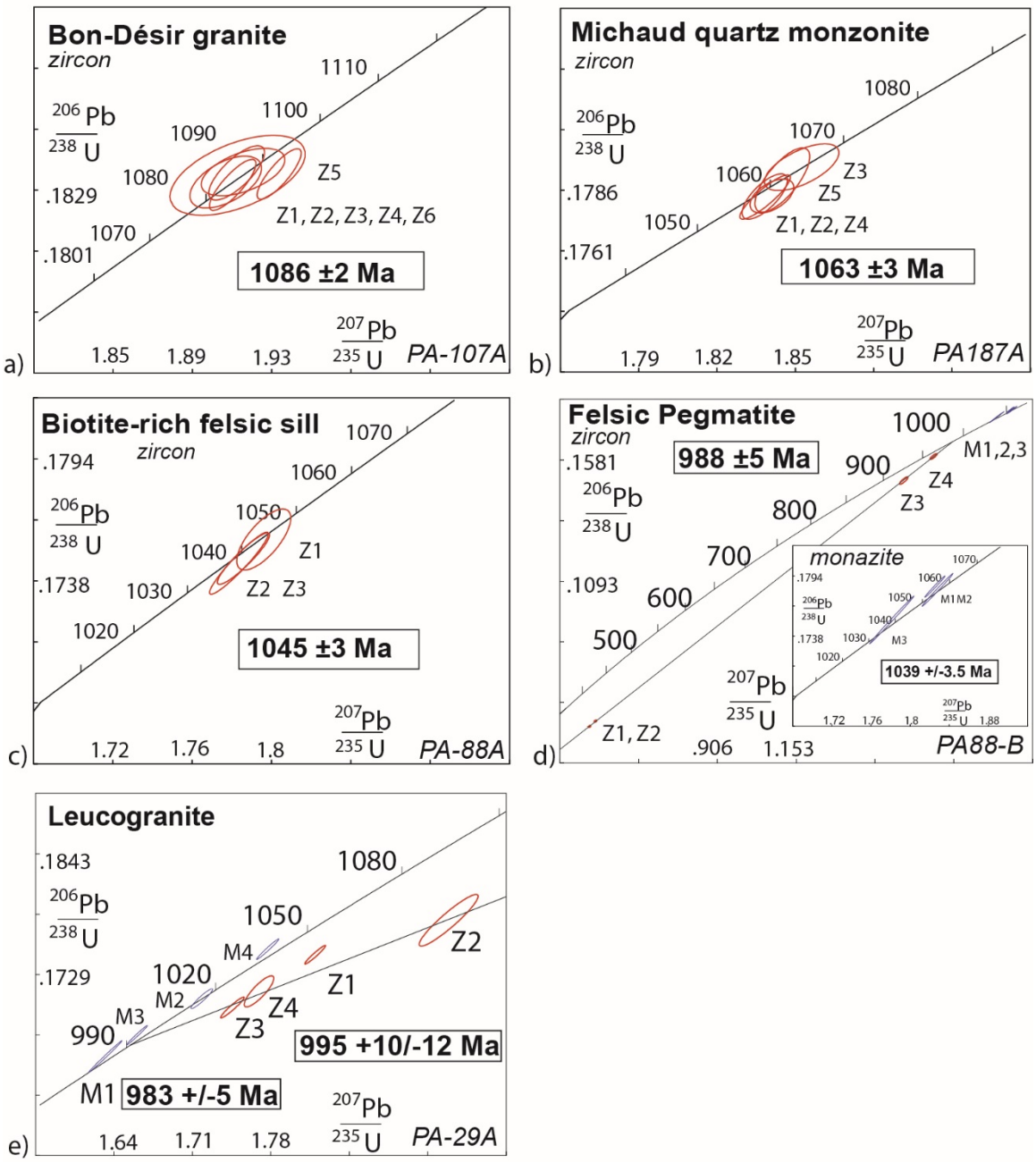

Figure 0.11: Concordia diagrams of TIMS U–Pb analyses of zircon and monazite grains from: **a)** Bon-Désir granite (zircon); **b)** Michaud quartz monzonite (zircon); **c)** the biotite-rich felsic sill (zircon); **d)** the felsic pegmatite; and **e)** the two-mica leucogranite.

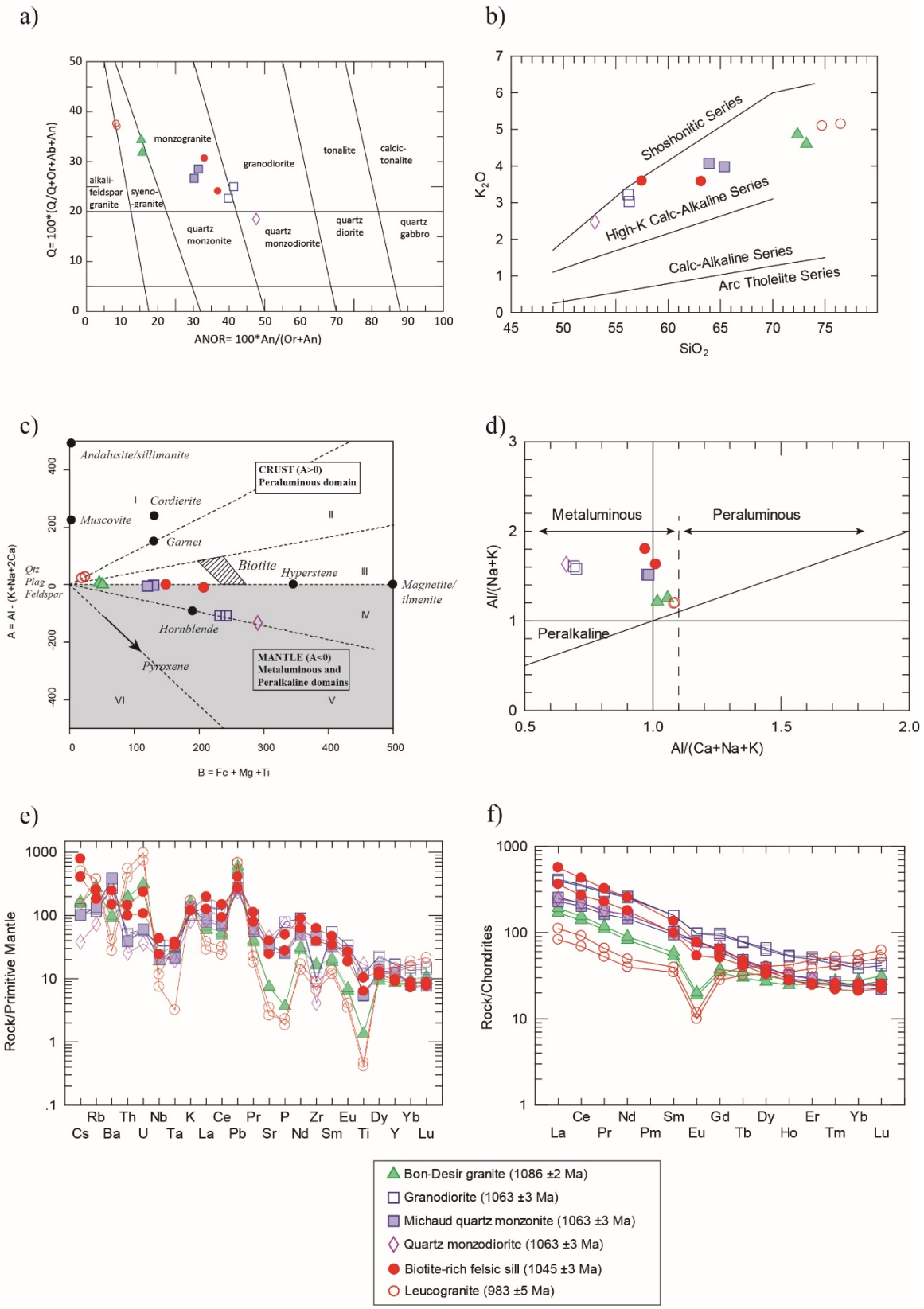
a)
Q= 100*(Q/Q+Or+Ab+An)
ANOR= 100*An/(Or+An)
monzogranite
granodiorite
tonalite
calcic-tonalite
alkali-feldspar granite
syeno-granite
quartz monzonite
quartz monzodiorite
quartz diorite
quartz gabbro
b)
K_2O
SiO_2
Shoshonitic Series
High-K Calc-Alkaline Series
Calc-Alkaline Series
Arc Tholeiite Series
c)
A = Al - (K+Na+2Ca)
B = Fe + Mg +Ti
Andalusite/sillimanite
CRUST (A>0)
Peraluminous domain
Cordierite
Muscovite
Garnet
Biotite
Hyperstene
Magnetite/ ilmenite
Qtz
Plag
Feldspar
Hornblende
Pyroxene
MANTLE (A<0)
Metaluminous and
Peralkaline domains
I
II
III
IV
V
VI
d)
Al/(Na+K)
Al/(Ca+Na+K)
Metaluminous
Peraluminous
Peralkaline
e)
Rock/Primitive Mantle
Rb Th Nb K Ce Pr P Zr Eu Dy Yb
Cs Ba U Ta La Pb Sr Nd Sm Ti Y Lu
f)
Rock/Chondrites
Ce Nd Sm Gd Dy Er Yb
La Pr Pm Eu Tb Ho Tm Lu
Bon-Desir granite (1086 ±2 Ma)
Granodiorite (1063 ±3 Ma)
Michaud quartz monzonite (1063 ±3 Ma)
Quartz monzodiorite (1063 ±3 Ma)
Biotite-rich felsic sill (1045 ±3 Ma)
Leucogranite (983 ±5 Ma)

(*Previous page*) **Figure 0.12: a)** Q-ANOR normative classification plot. **b)** K_2O vs SiO_2 diagram (Peccerillo and Taylor, 1976). **c)** Peraluminous index (A = Al-(Na+K+2Ca)) versus differentiation index (B = Fe+Mg+Ti) diagram from Debon and Le Fort (1988), the different sectors are defined in the text. **d)** A/CNK diagram (Maniar and Piccoli, 1989). **e)** Primitive mantle-normalized extended trace element diagram (Sun and McDonough, 1989). **f)** REE diagram normalized to chondrite (Sun and McDonough, 1989). Symbols: open circles – leucogranites (samples 54353, 54714); solid triangles – Bon-Desir granite (samples 54705, 54706); solid squares – Michaud quartz monzonite (samples 54745, 54746); solid dots – biotite-rich felsic sill (samples 54355, 43702); open squares – granodiorite (samples 54735, 54736); open pyramid – quartz monzodiorite (sample 54755).

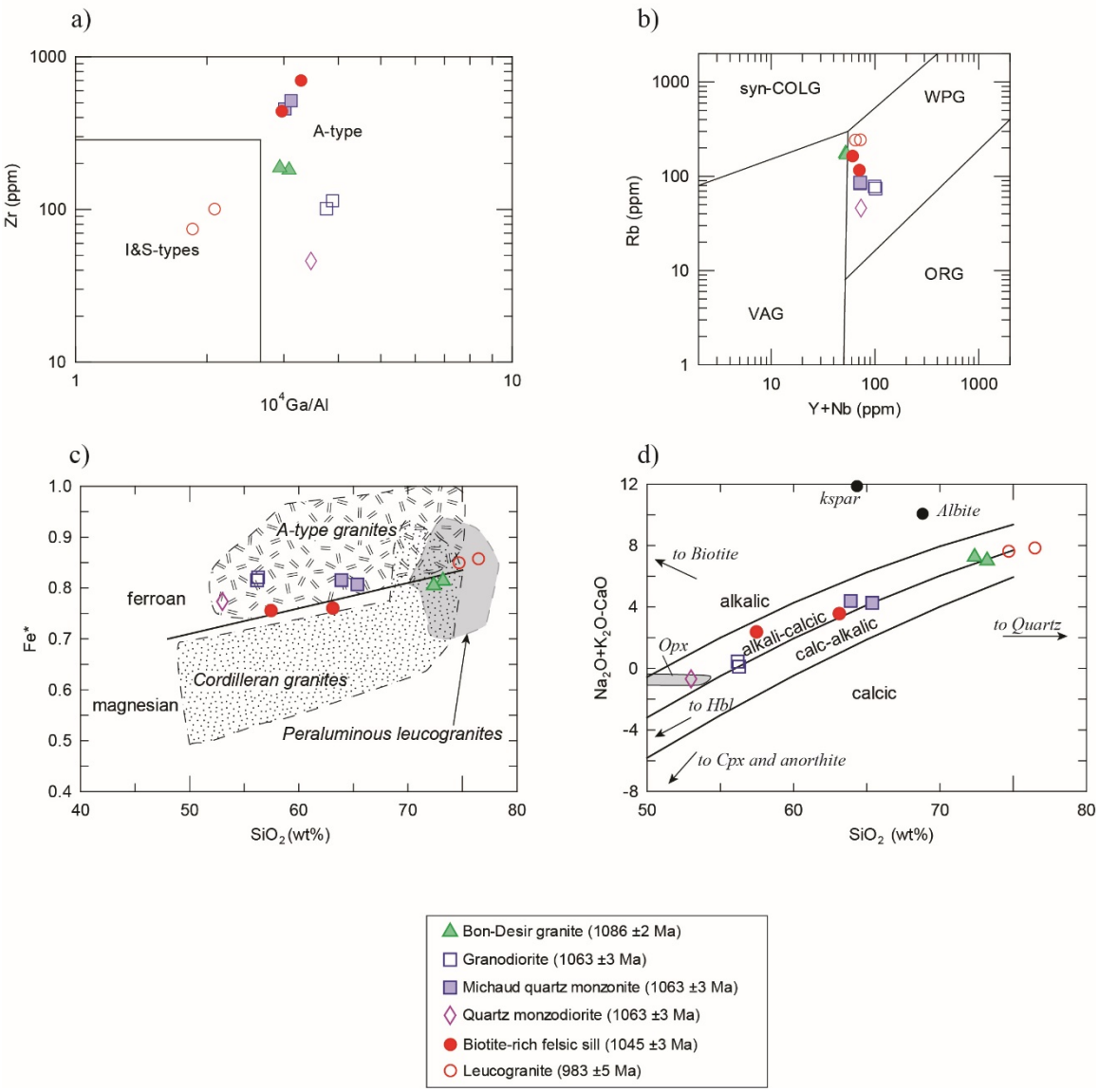

Figure 0.13: a) 10^4 Ga/Al vs Zr (Whalen et al., 1987). I-type = igneous source, S-type = crustal source, A-type = alkaline. **b)** Yb+Nb vs Rb plot for tectonic discrimination for granitoids (Pearce et al., 1984). VAG = Volcanic Arc Granitoids, WPG = Within-Plate Granitoids, ORG = Oceanic Ridge Granitoids and Syn-COLG = Syn-Collisional Granitoids. **c)** Fe-index = $(FeO + 0.9Fe_2O_3) / (FeO + 0.9 Fe_2O_3 + MgO)$ vs SiO_2 diagram illustrating the boundary between ferroan and magnesian rocks (Frost et al., 2001). **d)** Modified alkali-lime index against silica diagram (Frost et al., 2001). **e)** Sr vs Ba plot used to differentiate the possible type of source signature.

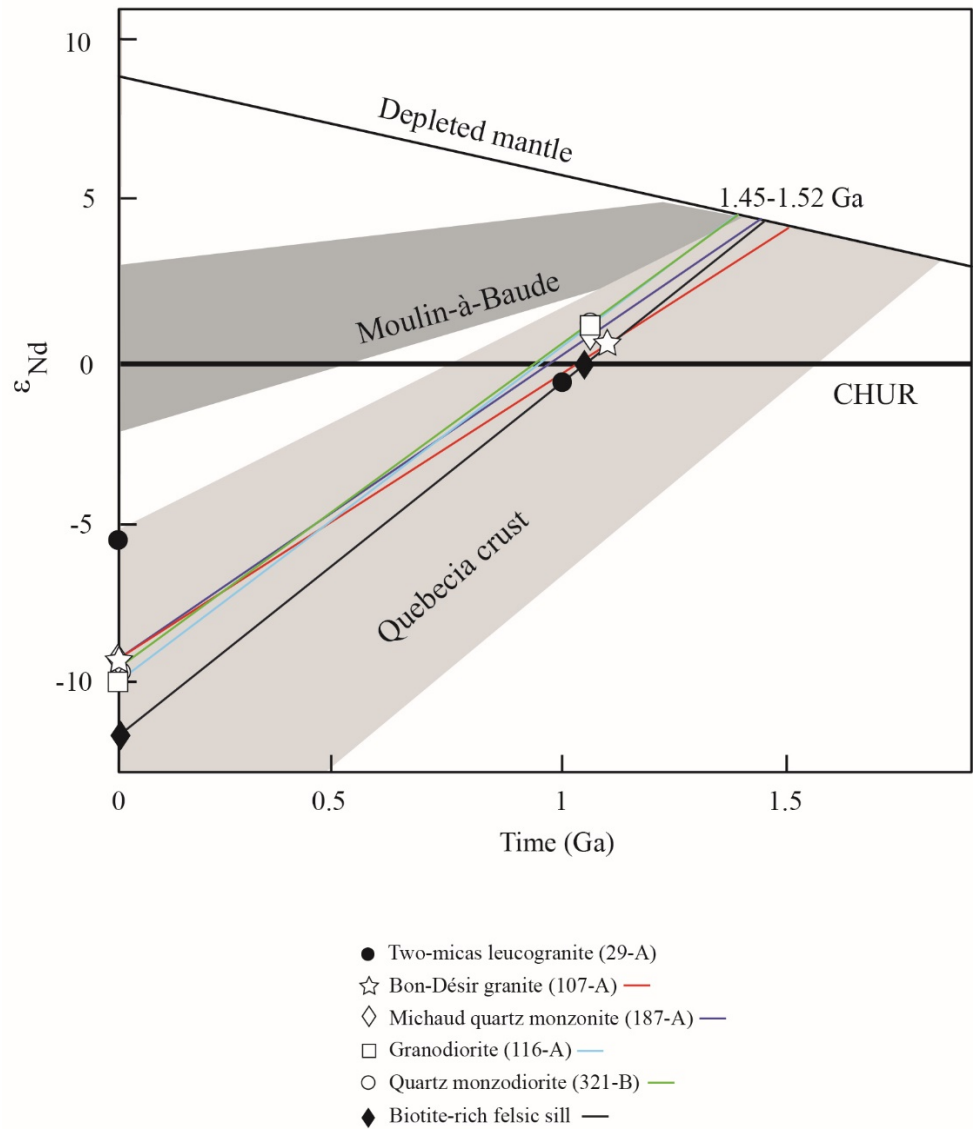

Figure 0.14: Initial εNd vs age diagram for intrusive rocks from the ESB. Data for Quebecia crust after Owens and Tomascak (2002) based on data by Dickin and Higgins (1992) and Dickin (2000). Data from the Moulin-à-Baude volcanic rocks are from Groulier et al. (submitted).

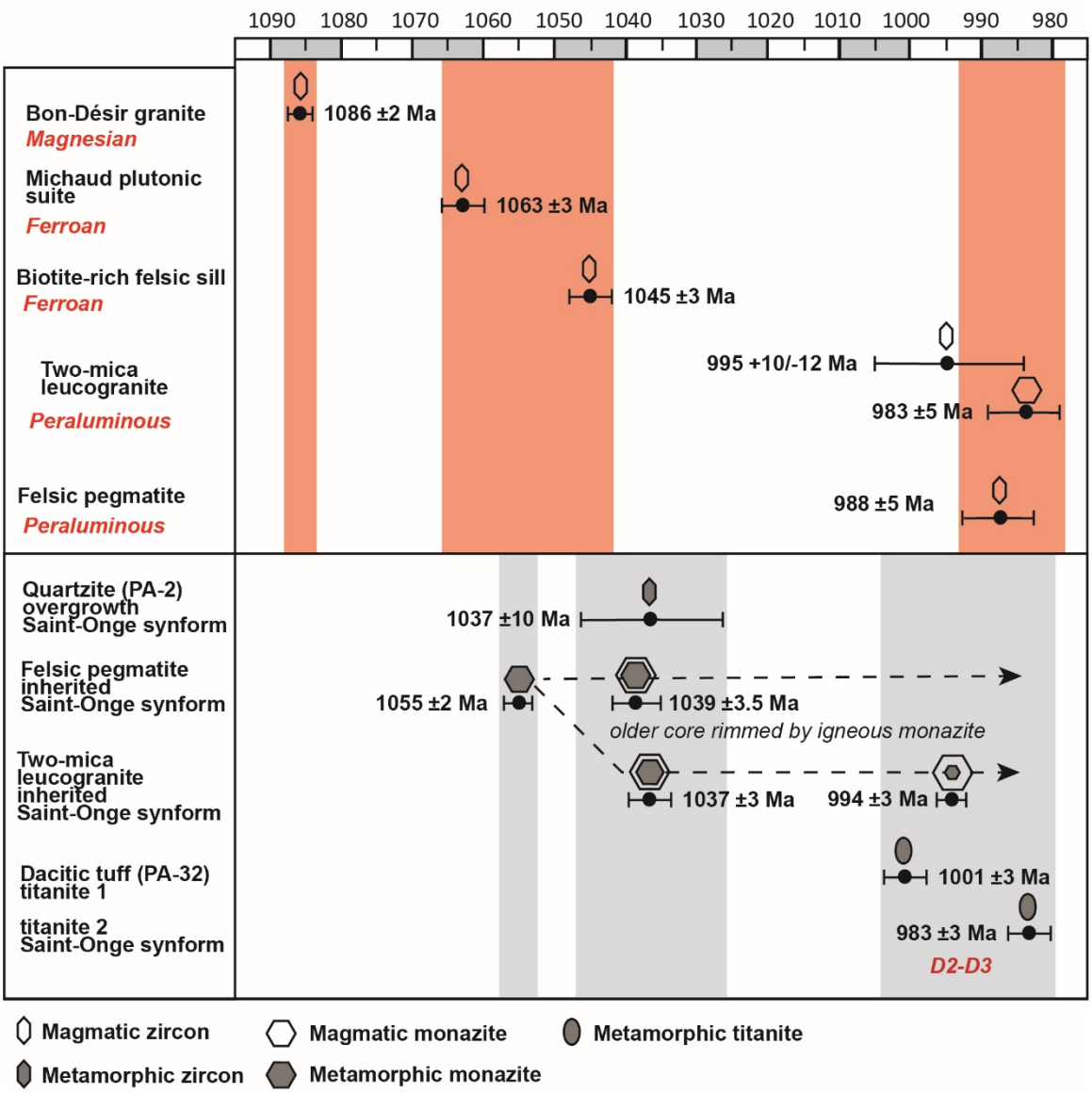

Figure 0.15: Summary of the U–Pb magmatic and metamorphic ages presented in this study.

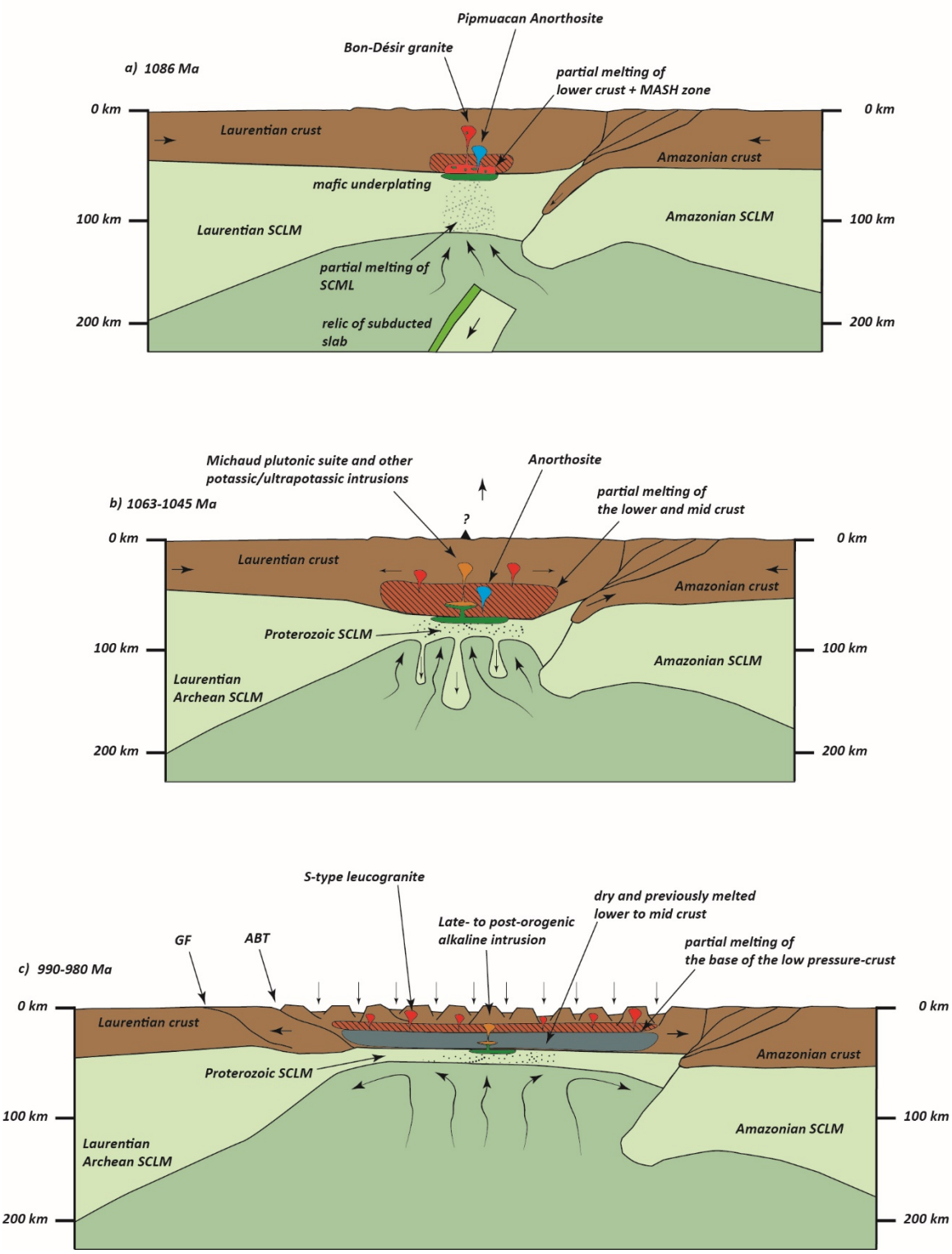

Figure 0.16: Proposed model for the tectono-magmatic evolution of the central Grenville Province during the Grenvillian orogeny.

Table 5.1: U-Pb Data for Zircon and Monazite

Fraction	Weight [mg]	Concentration U [ppm]	Concentration Pb rad [ppm]	Measured total common Pb [pg]	Measured 206Pb/204Pb	Corrected Atomic Ratios * 208Pb/206Pb	206Pb/238U	+/-	207Pb/235U	+/-	207Pb/206Pb	+/-	Age [Ma] 206Pb/238U	Age [Ma] 207Pb/235U	Age [Ma] 207Pb/206Pb
Bon- Desir Granite (PA-107A;465796 5347120)															
Z1 2 clr long prm	0.002	243	45.4	1.6	3561	0.1093	0.18374	102	1.9136	116	0.07553	30	1087	1086	1083
Z2 1 clr long prm	0.001	186	34.3	2.3	957	0.0928	0.18363	150	1.9143	280	0.07561	94	1087	1086	1085
Z3 2 clr long prm	0.002	512	93.4	2.9	4065	0.0832	0.18320	96	1.9116	96	0.07568	22	1084	1085	1087
Z4 2 clr long prm	0.002	103	18.9	2.3	1035	0.0858	0.18333	98	1.9083	148	0.07549	50	1085	1084	1082
Z5 3 long prm	0.003	332	62.3	1.9	6093	0.1121	0.18370	94	1.9350	90	0.07640	22	1087	1093	1106
Z6 1 long prm	0.001	198	36.9	3.0	785	0.1011	0.18378	88	1.9172	172	0.07566	58	1088	1087	1086
Z7 1 clr prm	0.001	414	47.9	3.0	1032	0.1354	0.11165	68	1.0500	106	0.06820	60	682	729	875
Michaud Qz-Monzonite (PA187A;461449 5369259)															
Z1 1 lrg prm	0.003	452	83.8	2.9	5310	0.1341	0.17837	74	1.8396	80	0.07480	16	1058	1060	1063
Z2 1 lrg prm	0.003	262	51.1	5.9	1499	0.1939	0.17841	58	1.8424	68	0.07489	26	1058	1061	1066
Z3 1 lrg prm	0.003	194	36.9	3.9	1692	0.1541	0.17960	78	1.8538	116	0.07486	36	1065	1065	1065
Z4 1 lrg prm	0.003	432	81.9	4.0	3621	0.1617	0.17839	76	1.8395	72	0.07479	22	1058	1060	1063
Z5 4 lrg clr prm	0.012	262	48.7	4.8	7419	0.1326	0.17907	108	1.8462	86	0.07477	30	1062	1062	1062
Biotite-rich monzonite (14PA-88A;469026 5359161)															
Z1 2 clr euh needles	0.003	1457	256.9	51	956	0.0926	0.17576	114	1.7976	112	0.07418	36	1044	1045	1046
Z2 5 clr elong prisms	0.007	1540	264.1	178	728	0.0664	0.17488	96	1.7875	108	0.07413	18	1039	1041	1045
Z3 3 clr euh elong	0.004	1060	178.6	35	1504	0.0480	0.17461	116	1.7836	122	0.07409	16	1037	1040	1044
Felsic Pegmatite (PA88-B; 469026 5359161)															
Z1 1 cloudy sml euh	0.000	1019	50.3	3.4	415	0.0125	0.05302	32	0.5239	32	0.07166	40	333	428	976
Z2 1 sml turbid prm	0.001	1826	86.9	4.6	1271	0.0163	0.05089	30	0.5056	28	0.07207	38	320	416	988
Z3 1 sml cloudy prm	0.001	2553	355.4	4.4	5434	0.0092	0.14980	122	1.4901	106	0.07215	30	900	926	990
Z4 1 sml cloudy prm	0.001	782	115.8	3.3	2390	0.0084	0.15951	96	1.5838	92	0.07201	22	954	964	986
M1 1 lrg clr yel	0.003	42590	35253.7	57	25270	4.2849	0.17839	82	1.8254	84	0.07421	4	1058	1055	1047
M2 1 lrg clr yel euh	0.003	41620	50937.3	50	27769	6.8579	0.17809	124	1.8281	128	0.07445	4	1057	1056	1054
M3 1 lrg yel clr euh	0.003	74332	95548.3	171	14358	7.3895	0.17530	180	1.7813	184	0.07370	4	1041	1039	1033
Leucogranite (13PA-29A; 467424 5356370)															
Z1 1 sml elong prm	0.002	1163	197.0	4.2	6124	0.0512	0.17477	72	1.8196	76	0.07551	8	1038	1053	1082
Z2 1 sml elong prm	0.002	174	27.6	4.7	838	0.0442	0.17802	200	1.9386	214	0.07898	32	1056	1095	1172
Z3 1 sml elong prm	0.002	1224	213.4	33	811	0.1188	0.16979	80	1.7457	86	0.07457	10	1011	1026	1057
Z4 1 sml prm	0.002	760	134.0	4.3	3819	0.1220	0.17131	120	1.7695	108	0.07491	28	1019	1034	1066
M1 1 lrg euh flat gem	0.003	46009	54019.7	56	25525	7.1337	0.16516	122	1.6323	122	0.07168	4	985	983	977
M2 1 sml euh gem	0.001	10181	15387.0	50	2189	9.1489	0.17062	76	1.7184	78	0.07304	12	1016	1015	1015
M3 1 lrg gem	0.003	25061	32050.5	42	18824	7.7567	0.16718	74	1.6607	76	0.07204	4	997	994	987
M4 1 tiny euh gem	0.001	21664	32438.4	17	13748	8.7829	0.17530	80	1.7772	82	0.07353	6	1041	1037	1029

Notes: Z=zircon, 1, 2 =number of grains, lrg=large, clr=clear, sml= small, prm =prism, euh=euhedral, yel= yellow.
All zircon was chemically abraded (cf. Mattinson, 2005). Weights were estimated so U and Pb concentrations are approximate.
* Atomic ratios corrected for fractionation, spike, laboratory blank of 1-2 picograms of common lead, and initial common lead at the age of the sample calculated from the model of Stacey and Kramers (1975), and 0.3 picogram U blank. Two sigma uncertainties are reported after the ratios and refer to the final digits.

Table 5.2: Whole rock geochemistry of the different plutonic rocks.

Intrusion/Field Name	Bon-Désir	Bon-Désir	Granod.	Granod.	Michaud	Michaud	Qtz mzd	Leucogranite	Leucogranite	Bt-rich felsic sill	Bt-rich felsic sill
Lab number	54705	54706	54735	54736	54745	54746	54755	54353	54714	54355	53072
Q-ANOR norm class	Syenogranite	Syenogranite	Monzogranite	Granodiorite	Monzogranite	Monzogranite	Quartz Monzodiorite	Alkali feldspar granite	Alkali feldspar granite	Monzogranite	Monzogranite
SiO_2	73,22	72,37	56,19	56,28	65,38	63,91	53,00	74,73	76,52	57,50	63,16
TiO_2	0,29	0,29	2,68	2,55	1,16	1,20	3,64	0,10	0,09	2,24	1,37
Al_2O_3	13,48	13,51	12,57	12,18	14,40	14,55	12,55	12,67	13,22	14,92	13,97
$Fe_2O_3(T)$	2,41	2,41	11,68	11,45	6,04	6,58	12,81	1,18	1,05	9,03	6,65
MgO	0,50	0,53	2,40	2,27	1,31	1,35	3,40	0,19	0,16	2,66	1,91
MnO	0,03	0,04	0,18	0,17	0,11	0,11	0,17	0,02	0,03	0,12	0,07
CaO	1,10	1,18	5,49	5,53	2,88	2,85	6,20	0,60	0,64	3,91	2,89
Na_2O	3,51	3,57	2,72	2,61	3,16	3,17	3,05	3,10	3,30	2,67	2,85
K_2O	4,60	4,86	3,22	3,03	3,98	4,07	2,47	5,10	5,15	3,59	3,58
P_2O_5	0,08	0,08	1,71	1,69	0,54	0,57	1,60	0,04	0,05	1,08	0,60
LOI	0,87	0,81	0,66	0,48	0,62	0,59	0,68	0,52	0,52	1,15	1,20
Total	100,09	99,65	99,50	98,24	99,58	98,95	99,57	98,25	100,73	98,87	98,25
Transition Elements											
Co	4	4	21	22	9	9	30			18	13
Cr	52	39	21	20	34	27	32	12	36	31	52
Cu	4	3	15	17	12	5	30	8	2	8	6
Ni	4	3	5	5	5	5	23	2	1	18	13
Sc	4,2	4,6	18,5	17,2	10,2	10,8	17,2	3	2	9	8,5
V	21	21	130	125	53	56	216		6	102	74
Zn	51	51	195	190	116	130	154	82	15	227	128
LFSE											
Ba	626	684	1915	1884	2641	2726	1538	290	193	1717	1038
Cs	1,2	1,3	1,0	0,8	0,8	0,8	0,3	1,2	4,0	3,2	6,2
Ga	22	21	25	25	23	24	23	14	13	26	22
Rb	174	169	78	74	84	86	46	241	240	115	162
Pb	42	36	25	24	18	19	17	49	47	19	29
Sr	153	158	658	646	720	727	941	74	55	837	516
Th	16,9	16,4	4,13	4,46	3,28	3,34	2,16	46,8	33,6	8,40	12,3
U	6,41	6,62	1,21	1,25	1,21	1,27	0,75	20,5	15,4	2,24	4,92
HFSE											
Hf	5,7	5,9	2,3	2,6	9,5	10,7	1,0	4,0	3,0	14,1	8,8
Nb	13,2	13,3	23,3	23,9	16,7	14,6	15,6	5,3	8,3	30,7	17,2
Ta	1,25	1,21	1,34	1,36	0,84	0,87	0,79	0,13	1,34	1,55	1,38
Y	39,1	39,8	76,0	77,7	55,3	57,6	57,8	67,9	57,2	40,9	44,5

Zr	181	187	101	114	456	515	46	100	74	694	436
REE											
La	40,2	45,6	94,2	98,0	54,3	60,5	58,4	26,4	19,7	135	86,2
Ce	85,1	94,8	212	220	124	135	136	56,3	42,4	263	165
Pr	10,3	11,2	27,8	28,7	15,5	16,9	17,1	6,20	5,00	30,8	21,7
Nd	38,4	41,9	119	123	67,7	75,0	75,1	23,0	18,6	120	83,9
Sm	8,10	9,00	24,2	24,2	14,4	15,6	15,4	6,10	5,30	20,7	15,1
Eu	1,08	1,17	5,67	5,72	4,68	4,63	3,96	0,68	0,58	4,47	3,12
Gd	7,03	7,69	19,1	20,2	12,5	13,2	13,8	6,71	5,78	13,2	10,5
Tb	1,12	1,31	2,88	2,94	1,66	1,81	1,78	1,49	1,20	1,76	1,56
Dy	6,82	7,91	15,9	16,8	9,13	9,97	9,81	10,3	8,50	9,46	8,34
Ho	1,39	1,60	2,98	3,08	1,65	1,81	1,78	2,37	1,97	1,61	1,57
Er	4,20	4,52	8,12	8,63	4,45	4,91	4,83	7,96	6,32	4,07	4,26
Tm	0,62	0,71	1,10	1,19	0,63	0,69	0,65	1,33	1,05	0,56	0,66
Yb	4,21	4,73	6,60	7,31	3,95	4,10	4,25	9,30	7,76	3,57	4,32
Lu	0,69	0,80	1,05	1,12	0,56	0,64	0,61	1,59	1,30	0,57	0,64
(La/Sm)n	3,22	3,27	2,52	2,62	2,44	2,51	2,45	2,81	2,41	4,21	3,69
(La/Yb)n	6,85	6,92	10,24	9,62	9,86	10,59	9,86	2,04	1,82	27,14	14,32
(Th/La)n	3,40	2,91	0,35	0,37	0,49	0,45	0,30	14,33	13,79	0,50	1,15
(Nb/La)n	0,32	0,28	0,24	0,23	0,30	0,23	0,26	0,19	0,41	0,22	0,19
A	13,9	4,2	-105,9	-107,3	-7,1	-5,4	-126,3	18,5	20,3	-9,6	2,6
B	46,3	47,0	239,5	231,7	122,8	131,0	290,6	20,8	18,2	207,4	148,0

Major elements in weight percent. Trace elements in ppm. (T) - total iron as Fe2O3. n - primitive mantle normalized ratios (Sun and McDonough, 1989).
A and B - parameters for Debon and LeFort plot (see Fig. 14c).
Granod. – Granodiorite; Qtz-mzd - quartz monzodiorite; Leucog - leucogranite; Bt-rich felsic sill - biotite-rich felsic sill

Table 5.3: Sm-Nd isotopic data of the different Grenvillian intrusions.

Sample	Rock type	Nd (ppm)	Sm (ppm)	$^{147}Sm/^{144}Nd$	$^{143}Nd/^{144}Nd(m)$	2sem	εNd(o)	εNd(t)	T_{DM}	Crystallization age (t)
107-A1	Bon-Désir granite	37.73	7.82	0.1253	0.512161	7	-9.3	0.6	1517	1085
29-A	leucogranite	20.34	5.27	0.1567	0.512361	7	-5.4	-0.4	-	984
116-A	quartz monzodiorite	121.06	23.48	0.1172	0.512123	8	-10.0	0.8	1450	1063
321-B	monzodiorite	83.72	16.46	0.1188	0.512135	6	-9.8	0.8	1456	1063
187-A1	Michaud qtz monzonite	71.72	14.56	0.1227	0.512159	7	-9.3	0.7	1478	1063
88-A	Biotite-rich monzonite	81.58	14.25	0.1056	0.512013	6	-12.2	-0.1	1450	1045

Epsilon Nd calculated using present day CHUR values: $^{143}Nd/^{144}Nd = 0.512638$ and $^{147}Sm/^{144}Nd = 0.1967$. T_{DM} after DePaolo (1988). 2 sem – 2 standard error of the mean. (o) – Epsilon Nd today. (t) – initial Epsilon Nd at time of formation based on (t) the crystallization age (in Ma). Note that due to the highly fractionated Sm/Nd ratio in the leucogranites, we do not calculate any model ages. CHUR – chondritic uniform reservoir. DM – depleted mantle.

Chapter 6 Conclusions and directions for future research

6.1 Conclusion and key findings

This thesis focused on the recently recognized Escoumins supracrustal belt (ESB) located in the southern central Grenville Province (Quebec) and combined field observations with microscopic and micro-analytical techniques to elucidate: (1) the age, nature and tectonic environment of the igneous and sedimentary rocks from the supracrustal belt and its basement; (2) their relations with other Geon 15 to 13 lithotectonic units from the central Grenville Province; (3) the types of hydrothermal alterations and their economic potential; (4) the relation between Grenvillian-age orogenic magmatism, metamorphism and deformation within the supracrustal belt. Key findings of this study include:

1) The ESB represents remnants of a Pinwarian (1.52–1.46 Ga; Gower and Krogh, 2002) oceanic arc, arc-rift and back-arc system (Chapters 2 and 4) that consists of supracrustal rocks (Saint-Siméon Group; SSG), and their structural basement (Tadoussac Intrusive Suite; TIS). Preserved primary features of supracrustal (Chapters 2 and 4) and plutonic rocks (Chapter 2), provide a detailed record of the evolution of a pre-Grenvillian oceanic arc system. The TIS consists of a polyphase 1.5 Ga calc-alkaline and alkaline batholith that records an evolution from a mature island arc toward an arc-rift environment (Chapters 2 and 3). The dated granodiorite from this suite has inherited zircon cores and an older Nd model age (~1.67 Ga), that together with positive εNd_t value (+2.66), suggest that the magma was derived from remelting of juvenile older crust (Chapter 2). The SSG tectonically lies above the TIS and is exposed in synclinal

structures. Its lower Saint-Paul-du-Nord Formation is a marine sedimentary sequence, the middle Moulin-à-Baude Formation is a submarine bimodal volcanic-dominated sequence typical of oceanic island arc, arc-rift and back-arc environments (Chapters 2 and 4), and finally the upper Port-aux-Quilles Formation is a sequence of quartzite–arkose–metapsammite–greywacke–metapelite emplaced in a shallow- to deep-water environment. A 1.49 Ga dacitic tuff from the lower part of the volcanic formation and a ~1.46 Ga rhyolitic to rhyodacitic lava flow or tuff from the upper part together with a younger age limit of deposition of ~1.47 Ga from a Port-aux-Quilles quartzite give age constraints to the Saint-Siméon Group (Chapter 2). The 1.49 Ga dacite has inherited zircon cores together with older Nd model age (1.9 Ga) and slightly negative εNd_t value (-0.8) consistent with remelting of older crust at depth (Chapter 2). Basalt and ferrobasalt from the upper part of the formation are however juvenile and consistent with direct melting of the asthenospheric mantle in an extensional arc-rift to back-arc environment (Chapters 2 and 4). The detrital zircon age distribution from the Port-aux-Quilles quartzite shows a typical back-arc basin spectrum with sources of Laurentian affinity (Chapters 2 and 3). The youngest and most prominent peaks indicate that the main source of material is the arc and that some of the zircon may be derived from coeval ash deposits (Chapter 2). The emplacement of a major ca. 1.43 – 1.37 Ga arc-related plutonic belt within or near the supracrustal belts (Escoumins and Montauban) is interpreted to mark the accretion of the island arc to Laurentia (Chapter 3). It is proposed that the preservation of the pre-Grenvillian supracrustal belts in the southernmost part of the Grenville Province can be linked to the structure of the orogen with potential embayments and promontories similar to the Appalachian orogen (Chapter 2).

2) The ESB, together with other Geon 15 to 13 supracrustal and plutonic rock units in the central Grenville Province provide new insights on arc dynamics along the SE Laurentian margin during this period and on the genetic link between Quebecia and Laurentia (Chapter 3). The data point to a major extensional event along the SE Laurentian margin during Geon 15 as a result of upper-plate extension in an active continent-ocean convergent setting. This event led to the formation along the Laurentian margin of an intra-arc and shallow marine continental back-arc basin and to the separation of crustal slivers, together with the opening of a seaway resulting in the formation of island arcs. Intrusion of ca. 1.5 to 1.49 Ga plutons in the sedimentary sequences previously formed during the rifting of the Laurentian margin suggests back-arc inversion (preserved in the eastern Grenville) and transformation of a passive margin into an active one (in the central Grenville). The island arcs experienced rifting and back-arc opening during Geon 14, and the emplacement of 1.43–1.37 Ga plutonic rocks in the central Grenville marks the closure of the seaway and the accretion of these arcs to Laurentia. It is proposed that: a) the emplacement of the 1.46–1.43 Ga Michael – Shabogamo gabbro in the northern central and eastern Grenville Province is linked to the formation of an asthenospheric window or back-arc extension; and b) the 1.36–1.33 Ga anorthosite suites in the central part of Quebecia reflect an episode of mafic underplating linked to the accretion of the arc. Such mechanisms are typical of modern-day arc dynamics and can be compared to the Andean active margin.

3) In term of economic potential, the volcanic sequence of the Moulin-à-Baude Formation was affected by syn-volcanic hydrothermal alteration typical of VMS deposits that was subsequently metamorphosed (Chapter 4). The field and petrographic

observations together with the alteration geochemistry and microprobe analyses of key metamorphic minerals from the alteration zones are consistent with: (1) a regional widespread semi-conformable quartz – epidote (epidosite) subseafloor alteration in the lower part of the sequence; in the upper part of the sequence the rocks are affected from the edge to the core and top by (2) Na-metasomatism (spillite) with varied enrichment in K–Fe–Mg–Si typical of albite – chlorite – sericite – quartz pre-metamorphic alteration assemblage, (3) K–Fe–Mg–Ca after sericite – chlorite – quartz – clinozoisite/zoisite – carbonate; (4) K-metasomatism (keratophyre) sericite ± quartz and potentially in some place kaolinite-pyrophyllite alteration zone), (4) Fe–Mg±K±Si alteration equivalent of chlorite ± sericite ± quartz assemblage, (5) silicification and (6) Ca–Mg±Si±K skarn alteration after dolomite – quartz ± sericite ± chlorite alteration). The metamorphosed chloritic and sericite-quartz alteration zones are associated with Cu-rich (±Au–Ag) mineral occurrences while the upper Ca-Mg skarn zones are linked to Zn–Pb mineralization. This zonation is consistent with a VMS-type of deposit with higher temperature mineralization in the core of the system and lower temperature mineralization closer to the seafloor. The recognition of a Zn–Pb-rich tuffite in the northern limb of the Grandes-Bergeronnes syncline represents an attractive horizon to follow in order to find massive sulfide lenses. The aluminosilicate-rich discordant pipe in the southern limb of the same syncline together with the presence of tourmaline (dravite type), Mn-rich garnet and white mica (wilsonite) and anomalies in magmatophile elements (i.e. W–Mo–As–B–Mn–Be) seems to indicate a potential magmatic input in the hydrothermal fluid that could have endowed gold and other economic commodities to the system. This detailed study is a first for the Grenville Province, it highlights the

underexploited potential of this province and shows the path for future studies in highly deformed and metamorphosed terranes.

4) In chapter 5, it has been shown that the ESB, which is part of the low-pressure belt (low-*P* Belt) of the Grenvillian hinterland, represents higher levels of the infrastructure of a large hot (long duration) orogen. The supracrustal rocks were deformed and metamorphosed to the amphibolite facies during the Grenvillian orogeny (1.09–0.98 Ga; Rivers 1997). Investigated Grenvillian-age plutonic rocks and metamorphic ages cover a time interval of ~100 My that represents the entire length of the orogeny (ca. 1090–980 Ma). The magmatic activity shows an evolution from magnesian to ferroan, followed by a peraluminous chemical affinity. The ~1.09 Ma magnesian Bon Desir granite is early-Ottawan, it bears similarities to the K-rich calc-alkalic granitoid-type (KCG) of Barbarin (1999) and in the context of early collision the source of heat to melt the crust could have been mantle-derived magma associated with slab-retreat or break-off. The ~1.06–1.04 Ga ferroan magmatism (e.g. Michaud monzonite) is temporally linked to metamorphic monazite growth and zircon overgrowth in the supracrustal rocks. The Ottawan-age magmatic rocks are potassic to ultrapotassic, Ba–Sr, LREE, Fe–Ti-enriched and show evidence of derivation from partial melting of a subduction-modified (metasomatized) mantle source induced by thinning (convective removal, or foundering) of the overthickened orogenic mantle lithosphere. Finally, the ~0.9–0.8 Ga Rigolet peraluminous magmatism is manifested by two-mica garnetiferous leucogranite and muscovite – tourmaline – garnet ± beryl pegmatite that are typical of crust-derived S-type igneous rocks. They are contemporaneous with the growth of titanite in a dacitic tuff and with magmatic monazite overgrowth on inherited grains in the leucogranite. This type of

magmatism, emplaced during the waning stage of the orogeny, is interpreted to have formed from the melting of metasedimentary rocks at the base of the low-*P* belt during heat transmission when it was juxtaposed with hot and weak middle-crust. The overall extensional tectonic setting (compared to the Basin and Range) is coupled to deformation in the ESB as the leucogranite is also deformed by the main D2 event that is potentially linked to the emplacement of the dome and basin pattern. Elsewhere in the Grenville, the emplacement of late-Rigolet alkaline to peralkaline small volume plutonic bodies is consistent with limited pulses of mantle-derived magma in a late- to post-orogenic and anorogenic tectonic environment. These data provide new insights into the low-*P* belt and show that the recorded deformation within the supracrustal rocks is late-Grenvillian, potentially linked to the final emplacement of the dome and basin structure during the late orogenic collapse. The studied igneous rocks cover the entire time range of the orogeny, they provide new insight on the close relation between metamorphism and magmatism in the higher levels of the orogenic infrastructure of the Grenville Province and they are consistent with Laurentia in the position of the upper plate during the continental collision with Amazonia.

6.2 Recommendations for future work

This study has provided new insights on the stratigraphic, volcanic, magmatic, alteration and structural history of the supracrustal rocks of the ESB. It has also provided new information about its basement and the crosscutting Grenvillian-age magmatic rocks. However, some questions remained unsolved and more work can be done in order to better comprehend this complex geologic environment.

1) The southern part of the ESB (south of the Saguenay River), seems to be characterized by a more primitive mafic volcanic sequence as no felsic volcanic rocks have been reported yet. It is characterized by a large layered mafic-ultramafic intrusion and by smaller ultramafic dykes. This sequence may represent a lateral variation of the volcanic arc and back-arc that needs to be assessed. Therefore, a new mapping and sampling campaign within the unexplored zones could provide new complementary information on the stratigraphy, extent and evolution of the Saint-Siméon Group, and would also allow the identification of new prospective zones for targeting base and precious metal deposits.

2) Two U–Pb ages have been obtained from a dacitic tuff (F1 unit) and a rhyodacite (F2 unit) from both the lower and upper parts of the Moulin-à-Baude Formation. The former age is highly precise however the latter has a larger uncertainty due to the presence of thick metamorphic overgrowth. The sample is also coming from a zone that experienced intense alteration (muscovite, sillimanite, tourmaline). Such alteration has the potential to remobilize high field strength elements and potentially alter the pristine signature of the igneous zircon. For this reason, new samples from both the upper intermediate (I1 unit) and felsic (F2 unit) rocks represent attractive geochronology targets. This would permit a more precise time constraint on the upper portion of the Moulin-à-Baude Formation and it will bring more information on the relative timing between these two units. They should also be analyzed for Sm-Nd isotopes in order to compare their source with the one from the lower F1 unit. Concerning the Tadoussac Intrusive Suite, an unpublished age of 1511 Ma was obtained using LA-ICP-MS U-Pb dating on zircon grains from an A-type granite (Solgadi, personal communication). A

more precise age using CA-TIMS would bring more information on the relation between the I- and A-types intrusive rocks of this complex.

3) A set of zircon grains from several igneous rocks from well-delimited intrusions and deformed igneous rocks should be dated by LA-ICP-MS in order to refine the magmatic history in the area. This technique can be coupled to in-situ Lu-Hf analyses in order to constraint the different types of sources. Depending on the LA-ICP-MS U-Pb results, CA-TIMS technic could be used in order to deliver more accurate ages.

4) Higher resolution maps can be produced in keys areas of the different synclines, with focus on the different types of volcanic, sedimentary and intrusive rocks together with their primary textures and the alteration that affected. A systematic sampling has to be done in order to increase the set of geochemical analyses and polished thin sections. The geochemical analyses can be used in order to better define the various types of hydrothermal alteration in term of major and trace elements and potentially to calculate mass balance changes. In addition, minerals (amphibole, garnet, epidote, biotite, muscovite, carbonate…) from the metamorphosed alteration zones can be analyzed by EPMA following what has been done in Chapter 4. They can provide key information relative to the alteration zones and they can outline high-temperature discordant pipes that can be linked to massive sulfides lenses.

5) The northern limit of the ESB is a major shear-zone, however no precise age constraint is available. The deformation zone is separating low-*P* rocks in the south (ESB) from rocks that experienced partial melting in the north. Some melt pockets from migmatitic gabbro have been sampled in order to obtain an age of these partial melting event. Such an age can provide an important addition to the understanding of the impact

of the Grenville in this area and it can be compared with the Grenvillian metamorphic and magmatic ages obtained on the southern side of the shear-zone. Pressure-temperature conditions from samples from both side of the shear-zone have to be modelled in order to fill the information gap for this part of the Grenville Province. Furthermore, a more detailed structural study within the supracrustal rocks has to be done.

6.3 References

Barbarin, B., 1999. A review of the relationships between granitoid types, their origins and their geodynamic environments. Lithos 46, 605–626. doi:10.1016/S0024-4937(98)00085-1

Gower, C.F., Krogh, T.E., 2002. A U–Pb geochronological review of the Proterozoic history of the eastern Grenville Province. Canadian Journal of Earth Sciences 39, 795–829. doi:10.1139/e01-090

Rivers, T., 1997. Lithotectonic elements of the Grenville Province: review and tectonic implications. Precambrian Research 86, 117–154. doi:10.1016/S0301-9268(97)00038-7

Bibliography and References

Agrawal, S., Guevara, M., Verma, S.P., 2008. Tectonic discrimination of basic and ultrabasic volcanic rocks through log-transformed ratios of immobile trace elements, International Geology Review, volume 50 (12), 1057–1079.

Allen, R.L, Lundström, I., Ripa, M., Simeonov, A., and Christofferson, H., 1996. Facies analysis of a 1.9 Ga, continental margin, back-arc, felsic caldera province with diverse Zn-Pb-Ag-(Cu-Au) sulfide and Fe oxide deposits, Bergslagen region, Sweden. Economic Geology, volume 91, 979–1008.

Ames, D.E., Galley, A.G., Kjarsgaard, I.M.K., Tardif, N., Taylor, B.E., 2016. Hanging-wall vectoring for buried volcanogenic massive sulfide deposits, Paleoproterozoic Flin Flon Mining Camp, Manitoba, Canada. Economic Geology, volume 111, 963–1000.

Augland, L.E., Moukhsil, A., Solgadi, F., Indares, A., 2015. Pinwarian to Grenvillian magmatic evolution in the central Grenville Province: new constraints from ID-TIMS U-Pb ages and coupled Lu-Hf S-MC-ICP-MS data. Canadian Journal of Earth Sciences, volume 52, 701–721.

Bailes, A.H., Galley, A.G., Paradis, S., Taylor, B.E., Pehrsson, S.J., Gibson, H.L., Gilmore, K., 2016. Variations in large synvolcanic alteration zones at Snow Lake, Manitoba, Canada, with proximity to associated volcanogenic massive sulfide deposits. Economic Geology, volume 111 (4), 933–962.

Ballouard, C., Poujol, M., Boulvais, P., Zeh, A., 2017. Crustal recycling and juvenile addition during lithospheric wrenching : the Pontivy-Rostrenen magmatic complex, Armorican Massif (France), Variscan belt. Gondwana Research, volume

49, 222–247. doi:10.1016/j.gr.2017.06.002

Barbarin, B., 1999. A review of the relationships between granitoid types, their origins and their geodynamic environments. Lithos 46, 605–626. doi:10.1016/S0024-4937(98)00085-1

Barret, T.J., MacLean, W.H., 1994a. Mass changes in hydrothermal alteration zones associated with VMS deposits of the Noranda Area. Exploration and Mining Geology, volume 3 (2), 131–160.

Barret, T.J., MacLean, W.H., 1994b. Chemostratigraphy and hydrothermal alteration in exploration for VHMS deposits in greenstones and younger volcanic rocks, in Lentz, D.R., ed., Alteration and Alteration Processes associated with Ore-forming Systems: Geological Association of Canada, Short Course Notes, volume 11, 433–467.

Barret, T.J, MacLean, W.H., 1999. Volcanic sequences, lithogeochemistry, and hydrothermal alteration in some bimodal volcanic-associated massive sulfide systems, in: C.T. Barrie and M.D. Hannington (Eds.), Volcanic-Associated Massive Sulfide Deposits: Processes and Examples in Modern and Ancient Environments. Society of Economic Geologists, Reviews in Economic Geology, volume 8, 101–131.

Barrie, T.C., and Pattinson, J., 1999. Fe-Ti basalts, High silica rhyolites and the role of magmatic heat in the genesis of the Kam-Kotia volcanic-associated massive sulfide deposit, Western Abitibi Subprovince, Canada. Economic Geology, Monograph 10, 577–592.

Beaumont, C., Nguyen, M.H., Jamieson, R.A., and Ellis, S., 2006. Crustal flow modes in large hot orogens. In Channel Flow, Ductile Extrusion and Exhumation in Continental Collision Zones. Edited by R.D. Law, M.P. Searle, and L. Godin. Geological Society, London, Special Publication 268, 91–145.

Beaumont, C., Jamieson, R., Nguyen, M., 2010. Models of large, hot orogens containing a collage of reworked and accreted terranes. Canadian Journal of Earth Sciences, volume 47, 485–515.

Benahmed, S., Intissar, R., 2015. Levé magnétique aéroporté dans le secteur des Escoumins, Côte-Nord, Province de Grenville. Ministère de l'Énergie et des Ressources naturelles, Québec, DP 2015-04.

Bernier, L.R., Pouliot, G., MacLean, W.H., 1987. Geology and metamorphism of the Montauban north gold zone: a metamorphosed polymetallic exhalative deposit, Grenville Province, Quebec. Economic Geology, volume 82, 2076–2090.

Bernier, L.R., MacLean, W.H., 1993. Lithogeochemistry of a metamorphosed VMS alteration zone at Montauban Grenville Province, Quebec. Exploration and Mining Geology, volume 2(4), 367–386.

Bickford, M.E., Van Schmus, W.R., Karlstrom, K.E., Mueller, P.A., Kamenov, G.D., 2015. Mesoproterozoic-trans-Laurentian magmatism: a synthesis of continent-wide age distributions, new SIMS U-Pb ages, zircon saturation temperatures, and Hf and Nd isotopic compositions. Precambrian Research, volume 265, 286–312.

Bonin, B., 2007. A-type granites and related rocks: Evolution of a concept, problems and prospects. Lithos, volume 97, 1–29. doi:10.1016/j.lithos.2006.12.007

Bonnet, A.-L., Corriveau, L., La Flèche, M.R., 2005. Chemical inprit of highly metamorphosed volcanic-hosted hydrothermal alterations in the La Romaine Supracrustal Belt, easttern Grenville Province, Quebec. Canadian Journal of Earth Sciences, volume 42, 1783–1814.

Bonnet, A.-L., Corriveau, L., 2006. Atlas et outils de reconnaissance de systèmes hydrothermaux métamorphisés dans les terrains gneissiques. DIVEX, 94 pages.

Bourne, J., 1991. The geochemistry of the La Galissonniere Pluton: a Middle Proterozoic late-orogenic intrusion from the eastern Grenville Province, Quebec. Canadian Journal of Earth Sciences, volume 28, 37–43.

Brisebois, D., Clark, T., 2003. Géologie et ressources minérales de la partie est de la Province de Grenville. Ministère des Ressources naturelles de la Faune et des Parcs, Québec, DV 2002-03, 419 p.

Brown, G.C., Thorpe, R.S., Webb, P.C., 1984. The geochemical characteristics of granitoids in contrasting arcs and comments on magma sources. Journal of the Geological Society of London, volume 141, 413–426.

Brueckner, S.M., Piercey, S.J., Sylvester, P.J., Maloney, S., Pilgrim, L., 2014. Evidence for syngenetic precious metal enrichment in an Appalachian volcanogenic massive sulfide system: the 1806 Zone, Ming Mine, Newfoundland, Canada. Economic Geology, volume 109, 1611–1642.

Cabanis, B., Lecolle, M., 1989. Le diagramme La/10-Y/15-Nb/8 ; un outil pour la discrimination des séries volcaniques et la mise en évidence des processus de mélange et/ou de contamination crustale. Comptes Rendus de l'Académie des

Sciences, Série 2, Mécanique, Physique, Chimie, Sciences de l'Univers, Sciences de la Terre, volume 309 (20), 2023–2029.

Campbell, I.H., Lesher, C.M., Coad, P., Franklin, J.M., Gorton, M.P., Thurston, P.C., 1984. Rare-Earth element mobility in alteration pipes below massive Cu-Zn sulfide deposits. Chemical Geology, volume 45, 181–202.

Carr, S.D., Easton, R.M., Jamieson, R.A., Culshaw, N.G., 2000. Geologic transect across the Grenville Orogen of Ontario and New York. Canadian Journal of Earth Sciences, volume 37, 193–216.

Caté, A., Ross, P.-S., Gagne, S., 2015. Hydrothermal history and gold mineralization at the Lalor volcanogenic massive sulphide deposit, Snow Lake camp, Manitoba, Canada. 13th SGA biennal meeting, Nancy, France.

Caté, A., 2016. Geology of the Paleoproterozoic Zn-Cu-Au Lalor volcanogenic massive sulphide deposit and its gold-rich lenses, Snow Lake, Manitoba. PhD thesis, Université du Québec, Institut National de la Recherche Scientifique, 384 p.

Cawood, P.A., Hawkesworth, C.J., Dhuime, B., 2012. Detrital zircon record and tectonic setting. Geology, volume 40, 875–878.

Cawood, P.A., Strachan, R.A., Pisarevsky, S.A., Gladkochub, D.P., Murphy, J.B., 2016. Linking collisional and accretionary orogens during Rodinia assembly and breakup: Implications for models of supercontinent cycles. Earth and Planetary Science Letters, volume 449, 118–126. doi:10.1016/j.epsl.2016.05.049

Černý, P., Ercit, T.S., 2005. The classification of granitic pegmatites revisited. Canadian Mineralogist 43, 2005–2026. doi:10.2113/gscanmin.43.6.2005

Chen, B., Xiaoping, L., Wilde, S.A., Yuan, C., Wang, Q., Xia, X., Zhang, Z., 2017.

Delamination of lithospheric mantle evidenced by Cenozoic potassic rocks in Yunnan, SW China: a contribution to uplift of the Eastern Tibetan Plateau. Lithos, 284-285, 709–729.

Colman-Sadd, S.P., Dunning, G.R., Dec, T., 1992. Dunnage-Gander relationships and Ordovician orogeny in central Newfoundland: a sediment provenance and U/Pb age study. American Journal of Science, volume 292, 317–355.

Condie, K.C., 2003. Incompatible element ratios in oceanic basalts and komatiites: tracking deep mantle sources and continental growth rates with time. Geochemistry Geophysics Geosystems, volume 4 (1), 1005. doi:10.1029/2002GC000333.

Corrigan, D., van Breemen, O., Hanmer, S., Nadeau, L., 1994. Arc accretion, crustal thickening, and post-collisional extension in the Grenville Province: constraints from the St. Maurice lithotectonic belt. Lithoprobe Meeting, Abitibi-Grenville Transect, Université de Montreal, Montreal, Quebec, Nov/Dec. 1994. Program with abstracts.

Corrigan, D., 1995. Mesoproterozoic evolution of the south-central Grenville orogen: structural, metamorphic, and geochronologic constraints from the Mauricie transect. PhD thesis, Carleton University, 282 p.

Corrigan, D., van Breemen, O., 1997. U-Pb age constraints for the lithotectonic evolution of the Grenville Province along the Mauricie transect, Quebec. Canadian Journal of Earth Sciences, volume 34, 299–316.

Corrigan, D., Hanmer, S., 1997. Anorthosites and related granitoids in the Grenville Orogen: a product of convective thinning of the lithosphere? Geology, volume 25,

61–64. doi:10.1130/0091-7613(1997)025<0061:AARGIT>2.3.CO;2

Corriveau, L., Heaman, L.M., Marcantonio, F., and van Breemen, O., 1990. 1.1 Ga K-rich alkaline plutonism in the SW Grenville Province. Contribution to Mineralogy and Petrology, volume 105, 473–485.

Corriveau, L., Morin, D., 2000. Modelling 3D architecture of western Grenville from surface geology, xenoliths, styles of magma emplacement, and Lithoprobe reflectors. Canadian Journal of Earth Sciences, volume 37, 235–251. doi:10.1139/e99-121

Corriveau, L., Bonnet, A.-L., 2005. Pinwarian (1.5 Ga) volcanism and hydrothermal activity at the eastern margin of the Wahekam Group, Grenville Province, Quebec. Canadian Journal of Earth Sciences, volume 42, 1749–1782.

Craddock, P.R., Bach, W., Seewald, J.S., Rouxel, O.J., Reeves, E., Tivey, M.K., 2010. Rare earth element abundances in hydrothermal fluids from the Manus Basin, Papua New Guinea: Indicators of sub-seafloor hydrothermal processes in back-arc basins. Geochemica et Cosmochimica Acta, volume 74, 5494–5513.

Culshaw, N.G., Beaumont, C., Jamieson, R.A., 2006. The orogenic superstructure-infrastructure concept: revisited, quantified, and revived. Geology, volume 34, 733–736.

Cuney, M., Kyser, K., 2009. Chapter 7: Hydrothermal Uranium Deposits Related to Igneous Rocks. Mineralogical Association of Canada.

David, J., Moukhsil, A., Clark, T., Hébert, C., Nantel, S., Dion, C., Sappin, A.-A., 2009. Datations U-Pb effectuées dans les provinces de Grenville et de Churchill en 2006-2007. Ministère des Ressources naturelles et de la Faune, RP 2009-03, 32 p.

David, J., Moukhsil, A., Dion, C., 2010. Datations U-Pb effectuées dans la Province de Grenville en 2008-2009. Ministère de l'Énergie et des Ressources naturelles du Québec, RP2010-10.

Davies, J.F., Whitehead, R.E., 1994. Molar ratios in the study of unaltered and hydrothermally altered greywackes and shales. Chemical Geology, volume 111, 85–100.

Davies, J.F., Whitehead, R.E., 2006. Alkali-Alumina and MgO-Alumina molar ratios of altered and unaltered rhyolites. Exploration and Mining Geology, volume 15 (1-2), 75–88.

Day, W.C., Slack, J.F., Ayuso, R.A., Seeger, C.M., 2016. Regional geologic and petrologic framework for iron oxide ± apatite ± rare earth element and iron oxide copper-gold deposits of the Mesoproterozoic St. Francois Mountains Terrane, Southeast Missouri, USA. Economic Geology, volume 111, 1825–1858.

Defant, M.J., Drummond, M.S., 1990. Derivation of some modern arc magmas by melting of young subducted lithosphere. Nature, volume 347, 662–665.

Defant, M.J., Drummond, M.S., 1993. Mount St. Helens: potential example of the partial melting of the subducted lithosphere in a volcanic arc. Geology, volume 21, 541–550.

Debon, F., and Le Fort, P. 1988. A cationic classification of common plutonic rocks and magmatic associations: principles, method, applications. Bulletin de Minéralogie, volume 111, 493–510.

DePaolo, D.J., 1981. Neodynium isotopes in the Colorado Front Range and crust-mantle evolution in the Proterozoic. Nature, volume 291, 193–196.

De Paolo, D. J. 1988. Neodymium isotope geochemistry. Springer-Verlag. 187 pp.

Dewey, J.F., 1988. Extensional collapse of orogens. Tectonics, volume 7(6), 1123–1139.

DeWolfe, Y.M., Gibson, H.L., Lafrance, B., Bailes, A.H., 2009a. Volcanic reconstruction of Paleoproterozoic arc volcanoes: the Hidden and Louis formations, Flin-Flon, Manitoba, Canada. Canadian Journal of Earth Sciences, volume 46 (7), 481–508.

DeWolfe, Y.M., Gibson, H.L., Piercey, S.J, 2009b. Petrogenesis of the 1.9 Ga mafic hanging-wall sequence to the Flin-Flon, Callinan and Triple 7 massive sulphide deposits, Flin-Flon, Manitoba, Canada. Canadian Journal of Earth Sciences, volume 46 (7), 509–527.

Dickin, A.P., Higgins, M.D., 1992. Sm /Nd evidence for a major 1.5 Ga crust-forming event in the central Grenville Province. Geology, volume 20, 137–140.

Dickin, A.P., 2000. Crustal formation in the Grenville Province: Nd-isotope evidence. Canadian Journal of Earth Sciences, volume 37, 165–181.

Dickin, A.P., McNutt, R.H., Martin, C., Guo, A., 2010. The extent of juvenile crust in the Grenville Province: Nd isotope evidence. Geological Society of America Bulletin, volume 122 (5-6), 870–883.

Douville, E., Bienvenu, P., Charlou, J.L., Donval, J.P., Fouquet, Y., Appriou, P., Gamo, T., 1999. Yttrium and rare earth elements in fluids from various deep-sea hydrothermal systems. Goechimica et Cosmochimica Acta, volume 63 (5), 627–643.

Dubé, B., Mercier-Langevin, P., Hannington, M., Lafrance, B., Gosselin, G., Gosselin, P., 2007. The LaRonde Penna World-Class Au-Rich Volcanogenic Massive Sulfide Deposit, Abitibi, Québec: Mineralogy and Geochemistry of Alteration and

Implications for Genesis and Exploration. Society of Economic Geologist, volume 102, 633–666.

Dubé, B., Gosselin, P., Mercier-Langevin, P., Hannington, M., Galley, A., 2007. Gold-rich volcanogenic massive sulphide deposits, in: W.D. Goodfellow (Ed.), Mineral Deposits of Canada; A synthesis of Major Deposit Types, District Metallogeny, the Evolution of Geological Provinces, and Exploration Methods. Geological Association of Canada, Mineral Deposits Division, Special Publication No. 5, 75–94.

Dubé, B., Mercier-Langevin, P., Kjarsgaard, I., Hannington, M., Bécu, V., Côté, J., Moorhead, J., Legault, M., Bédard, N., 2014. The Bousquet 2-Dumagami World-Class Archean Au-Rich Volcanogenic Massive Sulfide Deposit, Abitibi, Quebec: Metamorphosed Submarine Advanced Argillic Alteration Footprint and Genesis. Society of Economic Geologist, volume 109, 121–166.

Dunning, G., Indares, A., 2010. New insights on the 1.7–1.0Ga crustal evolution of the central Grenville Province from the Manicouagan – Baie Comeau transect. Precambrian Research, volume 180, 204–226. doi:10.1016/j.precamres.2010.04.005

Eilu, P.K., Mathison, C.I., Groves, D.I., Allardyce, W.J., 1999. Atlas of alteration assemblages, styles and zoning in orogenic lode-gold deposits in a variety of host rocks and metamorphic settings. Geology and Geophysics Department (Centre for Strategic Mineral Deposits) & UWA Extension, The University of Western Australia, Publication 30, 50 p.

Embley, R.W., Jonasson, I.R., Perfit, M.R., Franklin, J.M., Tivey, M.A., Malahoff, A., Smith, M.F., Francis, T.J.G, 1988. Submersible investigation of an extinct hydrothermal system on the Galapagos ridge: sulfide mounds, stockwork zone, and differentiated lavas. Canadian Mineralogist, volume 26, 517–539.

Fowler, M.B., Kocks, H., Darbyshire, D.P.F., Greenwood, P.B., 2008. Petrogenesis of high Ba-Sr plutons from the Northern Highlands Terrane of the British Caledonian Province. Lithos, volume 105, 129–148. doi:10.1016/j.lithos.2008.03.003

Frost, B.R., Barnes, C.G., Collins, W.J., Arculus, R.J., Ellis, D.J., Frost, C.D., 2001. A Geochemical Classification for Granitic Rocks. Journal of Petrology, volume 42, 2033–2048. doi:10.1093/petrology/42.11.2033

Frost, B.R., Frost, C.D., 2008. A geochemical classification for feldspathic igneous rocks. Journal of Petrology 49, 1955–1969. doi:10.1093/petrology/egn054

Frost, C.D., Frost, B.R., 2011. On ferroan (A-type) granitoids: Their compositional variability and modes of origin. Journal of Petrology, volume 52, 39–53. doi:10.1093/petrology/egq070

Galley, A.G., Hannington, M.D., Jonasson, I., 2007. Volcanogenic massive sulphide deposits, in: W.D. Goodfellow (Ed.), Mineral Deposits of Canada; A synthesis of Major Deposit Types, District Metallogeny, the Evolution of Geological Provinces, and Exploration Methods. Geological Association of Canada, Mineral Deposits Division, Special Publication No. 5, 141–161.

Gammons, C.H., Wood, S.A., Li, Y., 2002. Complexation of the rare earth elements with aqueous chloride at 200 °C and 300 °C and saturated water vapor pressure, in Hellmann, R. and Wood, S.A., eds., Water-Rock interactions, Ore Deposits, and

Environmental Geochemistry: A tribute to David A. Crerar. The Geological Society, Special Publication No. 7, 191–207.

Gauthier, M., Brown, A.C., 1986. Zinc and iron metallogeny in the Maniwaki-Gracefield District southwestern Quebec. Economic Geology, volume 81, 89–112.

Gauthier, M., Chartrand, F., Cayer, A., David, J., 2004. The Kwyjibo Cu-REE-U-Au-Mo-F property, Quebec : a Mesoproterozoic polymetallic iron oxide deposit in the northeastern Grenville Province. Economic Geology, volume 99, 1177–1196.

Gauthier, M., Chartrand, F., 2005. Metallogeny of the Grenville Province revisited. Canadian Journal of Earth Sciences, volume 42, 1719–1734.

Gehrels, G., Rusmore, M., Woodsworth, G., Crawford, M., Andronicos, C., Hollister, L., Patchett, J., Ducea, M., Butler, R., Klepeis, K., Davidson, C., Friedman, R., Haggart, J., Mahoney, B., Crawford, W., Pearson, D., Girardi, J., 2009. U-Th-Pb geochronology of the Coast Mountains batholith in north-coastal British Columbia: constraints on age and tectonic evolution. Geological Society of America Bulletin, volume 121, 1341–1361.

Genna, D., Gaboury, D., Roy, G., 2014. The Key Tuffite, Matagami Camp, Abitibi Greenstone Belt, Canada: petrogenesis and implications for VMS formation and exploration. Mineralium Deposita, volume 49, 489–512.

Gifkins, C., Herrmann, W., Large, R.R., 2005. Altered volcanic rocks: a guide to description and interpretation; Centre for Ore Deposits Research; University of Tasmania, Hobart, Tasmania, Australia, 275 p.

Ginsburg, A.I., 1984. The geological condition of the location and the formation of granitic pegmatites. International Geological Congress, 27th, Proceedings 15, 245–

260.

Gobeil, A., Hébert, C., Clark, T., Beaumier, M., Perreault, S., 2002. Géologie de la région du lac De La Blache (22K/03 et 22K/04). Ministère des Ressources naturelles et de la Faune, RG 2002-01, 49 p.

Gorton, M.P., Schandl, E.S., 2000. From continents to island arcs: a geochemical index of tectonic setting for arc-related and within-plate felsic to intermediate volcanic rocks. Canadian Mineralogist, volume 38, 1065–1073.

Gower, C.F., Erdmer, P., 1988. Proterozoic metamorphism in the Grenville Province: a study in the Double Mer – Lake Melville area, eastern Labrador. Canadian Journal of Earth Sciences, volume 25, 1895–1905.

Gower, C.F., Heaman, L.M., Loveridge, W.D., Sch.rer, U., and Tucker, R.D., 1991. Grenvillian granitoid plutonism in the eastern Grenville Province. Precambrian Research, volume 51, 315–336.

Gower, C.F., Krogh, T.E., 2002. A U-Pb geochronological review of the Proterozoic history of the eastern Grenville Province. Canadian Journal of Earth Sciences, volume 39, 795–829.

Gower, C.F., Kamo, S.L., Kwok, K., Krogh, T.E., 2008. Proterozoic southward accretion and Grenvillian orogenesis in the interior Grenville Province in eastern Labrador: Evidence from U-Pb geochronological investigations. Precambrian Research, volume 165, 61–95.

Groulier, P.-A., Indares, A., Dunning, G., Moukhsil, A., 2015. Géologie de la ceinture volcano-sédimentaire des Escoumins, Côte-Nord, Québec (rapport préliminaire), MB 2015-09, Énergie et Ressources naturelles, 57 p.

Groulier, P.-A., Indares, A.D., Dunning, G., Mouhksil, A., 2016. Géologie de la ceinture volcano-sédimentaire des Escoumins, Côte-Nord, Québec. MB 2016-07, Ministère de l'Énergie et des Ressources naturelles, 87 p.

Groulier, P.-A., Indares, A.D., Dunning, G., Mouhksil, A., Wälle, M., 2018a. Peri-Laurentian, Pinwarian-age oceanic arc crust preserved in the Grenville Province: insights from the Escoumins Supracrustal Belt. Precambrian Research, volume 311, 37–64.

Groulier, P.-A., Indares, A.D., Dunning, G., Mouhksil, A., Jenner, G., 2018b. Syn-orogenic magmatism over 100 m.y. in high crustal levels of the central Grenville Province: characteristics, age and tectonic significance. Lithos, volume 312-313, 128–152.

Groulier, P.-A., Turlin, F., André-Mayer, A.S., Ohbebstetter, D., Crépon, A., Boulvais, P., Poujol, M., Rollion-Bard, C., Zeh, A., Moukhsil, A., Solgadi, F., El Basbas, A., in review for Journal of Petrology. Silicate-carbonate liquid immiscibility: insights from the Crevier alkaline intrusion (Quebec).

Gunning, M.H., Hodder, R.W.H., Nelson, J.L., 2006. Contrasting volcanic styles within the Paleozoic Stikine assemblage, western Stikine terrane, northwestern British Columbia, in: M. Colpron and J.L. Nelson (Eds.), Paleozoic evolution and metallogeny of pericratonic terranes at the Ancient Pacific Margin of North America, Canadian and Alaskan Cordillera. Geological Association of Canada, Special Paper 45, 201–227.

Hanchar, J.M., Watson, E.B., 2003. Zircon saturation thermometry. Reviews in Mineralogy and Geochemistry, volume 53 (1), 89–112.

Harris, N.B.W., Pearce, J.A., Tindle, A.G., 1986. Geochemical characteristics of collision-zone magmatism. In: Coward, M.P., Reis, A.C. (Eds.), Collision Tectonics, Geological Society, London, Special Publications no. 19, pp. 67–81.

Hart, T.R., Gibson, H.L., Lesher, C.M., 2004. Trace element geochemistry and petrogenesis of felsic volcanic rocks associated with volcanogenic massive Cu-Zn-Pb sulfide deposits. Economic Geology, volume 99, 1003–1013.

Hastie, A.R., Kerr, A.C., Pearce, J.A., Mitchell, S.F., 2007. Classification of altered island arc rocks using immobile trace elements: development of the Th – Co discrimination diagram. Journal of Petrology, volume 48, 2341 – 2357.

Hawthorne, F. C., Kato, A., Kisch, H. J., Krivovichev, V. G., Linthout, K., Laird, J., Maresch, W. V., Schumacher, J. C., Stephenson, N. C. N., Whittaker, E. J. W. (1997). Nomenclature of amphiboles: report of the subcommittee on amphiboles of the International Mineralogical Association, Commission on New Minerals and Mineral Names. The Canadian Mineralogist, volume 35, 219–246.

Hébert, C., Lacoste, P., 1998. Géologie de la region de Bagotville (22D/07). Ministère des Ressources naturelles, Québec, RG 97-06, 17 p.

Hébert, C., van Breemen, O., 2004. Mesoproterozoic basement, the Lac-Saint-Jean anorthosite suite and younger Grenvillian intrusions in the Saguenay region (Quebec): structural relationships and U-Pb geochronology, in: R.P. Tollo, L. Corriveau, J. McLelland, and M. Bartholomew (Eds.). Geological Society of America, Memoir 197, 65–79.

Hébert, C., van Breemen, O., and Cadieux, A-M. 2009. Région du reservoir Pipmuacan (SNRC 22E): Synthèse géologique. RG 2009-01, Ministère des ressources

naturelles et de la faune, Gouvernement du Québec.

Hibbard, J., Karabinos, P., 2013. Disparate paths in the geologic evolution of the Northern and Southern Appalachians: a case for inherited contrasting crustal/lithospheric substrates. Geoscience Canada, volume 40, 303–317.

Higgins, M.D., van Breemen, O., 1996. Three generations of AMCG magmatism, contact metamorphism and tectonism in the Saguenay – Lac-Saint-Jean region, Grenville Province, Canada. Precambrian Research, volume 79 (3-4), 327–346.

Hoffman, P.F., 1989. Precambrian geology and tectonic history of North America. In The Geology of North America: an Overview. Geological Society of America, Boulder, Colo., The Geology of North America, Vol. A., 447–512.

Hughes, C.J., 1973. Spilites, keratophyres, and the igneous spectrum. Geological Magazine, volume 109, 513–527.

Hynes, E., 2010. Nd isotope delineation of crustal terranes in the Bancroft area of Ontario and the Saguenay and Baie Comeau regions of Central Quebec: ensialic rifting and arc formation. Msc thesis, McMaster University.

Hynes, A., Rivers, T., 2010. Protracted continental collision – evidence from the Grenville Orogen. Canadian Journal of Earth Sciences, volume 47, 591–620.

Indares, A., Moukhsil, A., 2013. Geon 12 crustal extension in the central Grenville Province, implications for the orogenic architecture, and potential influence on the emplacement of anorthosites. Canadian Journal of Earth Sciences 50, 955–966. doi:10.1139/cjes-2012-0161

Ishikawa, Y., Sawaguchi, T., Ywaya, S., Horiuchi, M., 1976. Delineation of prospecting targets for Kuroko deposits based on modes of volcanism of underlying dacite and alteration haloes. Mining Geology, volume 26, 105–117.

Jamieson, R.A., Beaumont, C., Nguyen, M.H., Culshaw, N.G., 2007. Synconvergent ductile flow in variable strength continental crust: numerical models with application to the western Grenville Province. Tectonics, volume 26, TC5005. https://doi.org/10.1029/2006TC002036.

Jamieson, R.A., Beaumont, C., Warren, C.J., Nguyen, M.H., 2010. The Grenville Orogen explained? Applications and limitations of integrating numerical models with geological and geophysical data. Canadian Journal of Earth Sciences, volume 47, 517–539.

Jansson, N.F., Erismann, F., Lundstam, E., Allen, R.L., 2013. Evolution of the Paleoproterozoic volcanic-limestone-hydrothermal sediment succession and Zn-Pb-Ag and Iron Oxide deposits at Stollberg, Bergslagen Region, Sweden. Economic Geology, volume 108, 309–335.

Jenner, G.A., 1996. Trace element geochemistry of igneous rocks: geochemical nomenclature and analytical geochemistry, in: D.A. Wyman (Ed.), Trace Element Geochemistry of Volcanic Rocks: Applications for Massive Sulfide Exploration. Geological Association of Canada, Short Course Notes, volume 12, 51–77.

Jiang, S.-Y., Wang, R.-C., Xu, X.-S., Zhao, K.-D., 2004. Mobility of high field strength elements (HFSE) in magmatic-, metamorphic-, and submarine-hydrothermal systems. Physics and Chemistry of the Earth, volume 30, 1020–1029.

Karlstrom, K.E., Ahall, K.-I., Harlan, S.S.,Williams, M.L., McLelland, J., Geissman, J.W., 2001. Long-lived (1.8-1.0 Ga) convergent orogen in southern Laurentia, its extensions to Australia and Baltica, and implications for refining Rodinia. Precambrian Research, volume 111, 5–30.

Ketchum, J.W.F., Heaman, L.M., Krogh., T.E., Culshaw, N.G., Jamieson, R.A., 1998. Timing and thermal influence of late orogenic extension in the lower crust: a U-Pb geochronological study from the southwest Grenville orogen, Canada. Precambrian Research, volume 89, 25–45.

Ketchum, J.W.F., Jackson, S.E., Culshaw, N.G., Barr, S.M., 2001. Depositional and tectonic setting of the Paleoproterozoic lower Aillik Group, Makkovik Province, Canada: evolution of a passive margin-foredeep sequence based on petrochemistry and U-Pb (TIMS and LAM-ICP-MS) geochronology. Precambrian Research, volume 105, 331–356.

Krogh, T.E., 1982. Improved accuracy of U-Pb zircon ages by the creation of more concordant systems using an air abrasion technique. Geochemica et Cosmochimica Acta, volume 46 (4), 637–649.

Large, R.R., Gemmell, J.B., Paulick, H., 2001. The alteration box plot: a simple approach to understanding the relationship between alteration mineralogy and lithogeochemistry associated with volcanic-hosted massive sulfide deposits. Economic Geology, volume 96, 957–971.

Lasalle, S., S., Fisher, C.M., Indares, A., and Dunning, G. 2013. Contrasting types of Grenvillian granulite facies aluminous gneisses: insights on protoliths and

metamorphic events from zircon morphologies and ages. Precambrian Research, volume 228, 117–130.

Lesher, C.M., Goodwin, A.M., Campbell, I.H., Gorton, M.P., 1986. Trace-element geochemistry of ore-associated and barren, felsic metavolcanics rocks in the Superior Province, Canada. Canadian Journal of Earth Sciences, volume 23, 222–237.

Li, Z.X., Bogdanova, S. V, Collins, A.S., Davidson, A., De Waele, B., Ernst, R.E., Fitzsimons, I.C.W., Fuck, R.A., Gladkochub, D.P., Jacobs, J., Karlstrom, K.E., Lu, S., Natapov, L.M., Pease, V., Pisarevsky, S.A., Thrane, K., Vernikovsky, V., 2008. Assembly, configuration, and break-up history of Rodinia: A synthesis. Precambrian Research, volume 160, 179–210. doi:10.1016/j.precamres.2007.04.021

Liu, D., Zhao, Z., Zhu, D.C., Niu, Y., DePaolo, D.J., Harrison, T.M., Mo, X., Dong, G., Zhou, S., Sun, C., Zhang, Z., Liu, J., 2014. Postcollisional potassic and ultrapotassic rocks in southern Tibet: Mantle and crustal origins in response to India-Asia collision and convergence. Geochimica et Cosmochimica Acta, volume 143, 207–231. doi:10.1016/j.gca.2014.03.031

Liu, Z., Liao, S.-Y., Wang, J.-R., Ma, Z., Liu, Y.-X., Wang, D.-B., Tang, Y., Yang, J., 2017. Petrogenesis of late Eocene Ba-Sr potassic rocks from Western Yangtze Block, SE Tibet : a magmatic response to the Indo-Asian collision. Journal of Asian Earth Sciences, volume 135, 95–109.

London, D., 2008. Pegmatites. Canadian Mineralogist Special Publication 10, 368.

MacLean, W.H., Seymour, K.S., Prabhu, M.K., 1982. Sr, Y, Zr, Nb, Ti, and REE in Grenville amphibolites at Montauban-les-Mines, Quebec. Canadian Journal of Earth Sciences, volume 19, 633–644.

MacLean, W.H., Barrett, T.J., 1993. Lithogeochemical techniques using immobile elements. Journal of Geochemical Exploration, volume 48, 109–133.

Madore, L., Verpaelst, P., Choinière, J., Dion, D.-J., David, J., Lefebre, D., Marquis, R., Hocq, M. 1997*a*. Géologie de la région du Lac Briend. Ministère des ressources naturelles du Québec, RG96-05.

Maniar, P.D., Piccoli, P.M., 1989. Tectonic discrimination of granitoids. Geological Society of America Bulletin doi:10.1130/0016-7606(1989)101<0635:TDOG>2.3.CO

Madore, L., Verpaelst, P., Brisebois, D., Choinière, J., Dion, D.-J., David, J. 1997*b*. Géologie de la région du Lac Cormier. Ministère des ressources naturelles du Québec, RG97-08.

Martignole, J., Machado, N., Nantel, S., 1993. Timing of Intrusion and Deformation of the Rivière-Pentecôte Anorthosite (Grenville Province). The Journal of Geology, volume 1, 652–658.

Mattinson, J.M., 2005. Zircon U-Pb chemical abrasion (‘‘CA-TIMS’’) method: combined annealing and multi-step partial dissolution analysis for improved precision and accuracy of zircon ages. Chemical Geology, volume 220, 47-66.

McDonough, W.F., Sun, S.S., 1995. The composition of the Earth. Chemical Geology, volume 120, 228 p.

McLelland, J.M., Selleck, B.W., Bickford, M.E., 2013. Tectonic evolution of the Adirondack Mountains and Grenville Orogen inliers within the USA. Geoscience Canada, volume 40, 318–352.

Mercier-Langevin, P., Caté, A., and Ross, P.-S. (2014a) Whole-rock oxygen isotope mapping, Lalor auriferous VMS deposit footwall alteration zones, Snow Lake, west-central Manitoba (NTS 63K16). Report of activities 2014, Manitoba Mineral Resources, Manitoba Geological Survey, 94–103.

Mercier-Langevin, P., Hannington, M.D., Dubé, B., Piercey, S.J., Peter, J.M., and Pehrsson, S.J., 2015. Precious metal enrichment processes in volcanogenic massive sulphide deposits — A summary of key features, with an emphasis on TIGI-4 research contributions, In: Targeted Geoscience Initiative 4: Contributions to the Understanding of Volcanogenic Massive Sulphide Deposit Genesis and Exploration Methods Development, (ed.) J.M. Peter and P. Mercier-Langevin; Geological Survey of Canada, Open File 7853, 117–130.

Meschede, M., 1986. A method of discriminating between different types of mid-ocean ridge basalts and continental tholeiites with the Nb-Zr-Y diagram. Chemical Geology, volume 56, 207–218.

Migdisov, A.A., Williams-Jones, A.E., Wagner, T., 2009. An experimental study of the solubility and speciation of the Rare Earth Elements (III) in fluoride- and chloride-bearing aqueous solutions at temperatures up to 300 °C. Geochemica et Cosmochimica Acta, volume 73, 7087–7109.

Miller, M.L., 1973. Région de Saint-Siméon Tadoussac, Ministère de l'Énergie et des Ressources naturelles, Québec ; GM 159, 94 p.

Miyashiro, A. 1974. Volcanic rock series in island arc and arctive continental margins. American Journal of Science, volume 274(4), 321–355.

Morin, G., 1987a. Gîtologie de la région de Montauban. Ministère des ressources naturelles du Québec, MM 86-02, 59 p.

Morin, G., 1987b. Gîtologie des régions de Sacré-Coeur et de Grandes-Bergeronnes, Ministère de l'Énergie et des Ressources naturelles, Québec ; ET 85-11, 25 pages.

Morrison, G.W., 1980. Characteristics and tectonic setting of the shoshonite rock association. Lithos, volume 13, 97–108.

Moukhsil, A., Lacoste, P., Gobeil, A., David, J., 2009. Synthèse géologique de la région de Baie-Comeau (SNRC 22F). Ministère des Ressources naturelles et de la Faune, RG 2009-03, 28 p.

Moukhsil, A., Solgadi, F., Lacoste, P., Gagnon, M., David, J., 2012. Géologie de la region du lac du Milieu (SNRC 22O03, 22O04, 22O06, 22J13 et 22J14). Ministère des Ressources naturelles et de la Faune, RG 2012-01, 31 p.

Nadeau, L., van Breemen, O., Hebert, C., 1992. Géologie, âge et extension géographique du groupe de Montauban et du complexe de La Bostonnais. Ministère de l'Énergie et des Ressources, Québec, DV 92-03, 35–39.

Nadeau, L., van Breemen, O., 1994. Do the 1.45-1.39 Ga Montauban Group and the La Bostonnais complex constitute a Grenvillian accreted terrane? In Program with abstracts. Geological Association of Canada, volume 19, p. A81.

Nadeau, L., Brouillette, P., Hébert, C., 2008. Arc magmatism, continental collision and exhumation : the Mesoproterozoic evolution of the south-central Grenville

Province, Portneuf-Mauricie region, Quebec. Field trip B3, GAC-MAC-SEG-GSA Joint Annual Meeting, Québec, Canada.

Nold, J.L., Dudley, M.A., Davidson, P., 2013. The Southeast Missouri (USA) Proterozoic iron metallogenic province - Types of deposits and genetic relationships to magnetite-apatite and iron oxide-copper-gold deposits. Ore Geology Reviews, volume 57, 154–171.

Owen, J.V., Erdmer, P., 1990. Middle Proterozoic geology of the Long Range inlier, Newfoundland: regional significance and tectonic implications. In: Gower, C.F., Rivers, T., Ryan, A.B. (Eds.), Mid-Proterozoic Laurentia-Baltica, Geological Association of Canada, Special Paper 38, 215–231.

Owens., B.E., Tomascak, P.B., 2002. Mesoproterozoic lamprophyres in the Labrieville Massif, Quebec: clues to the origin of alkali anorthosites? Canadian Journal of Earth Sciences, volume 39, 983–997.

Parada, M.A., Lopez-Escobar, L., Oliveros, V., Fuentes, F., Morata, D., Calderon, M., Aguirre, L., Feraud, G., Espinoza, F., Moreno, H., Figueroa, O., Munoz Bravo, J., Troncoso Vasquez, R., Stern, C.R., 2007. In: Moreno, T., Gibbons, W. (Eds.), The Geology of Chile. The Geological Society, London., 147–178.

Pearce, J.A., 1982. Trace element characteristics of lavas from destructive plate boundaries. In: Thorpe, R.S. (Ed.), Orogenic Andesites. Wiley, Chichester, U.K., 528–548.

Pearce, J.A., Harris, B.W., Tindle, A.G., 1984. Trace element discrimination diagrams for the tectonic interpretation of granitic rocks. Journal of Petrology, volume 25 (4), 956–983.

Pearce, J.A., Ernewein, M., Bloomer, S.H., Parson, L.M., Murton, B.J., Johnson, L.E., 1994. Geochemistry of Lau Basin volcanic rocks: influence of ridge segmentation and arc proximity. In: Smellie, J.L. (Ed.), Volcanism Associated with Extension at Consuming Plate Margins, Geological Society of London, Special Publication No. 81, 53–75.

Pearce, J.A., Peate, D.W., 1995. Tectonic implications of the composition of volcanic arc magmas. Annual Review of Earth and Planetary Sciences, volume 23, 251–285.

Pearce, J.A., Stern, R.J, 2006. Origin of Back-Arc Basin Magmas: Trace Element and Isotope Perspectives, in: D.M. Christie et al., (Eds), Back-Arc Spreading Systems: Geological, Biological, Chemical and Physical Interactions. AGU Washington D.C., Geophysical Monograph Series 166, 63–86.

Pearce, J.A., 2008. Geochemical fingerprinting of oceanic basalts with applications to ophiolite classification and the search for Archean oceanic crust. Lithos, volume 100, 14–48.

Pearce, J.A., 2014. Immobile element fingerprinting of ophiolites. Elements, volume 10, 101–108.

Peccerillo, A., Taylor, S.R., 1976. Rare earth elements in East Carpathian volcanic rocks. Earth and Planetary Science Letters, volume 32, 121–126. doi:10.1016/0012-821X(76)90050-9

Piercey, S.J., 2008. Lithogeochemistry of volcanic rocks associated with volcanogenic massive sulphide deposits and applications to exploration, in Submarine Volcanism and Mineralization: Modern Through Ancient, (eds.) B. Cousens and

S. Piercey; Geological Association of Canada, Short Course 29-30 May 2008, Quebec City, Canada, 25 p.

Piercey, S.J., 2010. An overview of petrochemistry in the regional exploration for volcanogenic massive sulphide (VMS) deposits. Geochemistry: Exploration, Environment, Analysis, volume 10, 1–18, doi 10.1144/1467-7873/09-221.

Piercey, S.J., 2011. The setting, style, and role of magmatism in the formation of volcanogenic massive sulfide deposits. Mineralium Deposita, volume 46 (5), 449–471.

Plank, T., Langmuir, C.H., 1998. The chemical composition of subducting sediment and its consequences for the crust and mantle. Chemical Geology, volume 145, 325–394. doi:10.1016/S0009-2541(97)00150-2

Prahbu, M.K., Webber, G.R., 1984. Origin of quartzofeldspathic gneisses at Montauban-les-mines, Quebec, Canadian Journal of Earth Sciences, volume 21, 336–345.

Raczek, I., Jochum, K.P., Hofmann, A.W., 2003. Neodynium and Strontium Isotope Data for USGS Reference Materials BCR-1, BCR-2, BHVO-1, BHVO-2, AGV-1, AGV-2, GSP-1, GSP-2 and Eight MPI-DING Reference. Geostandards and Geoanalytical Research, volume 27 (2), 173–179.

Rivers, T., Martignole, J., Gower, C.F., Davidson, A., 1989. New tectonic divisions of the Grenville Province, southeast Canadian shield. Tectonics, volume 8 (1), 63–84. doi:10.1029/TC008i001p00063.

Rivers, T., 1997. Lithotectonic elements of the Grenville Province: a review and tectonic implications. Precambrian Research, volume 86, 117–154.

Rivers, T., Corrigan, D., 2000. Convergent margin on southeastern Laurentia during the Mesoproterozoic: tectonic implications. Canadian Journal of Earth Sciences, volume 37, 359–383.

Rivers, T., 2008. Assembly and preservation of lower, mid and upper orogenic crust in the Grenville Province – Implications for the evolution of Large hot long-duration orogens. Precambrian Research, volume 167, 237–259.

Rivers, T., 2012. Upper-crustal orogenic lid and mid-crustal core complexes: signature of a collapsed orogenic plateau in the hinterland of the Grenville Province. Canadian Journal of Earth Sciences, volume 49, 1–42.

Rivers, T., Culshaw, N., Hynes, A., Indares, A., Jamieson, R., Martignole, J., 2012. The Grenville Orogen – A post-LITHOPROBE perspective, Chapter 3, in: Percival, J.A., Cook, F.A., and Clowes, R.M. (Eds.), Tectonic Styles in Canada: the LITHOPROBE Perspective. Geological Association of Canada, Special Paper 49, 97–236.

Rivers, T., 2015. Tectonic setting and evolution of the Grenville Orogen: an assessment of progress over the last 40 years. Geoscience Canada, volume 42, 77–124. http://dx.doi.org/10.12789/geocanj.2014.41.057

Roger, C., Cousens, B., Ernst, R.E., Söderlund, U., Phosphorus and potassium metasomatic enrichment in the mantle source of the c. 1450–1425 Ma Michael – Shabogamo gabbro of eastern Laurentia. Journal of Petrology, volume 60 (1), 57–84.

Rondot, J., Marleau, J.R., 1977. La silice de Charlevoix, CIM Bull. 70, 105-115.

Rondot, J., 1979. Reconnaissances Géologiques dans Charlevoix-Saguenay, Ministère de l'Énergie et des Ressources naturelles, Québec ; DPV-682, 44 p.

Rondot, J., 1986. Géologie de la région de Forestville-Les Escoumins, Ministère de l'Énergie et des Ressources naturelles, Québec ; ET 85-05, 47 p.

Rondot, J., 1989. Géologie de Charlevoix, Ministère de l'Énergie et des Ressources naturelles, Québec; MB 89-21, 606 p.

Rondot, J., Lavergne, G., 1984. Carte géologique de la région de Forestville-Les Escoumins, 2 cartes annotées, Ministère de l'Énergie et des Ressources naturelles, Québec ; DP 84-54.

Ross, P.-S., Bédard, J.H., 2009. Magmatic affinity of modern and ancient subalkaline volcanic rocks determined from trace-element discriminant diagrams. Canadian Journal of Earth Sciences, volume 46, 823–839.

Rucks, T.W., Piercey, S.J., Ryan, J.J., Villeneuve, M.E., Creaser, R.A., 2006. Mid- to Late Paleozoic K-feldspar Augen granitoids in the Yukon-Tanana Terrane, Yukon, Canda: Implications for crustal growth and tectonic evolution of the Northern Cordillera. Geological Society of America Bulletin, volume 118, 1212–1231.

Salvi, S., William-Jones, A.E., 1996. The role of hydrothermal processes in concentrating high-field strength elements in the Strange Lake peralkaline complex, northeastern Canada. Geochimica et Cosmochimica Acta, volume 60 (11), 1917–1932.

Sangster, A.L., Gauthier, M., Gower, C.F., 1992. Metallogeny of structural zones, Grenville Province, northeastern North America. Precambrian Research, volume 58, 401–426.

Sappin, A.-A., Constantin, M., Clark, T., van Breemen, O., 2009. Geochemistry, geochronology, and geodynamic setting of Ni-Cu±PGE mineral prospects hosted by mafic and ultramafic intrusions in the Portneuf-Mauricie Domain, Grenville Province, Quebec. Canadian Journal of Earth Sciences, volume 46, 331–353.

Sappin, A.-A., Constantin, M., Clark, T., 2011. Origin of magmatic sulfides in a Proterozoic island arc – an example from the Portneuf-Mauricie Domain, Grenville Province, Canada. Mineralium Deposita, Volume. 46 (3), 211–237.

Sappin, A.-A., Constantin, M., Clark, T., 2012. Petrology of mafic and ultramafic intrusions from the Portneuf-Mauricie Domain, Grenville Province, Canada: Implications for plutonic complexes in a Proterozoic island arc. Lithos, volume 154, 277–295.

Saunders, A.D., Tarney, J., 1984. Geochemical characteristics of basaltic volcanism within back-arc basins. In Marginal Basin Geology. Kokelaar, B.P. and Howells, M.F. (Eds.). Special Publication number 16 of the Geological Society, London, 59–76.

Shervais, J.W., 1982. Ti-V plots and the petrogenesis of modern and ophiolitic lavas. Earth and Planetary Science Letters, volume 59, 101–118.

Slagstad., T., Culshaw, N.G., Daly, J.S., Jamieson, R.A., 2009. Western Grenville Province holds key to midcontinental Granite-Rhyolite Province enigma. Terra Nova, volume 21, 191–187.

Sláma, J., Košler, J., Condon, D.J., Crowley, J.L., Gerdes, A., Hanchar, J.M., Horstwood, M.S.A., Morris, G.A., Nasdala, L., Norberg., N., Schlategger, U., Schoene, B., Tubrett, M.N., Whitehouse, M.J., 2008. Plešovice zircon – A new natural

reference material for U-Pb and Hf isotopic microanalysis. Chemical Geology, volume 249, 1–35.

Sparkes, G.W., Dunning, G.R, 2014. Late Neoproterozoic epithermal alteration and mineralization in the western Avalon zone: a summary of mineralogical investigations and new U/Pb geochronological results. Current Research, Newfoundland and Labrador Department of Natural Resources, Geological Survey, Report 14-1, 99–128.

Spear, F.S., 1993. Metamorphic phase equilibria and pressure-temperature-time paths. Mineralogical Society of America, Washington, D.C., short-course notes, Monograph, volume 1, 799 p.

Spitz, G., Darling, R., 1978. Major and minor element lithogeochemical anomalies surrounding the Louvem copper deposit, Val D'Or, Quebec. Canadian Journal of Earth Sciences, volume 15, 1161–1169.

Stacey, J.S., Kramers, J.D., 1975. Approximation of terrestrial lead isotope evolution by a 2-stage model. Earth and Planetary Science Letters, volume 26 (2), 207–221.

Stamatelopoulou-Seymour, K., MacLean, W.H., 1984. Metamorphosed volcanogenic ores at Montauban, Grenville Province, Quebec. Canadian Mineralogist, volume 22, 595–604.

Stern, C.R., de Wit, M.J., 1997. The Rocas Verdes "Greenstone Belt", Southernmost South America. In: de Wit, M.J., Ashwal, L.D. (Eds.), Greenstone Belts. Oxford monographs on geology and geophysics, volume 35, 791–801.

Stern, C.R., Moreno, H., Lopez-Escobar, L., Clavero, J.E., Lara, L.E., Naranjo, J.A., Parada, M.A., Skewes, M.A., 2007. Chilean volcanoes. In: Moreno, T., Gibbons, W. (Eds.), The Geology of Chile. The Geological Society, London., p. 147–178.

Sun, S.S., McDonough, W.F., 1989. Chemical and isotopic systematics of oceanic basalts: Implications for mantle composition and processes, in Magmatism in the Ocean Basins, in: A.D. Saunders and M.J. Norry (Eds.). Geological Society of London, Special Publication No. 42, 313–345.

Tanaka, T., Togashi, S., Kamioka, H., Amakawa, H., Kagami, H., Hamamoto, T., Yuhara, M., Orihashi, Y., Yoneda, S., Shimizu, H., Kunimaru, T., Takahashi, K., Yanagi, T., Nakano, T., Fujimaki, H., Shinjo, R., Asahara, Y., Tanimizu, M., Dragusanu, C., 2000. JNdi-1: A neodymium isotopic reference in consistency with LaJolla neodymium. Chemical Geology, volume 168, 279–281. doi:10.1016/S0009-2541(00)00198-4

Tomkins, A.G., 2007. Three mechanisms of ore re-mobilisation during amphibolite facies metamorphism at the Montauban Zn-Pb-Au-Ag deposit. Mineralium Deposita, volume 42, 627–637.

Tucker, R.D., Gower, C.F., 1990. Salient features of the Pinware terrane, Grenville Province, eastern Labrador. Geological Association of Canada, Mineralogical Association of Canada, Program with abstracts, volume 15, A133.

Tucker, R.D, Gower, C.F., 1994. A U-Pb geochronological framework for the Pinware terrane, Grenville Province, southeast Labrador. Journal of Geology, volume 102, 67–78.

Turlin, F., André-Mayer, A.-S., Moukhsil, A., Vanderhaeghe, O., Gervais, F., Solgadi, F., Groulier, P.-A., Poujol, M., 2017. Unusual LREE-rich, peraluminous, monazite- or allanite-bearing pegmatitic granite in the central Grenville Province, Québec. Ore Geology Reviews, volume 89, 627–667.

Turlin, F., 2017. Les granites pegmatitiques enrichis en éléments de terres rares légères marqueurs des processus de croissance et de différenciation crustale : Exemple de la Province Protérozoïque de Grenville, Québec. PhD thesis, Université de Lorraine, France, 448 p.

Valverde Cardenas, C., Indares, A., Jenner, G., 2012. Mafic and ultrapotassic rocks from the Canyon domain (central Grenville Province): geochemistry and tectonic implications. Canadian Journal of Earth Sciences, volume 49, 412–433.

van Breemen, O., Corriveau, L., 2005. U-Pb age constraints on arenaceous and volcanic rocks of the Wahekam Group, eastern Grenville Province. Canadian Journal of Earth Sciences, volume 42, 1677–1697.

Vanderhaeghe, O, 2012. The thermal–mechanical evolution of crustal orogenic belts at convergence plate boundaries: a reappraisal of the orogenic cycle. Journal of Geodynamics, volume 56–57, 124–145.

Van Schmus, W.R., Schneider, D.A., Holm, D.K., Dodson, S., Nelson, B.K., 2007. New insights into the north-central United States based on U-Pb, Sm-Nd, and Ar-Ar geochronology. Precambrian Research, volume 157, 80–105.

Vautour, S., 2015. A new model for the Quebecia terrane in the Grenville Province as a composite arc belt: Sm-Nd evidence. MSc thesis, McMaster University, 66 p.

Veizer, J., Ala, D., Azmy, K., Bruckschen, P., Buhl, D., Bruhn, F., Carden, G.A.F., Diener, A., Ebneth, S., Godderis, Y., Jasper, T., Korte, C., Pawellek, F., Podlaha, O.G., Strauss, H., 1999. $^{87}Sr/^{86}Sr$, $\delta^{13}C$ and $\delta^{18}O$ evolution of Phanerozoic seawater. Chemical Geology, volume 161, 59–88.

Watson, E.B., Harrison, T.M., 1983. Zircon saturation revisited: temperature and composition effects in a variety of crustal magma types. Earth and Planetary Science Letters, volume 64, 295–304.

Whalen, J.B., Currie, K.L., Chappell, B.W., 1987. A-type granites: geochemical characteristics, discrimination and petrogenesis. Contributions to Mineralogy and Petrology, volume. 95, 407–419.

Whalen, J., Jenner, G.A., Longstaffe, F.J., Robert, F. and Gariepy, C., 1996. Geochemical and isotopic (O, Nd, Pb, Sr) constraints on A-type granite petrogenesis based on the Topsails Igneous Suite, Newfoundland Appalachians. Journal of Petrology, volume 37, 1463–1489.

Whelan, J.F., Rye, R.O., DeLorraine, W., 1984. The Balmat-Edwards Zinc-Lead Deposits – Synsedimentary ore from Mississippi Valley-Type fluids. Economic Geology, volume 79, 239–265.

Whitmeyer, S.J., Karlstrom, K.E., 2007. Tectonic model for the Proterozoic growth of North America. Geosphere, volume 3(4), 220–259.

Wiedenbeck, M., Allé, P., Corfu, F., Griffin, W.L., Roddick, J.C., Spiegel, W., 1995. Three natural zircon standards for U-Th-Pb, Lu-Hf, trace element and REE analyses. Geostandards and Geoanalytical Research, volume 19, 1–23.

Winchester, J.A., Floyd, P.A., 1977. Geochemical discrimination of different magma series and their differentiation products using immobile elements. Chemical Geology, volume. 20, 325–343.

Williams, P.J., 1990. Evidence for a late metamorphic origin of disseminated gold mineralization in Grenville gneisses at Calumet, Quebec. Economic Geology, volume 85, 164–171.

Williams, N.C., Davidson, G.J., 2004. Possible submarine advanced argillic alteration at the Basin Lake prospect, Western Tasmania, Australia. Economic Geology, volume 99, 987–1002.

Wood, D. A. (1980) The application of a Th Hf Ta diagram to problems of tectonomagmatic classification and to establishing the nature of crustal contamination of basaltic lavas of the British Tertiary Volcanic Province. Earth and Planetary Science Letters, volume 50 (1), 11–30.